The Ageing Bone: PEPITEM as a Novel Inducer of Bone repair.

By

Kathryn Frost



UNIVERSITY OF BIRMINGHAM

A thesis submitted to the University of Birmingham for the degree

of

DOCTOR OF PHILOSOPHY

Department of Inflammation and Ageing

College of Medicine and Health

The University of Birmingham

September 2024

UNIVERSITY OF
BIRMINGHAM

University of Birmingham Research Archive

e-theses repository

This unpublished thesis/dissertation is copyright of the author and/or third parties. The intellectual property rights of the author or third parties in respect of this work are as defined by The Copyright Designs and Patents Act 1988 or as modified by any successor legislation.

Any use made of information contained in this thesis/dissertation must be in accordance with that legislation and must be properly acknowledged. Further distribution or reproduction in any format is prohibited without the permission of the copyright holder.

Abstract

Bone is a highly dynamic organ undergoing constant osteoblast-mediated bone formation and osteoclast-mediated bone resorption, allowing for balanced bone remodelling. This process is regulated by multiple endogenous factors, such as parathyroid hormone and oestrogen. Recently an endogenous peptide, known as PEPITEM has been shown to regulate bone remodelling through a dual action on osteoblasts and osteoclasts, making it a promising therapeutic for the treatment of bone loss in diseases such as osteoporosis.

In this thesis we expand on the current understanding of PEPITEM, investigating its molecular mechanism on osteoblasts and osteoclasts, whilst also exploring the therapeutic benefits of peptide memetics derived from PEPITEM. We hypothesised that PEPITEM is having direct actions on osteoblasts through membrane receptor signalling, causing changes in osteoblast maturation and osteoblast-osteoclast communication.

We identified through the use of *ex vivo* and both 2D and 3D *in vitro* experiments, that PEPITEM is able to act on osteoblasts to increase extracellular matrix production and mineralisation through actions on the membrane receptor, neural cell adhesion molecule 1 (NCAM-1). PEPITEM binding was shown to elicit increased β-catenin signalling, resulting in increased osteoblast maturation and activity. NCAM-1 mediated activation of osteoblasts was also shown to increase secretion of anti-osteoclastogenic molecule osteoprotegerin (OPG), which mediates the indirect anti-os²teoclastogenic actions of PEPITEM.

Previous experiments showing PEPITEMs limited half-life led us to explore the bioactive residues present in the PEPITEM sequence, in order to explore the therapeutic potential of PEPITEM mimetics. Here we show that PEPITEM memetics are able to partially mimic PEPITEM actions both *in vitro* and *in vivo*. *In vitro* memetics were able to increase

osteoblast maturation, however not all memetics were able to increase OPG secretion. Comparatively *in vivo* both memetics tested were able to increase bone formation and reduce osteoclast number during homeostasis increasing trabecular bone length. The bioactivity of these peptides was maintained during disease, where ovariectomised show reduced trabecular bone loss in response to peptide treatments.

This project offers new insights into how the endogenous peptide PEPITEM functions and its role in bone homeostasis and disease. The identification of the PEPITEM-NCAM-1 pathway enhances our understanding of osteoblast activity and opens up potential new avenues for therapeutic intervention. Additionally, the discovery of bio-active regions within the PEPITEM sequence, regions that retain partial PEPITEM function both *in vitro* and *in vivo*, provides further understanding of the peptide's mechanism. These findings suggest potential new therapeutic targets for bone loss, as these bio-active regions could enable less frequent treatments compared to the full PEPITEM peptide.

Acknowledgements

Firstly, I'd like to thank my wonderful funders the British Society for Research on Ageing and the Chernajovsky biomedical research foundation, without whom none of this research would have been possible. I'd also like to thank all the BMSU staff for all their help with the animal work involved in this thesis.

To my primary supervisors, Helen McGettrick and Amy Naylor, thank you for your patience, expertise and support over the last 3 years. From our initial discussions to the final revisions, you have provided not only insightful feedback and constructive criticism but also provided me with encouragement giving me the confidence in my own abilities that I'll be forever grateful for. Also, thank you to my additional supervisor James Edwards for all your help along the way.

To all the people who I've had the pleasure of working with during this PhD, thank you for all of your help and endless support. A special thanks to the members of the IVB and LTG past and present, Ladi, Mussarat, Julia, Poppy, Abbey, Jenefa, Areeba and Alyssa, thank you for always listening and supporting me inside and outside of the lab, your advice and laughter was always needed and greatly appreciated. The Naylor group, Ellie, Mel, Georgiana, Miruna, Maryam and Joe, thanks for always helping me navigate the world of bone, our meetings will always be the best way to start a Monday. Kate, Annie, Chloe and Liv, we basically started this journey together and I can't believe it's over, thank you for always being there for a chat or a vent, honestly the number of times I would have quit without you all. And Jonny, thank you for starting this project and teaching me even when you were writing your thesis, I'm only now appreciating how annoying that must have been.

I would like to express my deepest gratitude to my family for their unwavering support. Mum and dad, thank you for always being there, both in moments of joy and in times of doubt. Your guidance and encouragement have been invaluable, and I am deeply grateful for everything you have done. Nicky, thank you for always making me laugh and always looking out for me, you're the best big siter anyone could ask for. Gramps, you will always be one of my biggest inspirations. To Nana and Granny, I did it, I finally finished school! I wish you both could be here to see it, but I know you'd be proud, and I miss you every day.

Finally, Mev I am so sorry for the emotional wreck you've had to deal with over the past few months (maybe years). I cannot thank you enough for always being there, even when you didn't know what I was wittering on about.

Outputs from Thesis

First Author Manuscripts

- Lewis, J.W.*, **Frost, K**.*, Neag, G., Wahid, M., Finley, M., Northall, E., Abudu, O., Davis, E.T., Powell, E., Plamer, C., Lu, J., Edwards, J.R., Iqbal, A., Chimen, M., Mahmood, A., Jones, S.W., Edwards, J.R., Naylor, A.J., McGettrick, H.M (2024) New therapeutic avenues in bone repair: Harnessing a novel endogenous molecule to boost bone growth and prevent bone loss. *Cell Reports Medicine*, 2024, 5(5), 101574, ISSN 2666-3791, https://doi.org/10.1016/j.xcrm.2024.101574.
- **Frost, K***., Lewis, J.*, Edwards, J.R , Naylor, A.J , McGettrick, H.M (2024). Analysis of differences in bone responses to Sphingosine-1-Phosphate in murine and human. I*nt. J. Mol. Sci.* 2024, *25*(10), 5118; https://doi.org/10.3390/ijms25105118

Reviews

- **Frost K**, Naylor AJ, McGettrick HM. The Ying and Yang of Sphingosine-1-Phosphate Signalling within the Bone. *International Journal of Molecular Sciences*. 2023; 24(8):6935. https://doi.org/10.3390/ijms24086935

Science communications

- **Frost, K**. , Insch,E , Naylor, A.J , McGettrick, H.M (2024). Unlocking new treatments for bone diseases: using PEPITEM to strengthen bones and prevent loss. *Atlas of Science. 2024*
- Nathan, P., Hopkin, S., Wilson, I., Lightfoot, A., Lezama, D., Begum, J., Manning, J., **Frost, K**., Abudu, O., Wahid, M. and Sevim, M. Hitting the road at last: ECRs at an international conference, British Society for Immunology Newsletter Sept 2022.

Oral Presentations

- The Ageing Bone: PEPITEM as a Novel Inducer of Bone repair. Birmingham Inflammation Repair and Ageing Conference, 2024
- The Ageing Bone: PEPITEM as a Novel Inducer of Bone repair. Connect Immune Conference, Birmingham, UK, 2023.

- Endogenous osteoanabolic peptide as a therapeutic for ageing and inflammation-induced bone loss. European Calcified Tissue Society Congress, Liverpool, UK, 2023.
- Endogenous osteoanabolic peptide as a therapeutic for ageing and inflammation-induced bone loss. PEPITEM symposium, Birmingham, UK, 2023.

Poster Presentations

- **Frost, K.,** Lewis, J.W., Wahid, M., Chimen, M., A., Edwards, J.R , Naylor, A.J , McGettrick, H.M (2024), Endogenous osteoanabolic peptide as a therapeutic for inflammatory mediated bone loss. European Workshop for Rheumatology Research, Genoa, Italy
- **Frost, K.,** Lewis, J.W., Wahid, M., Chimen, M., A., Edwards, J.R , Naylor, A.J , McGettrick, H.M (2023), Endogenous osteoanabolic peptide as a therapeutic for ageing induced bone loss. Institute of Inflammation and Ageing Away Day.
- **Frost, K.,** Lewis, J.W., Wahid, M., Chimen, M., A., Edwards, J.R , Naylor, A.J , McGettrick, H.M (2023), Endogenous osteoanabolic peptide as a therapeutic for ageing induced bone loss. British Society for Research on Ageing Annual Meeting, London, UK, 2023.
- **Frost, K.,** Lewis, J.W., Wahid, M., Chimen, M., A., Edwards, J.R , Naylor, A.J , McGettrick, H.M (2023), Endogenous osteoanabolic peptide as a therapeutic for ageing and inflammation-induced bone loss. Bone Research Society Congress, Liverpool, UK, 2023.
- **Frost, K**., Lewis, J.W., Wahid, M., Chimen, M., A., Edwards, J.R , Naylor, A.J , McGettrick, H.M (2022), PEPITEM enhances bone remodelling in health and musculoskeletal disease. British Society for Inflammation Congress, Liverpool, UK, 2022.
- **Frost, K.,** Lewis, J.W., Wahid, M., Chimen, M., A., Edwards, J.R , Naylor, A.J , McGettrick, H.M (2022), PEPITEM enhances bone remodelling in health and musculoskeletal disease. Institute of Inflammation and Ageing Away day, University of Birmingham, UK, 2022.

- Lewis, J.W., **Frost, K.**, Neag, G., Jones, S.W., Mahmood, A., Edwards, J.R , Naylor, A.J , McGettrick, H.M (2022). Osteoregulatory Peptide Repairs Bone in Health and Age Related Musculoskeletal Diseases. Mechanisms of Inflammation Symposium (MIDAS), University of Birmingham, UK, 2022.
- Lewis, J.W., **Frost, K.**, Neag, G., Jones, S.W., Mahmood, A., Edwards, J.R , Naylor, A.J , McGettrick, H.M (2022). Osteoregulatory Peptide Repairs Bone in Health and Age Related Musculoskeletal Diseases. The World Congress of Inflammation, Rome, 2022.

Table of Contents

Table of Contents ..... *IX*

1 General Introduction: *1*

1.1 Bone Structure **2**

1.2 Cellular components **3**

1.2.1 Osteoclasts 3

1.2.2 Osteoblasts 4

1.2.3 Osteocytes 7

1.2.4 Bone Lining Cells 8

1.3 Bone Formation **8**

1.3.1 Intramembranous ossification 8

1.3.2 Endochondral ossification 9

1.3.3 Bone Vasculature 13

1.4 Bone Remodelling **16**

1.5 Regulation of Bone Remodelling **19**

1.5.1 Mechanical Loading 19

1.5.2 Endogenous stimulating factors 21

1.5.3 14-3-3 Family Proteins 42

1.6 Dysregulation of bone remodelling **46**

1.6.1 Ageing 47

1.6.2 Osteoporosis 51

1.6.3 Pharmacological interventions for bone remodelling 52

1.7 Future Therapeutics **61**

1.7.1 PEPITEM as a novel therapeutic 61

1.8 Modelling bone remodelling in health and disease 65

1.8.1 *In vivo* 65

1.8.2 *Ex vivo* 67

1.8.3 In vitro 68

1.9 Aims and Objectives 72

2 Methods 73

2.1 Animal Studies 74

2.1.1 Mice 74

2.1.2 Homeostatic conditions 74

2.1.3 Ovariectomy (OVX) model of osteoporosis 75

2.2 Ex vivo μ-CT analysis 75

2.2.1 Imaging 75

2.2.2 Image reconstruction 76

2.2.3 Analysis and 3D mesh generation 77

2.3 Ex vivo tissue processing and Staining 79

2.3.1 Decalcification and Paraffin Embedding 79

2.3.2 Sectioning 79

2.4 Tissue Histomorphometry 80

2.4.1 Haematoxylin and Eosin (H&E) 80

2.4.2 Sirius red staining 81

2.4.3 Tartrate resistant acid phosphatase (TRAP) 82

2.5 Ex vivo metatarsal culture 82

2.6 Murine Osteoblast Cell Culture 83

2.6.1 Murine Calvaria Osteoblast Isolation 83

2.6.2 Detachment of cells 84
2.6.3 Freezing and storage of cells 85
2.6.4 Osteoblast cell lines 85
2.6.5 Self-Structuring Bone Model (SSBM) Culture 86
2.6.6 Induction of osteoblast mineralisation 89
2.6.7 Measures of osteoblast maturation and function 90
2.6.8 Identification of downstream PEPITEM signalling 94
2.7 Assessment of gene expression 102
2.7.1 RNA Extraction and cDNA Conversion 102
2.7.2 PCR 103
2.7.3 RNAseq 104
2.8 In Silico Analysis (AlphaFold and ChimerX) 107
2.9 Osteoclast cell culture: 108
2.9.1 Murine osteoclast cell line 108
2.9.2 Media transfer 108
2.9.3 Osteoprotegerin Neutralising Antibody Treatment 108
2.9.4 Tartrate Resistant Acid Phosphatase (TRAP) staining of osteoclasts in culture 109
2.10 Statistical analysis 109
3 Mechanistic action of PEPITEM in osteoblasts 111
3.1 Introduction 112
3.2 Results: 113
3.2.1 PEPITEM acts to increase bone morphometric parameters in male and female mice 113
3.2.2 PEPITEM increases bone formation in 3D *in vitro* and ex vivo bone models 125
3.2.3 Investigating known components of the PEPITEM Pathway 135
3.2.4 Identification of Novel PEPITEM pathway in osteoblasts 140

3.2.5 NCAM-1 signalling 154

3.2.6 PEPITEM increases gene related to bone formation following 6hr of treatment (RNAseq) 169

3.3 Discussion: 172

3.3.1 Sexual dimorphism in PEPITEM function 172

3.3.2 Cortical and trabecular bone remodelling 176

3.3.3 S1P in Bone remodelling 179

3.3.4 Cdh15 in Osteoblasts 180

3.3.5 NCAM-1 in bone remodelling 183

3.3.6 β-catenin mediates NCAM-1-PEPITEM signalling in osteoblasts 186

3.3.7 Intracellular function of peptide therapies 188

3.3.8 Conclusion 189

4 PEPITEMs effect on Osteoblast–Osteoclast Communication 190

4.1 Introduction 191

4.2 Results 192

4.2.1 Osteoblasts secrete a soluble mediator in response to PEPITEM 192

4.2.2 Inhibition of S1P production results in altered osteoblast-osteoclast communication independent of PEPITEM. 194

4.2.3 Osteoblasts increase OPG secretion in response to PEPITEM 196

4.3 Discussion 203

4.3.1 S1P signalling in osteoblast-osteoclast communication. 203

4.3.2 Osteoblast-Osteoclast paracrine interactions 204

4.3.3 Directed Osteoblast-Osteoclast communication 206

4.3.4 Role of PEPITEM in macrophage biology and differentiation 207

4.3.5 How does PEPITEM alters RANK-RANKL-OPG signalling to influence bone remodelling? 208

4.3.6 How is RANKL-OPG signalling disrupted in bone diseases 209
4.3.7 PEPITEM compared to other treatments which alter RANKL signalling 211
4.3.8 Conclusion 212

5 Identifying PEPITEM bioactivity to improve therapeutic capacity 214

5.1. Introduction 215

5.2. Results 216

5.1.1 PEPITEM contains bioactive regions with differing biological function 216
5.1.2 Investigation of small PEPITEM derived memetics 222
5.1.3 Peptide memetics partially to mimic PEPITEM function during homeostatic remodelling 232
5.1.4 Peptide partially mimic PEPITEM function in models of osteoporosis.....242

5.2 Discussion 251

5.2.1 PEPITEM contains bioactive regions 252
5.2.2 PEGylation increases PEPITEM bioactivity.....254
5.2.3 PEPITEM and peptide memetics alter trabecular bone patterning.....256
5.2.4 Do peptide memetics mimic PEPITEM function during homeostasis? 259
5.2.5 Peptide memetics compared to PEPITEM and current therapeutic for osteoporosis 261
5.2.6 Conclusion 265

6 General Discussion..... 266

6.1 Summary of Findings 267

6.2 Mechanistic action of PEPITEM in Bone 269

6.3 Therapeutic potential of PEPITEM and Peptide memetics 271

6.4 Study Limitations..... 277

6.5 Future Experiments 279

6.6 Conclusion..... 280

7 Bibliography:..... 281

8 Appendix..... 352

Table of Figures

Figure 1.1 Life cycle of osteoblasts. 6

Figure 1.2 Diagram of endochondral ossification and growth plate development. 11

Figure 1.3 Diagram of bone vasculature development. 15

Figure 1.4 Bone remodelling cycle. 18

Figure 1.5 Sphingosine metabolic pathway. 23

Figure 1.6 S1PR function in osteogenic cells. 26

Figure 1.7 Osteoblast-Osteoclast Communication via S1P. 40

Figure 2.1 Image of straws for μCT scanning. 76

Figure 2.2 Systematic diagram of the ROIs for analysing murine tibiae bone parameters. 78

Figure 2.3 Diagram of Self-Structuring Bone Model (SSBM). 89

Figure 2.4 RIN scores calculated for each sample. 106

Figure 3.1 PEPITEM increased osteoblast production of osteoid without increasing osteoblast number. 114

Figure 3.2 PEPITEM does not alter trabecular bone parameters by μ-CT in female mice following 2-week treatment. 116

Figure 3.3 PEPITEM does not alter cortical bone parameters by μ-CT in female mice. 117

Figure 3.4 PEPITEM treatment increases osteoid production in female homeostatic mice without effecting osteoblast number. 118

Figure 3.5 PEPITEM treatment significantly decrease osteoclast number in female homeostatic mice. 119

Figure 3.6 PEPITEM does not alter trabecular bone parameters by μ-CT in female mice following prolonged treatment. 121

Figure 3.7 PEPITEM increased cortical bone parameters by μ-CT in female mice following prolonged treatment. 122

Figure 3.8 PEPITEM treatment increased osteoid production in female homeostatic mice following 4 weeks of treatment. 123

Figure 3.9 PEPITEM treatment decreased osteoclast number in female homeostatic mice following 4 weeks of treatment. 124

Figure 3.10 PEPITEM acts to increase osteoblast maturation in hFOB 1.19 cells. 127

Figure 3.11 4-week SSBM constructs show altered gene profiles when treated with PEPITEM. 128

Figure 3.12 12-week SSBM constructs show altered gene profiles when treated with PEPITEM. 129

Figure 3.13 PEPITEM increased Pro-collagen type I production in 4-week SSBM constructs following short term treatment. 131

Figure 3.14 PEPITEM increases SSBM mineralisation when given at 4-wks. 132

Figure 3.15 PEPITEM increased mineralisation in ex vivo metatarsal model. 134

Figure 3.16 Activation of Cdh15 does not mimic PEPITEM treatment. 136

Figure 3.17 S1P Kinases inhibition results in increased cell death within ST2 cells. 139

Figure 3.18 Biotinylation of PEPITEM does not affect bioactivity of the peptide. 141

Figure 3.19 Graphical analysis of peptides from Co-IP. 144

Figure 3.20 PEPITEM binding models to top co-ip hits. 146

Figure 3.21 Alphafold predicted binding of PEPITEM and NCAM-1. 148

Figure 3.22 Alphafold predicted binding of PEPITEM and NCAM-1 Fibronectin-III domains. 150

Figure 3.23 Alphafold predicted binding of PEPITEM and Ehd2. 153

Figure 3.24 C.Obs express NCAM-1 at time of PEPITEM treatment. 155

Figure 3.25 Representative images of C.Obs stained for NCAM-1 and RUNX2, showing surface expression of NCAM-1. 157

Figure 3.26 Western blot of C.Ob lysates treated with or without PEPITEM stained of NCAM-1compared to actin. 158

Figure 3.27 PEPITEM treatment alters NCAM-1 expression. 159

Figure 3.28 Inhibition of NCAM-1 reduces the effect of PEPITEM. 161

Figure 3.29 PEPITEM mediated increase in mineralisation is inhibited by NCAM-1 antagonistic antibody in ex vivo metatarsal model. 162

Figure 3.30 Representative images of E15.5 metatarsals at with or without PEPITEM and NCAM-1 antagonistic antibody. 163

Figure 3.31 Representative images of β-catenin transnucleation following PEPITEM treatment. 166

Figure 3.32 PEPITEM increases transnucleation of β-Catenin. 167

Figure 3.33 PEPITEM increases levels of non-phosphorylated (active) β-Catenin. 168

Figure 3.34: Col1A1 expression increased following 6hr of treatment. 171

Figure 4.1 Osteoblasts release a soluble mediator in response to PEPITEM which inhibits osteoclastogenesis. 193

Figure 4.2 S1P signalling in osteoblasts impacts osteoclast formation independently of PEPITEM signalling. 195

Figure 4.3 Osteoblast secrete increase OPG in response to PEPITEM. 197

Figure 4.4 PEPITEM increases OPG secretion in 3D bone model. 199

Figure 4.5 Inhibition of OPG secretion reverses PEPITEM anti-osteoclastogenic effects. 201

Figure 4.6 Inhibition of NCAM-1 prevents PEPITEM induced OPG secretion. 202

Figure 5.1 Altering the PEPITEM sequence alters OPG secretion, but not ALP activity. 218

Figure 5.2 Diagram of AlphaFold predicted binding residues in PEPITEM. 220

Figure 5.3 PEPITEM sequence fragments alters OPG secretion and ALP activity. 221

Figure 5.4 Structural formula for PEPITEM and associated peptide memetics. Diagrams of the structural formula of PEPITEM and its memetics created using pepdraw.com 224

Figure 5.5 PEPITEM memetics alter OPG secretion and ALP activity. 225

Figure 5.6 Titration for peptide mimetics. 226

Figure 5.7 Peptide memetics increase pro-collagen type I secretion in 3D bone model. 229

Figure 5.8 *PEPITEM but not peptide memetics increase OPG secretion in 3D bone model*. 230

Figure 5.9 PEPITEM but not peptide memetics increase mineralisation 3D bone model. 231

Figure 5.10 Model to study the effect of PEPITEM memetics on bone homeostasis. 233

Figure 5.11 PEPITEM but not peptide memetics alter trabecular bone parameters by μ-CT in homeostatic male mice. 235

Figure 5.12 PEPITEM and peptide memetics enhanced trabecular bone elongation by μ-CT in homeostatic male mice. 236

Figure 5.13 PEPITEM and peptide memetics no not alter cortical bone parameters by µ-CT in homeostatic male mice. 237

Figure 5.14 PEPITEM memetics partially increased osteoblast production of osteoid. 239

Figure 5.15 PEPITEM memetics did not increase osteoblast number. 240

Figure 5.16 PEPITEM memetic treatments partially reduce osteoclast number in male homeostatic mice. 241

Figure 5.17 Model to study the effects of PEPITEM memetics on ovariectomized bone. 244

Figure 5.18 PEPITEM and peptide memetics partly restore trabecular bone parameters by µ-CT in female mice following ovariectomy induced bone loss. 245

Figure 5.19 Female wild type mice underwent an ovariectomy (OVX) on day 0 to initiate oestrogen dependent bone loss. 246

Figure 5.20 Non-PEGylated PEPITEM increased osteoblast production in OVX female mice. 248

Figure 5.21 PEPITEM increases osteoblast number in OVX model of osteoporosis. 249

Figure 5.22 PEPITEM memetic treatments partially reduce osteoclast number in female OVX mice. 250

Figure 6.1 Schematic of proposed PEPITEM signalling pathways in bone. 276

Figure 8.1 Preprocessing of PEPITEM vs Control peptide RNAseq in iDEP. 356

Table of Tables

Table 2.1 Antibodies used for immunofluorescence, neutralisation and western blotting 94
Table 2.2 Murine basal media 83
Table 2.3 Murine osteogenic media 83
Table 2.4 Human basal culture media 86
Table 2.5 Human osteogenic culture media 86
Table 2.6 Peptides used for *in vitro* and *in vivo* assays 90
Table 2.7 Taqman™ Primers used for qPCR 104
Table 3.1 Hits from PEPITEM only Co-IP analysis. Proteins which were only identified to bind to PEPITEM not control peptide. 143
Table 3.2 AlphaFold-Multimer predicted binding residues for PEPITEM interacting with NCAM-1 151
Table 3.3: Top upregulated genes related to bone when comparing PEPITEM to control peptide following 6hr of treatment 170
Table 5.1 Alanine sweep peptides and the amino acid substituted 217
Table 8.1 All upregulated and downregulated genes following PEPITEM treatment compared to control peptide 356

Abbreviation

ALA	Alanine
ALP(L)	Alkaline Phosphatase (Ligand)
ANXA6	Annexin6A
APC	Axin-adenomatous polyposis coli
APPL1	adaptor protein, phosphotyrosine interacting with PH domain and leucine zipper 1
ARS	alizarin red standard
ASN	Asparagine
ASP	Aspartic Acid
ATCC	American Type Culture Collection
ATP	Adenosine triphosphate
AUC	Area under curve
B2M	Beta-2-microglobulin
BFR	Bone formation rate
BGLAP1	Osteocalcin gene
BMD	Bone mineral density
BMDM	Bone marrow derived macrophage
BMM	Bone marrow macrophage
BMP	Bone morphogenic protein
BMSC	bone marrow stromal cell
BMSU	Biomedical service unit
BMU	bone modelling unit
BS	Bone surface
BSA	Bovine serum albumin
BV	Bone volume
CO-IP	Co-immunoprecipitation
COL1A1	Collagen type 1 alpha chain-1
COLLD	Collagen D
COX2	Cyclooxygenase-2
CT	computed tomography
CTF	Cytoplasmic tail fragment
CTSG	cathepsin G
CTX	carboxy-terminal collagen crosslinks
CXCL(X)	CXC motif chemokine ligand (X)
DAPI	4',6-diamidino-2-phenylindole
DMEM	Dulbecco's Modified Eagle Medium
DMP1	Dentin Matrix Acidic Phosphoprotein 1
DMSO	Dimethyl sulfoxide
DNA	Deoxyribonucleic acid

DPP3	Dipeptidyl-peptidase 3
ECM	Extra cellular matrix
EDA	Experimental design assistant
EDTA	Ethylenediaminetetraacetic acid
EFNB2	Ephrin B2
EHD2	EH domain containing 2
ELISA	enzyme-linked immunosorbent assay
ER	Endoplasmic reticulum
ERK	extracellular signal-regulated kinase
FASTQC	Fast Quality Control
FBS	Foetal bovine serum
FGFR	Fibroblast growth factor receptor
FIJI	Fiji is just imagej
GLN	glutamine
GLU	Glutamic acid
GLY	Glycine
GSK	Glycogen synthase kinase
GWAS	Genome wide association study
HRP	Horse radish peroxidase
HRT	Hormone replacement therapy
ILE	Isoleucine
KO	Knockout
LEU	Leucine
LYS	Lysine
MMRN2	Multimerin-2
NC3R	National centre for the 3Rs
NCAM	Neural cell adhesion molecule
NFAT	Nuclear factor of activated T-cells
MCSF	macrophage colony stimulating factor
NXN	Nucleoredoxin
OB	osteoblast
OC	osteoclast
OCN	osteocalcin
OPG	Osteoprotegerin
OVX	Ovariectomy
P1NP	Total procollagen type 1 N-terminal propeptide
PAE	Predicted aligned error
PBMC	Peripheral Blood Monocytic Cell
PBS	Phosphate Buffered Saline
PCA	Principal Component Analysis
PCR	polymerase chain reaction

PDPN	podoplanin
PEPITEM	Peptide Inhibitor of Transendothelial Migration
PEG	Pegylation
PRO	Proline
plDDT	predicted local distance difference test
PTH	Parathyroid hormone
RANK(L)	Receptor activator of nuclear factor-κB (ligand)
RIPA	Radioimmunoprecipitation assay buffer
RNA	Ribonucleic acid
ROI	Region of interest
RUNX2	Runt-related transcription factor 2
S1P	Sphingosine-1-phosphate
S1PR	Sphingosine-1-phosphate receptor
SD	Standard deviation
SDS	Sodium dodecyl sulphate
SEM	Standard error of the mean
SOST	Sclerostin
SOX	SRY-box transcription factor
SP7	Specificity protein-7
SPARC	Secreted Protein Acidic and Cysteine Rich
SPHK	Sphingosine Kinase
SPNS2	Spinster homolog
SPP	Secreted phosphoprotein
SSBM	Self-structuring bone model
TGF	Transforming growth factor
TNF	Tumour Necrosis Factor
TRAP	Tartrate Resistant Acidic Phosphatase
TV	Tissue volume
TYR	Tyrosine
VAL	Valine
WNT	Wingless and Int-1
YWHAZ	Tyrosine 3-Monooxygenase/Tryptophan 5-Monooxygenase Activation Protein Zeta

1 General Introduction:

Part of this chapter (section 1.5.2.1 – Sphingosine-1-Phosphate) is based on Frost et al, 2023, for which I carried out the literature review, wrote the text and created the figures.
Co-authors Naylor and McGettrick made corrections and minor revisions.
The full review can be found in Appendix 305-324

The bone is a highly dynamic structure, which cycles through periods of formation and resorption allowing for adaption to mechanostimulation[1–4] and damage[5,6]. In this general introduction, the structure of bone will be discussed from its macro-architecture to its micro-architecture and cellular components. Here we will also discuss cases where bone structure is compromised and current therapeutic strategies available to treat these issues. This thesis will explore the involvement and mechanism of action of the endogenous peptide inhibitor of transendothelial migration (PEPITEM) in bone homeostasis and look at its therapeutic potential in diseases of bone loss.

1.1 Bone Structure

The adult human body consists of 206 bones that act together with cartilage, ligaments and tendons to make up the skeletal system[7]. The bone is integral to many bodily functions, such as providing structural support, protection of soft tissue and regulation of calcium and phosphate homeostatsis[8]. The formation of bone first begins within the seventh week of embryogenesis[9], by the process of ossification (new bone formation) that continues in humans up to 25 years of age[10]. However, the bone continues to adapt and repair throughout life, as bone is repeatedly replaced in a process called bone remodelling[11].

The bone is comprised of two types of tissue, compact or cortical bone, which forms the hard outer layer[12], and trabecular bone, which is spongy in appearance and consists of a network of trabeculae structures[13]. The ratio of cortical and trabecular bone varies between individual bone types[12], with the vertebrae consisting predominantly of trabecular bone at a 25:75 ratio compared to the 50:50 ratio seen in the femoral head[14]. The composition of bone can be separated into the organic (90%) and inorganic matrix[15]. The organic matrix is

predominantly type 1 collagen with the addition of non-collagenous proteins, such as osteocalcin[16]. The inorganic components of bone are mainly calcium and phosphorus in the form of hydroxyapatite crystals, however, there are other elements including sodium and potassium[17]. The organic matrix creates a scaffold for the deposition of hydroxyapatite in the process of mineralisation[18].

1.2 Cellular components

The formation, modelling and remodelling of bone is primarily carried out by two cell types: Osteoclasts, the bone-resorbing cells, and osteoblasts, the bone-forming cells[19,20]. With the addition of other osteogenic cells, including osteocytes and bone lining cells, that can also impact bone remodelling through the regulation of osteoclast and osteoblast function[19,20].

1.2.1 Osteoclasts

Osteoclasts are multinucleated cells that originate from mononuclear hematopoietic stem cells[21]. Osteoclast precursors differentiate when stimulated by various factors, such as macrophage colony stimulating factor (M-CSF)[22] and receptor activator of nuclear factor kappa-B ligand (RANKL)[23], secreted by osteoblasts and other local cells[24]. Whilst M-CSF is known to stimulate proliferation and promote survival of osteoclast precursors[25], RANKL is essential for osteoclastogenesis[26]. RANKL binds to its receptor RANK on osteoclast precursors[27], which promotes the expression of osteoclastogenic factors, such as the nuclear factor of activated T-cells (NFATc1)[28]. NFATc1 regulates osteoclast specific genes, such as tartrate resistant acid phosphatase (TRAP) and cathepsin-K[29] that are important in

the degradation and cleavage of proteins within the extracellular matrix (ECM)[30,31]. The activity of RANKL/RANK is regulated through the release of the RANKL decoy receptor osteoprotegerin (OPG), which is produced by osteoblasts and other stromal cells[23]. OPG prevents the binding of RANKL to RANK, therefore reducing RANKL mediated osteoclastogenesis.

During bone resorption, osteoclasts become polarized and express four observable membrane domains[19]. Two of these membranes are found in contact with the bone, forming the sealing zone and the ruffled border, and the basolateral and secretory membranes that do not contact the bone surface[32,33]. The ruffled border domain is formed of microvilli and is isolated by the sealing zone, which is devoid of organelles[34]. At the ruffled border there is the release of vacuolar-type H^+-ATPase[35], causing acidification of the resorption lacuna resulting in the dissolution of hydroxyapatite crystals within the ECM[24]. Enzymes and proteins, such as TRAP and cathepsin-K, are also secreted across this membrane allowing for further degradation of the ECM[30,31].

1.2.2 Osteoblasts

Derived from mesenchymal stem cells (MSC), osteoblasts are an osteogenic cell type responsible for bone formation[36]. MSCs are non-haemopoietic stem cells that can be produced from various locations, including the bone marrow, and can differentiate into mesenchymal tissues, such as bone, cartilage, muscle and adipose[37,38]. As MSCs can differentiate into several cell types, the activation of specific transcription factors is required to allow for successful osteoblastogenesis[38]. This includes the synthesis of bone morphogenic proteins (BMP) specifically BMP2/4[39] and activation of members of the wingless

(WNT) pathways[40]. Runt related transcription factor 2 (RUNX2)[41] and Osterix (OSX)[42] are essential in this process. RUNX2 has been shown to upregulate osteoblast genetic markers, such as alkaline phosphatase (ALP), bone gamma-carboxyglutamate protein (BGLAP), osteocalcin (OCN) and collagen (COL1A1)[41,43]. Within cell culture, osteoblastogenesis can be triggered in the presence of ascorbic acid, an essential for extracellular matrix production and transcription of regulatory genes such as RUNX2[44–47]. Whilst β-glycerophosphate[48], can be added to provide essential phosphates for the production of hydroxyapatite and regulates osteoblast differentiation through regulation of genes such as BMP-2[49–52].

The process of osteoblastogenesis can be separated into stages (Figure 1.1). Firstly MSCs are recruited to the site of bone remodelling, where cells initially proliferate and commit to the osteoblast lineage through the expression of RUNX2 and COL1A1[36]. At this stage, cells are termed pre-osteoblasts, which are highly proliferative cells with ALP activity that are incapable of secreting extracellular matrix (ECM). Pre-osteoblasts then exit the cell cycle and become mature osteoblasts, which is characterised by increased OSX gene expression[53]. Mature osteoblasts show alterations in morphology, becoming large polarised cuboidal cells that can secrete osteoid; a non-mineralised collagen matrix containing a mixture of non-collagenous proteins, such as osteocalcin (OCN) and osteopontin[54]. These cells adhere to the bone surface and form tight gap junctions with neighbouring osteoblasts, which facilitates ionic transfer, cell synchrony and regulation of future differentiation[55]. Once sufficient osteoid has been deposited, mineralisation of the ECM can take place. Mineralisation refers to the deposition of calcium phosphate crystals into the ECM, and this process is thought to involve the release of matrix vesicles from osteoblasts[56]. Mature osteoblasts will then undergo apoptosis or differentiate into osteocytes or bone lining cells[57].

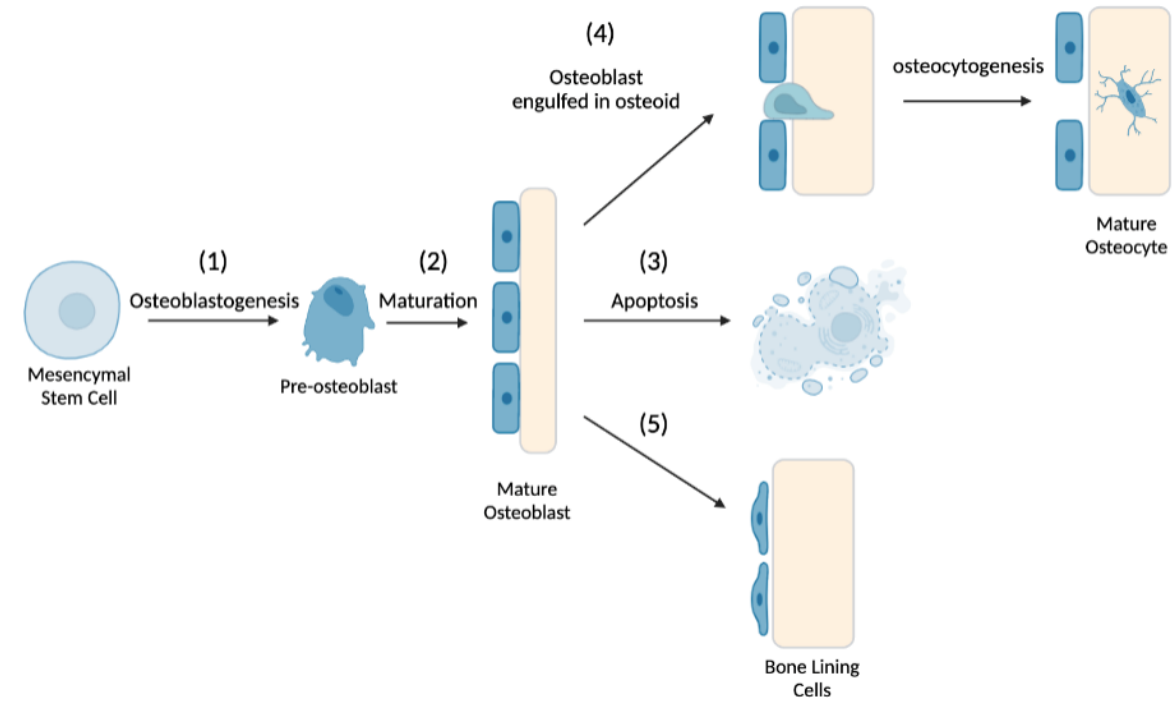


Figure 1.1 **Life cycle of osteoblasts.** Osteoblasts are derived from mesenchymal stem cells, which are non-haemopoietic stem cells capable of differentiating into mesenchymal tissues[36]. These cells undergo osteoblastogenesis (1) into pre-osteoblasts in the presence of BMPs, ascorbic acid and β-glycerophosphate (within cell culture) [44–47]. This causes the upregulation of genes including ALP and osteopontin. Over time these cells develop into mature osteoblasts (2) through the expression of genes such as osteocalcin and Col1a1[54]. Following the production of ECM these cells then undergo one of 3 processes: Apoptosis (3), osteocytogenesis (4) or differentiation into bone lining cells (5) [57]. Diagram created using biorender.com

1.2.3 Osteocytes

Osteocytes comprise 90-95% of the total cells within the bone[57], however, for many years the function of these cells was unclear as they were initially thought to be a passive cell type[58]. The development of new technologies has since debunked this belief and osteocytes are now known to have many valuable functions within bone[59] such as responding to mechanical strain, maintaining balanced osteoblast and osteoclast function and regulation of mineral homeostasis[59]. Osteoblasts may undergo osteocytogenesis and become embedded within the ECM, this results in dramatic changes in their morphology and genetic expression[60]. Osteocytes, unlike osteoblasts, have many dendritic projections that can extend through canaliculi; narrow fluid-filled channels[60]. These projections form connections with neighbouring bone cells, including other osteocytes, bone lining cells, osteoblasts and osteoclasts, creating a 3D cellular network[61]. This complex network allows for communication within the bone; however, studies have demonstrated that this network weakens with age as the number of dendritic processes decreased[62].

Alongside this dendritic network, osteocytes are also able to secrete signalling molecules that regulate osteoclast and osteoblast activity[63]. An example of this is the release of sclerostin, a potent WNT antagonist[64], which inhibits bone formation through the prevention of osteoblast proliferation and differentiation[63]. Additionally, osteocytes are known to secrete the osteoclast regulatory proteins, RANKL and OPG[65]. Further osteocyte-osteocyte communication can also take place through the release of signalling molecules into the interstitial fluid within the canaliculi[66].

1.2.4 Bone Lining Cells

Bone lining cells are quiescent flat cells that can be found to cover the bone surface where neither bone formation nor resorption takes place[67]. The function of bone lining cells is not well understood; however, due to some of these cells forming connections with osteocytes it has been suggested that they are involved in communicating about the bone environment[68]. These cells also have secretory functions that are dependent on the physiological status of the bone, as they gain the ability to produce osteoclastogenic molecule RANKL, as well as anti-osteoclastogenic OPG[69].

1.3 Bone Formation

For bone to form, it requires a developmental template of cartilage which is derived from the embryonic mesoderm[70]. Over embryonic development, this cartilaginous structure will be replaced by hardened mineralised bone in a process called ossification[10]. There are two types of bone formation, intramembranous ossification and endochondral ossification[10].

1.3.1 Intramembranous ossification

Intramembranous ossification is the process characteristically defined to form flat bones such as the skull[71]. This is a process of direct bone formation, where mesenchymal cells derived from the neural crest proliferate to form compact nodules[72,73], which go onto develop into osteoblastic[74,75] or vascular cells[76] . The osteoblasts produced begin to deposit osteoid, collagen-proteoglycan matrix, which binds calcium salts resulting in calcification[74,75]. The calcification process results in the formation of bony spicules which expand out from the initial point of ossification. Intramembranous ossification is primarily

regulated by BMP-mediated expression of the transcription factor, *CBFA1* also known as *RUNX2*, which triggers mesenchymal osteogenesis through activation of genes such as *OCN*[77,78]. The absence of RUNX2 prevents osteoblast formation, resulting in a solely cartilaginous skeletal structure[77,78].

1.3.2 Endochondral ossification

Endochondral ossification is the typical process that results in the formation and growth of bones in the axial skeleton[79]. The main differentiating factor between intramembranous and endochondral ossification is the presence of cartilage[80]. Whereas intramembranous ossification is the direct formation of bone through osteoblast secretion of osteoid, endochondral ossification first requires a developmental template of cartilage which is derived from the embryonic mesoderm[80]. Over embryonic development this cartilaginous structure will be replaced by hardened mineralised bone.

Endochondral ossification occurs in two sites, diaphyseal (primary) and epiphyseal (secondary), with bone formation beginning within the primary diaphyseal site[81]. Cartilage is formed from the differentiation of mesenchymal condensations into chondrocytes, which can proliferate rapidly, secreting large amounts of cartilage-specific matrix as they divide[82]. The cells surrounding the newly formed chondrocytes form the perichondrium, which serves to protect the newly formed cartilage[83]. The proliferation of chondrocytes is tightly controlled by various secreted and systemic factors, including growth hormones (GHs) and BMPs[82]. Due to the presence of factors, such as the thyroid hormone, triiodothyronine (T3)[84], the chondrocytes closest to the perichondral boarder begin to hypertrophy. These large hypertrophic chondrocytes produce an altered matrix consisting of predominantly collagen X

and fibronectin, which allows for the matrix to be mineralised by calcium carbonate[79,85]. Hypertrophic chondrocytes also triggers vascular invasion of the cartilage resulting in osteoblast differentiation, facilitation of chondro-resorptive cells and results in the formation of the bone marrow cavity[86]. The area of blood vessel infiltration becomes known as the primary ossification centre[86,87], which is formed within the diaphysis (midshaft).

The primary ossification continues to expand during embryonic development (Figure 1.2). Following primary ossification there is the formation of the secondary ossification centres which develop at the bone epiphyses (end of the bone)[88]. Between these two regions of ossification is the epiphyseal growth plate, which can be split into different zones (Figure 1.2). The reserve zone contains quiescent chondrocytes, whereas chondrocytes within the proliferation zone are undergoing high levels of proliferation[86]. In the proliferation zone the chondrocytes begin to orientate themselves into column-like structures. As cells migrate further towards the diaphysis, they enter the hypertrophic zone, when they stop proliferation and become enlarged[86]. These enlarge cells then undergo apoptosis, releasing large levels of extracellular matrix which is then calcified in the calcification zone[86] (Figure 1.2). Remaining chondrocytes differentiate into osteoblasts[86]. The invasion of vessels then allows for the introduction of osteoclasts which breakdown the cartilage matrix, osteoblasts begin to mineralise the remaining cartilage, resulting in new bone formation[79,86]. The growth of long bones in humans[89] and other mammals such as dogs[89] and rabbits[90] will eventually close resulting in fusion of the epiphysis and the diaphysis. However, in other animals such as rodents[91] and zebrafish[92], the growth plate fails to fuse, allowing for continuous bone growth.

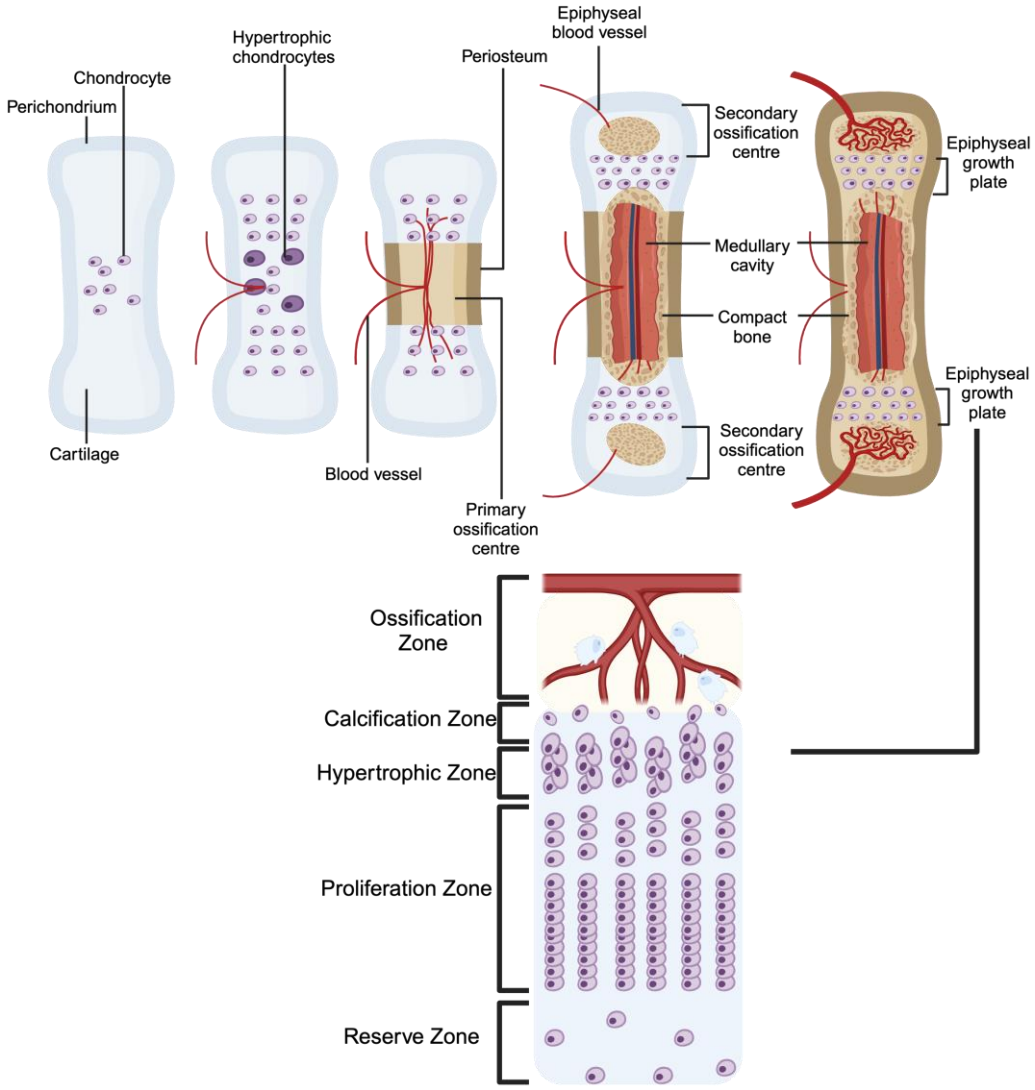


Figure 1.2 **Diagram of endochondral ossification and growth plate development.** Mesenchymal cells condense and differentiate into chondrocytes which create a cartilaginous model surrounded by the perichondrium. Chondrocytes become enlarged allowing for blood vessels infiltration[86,87]. With blood vessel infiltration comes the invasion of osteoprogenitors resulting in the formation of the primary ossification centre, which develops in the diaphysis (midshaft) of the long bone. Within the primary ossification centre there is the calcification of woven bone and remodelling of compact bone by osteoblasts and osteoclasts. Invasion of other cell types, results in the formation of the bone marrow cavity. Alongside the primary ossification centre, two secondary ossification centres develop at the bone epiphysis (ends) as blood vessels independently innervate these regions. Between the primary and secondary centres there is the epiphyseal growth plate, which allows for the production of new cartilage structures. The growth plate can be split into five developmental regions: (1) Reserve

zone, which contains quiescent chondrocytes[86], (2) proliferation zone, where chondrocytes form organised columns of highly proliferative cells with cells migrating towards the bone diaphysis[86], (3) hypertrophic zone, where chondrocytes closest to the diaphysis enlarge and apoptose resulting in high levels of ECM secretion[86], (4) Calcification zone, where cartilage matrix becomes calcified, and (5) the ossification zone, where invasion of vessels recruits osteoclasts to resorb the calcified cartilage matrix and osteoblasts to lay down new mineralized bone tissue[79,86]. Created using Biorender.com

1.3.3 Bone Vasculature

The vascular system within the bone is highly complex and crucial for orchestrating controlled and organised bone development and growth, through the regulation of osteogenesis and hemopoiesis[93,94]. The bone vascular network is composed of arterioles, arteries, a large central draining vein, and capillaries[95]. The importance of angiogenesis to osteogenesis coupling has been previously demonstrated, especially in embryogenesis and has been recently shown to be tightly regulated by bone specific capillary subsets[93,94]. These vessels have been split into type-H, type-L and type-E vessels[93,94,96]. The patterning and protein profile of the endothelial cells which make up these vascular structures have been used to look at changes in vascularisation during development and age.

Blood vessels have been shown to enter the avascular cartilage at the primary ossification centre by E14.5 in mouse and are highly branched by E15.5 (Figure 1.3)[96]. At this stage the vessels within the bone lack defined patterning and spread throughout the long bone. These vessels were shown to belong to the type-E capillary subset[96]. These vessels are highly associated with osterix positive osteoprogenitors, indicating an association with pre-osteoblast like cells[96]. Co-culture experiments show that isolated type-E vessels are able to enhance differentiation of C3H10T1/2 cells[96], suggesting that type-E promote osteogenesis and therefore are likely supporting initial bone formation within the long bone. At P6, there was shown to be a noticeable morphological change in the bone vasculature, with there being a distinct difference in the vessels within the metaphysis (directly under the growth plate) and the diaphysis (Figure 1.3)[96]. It is at this point where type H and L vessels become more identifiable, with type H vessels being located within the metaphysis and type L in the diaphysis[96].

Vessels can be identified by morphology as well as their relative expression of the proteins, CD31 and endomucin (Emcn), with type H(igh) vessels expressing high levels of CD31 and Emcn and type L(ow) expressing low levels of these proteins. Type E vessels express both CD31 and Emcn at similar levels to that of type H but can be gated for using flowcytometry[96]. The expression of type E vessels is almost completely lost at P14, however lineage tracing has demonstrated that these vessels do not disappear but rather have likely matured into either type H or L vessels[96]. Similarly to that of type E vessels, type H vessels are closely associated with osterix positive cells and therefore can increase osteoblast differentiation, whereas type L vessels are not. Suggesting that type H vessels are important for bone formation[93,94] in both development and remodelling.

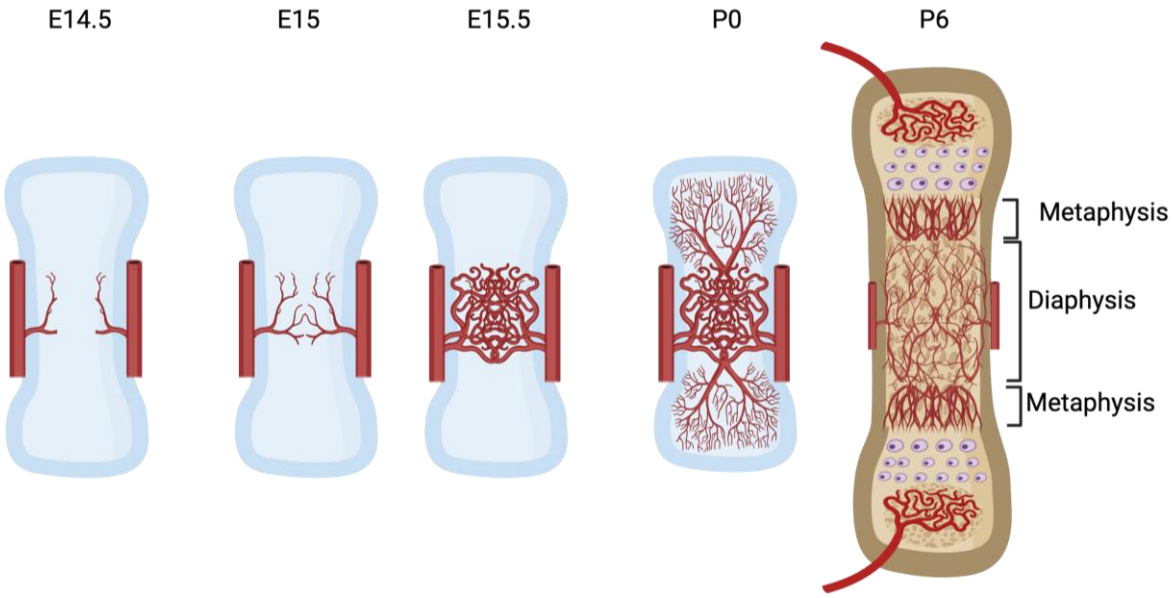


Figure 1.3 **Diagram of bone vasculature development.** Vascularisation of bone begins at embryonic day (E)14.5. The capillary network continues to expand through the cartilaginous tissue from the primary ossification centre in the metaphysis. At P0 the whole bone is vascularised. At P6 the vascularisation begins to become more organised with vessels within the metaphysis, termed type H vessels, form column structure down perpendicular to the growth plate. Whereas the vessels within the diaphysis are less organised, these are the type L vessels. Adapted from imaging in Langen et al 2019[96]. Created using Biorender.com

1.4 Bone Remodelling

Despite its static appearance, the bone remains highly dynamic after initial formation and undergoes constant phases of resorption and formation, in a process called bone remodelling. The bone remodelling cycle is essential for the maintenance and repair of the skeleton, and also acts to allow for the rapid release of calcium and phosphate, required for mineral homeostasis[8]. This cycle is tightly regulated and occurs in temporary anatomical structures called basic multicellular units (BMU), consisting of osteoclasts, osteoblasts and capillary vessels[97]. The BMU is separated from the surrounding bone by a canopy of cells creating the bone remodelling compartment (BRC), which allows for regulated osteoblast-osteoclast communication within the BMU.

The bone remodelling cycle can be separated into five overlapping stages, tightly regulated by osteocytes (Figure 1.4). The cycle begins with the activation phase, primarily triggered by the detection of strain or damage by mechanoreceptors present on local osteocytes resulting the secretion of paracrine factors and recruitment of osteoclast and osteoblast precursors[98].

In cases of severe bone damage, osteocyte apoptosis has also been found to act as a chemotactic signal to promote BMU formation, increasing osteoclast migration and differentiation[99]. Apoptotic osteocytes are then engulfed by the osteoclasts upon arrival[100].

Following the activation phase there is the resorption phase that involves the maturation of osteoclasts that resorb bone within the BMU[98]. The resorption of old bone is thought to result in the recruitment of osteoblasts, due to the release of growth factors from the bone matrix which become solubilised following resorption[101]. Once both the mineral and extracellular matrix has been removed, osteoclasts undergo programmed cell death[102]. The

following stage of remodelling is less well understood, this is the reversal phase. It is within this time where the newly exposed bone surface is prepared for the deposition of extracellular matrix, and remaining collagen matrix is removed and replaced by a cement line, consisting of non-collagenous mineral[103,104]. The formation phase begins once the osteoblasts attach to the bone surface, osteoblast deposit osteoid, consisting of primarily type 1 collagen that is later mineralised[105]. The termination of the bone remodelling cycle is not fully understood, however; it is thought to be initiated through the actions of osteocytes and bone lining cells, where upon completion of mineralisation osteoblasts undergo one of the three fates described in Figure 1.1.

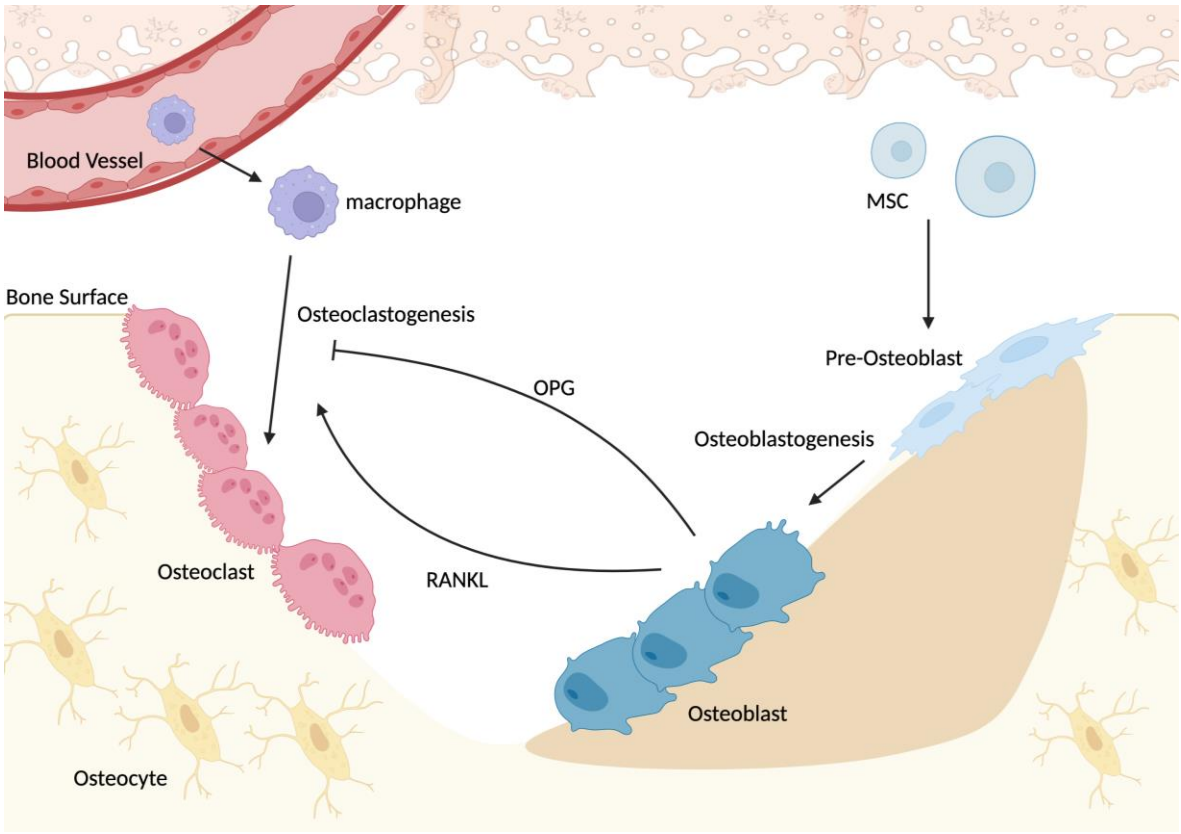


Figure 1.4 **Bone remodelling cycle**. Bone remodelling consists of five major phases: activation, resorption, reversal, formation/mineralisation and termination. This process can be activated by a variety of different stimuli including the activation of mechanosensors or the presence of inflammatory mediators, causing the recruitment of pre-osteoclasts (macrophages)[98]. These cells undergo osteoclastogenesis to form mature osteoclasts which adhere to the bone surface and resorb the bone matrix through the secretion of enzymes[101]. The reversal phase is less understood but during this phase, there is the migration of MSCs to the BMU[103,104]. These cells undergo osteoblastogenesis into pre-osteoblasts which later mature into mature osteoblasts which secrete ECM and mineralise it within the formation phase[105]. Termination occurs when the bone has been replaced. Diagram created using biorender.com

1.5 Regulation of Bone Remodelling

Bone remodelling is a complex process. The bone is undergoing different stages of remodelling simultaneously, therefore requires constant regulation to allow for balanced bone formation and resorption.

1.5.1 Mechanical Loading

One trigger for bone remodelling comes from mechanical loading, this can be through everyday movement and weightbearing exercise[106]. Comparatively a loss of loading results in accelerated bone turnover with enhanced bone resorption causing a loss of bone mass. This type of bone loss is observed in astronauts who spend extended periods of time in space where the absence of gravity prevents mechanical loading[107], or more commonly this occurs in bed bound patients[108], such as following surgery or in comatose patients.

The cell which is most commonly associated with mechanical loading are osteocytes[109,110], which are able to sense local mechanical stimulation and respond to these cues by regulating a number of cellular functions, such as gene expression, protein synthesis, cell proliferation, and differentiation[109]. Ablation of osteocytes within the bone prevents increased bone formation in response to mechanical loading, but also results in osteoporosis due to rapid bone turnover[111]. The mechanism in which osteocytes detect mechanical stimulation is largely through the shear stress caused by fluid flowing over the osteocyte surface[112]. Osteocytes are embedded within the bone in a lacuno-canalicular system (LCS). The LCS allows for a vast network of osteocyte dendrites to be connected within the bone through a series of small channels (canaliculi)[113]. As the bone is an extremely stiff tissue, these channels also allow for shear stress to occur as the movement of fluid within the canal stimulates osteocytes opposed to direct compression which is detectable by

other cell types in other organs like the skin. Changes in shear stress are detected by a multitude of different signalling proteins, including integrins[113], connexins[114] and ion channels[115–117]. In response to these changes osteocytes are able to alter secretion of various regulators of bone remodelling including OPG and sclerostin, allowing for mechanically mediated control of local bone remodelling[109].

Although osteocytes are known to be major sensors of mechanical stimulation in the bone, it is also known that osteoblasts and osteoclasts can detect changes in mechanical load. Research has demonstrated that appropriate mechanical stress stimulation has significant effects on bone metabolism and structure. Following mechanical load there is a reduction in osteoclast numbers and activity, inhibiting bone resorption[118]. The mechanism in which osteoclasts are able to directly detect mechanical loading has been recently identified and has been shown to require the chloride ion channel, Anoctamin-1 (ANO1), also known as TMEM16A. In this study they demonstrated *in vitro* that fluid shear stress and hyper gravity were able to reduce the number of TRAP+ multinucleated osteoclasts that formed[119]. The reduction in osteoclasts was coupled with a reduction in expression of ANO1, which was previously shown by the same group to be required for osteoclast formation[120]. Comparatively in states of unloading there was a coupling of increased osteoclast formation and ANO1 expression, suggesting that ANO1 is able to regulate osteoclast responses to mechanical stimulus. Conditional knockout of ANO1 was able to blunt osteoclast responses to mechanical loading and unloading in vitro and in vivo whereby the reduction in trabecular bone caused by hind limb suspension was lost in the ANO1 knockout mice. These data show that direct osteoclast responses to mechanical stimulus in the absence of osteocyte intervention.

Mechanical loading has also been shown to directly promote osteoblast differentiation and osteogenic function[118]. Additionally, loading inhibits the differentiation of bone marrow stromal cells (BMSCs) into adipocytes resulting in increased osteoblast numbers and prevention bone loss[118]. One key mechanism involves ion channels, particularly mechanosensitive channels like Piezo1. Piezo1 is crucial for osteoblasts to sense and respond to mechanical load changes, and it is required for gene expression alterations caused by fluid shear stress. Mechanical tensile force can promote Piezo1 expression in osteoblasts, and its deficiency in these cells can contribute to osteoporosis in mice[115,116]. Integrins also play a role in mechanotransduction in bone cells. They act as mechanoreceptors, helping osteoblasts perceive and respond to mechanical stress through various pathways[118].

Current research demonstrates the importance of mechanical stimulation for bone remodelling, leading to further research exploring how manipulation of detectors or mechanical stimulation such as piezo1[121] can be used in the treatment of diseases such as osteoporosis[122].

1.5.2 Endogenous stimulating factors

Alongside mechanical stimulation there are a variety of factors which are able to regulate bone remodelling, including systemic factors, such as parathyroid hormone (PTH)[123] and oestrogen[124], which are able to regulate overall bone homeostasis. Additionally, bone remodelling can be regulated by local factors such as growth factors, cytokines and prostaglandins, that alter cellular function through autocrine or paracrine signalling[125,126].

In addition to the local and systemic factors mentioned above, increasing evidence points to the role of sphingosine-1-phosphate (S1P)[127] and 14-3-3ζ derived Peptide Inhibitor of TransEndothelial Migration (PEPITEM)[128], in the regulation of bone remodelling.

1.5.2.1 Sphingosine-1-Phosphate

S1P is part of the sphingolipid metabolic pathway that also includes sphingosine and ceramide (Figure 1.5). S1P is metabolised from ceramide via two reactions. Firstly ceramidase (CDase) converts ceramide into sphingosine in a reversible reaction with ceramide synthase (CerS) (reviewed by[129]). Sphingosine kinases (SPHK1 and SPHK2) then phosphorylate sphingosine to form S1P. Phosphorylation of sphingosine can be reversed in the presence of sphingosine phosphate phosphatases (SPPase) or S1P lyase can irreversibly break down S1P into ethanolamine phosphate and hexadecenal[130]. Collectively these reactions regulate extra- and intra-cellular sphingolipid concentrations and thus the functional consequence of their signalling on the cell and surrounding cells (extensively reviewed by[131]).

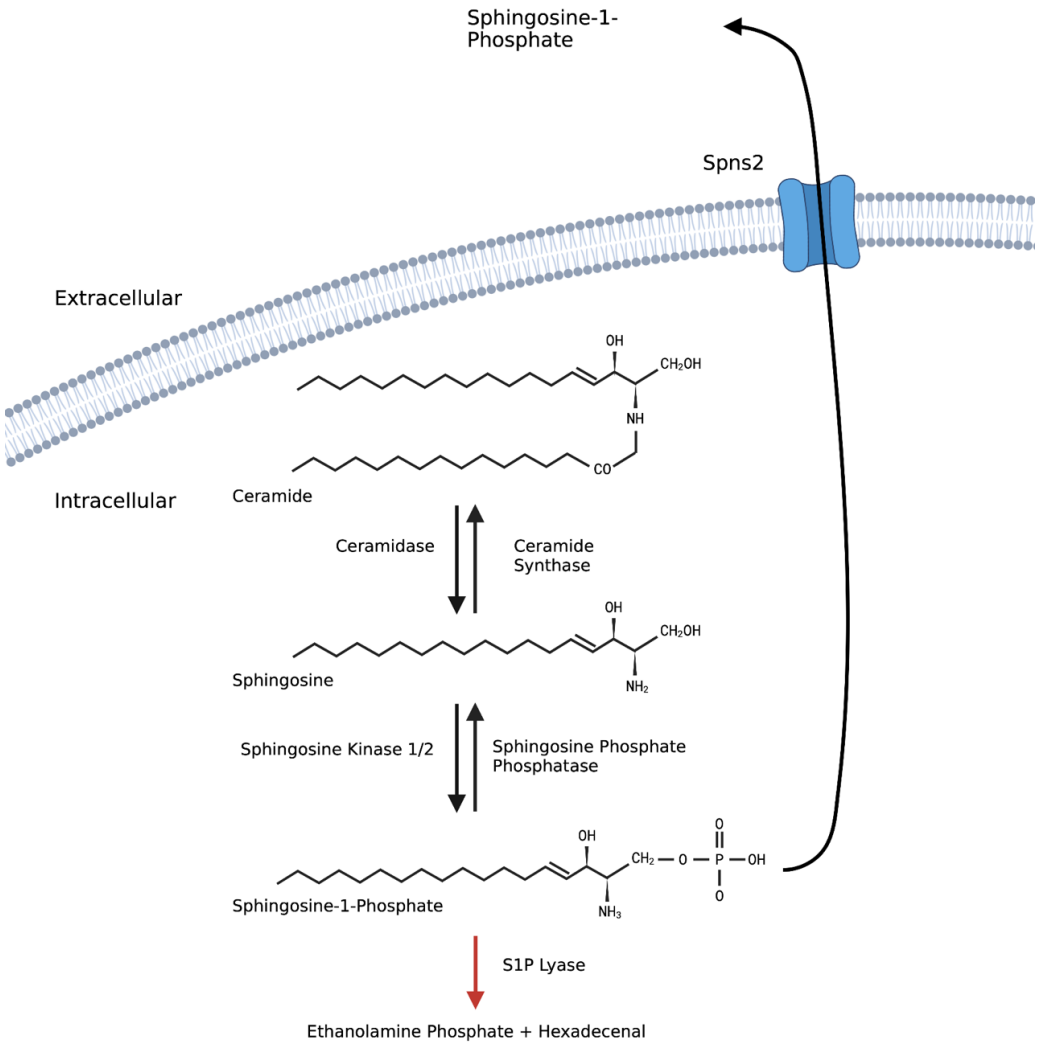


Figure 1.5 **Sphingosine metabolic pathway.** Ceramide, Sphingosine, and Sphingosine-1-phosphate can be metabolised into each other via various enzymes. Ceramide increases cell senescence and apoptosis. It is converted into Sphingosine through a reversible reaction by Ceramidase (CDase) and Ceramide synthase (CerS)[18]. Sphingosine has also been shown to increase cell apoptosis and endocytosis, however, is frequently converted to Sphingosine-1-phosphate via the two Sphingosine kinases (SPHK1/2)[19]. S1P can alter cell proliferation, migration, differentiation and oppose the apoptotic effects of Ceramide, however there is conflicting data surrounding its exact function. S1P is metabolised back to Sphingosine via Sphingosine phosphate phosphatases (SPPase) or by an irreversible reaction by S1P lysase[19]. S1P is then exported out of the cell via Spinster 2 (SPNS2). Diagram created using biorender.com

1.5.2.2 S1P signalling

S1P has both intracellular and extracellular functions in a variety of tissues (reviewed by[132]). One accepted principle is the sphingosine rheostat: here the intracellular levels of ceramide and S1P influence cell survival and proliferation, with ceramide being considered pro-apoptotic and S1P acting in an anti-apoptotic fashion[133]. Currently, no studies have looked at this rheostat directly in osteogenic cells. Indeed, there are few studies that directly investigate the role of intracellular S1P within bone cells[134,135] and therefore reviews on the subject tend to infer function based on other studies performed in other cell types.

1.5.2.2.1 Intracellular S1P signalling

Most of the data on intracellular S1P within bone focuses on the action of the enzymes required for its production (SPHK1 or 2) rather than the bioactivity of S1P itself. Alterations in SPHK1 activity and/or expression result from altered autocrine signalling of the extracellular S1P receptors (S1PR1-5), rather than altered intracellular S1P signalling[136]. Indeed, alterations in SPHK1 expression during osteoblast differentiation have been linked to the activation of S1PR1 signalling[134]. To the best of our knowledge, no studies have investigated the impact of intracellular osteoblastic SPHK1 and/or S1P signalling, however, it has been shown that osteoclast-specific deletion of SPHK1 has no effect on bone mass in male or female mice[137]. Similarly, siRNA knockdown of Sphk1 in a murine macrophage cell line (RAW264) or in primary murine bone marrow-derived macrophages had no effect on osteoclast maturation in response to RANKL[135]. Conversely upregulation of Sphk1, through retroviral transfection of HA-tagged SPHK1, resulted in a moderate decrease in osteoclast maturation[135], suggesting that SPHK1 in osteoclasts acts as a negative regulator of

osteoclastogenesis. The authors suggested that RANKL-mediated osteoclast activation results in an upregulation of SPHK1, which regulates osteoclast function through the inhibition of c-FOS and NFATc1 via p38-dependent signalling[135]. Crucially, these differences were not observed in the presence of extracellular S1P, suggesting that they are mediated by either the intracellular action of SPHK1 or intracellular S1P[135]. These findings demonstrate the importance of intracellular S1P on osteogenesis and bone resorption and underscore the need for additional investigations into intracellular receptors of S1P and their function in osteoclasts.

Inhibition of SPHK2 in the murine macrophage cell line RAW264 resulted in a reduction in c-FOS expression and subsequent osteoclastogenesis[138], identifying intracellular SPHK2 signalling as essential during the initial stages of osteoclastogenesis. In contrast, SPHK2$^{-/-}$ osteoclasts had normal resorptive activity, despite the observation that global SPHK2$^{-/-}$ mice have reduced trabecular bone mass[137]. This finding led to the phenotype being attributed to alterations in osteoblast formation, which was demonstrated by a reduction in Col1a1 gene expression and a significant impairment of the anabolic response to PTH within these mice[137]. Crucially the impact of SPHK2 on PTH signalling was not determined, making it difficult to draw any firm conclusions about the exact role of intracellular S1P signalling in this process. These studies both postulate a role for SPHK2 in altering osteoclast or osteoblast function to drive changes within the bone architecture. However, further research into the intracellular actions of S1P is urgently needed to resolve the conflicting nature of the findings to enable identification of potential intracellular targets that inhibit intracellular S1P function.

1.5.2.2.2 Extracellular S1P signalling

In comparison to intracellular signalling, significantly more research has been conducted into the role of extracellular S1P signalling in the bone. S1P is secreted by osteoblasts and osteoclasts, predominantly through the spinster 2 (SPNS2) transporter[139,140], allowing binding to one of the G-coupled protein S1PR. Osteoblasts, osteoclasts and their precursors express four types of S1PR (S1PR1, -2, -3 and –4), which vary in expression levels across the maturation/differentiation status of the cells[140,141] and are thought to play critical roles in bone cell migration, differentiation and communication (Figure 1.6).

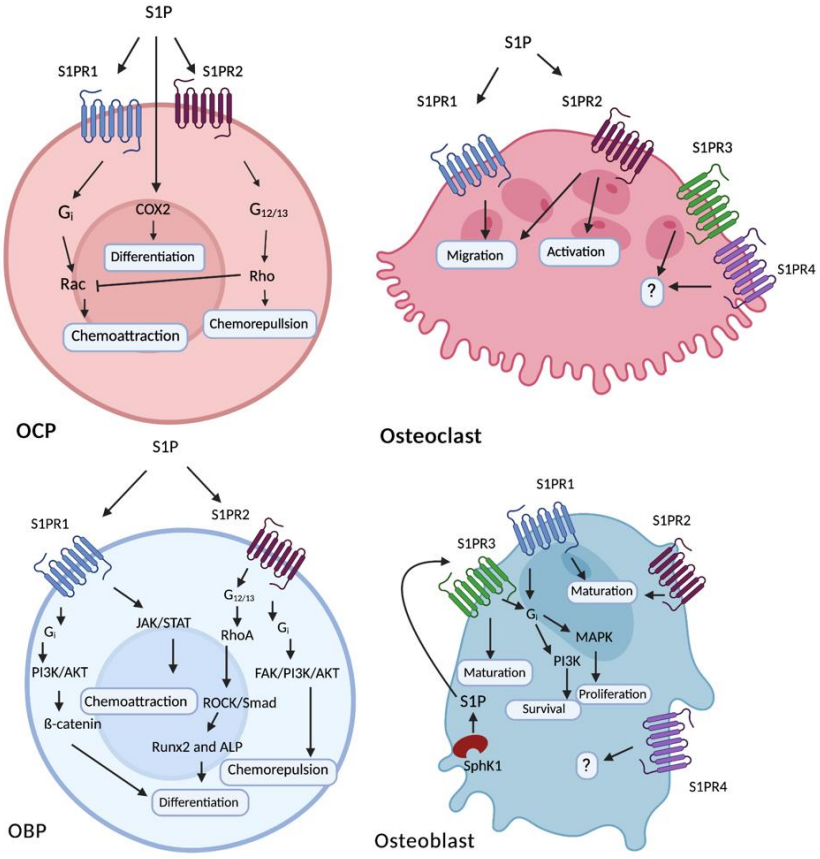


Figure 1.6 **S1PR function in osteogenic cells.** S1PRs are g-protein coupled receptors that activate various pathways. This diagram denotes what is known about the downstream signalling of these

receptors in osteoclast precursors (OCP), osteoclasts (OCs), osteoblast precursors (OBP) and osteoblasts (OBs). Within OCPs S1PR1 and S1PR2 have been shown to alter osteoclast maturation via activation of Rho and Rac signalling pathways[135]. S1P has also been shown to increase OCP differentiation via Cox2 however the complete mechanism is not understood. In OCs, although S1PR1-4 are expressed the role of S1PR1 and S1PR2 are not currently understood[142]. S1PR1/2 can alter osteoclast migration however the signalling pathway behind this is so far unknown. S1PR2 appears to be essential for osteoclast activation. Within osteoblasts S1PR1 has shown to mediate osteoblast differentiation via PI3K/AKT signalling as well as regulate migration via JAK/STAT signalling[143], resulting in chemoattraction in response to S1P[143]. Whereas S1PR2 has been shown to increase osteoblast differentiation via RhoA/ROCK/Smad signalling[142], additionally S1PR2 is shown to act through FAK/PI3K/AKT signalling to promote chemorepulsion. In OBs, S1PR1 was shown to increase OB proliferation[144] and survival via MAPK and PI3K signalling. S1PR1-3 have demonstrated involvement in osteoblast maturation however the complete mechanism is unknown. Additionally activation of SphK1 in OBs has been shown to promote osteoblast maturation via autocrine S1P signalling through S1PR3[134]. The function of S1PR4 in OB is currently unknown. Diagram created using biorender.com

1.5.2.3 S1P in bone precursors and resident cells

1.5.2.3.1 S1P as a chemoattractant and chemorepellent for osteoclast precursors

Osteoblast precursors (mesenchymal stem cells) and osteoclast precursors (monocytes/macrophages) are recruited into the bone tissue during periods of remodelling (reviewed by[145]) in response to CXCL12-CXCL4 and S1P-S1PR signalling (reviewed by[146]). S1P is detected in many different tissues, however under homeostatic conditions blood holds the highest concentration of S1P, due to the secretion from red blood cells, thrombocytes, endothelial cells and platelets (reviewed by[147]). Within blood, S1P is found bound to albumin and lipoproteins, particularly HDL. Studies have demonstrated that S1P bound to albumin or HDL does not impact its ability to activate S1PRs, but rather creates a reservoir of S1P keeping the S1P within circulation (reviewed by[147]). As total S1P is detected at higher

concentrations in blood[148] and at lower concentrations within the bone[142], a concentration gradient is created along which osteogenic precursors migrate. The importance of this gradient in osteogenic precursor migration was demonstrated when S1P breakdown was inhibited by either the inhibition or deletion of S1P lyase, causing the gradient to dissipate, resulting in increased bone mass and strength coupled with decreased osteoclast number[149].

1.5.2.3.2 Osteoclast progenitors

Osteoclast precursor chemotaxis/migration has been shown to be dependent on the local S1P concentration: at low concentrations ($<10^{-7}$M) osteoblast precursors (murine macrophages, RAW624.7) efficiently move through a transwell filter towards S1P[150]. However, at higher concentrations (10^{-6}M) S1P repels the RAW624.7 cells, resulting in greater numbers remaining in the filter unable to move[150]. This observation raises a key question: How does S1P simultaneously attract and repel osteoclast precursors (monocytes)?

Osteoclast precursors express two of the S1P family of receptors, S1PR1 and S1PR2[150]. siRNA knockdown of S1PR1 reduced osteoclast precursor migration at low S1P (10^{-9}M) concentrations, a phenomenon not observed following S1PR2 knockdown, indicating that S1P chemoattraction was mediated by S1PR1[150]. Similar observations were made in wild-type mice treated intravenously with the S1PR1 agonist, SEW2871 (which causes receptor internalisation and mimics inhibition of S1P activity), where increased numbers of osteoclast precursors were detected in the bloodstream[151], suggesting S1PR1 is responsible for keeping cells within circulation. These data suggest that S1PR1 is responsible for retaining osteoclast precursors within the circulation, where the S1P concentration is greater. Conversely, S1PR2 knockdown in osteoclast precursors (RAW264 cell line) enhanced migration towards S1P

irrespective of S1P concentration, suggesting that S1PR2 negatively regulates osteoclast precursor migration[151]. Similarly, administration of the S1PR2 antagonist, JTE013, increased monocyte migration into circulation . Thus, S1PR2 is responsible for retaining osteoclast precursors within the tissue[150]. Collectively, the studies from this group have demonstrated opposing functions of S1PR1 and S1PR2 expressed by osteoclast precursors, through facilitation of chemotactic responses to S1P and thus regulating the migration of osteoclast precursors.

As previously described, RANKL is required for the differentiation of osteoclast precursors and is secreted from both osteoblasts and osteocytes (reviewed by[152]). Additionally, RANKL may also influence osteoclast precursor migration via its actions on S1PR1[153,154]. For example, intraperitoneal injection of RANKL induced a severe osteoporotic phenotype in mice that was reversed in the presence of the S1PR2 antagonist, JTE013[153,154], indicating that RANKL directly impact S1P-related chemotaxis of osteoclast precursors. Therefore, RANKL appears to have a dual role in enhancing bone remodelling through (i) promoting differentiation of osteoclast precursors and (ii) facilitating their migration into the bone.

1.5.2.3.3 Osteoblast progenitors

S1P has also been investigated for its effect on osteoblast precursors (MSC). Primary murine MSCs express gene transcripts for all five of the S1PRs[155], whereas human bone marrow-derived MSCs were only shown to express S1PR1-3 transcripts[156,157]. Of note, additional amplification revealed extremely low-level expression of S1PR4 and S1PR5 transcripts in human MSC[156], indicating that they are expressed at much lower levels

compared to the murine MSC. It should be noted that the expression of S1PRs have also been shown to be influenced by culture density (3,000-5,000 cells/cm^2 vs 15,000-20,000 cells/cm^2), where a marked increase in S1PR1 and S1PR3, but not S1PR2, gene expression was detected in the high-density cultures[156]. Therefore, alterations in cell culture protocols and crosstalk between cells in culture may explain the conflicting findings within the literature. Unfortunately, exact seeding density or plate sizes used are not always reported in sufficient detail within the current literature to establish this.

Similar to that described for the osteoblast progenitors, MSCs also display a concentration-dependent response[157] where human BM-MSC migrate towards low concentrations (1-10 nM) of S1P in a transwell migration assay, whilst no migration was seen at higher concentrations (50-1000 nM)[157]. These data suggest that an S1P gradient is necessary for MSC migration. The opposing migratory properties of S1P on MSC movement have been, in part, attributed to the downstream signalling mediated by the different S1PRs - For instance, at low S1P concentrations, S1PR1 and S1PR3 downstream signalling occurred via Gi/ERK and supported migration, which was sensitive to S1PR1/3 or ERK1/2 pharmacological inhibitors in transwell experiments[158]. By contrast, S1PR2 signalling via the $G_{12/13}$-RhoA-ROCK pathway inhibited migration, whilst pharmacological inhibition of ROCK with Y27632 allowed for increased migration at 1 nM[157]. JTE-013-mediated inhibition of S1PR2 or genetic deletion (S1PR2$^{-/-}$) also inhibited migration in MSC scratch wound and Boyden chamber assays[155].

Despite the evidence above that activation of S1PR2 results in chemorepulsion of MSC in response to S1P, conflicting data indicate a role for S1PR2 in enhancing MSC migration via signalling crosstalk with S1PR1[143]. Quint et al showed that the pro-migratory response of the

FAK/PI3K/AKT signalling is lost when JAK/STAT activity is inhibited, suggesting that S1PR2-mediated activation of the FAK/PI3K/AKT signalling pathway induces activation of S1PR1-mediated JAK/STAT signalling[143]. These data suggest that S1PR2 works in concert with, rather than against, S1PR1 to increase MSC migration.

The differences in S1P receptor roles in migration may be due to the origin of the progenitors (e.g., blood or tissue resident) and the experimental concentration of S1P used to activate the receptor. Unlike osteoclast progenitors, which originate in the blood, the majority of MSC that differentiate into osteoblasts for bone remodelling are derived from the bone marrow or periosteum. These cells are not subjected to the high concentrations of S1P found within the blood. As such, the strength of any concentration gradient along which MSC are migrating is substantially reduced compared to that experienced by osteoclast progenitors.

Moreover, the Quint study demonstrated that osteoclast-conditioned media acts as a chemoattractant to MSCs, increasing chemotaxis in an S1P-dependent manner (where migration was blocked in the presence of S1PR antagonists) – thus suggesting that osteoclasts can recruit MSCs to the site of resorption[143]. Given that MSC responses to S1P vary dependent on S1P concentration, researchers should take care to use biologically relevant concentrations for their tissue of interest. One hypothesis is that smaller gradients in S1P concentrations are responsible for MSC chemotaxis to the bone surface opposed to those responsible for MSC recruitment from the blood.

1.5.2.4 Role of S1P in mature bone-resident cells

1.5.2.4.1 S1P on Osteoclasts

Osteoclasts are multinucleated cells involved in bone matrix demineralisation by releasing protons via vacuolar H^+-adenosine triphosphatase (H^+-ATPase), resulting in acidification of the resorption compartment and release of calcium and phosphates (reviewed by[159]). The differentiation of monocytic osteoclast precursors into osteoclasts occurs within the bone remodelling compartment, where several molecules (M-CSF, RANKL and OPG) drive osteoclastogenesis (reviewed by[160]) The most well-studied of these factors, RANKL, appears to elicit its osteogenic response via S1P.

Following RANKL-induced osteoclastogenesis, there is an enhanced gene expression and activity of SPHK1 and SPHK2, resulting in increasing in both intracellular and extracellular S1P[135]. Intracellular S1P was assessed by comparing extracellular S1P levels in culture media with concentrations within the cells cell lysates[135]. Mature osteoclasts express tartrate resistant acid phosphatase (TRAP), therefore expression of this enzyme is used as a marker of differentiation. SPHK1-induced intracellular S1P inhibited TRAP expression, as did overexpression of SPHK1, whilst siRNA knockdown of SPHK1 increased TRAP[135]. Ryu et al demonstrated that RANKL increases expression and also activation of p38 and ERK MAPKs in osteoclast precursors to promote osteoclastogenesis[135]. In cells treated with SPHK1 siRNA, there was an increase in p38 protein expression compared to those treated with control siRNA, whereas in SPHK1 overexpressing Mx-HA-SPHK1 cells there was a significant decrease in p38[135]. From these data, it is postulated that the SPHK1 upregulation and activation seen in response to RANKL results in increased intracellular S1P to induce a negative feedback loop, suppressing p38 signalling in osteoclast precursors and allowing

tight regulation of osteoclast differentiation[135]. Collectively, these studies suggest RANKL mediated osteoclastogenesis is regulated though intracellular S1P, therefore alterations in osteoclast S1P responses may result in osteoclastogenesis being unregulated causing increased bone resorption. Enhanced understanding of how intracellular S1P inhibits p38 may enable identification of new therapeutic targets to inhibit osteoclast formation and reducing bone formation.

The literature examining the effects of extracellular S1P on osteoclast precursors is both limited and conflicting: one study showed that exogenous S1P has no effect on osteoclastogenesis in bone marrow macrophages (BMM) in culture[135]. Whilst we have observed increased differentiation of murine macrophage-like cell line, RAW264.7 in response to S1P (unpublished observations). One possible explanation for this conflict could be the fact that the expression pattern of S1PR1 and S1PR2 alters during BMMs differentiation[137], but not during RAW264.7 differentiation[135]. That said, the concerted actions of RANKL and S1P appear to be important for BMMs osteoclastogenesis[154]. The S1PR2 antagonist (JTE013) inhibited TRAP positive osteoclast formation and absence of activity/ bone resorption pits[154]. Therefore, S1PR2 appears to be essential for both osteoclastogenesis and osteoclast function[154]. Hsu et al further demonstrated that S1PR2 regulates osteoclastogenesis via regulation of podosome adhesive proteins that are required for the fusion of monocytes to form multinucleated osteoclasts[154]. siRNA knockdown of S1PR2 reduced the levels of the protein kinases, p-PI3K, p-SRC, or p-PYK2, required for the adhesion and fusion of monocytes[154]. Extracellular S1P and its receptors may play a role in osteoclastogenesis, however further research is required to understand the differences in

responses to exogenous S1P between studies and how other S1PRs may impact osteoclast formation.

1.5.2.4.2 S1P on Osteoblasts

Expression of S1PRs appears to vary during osteoblast differentiation, however, which receptors are expressed at what stage of differentiation remains somewhat contradictory in the literature. It is frequently reported that S1PR1-3 are the most highly expressed[163], more contentious is whether S1PR4 is also expressed[140]. Analysis of publicly available mouse bone marrow stromal cell RNAseq datasets (GSE128423) allowed interrogation of osteoblast populations at distinct stages of maturation. Early osteoblast progenitors, pre-osteoblasts and mature osteoblasts were detected by looking at osteoblast differentiation genes, such as COL1A1, RUNX2 and BGLAP1. Only S1PR1, S1PR2 and S1PR3 were identified to be expressed in immature osteoblast populations and their expression decreased as osteoblasts mature, with no detection of S1PR4 at any stage (unpublished observations). S1PR1 and S1PR3 expression appeared to increase during the initial stages of osteoblastogenesis[140,141], but may wain following differentiation (unpublished observations). Differences in S1PR expression on osteoblasts during maturation may account for the stark differences in responses of osteoblasts to S1P.

S1P has been reported to act as an osteoanabolic, increasing osteoblast differentiation and proliferation[144,155,164–167]. Hashimoto et al demonstrated that the addition of exogenous S1P to early osteoblast progenitors (C3H10T1/2 pluripotent stem cells) resulted in increased expression of genes linked to osteoblast differentiation e.g. LRP5/6, ALPL and BGLAP[164]. Additionally, S1P increased mineralisation (alizarin red staining) suggesting it

promotes MSC-like cells to differentiation towards an osteoblast lineage[164,165]. A recent study into the effect of S1P on murine dental pulp stem cells, which display a MSC like phenotype and express S1PR1 and 2, showed that low levels of osteoblastic differentiation can be induced in response to S1P at various concentrations (1 – 10 μmol-L^{-1})[168]. These cells also displayed decreased expression of several osteoblast-specific genes (including ALP, RUNX2 and COL1A1), as well as decreased mineralisation following 3-weeks of culture with S1P[168]. The differences between these two studies may stem from differences between the two cell types used, with the S1PR expression on C3H10T1/2 yet to be reported.

Studies have also looked at S1P in pre-osteoblasts and osteoblast-like cell lines[144,166–168]. Murine MC3T3-E1 cells are an immature osteoblast cell line that matures in response to S1P[166,168]. Matsuzaki et al first showed that S1P increased protein expression and activation of PI3K/Akt/GSK-3β signalling at increasing concentrations of S1P (0.1-2 μM), resulting in increased ALP activity (p-nitrophenyl phosphate substrate levels) and increased alizarin red stained mineral[166]. Increased mineralisation in response to increasing concentrations of S1P (1-10 μmol-L^{-1}) was replicated in MC3T3-E1 cells by Choi et al[168]. SaOS-2 cells, a human osteoblastic osteosarcoma cell line, also show increased PI3K/Akt/GSK-3β signalling in response to S1P stimulation, which resulted in enhanced ALP levels and mineralisation[166]. Addition of S1P also increased proliferation of primary rat calvarial osteoblasts, as measured using [H^3]-thymidine incorporation[144]. Unfortunately, this study did not look at markers of differentiation so no comments on this can be made. In our hands, S1P reduced ALP activity and alizarin red staining, thus differentiation of primary mouse calvarial osteoblasts (unpublished observations). By contrast, we were unable to detect the increases in osteoblast maturation and mineralisation previously reported using MC3T3s. These

disparities may be due to differences in the osteogenic media used as both Higashi et al and Choi et al supplemented with steroids (dexamethasone or hydrocortisone), whilst neither Matsuzaki et al nor we did[166–168].

Of all the S1P receptors expressed by MSCs and osteoblasts, the most well-studied in the context of osteoblastogenesis is S1PR2. Isolated murine BMSC from wildtype mice treated with JTE-013 or S1PR2$^{-/-}$ mice exhibited enhance proliferation as assessed using an MTA assay[155]. Moreover, these cells had lower levels of the osteoblast differentiation marker, osteopontin, compared to wildtype untreated cells[155], suggesting S1P/S1PR2 signalling enhances osteoblastogenesis and that the inhibition of S1PR2 retains osteoblasts in a prolonged proliferative state.

Members of the SMAD signalling family are required for osteoblastogenesis[166] – where SMAD4 forms heteromeric complexes with phosphorylated SMAD1/5/8 resulting in nuclear translocation and regulation of gene expression (e.g., RUNX2[169]). At high S1P concentrations (2 μM), downstream signalling through ROCK and SMAD1/5/8 signalling led to enhanced RUNX2 gene expression and increased von Kossa staining (a measure of mineralisation) in MC3T3 murine osteoblastic cell line[164]. These data suggest that S1PR2 is required for the differentiation and maturation of osteoblasts. By contrast, others have shown that S1PR2 inhibition increased adipocyte genetic markers FABP4[155], suggesting that whilst S1PR2 promotes MSC differentiation its function is not necessarily osteogenic-lineage specific.

Whilst S1PR2 appears dispensable, S1PR1 global knockout in mice is embryonic lethal[164]. Osteoblast-specific S1PR1 deletion results in viable pups that have no detectable differences in bone formation at either 3 or 8 months[140]. Conversely, S1PR3 global knockout mice are viable and exhibit no developmental defects at 3 months, however osteopenia is

seen at 8 months[140]. This S1PR3$^{-/-}$-induced osteopenia is a result of reduced bone formation rate demonstrated by reduced BV/TV (a measure of bone volume) and BFR/BS (a measure of bone formation over time), whilst parameters linked to resorption e.g. serum osteocalcin (OCN)/bone morphogenic protein (BMP) and collagen degradation products (carboxy-terminal collagen crosslinks: CTX) remained unaffected[140]. Furthermore, when S1PR3$^{-/-}$ calvarial and bone marrow-derived osteoblasts were cultured in the presence of S1P there was a reduction in mineralisation compared to wildtype cells, suggesting reduced osteoblast maturation although no other measurements of osteoblast maturation were assessed[140].

Although S1PR1 appears to have no role in post-natal bone remodelling, S1PR3 signalling is required for continued remodelling following skeletal maturation in mice i.e., mid-life onwards. Brizuela et al. demonstrated that SPHK1 mRNA expression increased with osteoblast maturation and that inhibition of SPHK1 using an inhibitor (SK-II) or by sequestration of S1P with a neutralising antibody reduced osteoblast maturation (as identified through reduced alkaline phosphatase activity and RUNX2 mRNA expression)[139]. A similar reduction in maturation was observed when the S1PR1/3 antagonist (VPC23019) was applied, but not when using specific S1PR1 (W146) or S1PR2 (JTE013) antagonists[139]. Taken together, these data suggest that S1P is essential for osteoblast maturation via S1PR3. As such S1PR3 agonists may offer therapeutic benefit in the treatment of catabolic bone disease in adults but are not expected to offer the same benefits to children.

1.5.2.5 Role in osteogenic communication

To regulate bone remodelling, osteoclasts and osteoblasts secrete a variety of factors that attract, activate, and inhibit each other (reviewed by[170]). This crosstalk is essential for

normal bone remodelling, and if communication is disrupted it results in altered bone formation and resorption. There is some evidence of the impact of S1P on this bidirectional crosstalk. Culturing naïve or activated macrophages with murine bone marrow derived stem cells (BMSCs) was sufficient to induce the upregulation of SPHK1 and S1PR1 mRNA expression[134], suggesting that macrophages secrete molecules that induce SPHK1 and S1PR1 expression in the bone marrow niche. Additionally, co-culturing activated macrophages with BMSCs resulted in increased RANKL production that was dependent on the activation of S1PR1, where secretion of RANKL was lost following siRNA knockdown of S1PR1[134]. The authors postulate that osteoblast-osteoclast signalling activates S1PR1 and SPHK1, resulting in autocrine S1P/S1PR1 signalling that triggers increased RANKL production, which subsequently stimulates osteoclastogenesis within the co-culture[134]. This example highlights the complexity of S1P communication between osteogenic cells and emphasises the importance of such co-culture experiments.

The molecular mechanisms by which S1P acts as a communication molecule within bone is complex due to its varying roles in migration and differentiation and the sensitivity of its receptors to fluctuating S1P concentration. S1P-induced differentiation of MSCs into osteoblasts triggers the release of RANKL and subsequently the osteoclastic release of S1P[135]. This feed-forward mechanism allows for the coupling of osteoblasts and osteoclasts, which is important for the regulation of bone remodelling. S1P has also been shown to stimulate RANKL expression in osteoblasts through the upregulation of COX2 via ERK and p38 MAPK pathways[135]. However, a model in which S1P purely stimulates osteoblast release of RANKL, and its subsequent stimulation of osteoclastogenesis, does not explain the

increased bone mass seen in response to S1P lyase inhibition or deletion[149]. Activation of osteoblast-expressed S1PR2 has been reported to cause the release of the soluble RANKL decoy molecules, OPG, via p38-GSK3b-β-catenin and noncanonical WNT5A-LRP5 signalling [134,149,167]. Given that S1PR2 has a lower affinity for S1P compared to S1PR1[171], one hypothesis is that at low concentrations of S1P S1PR1/3 activation induces RANKL release. RANKL serves to activate osteoclasts and promote further S1P release. As S1P concentrations increase there is a shift in S1PR activation towards S1PR2, resulting in an alteration in RANKL/OPG ratio in favour of OPG, which reduces bone resorption rates. An alternative explanation is that increased S1P results in S1PR1 internalisation, thereby reducing RANKL production and altering the RANKL/OPG ratio in favour of bone formation (Figure 1.7). Collectively, S1P bioavailability regulates the activation and the cessation of bone resorption.

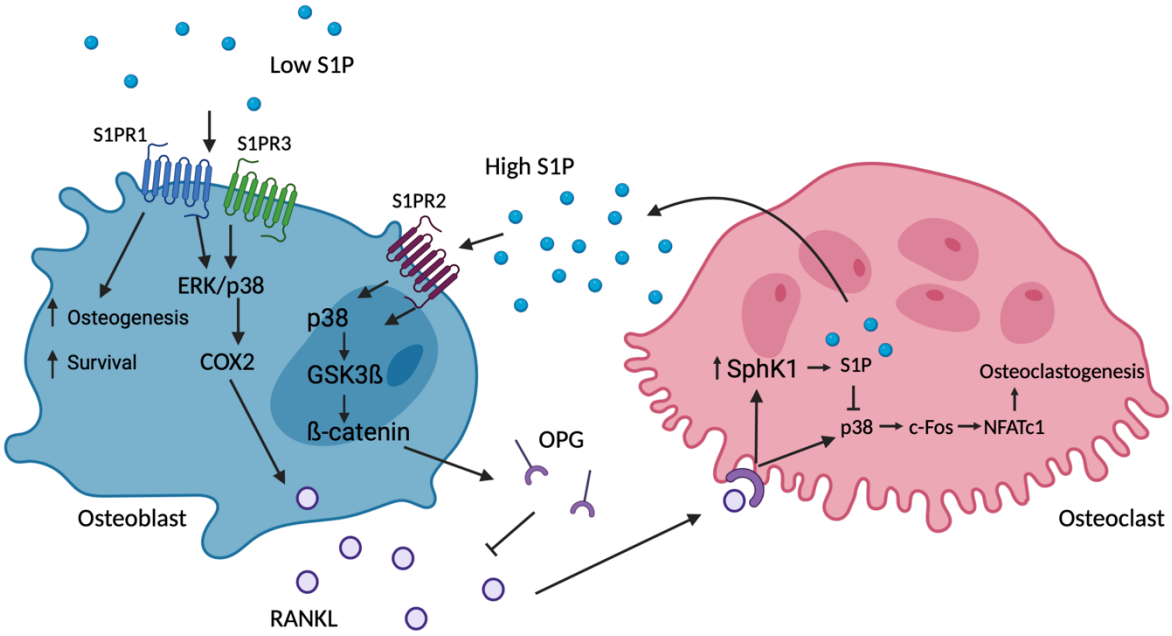


Figure 1.7 **Osteoblast-Osteoclast Communication via S1P**. S1P can act directly on osteoblasts via S1PR1/3 receptors to enhance osteoblast maturation and mineralisation. S1PR1/3 also activates the ERK/p38 signalling pathway to enhance COX2 production[135,138]. COX2 then elicits the release of RANKL from osteoblasts to enhance osteoclastogenesis via p38-cfos-NFATc1 signalling[135]. RANK/RANKL also upregulates SPHK1 expression and production resulting in increased intracellular S1P which inhibits p38. S1P released from osteoblasts increases extracellular S1P, which may act as a break on osteoclastogenesis through the S1PR2 receptor on osteoblasts. S1PR2 acts to enhance the secretion of the RANKL decoy receptor, osteoprotegerin (OPG) [172], which reduces further RANKL-mediated osteoclastogenesis. Diagram created using biorender.com

Calcitonin has been shown to impact osteoclast-osteoblast communication via S1P. Calcitonin downregulates gene expression of the S1P transporter, SPNS2, on primary murine osteoclasts[140] and is a negative regulator of bone formation. Calcitonin receptor knockout mice ($CALCR^{-/-}$) have increased trabecular bone volume and evidence of increased bone formation rate (serum alkaline phosphatase levels are increased)[140]. No effect on bone resorption markers (e.g. collagen breakdown products - CTX assay) were detected in these mice[140]. In response to calcitonin, Keller et al observed that SPNS2 gene expression was downregulated in wild type osteoclasts[140]. This reduction in SPNS2 gene expression was coupled with a reduction in extracellular S1P, a difference that was not observed in the osteoclasts from $CALCR^{-/-}$ mice. These data indicate that calcitonin reduces S1P secretion from osteoclasts, via inhibition of SPNS2. The phenotype was lost in $CALCR^{-/-}$ mice when S1PR3 was knocked out in osteoblasts[140], suggesting that S1P secreted by osteoclasts in response to calcitonin acts to increase osteoblast maturation and mineralisation via S1PR3. Calcitonin acts to negatively regulate this circuit via inhibition of osteoclastic secretion of S1P. Together, these data imply that calcitonin naturally regulates bone remodelling through altering S1P-mediated osteoclast-osteoblast communication.

As detailed above, the mechanisms by which S1P acts as a key regulator of bone remodelling (through communication between osteoblasts and osteoclasts) are starting to be uncovered. Challenges in the isolation and culture of osteocytes have limited research into how this S1P-mediated communication affects osteocytes. A recently developed osteocyte cell line (Ocy454[173]) has been shown to increase production of S1P in response to mechanical stimulation, which triggers the upregulation of SPHK1 and downregulation of SPPases (SGP11

and SGPP11)[174,175]. If confirmed, these data could indicate that S1P functions in the activation of the bone remodelling cycle, attracting osteoclast and osteoblast precursors to the site of injury and promoting osteogenesis within the bone modelling unit. These findings suggest the existence of a positive feedback loop, whereby S1P is produced by osteocytes in response to mechanical stimulation acts directly on osteocyte S1PRs to further increase S1P release[175]. Moreover, intracellular levels of S1P enhance calcium and prostaglandin E2 signalling in osteocytes (Ocy454[176]), raising the possibility that S1P influences other osteocyte functions. Exactly how extracellular S1P and S1PR expression on osteocytes impacts communication with other bone resident cells following activation is unclear and further research is urgently required.

1.5.3 14-3-3 Family Proteins

14-3-3 proteins are a family of seven phosphoserine and phosphothreonine binding proteins[177]. This family of proteins is ubiquitously expressed throughout the body and have major roles in most cellular signalling pathways, most often acting as scaffolds for protein interactions[177]. The seven human isoforms are represented by the Greek letters β, γ, ε, τ, η and ζ[178]. The interactions of these proteins are vast with over 1200 independent binding partners being identified, including cytoskeletal proteins and G-proteins[179]. 14-3-3 proteins are able to alter interactions through altering the cellular location and stability of its binding protein[179].

Of particular relevance is the involvement of 14-3-3η[180], 14-3-3β[181] and 14-3-3ζ[182–184] as all have been shown to impact bone remodelling. 14-3-3η and β, have both been shown to negatively regulate bone formation and 14-3-3η has recently been linked to progression of

osteoporosis[180]. The cause of this is thought to be linked to the roles of 14-3-3η in the MSC differentiation[185]. 14-3-3η knockout in BMSCs caused increased expression of multiple osteoblast related markers including BMP-2 and OPN and increased BMSC migration in scratch wound assays[185]. Similarly, downregulation of the 14-3-3β protein has been shown enhance osteogenesis in MSCs[181], whilst the presence of 14-3-3β negatively regulates MSC osteogenesis, however the mechanism behind this function is still unclear[181]. One study observed that 14-3-3 proteins are able to modulate differentiation of MSCs through binding to TAZ (transcriptional coactivator with PDZ-binding motif). TAZ coactivates RUNX2 mediated gene transcription while inhibiting PPARγ which is required for adipogenesis, therefore promoting an osteogenic differentiation. The binding of 14-3-3 proteins to TAZ sequesters it within the cytoplasm, therefore inhibiting activation of RUNX2. These studies suggest that 14-3-3 proteins can act as negative regulators of osteoblast formation.

Comparatively, 14-3-3ζ is expressed by and impacts the functions of both osteoclasts[184] and osteoblasts[182,183]. Within osteoclasts, 14-3-3ζ has been shown to impact RANKL mediated osteoclast differentiation, however the mechanism in which it has these effects is so far unclear. One study described that 14-3-3ζ interactions with microphthalmia-associated transcription factor (MITF) prevented MITF translocation to the nucleus following RANKL stimulation[184]. With 14-3-3ζ overexpression within these cells causing a reduction in TRAP and cathepsin-k mRNA[184], suggesting that the binding of 14-3-3ζ with MIFT may reduce osteoclastogenesis and therefore regulate bone resorption. Whereas a more recent study suggests that 14-3-3ζ is able to reduce RANKL mediated osteoclastogenesis through inhibition of downstream TRAF6 signalling[186]. TRAF6 is an adaptor protein which forms a complex with RANK, and is essential for RANKL mediated osteoclast activation, with TRAF6

knockout mice showing an osteopetrosis phenotype similar to that seen in RANK knockout mice[187]. Upon binding 14-3-3ζ triggered TRAF6 ubiquitination and subsequent degradation, preventing MAPK and AKT mediated transcription of osteoclast genes such as Ctsk and Acp5[186]. Although the mechanism behind 14-3-3ζ inhibition of RANKL mediated osteoclast formation is unclear, both studies suggest that 14-3-3ζ plays an important role in osteoclast differentiation.

Within osteoblasts, 14-3-3ζ has been found related to the 3 binding-protein 2 (3BP2)[188], which is essential for homeostatic bone remodelling, as 3BP2 deficient mice display an osteoporotic phenotype[189]. Importantly as osteoblasts have been shown to express 14-3-3ζ on vesicles[182] and exosomes[183], thereby allowing for potential osteoblast-osteoclast communication to occur. Further evidence of the importance of 14-3-3ζ in bone remodelling is that 14-3-3ζ knockout mice show significant shortened tibia[190] and significant trabecular and cortical bone loss, which can be reversed when mice were immunized with 14-3-3ζ[191]. Additionally, 14-3-3ζ treatment was able to increase trabecular and cortical bone parameters in wildtype mice[191]. These data state the important role of 14-3-3 proteins in the regulation of bone remodelling, and further work is required to identify the mechanism of these proteins to identify potential therapeutic targets.

Although previously described as scaffold proteins, an additional role of these proteins has come to light in recent years with 14-3-3ζ acting as the parent protein for the endogenous PEPITEM[192].

1.5.3.1 PEPITEM

Our group previously identified an immunoregulatory peptide, PEPITEM, as an inhibitor of T-cell transmigration across inflamed endothelium in an S1P dependent manner[192]. Here PEPITEM was shown to act on cadherin-15 to increase Sphk2 activity results in increased S1P release from endothelial cells, inhibiting T-cell migration via actions on S1PR4. PEPITEM is an endogenous 14 amino acid peptide, that is cleaved by MMP-2 and MMP-9[193], from the ubiquitously expressed 254 amino acid protein 14-3-3ζδ[192], encoded by tyrosine 3-monooxygenase activation protein zeta gene (YWHAZ) gene[194,195].

As described above both S1P and the 14-3-3 proteins play a major role in bone. Additionally, PEPITEM has previously been shown to significantly reduce the bone erosion within an inflammatory collagen-induced model of rheumatoid arthritis[196], therefore PEPITEM was tested as a potential pro-osteogenic molecule[128].

To observe the homeostatic function of PEPITEM on bone remodelling WT were treated once daily with 300 μg of pegylated PEPITEM via intraperitoneal (i.p.) injection for 14 days. Tissues were collected on day 15 and analysed using μ-CT, where PEPITEM showed a significant increase in trabecular bone parameters including bone volume / total volume (BV/TV), trabecular thickness (Tb.th) and trabecular number (Tb.n) compared to vehicle control[197]. In order to address how PEPITEM was increasing bone volume, methods for interpreting osteoblast and osteoclast activity were used. Effects on osteoblast activity were assessed by, dynamic histomorphological. Analysis of calcein labelling was performed which demonstrated an increase in the levels of mineralisation following PEPITEM treatment, indicating higher levels of osteoblast activity[197]. Interestingly although it is often seen that increasing osteoblast activity also increases osteoclast activity, analysis of TRAP positive

osteoclast suggests a significant decrease in osteoclast number compared to vehicle control[197]. Suggesting that PEPITEM is having dual action on both osteoblast and osteoclast functions.

In vitro, PEPITEM was shown to increase the maturation and mineralisation of both murine and human osteoblasts, as evidenced by an increase in alkaline phosphatase (ALP) activity and increased alizarin red staining of deposited mineral[128]. These data suggest that PEPITEM is having a direct action on osteoblasts to increase maturation and mineralisation, however the mechanism behind this is so far unknown.

Within osteoclasts PEPITEM treatment had no direct effect. However, when PEPITEM was added to whole bone cell cultures, there was a significant decrease in osteoclastogenesis. PEPITEM had the same indirect effect when transferring the media of PEPITEM treated osteoblasts on to monocytes, resulting in decreased osteoclastogenesis as shown by a reduced number of multinucleated cells stained using TRAP. These data suggest that PEPITEM causes the release of a secondary molecule which acts to decrease osteoclastogenesis, however, the identity of this molecule remains unclear.

1.6 Dysregulation of bone remodelling

As is seen in all organs there are cases where normal cell function is lost resulting in homeostasis being lost, in the case of bone this can occur for a variety of reasons including age and disease.

1.6.1 Ageing

With age comes numerous cellular and structural changes throughout the body, and bone is no exception. It is well known that aging induces multiple structural modifications within bone, resulting in a loss of skeletal integrity[198]. These changes include a reduction in bone mineral density and alterations in microarchitecture, characterized by trabecular thinning and increased cortical porosity[198]. In addition to a reduction in bone formation, there are significant changes in the structure of newly produced bone[199]. As bone ages, notable shifts occur in its composition, including alterations in the collagen matrix and mineral content. An increase in collagen cross-linking with age results in enhanced bone rigidity but diminished mechanical resilience[200]. Together, these changes decrease bone integrity and increase the risk of fracture. Therefore, it is paramount that we strive to understand the mechanisms of bone aging and develop interventions to prevent further bone loss.

1.6.1.1 Osteoblast Ageing

With age, the number of osteoblasts present within bone decreases due to alterations in the differentiation and proliferation of osteoblast progenitors[201]. The regenerative capacity of bone marrow stromal cells (BMSCs) diminishes, primarily due to telomere shortening, resulting in DNA damage and growth arrest[201]. This loss of mesenchymal stem cells (MSCs) leads to a significant reduction in osteoblast numbers and, consequently, decreased bone formation.

Moreover, the remaining osteoblasts undergo substantial age-related changes, characterized by DNA damage, cell cycle arrest, and elevated p53 and p21CIP1 levels, all of which impact bone regeneration and create a proinflammatory microenvironment[202]. Multiple

pathways, including ROS/PADI2 and mTORC1/Scn1a, have been implicated in osteoblast aging[203]. Additionally, age-related changes in the senescence-associated secretory phenotype (SASP) of both osteoblasts and BMSCs significantly affect osteoclastogenesis and angiogenesis, shifting the balance towards increased bone resorption[204].

1.6.1.2 Osteocyte Ageing

The osteocyte network undergoes substantial changes with age, as studies have identified an increased number of empty lacunae, altered lacunar patterning (changes in directionality and orientation), and an overall reduction in the number and length of osteocyte dendrites[205], indicating a decrease in osteocyte connectivity. These changes result in osteocytes failing to adequately transmit mechanical signals, leading to further dysregulation of bone remodelling and an impaired ability to respond to mechanical stimuli or injury.

1.6.1.3 Osteoclast Ageing

As osteoclasts age, they undergo molecular changes driven by factors such as oxidative stress accumulation and DNA damage. This results in delayed osteoclastogenesis while maintaining bone resorption capacity[206], as the delayed osteoclastogenesis impairs the removal of damaged bone tissue, hindering its replacement with new bone. Additionally, imbalances in key molecules like cathepsin K and integrins leads to impaired apoptosis, resulting in a disproportionate number of osteoblasts to osteoclasts[207]. Consequently, bone microarchitecture is altered, increasing fracture risk. Additionally, aged osteoclasts as with osteoblasts, exhibit an altered SASP, promoting a proinflammatory bone microenvironment and contributing to the chronic low-grade inflammation associated with aging[204].

These age-related changes in bone cell function collectively impair the bone remodelling system, ultimately leading to age-related osteoporosis, resulting in increased bone fragility and fracture risk[208,209]. In older individuals, not only is the risk of fracture higher, but also compromised wound healing[210,211]. This delayed healing and subsequent incapacitation can have more severe and wide-ranging consequences in the elderly population.

1.6.1.4 Fracture healing and Ageing

There are multiple stages involved in fracture healing[211] starting with the inflammatory stage which is required for the removal of debris from the fracture site, whilst also signalling other cells for later stages in the healing process[212]. Once debris has been removed, progenitors move in and chondrocytes form a soft callus which becomes vascularised[213] and mineralised to form new bone via endochondral ossification, this is known as the anabolic phase[214]. Once new bone has formed the catabolic can stage begin, in order to remodel the newly formed callus. Once the callus is reduced, osteoblasts and osteoclasts reestablish a typical remodelling cycle allow the bone to return to a pre-injured homeostatic state[215].

The process of fracture healing is severely impaired in older animals including humans, with each stage being shown to be impacted with age[216,217]. One of the causes of delay is due to the loss of stemness of osteochondral stem cells[218,219], resulting in impaired callus formation but also reduced osteoblast mediated bone formation and mineralisation. During fracture healing these stem cells primarily arise from the periosteum[212,220], when periosteal cells were isolated from older and younger patients, researchers found that

significantly less cells could be collected[220]. Additionally, when comparing periosteal cells from aged mice there was a significant reduction in osteogenic and chondrogenic capacity with age[221]. These data therefore suggest that not only are their fewer stem cells available but of the stem cells present they are less likely to promote fracture healing. This is also true for other sources of stem cells which may be involved in fracture healing such as cells from the muscle[222] or bone marrow[223].

In addition to changes in stem cell number and capacity, a major factor in delayed healing is due to an impaired inflammatory response. To allow for the fracture healing process to being a robust inflammatory response is required[224], this response is tightly controlled as the temporal release of pro-inflammatory cytokines is required for adequate recruitment of cells to the site of injury. Following the initial inflammatory response there must be resolution to allow for the anabolic stage to continue. However, with age the immune system becomes maladaptive, resulting in chronic inflammation with failure to resolve inflammation. In fracture healing this prolonged inflammatory process has resulted in delayed and impaired callus formation[225,226]. Age related changes to the immune system and how this affects fracture healing has been reviewed here[211].

The impairment of the healing process following fracture can have profound complications on skeletal health and recovery, predominantly due to prolonged bedrest resulting a loss of bone mass and strength. This self-fulfilling cycle results in an increased risk of secondary fracture following recovery, putting an additional strain on the patient and health services. Therefore, it is paramount that new treatments are created to improve facture healing but also improve bone health to prevent osteoporosis especially in the older population.

1.6.2 Osteoporosis

One of the main co-morbidities for fracture risk in the elderly is osteoporosis. Osteoporosis is the most common metabolic bone disorder characterised by a reduction in bone mineral density, resulting reduced bone strength and increase fracture risk[227].

1.6.2.1 Pathophysiology

Osteoporosis is caused by an imbalance of bone formation and bone resorption. There are two types of osteoporosis, primary and secondary. Secondary osteoporosis is where bone loss occurs as a result of medications such as glucocorticoids[228] or from other diseases such as anorexia nervosa[229]. Primary osteoporosis consists of two groups, type 1 that is caused by a loss of oestrogen or androgen, and type 2, age-associated osteoporosis (AAOP).

1.6.2.1.1 Postmenopausal Osteoporosis (Type 1)

Menopause is defined by the world health organisation as the complete cessation of menstruation (amenorrhea) for over 12 months, in the absence of physiological or pathological cause[230]. The onset of menopause can vary, averaging at 51 years in industrialised nations although it can occur as early as 40 in women with premature menopause. With the onset of menopause there is a gradual decline and cessation in the production of oestrogen and progesterone from the ovaries[230]. As oestrogens have long been shown to have a profound impact on bone remodelling with oestrogen receptors (ERs) being expressed on osteoblast, osteoclasts and their precursors[124]. Therefore, the rapid decline in oestrogen during menopause can have devastating consequences on bone remodelling.

1.6.2.1.2 Age-associated Osteoporosis (Type 2)

As life-expectancy increases and longevity treatments advance, there has been a dramatic shift in the age of our population. The world health organisation has predicted that by 2030 1 in 6 people will be aged 60 or over, with the number of aged individuals increasing by 400 million[231]. Although ageing has multiple comorbidities, osteoporosis is one of the most prevalent with 1 in 2 women over the age of 50 in the UK, estimated to experience on osteoporotic fracture in their lifetime.

As mentioned, causes of age-associated osteoporosis are multifaceted. At a cellular level as the bone ages there is a significant decrease in the number of active osteoblasts, and increased number of osteoclasts[232,233]. MSCs are the precursor of multiple cell types, including osteoblasts, chondrocytes and adipocytes. However, ageing has been shown to result in an impairment to MSC proliferation and differentiation into osteoblasts, with cells shifting to favour adipogenesis[234].

1.6.3 Pharmacological interventions for bone remodelling

The decreased bone mass seen in osteoporosis results in increased risk of fracture. Fractures are associated with substantial pain, chronic disability and high mortality[235,236]. Additionally in 2022 it was estimated that 3.5 million people in the UK were affected by osteoporosis[237], this results in a significant financial burden on the NHS costing £4.6 billion per year[237], expected to rise to £6 billion by 2030. Due to this several treatments for osteoporosis have been developed in order to prevent risk of fracture.

Prior to the 1980s there were few interventions for patients with osteoporosis, with the primary treatment being oestrogen, calcium and vitamin D supplementation[238]. Whereas now

there are over five approved osteoporosis treatments with others on the horizon. These treatments can be broadly split into anti-resorptive and pro-formative therapies.

1.6.3.1 Anti-resorptive

Anti-resorptive therapies are the most commonly used treatment of osteoporosis with bisphosphonates being the first pharmacological intervention[238]. These therapies act to inhibit the osteoclast function and/or formation therefore reducing resorption.

1.6.3.1.1 Bisphosphonates

Despite being the first line of defence in the treatment of osteoporosis, the discovery of bisphosphonates (BPs) and their original uses is far removed from the biological intervention seen today[239]. BPs are synthetic analogues of inorganic pyrophosphate (PPi)[240–242] and are strong chelators of divalent metal ions, with a particular affinity for calcium ions. These properties made them ideal for their initial use as water softeners[239], but later showed great potential for the treatment of bone disorders with their high affinity for hydroxyapatite, allowing BPs to specifically target bone tissue[240,243]. Once bound to bone BPs would be internalised by active osteoclasts during resorption and once internalised BPs are toxic to osteoclast inducing apoptosis[243].

Although there have been multiple generations of bisphosphonates, their action has remained the same with their primary target being osteoclasts[242]. The use of oral bisphosphonates have been shown to reduce the number of hip[242,244,245] and vertebral[242,244,246–248] fractures. The use of BPs comes with a myriad of side effects including gastrointestinal issues, osteonecrosis of the jaw and flu like symptoms, however the recent availability of

intravenous bisphosphonates, that can be given yearly can reduces associated gastrointestinal symptoms[249].

The main issue with the use of bisphosphonates is that they are not an anabolic therapy, therefore do not increase bone formation and primarily preserve existing bone. However long term use has been shown to increase bone mineral density in the spine, hips and femoral head[250], suggesting they do have some anabolic capacity. Due to having no action on osteoblasts, prolonged bisphosphonate treatment has been shown to lead to over mineralisation, which can cause bones to become brittle and increase the risk of microdamage as damaged bone can no longer be removed by osteoclast[251].

1.6.3.1.2 Denosumab

The development of anti-resorptive treatments stalled for years until the isolation of osteoprotegerin (OPG) in 1997[252]. Following this and the subsequent finding of OPG binding molecule, RANKL, led to the discovery and understanding of the osteoclast regulatory RANK-RANKL-OPG axis, which could be used as a therapeutic target.

Denosumab is a human monoclonal antibody therapy against the pro-resorptive molecule RANKL[253]. Through the competitive binding to RANKL, denosumab acts similarly to OPG, preventing RANKL binding to the RANK receptor on the osteoclast surface[253]. This inhibition results in a reduction in osteoclast formation, activity and survival.

Unlike bisphosphonates denosumab has been shown to increase structure and thickness of cortical bone[254], however it has also been shown to reduce bone turnover. Although effective at increasing bone mineral density (BMD), denosumab has been shown to increase infections such as urinary tract and ear infections, this is likely caused by RANK

expression on B-lymphocytes and T-lymphocytes[255]. One of the primary issues with denosumab treatment is that upon cessation of treatment there is a dramatic reversal of therapeutic benefit resulting in increased bone turnover, shown though increase in both Serum C-telopeptide (CTX) a marker of increased bone resorption and increased serum levels of N-terminal propeptide of type 1 procollagen (P1NP), a marker of increase bone formation[256–259]. Because of this the stopping of denosumab is often coupled with additional treatment such as bisphosphonates, to slow the decline in bone loss[260].

1.6.3.1.3 Hormone therapies

As described in section 1.6.2.1.1 osteoporosis is often caused due to a hormonal imbalance caused by the onset of menopause. For this reason, many therapeutics have been aimed to target the oestrogen pathway to reverse bone loss as a result of oestrogen deficiency. Hormone replacement therapy (HRT), although not used as the first line of defence is a common treatment for postmenopausal osteoporosis[261]. Oestrogen treatment is able to increase the BMD in all skeletal sites including the lumbar spine[262,263]. Oestrogen replacement is a relatively simple to take through the use of oral contraceptive treatments; however many women reduce their use of the standard oestrogen dose due to increased side effects[264]. Following discontinuation of treatment, the improvement in patient bone mass is seen to decrease after a few years[264]. More recent studies have therefore looked at the use of lower dose (LD-HRT) replacement of alternative treatments[265]. The health, osteoporosis, progestin, oestrogen (HOPE) trial, showed that LD-HRT is able to prevent bone loss in the hip and spine, with reduced side effects compared to the standard dose[266]. Therefore LD-HRT may be an effective treatment with higher patience adherence.

Due to concerns surrounding pro-longed oestrogen treatment use and cancer risk[267], compounds have been developed which modulate oestrogen receptors without the steroidal structure of oestrogens[268]. Selective oestrogen receptor modulators (SERMs) represent a class of compounds that act as agonists or antagonists of oestrogen receptors in a tissue dependent manner. SERMs can be currently separated into two classes, triphenylethylene derived (e.g. tamoxifen) or benzothiophene derivatives (e.g. raloxifene)[268]. Raloxifene is currently used to treat osteoporosis and has been shown to be effect antiresorptive agents, decreasing bone turnover and maintain or increasing BMD[269–271]. Additionally, tamoxifen although is not used as a treatment of osteoporosis has been shown to decrease risk of osteoporosis following use in the treatment of breast cancers[272]. SERMs have been given in combination with HRT, called the tissue selective oestrogen complex (TSEC), decreasing menopausal symptoms whilst being safer and better tolerated compared to conventional HRT[273].

1.6.3.2 Pro-formative

Although some anti-resorptive therapies have the capacity to increase bone mineral density through reducing osteoclast activity therefore switching the balance towards formation. They do not actively act to increase bone formation therefore cannot improve osteoporosis only prevent the disease from worsening. Therefore, more research has focussed on the development of pro-anabolic therapies as novel osteoporosis treatment.

1.6.3.2.1 Parathyroid hormone related protein

Human parathyroid hormone (hPTH) is an endogenous 84aa peptide hormone that plays a key role in calcium homeostasis[274]. PTH release from the parathyroid gland is triggered by a decrease in extracellular calcium levels[275], PTH is then able to alter bone turnover to allow for calcium release and storage. The effect of PTH on bone has been shown to be two-fold dependent on the length of exposure the PTH treatment. Prolonged PTH exposure has been shown to increase osteoclastic activity resulting in a net release of calcium from the bone compartment[276]. PTH has been shown to act directly on osteoclasts through increasing cell apoptosis and indirectly on osteoclasts through increasing osteoblast secretion of RANKL and repressing OPG secretion, through binding to parathyroid hormone receptor 1 (PTH1R)[277–281]. However, transient exposure to PTH increases osteoblast activity to cause a net increase in bone mineral density[282]. Transient exposure to PTH has been shown to effect multiple levels of osteoblast function including proliferation and differentiation[283–290]. The mechanism of action of this function is widely disputed due to difficulty developing *in vitro* systems which mimic the transient effect of PTH. However partial effects of PTH have been linked to the reductions of osteoblast inhibitor sclerostin[291].

Studies found that the biological effects of PTH come from the N-terminal 34aa, (hPTH(1-34))[292], now called teriparatide. Teriparatide, but not the whole length recombinant hPTH has been approved for the treatment of osteoporosis, this may be due to suspected additional impacts of the C-terminal fragment, which has been shown to enhance osteocyte apoptosis[293]. Teriparatide has been shown to be an effective treatment for osteoporosis with trials showing a reduced risk of one or more vertebral fractures by 69% and risk of non-vertebral fractures by 54%[294].

Despite being an effective therapy for bone formation there are several limitations to the use of teriparatide. Firstly, similarly to other therapeutics there are several side effects including pain, weakness and risk of hypercalcemia[294]. Unlike bisphosphonates which can be taken as daily oral tablets or once a year treatments teriparatide requires daily subcutaneous injections which causes issues with patience compliance[295]. The primary issue with teriparatide is due to safety concerns surrounding development of osteosarcoma[296], which limits its use to a maximum of 24 months, after which bone loss continues. Meaning teriparatide is often suggested to be followed up with bisphosphonate treatment to reduce resorption following cessation of teriparatide[297].

Some of these issues have been addressed with the recent approval of a new PTH analogue, Abaloparatide, a synthetic agonist for PTHR1[298]. Comparatively to teriparatide Abaloparatide is able to increase bone formation but has less effects on bone resorption, therefore reducing risk of hypocalcemia[299]. Although risk of hypercalcemia is reduced, the risk of osteosarcoma remains[300] and both treatments still require daily injections resulting in poor patient compliance[301]. Finally, other treatments are required for the treatment of osteoporosis in patients with additional co-morbidities such as severe kidney diseases[302] or other bone diseases such as Paget's disease[303].

1.6.3.2.2 Anti-sclerostin antibody (Romosozumab)

Romosozumab is a humanized anti-sclerostin antibody that was approved for the treatment of osteoporosis in the UK in 2022[304]. Sclerostin is a glycoprotein produced by osteocytes and is a key inhibitor of the canonical WNT signalling pathway, which is important for osteoblast differentiation[40,173]. In the absence of sclerostin WNT ligand binds specifically

to the Frizzled family receptor and its LDL-receptor related protein (LRP) coreceptor, LRP-5/LRP-6[64]. The binding of Wnt triggers the inhibition of GSK-3β, the destruction complex of β-catenin. The inhibition of β-catenin degradation results in accumulation within the cell, allowing for transnucleation and binding to the T-cell factor transcription factor, thus activating Wnt-responsive genes resulting in osteoblastogenesis[305].

The presence of sclerostin is essential for regulation of bone remodelling particularly in response to mechanical stress. Osteocytes have been shown to enhance secretion of sclerostin in periods of unloading[306], decreasing osteoblast formation leading to increased bone resorption. Comparatively, when mechanical load is high, as seen in weight-bearing exercise, osteocytes downregulate sclerostin and promote bone formation[173]. The importance of sclerostin in the regulation of bone remodelling is highlighted in two rare autosomal diseases, Sclerosteosis and van Beachem's disease, where sclerostin production is significantly decreased. Sclerosteosis results in a more severe phenotype due to the gene mutation being within the SOST gene, whereas van Beachem's disease is caused by a mutation within the regulatory elements involved in SOST transcription. In both diseases patients have generalised osteosclerosis, increased bone mass as a result of unregulated bone formation. This abnormal bone remodelling is replicated in the SOST-KO mouse, that display increased bone mass and density[307,308]. Whereas the SOST overexpression results in decreased bone mass and increased bone fragility[309].

Sclerostin has indirect effects on osteoclasts as increased osteoblast maturation through activation of WNT-β -catenin signalling results in the upregulation of OPG. Therefore, inhibition of sclerostin will allow for increased bone formation through increased osteoblast differentiation, whilst also inhibiting osteoclast formation through increased secretion of

OPG. Due to this sclerostin became a target for therapeutic intervention in osteoporosis. Animal studies showed the effectiveness of anti-sclerostin antibodies in OVX rodents[310–313]. The effects of anti-sclerostin treatments on animal models of osteoporosis has been extensively reviewed[314]. These studies predominantly showed that anti-sclerostin antibody treatment is able to cause an increase the number of osteoblasts and osteoprogenitors, thought to be partially due to reactivation of quiescent bone lining cells[315], resulting in increased matrix deposition and mineralisation[316]. However, the initial increase on osteoblast numbers is later lost, however the remaining osteoblast have higher levels of activity[317]. In addition to alterations in bone formation through changes in osteoblast function, anti-sclerostin treatment is also able to alter bone resorption through altering the OPG:RANKL ratio as well as causing reductions in M-CSF[318]. Together these changes in bone turnover result in several studies showing a significant increase in both trabecular and cortical parameters following anti-sclerostin treatment[310–313,319–321]. Short term changes in bone formation seen with antibody treatment, studies have suggested that anti-sclerostin antibody treatment may cause long term effects through altering osteocyte transcription[322].

One anti-sclerostin treatment, Romosozumab, has been approved for the treatment of severe post-menopausal osteoporosis, with NICE guidelines suggesting Romosozumab to only be given in cases of imminent fracture risk[323]. However, studies have reported higher cardiovascular risk following Romosozumab compared to bisphosphonates[324,325], but not compared to placebo[326]. A recent GWAS study suggests that low circulating sclerostin levels may increase risk of cardiovascular events following treatment[327], therefore suggesting additional screening may be required to mitigate potential risk factors.

1.7 Future Therapeutics

The current therapeutics for osteoporosis described above have been shown to be effective at increasing BMD in the short term but each pose issue following continuous use[328]. Many of these therapies have been given in combination such as hPTH and bisphosphonates in order to provide both anabolic and anti-resorptive functions[297]. However, novel treatments which are able to act on both osteoblasts and osteoclasts to increase bone formation and reduce bone resorption are required.

1.7.1 PEPITEM as a novel therapeutic

In addition to PEPITEMs role in bone homeostasis, PEPITEM has been explored to look at its potential therapeutic values in the treatment of bone loss. Using the OVX model of osteoporosis it has been shown that PEPITEM is able to prevent further bone loss when given for 14-days after the onset of osteoporosis[197]. In this model PEPITEM prevented further decline in BV/TV and trabecular number compared the vehicle treated controls[197]. Additionally, PEPITEM mice showed no difference from baseline pre-treatment controls, suggesting PEPITEM treatment prevented additional bone loss[197]. Unlike many of the current therapeutics described PEPITEM is able to have dual action on both osteoblasts and osteoclasts, which allows for increased formation whilst decreasing overall resorption without completely inhibiting resorption as seen in the use of bisphosphonates.

PEPITEM is an endogenous peptide which has so far only been reported to be secreted from b-cells in response to adiponectin stimulation[192]. However, it has been reported that the ability for b-cells to produce PEPITEM, declines with age which has been linked to an age related dysregulation in leukocyte trafficking[329]. The loss in PEPITEM production is caused by

a reduction in the expression of adiponectin receptor 1 (AdipoR1) coupled with a reduction in the proximal adaptor protein (APPL1), which is required for adiponectin signalling. In addition aged b-cells show a much reduced expression of PEPITEM parent protein, 14-3-3ζ, thus indicating that the PEPITEM pathway is impaired in aged individuals[329]. The age related dysregulation can be rescued through the administration of supplemental PEPITEM[329], suggesting that although the PEPITEM production is impaired, downstream signalling remains unaltered.

It is currently unknown whether osteoblasts are able to produce PEPITEM or whether b-cells within the bone marrow secrete PEPITEM and/or 14-3-3ζ in response to surrounding adipocyte derived adiponectin during homeostasis. Due to these unknowns, it is unclear whether an impaired PEPITEM production mediates dysregulation in bone remodelling with age. We have demonstrated that age does impact osteoblast responses to PEPITEM, in osteoarthritis patients aged 59-77 we saw increased ALP activity and mineralisation in response to PEPITEM compared to untreated controls[197]. However in older individuals aged 80< we saw no effect of PEPITEM, suggesting that there is an age related decline in PEPITEM response but this occurs at a later point than average onset of osteoporosis at the age of 50[235]. This decline with age is not due to decreases in the previously identified PEPITEM receptor, Cdh15, suggesting a separate mechanism is involved in PEPITEM signalling within osteoblasts[197].

Together these data provide strong evidence towards the therapeutic potential of PEPITEM in the treatment of musculoskeletal diseases, however as with all peptide treatments there are issues which must be addressed before clinical use. Peptide therapeutics have been used since 1923, with the commercial use of insulin[330], and many

peptide drugs have been developed since including one treatment for osteoporosis, PTH (section 1.6.3.2.1). The use of peptide drugs are favourable due to their often high target specify and efficacy, additionally due to endogenous function peptide therapeutics are often viewed as safer[330]. However, the primary drawbacks of peptide therapeutics is their low stability and short half-life, as a result of the body being readily equipped to cleave and degrade endogenous peptides[330]. Our group has previously investigated the pharmacokinetics of PEPITEM through the use of radioactive and florescence labelling[331]. These studies showed a rapid clearance of PEPITEM from the bloodstream following intravenous injection with 94% of ^{3}H PEPITEM injected being undetectable in the blood after 2 minutes. Additionally, after 15 minutes of treatment fluorescence labelled PEPITEM (AF680), could be detected in multiple tissues including lungs and spleen, however most prominently in the kidney, suggesting rapid renal clearance[331]. Due to rapid clearance, PEPITEM must be dosed daily, which sparks issues when moving forward therapeutically due to poor patient adherence. Due to this other disease avenues may benefit more from the use of PEPITEM such as short term treatment following fracture.

However, as described previously there are current osteoporosis therapeutics, such as teriparatide, that require daily subcutaneous (S.C.) injection. Investigations into adherence to teriparatide treatment, shows high initial adherence with 89% of patients who started the trail adhering within the first 6 months[295]. However adherence decreases with prolonged treatment where by 18months adherence drops to 75%[295], therefore showing that many patients are willing to have daily injections. Additionally, adherence increased with osteoporosis severity suggesting that there is a clinical desire for effective treatment that is not hindered by drug delivery[295]. However, PEPITEM is currently administered via I.P. not S.C.

There are multiple ways to improve the efficacy of peptide drugs this includes adding various side chains which increase the half-life of the peptide[330]. One way in which PEPITEM has been previously modified is through PEGylation, this is the addition of repetitive ethylene oxide units. The addition of a PEG is able to enhance half-life through increasing the molecular weight of the peptide which reduces renal clearance[332]. In addition, PEGylation can reduce enzymatic degradation of the protein through increased steric hinderance[332]. However, we have found that even with the PEG-PEPITEM, in order to see changes in bone parameters, daily PEPITEM treatment is still required.

Studies have also looked at the bioactive regions of the PEPITEM sequence in order to decipher which regions are required for activity. Reducing the size of the PEPITEM protein would reduce the enzymatic degradation due to reduced number of cleavage sites available. Two bioactive regions of PEPITEM have been identified, SVT and QGA[333], both of which show the ability to reduce the migration of leukocytes across the endothelium[333]. However, it is not yet clear whether the same bioactive regions are involved in PEPITEM function within osteoblasts. Identification of PEPITEM bioactive regions will provide biological information towards PEPITEM functioning but also great potential therapeutic peptides with potentially increased half-life and potency. As part of this thesis look at the development of therapeutics for the treatment of osteoporosis due to the access to a commonly used osteoporosis model, the ovariectomy model, which mimics postmenopausal bone loss due to the loss of oestrogen. However, due to the frequency of treatment currently required for PEPITEM treatment we believe that further testing should be done to examine the use of PEPITEM as a post-surgical intervention in the treatment of fractures, as the models required for this work were not possible during this thesis. Currently there are few models which accurately model

bone due to its complex structure, with many bone models requiring extensive animal research using severe models such as the bone fracture model. Due to this we use aimed to use a multitude of techniques to allow us to analyse different aspects of PEPITEM function in bone.

1.8 Modelling bone remodelling in health and disease

The different ways of modelling bone can be broadly split into three categories: (1) *In vivo,* (2) *Ex vivo* and (3) *In vitro*.

1.8.1 *In vivo*

The term in vivo is Latin for within the living and is used to describe research. Which requires live animal experimentation. Preclinical bone research employs a variety of in vivo models, each with its own strengths and limitations. Large animal models, which rely on animals such as sheep, rabbits, dogs, pigs, and non-human primates, are less frequently used primarily due to ethical considerations, time and high costs[334]. Due to these limitations' smaller animal models, such as rodents and bony fish, are more frequently used especially in basic molecular research and early drug development. However large animals are invaluable for translational research as they closely mimic human bone characteristics[335,336]. Currently the most commonly used large animal model is the sheep, this is primarily due to them sharing bone dimensions similar to humans[335,337,338] and similar rates of bone formation and healing[339], therefore allowing sheep to be used as more biologically accurate models of human fractures[340]. Despite closely resembling human bone in multiple ways as with all models, adjustments in experimental design must be used to consider existing biological differences such as increased bone mass and bone strength[338]. Large animal models are

particularly useful for advancing surgical techniques, testing orthopaedic implants and evaluating biomaterials[341], which are much harder to study in smaller animal models such as rodents due to their reduced size.

Rodents, especially rats and mice, form the cornerstone of skeletal research and drug development[334,342–344]. The advent of reverse genetics in rodents has been crucial in unravelling the complexities of bone growth and remodelling[343,344]. Key discoveries, such as the role of the RANKL/OPG system in osteoclastogenesis[345–347], have led to the development of important treatments like denosumab[348]. In addition to the use of rodent models in the understanding of drug mechanisms and safety the use of mouse models have also been instrumental in validating human GWAS candidates and understanding monogenic skeletal diseases through knockout and knock-in techniques[334].

Zebrafish (and other bony fish) have emerged as a powerful complement to rodent models, offering unique advantages for genetic studies[349]. Their small size, low cost, and ease of genetic manipulation make them ideal for both forward and reverse genetic screens[350–353]. The availability of advanced tools like CRISPR-based gene editing and extensive mutant resources has positioned zebrafish as an excellent model for high-throughput screening[354,355]. They can effectively complement ongoing mouse phenotyping projects and aid in prioritizing genes for functional studies following GWAS or sequencing studies[356–358].

The choice of model in bone research ultimately depends on the specific research question and experimental requirements, with each model type contributing uniquely to our understanding of bone biology and pathology.

1.8.2 *Ex vivo*

Ex vivo refers to the research on tissues which are derived from living tissue, this can refer to experimentation on animal tissue post in vivo experimentation or refer to tissue taken surgically from living animals or humans.

Bone organ cultures offer a solution to the limitations of traditional animal research methods. In these cultures, harvested bone tissue is maintained in a nutrient-rich medium, preserving its viability and functionality for extended periods[341,359,360]. This approach allows for the study of bone growth, remodelling, and repair processes while eliminating confounding factors present in vivo. It also enhances animal welfare by enabling substance testing on isolated tissue rather than whole organisms[341,359,360]. However, the tissue removal process may induce changes in the sample[334]. Unlike traditional cell culture, these models involve multiple cell types to simulate tissue remodelling, immune responses, vascularization, and bone marrow niche formation [341,359,360]. Despite these advancements, isolated bone tissue may not fully capture the intricate interactions between different cell types and surrounding tissues as observed in living organisms.

The mouse metatarsal organ explant culture serves as a highly physiological ex vivo model for studying endochondral ossification and bone growth[361]. This model closely mimics in vivo growth rates and allows for the examination of chondrocytes at various stages of chondrogenesis while maintaining cell-cell and cell-matrix interactions[361]. The protocol involves the careful dissection of embryonic metatarsals from E15 murine embryos and subsequent analyses to investigate endochondral ossification and longitudinal bone growth[361]. This method can allow for the treatment with pro-anabolic or anti-catabolic drugs in order to investigate how endochondral ossification and mineralisation is affected[362].

Zebrafish have emerged as valuable models due to their genetic tractability and the translucency of certain skeletal tissues into adulthood, enabling dynamic imaging[363]. Zebrafish scales, which contain both osteoblasts and osteoclasts, provide an abundant and easily accessible source of independent bone units. The ability of adult zebrafish to fully regenerate removed scales offers an opportunity to study the spatiotemporal growth of mineralized tissue in vivo[363]. These methods also allow for the observation of healing responses following controlled damage to the scale's mineralized matrix over time[363], making the zebrafish scale a valuable and may partially reduce the number of animals required for experimentation.

Despite these models aim to reduce the number of animals used in research, they still often require animal sacrifice. Additionally, as these models are often based on animal tissue the limitations of the accuracy and interspecies differences in bone still apply.

1.8.3 In vitro

In vitro research refers to cell culture techniques, referring to research performed in ‘glass’ (vitro) dishes, although many current techniques favour the use of plastic.

1.8.3.1 2D Cell culture

The use of 2D cell culture has been pivotal for understanding bone biology, with osteoblasts being obtained from primary mouse sources (i.e. Calvarial osteoblasts[364,364]), or primary human samples being derived from stromal mesenchymal cells from bone marrow[365], and outgrowths from human bone specimens[366]. Whilst primary mouse and human osteoclasts can be derived from bone marrow cells or peripheral blood samples[367]. The most challenging bone cell to culture in 2D is the osteocyte, as often once cultured

osteocytes revert back into an osteoblast-like phenotype[368]. A solution for this is the use of osteocyte cell lines such as MLO-Y4[368]. The use of primary cells and development of different cell lines has allowed for the study of bone cells in vitro, allowing for the study of processes such as differentiation in order to find potential targets for the regulation of bone remodelling.

However as in other areas of biology the use of 2D cell culture in bone research comes with its limitations, with a major limitation being a lack of biological complexity[369]. Frequently 2D cell culture is performed as monocultures focussing on a single cell, which results in a loss of understanding for the interactions between cells. Simple cell culture has been manipulated to add more complexity, through the addition of multiple cell types or altering O_2 concentration to mimic the hypoxic bone environment[370]. Despite this, researchers still are unable to support the long term culture of bone cells especially osteocytes and osteoclasts in 2D, predominantly due to the 2D environment[334]. Therefore, although 2D cell culture is more readily available and allows for high throughput screening, the lack of biological complexity often results in drug failure in vivo, as primary outputs of 2D culture is not necessarily indictive of the entire bone remodelling process[334]. Leading to a push towards more complex culture techniques.

1.8.3.2 3D Cell culture

Due to the aforementioned limitations for 2D cell culture, in the past few years there has been a dynamic push to development more biologically accurate bone models using 3D culture techniques[371]. Bone organoids are 3D, self-organising and self-renewing cultures which allow for biomechanical and spatial properties of bone to be mimicked, increasing the accuracy of in vitro modelling and reducing the reliance on animal models[372]. There are

currently multiple bone organoid systems, which are able to effectively mimic different aspects of the bone environment, with models focussing on mimicking the bone marrow microenvironment or the calcified bone tissue environment[372]. The model used is highly dependent on the experimental question.

Models have been created using multiple different cell types including those described in 2D cell culture which provides insight into how cells can behave differently in 2D and in 3D environments[373–375]. The 3D environment has been created using various biomaterials which are designed to recapitulate the natural extracellular matrix (ECM) conditions, which guide cell fate. The ECM is mixture of proteins, including fibrillar proteins (e.g., collagens), glycoproteins (e.g., fibronectin), proteoglycans (e.g., syndecan), glycosaminoglycans (e.g., hyaluronan)[373–375]. Therefore, biomaterials which contain these compounds are often used, most commonly collagen, gelatine, alginate, fibrin, and hyaluronic acid have been used in organoid development. Another common material used in organoid development is Matrigel, a natural ECM that is produced by mouse osteosarcoma, which is able to mimic the ECM and also contains various growth factors[372,376]. However, as Matrigel a naturally produced substance there is a high level of batch-to-batch variation, thereby limiting reproducibility[372,376]. Additionally, Matrigel as with many other components used to created organoids can be expensive and therefore limit the accessibility of these models[376].

Although there are multiple bone organoids, in this thesis we focus on the use of the self-structuring bone model (SSBM) which was developed in our lab at the University of Birmingham[377,378]. Unlike other organoids which primarily use stem cells this model has been created to use stromal mesenchymal cells including primary rat calvaria, MC3T3 cell line and

the human osteoblast cell line HFOB 1.19. This model is based on aspects of the fracture healing process, which first involves the formation of a fibrin-containing haematoma that is gradually replaced with a mineralising collagen-rich matrix. SSBMs have been shown to develop a collagen-based matrix containing hydroxyapatite mineral by 12-weeks of culture and contain dendritic cells with the ability to secrete sclerostin and FGF23 within 20-weeks of culture, indicating a osteocyte like phenotype[377,378]. Allowing us to explore how PEPITEM effects cells within a 3D matrix at different stages of maturity. A limitation of this model however is that it lacks osteoclast-like cells therefore is only used to look at osteoblast function.

1.9 Aims and Objectives

As previously described PEPITEM has been shown to be a key regulator of bone remodelling during homeostasis as serve as a potential therapeutic agent in *in vivo* models of osteoporosis. However, the mechanism in which PEPITEM acts within the bone is so far unknown. Therefore, we sought to explore how PEPITEM elicits changes in bone remodelling using multiple *in vivo, ex vivo* and *in vitro* models.

In this thesis we test the following hypotheses:

I. PEPITEM acts directly though osteoblasts via mechanisms differing to that described in endothelial cells
II. PEPITEM acts via indirect mechanisms to elicit osteoclast responses
III. PEPITEM consist of bioactive components which can serve as novel therapeutics for dysregulation in bone remodelling

These hypotheses will be investigated with the following aims:

- To identify PEPITEM binding partners of PEPITEM in osteoblast to locate potential PEPITEM receptors
- To explore potential mediators of PEPITEMs indirect actions on osteoclast function
- To characterise the bioactive components of the PEPITEM sequence for investigation into therapeutic benefit.

Each of these aims will be addressed in individual chapters within this thesis.

2 Methods

2.1 Animal Studies

All animal experiments were run in accordance with Home Office regulations and the University of Birmingham animal welfare and ethical review body. Under the project licences PE5985209, PP0156739 or PP1339258.

2.1.1 Mice

Mice were purchased from Charles River (Kent, UK), and were maintained in a specific pathogen free facility, with free access to food and water. Environmental conditions were: 21 ± 2˚ C, 55 ± 10% relative humidity and a 12 h light-dark cycle. In all experiments, littermates were randomly assigned to experimental groups within the same cages.

2.1.2 Homeostatic conditions

Eight-week-old, female or male, resting C57Bl/6J resting wild type (WT) mice were given daily intra-peritoneal (IP) injections of equivalent volume of vehicle control (PBS), pegylated PEPITEM (300 µg, sequence SVTEQGAELSNEER- PEG(352)-Amide; Biosynth Limited; Cambridge, UK), control peptide (300 µg, sequence: EQAERYDDMAACMK, Biosynth Limited; Cambridge, UK) PEPITEM (300 µg, sequence SVTEQGAELSNEER; Biosynth Limited; Cambridge, UK), QGA (56.3 µg, sequence QGA; Biosynth Limited; Cambridge, UK) or *tvs* (56.3 µg, sequence *tvs*; Biosynth Limited; Cambridge, UK) for 14 or 28 days. After 14 days mice were culled via cardiac puncture and tissues were collected. Hind limbs were dissected and cleaned of muscle and fat before fixation in 10% buffered formaldehyde (cat: HT5011; Sigma-Aldrich,) overnight. The tibias were then processed as described in in 2.2.1 or 2.3.1.

2.1.3 Ovariectomy (OVX) model of osteoporosis

Alternatively, 11-week-old, female C57Bl/6J underwent ovariectomy. Ovariectomy (OVX) surgical procedures were performed by University of Birmingham BMSU staff. Following 7-days of acclimatisation to BMSU conditions, OVX was performed, where ovaries were removed via ligation of the distal uterine horn[379]. 14-days later, mice were given daily I.P. injections of either vehicle control (PBS), PEPITEM (300 µg, sequence SVTEQGAELSNEER; Biosynth Limited; Cambridge, UK), QGA (56.3 µg, sequence QGA; Biosynth Limited; Cambridge, UK) or tvs (56.3 µg, sequence tvs; Biosynth Limited; Cambridge, UK) for 14-days. After 14-days mice were culled via cardiac puncture and tissues were collected. Hind limbs were dissected and cleaned of muscle and fat before fixation in 10% buffered formaldehyde (cat: HT5011; Sigma-Aldrich,) overnight. The tibias were then processed as described in in 2.2.1 or 2.3.1.

2.2 Ex vivo µ-CT analysis

2.2.1 Imaging

Following fixation tibias were moved to 70% ethanol (Cat: 20821.365DP, VWR Chemicals, Leicestershire). In order to scan multiple tibiae at once, three polystyrene straws were glued into place as imaged in Figure 2.1. Each straw contained one tibia and was filled with 70% ethanol (Cat: 20821.365DP, VWR Chemicals, Leicestershire). Polystyrene straws allowed for tibiae to be imaged in a vertical position and held sample in place to prevent movement during scanning. Samples were placed on to the stage of the Skyscanner 1172 m-CT scanner (Bruker; Kontich, Belgium) and fixed to stage with Blue Tak. Using the Skyscanner1172 software version 1.5, images were taken every 0.45° with an X-ray voltage of

60kV, current of 100µA through a 0.5mm aluminium filter at a resolution of 2000x1200 pixels[380,381]. Images were saved following scan.

2.2.2 Image reconstruction

Images were opened and reconstructed was using the NRecon 1.6.1.5 software (Bruker). Prior to reconstruction, scans were previewed for misalignment[382], if misalignment was ±2.5 pixels, samples were rescanned. Beam hardening correction of 20% and ring artifact correction of 4 was applied to reduce distortions produced during the scan. The images were then reconstructed using the Feldkamp algorithm[383]. Reconstruction was saved as .bmp files for analysis.



Figure 2.1 **Image of straws for µCT scanning.** Straws cut into sections and fixed in place within bijou lid with glue. Murine tibia added to each and filled with 70% ethanol 5mins before scanning. Copper tape used to mark first straw allowing the tibias to be identified in the scanned image.

2.2.3 Analysis and 3D mesh generation

Reconstructed images were analysed using the CTan v1.12 software (Bruker)[384], that allowed for trabecular and cortical parameters to be calculated and 3D generation of representative mesh. CTan provided cross-sectional mages of the whole bone allowing region of interests (ROIs) to be created for different bone parameters. For the trabecular bone parameters an ROI was drawn around the inside of the cortical bone (ROI 1, Figure 2.2), 100 slices down from the end of the growth plate. For investigations into trabecular elongation the ROI for trabecular bone was extended from 100 slices to 300 slices. For the cortical bone two ROIs were created, one encompassing the whole tissue (ROI 2, Figure 2.2) and one encompassing only the cortical bone (ROI 3, Figure 2.2), these were created for 100 slices starting from 250 slices below the growth plate. Following ROI creation, a global threshold by comparing the thresholded image to the original CT image, differentiated the bone from the background noise. Analysis was then performed by first applying the threshold, followed by "despeckle" to remove all white speckles < 10 voxels to remove background noise[385]. For trabecular bone, 3D analysis was used looking at trabecular bone volume (BV/TV, %), trabecular number (1/μm), trabecular separation (μm) and trabecular thickness (μm). For cortical analysis, 2D analysis was used to analyse cortical area (μm^2), total bone area (μm^2) and cross-sectional thickness (μm). A 3D mesh was generated using the marching cube algorithm 33[386] and saved as .ply files. Meshes were then opened in MeshLab 1.3.2[387] (ISTI-CNR, Italy) and processed using a quadratic edge collapse decimation of 0.2% to simplify the image by reducing the number of vertices in the mesh; smooth rendering and ambient

occlusion per face to generate soft shadows. Snapshots of 3D models were taken and saved as .JPG.

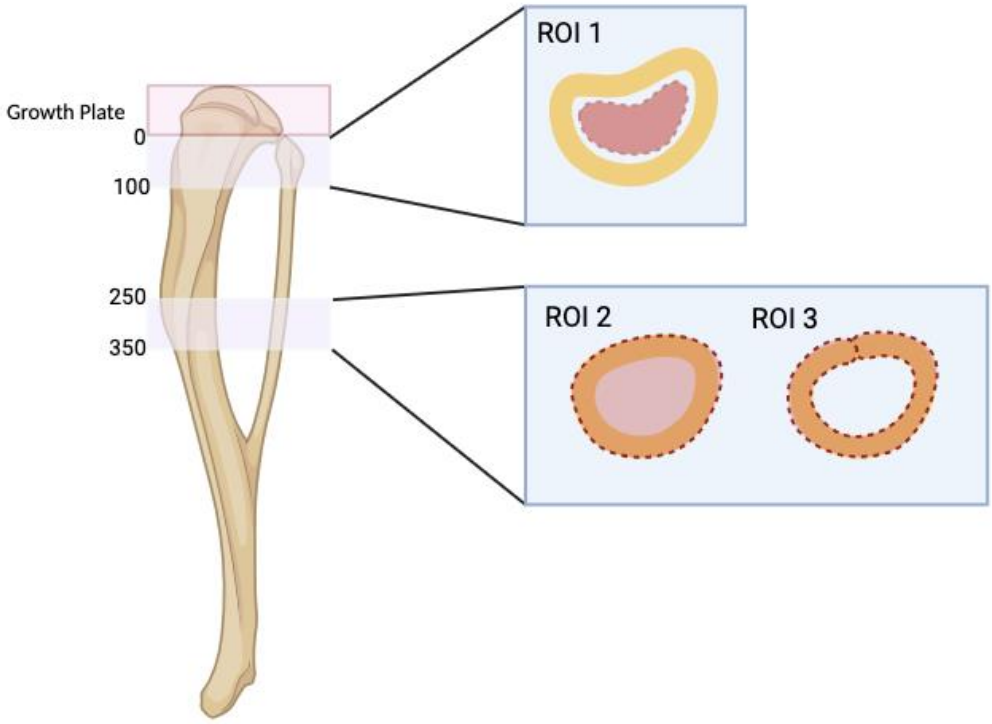


Figure 2.2 Systematic diagram of the ROIs for analysing murine tibiae bone parameters.
For analysis of trabecular bone, regions of interest (ROI) were drawn around the trabecular bone for 100 slices below the tibia growth plate (ROI 1). Analysis of cortical bone required two ROIs, which began 250 slices below the growth plate and continued for 100 slices. ROI 2 included the cortical bone and trabecular bone. ROI 3 surrounded the cortical bone and excluded the trabecular bone. Diagram created using biorender.com

2.3 Ex vivo tissue processing and Staining

2.3.1 Decalcification and Paraffin Embedding

Following fixation, the tibia which did not undergo μCT scanning was washed in PBS and moved into 10 times sample volume of 10% w/v ethylenediaminetetraacetic acid (EDTA; cat: T4174; Sigma-Aldrich) diluted in ultra-pure water and buffered to a pH of 7.4 using NaOH (cat: 221465; Sigma-Aldrich)[388,389]. Tibias were decalcified in EDTA for 3-weeks under constant agitation, changing the EDTA solution daily.

Once the tibias are completely decalcified (measured using μ-CT analysis), bones were dehydrated by being moved through beakers containing 10 times volume of rising concentration of ethanol (70%, 95%, 95%, 100%, 100%, 100%), for 1 hour per concentration. Following dehydration, samples were moved into 10 times sample volume of xylene for 2 hours with a change to fresh xylene after 1 hour. Samples were placed in 60°C paraffin wax for an hour to allow infiltration into the tissue. To embed the bone, a coating of paraffin (cat: 3801360, Leica) was placed on the bottom of a tissue mould (cat: 380380, Leica) and the tibia was placed flat in the paraffin layer. A tissue cassette (cat: EAD-02, CellPath) was placed inverted on the top of the mold and was filled with paraffin. Paraffin was then allowed to harden on a cold block for 1 hr and left in the fridge overnight before sectioning.

2.3.2 Sectioning

To section, paraffin blocks were placed on ice for 10 minutes before sectioning. The cassette was placed in the holder of a HistoCore MULTICUT Semi-Automated Rotary Microtome (cat:149MULTI0C1; Leica). Feather R35 microtome blades (cat: JDA-0300-00A, Cell Path, Newtown, Mid Wales) were used to trim blocks at 10μm until the bone could be

seen, at which point the microtome was changed to section at 4µm per section taking sections from half-way through the tibia. Sections were then transferred into a water bath set at 40°C (cat: HI1210, Leica) and placed on X-tra ADHESIVE slide (cat: 3800050; Leica). Slides were baked in a high-capacity section dryer (cat: JAX-0400-00A; Cell Path) set at 60°C for at least 1 hour to bake the sections onto the slide and stored until staining.

2.4 Tissue Histomorphometry

Slides were deparaffinised using Xylene (cat: 28975.325; VWR), followed by rehydration in decreasing concentrations of ethanol (100%, 90%, 80%, 70%; cat: 20821; VWR) and finished with two washes with de-ionised water (diH20).

2.4.1 Haematoxylin and Eosin (H&E)

For analysis of osteoblast numbers[390], rehydrated tissues stained with haematoxylin solution (cat: PRC-R51, Pioneer Research Chemicals) for 3 mins, followed by a wash in running tap water for 5 minutes. Tissue sections were differentiated in 1% acid alcohol (cat: PRC-R75, Pioneer Research Chemicals) for 30 seconds and washed in running tap water for 1 minute. Sections were placed in 0.2% ammonia water (cat: 09859, Sigma), for 1 minute and washed in running tap water for a further 5 minutes and rinsed in 95% alcohol. Sections were then counterstain in eosin (aqueous) (cat: PRC-661, Pioneer Research Chemicals) for 5 minutes.

Sections were dehydrated in increasing concentrations of ethanol (70%, 95%, 95%, 100%) for 2 minutes each and two times xylene for 5 minutes and 2 minutes. Samples were allowed to dry for 2 minutes and mounted using DPX mounting solution (cat: SEA-1304-00A)

and covered in a coverslip (cat: 631-0146, VWR). Slides were imaged using the slide scanner axioscan Z1 (ZEISS, Cambridge, UK) and stored as .Zen files.

For analysis osteoblast number, samples were manually analysed by drawing a ROI around the trabecular bone in the diaphysis, which was measured using ImageJ. Areas lined with osteoblasts, identified as cuboidal cells on the bone surface, were measured using the same imagej tool, converted to percentage of osteoblast coverage over total area, and presented as percentage bone osteoblast coverage (Ob.S/BS)[391].

2.4.2 Sirius red staining

For analysis of osteoid deposition[392], rehydrated slides were stained with 0.04% Fast Green (cat: F7252-5G, Sigma) for 30 minutes before being rinsed in running water for 1 minute. Sections were then stained with 0.1% Sirius red (cat: 365548, Sigma) dissolved in picric acid (0.18M, cat: P6744, Sigma) for a total of 1hr. Sections were rinsed in water for 5 mins. Sections were dehydrated as described in section 2.4.1. Slides were imaged using the slide scanner axioscan Z1 (ZEISS, Cambridge, UK) and stored as .Zen files.

For analysis osteoid, samples were manually analysed by drawing a ROI around the trabecular bone in the diaphysis, which was measured using ImageJ. Areas positive for osteoid were measured using the same imagej tool, converted to percentage of osteoid coverage over total area , and expressed as percentage of osteoid compared to trabecular bone surface area (OB/OS)[391].

2.4.3 Tartrate resistant acid phosphatase (TRAP)

Osteoclasts number in each section was analysed using, tartrate-resistant acidic phosphatase (TRAP)[393] staining. TRAP basic incubation medium was made using sodium acetate anhydrous (0.11mM, cat: 10236; VWR), L+ Tartaric acid (0.074mM, cat: 137855000; Fisher Scientific) and glacial acetic acid (2%, cat: 1005706; Sigma-Aldrich) to deionised water (diH2O). Make TRAP staining solution, 98% (V/V) TRAP basic incubation mix; 1.6M Fast Red Violet LB salt (cat:F3381; Sigma-Aldrich); and 2% (V/V) of Naphthol AS-MX phosphate substrate mix (58mM Naphthol AS-MX (cat: N4875; Sigma-Aldrich) in 2- ethoxyethanol (cat: 16100; Alfa Aesar, Lancashire, UK)). TRAP staining solution was warmed at 37°C on the digital orbital shaker (Heathrow Scientific; Illinois, USA). Deparaffinised slides were incubated in TRAP staining solution for 30 minutes at 37°C and mounted using immu-mount (cat: 1900331; Fisher Scientific) and covered with a coverslip (cat: 631-0146, VWR). Slides were imaged using the slide scanner axioscan Z1 (ZEISS, Cambridge, UK) and stored as .Zen files.

For analysis of tibias, samples were manually analysed by drawing a ROI around the trabecular bone in the diaphysis, which was measured using ImageJ. TRAP positive osteoclasts were counted manually as using the ImageJ cell counter plugin, normalised to the area of the ROI, and expressed as osteoclasts/mm^2[391].

2.5 Ex vivo metatarsal culture

Hind limbs from embryonic day (E)14.5-15.5 mice were removed, and metatarsals dissected under a dissection microscope in a-MEM (Sigma-Aldrich) diluted 1:13 with sterile PBS, plus 2 mg/ml BSA[361]. The metatarsals were cultured in a-MEM, supplemented with 2 mM L-glutamine, 100 mg/ml streptomycin, 100 U/ml penicillin, 0.2% BSA, 5 mg/ml L-ascorbic

acid and 1 mM b-glycerol phosphate (all from Sigma-Aldrich) for 5 days prior to the start of the experiment. Subsequently, metatarsals were treated ± PEPITEM alone, with IgG1 or anti-NCAM-1 antibody. Metatarsals were imaged every other day and data expressed as increase in mineralisation zone in μm.

2.6 Murine Osteoblast Cell Culture

Murine (primary and cell line) osteoblasts were cultured in basal proliferative media (Table 2.1) or osteoblastogenic culturing media (Table 2.2).

Table 2.1 **Murine basal media**

Reagent	Concentration	Company	Catalogue Number
a- MEM1*	90%	Sigma-Aldrich	M8042
L-Glutamine	2mM	Sigma-Aldrich	G1146
Streptomycin	100ul/ml	Sigma-Aldrich	G1146
Penicillin	100U/ml	Sigma-Aldrich	G1146
Foetal Bovine Serum	10%	Biosera	FB1001

[1]Minimum Essential Medium Eagle. *For ST2 cell culture replace with RPMI-1640, Sigma-Aldrich (Cat: R0883)

Table 2.2 **Murine osteogenic media**

Reagent	Concentration	Company	Catalogue Number
Murine Basal Media	100%	N/A	N/A
b- Glycerol Phosphate	10nM	Sigma-Aldrich	G9422
L-Ascorbic Acid	50ug/ml	Sigma-Aldrich	A5960

2.6.1 Murine Calvaria Osteoblast Isolation

Calvarial osteoblasts (C.Ob) were isolated following a previously described procedure[394]. C56Bl/6 WT mouse pups were culled via decapitation postnatal day (p)3-5, heads were washed briefly in 70% ethanol and kept hydrated in murine basal media (Table 2.1) without FBS. The skin was separated from the calvaria using forceps, the calvaria were

dissected and cleaned of any residual tissue and washed in murine basal media without FBS. Calvaria added to 1.5ml per calvaria of non-FBS basal media (Table 2.1) and 1mg/ml of collagenase d (cat: COLLD-RO; Merck, Feltham, UK) at 37°C for 10 minutes whilst shaking. The calvaria filtered out of from the supernatant and washed in non-FBS basal media. The collagenase step was then repeated for a further 30 minutes. After 30 minutes the supernatants were collected and stored on ice. The calvaria were then washed and incubated in a- MEM and 5mM EDTA for 10 minutes at 37°C. Supernatants were collected and stored on ice. Calvaria were washed for a final time and incubated in 1.5ml per calvaria of non-FBS basal media (Table 2.1) and 1mg/ml of collagenase d for 30 minutes. The supernatant was then filtered and stored on ice. Supernatants were centrifuged at 400g for 5 minutes, media removed, and cells resuspended in murine basal media (Table 2.1), and incubated at 37°C, 5% CO2. The media was changed within 5-24 hours to remove non-adhered and contaminated cells, following this media was changed every 2 days. Primary C.Obs were used at P1 or frozen down and stored in liquid nitrogen storage for future analysis (Section 2.6.3).

2.6.2 Detachment of cells

Cells were detached from flasks using 2X Trypsin-EDTA (1g/L porcine trypsin and 400mg/L EDTA, cat: T4717; Sigma-Aldrich) diluted (1:5) in sterile PBS and incubated at 37°C for 3 minutes. Trypsin was neutralised (1:2) using the appropriate basal media dependent on cell type, cells were then centrifuged at 400g for 5 minutes. Media was eluted from the cell pellet and the cells were resuspended in 1ml of basal media and counted using a

haemocytometer. Cells were diluted to the desired concentration for experimental plating or split 1:4 for expansion.

2.6.3 Freezing and storage of cells

For long term storage, trypsinised cells were centrifuged (Section 2.6.2) and all media was removed. Cell pellet was resuspended in 20% dimethyl sulfoxide (DMSO, cat: D2650; Sigma-Aldrich) and 80% cell type appropriate basal media. 1.5ml cryovials (cat: 122280; Greiner Bio-one, Kremsmünster, Austria) were filled with 500ml of 80% FBS and 20% cell type appropriate basal media. The cryovial was then slowly filled with 500ml of cell suspension. The cryovials were then transferred into a freezing container (cat: C1562, Sigma-Aldrich) and placed in -80°C freezer for 24 hours allowing for gradual freezing. Once frozen cryovials were transferred to liquid nitrogen storage.

2.6.4 Osteoblast cell lines

Murine ST2 cells, a bone marrow derived stromal clone cell line (provided by Dr James Edwards, University of Oxford, UK), were brought up from liquid nitrogen at passage (P) 3-6. Cells were thawed by gentle heating at 37°C in a water bath for 30 seconds. Once thawed cells were added to 10ml of basal media (Table 2.1) warmed to 37°C and centrifuged at 400g for 4 minutes. Supernatant discarded and cells were resuspended in 10ml of 37°C basal media and moved to a p75 flask (Corning, USA) and cultured at 37°C, 5% CO2 in basal media until 80% confluent, media changed every 2 days.

2.6.5 Self-Structuring Bone Model (SSBM) Culture

2.6.5.1 Human Osteoblast Cell line (hFOb 1.19) Culture

Human osteoblast cell line (hFOb 1.19) from American Type Culture Collection (ATCC, USA) were cultured in basal media (*Table 2.3*). Cells were cultured at 33.5°C, 5% CO_2 and passaged to P10 before use in SSBM[377].

Table 2.3 hFOb 1.19 basal culture media

Reagent	Concentration	Company	Catalogue Number
DMEM/F-12, no phenol red	90%	Fisher scientific	21041025
G418	0.3 mg/ml	Sigma-Aldrich	4727878001
Foetal Bovine Serum	10%	Biosera	FB1001

Table 2.4 hFOb 1.19 osteogenic culture media

Reagent	Concentration	Company	Catalogue Number
Basal culture media	N/A	N/A	N/A
Menadione	10-8M	Sigma-Aldrich	M5625
Ascorbic acid	100µg/ml	Sigma-Aldrich	A5960

2.6.5.2 Anchor and plate preparation

Anchors and plates prepared at least 5 days before making constructs. Anchor mold created using method in Finlay et al[377]. Anchors were made using 1.25 ± 0.005 g of beta-tricalcium phosphate (β-TCP) (Plasma Biotal Limited., Tideswell, UK) and 1ml 3.5 M orthophosphoric acid (23.2ml Orthophosphoric acid (85-90% purity) (cat no.: 20624.262; supplier: VWR Chemicals, Leicestershire, UK); 76.8ml diH2O). Solution mixed quickly with a metal spatula on ice. Paste scrapped into anchor mold and one pin per anchor (cat no.: 26002-20; supplier: InterFocus Ltd., Linton, UK). Anchors allowed to set for 5 days before removal from mold and store at room temperature till needed.

Plates made using the Sylgard 184 silicone elastomer kit by mixing 10 ± 0.1 g of the base component and 1.0 ± 0.1 g of the curing component (Cat no.: 634165S; supplier: VWR). 1.5ml of elastomer mixture per well in a 6-well plate (Cat no.: CLS3516; supplier: Corning, Flintshire, UK) and left on a flat surface with the lid on the plate at room temperature for 5 days. After the anchors and plates have set two anchor pins inserted into the elastomer plate 1.5cm a part per well as described in[377] shown in Figure 2.2.

2.6.5.3 Fibrin hydrogel and plate set up

Fibrinogen solution made using 100mg Fibrinogen (cat no.: F8630; supplier: Sigma-Aldrich, Gillingham, UK) in 5ml Ham's F-12K (Kaighn's) Medium (F-12K medium) (cat no.: 21127-022; supplier: Fisher Scientific), mixture incubated in a water bath at 37°C for 1hr with gentle agitation every 15 minutes[377]. Once dissolved stored at -20°C or used instantly. Thrombin solution (for one plate) made up using 162.5ml Thrombin (200 U/mL, cat no.: 605157 – 1KU; supplier: Sigma-Aldrich) diluted in 0.1% BSA (cat no.: A8806-5g; supplier: Sigma-Aldrich), 6.5ml Aminohexanoic acid (200 mM in PBS, cat no.: 07260-10g; supplier: Sigma-Aldrich), 6.5ml aprotinin (10 mg/mL in PBS, cat no.: A4529-10mg; supplier: Sigma-Aldrich) and 3074.5ml basal media[377] (Table 2.3).

Construct plates sterilised using 70% ethanol spray and allowed too completely dry (aprox. 10 minutes). 500ml of thrombin solution added per well and manipulated to cover entire well, avoiding interaction with the well wall. 200ml of fibrinogen added and mixed with the thrombin solution[377]. Plates incubated at 37 °C for 20-30 min to allow for polymerisation. Once polymerised hFOb seeded into plate at $2.5x10^5$ per well in 3ml of basal media (Table 2.3).

2.6.5.4 Construct maintenance and treatments

24hr after seeding fibrin hydrogen detached from well walls using a P1000 pipette tip. 1.5ml of media removed and replaced from each well every 3-4 days. For 8-day treatments 10ng/ml PEPITEM (sequence SVTEQGAELSNEER; Cambridge Biosynth Limited; Cambridge, UK), 1ng/ml QGA (sequence QGA; Cambridge Biosynth Limited; Cambridge, UK), 1ng/ml SVT(sequence SVT; Cambridge Biosynth Limited; Cambridge, UK) or 1ng/ml tvs (sequence tvs; Cambridge Biosynth Limited; Cambridge, UK) cells treated every 3-4 days for 8 days.

Constructs isolated one day before collection to avoid interference of secretome from 2D osteoblast on well surface[377]. Scalpel used to cut the elastomer and isolate the construct[377]. Constructs moved into new plate and media replaced and treated with treatments as described above. On day of collection media collected and stored in -80 before use in ELISA (section 2.6.7.2 & 2.6.7.3). For mineral analysis constructs were fixed in 10% buffered formaldehyde (cat: HT5011; Sigma-Aldrich,) for 4hr at 4°C. Constructs washed after 4hr and stored in PBS at 4 °C before alizarin red staining (Section 2.6.7.4). For RNA extraction constructs were isolated and for RNA extraction preparation constructs were unhooked from anchors and placed in 2mL RNAse-free Eppendorf tubes containing glass beads and 600ml 10% β- mercaptoethanol (v/v) (cat no.: M6250; supplier: Sigma) RLT buffer after which each sample was vortexed for 1-2mins then shredded using a 5ml syringe (cat no.: 15295083; supplier: Fisher Scientific) along with, initially, a 16G needle (cat no.: 11532445; supplier: Fisher Scientific), followed by a 19G needle (cat no.: 15341537; supplier: Fisher scientific). Samples then underwent the same protocol as described in (Section 2.7.1).

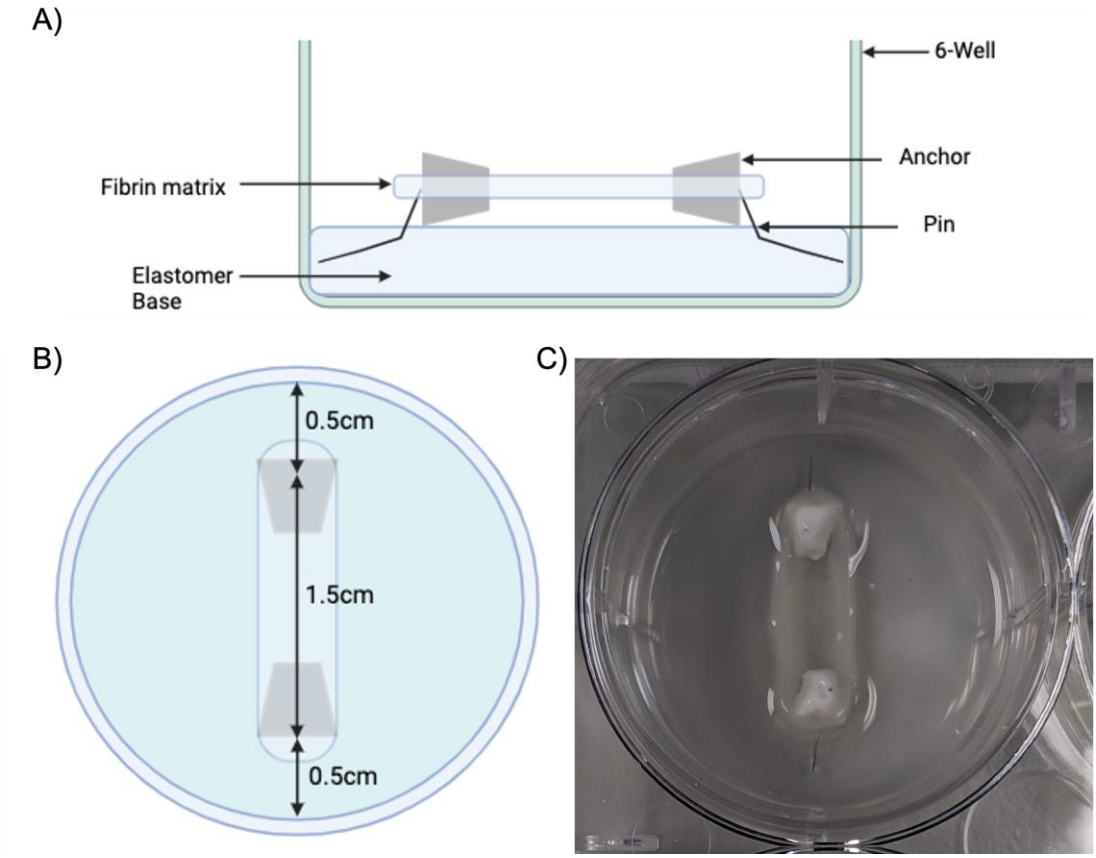


Figure 2.3 **Diagram of Self-Structuring Bone Model (SSBM).** (A-B) Diagrams of SSBM model from a (A) side profile and (B) birds eye view, showing the positioning of the anchors within the elastomer base and how the fibrin matrix forms around the anchors. (C) Representative image of SSBM construct at 4-weeks in culture. Diagram created using biorender.com

2.6.6 Induction of osteoblast mineralisation

C.Ob and ST2 were detached from flask as previously described (Section 2.6.2). Once released cells were counted using a haemocytometer and seeded into 48 well plates ($10x10^3$ cells/well) and cultured in basal or osteoblastogenic media. After 24 hours cells were treated with or without peptide treatments described in (Table 2.5) or 0.125-1μM S1P (cat: S9666; Sigma-Aldrich). Cells were incubated up to 21 days at 37°C and 5% CO_2. Media and treatment

were changed every 2 days. Maturation was assessed using alkaline phosphatase assay (Section 2.6.7.1) or alizarin red staining (Section 2.6.7.4).

Table 2.5 **Peptides used for *in vitro* and *in vivo* assays**

Peptide ID	Peptide sequence	Working concentration	Application
PEPITEM	SVTEQGAELSNEER	10ng/ml	ALP, SSBM, ELISA & Ex-vivo models
Control Peptide	EQAERYDDMAACMK	10ng/ml	ALP, SSBM, ELISA & Ex-vivo models
Alanine Substitution	AVTEQAAELSNEER	10ng/ml	ALP, ELISA
Alanine Substitution	SVTAQGAELSNEER	10ng/ml	ALP, ELISA
Alanine Substitution	SVAEAGAELSNEER	10ng/ml	ALP, ELISA
Alanine Substitution	SVTEQGAEISAEEA	10ng/ml	ALP, ELISA
Alanine Substitution	AVTEQGAELANEEA	10ng/ml	ALP, ELISA
PEPITEM Fragment	SVTEQGA	5ng/ml	ALP, ELISA
PEPITEM Fragment	LSNEER	5ng/ml	ALP, ELISA
PEPITEM Trimer (SVT)	SVT	0.1-10ng/ml	ALP, SSBM, ELISA & Ex-vivo models
PEPITEM Trimer (QGA)	QGA	0.1-10ng/ml	ALP, SSBM, ELISA & Ex-vivo models
SVT Memetic	SVT[NH-Ethyl]	2ng/ml	ALP, ELISA
SVT Memetic	Tvs	0.1-10ng/ml	ALP, SSBM, ELISA & Ex-vivo models
QGA Memetic	[pGlu]-GA	2ng/ml	ALP, ELISA
QGA Memetic	aGq	2ng/ml	ALP, ELISA

2.6.7 Measures of osteoblast maturation and function

2.6.7.1 Alkaline phosphatase assay

Alkaline phosphatase activity was assessed at two time points unless stated otherwise, on day 4 and day 8 after treatment. Media was removed and cells were washed in PBS. Cells were lysed using 100ml/well RIPA buffer (cat: R0278; Sigma-Aldrich) and left on ice for 30 minutes[395,396]. A cell scraper was used to harvest and further lyse the cells, which were then transferred into an Eppendorf tube and centrifuged at 13000g for 10 minutes. Cell

lysates were added to room temperature alkaline phosphatase yellow (pNPP) liquid substrate ELISA (cat: P7998; Sigma-Aldrich) at a 1:4 ratio in a 96-well plate[397]. The plate was wrapped in foil and incubated at 37°C in an incubated shaker (SciQuip, Shropshire, UK) for 30-45 minutes. Following incubation, the ELISA was quantified using a synergy HT plate reader at 405nm absorbance, plate then ran at 540nm, which was subtracted as a wavelength control. Data presented as percentage of differentiated control.

2.6.7.2 Osteoprotegerin ELISA

Osteoprotegerin (OPG) ELISA (Mouse, cat: MOP00, R&D systems) (Human, cat: DY805, R&D systems) was carried out per manufacturer's instructions. The samples tested were osteoblast or SSBM supernatants treated with or without peptide treatments detailed in (Table 2.5). Human OPG plate coated with human OPG capture antibody, 24hr and blocked with 1% BSA for 1hr before use. Murine osteoblast supernatants were diluted 1:50 and SSBM supernatants were diluted 1:20. The 50 μl assay dilutant and 50 μl of standard, control or cell supernatant sample were added to the provided 96 well microplate coated with monoclonal mouse OPG antibody or 100ml of standard or sample into coated human OPG 96 well plate and incubated for 2 hours at RT in the dark. Following incubation wells were washed 5 times using the provided wash buffer and 100ml of OPG Conjugate was added to each well and incubated for a further 2 hours at RT. The washing step was repeated at 100μl of substrate solution was added to each well and incubated at RT protected from light for 20-30minutes. After 20-30 minutes 100μl of stop, solution was added to each well. The plate was then read at 405nm using a synergy HT plate reader. A standard curve was created by measuring the absorbance of OPG standard from 0 – 2000 pg/ml. The standard curve equation was used to

calculate the concentration of OPG within each sample. Data were expressed as concentration (pg/ml) of OPG in each well or as a percentage compared to the differentiated untreated control.

2.6.7.3 Pro-collagen type I alpha 1 ELISA

Human pro-collagen type I alpha 1 ELISA (Human, cat: DY6220, R&D systems) was carried out per manufacturer's instructions. The samples tested were SSBM supernatants treated with or without peptide treatments detailed in (Table 2.5). 96-well plate was coated with the diluted capture antibody 100 µl overnight. Capture antibody removed and plate wash in wash buffer before blocking in 200 µl of 1% BSA for 1hr. SSBM supernatants were diluted 1:50. 100ml of standards (made up using serial dilution) or sample into coated 96 well plate and incubated for 2 hours at RT in the dark. Following incubation wells were washed 5 times using the provided wash buffer and 100ml of detection antibody was added to each well and incubated for a further 2 hours at RT. Wash step repeated and 100 µl of diluted Streptavidin-HRP to each well incubated for 20 minutes at room temperature. The washing step was repeated at 100ml of substrate solution was added to each well and incubated at RT protected from light for 20 minutes. After 20 minutes 100 µl of stop, solution was added to each well. The plate was then read at 405nm using a synergy HT plate reader. A standard curve was created by measuring the absorbance of standard from 0 – 2000 pg/ml. The standard curve equation was used to calculate the concentration of pro-collagen type I alpha 1 within each sample. Data were expressed as concentration (pg/ml) of pro-collagen type I alpha 1 in each well.

2.6.7.4 Alizarin red staining

The alizarin red standard was prepared via serial dilution. 100mL of 40mM ARS (ScienCell, Cat. 8678a) was added to 900 μl standard dilution solution (Cat. 8678d) to make 1 ml of 4mM ARS. 500 μl of standard dilution solution was added to eight 1.5 μl Eppendorf tubes. 500 μl of 4mM ARS was added to the first Eppendorf, and 500mL of the latter solution was added to the next Eppendorf. This step was repeated until the final Eppendorf, which remained as a blank control. 150 μl of each ARS standard was pipetted in triplicate into a 96-well plate.

PBS or media was removed from fixed constructs (2.6.5.4) or cells from the wells and wells were washed three times with diH_2O. For 2D cultures in 6-well plates, 1 ml alizarin red stain (ARS) was added directly to cells and incubated at RT for 30 minutes. Constructs were detached from anchors and placed in 12-well plates. 1ml ARS was added to each well and plate was placed on an orbital shaker for 24 hours at room temperature. Dye was removed and wells were washed with diH2O until the stain was completely removed. Once the plate was completely clear, 2D cell culture wells were scraped to removed stain or constructs were dissected into 3-5mm fragments. After which 800mL of 10% acetic acid (ScienCell, Cat. 8678b) was added to each well and plate was incubated at room temperature on a rocking incubator for 2 hours. Samples and liquid were transferred to separate 2 ml Eppendorf tubes. Each Eppendorf was vortexed for 30 seconds. Tubes were sealed with parafilm and heated for 10 minutes at 85°C. After 10 minutes, the samples were incubated on ice for 5 minutes then centrifuged at 20000g for 15 minutes. 500mL of each supernatant was added to 1.5 ml Eppendorf tubes along with 500 ml of 10% ammonium hydroxide (ScienCell, Cat.8678c). 150 μl of each neutralised solution was pipetted in triplicate into the empty wells of the 96-well

plate containing previously made standards. The plate was read by a Synergy HT plate reader at 405nm. Each sample was run in technical replicates (n = 3) from which a mean was calculated. A standard curve was generated in Excel using the alizarin red standard from concentrations 0 mM to 2 mM. Once the equation of the standard curve was generated the unknown concentrations of the alizarin red was calculated. Data was expressed as the percentage of Alizarin red stain relative to the control.

2.6.8 Identification of downstream PEPITEM signalling

Table 2.6 Antibodies used for immunofluorescence, neutralisation and western blotting

Antibodies	Manufacture	Catalogue number	Dilution
Anti-Cadherin-15 Antibody, clone: 12G4	Sigma-Aldrich	Cat: 05-852	10µg/ml (NEU)
Anti-NCAM-1 Antibody, clone: MEM-188	Thermo Fisher Scientific	Cat: MA1-19129	3µg/ml (NEU)
Rabbit IgG1 Isotype Control Antibody	Invitrogen	Cat: 02-6102	3µg/ml (NEU)
Anti-RANKL Antibody, clone: 3F2E1	Proteintech	Cat: 66610-1-Ig	1:3000 (WB)
Anti-OPG polyclonal Antibody	Bio-Techne	Cat: AF459-SP	1:3000 (WB)
Anti-β-actin polyclonal Antibody	Sigma-Aldrich	Cat: A2066	1:1000 (WB)
Goat Anti-Mouse IgG HRP-conjugated Antibody	Bio-Rad	Cat: 1706516	1:3000 (WB)
Goat Anti-Rabbit IgG HRP-conjugated Antibody	Merck Millipore	Cat: 401393	1:1000 (WB)
Anti-β-catenin polyclonal Antibody	Merck Millipore	Cat: 06-734	4 µg/ml (IHC)
Donkey Anti-Goat IgG 647-conjugated Antibody	Thermo Fisher Scientific	Cat: A21447	5µg/ml (IHC)
Goat anti-Rat IgG 546-conjugated Antibody	Thermo Fisher Scientific	Cat: A11081	1:2000 (IHC)
Goat anti-Rabbit IgG 488-conjugated Antibody	Thermo Fisher Scientific	Cat: A11034	1:4000 (WB)
NCAM-1 primary antibody, Polyclonal Goat IgG	Bio-techne	Cat: AF2408	10 µg/ml (IHC)

Anti-RUNX2 Antibody, clone: 232902	Bio-Techne	Cat: MAB2006-SP	10 mg/mL (IHC)
Rabbit Non-phospho (Active) β-Catenin (Ser33/37/Thr41) (D13A1) Antibody	Cell Signalling	Cat: 8814T	1:10000 (WB)

2.6.8.1 Sphingosine-1-phosphate kinase inhibition

SphK1 and SphK2 inhibitors CAY10621 (SphK1, cat; 13371, Cayman Chemicals), SLM-60314340-hydrochloride (SphK2, cat; 6281/10, R&D Systems) and N,N-Dimethylsphingosine (d18:1) (SphK1&2, cat; 62575, Cayman Chemicals) were applied to ST2 cells at varying concentrations to determine an appropriate concentration. Optimal concentrations were determined to be 5 mM, 1.12 mM and 3 mM respectively and were used in all subsequent assays.

ST2 cells were seeded into 48 well plates ($10x10^3$ cells/well) and cultured 10ng/ml non-pegylated PEPITEM (sequence: SVTEQGAELSNEER , Cambridge Biosciences) in the presence of one of the three kinase inhibitors, for osteoblast differentiation. For osteoblast function, cells were treated with or without PEPITEM for 2 days. On the third day cells were treated with SphK1 and SphK2 inhibitors for 24 hours. Maturation of osteoblasts was assessed using alkaline phosphatase assay (Section 2.6.7.1) following 4 day treatment and data were presented as a percentage change from untreated differentiated control. Cell viability was assessed using trypan blue staining following 4 days of treatment. Cells were detached from well (Section 2.6.2) and mixed with equal parts trypan blue, cell suspension mixture was then counted using a haemocytometer. Ratio of stained and unstained cells were counted, and percentage of dead cells was calculated. The 24hr treatment group, was used for media collection for media transfer.

2.6.8.2 Brefeldin-A Golgi stop treatment

ST2 cells were seeded in 48 well plates ($10x10^3$ cells/well) with or without 10 ng/ml non-PEG PEPITEM in the presence of 10nM of Brefeldin-A (cat: B6542-5MG, Sigma-Aldrich)[398] for 4 days. Maturation was assessed using ALP assay (Section 2.6.7.1) for the 10 nM Brefeldin-A treated cells. Alternatively, cells were treated with PEPITEM for 3 days after which they received 5 mM of Brefeldin-A for 1 hour. Media was collected from cells following 1 hour Brefeldin-A treatment to be used for future media transfer experiments (Section 2.9.2).

2.6.8.3 Cdh15 activation

C.Obs were plated at seeded into 48 well plates ($10x10^3$ cells/well) and cultured in basal or osteoblastogenic media. After 24 hours cells were treated with or without 100ng/ml non-pegylated PEPITEM (sequence: SVTEQGAELSNEER, Cambridge Bioscience), 10µg/ml Anti-Cadherin-15 antibody (cat: 05-852; Sigma-Aldrich) or IgG1 control. Cells were incubated for 8 days at 37°C and 5% CO_2. Media and treatment were changed every 2 days. Maturation was assessed using alkaline phosphatase assay (Section 2.6.7.1).

2.6.8.4 Co-Immunoprecipitation and Mass Spectrometry Identification:

2.6.8.4.1 Treatment and protein extraction

Calvaria Osteoblasts grown to 75% confluency in T75 flask in basal media (Table 2.1). Once confluent cells were moved into osteoblastogenic media (Table 2.2) for 24hr, followed by x4 wash in PBS. Cells were then moved into FBS free media with 0.1mg BSA with or without 3 µg/ml biotinylated PEPITEM (Cambridge Bioscience) or biotinylated control peptide 1, for

4hr in 4°C. Media was then removed, and cells were washed in cold PBS. Cells were then washed in 1.5 ml of cold triton phosphate lysis buffer (50 mM Tris-HCL pH 7.5, 150 mM NaCl, 1% Triton X100, protease and phosphatase inhibitor). Cells were then lysed further through scraping after 10mins and move to Eppendorf put on ice and left for 30 minutes. After 30 minutes, lysates were collected and centrifuged 20 minutes at 600 g at 4°C and the supernatant collected. Samples stored in -80 for future use.

2.6.8.4.2 Streptavidin Column collection

Pierce™ High Capacity Streptavidin Chromatography Cartridges (Thermofisher Scientific, cat: 87739) were used to separate out proteins bound to biotinylated PEPITEM or control peptide. Streptavidin columns were equilibrated with triton phosphate lysis buffer (50 mM Tris-HCL pH 7.5, 150 mM NaCl, 1% Triton X100, Protease and phosphatase inhibitor), at a flow rate of 0.5-2ml/minute. Samples were then passed through the column at a flow rate of 0.5-1 ml/minute, fractions were collected. Column washed x5 with triton phosphate lysis buffer. Bound proteins were then eluted using 50% ACN with 1% TFA, fractions collected. Fractions containing the eluted proteins were then dried in a vacuum centrifuge overnight. Samples resuspended in 8M urea/2% SDS.

2.6.8.4.3 Western and Mass Spectrometry

Following resuspension 20µl of sample was added to 5 µl of SDS laemelli buffer (Bio-Rad, Cat; 1610737) and heated at 95°C for 10mins. Samples were then loaded into 4-12% gels (Nu-Page, cat; NP0326BOX). Proteins were separated using a 100V current PowerPac Basic Power supply (cat: 1645050; BioRad) for 90 minutes. Following protein separation gels were removed and stained with Bio-Safeä Coomassie stain (cat: 1610786, BioRad) for 1hour

room temperature with shaking. The gel was washed x4 in PBS, bands from each sample run were cut and stored in PBS. Samples were then sent for peptide identification, performed by the functional genomics and proteomics laboratories (School of Biosciences, University of Birmingham, UK).

Briefly, trypsin digested samples (%10mg of protein) were incubated in 100 mM ammonium bicarbonate (pH 8) and 10 mM dithiothreitol for 30 min at 56o C. Cooled samples were incubated at room temperature in 50mM iodoacetamide for 30 min, prior to addition of trypsin gold (6 ng/mL; Promega, Southampton, Hampshire, UK) and incubation 37o C overnight. Peptide concentration and separation was performed using UltiMate 3000 HPLC series (Dionex, Sunnyvale, CA USA). Samples were added to precolumn (Thermo Scientific Acclaim PepMap 100 C18 HPLC Columns) and separated in Nano Series Standard Columns using a gradient of 3.2%–44% solvent B (0.1% formic acid in acetonitrile) for 30 min. Columns were washed with 90% mobile phase B, re-equilibrated with 3.2% mobile phase B and eluted directly (#350 nL/min) via a Triversa Nanomate nanospray source (Advion Biosciences, NY) into a QExactive HF Orbitrap mass spectrometer (ThermoFisher Scientific). Data were analysed using Uniprot database using Protein Discovery 2.2 software, Sequest HT algorithm (Thermo Fisher). Precursor mass tolerance was 10 ppm, and the MS/MS mass tolerance was 0.02 Da. Data were filtered with a false discovery rate of 0.01, and proteins with at least two high confidence peptides were accepted as a real hit. Quality control screening was performed on protein/peptide hits to remove expected contaminants and also hits that appeared in both control peptide and PEPITEM samples. The remaining potential PEPITEM binding partners were initially ranked using Sequest score and subsequently filtered based on an isoelectric point score of 4–7 corresponding to proteins associated with the plasma

membrane. Extensive literature analysis was performed on the top 10 binding partners looking for specific roles in bone biology.

2.6.8.5 Immunohistochemical staining of cultured cells

C.Obs were seeded onto coverslips in 6 well plates ($8x10^3$ cells/well) and cultured in basal media for 24hr and treated with or without PEPITEM for differing lengths of time. Cell was then fixed in 10% buffered formaldehyde for 15 minutes at room temperature followed by three washes in PBS. NCAM-1 primary antibody (Bio-techne, cat;AF2408) was made up in PBS at 10 µg/ml. 100µl of the diluted primary antibody was added to the coverslips for 1hr at room temperature. Following incubation primary antibodies were removed and coverslips were washed three times in PBS. Secondary antibody (Thermofisher, cat; A21447) and diluted to 5µg/ml, 100 µl of solution was added per coverslip and incubated for 40mins at room temperature in the dark. Antibodies were removed and coverslips were washed three times in PBS. Coverslips were then gently removed from the wells and tapped dry on paper towel to remove excess liquid. DAPI mounting media was then added onto slides and the coverslips were placed facedown into the mounting media. Slides were left to dry overnight and then moved to -20 for long term storage before imaging. Images were taken on Zeiss LSM 780 (Imaging Suite, University of Birmingham) and analysed using Zen Blue software (ZEISS).

2.6.8.6 β-catenin signalling

C.Obs seeded onto coverslips in 6 well plates ($1x10^4$ cells/well) were cultured in osteogenic media for 24h before treating with PEPITEM (10ng/ml, for up to 1h) or lithium chloride (20mM for 3 hour). Cells were fixed in 10% buffered formaldehyde for 15 minutes at

room temperature, followed by three washes in PBS. Samples were stained with a polyclonal β-catenin primary antibody (4 µg/ml in PBS, Merck, cat: 06-734) for 2 hours at room temperature. Coverslips were washed three times in PBS before incubation with secondary antibody (1:4000; ThermoFisher Scientific, cat: A11034) for 40min at room temperature in the dark. Coverslips were washed as described before being gently removed from the wells and excess liquid removed. Coverslips were mounted using DAPI mounting media (Invitrogen), dried overnight prior to storage at -20°C. Images were taken on a ZEISS LSM 780 confocal microscope and analysed using Zen Blue software (ZEISS). Using ImageJ FIJI software (v2.3.1/1.53f), masks were created for individual cells and their nuclei. Relative intensity was measured in both the whole cell and DAPI positive regions, DAPI measurements were then subtracted from the whole cell recordings. Data presented as average integrated density per nucleus

2.6.8.7 NCAM Neutralising Antibody

C.Obs were plated at seeded into 48 well plates ($10x10^3$ cells/well) and cultured in basal or osteoblastogenic media. After 24 hours cells were treated with or without 10 ng/ml non-pegylated PEPITEM (sequence: SVTEQGAELSNEER, Cambridge Bioscience), 3µg/ml Anti-NCAM-1 antibody (cat: MA119129; Thermo Fisher) or IgG1 control. Cells were incubated for 8-days at 37°C and 5% CO_2. Media and treatment were changed every 2 days. Maturation was assessed using alkaline phosphatase assay (Section 2.6.7.1).

2.6.8.8 Western Blotting

Cells were incubated in RIPA buffer (Sigma-Aldrich) for 30mins on ice, prior to storage at "80!C. Total protein was assessed using BCA assay (ThermoScientific) according to manufacturer's guidelines. Samples were diluted 1:5 with SDS Laemmli buffer (Bio-Rad, cat-1610737), heated at 95°C for 10min prior to loading into 10% gels (Nu-Page, cat - NP0326BOX). Proteins were separated using a 170V current PowerPac Basic Power supply (cat-1645050) for 50 min, then the gel was transferred on to a PVDF membrane using the Trans Blot Turbo mini 0.2 mm (cat-1704156) and Trans-Blo turbo transfer system (all from BioRad). Membranes were blocked with 5% milk (Marvel – Premier Foods, Ireland) diluted in PBS containing 1% TWEEN 20 (Sigma-Aldrich) for 1h under agitation, then incubated with the following primary antibodies diluted in 5% milk overnight at 4!C: anti-RANKL (1:3000, clone:3F2E1, Proteintech); anti-OPG polyclonal (1:3000, cat: AF459-SP Bio-techne); anti-NCAM-1 (1:1000 clone MEM-18, ThermoFisher Scientific); or anti-b-actin polyclonal (1:1000, cat:A2066, Sigma-Aldrich) or anti-none-phosphorylated b-catenin (1:10000, cat:8814T, Cell Signalling). Membranes were then washed with PBS-T and incubated with the relevant HRP-conjugated antibodies for 1hr: mouse, 1:3000, cat:1706516, BioRad) or rabbit (1:5000, cat:401393, Millipore). Membranes were washed as described and treated with Clarity Western Peroxide Reagent and Clarity Western Luminol/Enhancer Reagent 1:1 (cat: 1705061) prior to imaging using ChemiDOC MP Imaging System (both from BioRad). Band intensity was measured using ImageJ FIJI software.

2.7 Assessment of gene expression

2.7.1 RNA Extraction and cDNA Conversion

RNA extraction from C.Obs and hFOb 1.19 constructs was performed using the RNeasy kit (cat: 74104; Qiagen) following the manufacturer's instructions. For C.Obs, RLT buffer supplemented with 1% β-mercaptoethanol (cat:M6256; Sigma-Aldrich) was added to wells for 10 minutes before they were scraped. Samples were vortexed to further break up the cell suspension. For hFOb 1.19 constructs RNA lysis was performed as described in (section 2.6.5.4). From this point on Extract for both samples are the same. Cell suspensions were transferred to QIAshredder spin columns (cat no.: 79654; supplier: QIAGEN) and centrifuged for 2 minutes at 13000 rcf. Ethanol (70%) was added to the resulting supernatant of each sample and cells were transferred to RNA easy spin columns and spun for 2 minutes before addition of RW1 buffer was added to the top of the column and spun again. DNase incubation mix, constating of 1 part DNase to 7 parts Buffer RDD (cat: 79254; Qiagen) was added to samples for 15 minutes. RW1 was added, samples spun for 1 minute, washed with 500µl of RPE and spun for a further minute. RNAse free water (cat: 129112; Qiagen) was then added to the top of the filter and run through twice, each time spinning for 2 minutes. The RNA samples were then run on the NanoDrop™ One Microvolume UV-Vis Spectrophotometer (cat no.: ND-ONE-W; supplier: Fisher Scientific) to detect RNA concentration and quality.

mRNA from each sample was converted to cDNA using a high capacity cDNA reverse transcription kit as per the manufacturer's instructions (cat: LT-02241; Applied Biosystems, Cheshire, UK). A master mix was made up containing 1x RT buffer, 1x dNTP mix, 1x random primers and 50 units random primers. mRNA (500 ng) was added to 5.8 µl of master mix and nuclease free water (cat: 129114, Qiagen) was used to bring the total volume to 20 µl. Using

the mastercycler nexus GSX1 (Eppendorf), samples were heated to 25°C for 10 minutes, 37°C for 120 minutes and then 85°C for 5 minutes before being held at 4°C. Following conversion to cDNA, samples were stored at -20°C until required for polymerase chain reaction (PCR) analysis.

2.7.2 PCR

cDNA from Section 2.7.1 was diluted 1:4 in nuclease free water. Gene specific Applied Biosystems Assay on Demand TaqMan primers (Table 2.7) were diluted 1:10 in master mix (cat: 4369016; Applied Biosystems). Using a E1-Clip Tip Electronic Pipette (ThermoFisher), 2.3 µl/well of cDNA and 2.7 µl/well of the primer/master mix solution was added to each well of a 384 PCR Plate (cat: 04729749001; Roche, Hertfordshire, UK). Three technical repeats were conducted for each sample. The plate was sealed with an adhesive film (cat: 4311971; Applied Biosystems) and centrifuged at 1200rcf for 2 minutes at 20°C. The quantitative PCR was run on the CFX384 Touch real-time PCR system (cat no.: 1855484; supplier: Bio-Rad Laboratories, USA). The pre-programmed thermal cycling steps were as followed; samples initially heated to 50°C and held for 2 minutes, followed by heating to 95°C and holding for 10 minutes. Denaturing and annealing cycles of 95°C for 15 seconds, followed by cooling to 60°C for 1 minute were performed for a total of 40 cycles.

A mean of the three technical repeats was calculated to provide the average cycle threshold (CT) value. Any values greater than 1 SD different from the other two values, or >35 cycles were omitted from the average; sample discarded if the other two repeats were not within 1.5 cycles. The ΔCt value was calculated by subtracting the Ct value for the housekeeping gene (*B2M*) from the Ct value for the gene in question, $2^{-\Delta CT}$ was plotted graphically.

Table 2.7 **Taqman™ Primers used for qPCR**

Taqman™ Primers		
Ncam1 (Mm01149710_m1)	Thermo Fisher Scientific	Cat: 4331182
Alpl (Mm00475834_m1)	Thermo Fisher Scientific	Cat: 4331182
Col1a1 (Mm00801666_g1)	Thermo Fisher Scientific	Cat: 4331182
B2M (Hs99999907)	Thermo Fisher Scientific	Cat: 4369016
ALPL (Hs01029144)	Thermo Fisher Scientific	Cat: 4369016
BMP2 (Hs00165814)	Thermo Fisher Scientific	Cat: 4369016
RUNX2 (Hs00231692)	Thermo Fisher Scientific	Cat: 4369016
SP7 (Hs01866874)	Thermo Fisher Scientific	Cat: 4369016
SPARC (Hs00234160)	Thermo Fisher Scientific	Cat: 4369016
BGLAP (Hs01587814)	Thermo Fisher Scientific	Cat: 4369016
COL1A1 (Hs00164004)	Thermo Fisher Scientific	Cat: 4369016
SPP1 (Hs00959010)	Thermo Fisher Scientific	Cat: 4369016
PDPN (Hs00366764)	Thermo Fisher Scientific	Cat: 4369016
SOX9 (Hs00165814)	Thermo Fisher Scientific	Cat: 4369016
TNFSF11 (Hs00243522)	Thermo Fisher Scientific	Cat: 4369016
Col2A1 (Mm01309565_m1)	Thermo Fisher Scientific	Cat: 4331182
Alpl (Mm00475834_m1)	Thermo Fisher Scientific	Cat: 4331182
Sp7 (Mm04933803_m1)	Thermo Fisher Scientific	Cat: 4331182
Spp1 (Mm00436767_m1)	Thermo Fisher Scientific	Cat: 4331182
Runx2 (Mm00501584_m1)	Thermo Fisher Scientific	Cat: 4331182
Bmp2 (Mm01340178_m1)	Thermo Fisher Scientific	Cat: 4331182
Nfatc (Mm01265944_m1)	Thermo Fisher Scientific	Cat: 4331182
Tnfsf11 (Mm00441906_m1)	Thermo Fisher Scientific	Cat: 4331182
B2m (Mm00437762_m1)	Thermo Fisher Scientific	Cat: 4331182

2.7.3 RNAseq

Following isolation of RNA, samples were given to the University of Birmingham Genomics Service (Birmingham, UK), where the following step were carried out. Samples had their RNA integrity number (RIN) calculated using the High Sensitivity RNA ScreenTape® (Agilent, California)[399]. All samples had RIN scores >7 (Figure 2.1), allowing library prep to occur[400]. Library prep was performed using the Lexogen QuantSeq 3' mRNA-Seq Library Prep Kit FWD for Illumina (Illumina, California). Samples with successful library prep (24/24) were pooled and quality checked by the Genomics service using the Agilent TapeStation DNA 1000

tape (Aligent) and DNA HS Qubit™ (Fisher Scientific). Sequencing was then performed using the NextSeq 500 (Illumina), where the run had a Yield (Gbp) of 43.58 and an average %Q30 of 91.17, indicating a successful run and analysis could be performed in house[401,402].

Scripts used in this analysis were created by Julia Manning and edited to fit current data (Appendix**,** Figure 8.1-Figure 8.5). Data generated were provided in .fastq format, and quality of each sample was checked using FASTQC and MULTIQC packages in Rstudio (RStudio Public-benefit corporation)[403]. Four reads were generated for each sample. Trimming was performed using BBMap to remove the polyA tail, low quality RNA (Using the Phred quality score algorithm) and contaminating adaptor regions[404]. FASTQC was performed to visualise the changes in RNA quality. In order to align the genome, a previously generated mouse genome was used[128]

Trimmed sequences were then aligned to the genome using the STAR align package and the Encode standard settings[405]. MultiQC was performed on FastQC files generated from the aligned samples and each parameter was checked to ensure quality of pre-processing.

Feature counts were produced using the Subread package to generate a table of gene counts[406,407].The produced feature counts were then loaded and analysed using iDep[408]. IDep correctly identified he samples as *Mus musculus* and rlog transformation was selected. Genes were then ranked by standard deviation using hierarchical clustering. Samples were then plotted on a PCA plot using first and second principal components. The Dseq2 package was then used to identify upregulated and downregulated genes. Genes were analysed using GO term analysis.

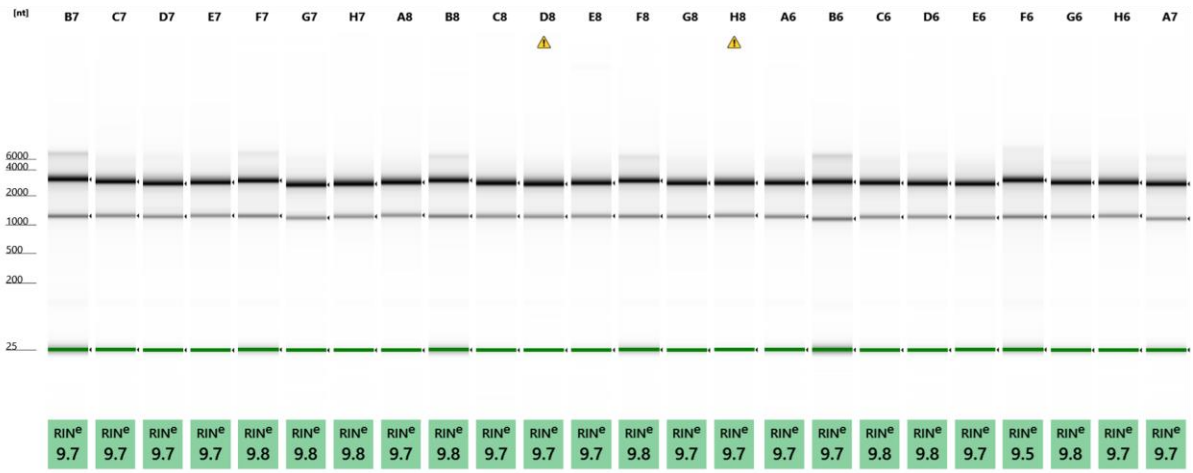


Figure 2.4 **RIN scores calculated for each sample.** Isolated RNA was analysed for RIN score using High Sensitivity RNA ScreenTape® to ensure all samples had a RIN >7.

2.8 In Silico Analysis (AlphaFold and ChimerX)

For this analysis we used programmes AlphaFold2[409,410] and ChimeraX[411,412], to create a predicted 3D rendering of both the binding protein and PEPITEM to assess location and predicted strength of binding. AlphaFold2 recently underwent an software update which gave rise to a new tool called AlphaFold-Multimer[413,414], which now allows the prediction protein-protein interactions without the need for a linker as used previously[413,415]. Which has been shown to have higher prediction capacity. Each co-IP protein Uniprot sequence was ran with PEPITEM (SVTEQGAELSNEER) in AlphaFold2.ipynb using Google colab[409,415]. This resulted in the prediction of 5 different. For each model AlphaFold produces a per-residue estimate of its confidence on a scale of 0-100, where a prediction >90 refers to a high confidence, 70-90 has good confidence, 50-70 should be treated with caution and <50 is unreliable. The conference measure is referred to as predicted local distance difference test (pLDDT), which evaluates the distance differences of all atoms within the model[416].

Based the plDDT plot the best model was selected for each protein and loaded onto ChimerX for analysis. Using ChimerX 3D rendering of the protein model were created and displayed as coloured by chain, co-IP protein (green) and PEPITEM (Purple) or coloured based on pLDDT based in the proteins predicted align error on a scale of red (low) and blue (high). We then focused on the co-IP protein residues which are in close proximity to PEPITEM allowing us to look at predicted hydrogen bonds or pseudobonds. Hydrogen bonds were identified using the "ui tool show H-Bonds" feature, where predicted bonds with a distance < 0.075Å were shown in blue and hydrogen bonds that didn't fit these criteria in orange. Pseudobonds were detected based on AlphaFold predictions and shown using the "alphafold

contacts /A to Residues /B distance" with distance set to 3Å, each pseudobond was coloured based on plDDT with red (low) and blue (high).

2.9 Osteoclast cell culture:

2.9.1 Murine osteoclast cell line

Murine macrophage-like cell line Raw.624 cells derived from Balb/c mice (cat: ATCC TIB-71; ATCC, Manassas, Virginia) were cultured in basal media (*Table 2.1*) at 37°C and 5% CO_2 until 60-70% confluent, with media changes every 3 days. Cells were detached (Section 2.6.2) if cells did not detach after 5 minutes of trypsin treatment a cell scraper was used to remove adhered cells. Cells were centrifuged at 400g for 5 minutes, the supernatant was discarded, and the pellet resuspended in 1ml basal media and counted using a haemocytometer prior to seeding into a 98 well plate ($8x10^3$ cells per well).

2.9.2 Media transfer

Raw.624 were cultured (Section 2.9.1) and plated in 98 well flat bottomed plates for 24 hours. After 24 hours media was replaced with basal osteoblast media (*Table 2.1*) or osteoblast supernatants each supplemented with 50ng/ml RANKL (cat: 390-TN-010, R&D Systems). At day 5 differentiation was measured using (TRAP) staining (Section 2.9.4).

2.9.3 Osteoprotegerin Neutralising Antibody Treatment

Media transfer was performed (Section 2.9.2). Media was supplemented with or without osteoprotegerin (OPG) antibody (cat: AF459-SP; Bio-techne, UK), at 0.15µg/ml or 0.5µg/ml or

in the presence of 0.5µg/ml mouse IgG control (cat: 31205; Invitrogen). Media was replaced and re-supplemented every two days. At day 5 differentiation was measured using (TRAP) staining (Section 2.9.4).

2.9.4 Tartrate Resistant Acid Phosphatase (TRAP) staining of osteoclasts in culture

Osteoclasts were fixed in 10% paraformaldehyde for 15 minutes at room temperature (RT). TRAP basic incubation medium was made up by adding sodium acetate anhydrous (0.11mM, cat; 10236, VWR, L+ Tartaric acid (0.074mM, cat: 13785000; Fisher scientific) and glacial acetic acid (2%, cat: 1005706; Sigma-Adrich) to distilled water[417].TRAP staining solution was then made with 98% TRAP basic incubation medium, 1.6M Fast Red Violet LB salt (cat: F3381; Sigma-Aldrich) and 2% Napthol AS-MX phosphate substrate mix containing 58 mM Napthol AS-MX (cat: N4875; Sigma-Aldrich) dissolved in 2-ethoxyethanol (cat: 16100; Alfa Aesar, Lancashire, UK). Following fixation paraformaldehyde was removed and cells were washed 3 times in distilled water. TRAP solution warmed to 37°C was added to each well and incubate at 37°C for 30 minutes, after which the TRAP solution was removed, and cells were washed 3 times with distilled water. Fixed and stained cells stored in distilled water at 2°C before imaging. Wells were imaged using the cytation5 microscope using Gen5 software and analysed in ImageJ, where the number of osteoclasts were manually calculated as osteoclasts per 1000μm^2.

2.10 Statistical analysis

All statistics were performed in Graphpad Prism 10 (GraphPad, San Diego, USA). All data are mean ± standard error of mean (SEM). Tests for normality were first preformed using

the Shapiro-Wilks test. For *in vivo* experiments, comparing unpaired data was analysed using unpaired student's t-test or one-way ANOVA with Dunnett's multiple comparison compared to PBS Vehicle control. For *in vitro* experiments if data is normalised to untreated group (non-parametric) either Wilcoxon, Kruskal-Wallis or Friedmans test with Dunn's multiple comparison was used. For parametric data unpaired/paired t-tests, or one-way ANOVA with Holm-Sidak's multiple comparison. Significance levels were set at $P<0.05$, only significant values represented by * on figures values close to significance were also indicated on graphs, if no value is shown $P = <0.09$.

3 Mechanistic action of PEPITEM in osteoblasts

This chapter is an expanded version of the article Lewis & Frost et al, 2024, for which the experiments I carried out are included here.
The full paper can be found in Appendix 325-351

3.1 Introduction

Previous studies have shown that PEPITEM directly enhances osteoblast maturation and mineralization, as evidenced by increased alkaline phosphatase activity and alizarin red staining[197,418]. However, the underlying mechanism remains unclear. The original study that characterised PEPITEM biology used co-immunoprecipitation (co-IP) to identify cadherin-15 (Cdh15) on endothelial cells as a binding partner of PEPITEM[192]. PEPITEM-Cdh15 binding induced Sphingosine-1-Phosphate (S1P) secretion through upregulation of S1P kinases, Sphk2. While S1P has been shown to enhance MSC differentiation in osteoblasts[419], literature on Cdh15 expression or function in osteoblasts were lacking. Our groups investigations revealed that osteoblasts express Cdh15 at both RNA and protein levels, with localization in focal adhesions[197,418]. However, siRNA knockdown of Cdh15 in osteoblasts was unable to downregulate protein expression, therefore the role of Cdh15 in the PEPITEM response is still unclear[128].

This chapter aims to test the hypothesis that PEPITEM acts directly though osteoblasts via mechanisms differing to that described in endothelial cells. Firstly, we'll further explore *in vivo* the responses to PEPITEM looking at potential sex differences in responses. Then we move into the functional mechanism of PEPITEM first looking at known targets of PEPITEM, S1P and Cdh15, followed by investigation into novel PEPITEM interactions in osteoblasts.

3.2 Results:

3.2.1 PEPITEM acts to increase bone morphometric parameters in male and female mice

PEPITEM was previously shown to increase trabecular bone parameters, including BV/TV and trabecular thickness (Tb.th), and showed increased histomorphological changes with increased rate of bone formation coupled with decrease osteoclast number[197]. Here we look at additional parameters, osteoid production and osteoblast number, to further understand that action of PEPITEM *in vivo*. Using tissue from previous experiments where male mice have been treated for 2-weeks with PEPITEM[100,170], we show increased deposition of unmineralized bone matrix (osteoid) when compared to PBS treated mice (Figure 3.1, A, B). Additionally, PEPITEM treatment tended towards an increase in the number of osteoblasts, however not significantly (Figure 3.1, C, D). Collectively, these data suggest that PEPITEM is acting predominately to increase osteoblast activity and osteoid production rather than absolute number.

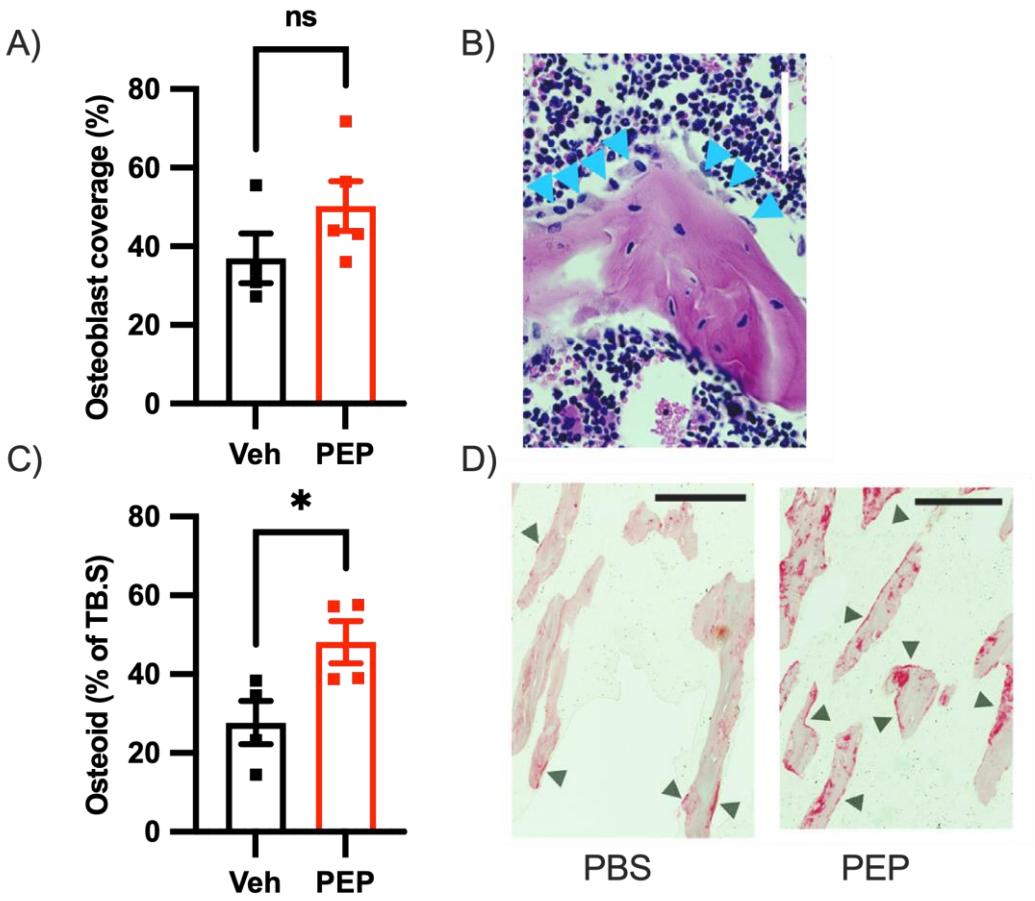


Figure 3.1 PEPITEM increased osteoblast production of osteoid without increasing osteoblast number. Homeostatic male mice injected with daily i.p. injections of PBS vehicle (black, n=4) or 300 µg PEPITEM (red, n=4) for 14 days. Tibiae were decalcified, paraffin embedded, sectioned and stained for osteoid (Sirius red) or H&E. (A) Osteoblasts were quantified and measures as percentage of the total bone surface area, OB.S/BS. (B) Representative image of H&E stained tibia where cyan arrows point to osteoblasts. (C) Levels of osteoid were measured as % of trabecular surface (TB.S). (D) Representative images of Sirius red staining from PBS or PEPITEM treated mice. Scale bar, 50 µm. Data are mean ± SEM. $* = P < 0.05$, by unpaired t test.

Initially the effects of homeostatic PEPITEM were only observed in male mice[197]. There have been multiple studies showing sex differences within the bone of both mice and human[9420–424]. Additionally, many musculoskeletal diseases, including osteoporosis, disproportionately effect females over males[425]. Therefore, we explored the effect of PEPITEM in female mice under homeostatic conditions. Female mice were treated with PEPITEM, PBS or control peptide for 2-weeks prior to tibia analysis for trabecular and cortical parameters. As expected, no differences were seen in cortical bone parameters (Figure 3.3), however contradictory to male mice, we saw no difference in trabecular bone parameters (Figure 3.2) measured using μ-CT following 2-weeks of PEPITEM treatment.

We explored changes in histomorphology allowing us to observe changes in matrix formation (osteoid), which is undetectable using μ-CT. As seen in male mice, there was a significant increase in osteoid production in the PEPITEM treated female mice comparative to the untreated and control peptide treated mice (Figure 3.4, A, B). The levels of osteoid observed in females was also on averagely higher than in males (76±11.8vs50±14.1,%), suggesting female mice have higher bone turnover than males. This difference was not due to an increase in osteoblast number, with no difference being detected between untreated or control peptide mice compared to PEPITEM (Figure 3.4, C, D). These data suggest that PEPITEM impacts bone formation in homeostatic female mice, despite not detecting differences in the μ-CT following 2-weeks of treatment.

To investigate the effect of PEPITEM on resorption we looked at osteoclast number following PEPITEM treatment. Similarly to that observed in males, we saw a significant decrease in TRAP positive osteoclasts following 2-week PEPITEM treatment (Figure 3.5), suggesting a reduction in resorption following PEPITEM treatment in female mice.

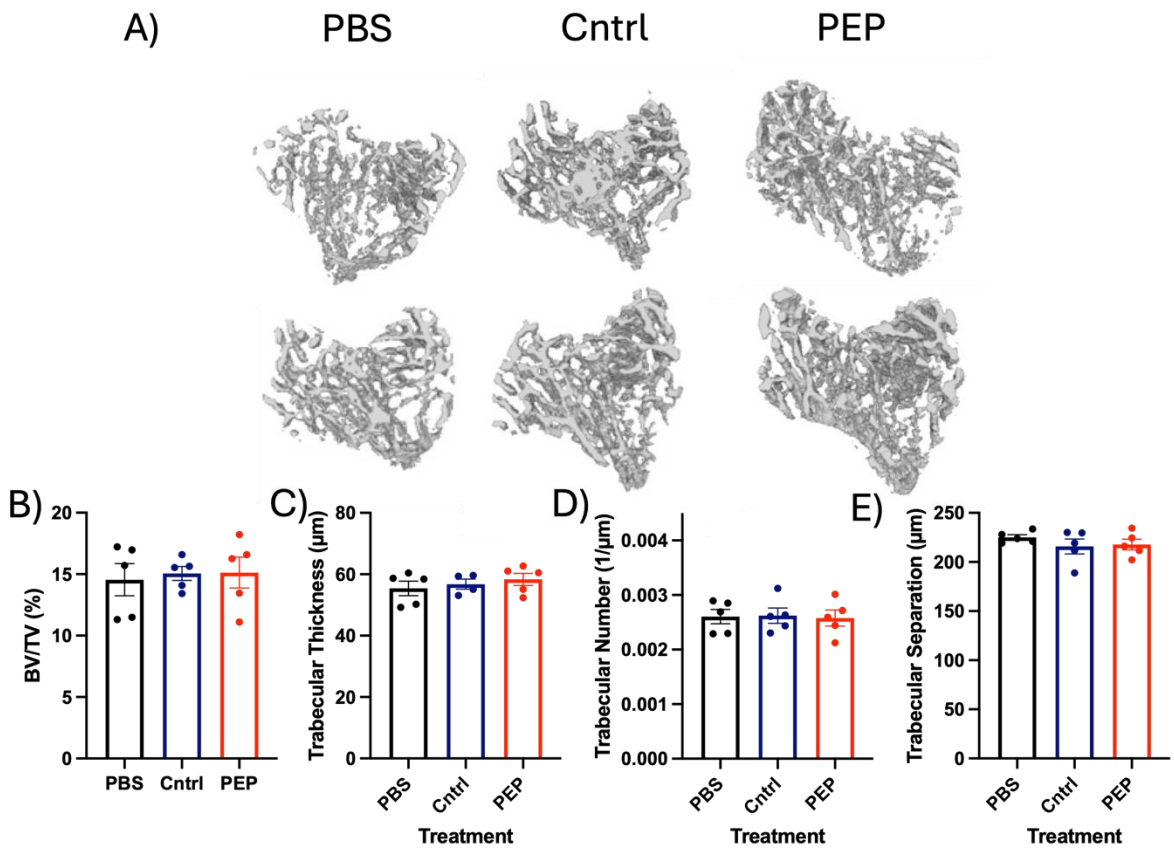


Figure 3.2 **PEPITEM does not alter trabecular bone parameters by µ-CT in female mice following 2-week treatment**. Homeostatic female mice injected with daily i.p. injections of PBS vehicle (black, n = 4), or 300 µg of control peptide (blue, n = 5) or PEPITEM (red, n = 5) for 14 days. Tibiae scanned by µ-CT and regions of interest were drawn around trabecular bone in the metaphysis to analyse trabecular parameters. (A) Representative images of transverse µ-CT 3D reconstructions from 2 PBS, control (cntrl) or PEPITEM treated mice. (B-E) trabecular bone was quantified and analysed for (B) trabecular bone volume (BV/TV, %), (C) trabecular thickness (µm), (D) trabecular number (1/µm), **(**E**)** trabecular separation (µm). Data are mean ± SEM for n = 5 mice per treatment group.

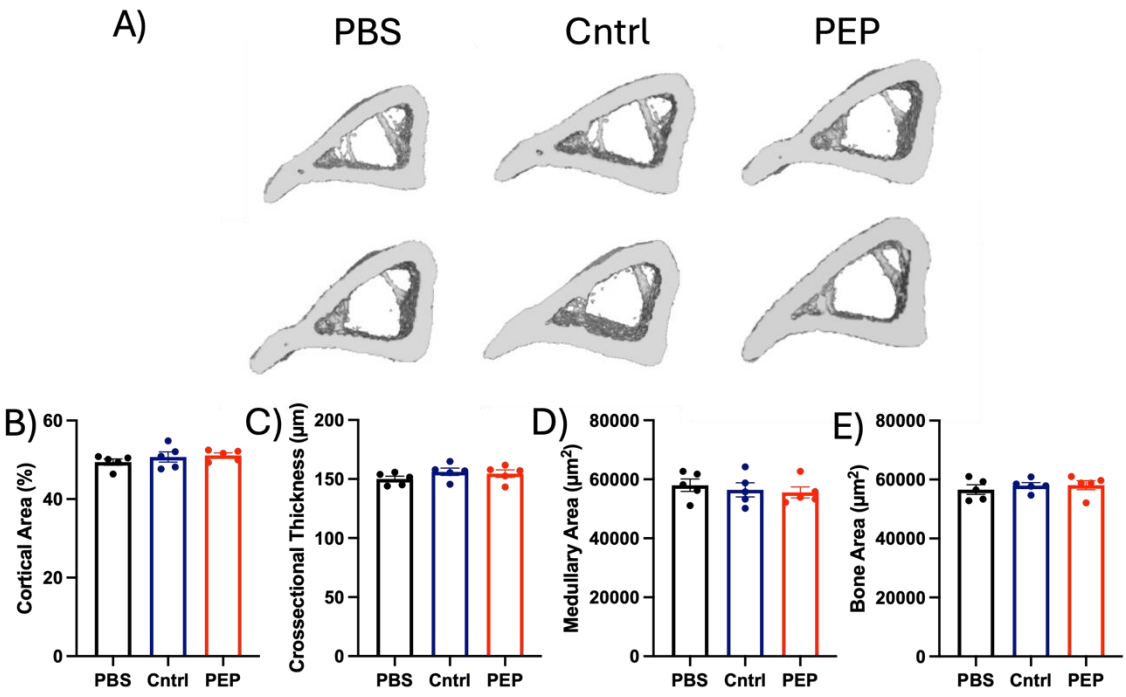


Figure 3.3 **PEPITEM does not alter cortical bone parameters by µ-CT in female mice**. Homeostatic female mice injected with daily i.p. injections of PBS vehicle (black, n=4), or 300 µg of control peptide (blue, n=5) or PEPITEM (red, n=4) for 14 days. Tibiae scanned by µ-CT and regions of interest were drawn around cortical bone in the epiphysis to analyse cortical parameters. (A) Representative images of transverse µ-CT 3D reconstructions from 2 PBS, control (cntrl) or PEPITEM treated mice. (B-E) Cortical bone was analysed for (B) cortical area (%), (C) Cross sectional thickness (µm), (D) Medullary area (μm^2) and (E) total bone area (μm^2). Data are mean ± SEM for n = 5 mice per treatment group.

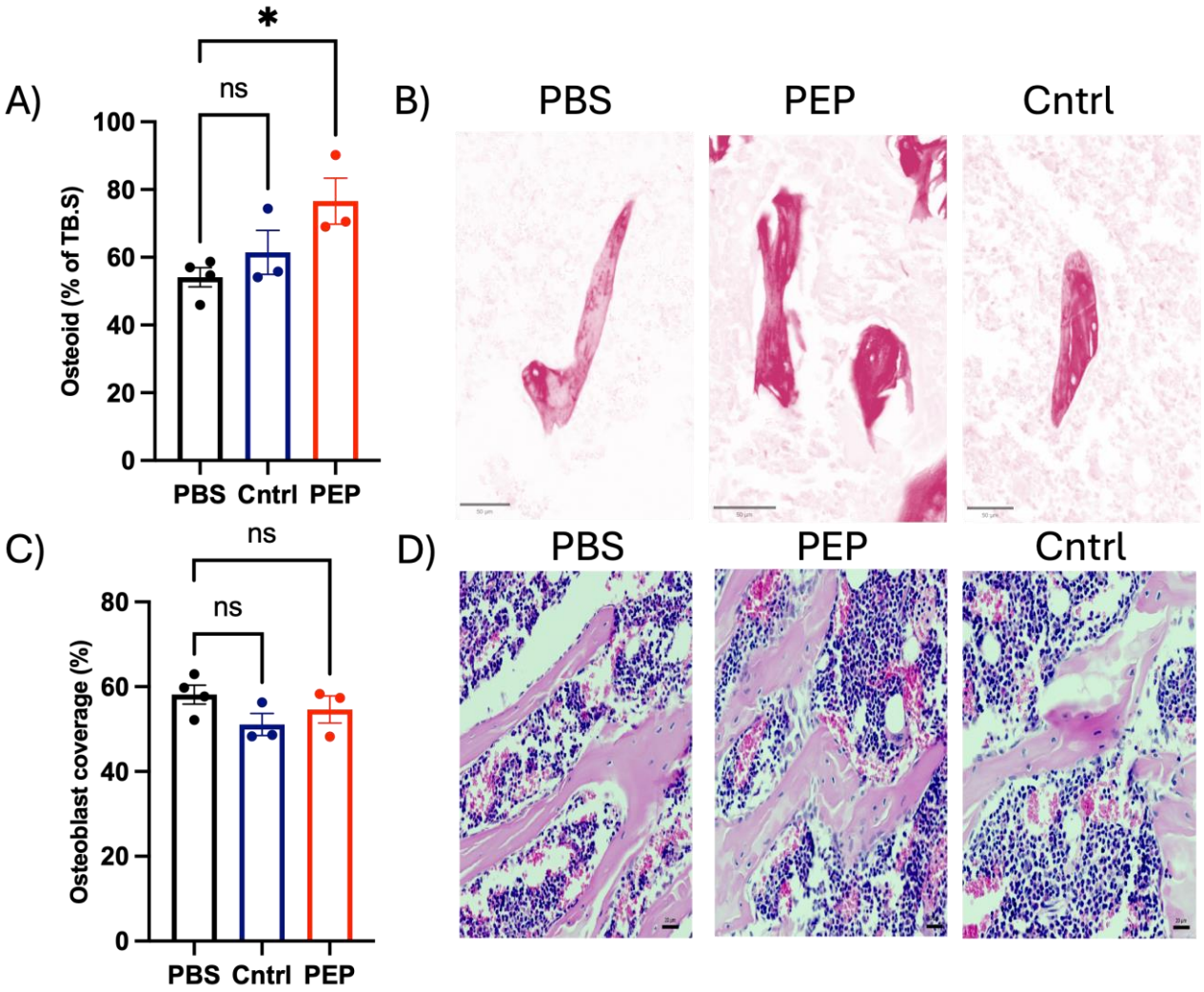


Figure 3.4 **PEPITEM treatment increases osteoid production in female homeostatic mice without effecting osteoblast number.** Homeostatic female mice injected with daily i.p. injections of PBS vehicle (black, n = 4), or 300 µg of control peptide (blue, n = 3) or PEPITEM (red, n = 3) for 14 days. Tibiae were decalcified, paraffin embedded, sectioned and stained for osteoid (Sirius red) or H&E. (A) Levels of osteoid were measured as % of trabecular surface (TB.S). ANOVA showed a significant effect of treatment on osteoid production, $p<0.05$ (B) Representative images of Sirius red staining from PBS, PEPITEM or control peptide treated mice. (C) Osteoblasts were quantified and measures as percentage of the total bone surface area, OB.S/BS. (D) representative images of H&E sections from PBS, PEPITEM or control peptide treated mice. Data are mean ± SEM for n = 3-4 mice . * = $P < 0.05$ by Dunnett's multiple comparison. B) Scale bar = 50 µm D) Scale bar = 20 µm

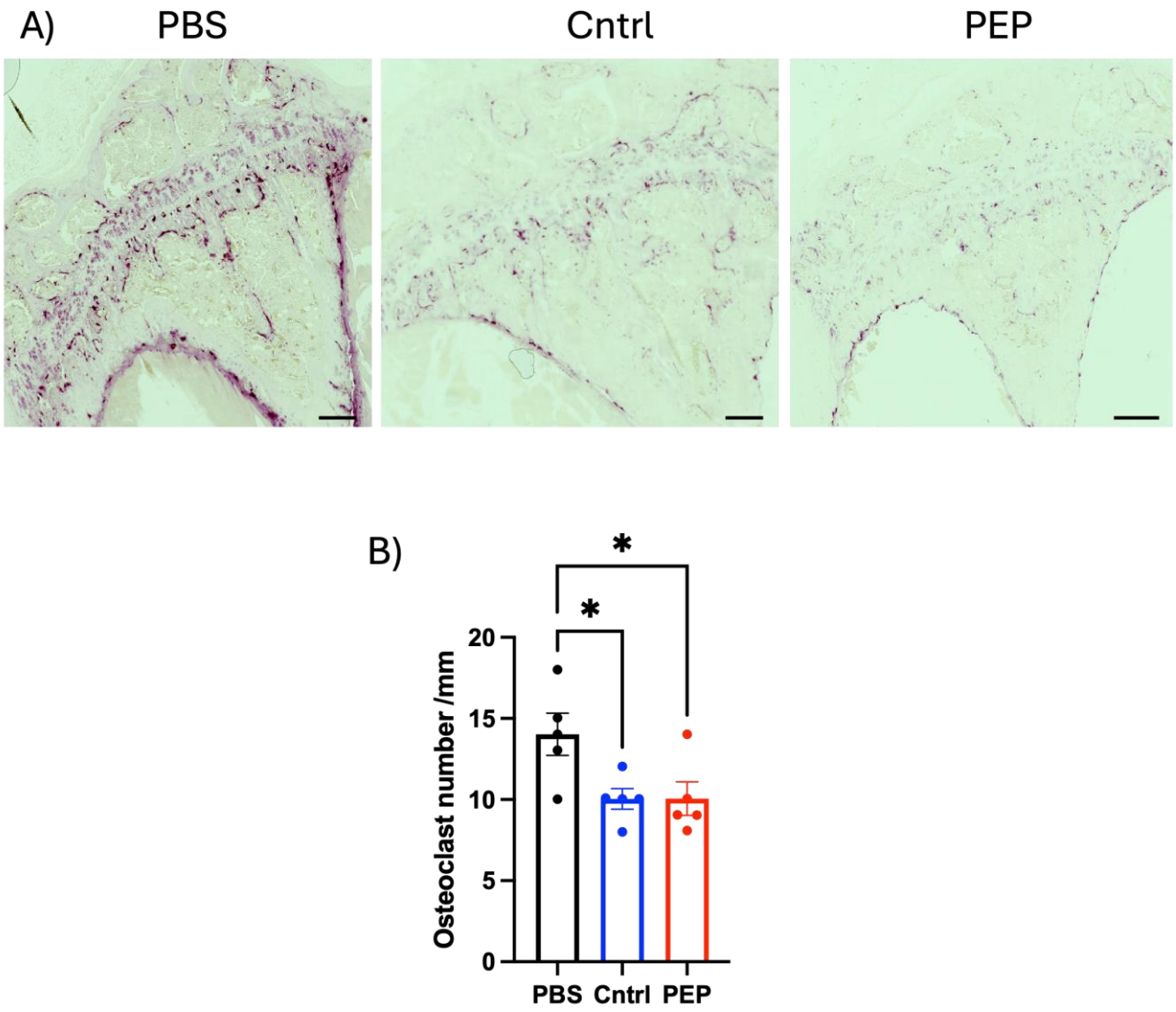


Figure 3.5 **PEPITEM treatment significantly decrease osteoclast number in female homeostatic mice**. Homeostatic female mice injected with daily i.p. injections of PBS vehicle (black, n = 5), or 300 µg of control peptide (blue, n = 5) or PEPITEM (red, n = 5) for 14 days. Tibiae were decalcified, paraffin embedded, sectioned and stained for TRAP. (A) Representative images of TRAP staining from PBS, PEPITEM or control peptide treated mice. (B) the number of TRAP positive cells were measured as osteoclast number /mm surface of trabecular bone. Data are mean ± SEM for n = 5 mice. * = $P < 0.05$ by Dunnett's multiple comparison. Scale bar = 150µm

As we saw no changes in cortical bone in male[197] or female mice, we explored the possibility that this is due to longer turnover time of cortical bone[426] and therefore a longer treatment regime maybe required. To further investigate the role of PEPITEM in homeostatic remodelling of cortical bone in female mice we looked at the effects of a 4-week PEPITEM treatment regime. Despite increased treatment period, we still saw no differences in trabecular bone formation using μ-CT (Figure 3.6), however we observed significant changes in the cortical bone (Figure 3.7). After 4-weeks PEPITEM significantly increased cortical area, cross-sectional thickness and bone area, whilst reducing medullary area compared to PBS treated mice (Figure 3.7).

As previously, we looked at changes in osteoblast number and osteoid production to investigate changes in bone formation which were non-detectable via μ-CT. Sirius red staining shows a significant increase in osteoid production in the PEPITEM treatment group compared to the PBS treatment control (Figure 3.8, A), matching that seen in the male mice and that seen following 2-weeks treatment in female mice. As expected, H&E staining showed no differences in osteoblast number following 4-week PEPITEM treatment compared to control(Figure 3.8, B), suggesting PEPITEM does not increase osteoblast proliferation following 4-weeks treatment.

In order to look at whether prolonged (4-week) PEPITEM treatment resulted in a change in osteoclast number we preformed TRAP staining on these sections. Counts of TRAP positive cells show a significant decrease following 28-day PEPITEM treatment compared to PBS treated mice (Figure 3.9), suggesting that PEPITEM is acting to resorption in female mice.

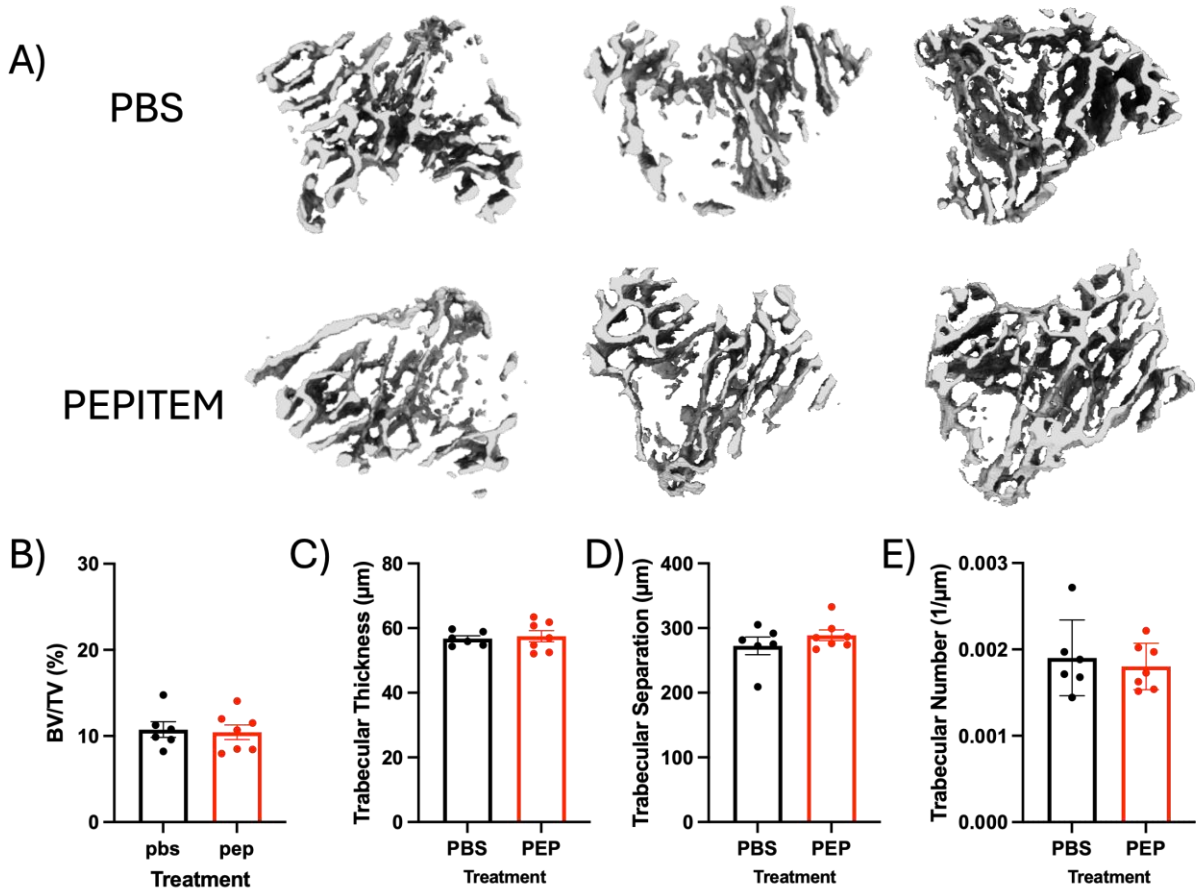


Figure 3.6 **PEPITEM does not alter trabecular bone parameters by µ-CT in female mice following prolonged treatment**. Homeostatic female mice injected with daily i.p. injections of PBS vehicle (black, n = 6), or 300 µg of PEPITEM (red, n = 7) for 28 days. Tibiae scanned by µ-CT and regions of interest were drawn around trabecular bone in the metaphysis to analyse trabecular parameters. (A) Representative images of transverse µ-CT 3D reconstructions from 3 PBS, or PEPITEM treated mice. (B-E) trabecular bone was quantified and analysed for (B) trabecular bone volume (BV/TV, %), (C) trabecular thickness (µm), (D) trabecular separation (µm), (E) trabecular number (1/µm). Data are mean ± SEM for n = 6-7 mice per treatment group.

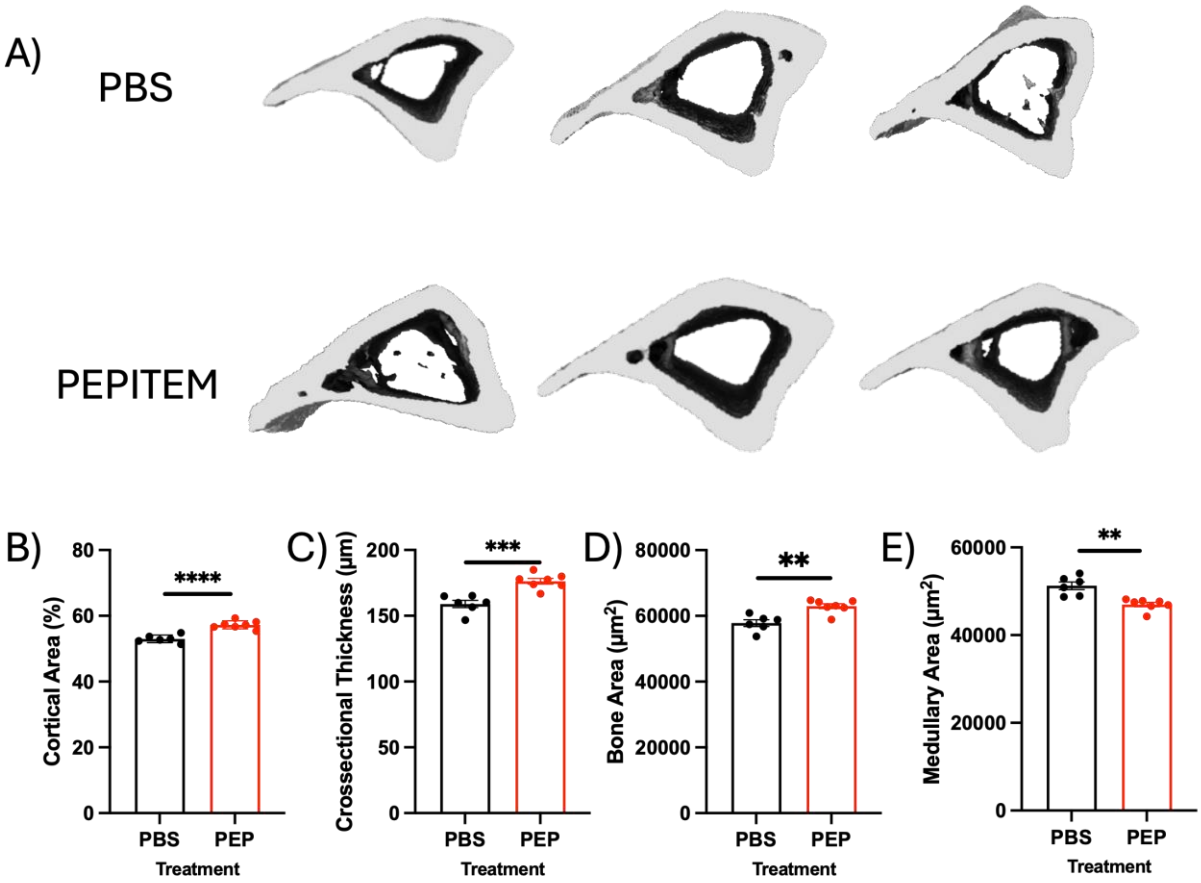


Figure 3.7 **PEPITEM increased cortical bone parameters by µ-CT in female mice following prolonged treatment.** Homeostatic female mice injected with daily i.p. injections of PBS vehicle (black, n = 6), or 300 µg of PEPITEM (red, n = 7) for 28 days. Tibiae scanned by µ-CT and regions of interest were drawn around cortical bone in the epiphysis to analyse cortical parameters. (A) Representative images of transverse µ-CT 3D reconstructions from 2 PBS, control (cntrl) or PEPITEM treated mice. (B-E) Cortical bone was analysed for (B) cortical area (%), (C) Cross sectional thickness (µm), (D) total bone area (µm^2) and (E) Medullary area (µm^2). Data are mean ± SEM for n = 6-7 mice per treatment group. ** = P < 0.01, *** = P < 0.001 and **** = P < 0.0001 by unpaired students t-test.

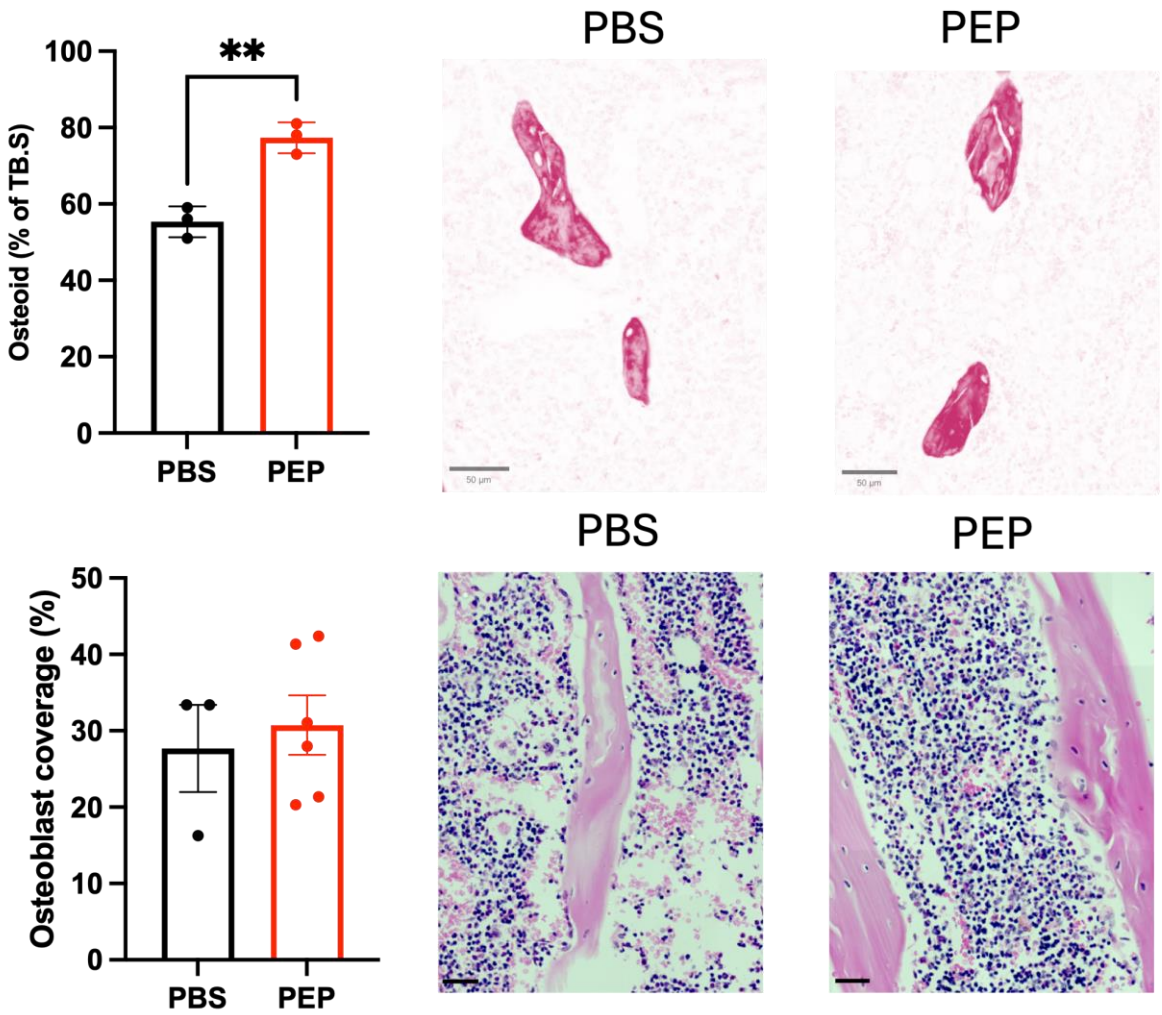


Figure 3.8 **PEPITEM treatment increased osteoid production in female homeostatic mice following 4 weeks of treatment**. Homeostatic female mice injected with daily i.p. injections of PBS vehicle (black, n = 4), or 300 µg of PEPITEM (red, n = 3) for 28 days. Tibiae were decalcified, paraffin embedded, sectioned and stained for osteoid (Sirius red) or H&E. (A) Levels of osteoid were measured as % of trabecular surface (TB.S). (B) Representative images of Sirius red staining from PBS or PEPITEM treated mice. (C) Osteoblasts were quantified and measures as percentage of the total bone surface area, OB.S/BS. (D) representative images of H&E sections from PBS or PEPITEM treated mice. Data are mean ± SEM for n = 3-6 mice. * = $P < 0.05$ by unpaired t-test. Scale bar = 50 µm

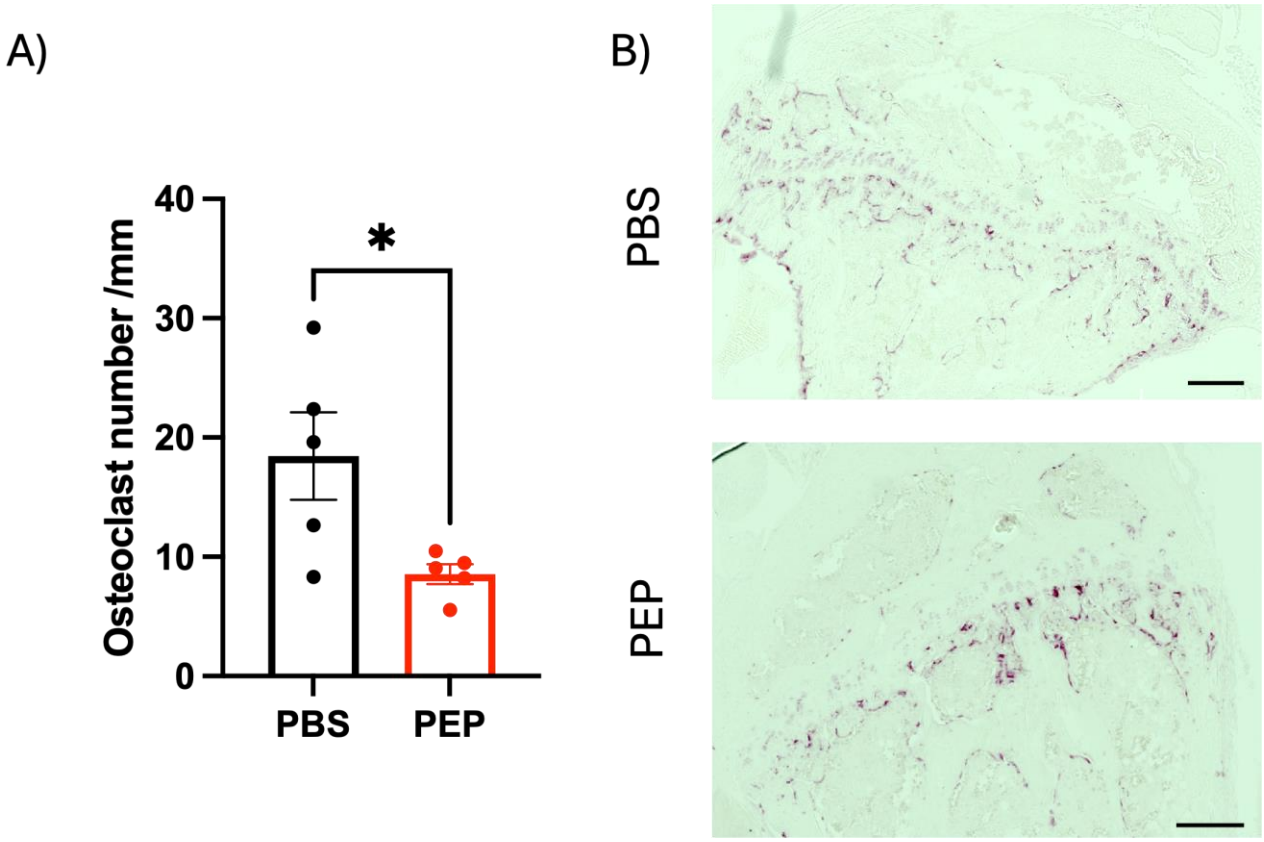


Figure 3.9 **PEPITEM treatment decreased osteoclast number in female homeostatic mice following 4 weeks of treatment.** Homeostatic female mice injected with daily i.p. injections of PBS vehicle (black, n = 5), or 300 µg of PEPITEM (red, n = 3) for 28 days. Tibiae were decalcified, paraffin embedded, sectioned and stained for TRAP. (A) the number of TRAP positive cells were measured as osteoclast number /mm surface of trabecular bone. (B) Representative images of TRAP staining from PBS or PEPITEM treated mice. Data are mean ± SEM for n = 5 mice. * = $P < 0.05$ by unpaired t-test. Scale bar = 250 µm

3.2.2 PEPITEM increases bone formation in 3D *in vitro* and ex vivo bone models

Previously PEPITEM was shown to have pro-osteoblastogenic properties on a variety of cell types, including primary mouse and human osteoblasts. In these studies, alkaline phosphatase (ALP) activity, a marker of osteoblast maturation, and alizarin red staining of mineral were shown to increase following PEPITEM treatment. However, these experiments were done using conventional cell culture techniques, where cells are cultured in 2D on a plastic surface, failing to mimic the 3D structure of bone. Therefore, we used of the self-structuring bone model (SSBM)[377] to observe how PEPITEM effects cells in a more accurate *in vitro* environment.

We first assessed whether the hFOb 1.19 cell line responded to PEPITEM in 2D, looking at ALP activity after 4 days of treatment (Figure 3.10, A) and mineralisation after 12 days of (Figure 3.10, B), showing that hFOb 1.19 cells response to PEPITEM.

To investigate PEPITEM treatment on SSBM hFOb 1.19 constructs[377] were cultured for 4- or 12-weeks then treated for 8-days with PEPITEM or control peptide, these constructs or their conditioned media were then analysed by qPCR, ELISA or alizarin red staining.

In order to assess the effects of PEPITEM on 3D osteoblasts we ran qPCR looking at markers of osteoblast, chondrocyte and osteocyte differentiation, for qPCR PEPITEM treated constructs were compared to previously attained data for untreated hFOb 1.19 SSBM constructs[427]. qPCR analysis of osteoblast differentiation markers from 4-wk constructs following treatment (Figure 3.11, A), shows a significant decrease in *ALPL* but a significant upregulation of *SPP1* (Osteopontin). When looking at markers of chondrogenesis (Figure 3.11, B), there is no significant change in *SOX9* expression. Osteocyte/Mature osteoblast markers (Figure 3.11, C), shows an upregulation in *BGLAP* (osteocalcin) coupled with a reduction in

PDPN (podoplanin). Together these data may suggest PEPITEM is increasing osteoblast maturation but not osteocyte formation, with *SPP1* being a marker of mid to late osteoblast differentiation and *BGLAP* being a marker of mature osteoblasts.

Comparatively when constructs are treated at 12-weeks, we see a decrease in osteoblast differentiation markers (Figure 3.12, A), *ALPL, SPP1* and *SPARC* (osteonectin) and an increase in *TNFSF11* (OPG/RANKL). At 12-weeks there was no change in chondrocytic or osteocytic markers (Figure 3.12, B, C). These data may suggest that PEPITEM is having less effects on osteoblast maturation at later time points, but PEPITEM may alter OPG/RANKL expression in mature osteoblast/osteocyte cultures.

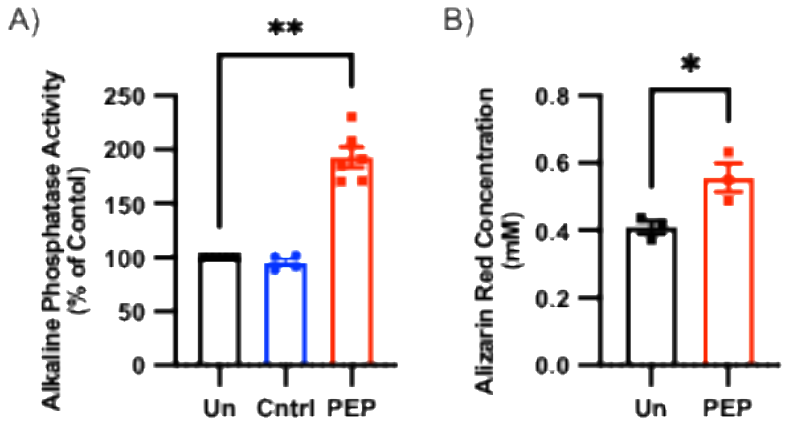


Figure 3.10 PEPITEM acts to increase osteoblast maturation in hFOb 1.19 cells. HFOb 1.19 cells were cultured for 7 days in non-osteogenic media, then moved to osteogenic media and untreated or treated with 10 ng/ml PEPITEM or cntrl peptide for (A) 4 days (n = 4-6) or (B) 14 days (n = 3). (A) Alkaline phosphatase activity was analysed on day 4 and displayed as % compared to untreated control . Kruskal-Wallis shows significant effect of treatment $P < 0.001$ (B) Alizarin red mineral stained and extracted from wells on day 14, displayed as nM conc. Data are mean ± SEM. (A) ** = $P < 0.01$ by Dunn's multiple comparison test (B) * = $P < 0.05$ by paired t-test.

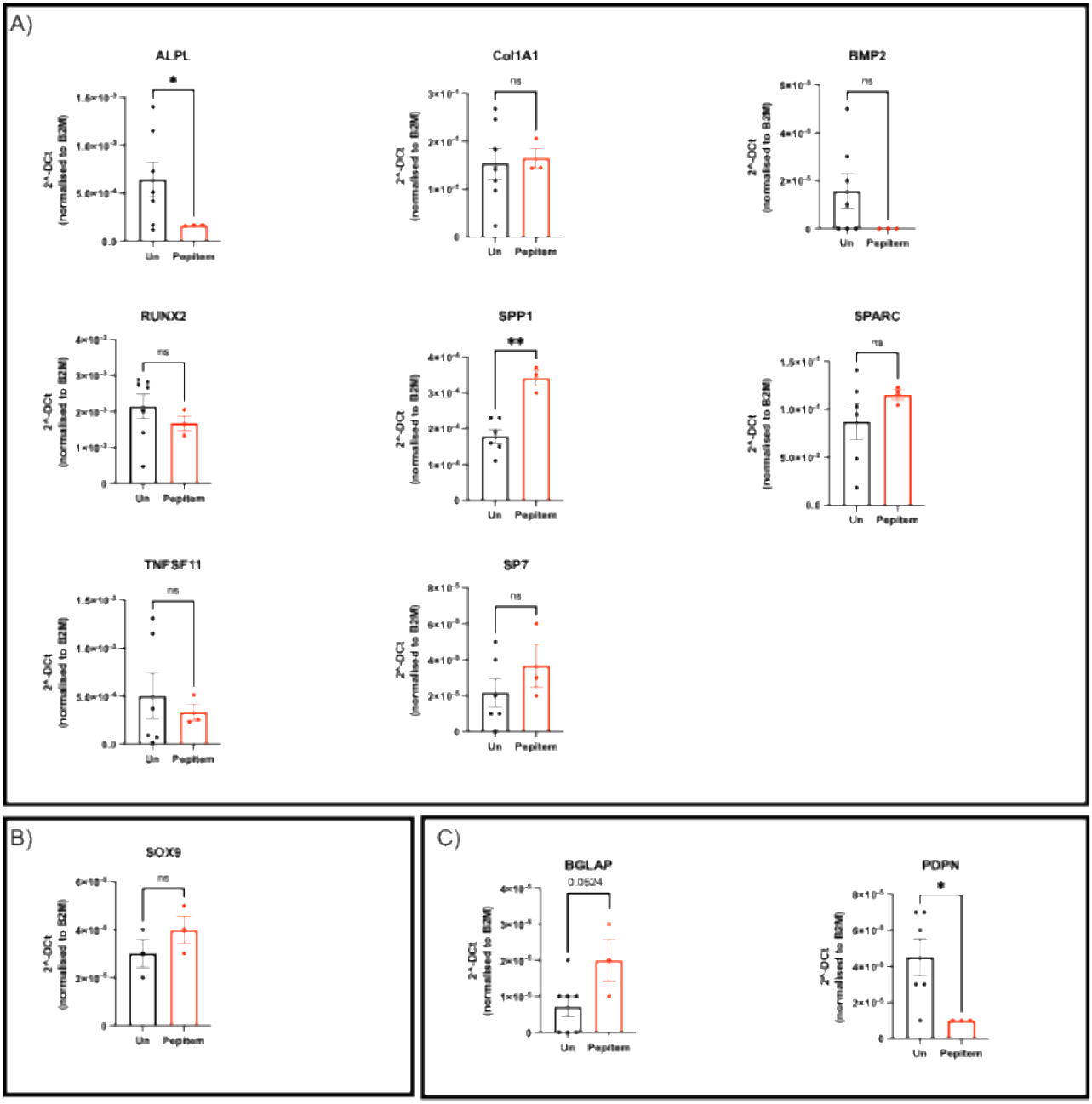


Figure 3.11 4-week SSBM constructs show altered gene profiles when treated with PEPITEM. SSBM hFOb 1.19 constructs were cultured for 4-weeks in non-osteogenic media, then treated for 8-days with PEPITEM (red, n = 3) or left untreated (black, n = 3-8). RNA was extracted from constructs after treatment and qPCR was performed looking at markers of (A) osteoblast differentiation (B) chondrocyte differentiation and (C) mature osteoblasts/osteocytes. Data expressed as Raw Ct values. Data are mean ± SEM. ** = $p<0.01$ by unpaired t-test with Welch correction if SD ratio = > 2.

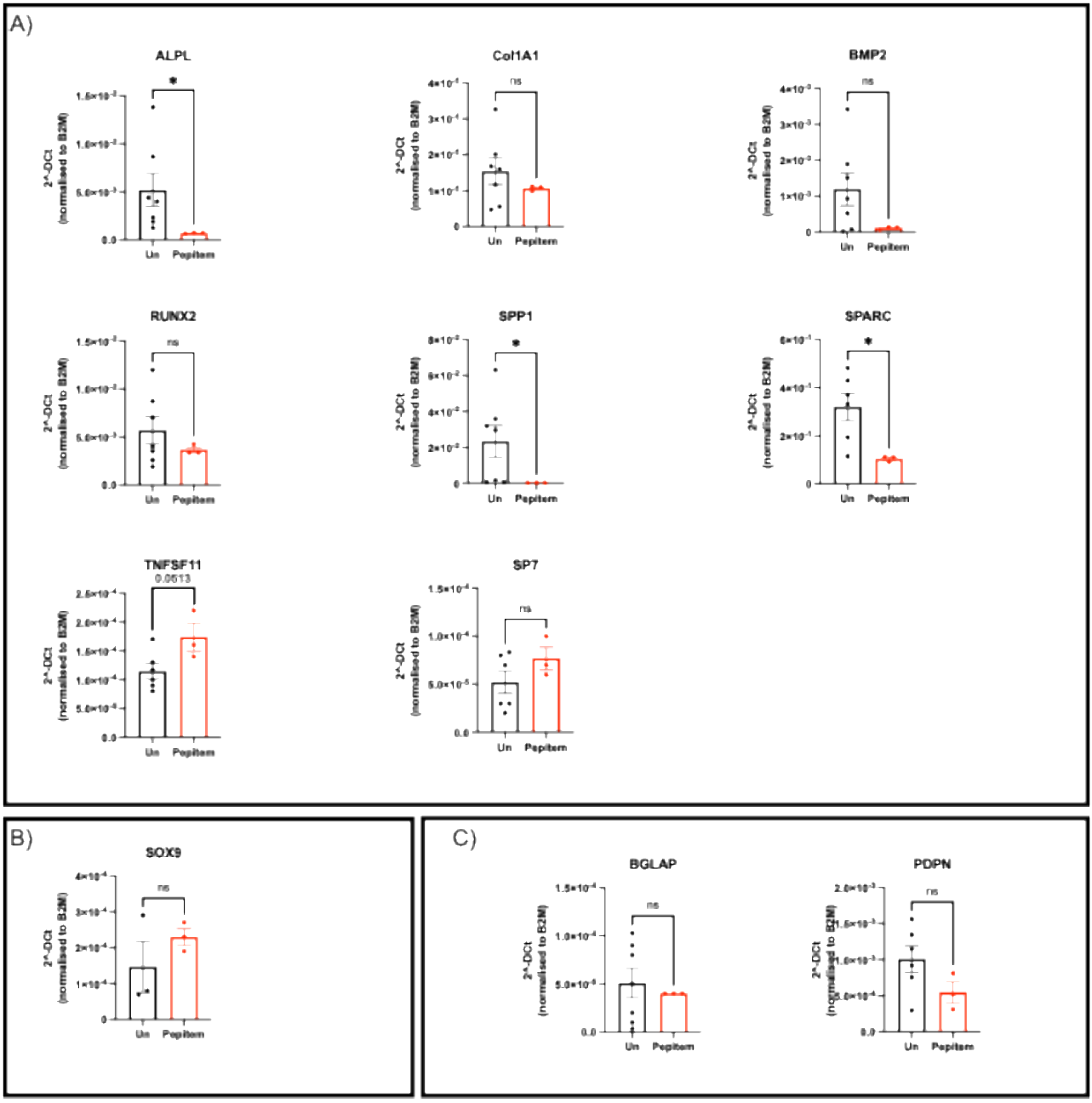


Figure 3.12 12-week SSBM constructs show altered gene profiles when treated with PEPITEM. SSBM hFOb 1.19 constructs were cultured for 4-weeks in non-osteogenic media and moved to osteogenic media for 8-weeks,at 12-weeks in culture constructs treated for 8-days with PEPITEM (red, n = 3) or left untreated (black, n = 3-8). RNA was extracted from constructs after treatment and qPCR was performed looking at markers of (A) osteoblast differentiation (B) chondrocyte differentiation and (C) mature osteoblasts/osteocytes. Data expressed as Raw Ct values. Data are mean ± SEM. * = $p < 0.05$ by unpaired t-test with Welch correction if SD ratio = > 2.

An ELISA for total procollagen type I alpha production as a surrogate marker of bone matrix production. We cultured SSBMs for 4-weeks in growth media before treating with PEPITEM or control peptide for 8 days. For 12-week cultures, at 4-weeks constructs were moved to osteogenic media and cultured for an additional 8-weeks before 8-days of PEPITEM or control peptide treatment (Figure 3.13, A). Following 8-days treatment, supernatants were collected and analysed for procollagen type I alpha. 4-week-old constructs treated for 8 days with PEPITEM showed a significant increase in procollagen type I alpha compared to untreated or control treated peptide (Figure 3.13, B). Comparatively at 12-weeks constructs appear to be less responsive to PEPITEM with no significant difference in procollagen type I alpha production being observed (Figure 3.13, C). These data suggest that PEPITEM can enhance matrix production in less mature constructs but not in older constructs, indicating that PEPITEM may have function on early osteoblasts but not more mature cells.

Changes in pro collagen type I production allowed us to look at extracellular matrix production within the SSBM models, however, fails to show changes in mineralisation. Therefore, we used alizarin red staining to quantify changes in mineralisation in 3D constructs at 4-wks following 8 day treatment. These data show an increase in alizarin red concentration in response to PEPITEM and in response to the control peptide (Figure 3.14), suggesting PEPITEM is able to increase osteoblast mineralisation in SSBM constructs and the cntrl peptide may be having additional effects.

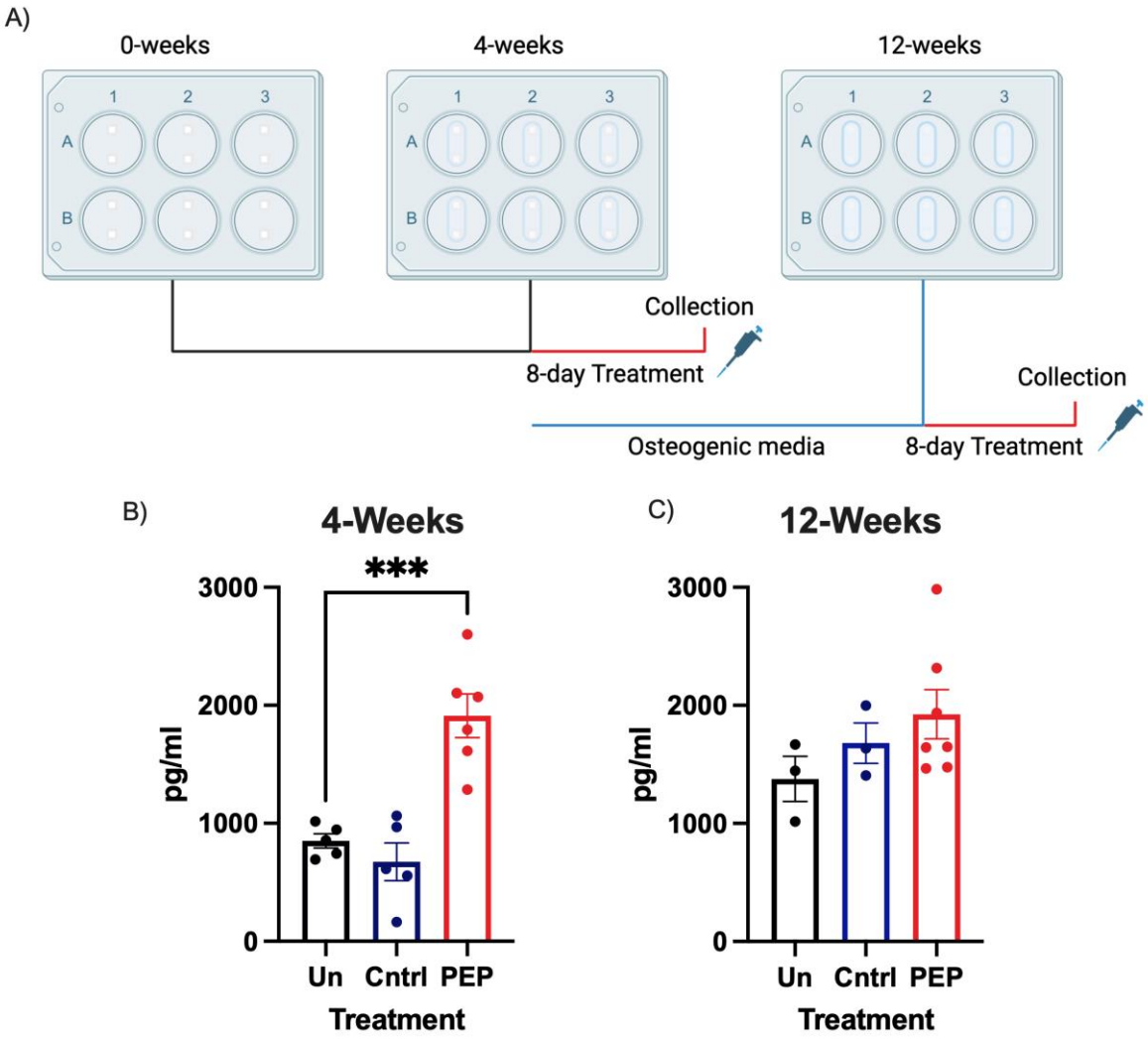


Figure 3.13 PEPITEM increased Pro-collagen type I production in 4-week SSBM constructs following short term treatment. Procollagen type 1 N-terminal propeptide (P1NP) ELISA of cell culture supernatants from SSBM constructs untreated (Un) (black, n = 3-5) or treated with 10 ng PEPITEM (PEP) (red, n = 3-5), or control peptide (Cntrl) (blue, n = 3-7), for 8 days at (B) 4 weeks or (C) 12 weeks. (A) Schematic diagram, detailing the formation of SSBM constructs in growth media and move to osteogenic media at 12 weeks. Constructs were then treated for 8 days at 4-weeks or 12-weeks. Media was collected at 5 weeks and 13 weeks following treatments. (B-C) Quantification of P1NP levels in cell culture supernatants from constructs treated at (B) 4-weeks and (C) 12-weeks, displayed as pg/ml. ANOVA showed significant effect of treatment on P1NP at (B) 4 weeks ($P < 0.001$). Data are mean ± SEM. *** = $P < 0.001$ by Dunnett's multiple comparisons. Diagram created using biorender.com

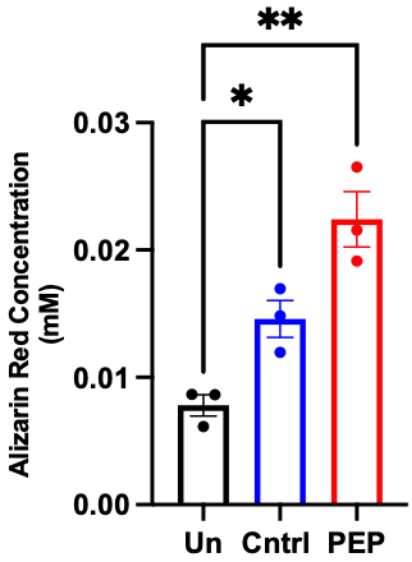


Figure 3.14 **PEPITEM increases SSBM mineralisation when given at 4-wks**. HFOb 1.19 SSBM constructs were cultured for 4-wks prior to 8-day treatment. After treatment SSBM constructs untreated (Un) (black, n = 3), control peptide (Cntrl) (blue, n = 3) or PEPITEM (PEP) (red, n = 3) were fixed and stained using alizarin red. Alizarin red dye was extracted from the constructs and measured against a standard curve. displayed as nM conc. One-way ANOVA shows a significant effect of treatment, $P < 0.01$. Data are mean ± SEM. * = $P < 0.05$ and ** = $P < 0.01$ by Dunnett's multiple comparison.

We have shown that PEPITEM can increase mineralisation in 2D[197] and 3D bone models. To further investigate the effects of PEPITEM on mineralisation we used the ex vivo metatarsal culture model. Culture of ex vivo embryonic (E15.5) metatarsals allowed for the measurement of the mineralisation zone and total bone length. Metatarsals treated with 10 ng PEPITEM, or control peptide for 10 days were imaged daily, and images analysed using ImageJ to analyse changes in mineralisation zone length and total bone length (Figure 3.15). Firstly, we mapped increase in mineralisation zone length over time (Figure 3.15, A) and measured the total change through analysis of area under the curve (Figure 3.15, B). Here we see a significant increase in mineralisation zone length over 10 days of treatment (Figure 3.15). To account for differences in metatarsal size we additionally plotted increase in mineralisation zone length over total bone length (Figure 3.15, C, D), where despite increases in bone formation we see observe significant increase in mineralisation. These data further show that PEPITEM enhances osteoblast mineralisation.

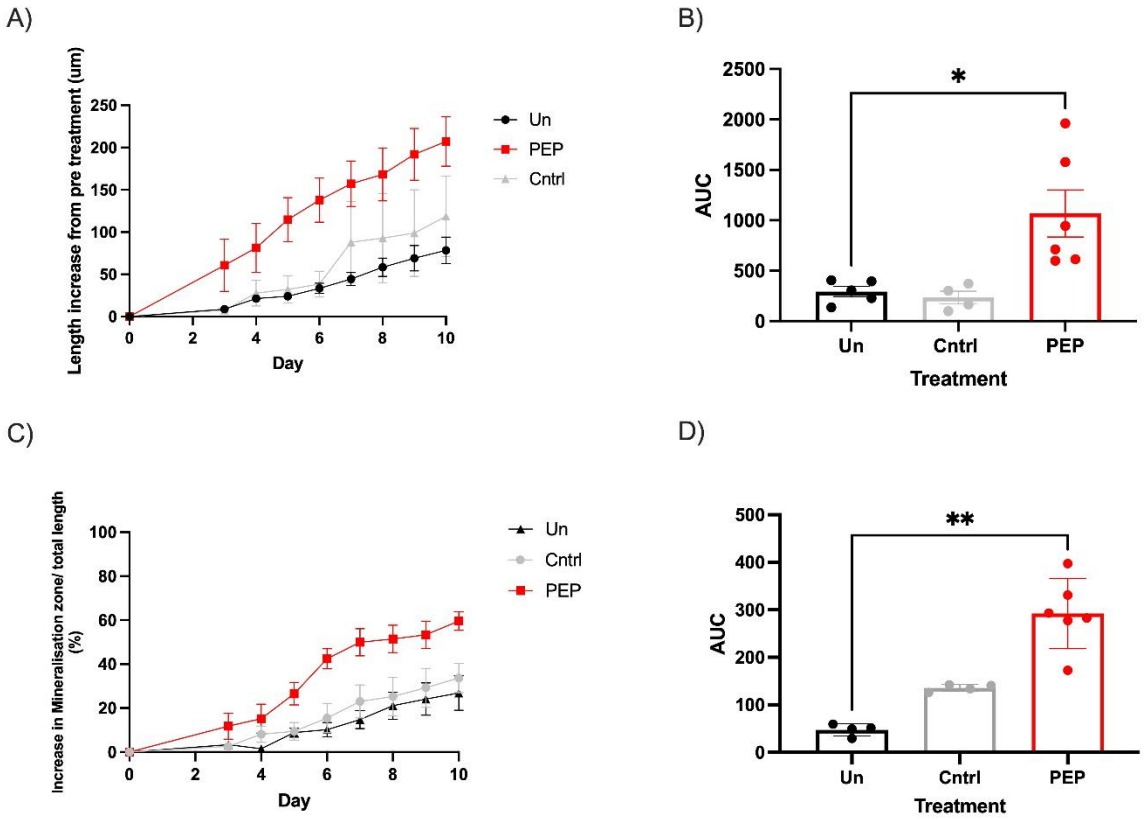


Figure 3.15 PEPITEM increased mineralisation in ex vivo metatarsal model. Metatarsals from E15.5 embryos were dissected and cultured for 5 days before treatment. After 5 days in culture metatarsals were moved into fresh plates and treated every 3 days with 100ng/ml PEPITEM (PEP) or Control peptide (Cntrl) for 10 days. Untreated (black, n = 5), cntrl (grey, n = 4) or PEP (red, n = 6) A) XY graph showing length increase from pre-treatment (μm) for untreated, cntrl, or PEP. B) Area under the curve (AUC) of length increases from pretreatment. C) XY graph showing increase in mineralisation zone over increase in total bone length (%). D) AUC of increase in mineralisation zone over total bone length. B) ANOVA shows significant effect of treatment (P = < 0.01) and D) Kruskal-Wallis shows significant effect of treatment (P = 0.001). Data are mean ± SEM for 3 independent experiments. B) * = P < 0.05 by Dunnett's multiple comparison D) ** = P < 0.01 by Dunn's multiple comparison.

3.2.3 Investigating known components of the PEPITEM Pathway

3.2.3.1 Activation of Cdh15 in osteoblasts does not enhance osteoblast differentiation.

Within endothelial cells it has been identified that PEPITEM acts through the activation of the adhesion molecule Cadherin-15 (Cdh15) to inhibit leukocyte trafficking. Little is known about the actions of Cdh15 on osteoblasts, however our group have previously described its presence at focal adhesion sites in murine osteoblasts. To assess the involvement of Cdh15, siRNA was used to inhibit Cdh15 functions. However, although siRNA was effective in knocking down *Cdh15* RNA in mouse and human, it failed to alter protein expression or location. Additionally, *CDH15* siRNA in human osteoblasts altered *ALP* gene expression in the absence of PEPITEM, suggesting that *CDH15* is required for typical osteoblast maturation and function. Therefore, to investigate the actions of Cdh15 on PEPITEM function we used agonistic antibodies to investigate whether the activation of Cdh15 could mimic the activity seen following PEPITEM treatment. Here we demonstrate that activation of Cdh15 did not cause an alteration in ALP activity (Figure 3.16). This coupled with the siRNA experiments therefore suggest that Cdh15 may not be the receptor involved in PEPITEM mediated maturation of osteoblasts.

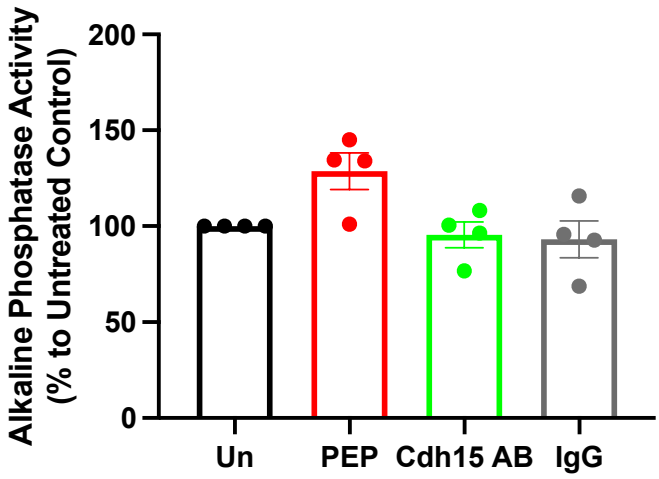


Figure 3.16 **Activation of Cdh15 does not mimic PEPITEM treatment.** C.Obs cultured in osteogenic media for 8 days with or without PEPITEM (10 ng/ml), anti-cdh15 antibody (3 µl/ml) or IgG control (3 µl/ml). Alkaline phosphatase activity was analysed on day 8 and displayed as % compared to untreated control. Kruskal-Wallis showed a significant effect of antibody treatment on alkaline phosphatase activity ($P < 0.0395$). Dunn's multiple comparison was used to analyse differences between untreated control and treatment groups.

3.2.3.2 S1P inhibits differentiation of murine osteoblasts at high concentrations.

Previous publications have discovered that PEPITEM activation of Cdh15 induces the release of S1P from endothelial cells[192]. In addition, S1P has been shown to have both osteoanabolic and osteocatabolic effects on bone remodelling[429], making it a potential regulator of PEPITEM function. Therefore, S1P was investigated as potential secondary molecule within the osteoblastic PEPITEM pathway. To assess this, exogenous S1P was added to ST2 osteoblast in culture for 4 days (Figure 3.17, A). The addition of high (0.5-1mM) concentrations of S1P resulted in a decrease in ALP activity within ST2 murine osteoblasts after 4 days of treatment opposite to that seen with PEPITEM treatment (Figure 3.17, A). Whereas at lower concentrations of S1P (0.125-0.25 μM), S1P had no effect on alkaline phosphatase activity comparatively to untreated controls (Figure 3.17, A). The effects of S1P on murine and human cells has been called into question, with S1P having a pro-osteoblastogenic function in human cells whilst inhibiting murine cells at the same concentration[429]. As PEPITEM does not have differing effects on ALP in mouse and human cells, these data suggest that PEPITEM is not acting through autocrine S1P activity.

3.2.3.3 Inhibition of S1P kinases in ST2 cells causing increased cell death.

Although we see differing effects of exogenous S1P on osteoblasts, PEPITEM may be acting through intracellular S1P signalling, which has been shown to impact many cell functions, including differentiation[142]. To assess whether PEPITEM function was driven by intracellular S1P production, S1P kinases (SphK1 and SphK2) were inhibited using different kinase inhibitors.

The addition of Sphk2 inhibitors, there was an increase in ALP activity in response to PEPITEM, however Sphk1 inhibitors alone did not (Figure 3.17, B). In the presence of PEPITEM, Sphk2 loss of ALP activity was reverted, suggesting that PEPITEM is able to act in the absence of Sphk2. Comparatively, no effect of PEPITEM treatment was seek following Sphk1 or Sphk1+2 inhibition, which may suggest PEPITEM requires Sphk1 for functions (Figure 3.17, B).

However, as S1P is involved in the survival of cells a viability analysis was preformed using trypan blue staining (Figure 3.17, C). Both CAY10621 (SphK1) and N,N-Dimethylsphingosine (d18:1) (SphK1&2) resulted in a significant increase in cell death following prolonged treatment with and without PEPITEM comparatively to differentiated control (Figure 3.17, C). SLM-60314340-hydrochloride (SphK2, cat; 6281/10, R&D Systems) did slightly increase cell death (Figure 3.17, C). Due to the increase in cell death following prolonged Sphk1 inhibition, the effect these kinases have on osteoblast maturation cannot be reliably interpreted. However, as there was limited cell death following Sphk2 inhibition and we saw PEPITEM mediated increase in ALP despite inhibition of Sphk2, it is unlikely that PEPTEM is acting through differences in Sphk2 function as seen previously[192].

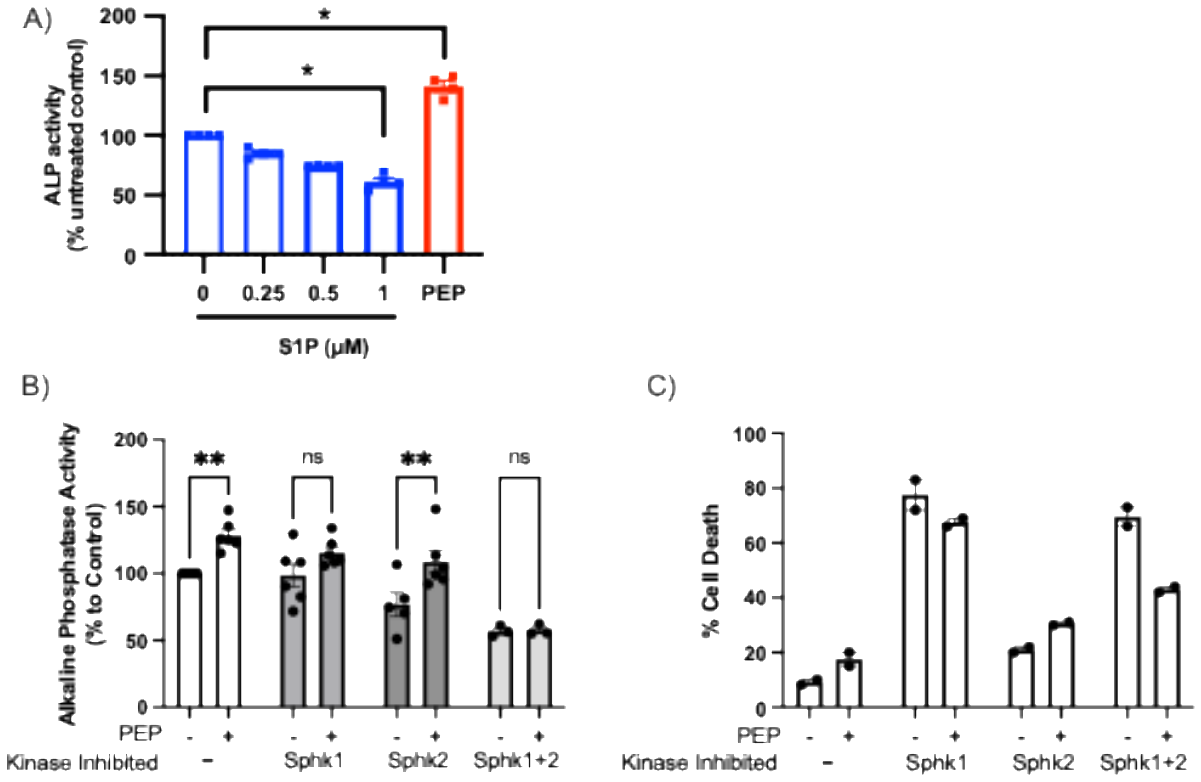


Figure 3.17 S1P Kinases inhibition results in increased cell death within ST2 cells. ST2 cells, bone marrow derived stromal clone cell line, were treated with either A) increasing concentration of sphingosine-1-phosphate (0.125-1 μM) or B-C) inhibitors against SPHK1 or 2 [CAY10621 (Sphk1), SLM-60314340-hydrochloride (Sphk2) and N,N-Dimethylsphingosine (Sphk1+2)] in the presence or absence of exogenous PEPITEM for four days. (A,B) Alkaline phosphatase activity was quantified and expressed as a percentage of the differentiated untreated osteoblast control. (C) Trypan blue staining was used to quantify cell death and was plotted as number of trypan blue positive cells as a percentage of total cells. A) Kruskal-Wallis test showed a significant effect of treatment on alkaline phosphatase activity, P = < 0.001. B) Two-way ANOVA showed a significant effect of SphK inhibitor treatment (P = < 0.0001), and PEPITEM treatment (P = 0.0003), on alkaline phosphatase activity. Data are mean ± SEM, where n = 3 independent experiments, except B where n = 2. In A, * = < 0.05by Dunn's multiple comparison. In B, **=P<0.001 by Sidak's multiple comparisons test.

3.2.4 Identification of Novel PEPITEM pathway in osteoblasts

3.2.4.1 Co-immunoprecipitation and Mass spectrometry analysis detected several PEPITEM binding partners.

Based on the data described above, we hypothesis that PEPITEM is acting through alternative mechanisms than those described in endothelial cells. Therefore, we sought to identify novel targets of PEPITEM using co-immunoprecipitation (co-IP) experiments, as were used initially to identify Cdh15. Prior to co-IP pull down we first assessed the bio activity of the biotin conjugated peptide. To do these we used a known measurement of PEPITEM function, alkaline phosphatase activity (ALP). These data show that biotin-tagged PEPITEM induced the same increase on ALP activity as non-biotinylated PEPITEM when compared to untreated control (Figure 3.18). Therefore, suggesting that biotinylation does not affect PEPITEM function and therefore receptor-ligand interaction.

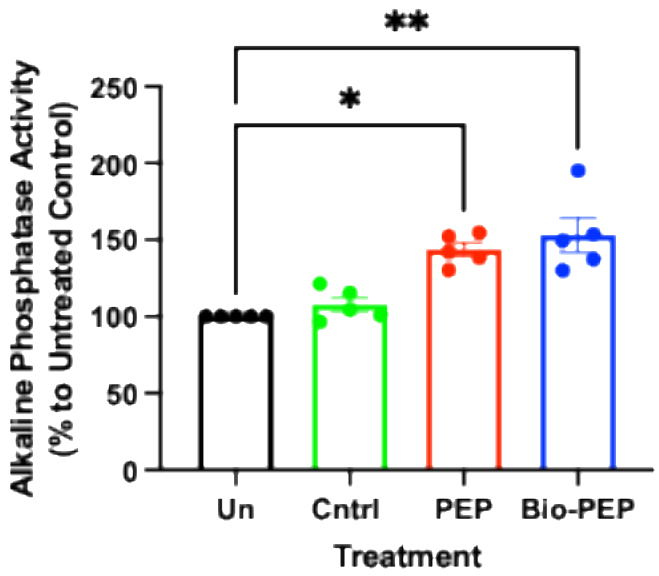


Figure 3.18 Biotinylation of PEPITEM does not affect bioactivity of the peptide. C.Obs untreated (black, n = 5), or treated with 10ng control peptide (blue, n = 5), PEPITEM (red, n = 5) or Biotinylated PEPITEM (green, n = 5), for 7 days. Cell maturity was analysed using ALP ELISA on day 8 and presented as percentage of untreated control. Friedman test analysis shows a significant effect of treatment ($P < 0.001$). Data are mean ± SEM for 4 independent experiments. * = $P < 0.05$ and ** = $P < 0.01$ by Dunn's multiple comparison test.

As we had a functional biotinylated peptide, we were able to perform pull down experiments to collect proteins which were bound to biotinylated PEPITEM or biotinylated control peptide. Following pulldown, peptides were analysed using mass spectrometry. The list of detected proteins was analysed to remove proteins that appeared more than once in the control peptide samples and filtered based on three criteria; (1) Isoelectric point (pI), an indicator of protein cell location due to protein charges, (2) sequest score, degree of correlation between expected and observed protein levels and (3) number of unique peptides detected. In addition, CRAPome[430] analysis was then used to remove proteins that appeared in >20% pulldown experiments. Remaining proteins are displayed in (Table 3.1) and presented in a graphical format (Figure 3.19). Following detection, an initial literature search of each protein was performed, investigating any known function for these peptides in cell differentiation or osteogenesis.

Table 3.1 **Hits from PEPITEM only Co-IP analysis**. Proteins which were only identified to bind to PEPITEM not control peptide. **Ave. # Peptides**, the number of unique peptides detected which have been identified within the parent protein sequence. **MW [kDa],** molecular weight of parent protein. **Calc. PI**, calculated isoelectric point of protein, providing indication of cellular location (4-7 indicates membrane association). **Ave. sequest HT score,** measure of amount of detected peptide compared to expected number of peptides detected, high sequest sore indicates there is a significant increase in the amount of peptide compared to what would usually be expected per mass spectrometry sample.

Description	Gene ID	Ave. # Peptides	MW [kDa]	calc. pI	Ave. Sequest HT Score
Annexin A6	*Anxa6*	25.5	75.8	5.5	110.9625
Neural cell adhesion molecule 1	*Ncam-1*	14.75	93.6	4.93	61.91
Protein transport protein Sec31A	*Sec31a*	17	133.5	6.76	49.59333333
EH domain-containing protein 2	*Ehd2*	16	61.1	6.51	48.02333333
Catenin delta-1	*Ctnnd1*	16	108.1	6.23	46.86333333
Catenin alpha-1	*Ctnna1*	11.66666667	100	6.23	38.67666667
Dipeptidyl peptidase 3	*Dpp3*	10.33333333	82.8	5.34	33.00666667
Serine/threonine-protein phosphatase 2A 65 kDa regulatory subunit A beta isoform	*Ppp2r1b*	10.33333333	76	5.19	26.80333333
Pleckstrin homology domain containing, family C (With FERM domain) member 1	*Fermt2*	11.5	77.8	6.7	23.7
Alpha-1,4 glucan phosphorylase	*Pygb*	10	96.6	6.65	23.43
Nucleoredoxin	*Nxn*	10.33333333	48.3	4.93	20.21333333

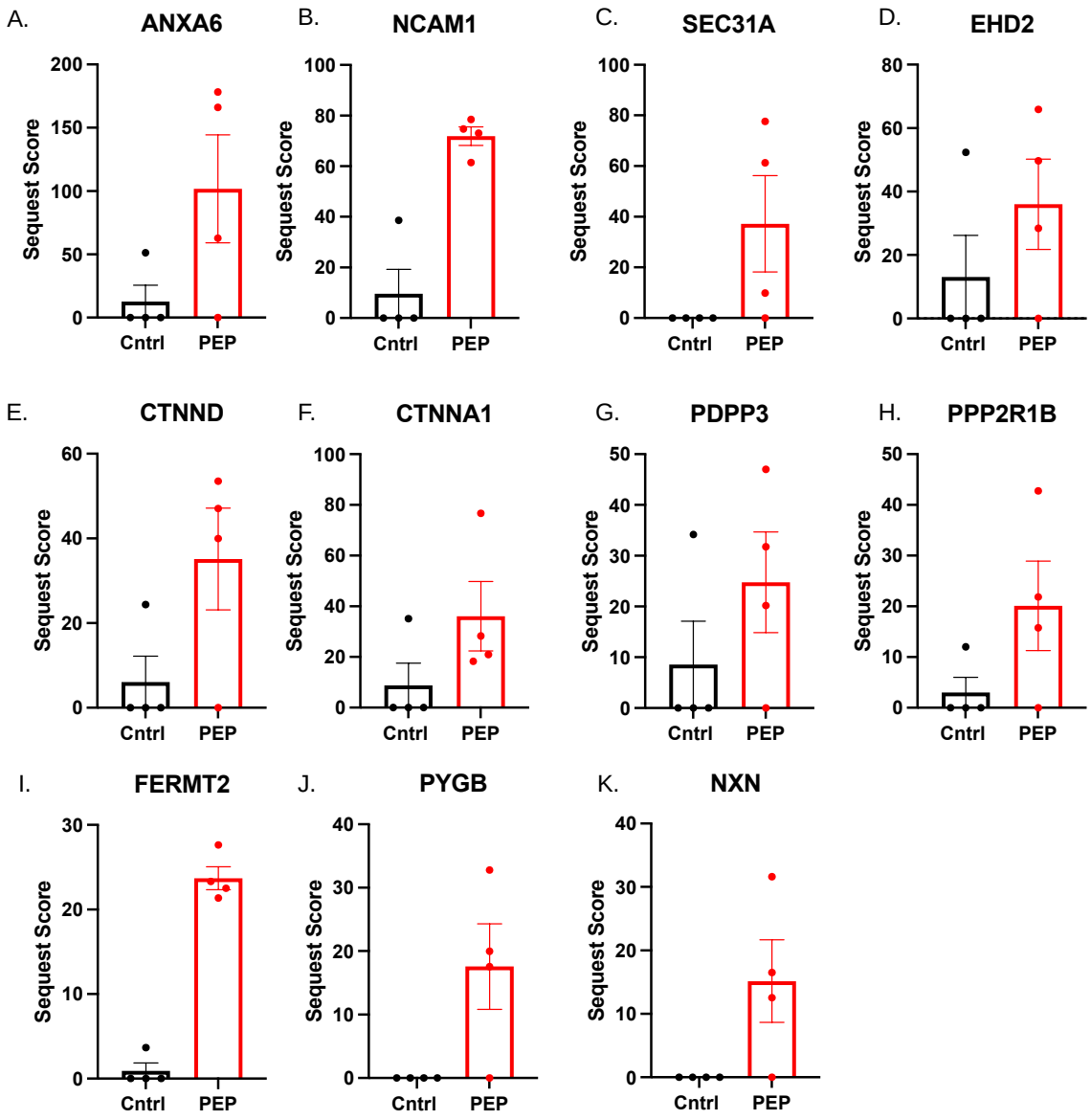


Figure 3.19 **Graphical analysis of peptides from Co-IP.** Peptides positive with in more than 3 PEPITEM samples but less than 2 Cntrl samples. A)Annexin A6 (AnxA6) B) Neural cell adhesion molecule 1 (NCAM-1) C) Protein transport protein Sec31A (Sec31a) D) EH domain-containing protein 2 (EHD2) E) Catenin delta-1 (CTNND1) F) Catenin alpha-1 (CTNNA1) G) Dipeptidyl peptidase 3 (DPP3) H) Serine/threonine-protein phosphatase 2A 65 kDa regulatory subunit A beta isoform (PPP2r1b) I) Pleckstrin homology domain containing, family C (With FERM domain) member 1 (FERMT2) J) Alpha-1,4 glucan phosphorylase (PYGB) K) Nucleoredoxin (nxn). Data are mean ± SEM for 4 independent experiments.

3.2.4.2 In Silico analysis of PEPITEM binding partners

To identify the most likely receptor, alongside our literature review we used in silico analysis to investigate protein interactions with PEPITEM. For this analysis we used programmes AlphaFold2[409,410] and ChimeraX[411,412] to create a predicted 3D rendering of both the binding protein and PEPITEM to assess location and predicted strength of binding. AlphaFold-Multimer[413,414] allows the prediction protein-protein interactions without the need for a linker as used previously[413,415]. This has been shown to have higher prediction capacity[413]. Following AlphaFold predictions, data were analysed in ChimeraX. Proteins have been split based on their known cellular location, (membrane, cytosolic, vesicles) or function (enzymes) (Figure 3.20), with predicted PEPITEM binding location annotated. Proteins are coloured based on their pLDDT score, where blue indicates high confidence and red is low. Although multiple proteins shown high predicted binding of PEPITEM (Figure 3.20), we focused on binding to cell membrane receptors as at the point of analysis we have not confirmed PEPITEM internalisation.

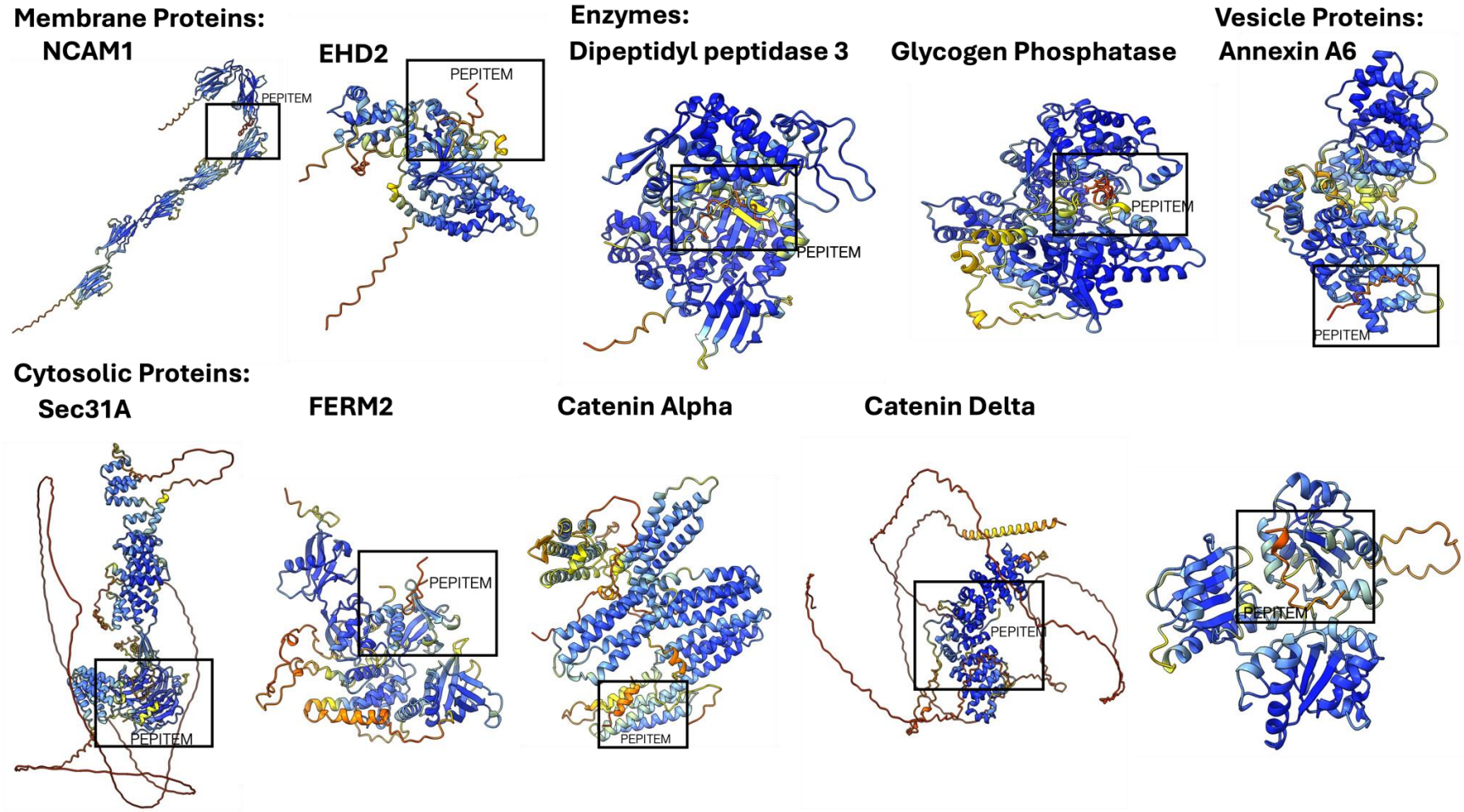


Figure 3.20 **PEPITEM binding models to top co-ip hits.** ChimerX modelling of AlphaFold2 binding predictions of PEPITEM to top co-IP proteins. Location of PEPITEM indicated by black box. Proteins separated into membrane proteins, enzymes, vesicle proteins and cytosolic proteins.

3.2.4.3 Neural cell adhesion molecule 1

Neural cell adhesion molecule 1 (NCAM-1) is a 120-190kDa glycoprotein and forms part of the Ig superfamily. NCAM-1 can be split into three major isoforms; 120, 140 and 180[431], all of which have been identified currently in MSCs[432]. The function of these isotypes has been shown to be different in with NCAM-180 and -140 being required for MSC migration[433]. Due to this when looking at computational models of PEPITEM binding we chose to use the extracellular tail of NCAM-180 (Uniprot: P13595).

Here we opted to only use the external portion of the protein as this is where we would usually expect ligand interactions. NCAM-1 can be split into 5 IgG-like domains as well as 2 fibronectin-III like domains[434]. AlphaFold[409] analysis show strong predicted alignment for the individual domains however the alignment to other domains was low (Figure 3.21, A). Additionally, the alignment for PEPITEM as with many of the other models was also low (Figure 3.21, A,B). Using chimera 3D modelling and sequence viewing it was identified that PEPITEM is binding to the fibronectin domain of the extracellular NCAM-1 protein (Figure 3.21,A). Bond analysis shows 1 predicted hydrogen bond forming between PEPITEM and NCAM-1 (Figure 3.21, B)(Table 3.2) and 8 pseudobonds (Figure 3.21, C)(Table 3.2), 75% of which have a pLTTD value of 70>50 suggesting low predicted binding. These data may suggest there is some interaction between PEPITEM and NCAM-1 via the fibronectin domain. Due to the size of NCAM-1 comparatively to the other proteins tested, we also looked at PEPITEM-fibronectin-III domain interactions to observe whether the size difference of the two peptides was diluting the potential for interaction detection (Figure 3.22), to allow us to decipher the amino acid residues involved in the binding interactions.

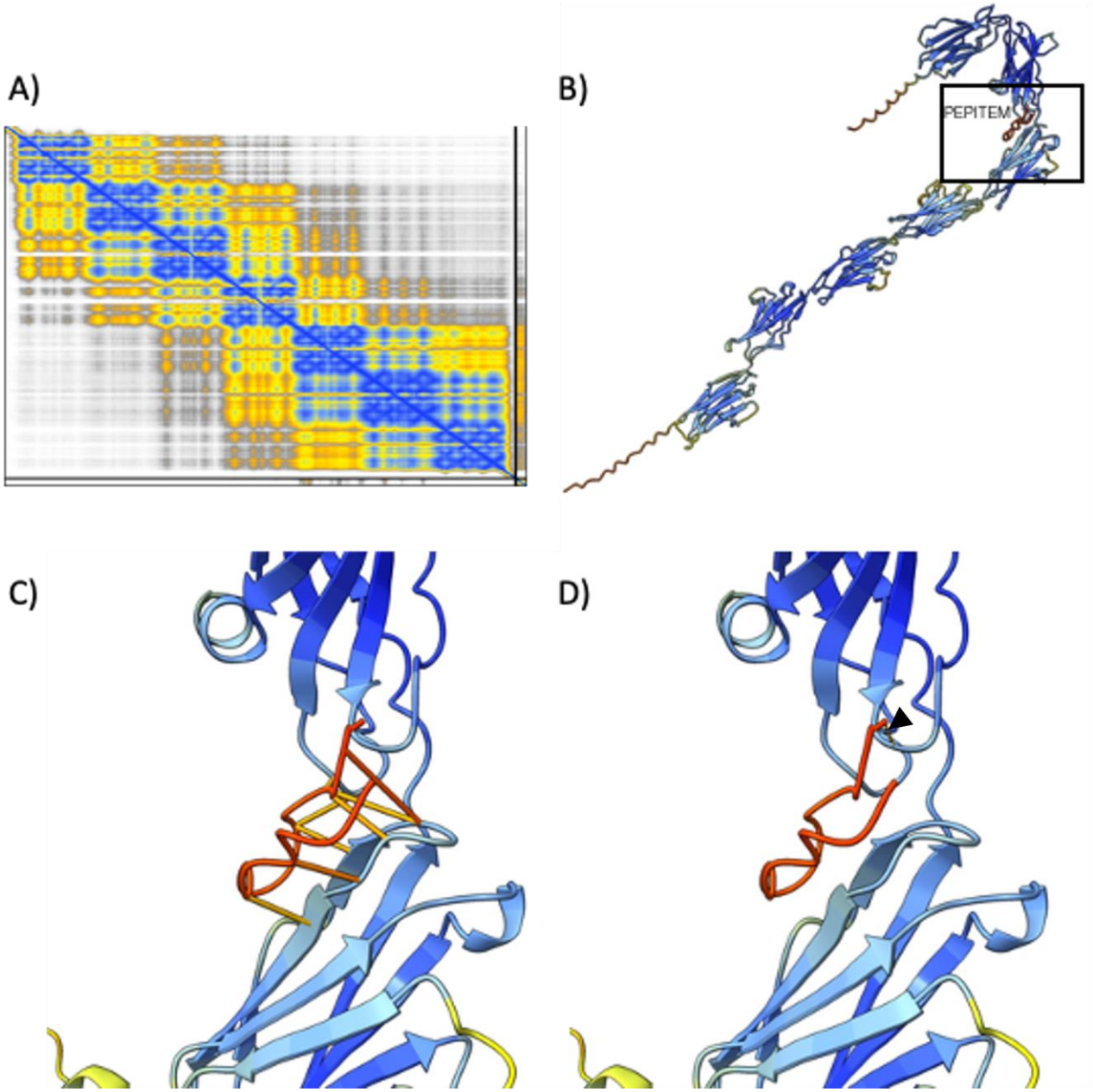


Figure 3.21 **Alphafold predicted binding of PEPITEM and NCAM-1.** The NCAM-1 sequence and the PEPITEM sequence were both ran together in AlphaFold-multimer. (A) Predicted aligned error (PAE) heat map for the top predicted model of NCAM-1 and PEPITEM, blue indicating low error and red indicating high error. B) 3D ChimeraX reconstruction of PEPITEM binding to NCAM-1, where the protein is coloured based on pLDDT, high confidence (blue) and low confidence (red). PEPITEM can be seen within the black square. C-D) Magnified view of PEPITEM binding site. C) Pseudobonds between PEPITEM and NCAM-1 with bonds represented as connecting lines falsely coloured based on pLDDT where blue is high binding predictability and red is low. D) Predicted hydrogen bonds between PEPITEM and NCAM-1, represented as dotted lines indicated with a black arrow.

The two fibronectin-III like domains from the NCAM-1 sequence along with one IgG-like domain (IgG5) were ran through AlphaFold alongside PEPITEM. Here you can see that the predicted residue alignment is much stronger comparatively to the whole extracellular NCAM-1 protein (Figure 3.22, A). As seen with the larger protein PEPITEM was predicted to bind to the fibronectin-III like domains, however the alignment prediction of PEPITEM was still low (Figure 3.22, B).

When looking at this 3D model the first thing to be noted was that PEPITEM was now binding to the second fibronectin-III like domain opposed to the first domain (Figure 3.22, A). This may suggest issues with AlphaFold when observing large-small protein interactions. When looking at bond interactions in this model we observe 9 predicted hydrogen bonds (Figure 3.22, B)(Table 3.2), significantly more that seen with the larger protein. However, this time we see a stark increase in the number of pseudobonds predicted: with 13 being predicted opposed to the 8 detected previously (Figure 3.22 C)(Table 3.2). Additionally, the pseudobonds have a pLDDT score of >70, shown in light/dark blue, suggesting high confidence in the predicted pseudobonds. The bonds found in the whole model are not identified in the fibronectin type-III only model (Figure 3.22 C)(Table 3.2). These data suggest that PEPITEM may be interacting with the fibronectin-III type domain on NCAM-1 to exert its function. This analysis also highlights the pitfalls when analysing a very small peptide and a large protein using AlphaFold.

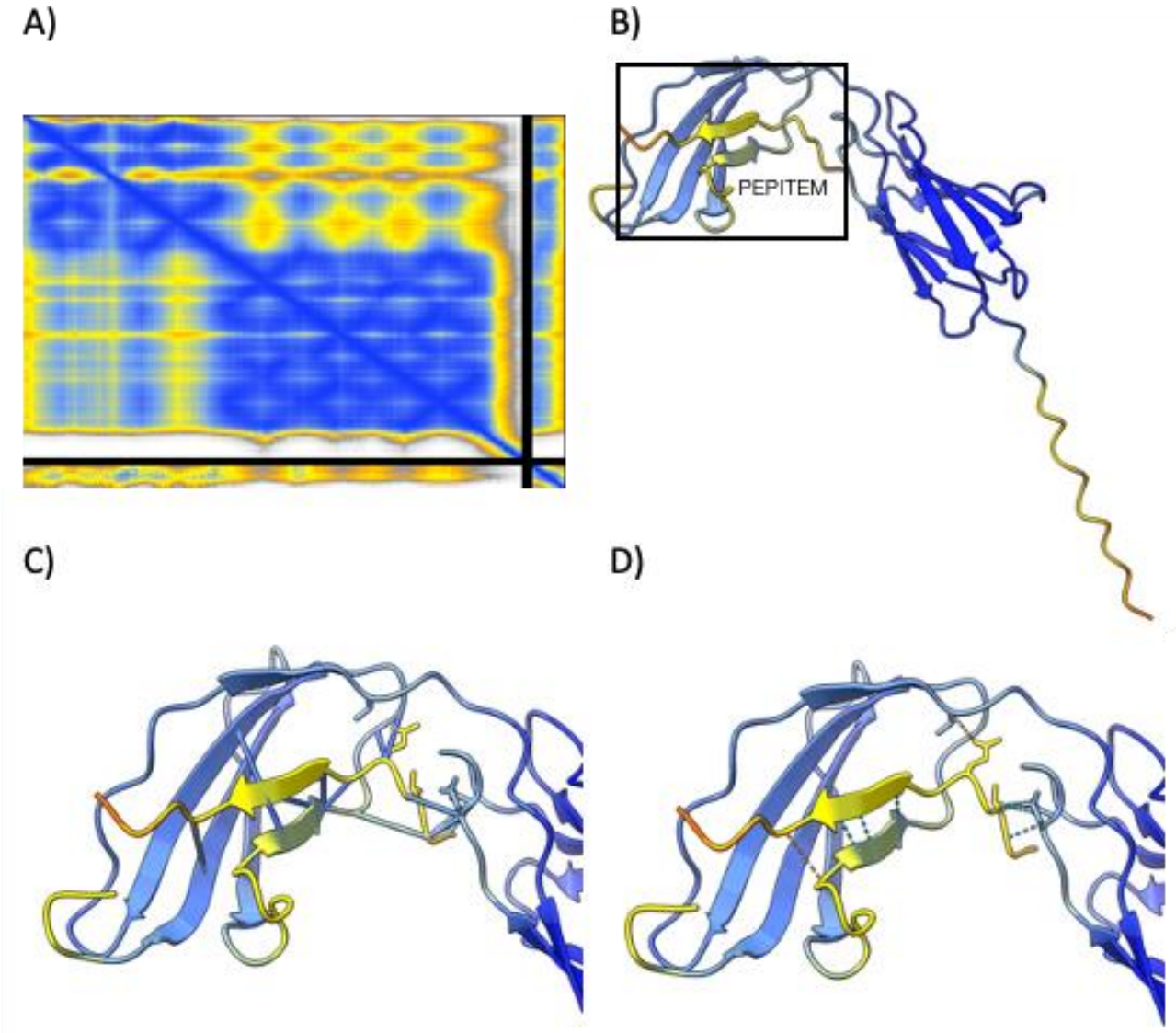


Figure 3.22 Alphafold predicted binding of PEPITEM and NCAM-1 Fibronectin-III domains. The NCAM-1 fibronectin domain sequence and the PEPITEM sequence were both ran together in AlphaFold-multimer. (A) Predicted aligned error (PAE) heat map for the top predicted model of NCAM-1 fibronectin domain and PEPITEM, blue indicating low error and red indicating high error. B) 3D ChimeraX reconstruction of PEPITEM binding to NCAM-1 fibronectin domain, where the protein is coloured based on pLDDT, high confidence (blue) and low confidence (red). PEPITEM can be seen within the black square. C-D) Magnified view of PEPITEM binding site. C) Pseudobonds between PEPITEM and NCAM-1 fibronectin domain with bonds represented as connecting lines falsely coloured based on pLDDT where blue is high binding predictability and red is low. D) Predicted hydrogen bonds between PEPITEM and NCAM-1 fibronectin domain, represented as dotted lines.

Table 3.2 AlphaFold-Multimer predicted binding residues for PEPITEM interacting with NCAM-1

Binding Protein	Bond Type	Protein residue	PEPITEM residue	Distance (Å)	pLDDT range score
NCAM-1	Hydrogen Bond	LYS 619 NZ	SER 10 OG	3.234	N/A
		SER 656 OG	GLY 6 O	2.746	N/A
		HIS 658 ND1	SER 10 N	3.017	N/A
		LEU 622 O	ASN 11 ND2	2.837	N/A
	Predicted Pseudobonds	SER 656	LEU 9	3	50-70
		SER 656	GLY 6	3	50-70
		SER 656	GLU 8	3	50-70
		SER 656	ALA 7	3	50-70
		PRO 653	GLY 6	3	50-70
		PRO 653	ALA 7	3	50-70
		ASP 657	ASN 11	3	50-70
		ASP 657	SER 10	3	50-70
		ASP 657	GLU 8	3	50-70
		ASP 657	LEU 9	3	50-70
		HIS 658	SER 10	3	50-70
		HIS 658	LEU 9	3	50-70
		HIS 658	GLU 8	3	50-70
		LEU 622	ASN 11	3	50-70
		LEU 622	LEU 9	3	50-70
		GLY 655	ALA 7	3	50-70
		GLY 655	GLU 8	3	50-70
Fibronectin-III Domains (from NCAM-1)	Hydrogen Bond	VAL 37 N	LEU 9 O	2.676	N/A
		ILE 39 N	ALA 7 O	2.755	N/A
		THR 71 OG1	GLN 5 OE1	3.358	N/A
		ASP 102 N	VAL 2 O	2.818	N/A
		ASP 102 OD1	THR 3 OG1	3.125	N/A
		ASP 102 OD2	THR 3 OG1	3.170	N/A
		ASP 101 OD1	GLU 4 N	2.499	N/A
		VAL 37 O	LEU 9 N	2.583	N/A
		GLY 35 O	ASN 11 N	3.341	N/A
	Predicted Pseudobonds	ASP 102	SER 1	3	70-90
		ASP 102	VAL 2	3	70-90
		ASP 101	VAL 2	3	70-90
		ASP 101	GLU 4	3	70-90
		TYR 9	ASN 11	3	70-90
		MET 40	VAL 2	3	>90
		PRO44	GLN 5	3	>90
		LYS 43	GLN 5	3	>90
		ILE 39	GLY 6	3	>90
		ILE 39	ALA 7	3	>90
		ILE 39	LEU 9	3	>90
		VAL 50	LEU 9	3	>90
		VAL 37	LEU 9	3	>90

3.2.4.4 EH domain-containing protein 2

EH domain containing protein 2 (EHD2) (Uniprot: Q8BH64) is a 61kDa membrane remodelling ATPase and is required for endosomes and the plasma membrane[435]. EHD2 consists of an N-terminal extended GTPase domain, a helical domain and a C-terminal Eps15-homology domain[435]. In silico analysis suggests PEPITEM binds to the GTPase domain of EHD2 (Figure 3.23, A,B). 12 pseudobonds were detected through Alphafold modelling, all with a pLTTD score of 70>50 (Figure 3.23, C). There are an additional 3 hydrogen bonds predicted between these two proteins (Figure 3.23, D).

Of these two proteins NCAM-1 shows stronger predicted binding to PEPITEM particularly to the fibronectin III-like domain of the protein. Additionally, NCAM-1 has been previously linked to osteoblast maturation and mineralisation[433,436,437]. Therefore, we chose to take NCAM-1 forward for *in vitro* testing.

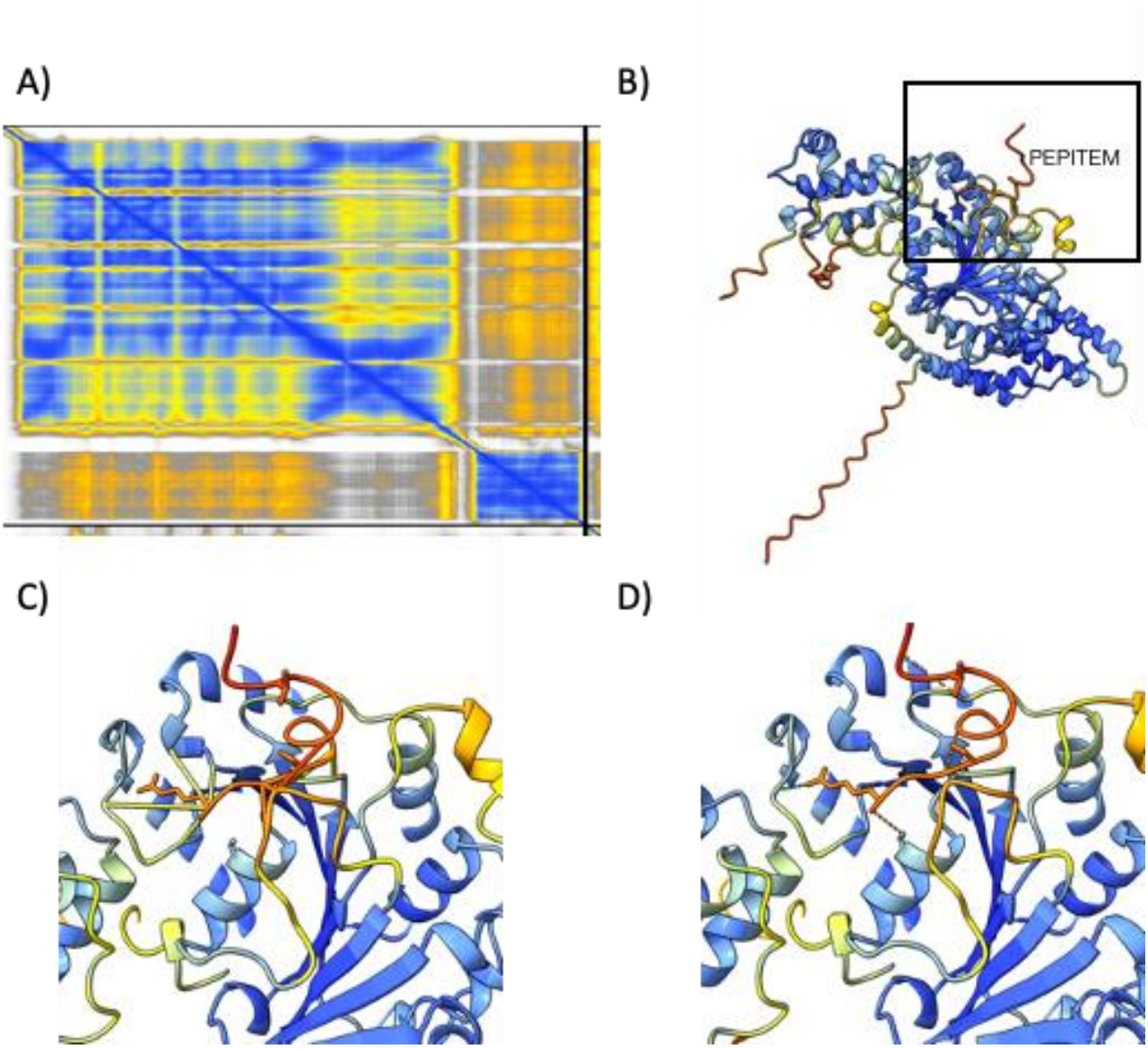


Figure 3.23 **Alphafold predicted binding of PEPITEM and Ehd2.** The Ehd2 sequence and the PEPITEM sequence were both ran together in AlphaFold-multimer. (A) Predicted aligned error (PAE) heat map for the top predicted model Ehd2 and PEPITEM, blue indicating low error and red indicating high error. B) 3D ChimeraX reconstruction of PEPITEM binding to Ehd2, where the protein is coloured based on pLDDT, high confidence (blue) and low confidence (red). PEPITEM can be seen within the black square. C-D) Magnified view of PEPITEM binding site. C) Pseudobonds between PEPITEM and Ehd2 with bonds represented as connecting lines falsely coloured based on pLDDT where blue is high binding predictability and red is low. D) Predicted hydrogen bonds between PEPITEM and Ehd2, represented as dotted lines.

3.2.5 NCAM-1 signalling

3.2.5.1 Confirming the presence and level of expression of NCAM-1 in Calvarial osteoblasts

NCAM-1 (also known as CD56) is a member of the immunoglobulin superfamily initially earned its name due to its high expression in neural cells within the central and peripheral nervous system[438]. However, NCAM-1 has been since shown to be a widely ubiquitous protein and can be identified in several cell types such as epithelial cells, natural killer cells, skeletal muscle and mesenchymal stem cells (MSCs)[432,433,436,439–441].

Current literature describes the transient expression of NCAM-1 on osteoblasts, with it being reported in osteoblast progenitors and early osteoblasts, however the expression of NCAM-1 decreases with osteoblast maturation[436]. Additionally, it has been demonstrated that the expression of NCAM-1 in calvarial osteoblasts (C.Ob) in culture reduces over time[442]. Therefore, we sought to confirm the expression of NCAM-1 in C.Obs at the point of PEPITEM treatment within our *in vitro* models. In order to do this, we look at NCAM-1 gene and protein expression.

Gene expression of *Ncam-1* in primary C.Ob was analysed by qPCR revealing that *Ncam-1* was expressed in C.Obs following 24hr of culture (Figure 3.24, A), this was shown comparatively to the additional osteoblast marker *Alpl*. Expression of *Ncam-1* within C.Ob was further observed in RNAseq data analysed using iDep[408], where RNA was collected at 6hr, 24hr and 8-day timepoints also shown comparatively to *Alpl* and *Col1a1* (Figure 3.24, A). These data confirm that *Ncam-1* is relatively highly expressed within C.Obs comparatively to other osteoblast markers (Figure 3.24, B). Additionally, the expression of *Ncam-1* does not significantly change during culture.

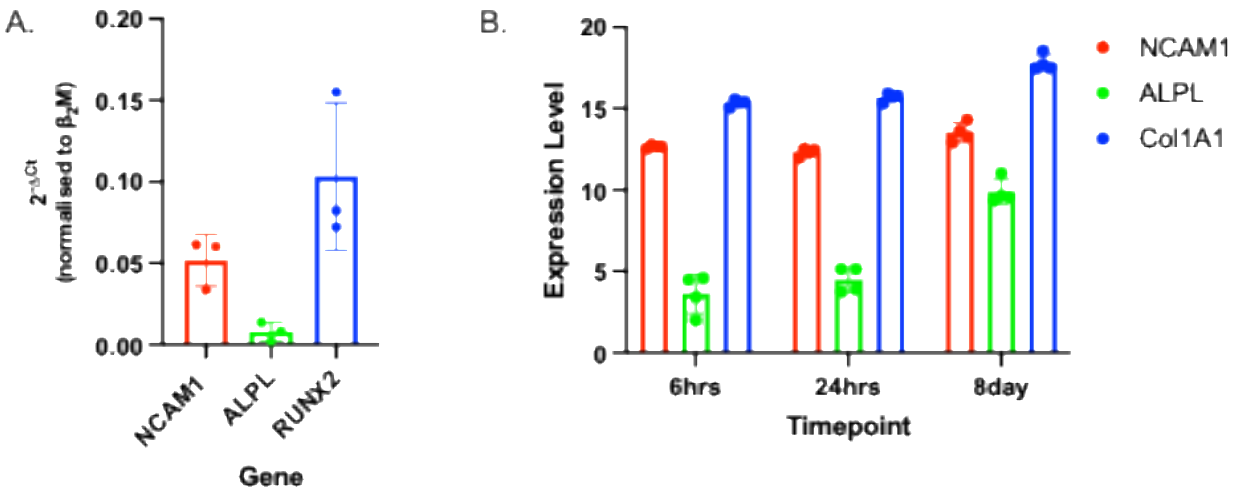


Figure 3.24 **C.Obs express NCAM-1 at time of PEPITEM treatment**. Primary C.Obs were cultured and analysed for NCAM-1 using (A) qPCR (B) RNAseq (A) Data are displayed as 2-ΔCt where ΔCt is the difference between NCAM-1, ALPL or RUNX2 expression and B2m housekeeping gene. (B) Data displayed as expression level following iDep analysis, displaying NCAM-1, ALPL and Col1A1 expression at 6hr, 24hr or 8 days of culture. Sidak's multiple comparison shows no significant difference in gene expression at 6, 24hr or 8 days in culture.

The cellular location of NCAM-1 on C.Obs was investigated using immunofluorescent imaging of *in vitro* cell cultures after 24hr of culture (Figure 3.25). Staining showed that Ncam-1 was predominantly found on the cell surface of C.Ob. Together these data suggest that C.Obs can produce and express NCAM-1 and are highly expressing this protein at time of PEPITEM treatment.

To determine protein expression of NCAM-1 on C.Obs western blotting was performed on C.Ob lysates which had been differentiated with or without PEPITEM for 8-days. Western blotting revealed the different isomers of NCAM-1 detected on C.Obs (Figure 3.26). NCAM-1 can be found as three full length FL isomers separated based on cytoplasmic tail length NCAM-180, NCAM-140 and a GPI-anchored isoform, NCAM-1-120[431]. Here we were to detect all three of these isoforms (Figure 3.26) based on their predicted molecular weight. Of these isoforms it appears NCAM-1-140 is most highly expressed and NCAM-180 least expressed (Figure 3.26). In addition to the full length isomers, NCAM-1 can be further separated into soluble fragments, where NCAM-1 has been cleaved from the membrane[434]. Here we detect three soluble NCAM-1 fragments (sNCAM-1) (Figure 3.26), soluble NCAM-1 has been found to interfere with NCAM-1 signalling through binding to membrane bound NCAM-1 protein[434]. The cleavage tail from NCAM-1 cleavage was also detected (Figure 3.26). To investigate whether PEPITEM influenced NCAM-1 expression we compared NCAM-1 expression of treated and untreated cells (Figure 3.27). Here we saw an increase in the levels of NCAM-180 isomer compared to control treated cells (Figure 3.27, A), without any difference in the other isomers, cleaved proteins or total NCAM-1 protein (Figure 3.27, B-F), suggesting PEPITEM may alter NCAM-1 expression, positively regulating PEPITEM activity.

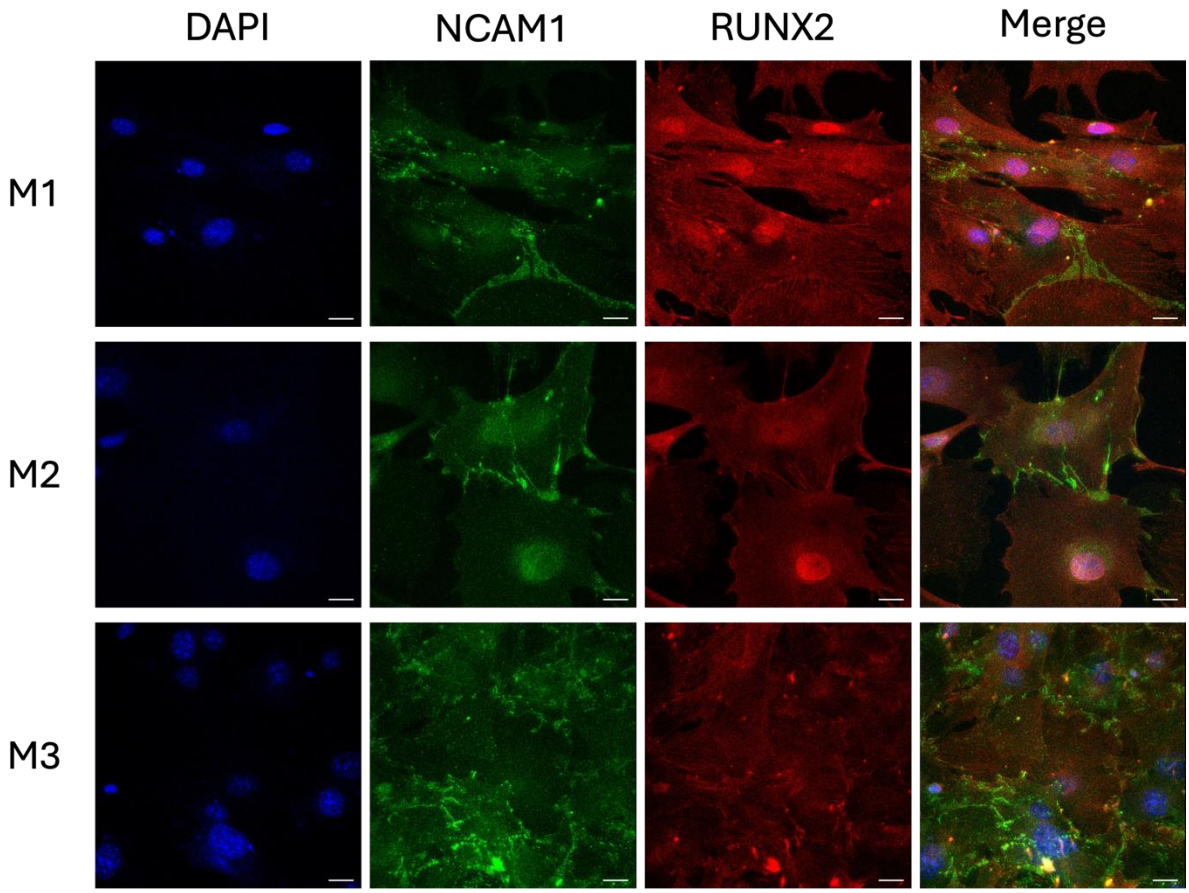


Figure 3.25 Representative images of C.Obs stained for NCAM-1 and RUNX2, showing surface expression of NCAM-1. C.Obs cultured on coverslips for 24hr and stained for NCAM-1 (green), RUNX2 (red) and nuclear DAPI staining (blue). Immunofluorescent images were captured and expressed as individual channels and merged. Scale bars = 20 μm. Data are images of 3 different murine samples (M1-M3) from 3 individual experiments.

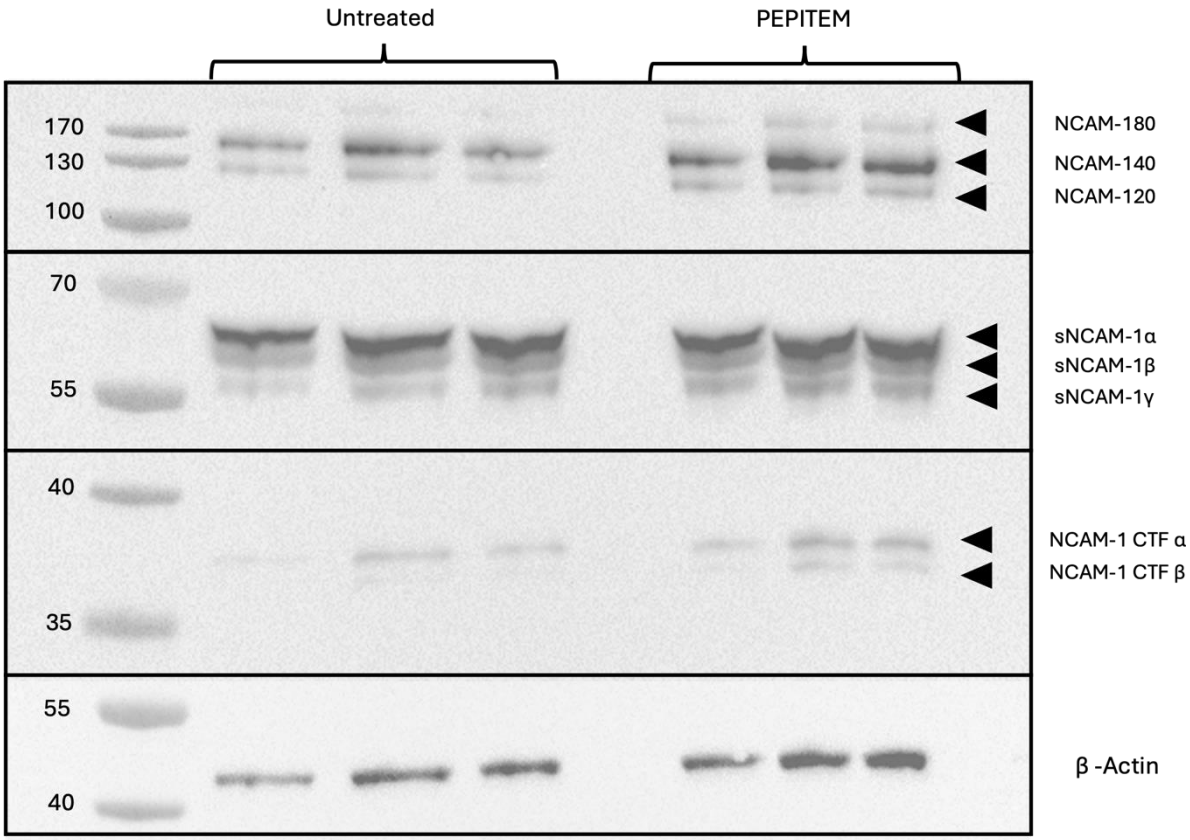


Figure 3.26 **Western blot of C.Ob lysates treated with or without PEPITEM stained of NCAM**-1compared to actin. C.Obs were cultures for 8 days without (untreated, n = 3) or with PEPITEM (PEPITEM, n = 3). Lysates were isolated and run via western blot and analysed for NCAM-1 and b-actin (control). Representative western blot showing expression of NCAM-1 isoforms indicated by black arrows showing whole protein (NCAM-180,-140 and -120), cleaved extracellular soluble protein (sNCAM-1α, β, γ) and cleaved cytoplasmic tail fragment (NCAM-1-CTFα, β) and β-actin control.

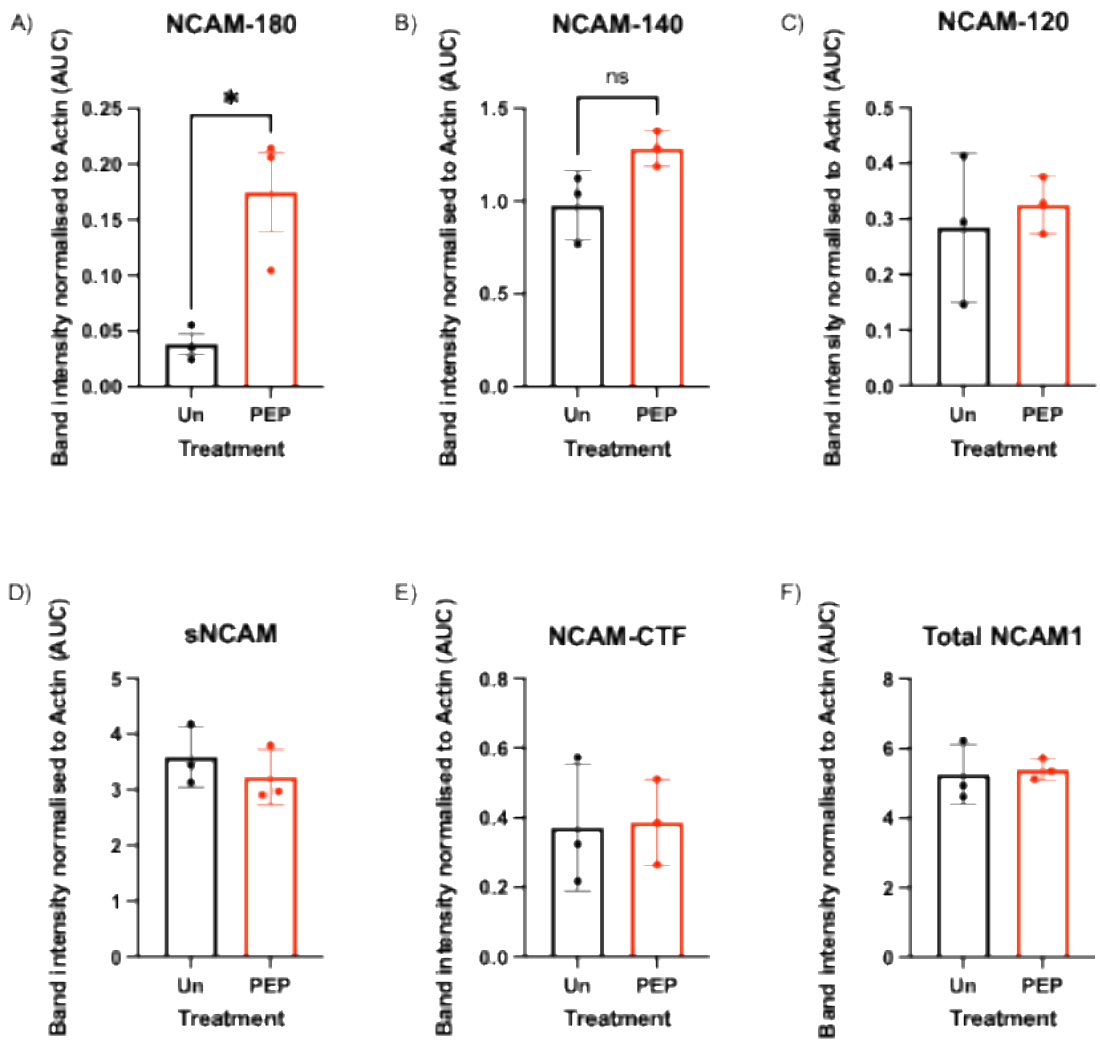


Figure 3.27 **PEPITEM treatment alters NCAM-1 expression.** C.Ob treated with or without PEPITEM for 8-days, after cells were lysed and proteins ran through a western blot. Blot was stained for NCAM-1. NCAM-1 isoforms were separated based on molecular weight and quantified compared to actin loading control. (A) NCAM-180 (B) NCAM-140 (C) NCAM-140 (D) soluble NCAM-1 (sNCAM) (E) NCAM-1 C-terminal fragment (NCAM-CTF) and (F) Total NCAM-1. Data are mean ± SEM. * = $P < 0.05$ by Wilcoxon test.

3.2.5.2 Investigating the effect of inhibiting NCAM on PEPITEM function.

Following confirmation of expression, NCAM-1 was taken forward as a potential receptor for PEPITEM within osteoblasts. We sought to inhibit NCAM-1 function, this was first attempted using an antibody against the NCAM-1 protein[443]. Treatment with NCAM-1 antagonistic antibody reduced the effect of PEPITEM on ALP activity in both ST2 (Figure 3.28, A) and C.Ob (Figure 3.28,B), suggesting that PEPITEM may act at least partially through NCAM-1 signalling.

In order to further investigate the role of NCAM-1 in osteoblast responses to PEPITEM, we applied the same NCAM-1 inhibitor to the ex vivo metatarsal model (Figure 3.29). Looking at the increase in mineralisation zone length, there was a significant increase following PEPITEM treatment with or without isotype control (Figure 3.29, A) quantified as area under the curve (Figure 3.29, B), whereas the was no increase in NCAM-1 AB and PEPITEM treated metatarsals compared to control (Figure 3.29, B). In order to control for differences in metatarsal length, increase in mineral length was normalised to total metatarsal length (Figure 3.29, D) quantified as area under the curve (Figure 3.29, D). Here we saw the same significant increase with PEPITEM with or without the isotype control, whereas in the presence of NCAM-1 AB there was no significant effect of PEPITEM (Figure 3.29, D). These data suggest NCAM-1 is required for PEPITEM mediated metatarsal mineralisation.

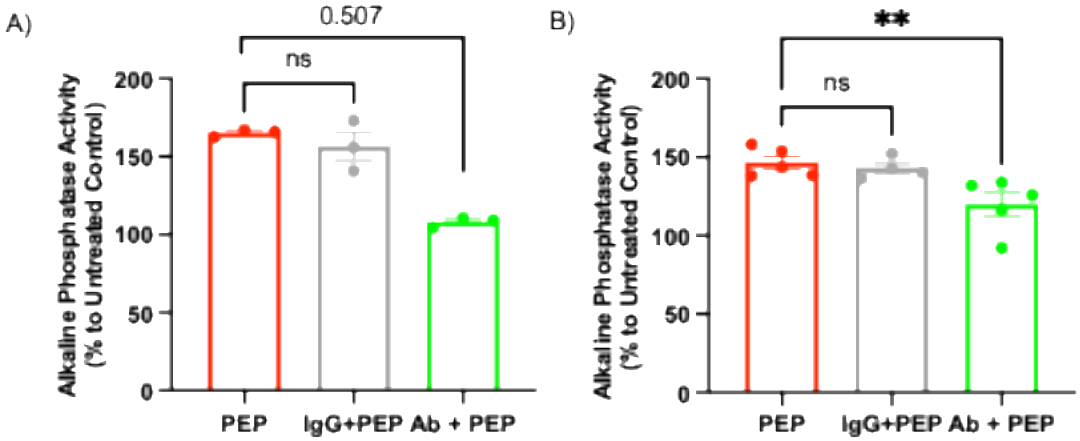


Figure 3.28 **Inhibition of NCAM-1 reduces the effect of PEPITEM.** ST2 (A, n = 3) or C.Obs (B, n = 5) cultured in osteogenic media for 8 days with PEPITEM (10 ng/ml) with or without anti-NCAM-1 antibody (2 μl/ml) or IgG control (2 μl/ml). Alkaline phosphatase activity was analysed on (A) day 4 or (B) day 8 of treatment and displayed as % compared to untreated control. Kruskal-Wallis showed a significant effect of antibody treatment on alkaline phosphatase activity (A) P = 0.05 or (B) P = 0.0019. Data are mean ± SEM. ** = P < 0.01 by Dunn's multiple comparison.

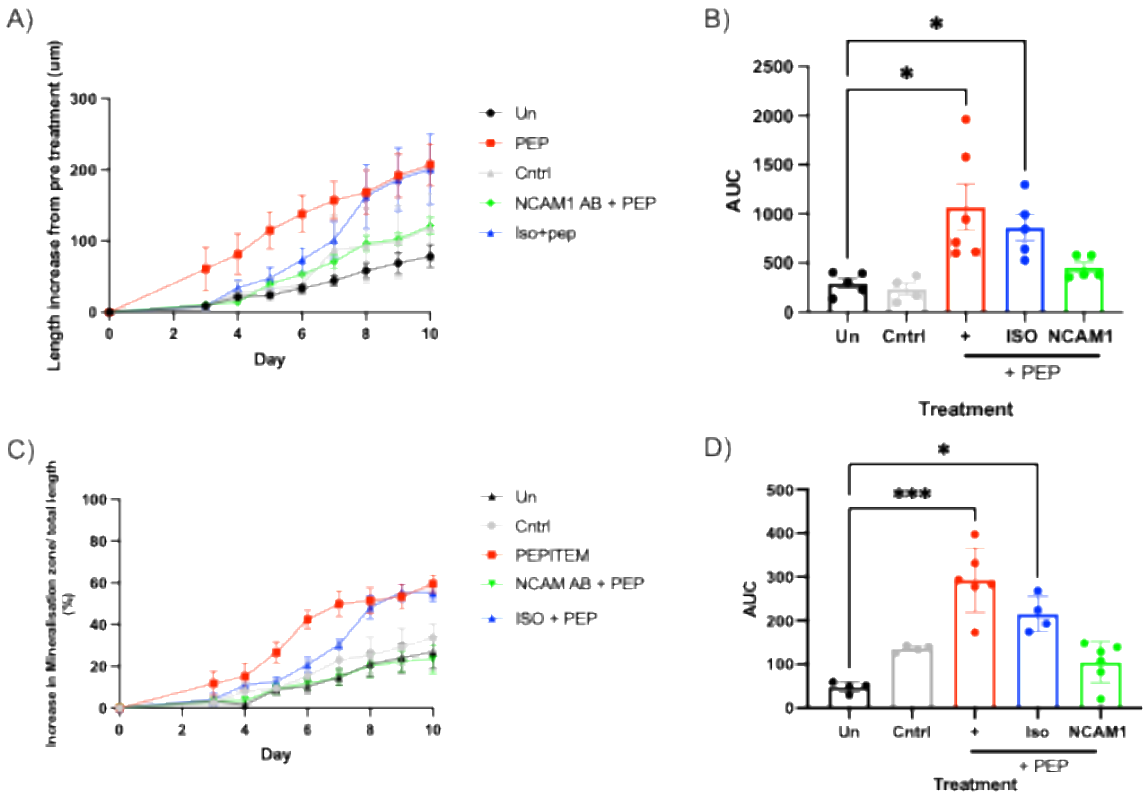


Figure 3.29 PEPITEM mediated increase in mineralisation is inhibited by NCAM-1 antagonistic antibody in ex vivo metatarsal model. Metatarsals from E15.5 embryos were dissected and cultured for 5 days before treatment. After 5 days in culture metatarsals were moved into fresh plates and treated every 3 days with 100 ng/ml Control peptide (Cntrl) or PEPITEM (PEP), with or without antibody isotype control (ISO) or NCAM-1 antagonistic antibody for 10 days. Untreated (black, n = 5), cntrl (grey, n = 4), PEP (red, n = 6), isotype (blue, n= 4) and NCAM-1 antibody (green, n = 6) A) XY graph showing length increase from pre-treatment (μm) for untreated, cntrl, or PEP. B) Area under the curve (AUC) of length increases from pretreatment. C) XY graph showing increase in mineralisation zone over increase in total bone length (%). D) AUC of increase in mineralisation zone over total bone length. Kruskal-Wallis test shows significance of treatment (B) $p<0.001$and (D) $p<0.001$. Data are mean ± SEM for 2 independent experiments. * = $P < 0.05$, ** = $P < 0.01$ and *** = $P < 0.001$ by Dunn's multiple comparison.

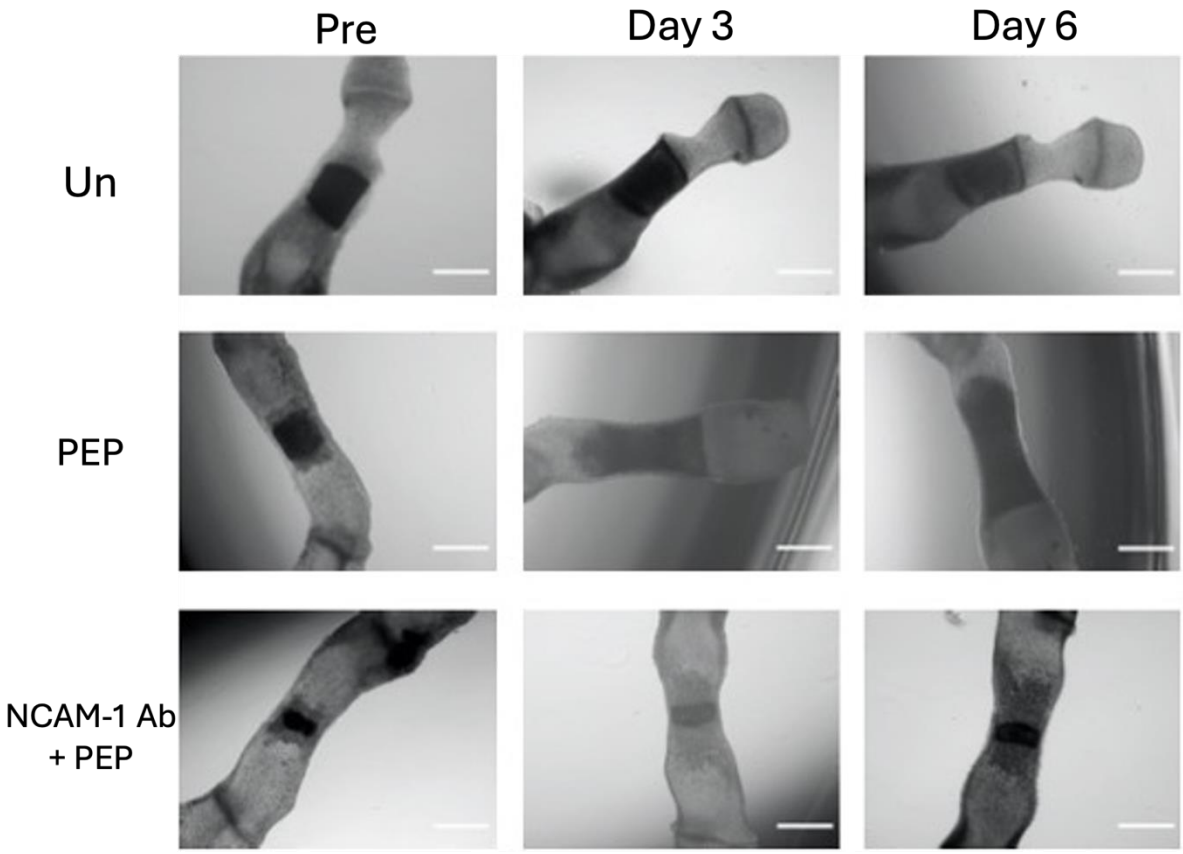


Figure 3.30 Representative images of E15.5 metatarsals at with or without PEPITEM and NCAM-1 antagonistic antibody. Metatarsals from E15.5 embryos were dissected and cultured for 5 days before treatment. On day 5 metatarsals which showed a positive mineralisation zone were moved to a new plate at random and treated with media alone (Un), PEPITEM (PEP) or NCAM-1 Ab + PEP. Metatarsals were imaged every day for 10-days. Representative images on Metatarsals from each treatment group pre-treatment (pre) and on days 3 and 6 post treatment. Scale bar = 100μm

3.2.5.3 PEPITEM acts via NCAM-1 to increase β-Catenin signalling.

NCAM-1 has been shown to activate multiple signalling pathways within mesenchymal stem cells and pre-osteoblasts such as MAPK/ERK[433], PI3K/Akt[437,439] and WNT/β-catenin[437]. Previous data has shown that PI3K/Akt[437,439] is involved in both MSC differentiation into adipocytes and osteoblasts, whereas WNT/β-catenin signalling has only been related to osteoblast maturation. Ex vivo studies using bone marrow stromal cells isolated from pre-osteoblast-specific β-catenin conditional knockout mice show reduced osteoblast differentiation, whilst increasing adipogenic differentiation[444]. These data show the importance of β-catenin in osteoblast differentiation therefore we assessed β-catenin signalling in response to PEPITEM.

Immunofluorescence staining was first used to stain for β-catenin at different time points following PEPITEM treatment (Figure 3.31). Quantification, shown as integrated density of β-catenin staining within DAPI positive nuclei, was used to investigate nuclear translocation of β-catenin (Figure 3.33 A), showing significant increase after 60minutes of PEPITEM treatment or the positive control LiCl treatment. Staining in the cytoplasm was also measured (Figure 3.33, B), also showing increased β-catenin staining following 60mins PEPITEM treatment compared to pre-treatment expression.

As β-catenin is active in its non-phosphorylated form, western blot analysis was performed to look at changes in levels of non-phosphorylated (active) β-catenin after PEPITEM treatment (Figure 3.33, C,D). Here we saw a significant increase at 30mins that reduced by 60 minutes but was still trending to higher than pre-treatment levels. These data

show that PEPITEM increases β-catenin activity, suggesting PEPITEM acts though downstream β-catenin activation.

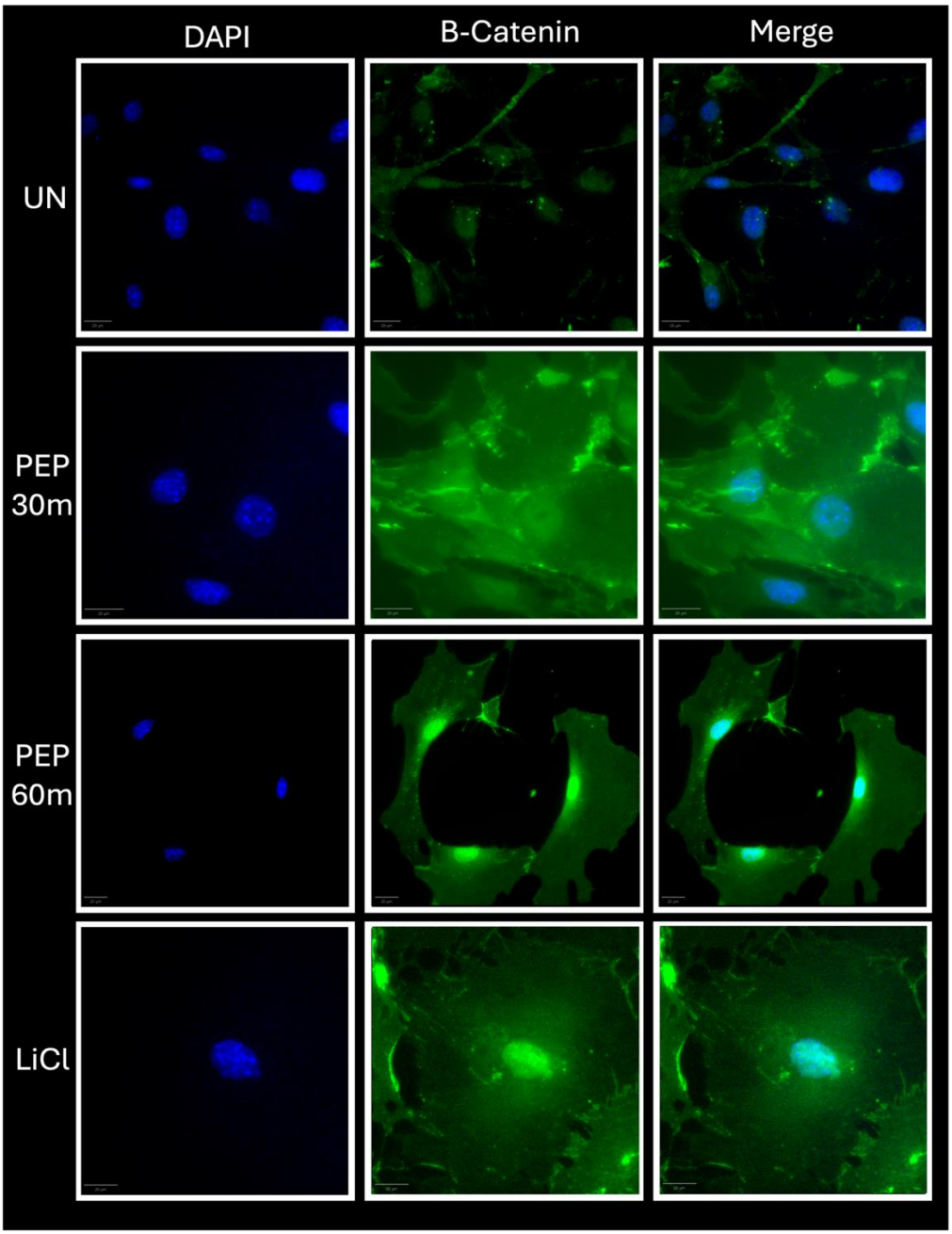


Figure 3.31 Representative images of β-catenin transnucleation following PEPITEM treatment. C.Ob were treated with osteogenic media 24hr before treatments, after 24hr cells were treated with LiCl (3hr) or PEPITEM (30-60min). After time media was removed and cells were fixed and stained for β-catenin (green) and DAPI (blue). Representative images from 2 independent experiments from 4 murine samples.

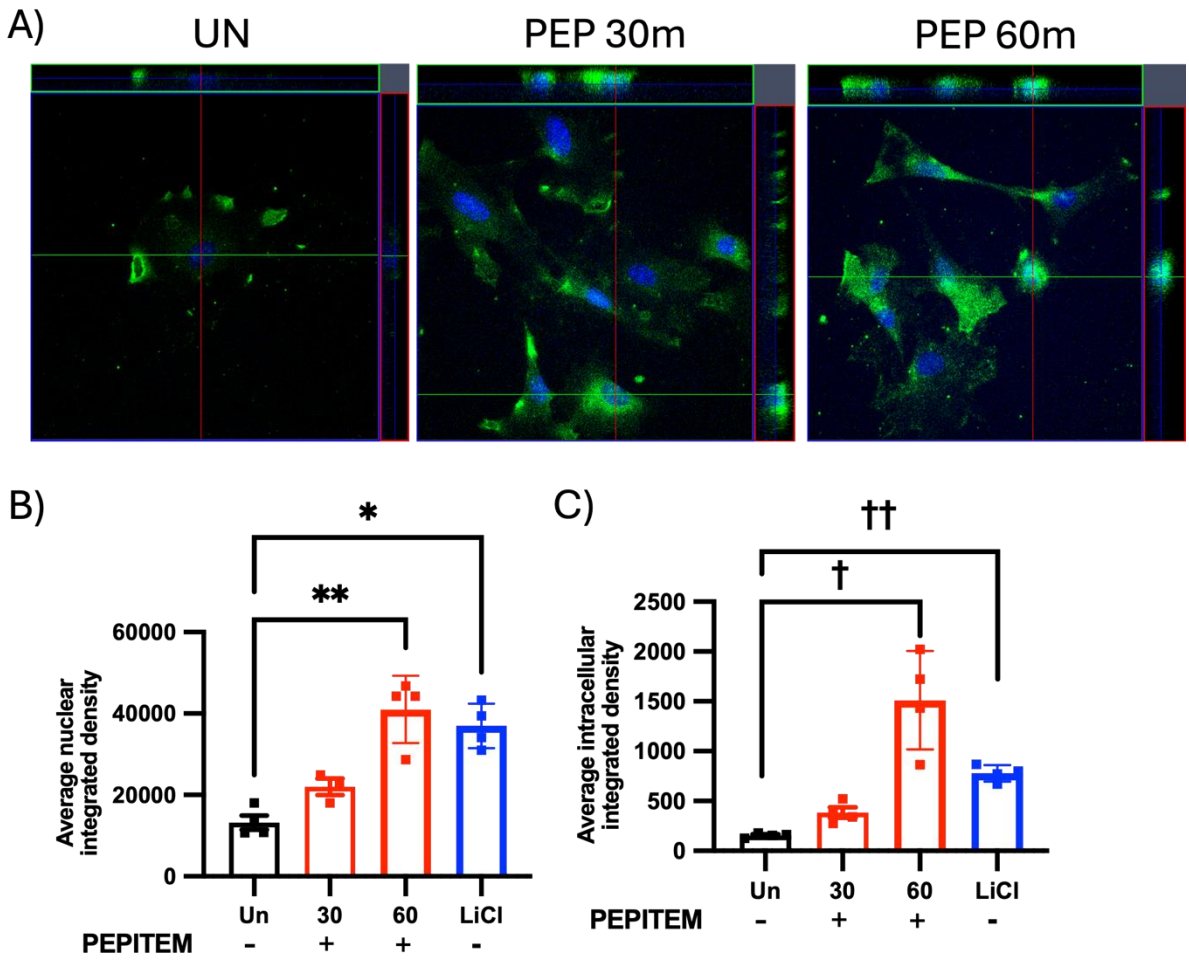


Figure 3.32 **PEPITEM increases transnucleation of β-Catenin.** C.Ob were treated with osteogenic media 24hr before treatments, after 24hr cells were treated with LiCl (3hr) or PEPITEM (30-60min). After time media was removed and cells were fixed and stained for β-catenin (green) . Analysis was preformed to look at (B) nuclear staining in relation to DAPI (blue) or (C) Cytosolic staining. Data presented as average integrated density. (B) Kruskal-Wallis shows significant effect of treatment $P < 0.001$ and (C) Welch's AANOVA shows significant effect of treatment $P < 0.0001$. Data mean ± SEM for 2 independent experiments, n = 4. * = $P < 0.05$ and ** = $P < 0.01$ by Dunn's multiple comparison or † = $P < 0.05$ and †† = $p < 0.01$ by Dunnett's multiple comparison.

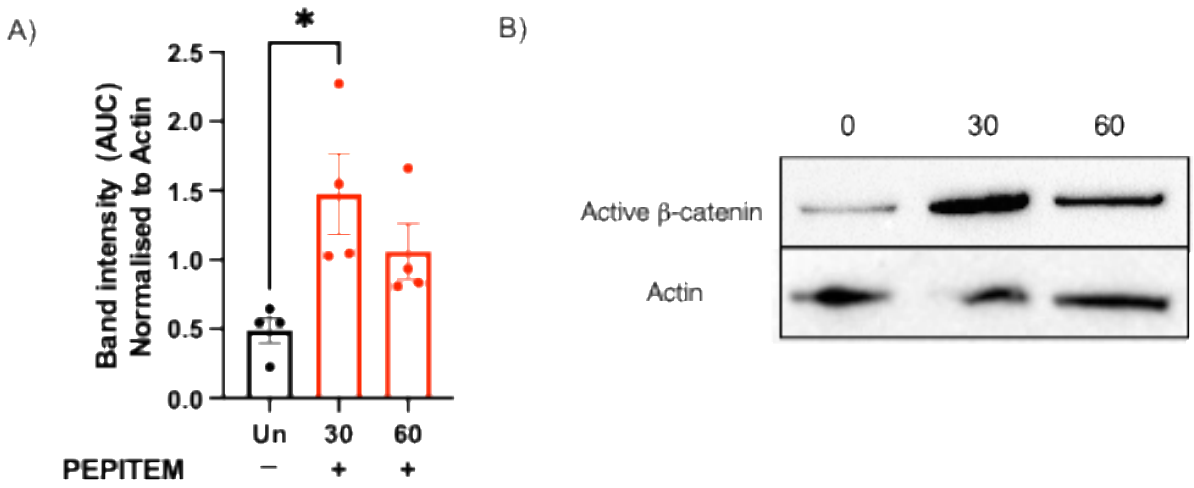


Figure 3.33 PEPITEM increases levels of non-phosphorylated (active) β-Catenin. C.Ob were treated with osteogenic media 24hr before treatments, after 24hr cells were treated with PEPITEM for 30 or 60min. After time media was removed and cells were lysed. Proteins ran in western blot staining for active β-Catenin and actin. (A) Analysis of β-Catenin staining normalised to actin. (B) Representative blot of active β-Catenin and actin stain. (A) Freidman test shows $p<0.05$. Data are mean ± SEM for 4 independent experiments. * = $P < 0.05$ by Dunn's multiple comparison

3.2.6 PEPITEM increases gene related to bone formation following 6hr of treatment (RNAseq)

In order to investigate the downstream signalling of PEPITEM in osteoblasts we used bulk RNA-sequencing to identify gene targets related to osteoblast differentiation, maturation and mineralisation. RNA from C.Obs which had been treated with PEPITEM or control peptide for 6hr was collected and sent for sequencing. Following pre-processing data was loaded into iDEP.16[408]. Hierarchical clustering and principal components analysis shows that the two treatment groups can be separated (Appendix, Figure 8.6). However, the PCA also shows that there was higher variation in responses between the PEPITEM treated cells. We used a threshold of minimum of 1 fold differences to detect small changes in genes that were up or down regulated, which showed 75 up regulated (Appendix, Table 8.1) and 36 down (Appendix, Table 8.1). Of the 75 upregulated genes, 19 were found to be involved in skeletal development and osteoblast differentiation (Table 3.3). The most significant increase was seen in the expression of *Kmt2d* and *Flt1*, both of which have been shown to be important in promoting osteoblast differentiation[445–447]. The genes upregulated by PEPITEM also including an increase in *Col1a1*, which is a major regulator of osteoblast maturation. Here, it should be noted that the increase in some of these genes was low, however this was to be expected as all of the cells used were undergoing osteoblast maturation due to the presence of osteogenic media.

To validate these responses, we looked at known gene markers of osteoblast maturation using qPCR. These data showed that there were very few genetic changes (Figure 3.34). However, we saw an increase in *Col1a1* (Figure 3.34, A) to a similar magnitude detected in the RNAseq data, suggesting PEPITEM acts to increase osteoblast maturation partially through increasing expression of *Col1a1*.

Table 3.3: Top upregulated genes related to bone when comparing PEPITEM to control peptide following 6hr of treatment

Genes related to osteoblast differentiation or skeletal maturation		
Gene symbol	**Log2 fold change**	**Chromosome**
Kmt2d	1.40430776556747	15q
Flt1	1.15024565487949	5q
Lama2	0.996559007758521	10q
Ptprm	0.952178517843655	17q
Pcnx3	0.78673474216748	19q
Nf1	0.728727334748264	11q
Zfhx4	0.698144342411609	3q
Ubr4	0.706757934426878	4q
Sp1	0.656539085200315	15q
Xrn1	0.649850897735021	9q
Ago3	0.600361833824849	4q
Col12a1	0.599971791753937	9q
Lrp1	0.57640041285326	10q
Fat1	0.518896007730861	8q
Dyrk2	0.510496882653584	10q
Herc2	0.493448659228275	7q
Macf1	0.489793110321781	4q
Pappa	0.457252945009879	4q
Huwe1	0.455546160489084	Xq
Col1a1	0.247360900416806	11q

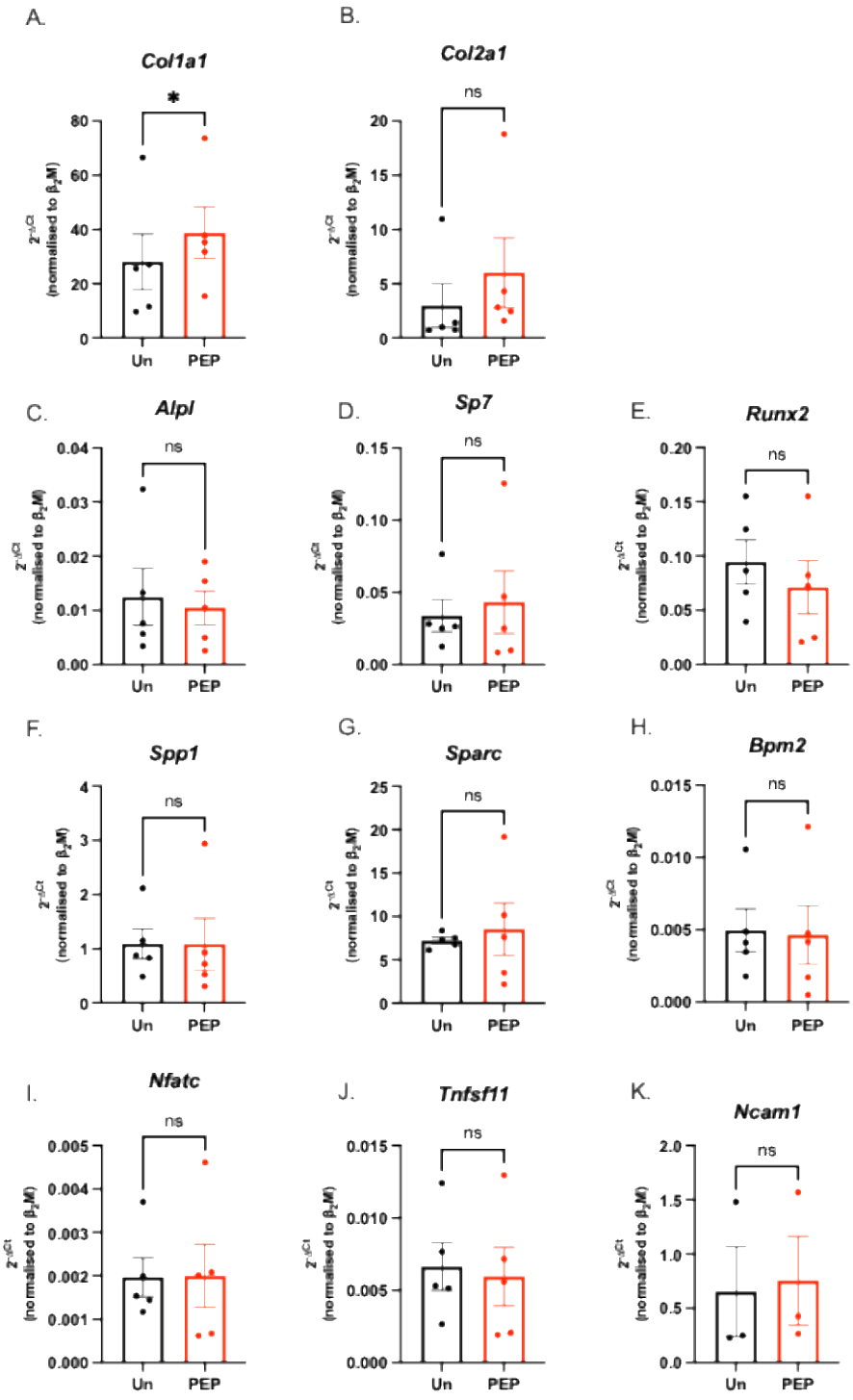


Figure 3.34: **Col1A1 expression increased following 6hr of treatment**. C.Obs treated with osteogenic medium for 24hr followed by treatment with or without PEPITEM for 6hr. RNA collected, and genes analysed using qPCR where untreated cells (black, n=5) or PEPITEM treated cells (Red, n=5) for (A)*Col1a1* (B) *Col1a2* (C) *Alpl* (D) *Sp7* (E) *Runx2* (F)*Spp1* (G) *Sparc* (H)*Bpm2* (I) *Nfatc* (J) *Tnfsf11* and (K) *Ncam-1*. Data are mean SEM, n=5 independent donors. * = P < 0.05 by paired t-test.

3.3 Discussion:

In this section we aimed to further understand the mechanism of PEPITEM in bone remodelling through further investigating PEPITEM function *in vivo* in both male and female homeostatic mice and identify downstream mechanism of PEPITEM in osteoblasts. Although we previously reported that PEPITEM increases trabecular bone parameters in male mice, PEPITEM did not increase the same parameter in female mice, however, does cause alteration in osteoblast production of extracellular matrix. Additionally, we saw that prolonged PEPITEM treatment had effects on cortical bone, suggesting that increasing treatment length allows for observable increases in cortical bone volume, which can explain increased bone strengthening seen previously[197]. We discover that PEPITEM is not acting though known pathways, with neither S1P nor CDH15 seeming to be involved in PEPITEM action in osteoblasts. Identification of PEPITEM binding partners on osteoblasts lead to the discovery of the NCAM-1. Inhibition of NCAM-1 resulted in a reduction in PEPITEM potency suggesting NCAM-1 is a novel target for PEPITEM. Investigation into the known downstream signalling of NCAM-1 molecule, β-catenin, we saw rapid translocation of active β-catenin into the nucleus of osteoblasts resulting in altered gene expression increasing osteoblast maturation. Overall, we have revealed the mechanism of PEPITEM in osteoblastic cells.

3.3.1 Sexual dimorphism in PEPITEM function

Sexual dimorphism of the skeletal system has been observed in most mammals[420–424], from differences in overall bone mass[420] to differences in responsiveness to mechanical loading[424]. This coupled with the higher incidence of musculoskeletal diseases in women comparatively to men[448], means it is imperative to look at differences in male and female

responses in research. The same traits can be recapitulated in the murine skeleton with male mice tending to have higher BV/TV and trabecular number[449], whereas female mice have increased trabecular number and trabecular separation, suggesting females have thicker but sparser trabeculae[449]. These sex differences in trabecular bone parameters were detected within our experiments (data not shown), however we did not detect differences in trabecular thickness. The differences in female and male mouse trabecular bone composition may account for us being unable to see trabecular changes in female mice following PEPITEM as the study was powered based on BV/TV increases in male mice.

Although we saw no effect of PEPITEM on trabecular bone in female mice, following 2- or 4-weeks of treatment we are able to see an increase in cortical bone parameters following 4-weeks of treatment. Additionally, we saw an increase in osteoid production following both 2- and 4-week treatment, suggesting that PEPITEM is affecting bone formation within female mice. Of note, the patterning of osteoid varies between experiments in this thesis, with staining carried out on tissues processed as part of this body of work looking different to those collected by Jonathan Lewis (JL) (cite) previously. Experiments looking at other tissue collected by JL (data not shown) showed similar staining to that seen when staining tissues in Figure 3.1, this may suggest that despite the tibias undergoing the same protocol following collection there was an issue in the processing of the tibias for osteoid analysis. Staining of osteoid is heavily dependent on decalcification process of the tissue, therefore as different researchers processed these tissues there may have been an experimental difference, not a biological difference due to incomplete or over decalcification. As picrosirius red staining should stain unmineralized osteoid the reduced staining in male tissue processed by JL may indicate incomplete decalcification of these bones are the mineralised bone is unstained.

Staining of tissues collected during this thesis stained similarly to that seen previously [450,451]. Due to the inconsistency of staining in this method it may benefit understanding to preform additional techniques to look at osteoid production/collagen deposition such as using immunofluorescence staining of collagen I in tissues[452] or using bone turnover markers such as osteocalcin or P1NP[453].

Differences between effects on trabecular bone vs cortical bone may be due to intrinsic differences between female and male bone structure. One study showed that male C57B1/6J mice have significantly higher trabecular bone parameters (BV/TV, Tb.th and Tb.n) whereas females displayed higher cortical parameters (Ct.th and Ct. Area/ Tt. Area) [454], this may explain the increase strength parameters also observed in female femurs. The same study showed significant differences in the metabolomic profile of female cortical bone compared to male cortical bone, indicating that females rely more heavily on fatty-acid metabolism whilst males rely on amino-acid metabolism[454]. As bone metabolism plays a large role in rate of bone turnover (reviewed by[455]) it is possible that sex differences in response to PEPITEM are caused by intrinsic sex differences in bone remodelling and metabolism. Supporting evidence to this hypothesis are the reports that the metabolome of the cortical bone changes following ovariectomy[456], which may indicate why following ovariectomy we are able to detect trabecular bone changes following PEPITEM treatment.

At a cellular level sex differences are also apparent with female mice having higher expression of osteoclasts[457] with higher resorption area, here we see a decrease in the number of osteoclasts in both males and females. At 2-weeks of treatment there is 28.5% decrease in females decrease compared to a 38% decrease previously seen in male mice after 2-weeks of treatment[197]. After 4-weeks of treatment we saw a 53.6% decrease,

suggesting that PEPITEMs actions on female osteoclasts may take longer than that seen in males. The cause of this may be due to higher starting numbers of osteoclasts or due to intrinsic female osteoclast responses. It has previously been postulated that there are sex differences in osteoclastogenesis, however the data surrounding this is conflicting [457–461]. Some studies have shown that osteoclast precursors from females have high osteoclastogenic capacity compared to cells isolated from males[457–459], whereas others have reported the reverse with males osteoclasts precursors being more readily differentiated to osteoclasts[460,461]. Desia and colleagues showed that there are differences in downstream pathways for RANKL mediated differentiation between males and females, showing that female derived BMDMs enhanced proliferation markers in response to RANKL stimulation whereas male mouse derived BMDMs increase differentiation markers[461]. Conflictingly, another similar study shows female mouse derived BMDMs differentiate more rapidly than male derived BMDMs due to upregulation in proinflammatory markers and faster activation of Nfatc1[458], despite both these studies using the same mouse strain and similar isolation protocols. One major difference between these studies is the amount of RANKL used with Desia et al using 10ng/ml and Mun et al using 50ng/ml, this difference may indicate that changes in RANKL concentration may alter cell responses. Supporting this one study looking at osteoclast formation of male and female human PBMCs show that male PBMCs differentiate in response to lower concentrations of RANKL (5-10ng/ml) compared to females, whereas at higher concentrations (30ng/ml) no difference is detected. Together these data suggest there is significant sexual dimorphism in macrophage responses to RANKL and osteoclast formation, which may partially account for sex differences with PEPITEM responses.

Despite slight differences in the magnitude of change detected, here we confirmed that PEPITEM can have a net osteoanabolic response on bone remodelling in homeostatic female and male mice, suggesting PEPITEM is an effective treatment in males and females. To assess whether PEPITEM is able to increase cortical bone in both sexes' experiments using longer treatment regimes in male mice are required.

3.3.2 Cortical and trabecular bone remodelling

Outside differences between sexes there are significant differences between the remodelling of cortical and trabecular bone which may shed light onto differences in trabecular and cortical changes we see in response to PEPITEM. Firstly, it is important to distinguish the differences between the two types of bones, including differences in their structure, mechanical properties and metabolic activity[462]. Structurally, cortical bone is solid and less porous than trabecular bone and contains osteons which run longitudinally in the bone[463]. Comparatively, trabecular bone is less uniform with pivots and struts of trabeculae running at various angle throughout the bone providing a larger surface area for metabolic activity and bone remodelling[464]. These structural differences may indicate why we see earlier changes in trabecular bone at 2-weeks, as trabecular bone has a high bone turnover rate comparatively to cortical bone[463], additionally due to increased proximity to blood vessels within the bone marrow cavity, cells lining the trabecular are likely to come in to contact with PEPITEM from the circulation.

Due to the slower turnover rate of the cortical bone, we may fail to detect changes in cortical bone following only 2-weeks of treatment in male mice, however previously we have reported that despite no changes in μ-CT we detect increased strength and stiffness of

femurs following PEPITEM as detected by three-point bend analysis[197,418]. Increases in strength and stiffness were detected in the diaphysis of the bone where trabecular bone is not present, therefore the increased strength can be attributed to increased cortical bone. These data suggest that PEPITEM is having an effect on cortical bone, following 2-weeks of treatment however it is not detectable by the measurements used for μ-CT[197,418]. Following 4-weeks of treatment these differences were now detectable which may suggest that longer treatment time is required in order to view these differences using μ-CT. Therefore, longer treatment regime experiments are required in male mice.

In addition to differences in remodelling time, studies have shown significant differences in the cellular signalling pathways in the cortical versus trabecular bone, including differences in responses to WNT/β-catenin signalling[464]. One study has previously shown the differences in WNT/β-catenin signalling between the cortical and trabecular bone, where wild type mice express significantly more β-catenin in the metaphyseal trabecular bone, comparatively to that in the diaphyseal cortical bone, suggesting there is increased β-catenin signalling within the trabeculae[464]. Additionally, stabilising β-catenin using a $Catnb^{lox(ex3)}$ reporter mouse[465] where when subjected to Cre recombinase, the mice are able to expression of a fully functional but stabilized β-catenin protein in osteoblasts[464]. Stabilisation of β-catenin led to increases in β-catenin pathway related genes in bone the cortical and trabecular bone, however the change was more significant within the trabecular bone compartments[464]. Additionally, these mice show a significantly increased trabecular bone volume (2.4 fold) whereas although there was a slight increase in the cortical bone (0.2 fold) the differences was significantly smaller than that of the trabecular bone[464]. These data

suggest that the WNT/β-catenin signalling pathway is important in both trabecular and cortical bone however is more prevalent in trabecular bone[464]. These data are supported by an additional study showing increased trabecular bone in β-catenin over expressing mice[466]. Together these data may suggest that the more pronounced effect on trabecular bone is due to PEPITEM signalling through β-catenin, resulting in cortical bone being slower to respond to the altered β-catenin signalling due to naturally lower signalling preferences.

The changes we see at 4-weeks may indicate the nature of remodelling taking place with increases in Cross sectional thickness (μm) being coupled with a decrease in Medullary area (μm^2), suggesting that remodelling is occurring on the endocortical surface opposed to the periosteal surface[462]. In order to look at these changes future work should reexamine images of the picrosirius red stained sections to examine changes in osteoid on the endocortical surface, as only changes in trabecular bone was analysed in this thesis. In addition to osteoid, we failed to look at changes in cortical porosity[467] due to resolution capacity of available micro-CT at the time this work was carried out. Cortical porosity increases with age and can be seen in osteoporosis[463], and increased porosity reduces the structural integrity of the bone. However, increase porosity may not indicate negative therapeutic benefit as porosity often equates to increased vascularisation of the tissue[468], which is thought to be required in order to sustain the osteocyte network. Therefore, alongside looking at cortical porosity it is important to look at vascularisation of the tissue and the osteocyte network[468].

In this thesis we focus on PEPITEM function on osteoblasts and osteoclasts, however when discussing cortical bone changes, it is important to also consider the effects on the embedded osteocytes. These cells are vital for the organised bone remodelling acting as a

key regulator of osteoblast and osteoclast activity. In order to look at how PEPITEM may be impacting these cells SEM[469] and IFC[470] is required to look at changes in the lacunae, osteocyte number and changes in osteocytic connectivity via canaliculi.

3.3.3 S1P in Bone remodelling

In the original PEPITEM pathway, PEPITEM was shown act on endothelial cells to increase S1P production through SphK2 and inhibit leukocyte migration. In addition to its role in leukocyte trafficking, S1P has been reported to act as an osteoanabolic, increasing osteoblast differentiation and proliferation[419,471–475].Hashimoto et al. demonstrated that the addition of exogenous S1P to early osteoblast progenitors (C3H10T1/2 pluripotent stem cells) resulted in the increased expression of genes linked to osteoblast differentiation, e.g., LRP5/6, ALPL, and BGLAP[472]. Additionally, S1P increased mineralisation (Alizarin red staining), suggesting it promotes MSC-like cells to differentiation towards an osteoblast lineage[144,472]. Previously our group was unable to observe these increases in osteoblast maturation following treatment with S1P on ST2, C.Ob or MC3T3 cells[140]. One study on murine dental pulp stem cells, which display a MSC-like phenotype, showed that low levels of S1P can induce osteoblastic differentiation whereas higher concentrations inhibited differentiation (1–10 μmol-L^{-1})[168]. These cells also displayed decreased expression of several osteoblast-specific genes (including ALP, RUNX2, and COL1A1), and decreased mineralisation following 3 weeks of culture with S1P[168]. Suggesting, the concentration of S1P impacts its effects on osteoblast function. Therefore, here we titrated S1P, although lower levels did prevent reduced ALP see with higher concentrations, we saw no increase in osteoblast differentiation. The differences between these two studies may stem from

differences between the two cell types used, with the S1PR expression on C3H10T1/2 yet to be reported.

As we didn't see the increases in osteoblast maturation or mineralisation as seen in previous studies, we concluded that PEPITEM wasn't acting through autocrine actions of S1P. Therefore, we decided to interrupt the intracellular S1P synthesis pathway to determine whether intracellular S1P was causing the increased mineralisation and maturation. PEPITEM has previously been described to act through Sphk2 in endothelial cells[172]. In this study we saw that PEPITEM mediated increases in S1P were still observed following Sphk2 inhibition, suggesting the same pathway was not involved. However, our data suggests that prolonged pharmacological inhibition of the S1P kinases (SphK1) causes increased cell death within osteoblasts. Therefore, due to S1P involvement in the regulation of cell survival, it may not be possible to disrupt S1P function via SphK1 inhibition to look at S1P in the involvement of PEPITEM effects on osteoblasts without causing alterations in cell function due to necrosis or apoptosis. Due to these data, we concluded that PEPITEM is likely not acting via increased S1P production or secretion.

3.3.4 Cdh15 in Osteoblasts

The cadherins are a family of calcium dependent adhesion receptors[476]. This family of adhesion molecules classically contain five extracellular domains (EC1-5), a transmembrane region and a cytoplasmic domain, and allow for cadherin-cadherin binding via EC1[477]. There are multiple forms of cadherins which have been shown to play various roles within different cell types (reviewed by [478–480]), however not all members have been described within osteoblasts. Cdh15 is predominantly known for its expression and role in myocytes and

formation of myotubules[481]. Prior to investigation in our lab little research had been carried out looking at the role of Cdh15 (M-Cadherin) in osteoblasts. It had been previously reported that there was an increase (5 fold) in gene expression of *Cdh15* in DMP1 positive osteocytes compared to osteoblasts, however the function of this difference was not taken further[482]. Our lab showed the positive expression of CDH15 at both the gene and protein level with CDH15 protein being predominantly located at cell adhesion sites. Here we show that the activation of CDH15 with agonistic antibodies did not mimic the ALP response seen with PEPITEM. Additionally, we did not detect CDH15 in the co-IP analysis, suggesting that PEPITEM may not be acting via CDH15 in osteoblasts.

Within osteoblasts multiple cadherins have been reported to play a role in MSC differentiation, osteoblast maturation and osteoclast activation, including CDH1-4 and CDH11[483–487]. The expression of these cadherins have been shown to be regulated by differentiation of MSCs as the cell differentiates into the various linages (reviewed by[488]), with *Cdh4* being downregulated[489] as cells enter the osteoblast lineage whilst *Cdh2* and *Cdh11* undergo a transient increase in expression[486,490–492]. However, both *Cdh11* and *Cdh2* are downregulated as osteoblasts mature further[489,493,494] and are undetectable in osteocyte line MLO-Y4[494]. Manipulation of both *Cdh2* and *Cdh11* expression *in vivo* has validated their importance in bone development and homeostasis[495 494,496–498].The germline depletion of *Cdh2* is embryonically lethal[495], but both the targeted overexpression of *Cdh2* via *Bglap* or *Col1a1* causes decreased bone formation and low bone mass[497,498]. Comparatively, the conditional depletion of *Cdh2* also causes smaller bones and age dependent osteopenia[494,496]. These contrasting results may shed light on the function of *Cdh2* at different stages of osteoblast maturation[496]. *Cdh11* depletion only resulted in modest osteopenia within young mice[497] and

no significant differences in adult mice[496], but these mice do show an increased number of adipogenic precursors, which may suggest an anti-adipogenic function of *Cdh11*[496]. Additionally, the partial ablation of *Cdh2* in *Cdh11* knockout mice causes much more severe skeletal deficits[496], suggesting that *Cdh2* and *Cdh11* may work in concert and *Cdh2* may rescue the skeletal phenotype in *Cdh11* mice.

Of note, CDH2 and CDH11 were both identified in the Co-IP analysis as binding to PEPITEM, but not the control peptide. Despite this, the Sequest score for these proteins fell at 5.07 and 9.2 respectively, suggesting the levels detected were only slightly more than theoretically predicted, therefore were discounted from the analysis. Although not investigated further, these data may suggest that PEPITEM was able to interact with multiple cadherins, however the low Sequest score suggest the binding potential is lower than seen in other proteins detected . Based on the current literature, the ability for PEPITEM to bind to CDH2 and CDH11 may allow for the activation of β-catenin as seen in this chapter (discussed in section 3.3.6). Cadherins have been shown to interfere with intracellular signalling in multiple cell types and are believed to act via canonical WNT signalling. Cadherins have been shown to bind to β-catenin, which is thought to allow for stabilisation of the adhesion structure[499], whereas disassociation leads to destabilisation[500], allowing for cell migration. The overexpression of *Cdh2* within osteoblasts has been shown to increase β-catenin sequestration at the cell surface, resulting in decrease translocation and decreased bone formation[497]. Based on this PEPITEM binding may cause destabilisation of the adhesion complex resulting in β-catenin dissociation and translocation, however due to the strength of PEPITEM-cadherin binding it is unclear whether this could be the case. To understand

whether PEPITEM may be functioning though other cadherins co-IP binding analysis or surface plasmon resonance (SPR) would be required.

3.3.5 NCAM-1 in bone remodelling

As shown above NCAM-1 can exist as multiple isoforms, NCAM-120, NCAM-140 and NCAM-180, based on alternative splicing of the *NCAM-1* gene[501]. NCAM-120 is most commonly found in glial cells and is linked to the cell membrane via a glycosyl-phosphatidylinositol anchor[431]. Whereas both, NCAM-140 and NCAM-180 are transmembrane glycoproteins with cytoplasmic tails[431]. Their differences in structure as lead to the belief of their role in different cellular processes[502,503].

Although NCAM-1 was initially shown to be widely expressed in both the central and peripheral nervous system, it has since been shown to be widely expressed outside the nervous system including on epithelial cells, and skeletal muscle[504,505]. Additionally, it has been shown to be expressed in osteogenic cells, with early papers identifying NCAM-1 in osteogenic condensations preceding intramembranous bone formation and additionally during endochondral bone formation[436,506]. NCAM-1 has been shown to be expressed in 95-99.1%[433,439] of murine bone derived MSCs. It's role has been discussed for its role in MSC proliferation[507], migration[433] and osteogenic differentiation[437,439,508]. These previous findings therefore made it an attractive initial target receptor when trying to identify the PEPITEM pathway within osteoblasts.

Within osteogenic cells the expression of NCAM-1 has been previously described as transient with *Ncam-1* - being expressed within pre-osteogenic condensations and later in osteoblasts and bone lining cells, after which expression is lost within mature osteocytes[436].

Additionally, *Ncam-1* has been shown to reduce in expression following long term culture in osteogenic media[442]. Therefore, we first ensured the presence of NCAM-1 on our cells at the time of PEPITEM treatment, demonstrating that NCAM-1 is highly expressed in these C.Obs at both the gene and protein level. Most recently NCAM-1 was shown to be involved in the maturation of a pre-osteoblast cell line (MC3T3s) to osteoblasts through WNT/β-catenin and PI3K/Akt signalling. Here we show that at the time of PEPITEM treatment C.Obs express NCAM-1 and inhibition of NCAM-1 disrupts PEPITEM function, indicating that NCAM-1 is required for PEPITEM signalling.

We are not the only group to have reported interactions between the 14-3-3 and NCAM protein families, with NCAM-2 being shown to effects neuronal differentiation through interactions with 14-3-3γ and ζ[509,510]. NCAM-2 was shown to interact with 14-3-3ζ at 4 distinct binding regions, including the 14aa sequence, SVTEQGAELSNEER[509]. Therefore, suggesting that NCAM2 can interact with the PEPITEM sequence. NCAM-1 and NCAM-2 have been shown to share 44% homology, each containing 5 Ig-like domains and 2 Fibronectin type-III domains[511]. NCAM-2 was not detected in our Co-IP analysis.

In silico analysis of PEPITEM binding to NCAM-1 suggests that PEPITEM may be able to bind to the fibronectin-III like domain. The binding to the fibronectin type-III domain of NCAM-1 has been previously linked to NCAM-1 activation through the binding of fibroblast growth factor receptor, resulting in activation of the FGFR[512–514]. FGFR1 is important in regulating osteoblastogenesis: deficiency in osteoblast precursors results in maintenance of stem-like properties and blockade of differentiation and mineral deposition[515]. Whereas within mature osteoblasts[515] and osteocytes, lack of FGFR1 drives bone formation by increasing the amount of active β-catenin leading to increase OPG release[516]. Thus, it is possible that PEPITEM

binding to NCAM-1 directly or indirectly inhibits FGFR1 activation, driving increased β-catenin activity, osteoblast maturation and mineralisation resulting in enhanced bone formation and reduced osteoclastogenesis. An alternative explanation may lie in the findings of Liu and colleagues looking at the involvement of NCAM-1 in proliferation of melanoma cells[517]. NCAM-1 signalling through β-catenin was reported to be independent of WNT or PI3K-AKT pathways, with no changes in canonical WNT signalling proteins and no effect of AKT inhibition[517]. Authors suggest NCAM-1 signals directly through increased β-catenin and reduced β-catenin inactivation by glycogen synthase kinase -3β (GSK-3β) with co-IP analysis showing binding of NCAM-1 with β-catenin and GSK-3β[517]. Additionally, FGFR1 was able so able to form a complex with NCAM-1, and FGFR inhibition prevented NCAM-β-catenin signalling[517]. These data may suggest that PEPITEM could potential mimic FGFR1 binding to increase β-catenin signalling. Therefore, further studies are required to confirm how NCAM-1 promotes β-catenin signalling within osteoblasts.

To confirm PEPITEM-NCAM-1 binding co-IP or SPR experiments are required. Previously when looking at binding to Cdh15 previously (unpublished), the large amount of noise meant it was difficult to confirm PEPITEM binding. To reduce noise, biotinylated PEPITEM could be used to increase the size of the peptide, whilst maintaining biological activity. Alternatively biotinylated PEPITEM could be used as the capture protein, increasing the signal but the importance of orientation of the peptide being so far unclear thereby immobilizing PEPITEM may not allow for the required binding.

3.3.6 β-catenin mediates NCAM-1-PEPITEM signalling in osteoblasts

β-catenin has long been known to be involved in bone formation (reviewed by[518]) and is an essential component of canonical WNT /β-catenin signalling[519]. β-catenin has been shown to be essential for the differentiation[520] and survival[521] of osteoblasts. In this chapter we decided to look at β-catenin signalling following PEPITEM treatment, as NCAM-1 has been previously suggested to act via WNT /β-catenin signalling[437]. Here we show increased β-catenin activity in response to PEPITEM treatment.

B-catenin signalling has been investigated as a potential therapeutic target for musculoskeletal diseases due the strong involvement of WNT signalling in bone formation. Lithium is a known activator of β-catenin signalling through the suppression of the axin-adenomatous polyposis coli (APC)-GSK-3β complex formation, thereby preventing β-catenin phosphorylation and subsequent degradation[522,523]. Multiple *in vitro*[524–526], ex vivo[362] and *in vivo* osteoporotic phenotype[524–530] studies have shown that lithium can improve bone formation and reduce bone loss. However, some *in vivo* studies have reported that in healthy bones lithium may have a detrimental or negligible effect[531–535]. Lithium is currently in clinical use as a mood stabiliser used as a treatment for bipolar disorder, allowing for research the secondary effects of lithium on these patients. Similarly to *in vivo* studies, the reports of the effects of lithium in humans is also contradictory. Some studies have reported a positive effect of lithium on bone health, showing increase bone mineral density compared to controls[536,537], coupled with an overall reduction in risk of osteoporosis[538]. Additionally, several studies have associated lithium treatment with an overall reduction in fracture risk[539–543]. By contrast, Wilting and colleagues also observed an increase in fracture risk upon discontinuation of lithium treatment[542]. Contradictory to these findings other observational

and clinical trials have found that lithium has no impact on bone health[544–546] or in some cases negative effect on bone, such as increasing fracture risker[547,548]. The differences in these findings are likely to do with study designs, however currently it is unclear to whether lithium can improve fracture risk and bone health in humans.

Based on this data it is apparent that targeting the β-catenin signalling pathway can be advantageous in the treatment of musculoskeletal diseases, however lithium treatment may not be the best treatment option[549]. Previously we have shown that similarly to lithium, PEPITEM was able to increase bone formation during homeostasis and in ovariectomy models[197], allowing for a wider range of disease treatment opportunities.

The mechanism in which β-catenin is activated following PEPITEM treatment is so far unclear. Previous studies have explored the role of 14-3-3 proteins in β-catenin signalling, showing that 14-3-3 proteins are able to modulate β-catenin function through direct bind to β-catenin[550,551] or through modulation of β-catenin interacting proteins[552,553]. PEPITEMs parent protein, 14-3-3ζ was shown to enhance β-catenin mediated gene expression through increasing steady-state expression of β-catenin within the cytosol, via direct interactions of β-catenin and 14-3-3ζ[550]. In our study we also observe increase cytosolic β-catenin staining following PEPITEM treatment, suggesting that PEPITEM may be acting similarly to its parent protein. Besides direct interactions with β-catenin, both 14-3-3ζ and 14-3-3σ have been shown to bind to GSK-3β[552,553], with 14-3-3σ sequestering GSK-3β and increasing GSK-3β phosphorylation, therefore enhancing β-catenin signalling[552]. These data suggest that PEPITEM may directly alter β-catenin signalling though direct binding or through modulation

of mediators of β-catenin signalling. However further work is required to look at intracellular functions of PEPITEM to investigate whether these interactions are able to take place.

Alternatively, NCAM-1 has been found to colocalise with β-catenin B16F0 melanoma cells[517], activation/interference with the adhesion molecule could cause detachment of β-catenin allowing for translocation[554]. In order to confirm this hypothesis, experiments must be performed to look at β-catenin-NCAM-1 colocalization, the effects of PEPITEM on GSK-3β activity and how inhibition of NCAM-1 affects β-catenin responses to PEPITEM.

3.3.7 Intracellular function of peptide therapies

NCAM-1 was selected as the likely PEPITEM receptor as its extracellular location and predicted AlphaFold interactions suggested it was likely to be involved, this was later confirmed with inhibition experiments showing that the effects of PEPITEM on ALP secretion was partially blocked by NCAM-1 antagonism. Our co-IP analysis also pulled down multiple intracellular binding partners of PEPITEM, including Annexin A6, Sec31A and CTNND1. As the cells were lysed it is possible that these binding interactions appeared after cell lysis, but it is possible that PEPITEM can pass through the cell membrane. Peptides can be transported into the cell via protein channels/carriers, or some small peptides are able to pass through the cell membrane in the absence of protein carriers. There are several cell-penetrating peptides (CPPs) (reviewed by[555–557]), these are small peptides (<30aa) that are able to permeate the cell membrane[558,559]. CPPs have been investigated extensively as their membrane permeability allows for the targeted delivery of drugs into the cell[555–557], and they can be predominantly split into two categories, cationic and amphipathic. Cationic CPPs contain predominantly cationic amino acids (Arg, Lys and His)[560,561] resulting in these CPPs having a net positive charge at

physiological pH. Whereas amphipathic CPPs are known to contain a combination of polar (Ser, Thr, Cys, Pro, Asn and Gln) and non-polar polar (Ala, Leu, Ile, Gly, Met and Val) amino acids, where the non-polar amino acids are thought to interact with non-polar lipid head and the polar regions are inserted into the membrane[555]. Based on these descriptions it is possible that PEPITEM falls into the amphipathic CPP category, as PEPITEM contains of four polar and four non-polar amino acids. Future experiments are required to test the internalisation capacity of PEPITEM. Additionally, if PEPITEM is found to internalise it will be essential to investigate additional intracellular PEPITEM binding partners.

3.3.8 Conclusion

In conclusion, PEPITEM increases bone formation in both male and female mice by enhancing osteoblast activity and reducing osteoclast number. For the first time this chapter defines the mechanism through which PEPITEM influences osteoblast function, discovering that PEPITEM can bind to multiple proteins expressed by osteoblasts. Among these proteins, NCAM-1 plays a crucial role in PEPITEM-mediated osteoblast maturation. We observe that PEPITEM increases β-catenin signalling, which in turn induces early osteoblast maturation markers *in vitro*. This chapter thus uncovers a novel pathway for PEPITEM signalling in osteoblasts, deepening our understanding of PEPITEMs function and providing potential new targets for therapeutic intervention for bone loss.

4 PEPITEMs effect on Osteoblast–Osteoclast Communication

This chapter is an expanded version of the article Lewis & Frost et al, 2024, for which the experiments I carried out are included here.
The full paper can be found in Appendix 325-351

4.1 Introduction

In the previous chapter we showed that PEPITEM has a direct action on osteoblasts through NCAM-1 activated β-catenin transnucleation. However, we have previously demonstrated that alongside increased bone formation there is a reduction in the number of osteoclast and therefore, reduced bone resorption following PEPITEM treatment [197]. In addition to this, PEPITEM has been shown to reduce osteoclast number and osteoclast activity in whole bone marrow cultures, suggesting that PEPITEM has dual action on both osteoblasts and osteoclast[562]. However, when PEPITEM was given to isolated osteoclast precursors we saw no effect on osteoclast formation or activity[197]. These data suggest that PEPITEM is unable to act directly on osteoclasts and instead acts on other cells within the bone niche to inhibit osteoclast formation in a paracrine manner[197].

In order to maintain controlled and balanced bone remodelling the interplay between osteoblast and osteoclast activity is heavily regulated, resulting in no net formation or loss during homeostatic conditions[563]. This control is maintained through a variety of cell-cell mediators, which can be membrane-bound (e.g. Ephrin B2-Ephrin B4)[564,565] or soluble factors (e.g. RANKL-RANK)[566], each allowing from the upregulation or the inhibition of osteoclast formation. Hence, in this chapter we test the hypothesis, PEPITEM acts via indirect mechanisms to elicit osteoclast responses by exploring the role of PEPITEM on osteoblast-osteoclast crosstalk, to evaluate the indirect effects of PEPITEM on osteoclast activity and formation.

4.2 Results

4.2.1 Osteoblasts secrete a soluble mediator in response to PEPITEM

PEPITEM caused a reduction in the number of osteoclasts within trabecular bone[128]. However, when macrophages are stimulated with PEPITEM, there was no alteration in osteoclastogenesis or osteoclast activity[197]. To allow for balanced formation and resorption, osteoblasts are able to control osteoclast maturation and activity through a number of surfaces expressed or secreted mediators[566]. Given this ability of osteoblasts to regulate osteoclastogenesis, we examined the possibility that the negative regulation of osteoclast function was through the production of a soluble agent released by osteoblasts in response to PEPITEM. To test this hypothesis, we collected the secretome/supernatant from PEPITEM treated osteoblasts and transferred this onto osteoclast precursors in addition to RANKL. Following media transfer number of TRAP positive osteoclasts were counted. Media from both primary murine C.Obs (Figure 4.1, A, B) and ST2 stromal cell line (Figure 4.1, C) treated with PEPITEM resulted in a decrease in the number of TRAP positive osteoclasts, compared to media transferred from untreated control cells (Figure 4.1, A-C). Additionally, when osteoblasts were treated with PEPITEM in the presence of Brefeldin A (a chemical inhibitor of the Golgi), they were no longer able to generate the osteoclast inhibitory agent(s), with no change in osteoclast formation being detected following media transfer compared to media from untreated cells (Figure 4.1, D,E). Together these data suggest that osteoblasts are releasing an anti-osteoclastogenic soluble mediator in response to PEPITEM.

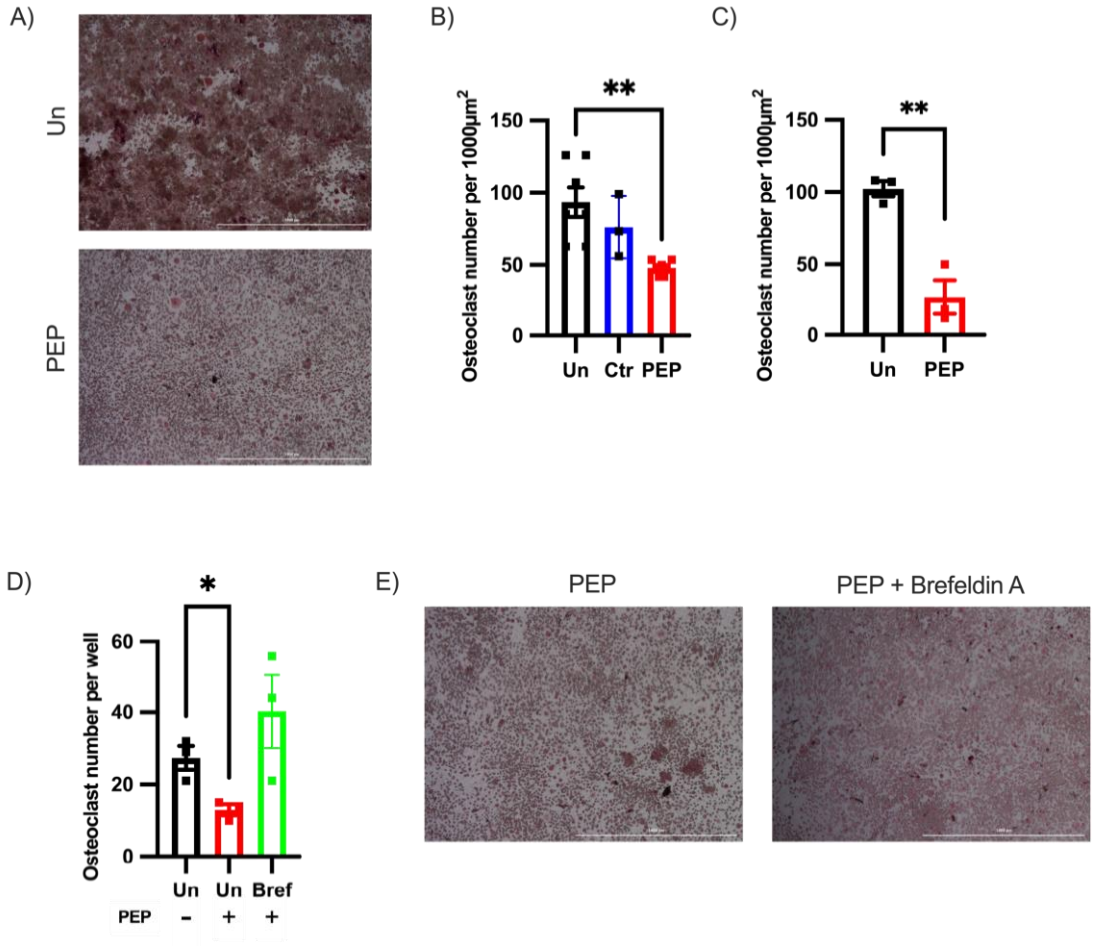


Figure 4.1 Osteoblasts release a soluble mediator in response to PEPITEM which inhibits osteoclastogenesis. Osteoblast conditioned media was collected from ST2 or C.Obs treated with PEPITEM, control peptide or brefeldin-A for (B) 4- or (C) 8-days. Media was then transferred on to Raw.624.7 cells, a macrophage cell line, for 5-days with RANKL supplementation. (A, E) Representative images of Raw.624 macrophages treated with osteoblast PEPITEM conditioned media and stained for TRAP, Scale bar = 1000 µm. (C-E) Counts of TRAP positive multinucleated osteoclasts per well following 5 day treatment with osteoblast media from (C, D) C.Obs or (C) ST2 cells untreated (Black), control peptide (blue) or PEPITEM alone (red) or in addition to brefeldin A (green) (B,D) ANOVA shows a significant effect of treatment $P < 0.05$. Data are mean ± SEM, from (C,D) n = 3 (B) n = 7 independent experiments, * = $P < 0.05$ and ** = $P < 0.01$ by (C) paired t-test or (D-E) Dunnett's multiple comparison.

4.2.2 Inhibition of S1P production results in altered osteoblast-osteoclast communication independent of PEPITEM.

PEPITEM has previously been described to act through S1P to regulate leukocyte trafficking, therefore we hypothesized PEPITEM results in an upregulation of S1P within osteoblasts. In chapter 3 we show that PEPITEMs action on osteoblasts is not through autocrine S1P signalling or increased S1P production. However, in addition to its effects on osteoblasts exogenous S1P has been reported to have multiple effects on osteoclasts, although the action it has on osteoclast differentiation are varied[127,429] .

Here we hypothesis that PEPITEM acts to alter S1P production and secretion altering osteoclast formation. Therefore, we investigated whether inhibiting S1P production within osteoblasts had an impact on osteoblast-osteoclast communication in response to PEPITEM. To do this we collected the media from osteoblasts that had been treated with PEPITEM in the presence or absence of SphK1/2 inhibitors for 24 hours, in order not to impact cell viability of the osteoblasts, as described in chapter 3. The media was then transferred onto Raw.624 cells for 5 days in the presence of RANKL, after which were stained for TRAP and multinucleated cells were counted (Figure 4.2). As expected, we observed a significant reduction in OC number following media transfer from PEPITEM treated OB, differences in OC number were detected between untreated and PEPITEM + inhibitor media transfer. Of note, baseline levels of OC numbers were dramatically reduced in the presence of just the inhibitors alone suggesting S1P/the enzymes are required for normal OC function (Figure 4.2,B). These data suggest that inhibiting SphK1/2 within osteoblasts impacts osteoblast-osteoclast communication, but this is independent of the actions of PEPITEM.

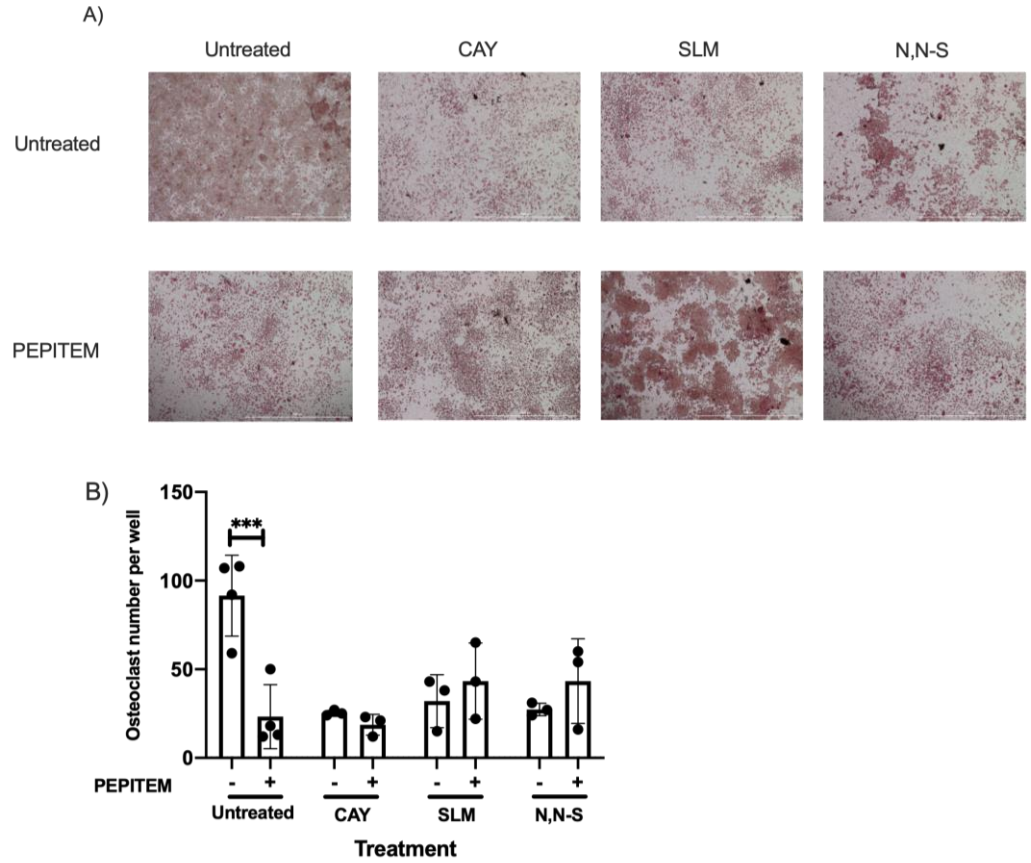


Figure 4.2 S1P signalling in osteoblasts impacts osteoclast formation independently of PEPITEM signalling. Inhibitors against SPHK1 (SLM-60314340-hydrochloride (SLM)) or SPHK2 (CAY10621 (CAY)), or both (N,N-Dimethylsphingosine (N,N-S)) were used to prevent the production of S1P from ST2 cells, bone marrow derived stromal clone cell line, in the presence or absence of exogenous PEPITEM for four days. The conditioned media was collected and (A-B) transferred on to Raw.624 macrophages for five days (A) Representative images of Raw.624 macrophages treated with osteoblast conditioned media and stained for TRAP. (B) TRAP staining was used to quantify the number of mature osteoclasts following media transfer from SphK inhibitor and PEPITEM treated osteoblasts and expressed as average number of osteoclasts per well. In B, two-way ANOVA shows a significant effect of SphK inhibitor treatment on osteoclast number ($p < 0.01$) and an interaction between the two variables (PEPITEM and inhibitor; $P < 0.001$). Data are mean ± SEM, where n = 3-4 independent experiments. *** = $P < 0.001$ by Sidak's multiple comparisons test.

4.2.3 Osteoblasts increase OPG secretion in response to PEPITEM

Osteoblasts can regulate osteoclastogenesis through paracrine signalling often through the RANKL-OPG axis[567,568]. Osteoblasts secrete both RANKL and OPG, which have opposing functions - RANKL binds to its receptor (RANK) on monocytes to induce their differentiation to osteoclasts; whilst OPG acts as a decoy receptor for RANKL inhibiting its binding to RANK and thus limiting osteoclast differentiation[569]. Given this, we next assessed OPG and RANKL levels in the conditioned media released from osteoblasts following PEPITEM treatment. After PEPITEM treatment of ST2 cells for 4-days or C.Obs for 8-days, conditioned media showed an increase in OPG secretion by ELISA (Figure 4.3, A,B). By ELISA we were unable to detect RANKL in our samples (data not shown), this was identified to be due to high OPG secretion in our samples in both treated and untreated, preventing binding of RANKL to the capture antibody. Therefore, we looked to detect OPG and RANKL levels by western blot from the same samples (Figure 4.3, C). Here we saw the same significant increase in OPG secretion following PEPITEM treatment when compared to untreated samples (Figure 4.3, D) as with ELISA. By contrast, we saw no significant change in RANKL levels compared to untreated controls (Figure 4.3, E).

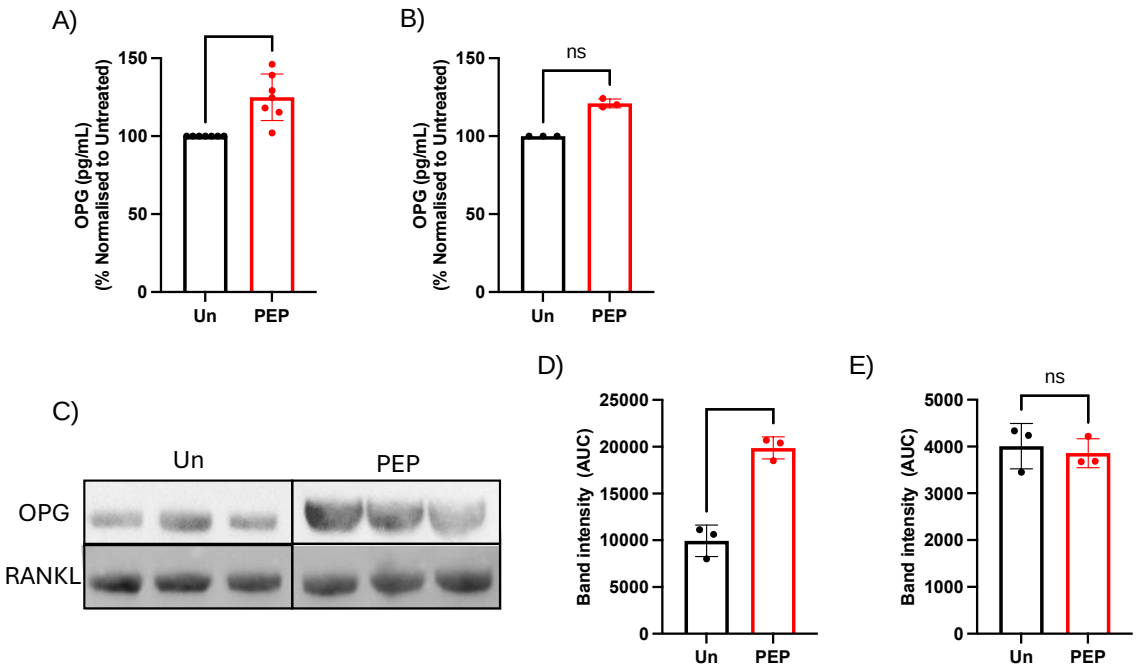


Figure 4.3 **Osteoblast secrete increase OPG in response to PEPITEM**. Media from (A) C.Obs treated for 8 days with PEPITEM or (B) ST2 cells treated with PEPITEM for 4 days, was analysed for concentration of OPG (pg/ml) by ELISA, presented as percentage of untreated controls. (C-E) Western blot of (D) OPG and (E) RANKL from the supernatants from C.Obs, presented as band intensity (AUC). Data are mean ± SEM from (A) n= 6 or (B,D,E) n=3 independent experiments. *=p<0.05 by (A) Wilcoxon and (D) paired students t-test.

To examine the effects of PEPITEM on long term human cultures we used the self-structuring bone model (SSBM) organoid using hFOb 1.19 cell line[377], allowing for the long term culture of osteoblasts in a 3D environment which has been shown to better mimic *in vivo* responses. Additionally, within this model cells which present a late-stage osteoblast phenotype or an early osteocytic phenotype have been detected, allowing us to investigate PEPITEM function on older osteocyte-like cultures. Here we treated 4- or 12-week-old SSBM constructs with PEPITEM for 8-days mimicking the treatment duration we have previously used in 2D cultures in which we have seen altered OPG secretion (Figure 4.4).

PEPITEM treated SSBM organoids showed a significant increase in the production of OPG at 4-weeks (Figure 4.4, A) and a tendency to be up-regulated in the 12-week constructs although the untreated cultures were very variable (Figure 4.4, B). These data demonstrate that PEPITEM can elicit the same OPG response in a humanised 3D model as in 2D murine cultures, suggesting PEPITEM is able to evoke a non-species dependent upregulation in OPG. Additionally, this effect does not appear to be affected by cell maturation, showing a response on both 4- and 12-weeks constructs.

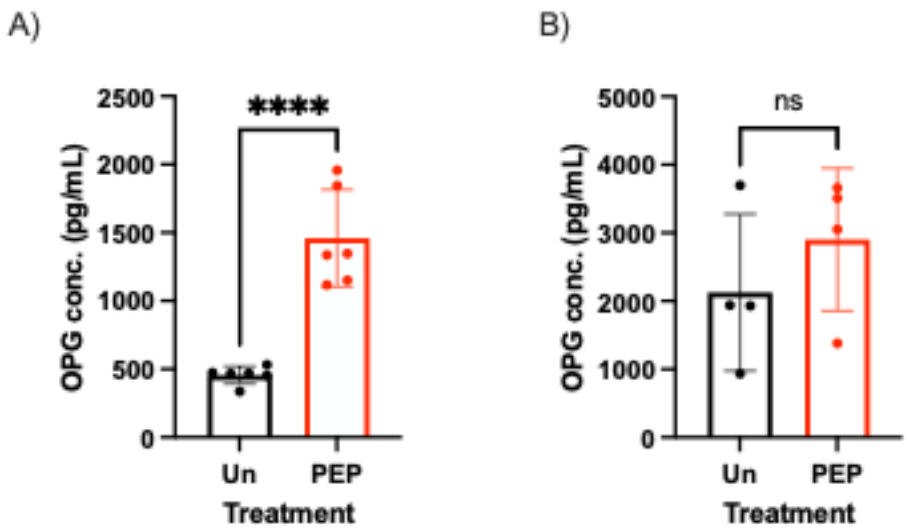


Figure 4.4 **PEPITEM increases OPG secretion in 3D bone model.** SSBM organoids cultured for 4 or 12 weeks, at 4 weeks constructs were treated with PEPITEM for 8 days before media collection or continued on till 12 weeks and media replaced with osteogenic media, at 12 weeks remaining constructs were treated for 8 days with PEPITEM. (A,B) OPG conc (pg/ml) from SSBM construct media following treatment at (A) 4 weeks or (B) 12 weeks. Data are Mean ± SEM from n = 4-6 constructs per group. ****= $p < 0.0001$ by unpaired student t test.

To ascertain whether OPG was truly the anti-osteoclastogenic agent responsible for the dual effects of PEPITEM, we undertook a competition assay adding increasing concentrations of RANKL to the OPG enriched PEPITEM-treated osteoblast conditioned media (Figure 4.5, A,B). As expected, RANKL was able to outcompete PEPITEM-induced OPG, such that at 500 ng/ml RANKL there was no longer a reduction in the number of TRAP positive osteoclasts in response to the PEPITEM conditioned osteoblast media. To further confirm these observations, we used an OPG neutralising antibody to deplete OPG from the PEPITEM-treated osteoblast conditioned media prior to transfer onto osteoclast precursors. Depleting OPG from the osteoblast conditioned media reversed the effects of PEPITEM on osteoclastogenesis, such that numbers of osteoclasts significantly increased compared to conditioned media in the absence of anti-OPG AB (Figure 4.5, C,D). Finally, we assessed whether blocking NCAM-1 signalling altered PEPITEM induced OPG in osteoblasts. Significantly lower OPG concentrations were detected in conditioned media from anti-NCAM-1+PEPITEM treated osteoblast supernatants compared to those from PEPITEM treatment in the presence of an IgG1 control antibody (Figure 4.6). Together these data indicate that PEPITEM acts to increase OPG secretion in osteoblasts through activation of NCAM-1, which in turn regulates osteoclast formation.

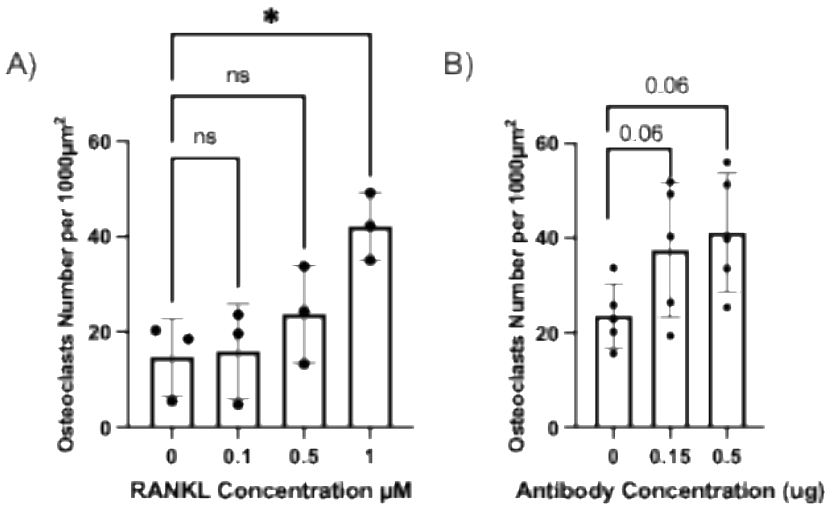


Figure 4.5 Inhibition of OPG secretion reverses PEPITEM anti-osteoclastogenic effects. Murine macrophage-like RAW264.7 cell line cultured with conditioned media from primary murine C.Obs cultured with PEPITEM in combination spiked with (A) increasing concertation of RANKL or (B) Anti-OPG antibody. (A,B) Number of TRAP positive osteoclasts expressed per 1000 μm^2. ANOVA shows significant effect of (A) RANKL, P = 0.024, (B) OPG Antibody, P = 0.0229. Data are mean ± SEM from (A) n = 3, (B) n = 5, * = P < 0.05 by Dunnett's post-test

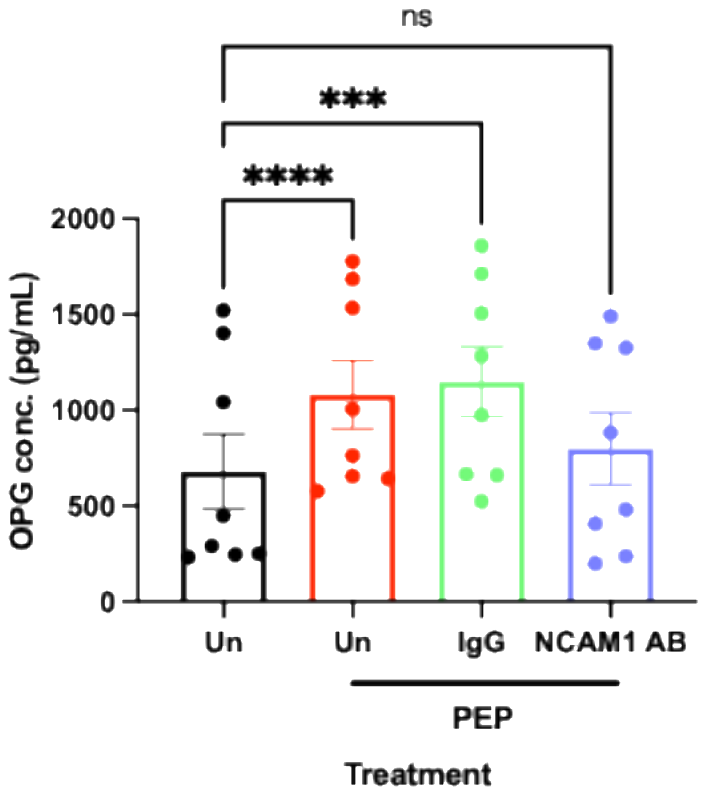


Figure 4.6 **Inhibition of NCAM-1 prevents PEPITEM induced OPG secretion**. C.Obs were treated with PEPITEM (red, n = 8) with or without anti-NCAM-1 (blue, n=8) antibody or IgG control (green, n = 8), for 8 days. Media was collected and analysed for concentration of OPG (pg/ml) by ELISA and compared to untreated osteoblasts (black, n=8) presented as OPG pg/ml. Data are mean ± SEM from, n = 8. *** = P < 0.001, **** = P<0.0001 by Dunnett's post-test

4.3 Discussion

Dysregulation in communication between osteoclast and osteoblasts often results in unbalance bone remodelling causing diseases, such as osteoporosis. Previously it has been reported that PEPITEM acts to inhibit leukocyte migration through the secretion of S1P[192], however the effects of S1P did not mimic the effects of PEPITEM in our hands, decreasing ALP activity and increasing osteoclast number[429]. Disrupting the S1P signalling pathway altered osteoblast-osteoclast communication independently of PEPITEM, reducing osteoclast formation. These data suggest the presence of other soluble mediators involved in PEPITEM mediated osteoblast-osteoclast cross talk. Here we describe the indirect function of PEPITEM on osteoclasts resulting in an anti-resorptive function. PEPITEM triggers the release of the anti-osteoclastogenic molecule, OPG, which disrupts the RANKL-OPG axis leading to decrease osteoclast formation and activity. This translates to the reduction in osteoclast number seen perviously[197], and additionally may contribute to the reduction in bone erosion seen in models of arthritis[570].

4.3.1 S1P signalling in osteoblast-osteoclast communication.

Based on previous finding of PEPITEM acting through altered S1P signalling we investigated whether inhibiting S1P production from osteoblasts altered osteoclast activity/number. S1P is often referred to as a clastokine and is known for its secretion from osteoclasts, however S1P is able to act on both osteoblasts and osteoclasts[127]. In the previous chapter we were unable to mimic the effects of S1P on osteoblasts seen previously[144,166] , with S1P reducing ALP activity in osteoblasts. Therefore, we instead moved to assess whether S1P acts as a paracrine signalling molecule on osteoclasts. The evidence

supporting a role for S1P on osteoclasts is limited and conflicting, with some studies suggesting S1P has no effect osteoclast formation, whereas other studies have reported the importance of S1P receptor, S1PR2[172]. S1PR2 was shown to be required for the adhesion and fusion of monocytes, and subsequently osteoclast formation[172]. Comparatively we have shown a species dependent response of S1P, where we reported an increased osteoclastogenic effect of S1P on murine osteoclast precursors whereas a reduced osteoclastogenic response in human osteoclast precursors[429]. These difference we hypotheses are due to differences in S1P receptors and kinases present across the species[429].

As expected, based on our previous data, we observed that inhibition of S1P production in osteoblasts resulted in a reduction in osteoclast formation, showing that S1P increases osteoclastogenesis in murine osteoclasts. As inhibition of S1P secretion caused a reduction in osteoclast number in the absence of PEPITEM, it suggests that osteoblast-secreted S1P is necessary for osteoclast formation. These data indicate that PEPITEM is not operating through increased secretion of S1P, therefore it is unlikely that PEPITEM is acting though increase Sphk2 signalling as seen in the original PEPITEM pathway. However, it does shed more light on the importance on the role of S1P in osteoblast-osteoclast communication, but this was out of the scope of the current thesis.

4.3.2 Osteoblast-Osteoclast paracrine interactions

Here we show that PEPITEM can have an indirect effect on osteoclasts through altering the osteoblast secretome, shown through the transfer of PEPITEM conditioned osteoblast media onto macrophages, thereby mimicking paracrine signalling. Paracrine signalling has

been shown to be vital in order to maintain balanced remodelling. Osteoblasts secrete both pro-osteoclastogenic molecules (e.g. RANKL and M-CSF) and anti-osteoclastogenic molecules (e.g. OPG and SEMA3A). Secretome analysis shows PEPITEM upregulated secretion of OPG without altering RANKL secretion, thereby skewing the RANKL:OPG ratio towards an anti-osteoclastogenic phenotype. 14-3-3ζ has recently been shown to be involved in mediating RANKL responses in osteoclast, however differently to that described here. 14-3-3ζ was shown to inhibit downstream RANK signalling in osteoclasts via inhibition of TRAF6, preventing RANKL/RANK-mediated osteoclast formation[186]. Previously we did not see an effect of PEPITEM on RANKL-mediated osteoclastogenesis, suggesting it may be a differing sequence within 14-3-3ζ that mediates these effects.

In addition to OPG:RANKL, osteoblasts are able to mediate osteoclast maturation through other soluble factors such as SEMA3A, which were not investigated within this thesis due to detected changes in OPG levels. SEMA3A is a member of the semaphoring family of proteins[571,572], which has been identified as a key regulator of osteoclast formation[573]. SEMA3A binds to Nrp1[574] on osteoclasts and inhibits RANKL induced PlxnA1-TRAM2-DAP12 complex formation, reducing expression of osteoclastic genes including Acp5 and Nfatc1[573]. In addition to an anti-osteoclastic effects, SEMA3A is also able to independently upregulate osteoblastogenesis through WNT mediated FARP2 activation of RAC1[575]. Thus, showing that SEMA3A has a dual effect on both osteoclasts and osteoblasts. Analysis of RNAseq at 6hr, 24hr and 8days following PEPITEM treatment shows no changes in expression of these gene or related pathways (data not shown), suggesting it is unlikely for SEMA3A to be involved in PEPITEM-mediated signalling.

4.3.3 Directed Osteoblast-Osteoclast communication

A caveat of this study is that we fail to look at direct osteoblast-osteoclast communication. In initial experiments we saw a significant effect of PEPITEM on whole bone marrow cultures, showing reduced osteoclast activity[128,197], but we did not look at gene or protein expression following co-culture. As osteoblasts and osteoclasts can communicate via direct interactions as well as soluble factors through the use of membrane bound proteins such as ephrinB2 (EFNB2) on osteoclasts and EphB4 on osteoblasts[576]. When EphB4 was used to stimulate Efnb2 on osteoclasts, there was a reduction in osteoclast number and activity in a dose dependent manner[576]. Conversely EphB4-Efnb2 signalling in osteoblasts enhanced osteoblast activity, increasing alkaline phosphatase signalling[576] and thus suggesting an important role of EphB4-Efnb2 in osteoclast-osteoblast communication. Therefore, in order to further understand the role of PEPITEM in osteoblast-osteoclast communication we must also examine changes in osteoclast function following, direct co-culture comparatively to indirect coculture to separate changes caused by secreted proteins, such as OPG, vs changes triggered by membrane bound proteins[371]. A recent review outlined the importance of the use of co-culture systems between osteoblasts and osteoclasts to allow for more accurate observation of drug responses. In this review[371] they highlight the importance of the use of 3D culture systems similar to the SSBM used in this thesis, suggesting that the responses in a 3D environment may differ to that in 2D. We observed a similar increase OPG secretion in both our 2D and 3D cultures providing increased reliability to our finding. That said, it is important to observe direct osteoblast-osteoclast effects, therefore future work should be carries out to investigate how PEPITEM effects

osteoclastogenesis in a 3D co-culture system, through the addition of osteoclast precursors to the SSBM.

4.3.4 Role of PEPITEM in macrophage biology and differentiation

Previously we have seen no direct effect of PEPITEM on osteoclastogenesis but have yet to explore the other effects that PEPITEM may exert on monocytes/macrophages. Previous studies have reported the importance of 14-3-3 proteins on macrophage responses, with 14-3-3ε promoting an anti-inflammatory phenotype through the regulation of TNFR2 signalling[577]. Additionally, our group and collaborators have identified that PEPITEM is able to alter macrophage phenotype/function skewing them towards an anti-inflammatory state and limiting their IL-6 and TNFα production (unpublished data). Macrophages that are polarised towards a pro-inflammatory phenotype are more readily able to differentiate into osteoclasts, particularly in the absence of oestrogen[578]. In the same study, they described an increase in the number of pro-inflammatory macrophages compared to anti-inflammatory macrophages in the bone marrow of OVX mice[578–580]. Recent studies have shown that treatments which alter macrophage polarisation, such as Pseudolaric acid B and isobavachalcone, are able to prevent osteoporotic phenotype in OVX mice, showing the importance of macrophage polarisation in osteoclastogenesis[579,580]. Whilst PEPITEM does not directly affect differentiation of macrophages into osteoclasts[128,197], it may alter macrophage polarisation to reduce osteoclastogenic potential[581].

To our best knowledge there is no direct evidence showing Cdh15 or NCAM-1 expression on macrophages. However, there is some evidence suggesting that macrophages have the capacity to express NCAM-1, but only following exposure to a tumour microenvironment[582].

These data suggest that PEPITEM acts on osteoclast progenitors, however the mechanism by which it mediates its effects may differ to those previously describe on endothelial cells, and that of osteoblasts describe in chapter 3. Therefore, further work should be carried out to investigate additional effects of PEPITEM on osteoclasts and their precursors outside the indirect effects carried out by osteoblasts.

4.3.5 How does PEPITEM alters RANK-RANKL-OPG signalling to influence bone remodelling?

In this chapter we show that PEPITEM increased osteoblast secretion of OPG (>25%) without increasing RANKL secretion, switching the ratio towards inhibition of osteoclastogenesis. The importance of the RANKL-RANK-OPG system has been long known for the regulation of osteoclast maturation[569], bone adherence[23] and activation[569], and heavily relies on the ratio of OPG:RANKL. Studies have demonstrated the importance of this ratio for bone development and modelling through inhibiting and sequestering OPG *in vitro*[252] and knocking down OPG *in vivo*[567], which result in a significant increase in osteoclast formation. Even partial reductions in OPG (+/-) has a significant impact on trabecular bone volume, suggesting that minor changes in the OPG:RANKL ratio can alter homeostatic bone remodelling[567]. Conversely the upregulation of OPG increases trabecular bone volume significantly[252]. Thereby, PEPITEMs ability to promote OPG secretion has an overall anti-osteoclastogenic effect resulting in a reduction in osteoclast cell number, as previously seen *in vivo*[197].

As shown in chapter 3, PEPITEM treatment alters β-catenin signalling, which suggest the involvement of the canonical WNT signalling pathway. WNT /β-catenin signalling plays a

significant role in osteoblast differentiation particularly in MSCs and immature osteoblasts, with β-catenin inactivation resulting in severe skeletal defects[520,583]. Inhibition of β-catenin signalling within mature osteoblasts and osteocytes, using Col1-, osteocalcin- and Dmp1-Cre mice, significantly upregulated bone resorption[584–586], suggesting that β-catenin signalling plays a significant role in osteoblast-osteoclast cross talk. The factor mediating this was later discovered to be OPG[587–589]. This dual effect of WNT /β-catenin signalling on both osteoblast maturation and osteoclast formation has resulted in significant investment into the development of WNT /β-catenin activators or inhibitors of β-catenin degradation, such as anti-sclerostin antibodies[310,311] and lithium treatments[526,530,535]. PEPITEM is able to act similarly to lithium therapies, increasing β-catenin signalling without the side effects which have been linked to lithium usage[590], making is an attractive therapeutic target.

Additionally, we saw that inhibition of NCAM-1 signalling caused a reduction in OPG secretions from osteoblasts. These data suggest that PEPITEMs ability to upregulate β-catenin via NCAM-1 activation on osteoblasts is likely to be the cause of increase OPG secretion and therefore PEPITEMs indirect actions on osteoclasts. However, to confirm this, we must examine the impact of PEPITEM following inhibition of β-catenin and observe whether PEPITEMs increase OPG secretion is mediated through the β-catenin signalling pathway.

4.3.6 How is RANKL-OPG signalling disrupted in bone diseases

Previously we have demonstrated that PEPITEM is able to restore the bone loss in a model of oestrogen deficiency induced osteoporosis (ovariectomy – OVX)[197]. The RANK-OPG

system has been shown to be alter or impaired in multiple bone diseases, resulting in ongoing pathogenesis, including sex hormone deficiency[591–597]. Oestrogen receptors (ERs) are expressed on osteoblasts, osteoclasts and osteocytes, therefore when oestrogen is lost there is a dramatic change in the functioning of these bone cells. When oestrogen is present activated ERs can regulate the expression of multiple genes, including IL-1[598] and IL-6[599]. In addition, ER activation can inhibit RANKL production in osteoblastic cells and stimulates OPG secretion[600], resulting in increased control of osteoclast formation. Therefore, in cases of oestrogen deficiency there is an upregulation in the production of RANKL[601], resulting in over activation of osteoclasts, which can be reversed in the presence of a RANKL inhibitor[602,603]. Together with these data we hypothesise that PEPITEM restores the homeostatic RANKL:OPG signalling, resulting in reduced osteoclast number and consequentially reduced resorption. However, to understand whether it is the increase osteoblast activity or the reduction in osteoclast formation that mediates PEPITEMs therapeutic role following OVX, we must investigate the number of osteoclasts present following OVX-PEPITEM treatment. In addition, we should observe serum changes in RANKL and OPG following PEPITEM treatment.

Fluctuations and changes in RANKL and OPG levels have also been observed in models of age[604–606] and glucocorticoid[607] (GC) induced bone loss. These data suggest that as PEPITEM may be able to restore homeostatic bone remodelling through re-establishing the RANKL:OPG ratio, it may also act as a potential therapeutic in age and GC induced bone loss. In order to prove this, PEPITEM needs to be tested in other models of osteoporosis and observe how treatment impacts the OPG:RANKL ratio and osteoclast formation.

4.3.7 PEPITEM compared to other treatments which alter RANKL signalling

As the RANKL-OPG system plays a large role in the regulation of bone remodelling it is no surprise that current treatments for osteoporosis have targeted this pathway. The first and most easily intervention for osteoporosis is increasing weight bearing exercise, the mechanism by which exercise increases bone formation is multi-faceted and has in part been attributed to increased OPG production. Several studies have demonstrated changes in RANKL and OPG levels following exercise in mouse[608–610] and in humans[611–616]. Unfortunately the effects of exercise on this system appears to vary based on the model used, the participants involved, and the type of exercise performed, with some studies showing no changes in OPG or RANKL[615–619].

In many cases exercise is not enough to prevent bone loss or the patients are unable to exercise due to other existing health problems. At this point patients are often moved on to pharmaceutical. Anti-RANKL antibody therapies (denosumab) specifically targets the RANKL-OPG system through binding to RANKL and inhibit its function, similarly to the mechanism of OPG[562]. The effectiveness of RANKL inhibition using denosumab was demonstrated in the FREEDOM trial[562], where it was shown to reduce the relative fracture risk for vertebral, hip and nonvertebral fractures to 6%, 40% and 20% respectively. One study looking at 1-week treatment with anti-RANKL antibody following ovariectomy showed no change in trabecular or cortical bone parameters[620]. Whereas at a cellular level there was a reduction in the number of osteoclasts, as expected with anti-RANKL treatment, coupled with a reduction in osteoblasts[620]. Comparatively PEPITEM was shown to increase trabecular bone parameters within a 2-week treatment window[197], similarly showing a reduction in osteoclasts without the reduction in osteoblasts as shown in chapter 3. Although denosumab can alter the

RANKL:OPG ratio, it has also been shown that cessation of denosumab treatment significantly increases risk of vertebral fracture[620,621]. Therefore, the switch to bisphosphonates following denosumab is often recommended. We have so far not observed the impacts of cessation following PEPITEM treatment, however as we only observe moderate reduction in the number of osteoclasts present and no changes in RANKL in response to the upregulated OPG secretion, we predict that there will be minimal rebound effects. However, experiments looking at long term treatment with PEPITEM followed by discontinuation of treatment are required to observe how quickly regained bone is lost and how this impacts fracture risk.

Although the use of denosumab indicates that targeting the RANKL-OPG signalling pathway is an effective treatment for osteoporosis, it is difficult to compare the results found with PEPITEM treatment as we see no change in RANKL secretion. Anti-sclerostin treatment also effects OPG secretion, in a similar way as hypothesized here for PEPITEM. As Sclerostin is a WNT inhibitor, inhibition of sclerostin causes an increase in conical WNT signalling, therefore resulting increased OPG secretion[466,622].

4.3.8 Conclusion

In completion these data show that altering the RANKL-OPG system is an attractive and effective therapeutic treatment for the treatment of osteoporosis. However, altering the balance of OPG:RANKL may cause long term changes within bone which must be assessed. Our data shows for the first time that PEPITEM is having dual action on the two bone cell types, through increasing the OPG:RANKL ration, providing a therapeutic strategy to increase the anti-catabolic actions OPG without the potential off target effects which come with the

use of inhibitors. However, it is important to assess how long term treatment and cessation of PEPITEM may alter osteoclast formation and OPG levels, to avoid rapid reversal in bone formation.

5 Identifying PEPITEM bioactivity to improve therapeutic capacity

5.1. Introduction

This thesis has so far described the function of PEPITEM and discussed its potential therapeutic value for musculoskeletal disorders such as osteoporosis. The use of peptide therapies has been researched for many years with the first therapeutic peptide, insulin, being synthesised in 1921[623,624]. Since then over 80 peptide drugs have been approved for clinical use worldwide[625–627], including one of the current treatments for osteoporosis, parathyroid hormone (PTH)[628]. There are multiple advantages of peptide treatments comparatively to small molecule therapies with peptides having higher specificity and efficacy[330]. However, the main drawbacks of peptide therapeutics are due to their low stability and short half-life, which we have previously observed when investigating the pharmacokinetics of PEPITEM *in vivo*[330]. The use of ^{3}H-PEPITEM allowed for radioactive tracing of PEPITEM following I.V. injection, revealing that PEPITEM is rapidly cleared from the circulation within 60 minutes post-injection with 95% leaving the circulation in 2 minutes in mouse[331]. It was identified that the main location for PEPITEM once out of the circulation was the kidneys, indicating renal clearance of the peptide[331]. Due to this, to see PEPITEM progress as a therapeutic agent, further research is required to alter its pharmacokinetic properties.

Peptide modifications to improve half-life have been extensively studied[330], and in this chapter we test the third hypothesis, PEPITEM consists of bioactive components which can serve as novel therapeutics for dysregulation in bone remodelling. Identifying the bioactive regions of the PEPITEM sequence and test peptide memetics for therapeutic value compared to PEPITEM.

5.2. Results

5.1.1 PEPITEM contains bioactive regions with differing biological function

PEPITEM is a 14aa peptide, which has previously been described to have biologically active trimers, located towards the N-terminus, SVT and QGA (unpublished data). These trimers were shown to mimic PEPITEM activity in the inhibition of leukocyte trans-endothelial migration[629]. In order to identify whether there are similar bioactive residues within the PEPITEM sequence we performed alanine mutagenesis[630]. This method allowed for site specific amino acid substitutions to decipher which, if any, of the amino acids within the PEPITEM sequence were required for peptide activity. Previous alanine mutagenesis experiments have shown that no singular amino acid substitution within PEPITEM affected peptide funtion[331], therefore we opted to substitute multiple amino acids to identify potential whole regions responsible for PEPITEM function (Table 5.1). As we have identified that PEPITEM has dual effects on osteoblast and osteoclasts through increase osteoblast maturation, measured using ALP, and osteoclast formation, measured through osteoblast OPG secretion, we will used both readouts as indicators of peptide activity.

C.Obs were treated for 8 days with PEPITEM or the edited sequence. Media subsequently was collected, and ALP activity was measured. ALP activity indicated that there is no effect of any alanine substitution on PEPITEM activity (Figure 5.1, A), with no significant decrease being detected when compared to PEPITEM. Comparatively altering different amino acid residues did impact PEPITEM mediated OPG secretion. When compared to PEPITEM, 4 of the altered peptide sequences showed a significance difference in OPG secretion (Figure 5.1, B), suggesting that these amino acid residues are required for PEPITEM mediated OPG secretion.

Table 5.1 Alanine sweeps peptides, and the amino acid substituted

Peptide Sequence	Amino Acid Substituted	Residue Number(s)
AVTEQAAELSNEER	S = Serine G = Glycine	1 & 6
SVTAQGAELSNEER	E = Glutamic acid	4
SVAEAGAELSNEER	T = Threonine Q = Glutamine	3 & 5
SVTEQGAELSAEEA	L = Leucine N = Asparagine R = Arginine	9, 11 & 14
AVTEQGAELANEEA	S = Serine R = Arginine	10 & 14

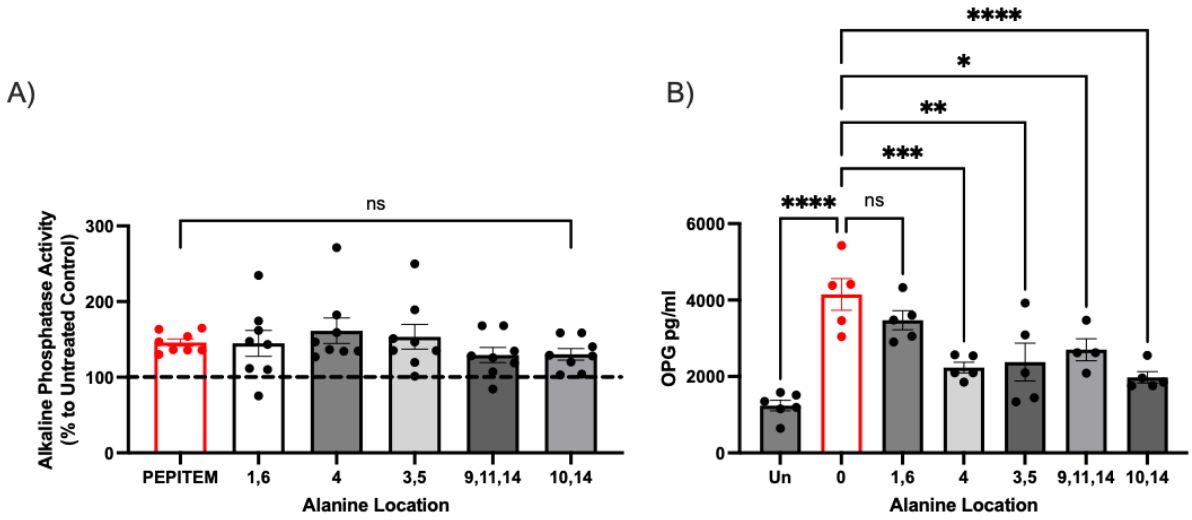


Figure 5.1 Altering the PEPITEM sequence alters OPG secretion, but not ALP activity. C.Obs were treated with 10 ng/ml synthesized PEPITEM versions with one or more alanine substitutions for 8 days. (A) Alkaline phosphatase activity was analysed on day 8 and displayed as % compared to untreated control. Friedman test shows a significant effect of treatments on ALP activity compared to untreated control, P<0.01. (B) OPG ELISA quantifying OPG secretions from conditioned media, displayed as OPG pg/ml. ANOVA shows a significant effect of treatments on OPG secretion, P < 0.0001. Data are mean ± SEM, from n=8 independent experiments. **** = P < 0 .0001, *** = P < 0.001, ** = P < 0.01 and * = P < 0.05 by Dunnett's multiple comparison compared to PEPITEM treatment.

The data above demonstrates that altering residues in the N-terminal and C-terminal regions, SVTEQGA and LSNEER, effects PEPITEM function. Coupled with previous data (Chapter 3, Table 3.2; Figure 5.2), where AlphaFold predictions for total NCAM-1 extracellular protein or Fibronectin type III domain protein interactions suggest the residues involved in binding fall either in the GAELSN sequence (Figure 5.2,A) or predominantly in the SVTEQGA sequence (Figure 5.2,A). Therefore, we treated osteoblasts with PEPITEM, SVTEQGA or LSNEER for 8-days in order to determine whether these segments mimicked or inhibited PEPITEM function. ALP activity was unaffected by the presence of the LSNEER peptide compared to untreated control, whereas both PEPITEM and SVTEQGA significantly increases ALP activity compared to untreated control (Figure 5.3, A). Comparatively, the OPG secretion appears to be regulated by LSNEER, with PEPITEM and LSNEER significantly increasing OPG secretion compared to untreated controls (Figure 5.3, B), whereas SVTEQGA has no significant effect on OPG secretion.

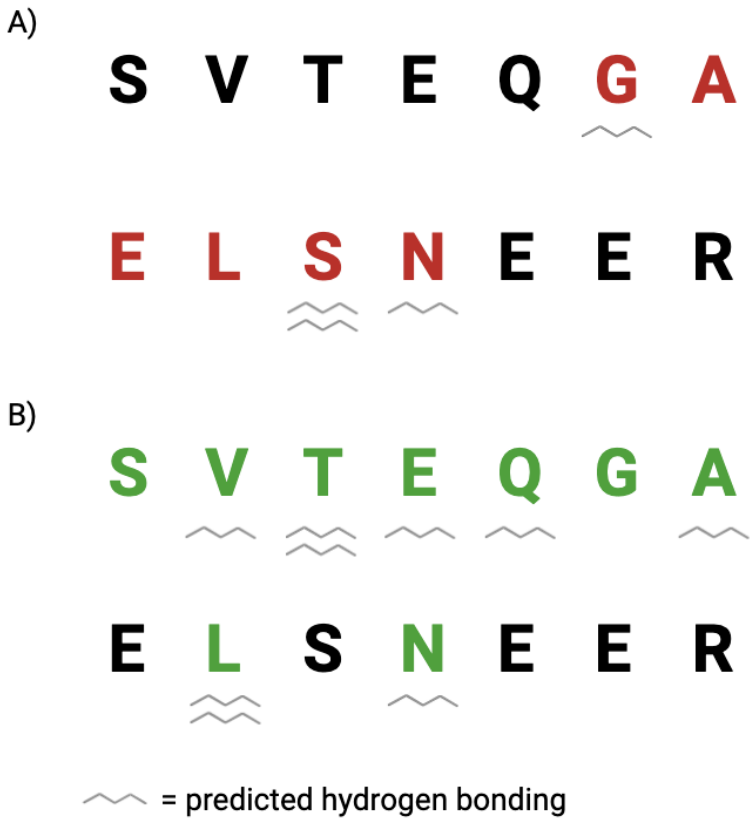


Figure 5.2 **Diagram of AlphaFold predicted binding residues in PEPITEM**. Predicted amino acid residues involved in binding of PEPITEM to (A) NCAM-1 extracellular or (B) Fibronectin type III domain proteins only, binding to PEPITEM. Red/green indicates predicted pseudobond formation. Predicted hydrogen bond formation is indicated by underlining.

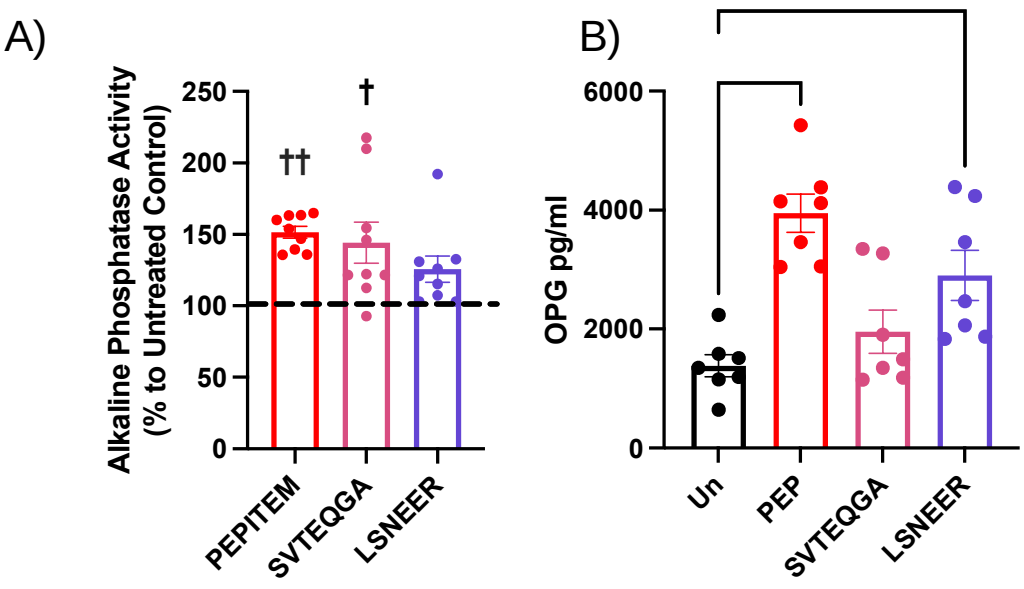


Figure 5.3 PEPITEM sequence fragments alters OPG secretion and ALP activity. C.Obs were treated with 12.9nM of PEPITEM or PEPITEM fragments SVTEQGA or LSNEER, for 8 days. (A) Alkaline phosphatase activity was analysed on day 8 and displayed as % compared to untreated control (dotted line). Friedman test shows a significant effect of treatments on ALP activity compared to untreated control P<0.01. (B) OPG ELISA quantifying OPG secretions from conditioned media, displayed as OPG pg/ml. ANOVA shows a significant effect of treatments on OPG secretion, P<0.0001. Data are mean ± SEM, from n=6-9 independent experiments. ††=P<0.01 and †=P<0.05 by Dunns multiple comparison compared to untreated control. ***=P<0.001 and *=P<0.05 by Dunnett's multiple comparison compared to PEPITEM treatment, all significant differences are shown.

5.1.2 Investigation of small PEPITEM derived memetics

Based on these results we investigated the first 7aa (SVTEQGA) of the PEPITEM sequence, which appears to have an osteoanabolic role. Previously a number of peptide memetics, based on the previously identified bioactive trimers (SVT and QGA) that play a role in leukocyte migration[629] were created (Figure 5.4). These memetics were designed to improve the bioavailability of the peptides *in vivo*. In total 6 peptides, consisting of the 2 trimers and 4 altered peptides, were assessed. Of the four engineered peptides, two were SVT based and two were QGA based (Figure 5.4). Peptides were altered to increase bioavailability, through modifications which increase peptide stability, permeability or decrease enzymatic cleavage. The techniques employed were: 1) Substitution of the C-terminal amide with a [NH-Ethyl] group, which has been shown to increase peptide stability and potentially increase membrane permeability[631], 2) substitution of QGAs N-terminal glutamine (Q) with pyroglutamate [pGlu], this process involves cyclization of glutamine to produce a more acidic variant, proteins with this modification have been shown to have an increased half-life due to reduced degradation by aminopeptidases[632,633] ; 3) use of D-isomers, which bare similar stereochemical properties to their more natural L-isomer enantiomer but are more resistant to enzyme cleavage[634].

Here we looked at how these trimers and their adapted memetics behave on osteoblasts and how these compares to PEPITEM. As before we use ALP and OPG as markers of peptide responses. ALP assessment shows that 3 of the peptides tested increased osteoblast maturation: SVT, *tvs* and QGA (Figure 5.5, A), whereas SVT[NH-Ethyl], pGlu]-GA-amide and aGq-amide did not significantly increase ALP compared to control. These peptides were also tested for OPG production, which was significantly increased in response to SVT-

related peptides (SVT and *tvs)* and showed a trend towards an increase in SVT[NH-Ethyl] compared to control (Figure 5.5, B). By contrast, the QGA-related peptides did not increase OPG secretions (Figure 5.5, B).

Based on these results, we focused our investigations on the three peptides that resulted in an increase in one or more of the outcome measures (Figure 5.5); SVT, QGA and *tvs*. Previously we used the peptides at the same molar concentration as used for PEPITEM treatment, therefore we wanted to look at optimum treatment dosage by carrying out a titration assessment. These data show that each peptide works at lower concentrations than that used for PEPITEM (10ng/ml) with the maximum response for SVT, *tvs* and QGA being between 0.1-1ng/ml (Figure 5.6, A-C). Using these data EC50s for each peptide was calculated SVT (21.4ng/ml), QGA (388.8 ng/ml) and *tvs* (7.7 ng/ml).

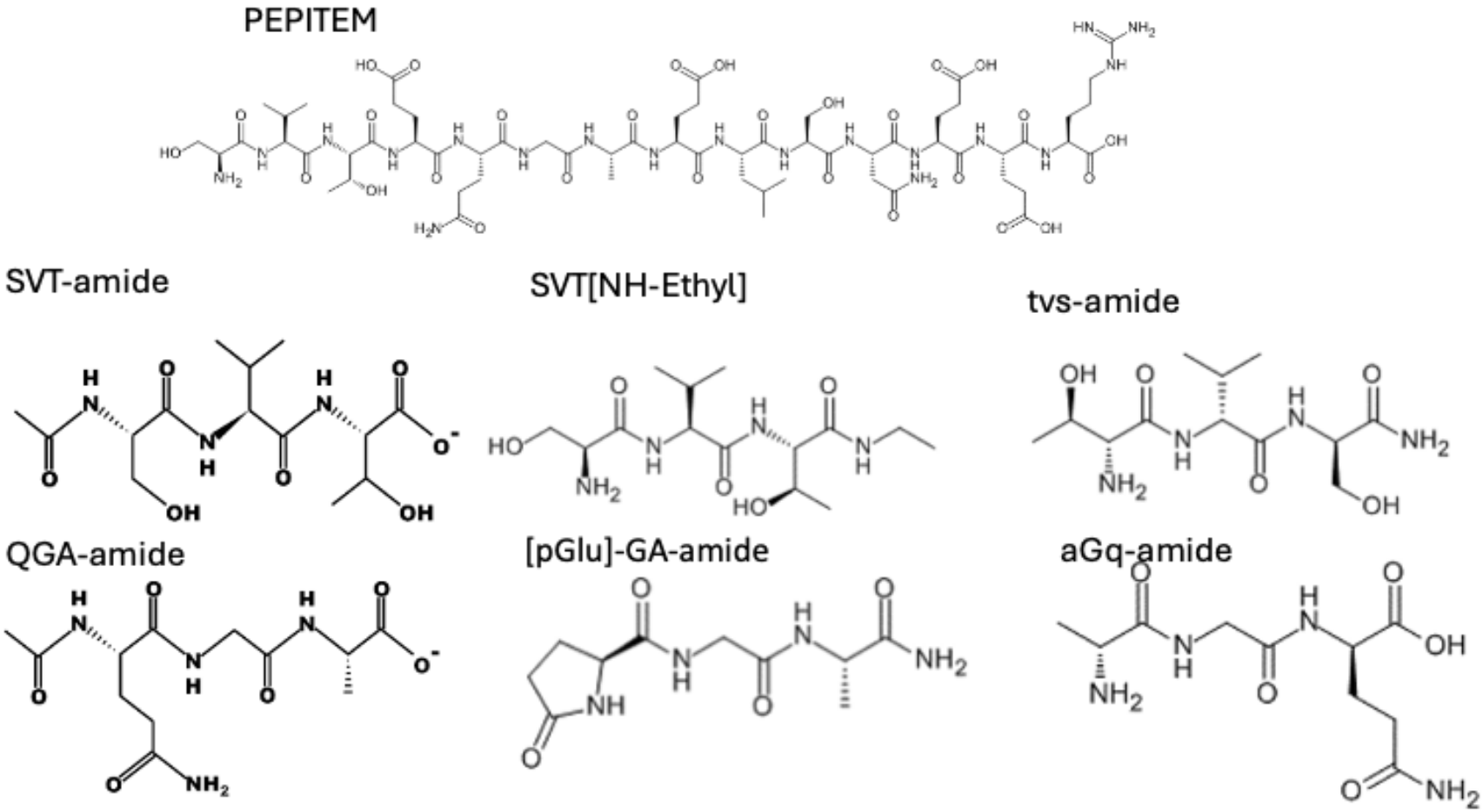


Figure 5.4 **Structural formula for PEPITEM and associated peptide memetics.** Diagrams of the structural formula of PEPITEM and its memetics created using pepdraw.com

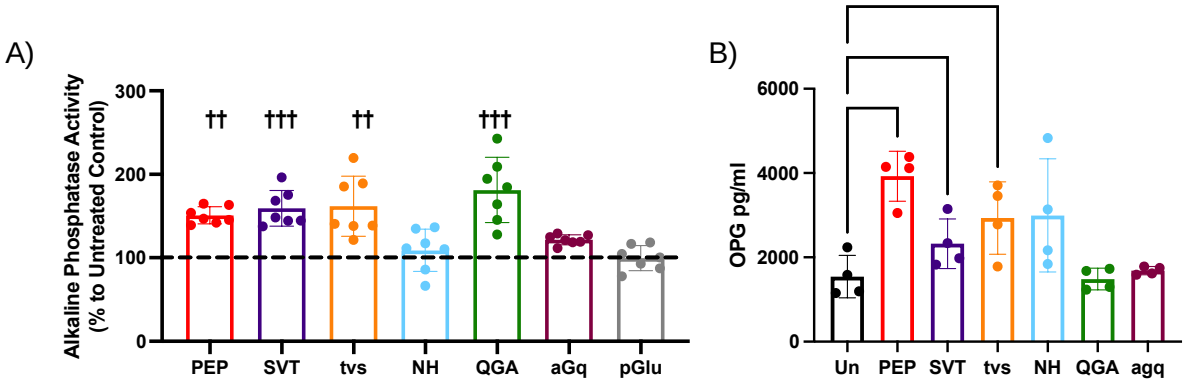


Figure 5.5 **PEPITEM memetics alter OPG secretion and ALP activity.** C.Obs were treated with 12.9 nM synthesized PEPITEM or each peptide memetic, for 8 days. PEPITEM (red), SVT (purple), *tvs* (orange) SVT[NH-Ethyl] (light blue, NH), QGA (green), aGq (magenta) and [pGlu]-GA-Amide (grey, pGlu). (A) Alkaline phosphatase activity was analysed on day 8 and displayed as % compared to untreated control. Friedman test shows a significant effect of treatments on ALP activity, compared to untreated control $P < 0.0001$. (B) OPG ELISA quantifying OPG secretions from conditioned media, displayed as OPG pg/ml. ANOVA shows a significant effect of treatments on OPG secretion, $P<0.05$. Data are mean ± SEM, from (A) n=6-9 (B) n= 4 independent experiments. ††† = $P < 0.001$ and †† = $P < 0.01$ by Dunns multiple comparison compared to untreated control. ** = $P < 0.01$ and * = $P < 0.05$ by Dunnett's multiple comparison compared to PEPITEM treatment, all significant differences are shown.

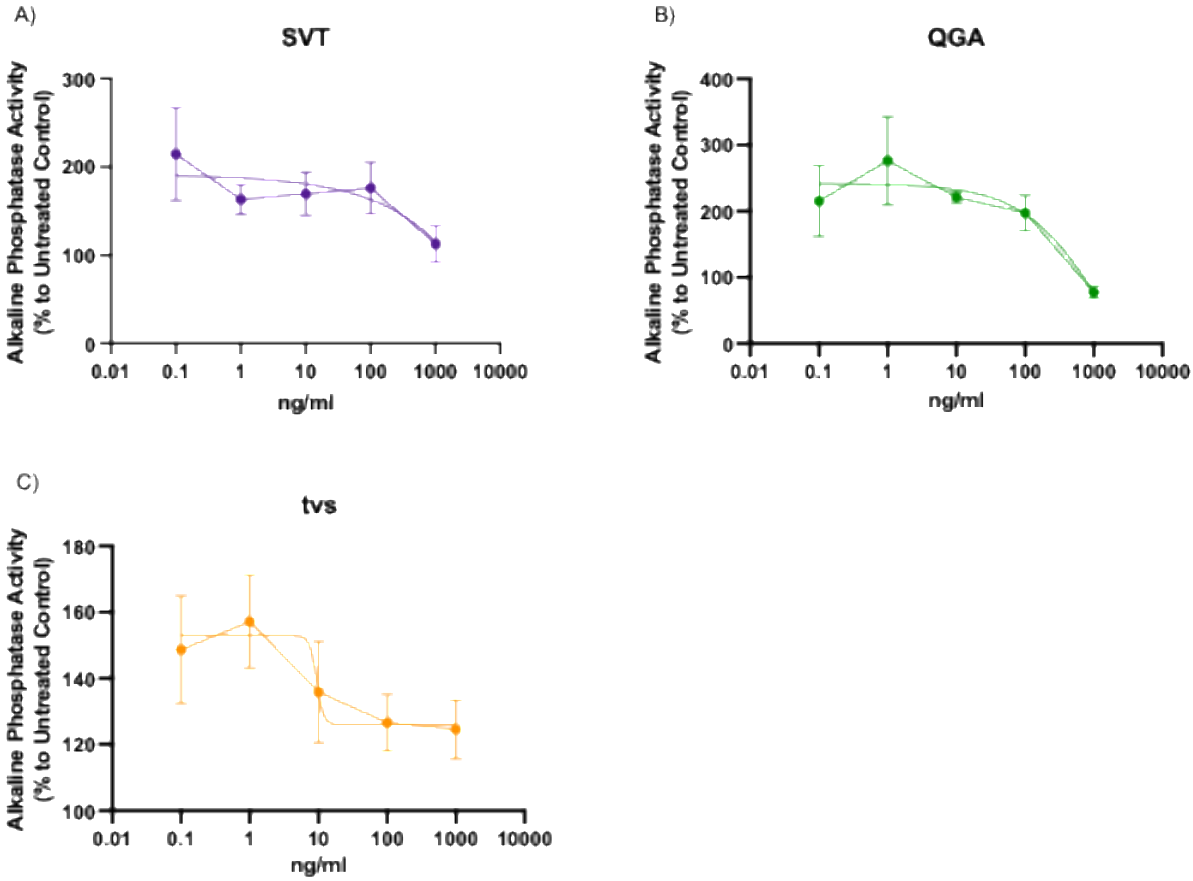


Figure 5.6 **Titration for peptide mimetics.** C.Obs were treated with 0.1-1000ng/ml synthesized PEPITEM of each peptide memetic, (A) SVT (purple), (B) QGA (green) or (C) *tvs* (orange) for 8 days. Alkaline phosphatase activity was analysed on day 8 and displayed as % compared to untreated control at each concentration. A non-linear 4PL regression curve fitted to each graph. Data are mean ± SEM, from n= 3 independent experiments.

5.1.2.1 3D *in vitro*

Once an optimum concentration of peptide was established, we moved to investigate the effects of each peptide in a 3D environment using the SSBM as describe previously in chapter 3 and 4. The outcome measures being pro-collagen type I secretion, OPG secretion and alizarin red staining. 4 – or 12-week-old SSBM constructs were treated for 8 days with PEPITEM (10ng/ml), SVT (0.5ng/ml), QGA (1ng/ml) or *tvs* (1ng/ml).

Pro-collagen type I ELISA showed a significant increase in secretion following 8-day treatment with SVT, QGA or *tvs* from 4-week-old constructs compared to control untreated constructs (Figure 5.7, A), whereas although there was a trend towards an increase in the PEPITEM treated group this increase was not significant. Comparatively the 12-week-old constructs were unaffected by any of the peptides(Figure 5.7, B), as seen previously in response to PEPITEM in chapter 3. These data suggest that each peptide can increase osteoblast secretion of extracellular matrix in the SSBM model of bone at earlier timepoints (4-weeks), whereas at later timepoints (12-weeks), neither PEPITEM nor the peptide memetics can alter pro-collagen production.

OPG secretion was significantly increased in PEPITEM treated 4-week SSBM constructs (Figure 5.8, A). Although there was a slight increase in OPG response to the peptide memetics, this increase was not significant (Figure 5.8, A). Comparatively, no differences were observed in OPG following treatment of the 12-week constructs (Figure 5.8, B).

In order to look at the memetics effects on mineralisation following media collection SSBM constructs were fixed and stained using alizarin red. The dye was then extracted and quantified as a measure of mineralisation (Figure 5.7). These data suggest that PEPITEM

treatment enhanced mineralisation as previously reported[197] and presented in previous chapters, however none of the memetic treatments increased mineralisation of the SSBM construct (Figure 5.7).

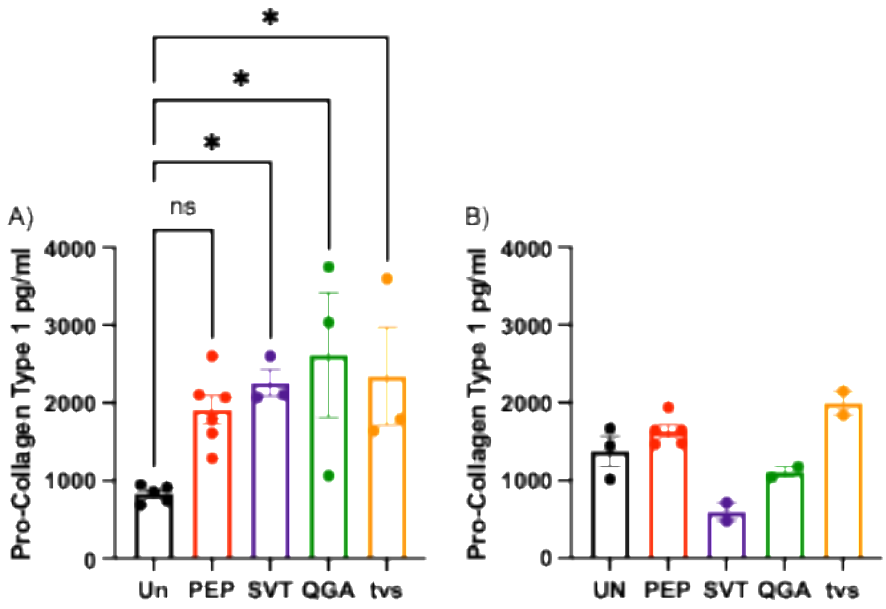


Figure 5.7 **Peptide memetics increase pro-collagen type I secretion in 3D bone model**. SSBM organoids cultured for 4 or 12 weeks, at each time point constructs were treated with PEPITEM, SVT, QGA or *tvs* for 8 days before media collection. (A,B) Pro-collagen type I (pg/ml) from SSBM construct media following treatment at (A) 4 weeks or (B) 12 weeks. (A) ANOVA showed significant effect of treatment $p < 0.05$. Data are Mean ± SEM from n=3-5 constructs per group. * = $P < 0.05$ by Dunnett's multiple comparison compared to Untreated control.

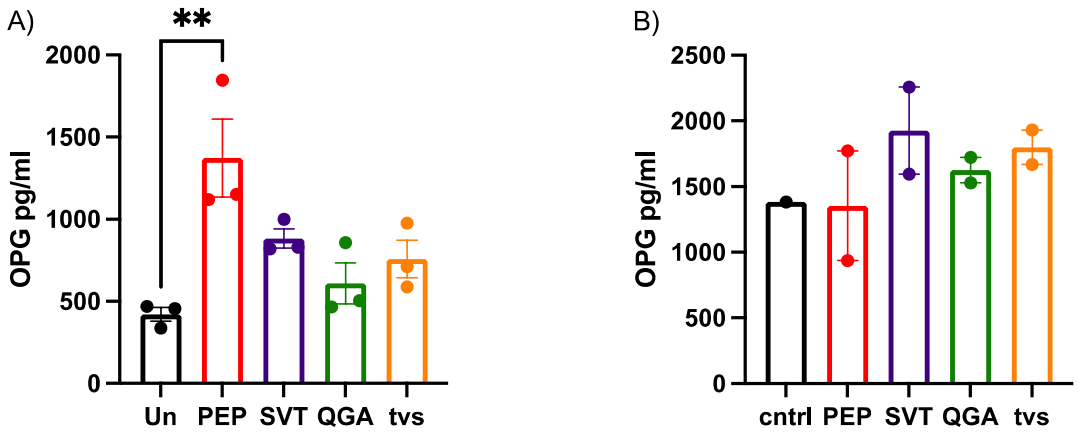


Figure 5.8 ***PEPITEM but not peptide memetics increase OPG secretion in 3D bone model***. SSBM organoids cultured for 4 or 12 weeks, at each time point constructs were treated with PEPITEM, SVT, QGA or *tvs* for 8 days before media collection. (A,B) OPG conc (pg/ml) from SSBM construct media following treatment at (A) 4 weeks or (B) 12 weeks. (A) ANOVA showed significant effect of treatment $P < 0.01$. Data are mean ± SEM from n = 1-3 constructs per group. ** = $P < 0.01$ by Dunnett's multiple comparison compared to untreated control

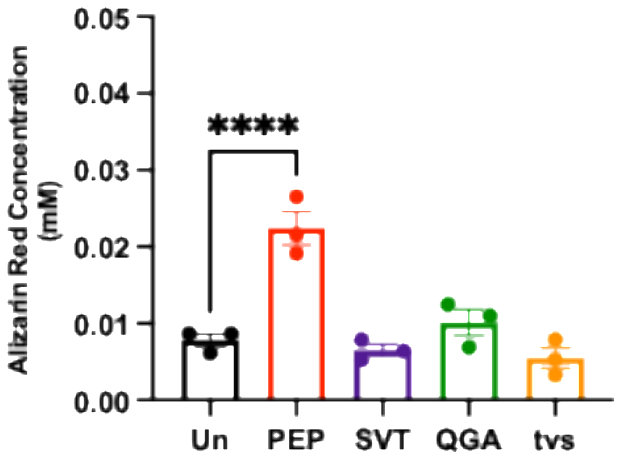


Figure 5.9 **PEPITEM but not peptide memetics increase mineralisation 3D bone model**. SSBM organoids cultured for 4-weeks, then treated with PEPITEM, SVT, QGA or *tvs* for 8 days before fixation. After fixation constructs were stained using alizarin red and concentration of dye extracted was determined from standard curve. Alizarin red concentration (mM) from SSBM construct following treatment at 4 weeks. (A) ANOVA showed significant effect of treatment $p < 0.0001$. Data are mean ± SEM from n = 3 constructs per group. ** = P< 0.0001 by Dunnett's multiple comparison compared to untreated control

5.1.3 Peptide memetics partially to mimic PEPITEM function during homeostatic remodelling

Following *in vitro* assessment of the peptide memetics we first wanted to compare their *in vivo* effects during homeostasis. Previously we have only tested this use of the PEGylated version of the PEPITEM peptide *in vivo*[197]. The PEGylation was thought to increase half-life and therefore increase bioavailability, however, as we have not PEGylated the peptide memetics we decided to use non-PEGylated PEPITEM as our control. Therefore, this study will also allow us to assessment of whether the natural form of the peptide is able to increase bone remodelling following supplementation.

Here we chose to investigate the actions of QGA and *tvs*. QGA was chosen due to its increased effects on ALP and collagen secretion. The *in vitro* data suggests that both SVT and *tvs* can both increase ALP activity and OPG secretion, however as *tvs* is the D-isomer we believe it may resist enzymatic degradation and therefore be cleared more slowly than SVT.

Based on our *in vitro* data we hypothesised that non-PEGylated PEPITEM, QGA and tvs would be able to alter homeostatic bone remodelling as seen with PEGylated PEPITEM previously[197]. To do this we use the same experimental design where 8-10-week old only WT mice were treated with daily I.P. injections of PBS (control), PEPITEM, QGA or *tvs* using the same molar concentration previously used for PEPITEM treatment (645.8 μM) for 14-days (Figure 5.10). Following, 14 days of treatment, tissues were collected. The number of mice used in this experiment was calculated using the NC3Rs EDA software[635,636], where the power calculation was based on the BV/TV values from the previous PEGylated PEPITEM experiments[197].

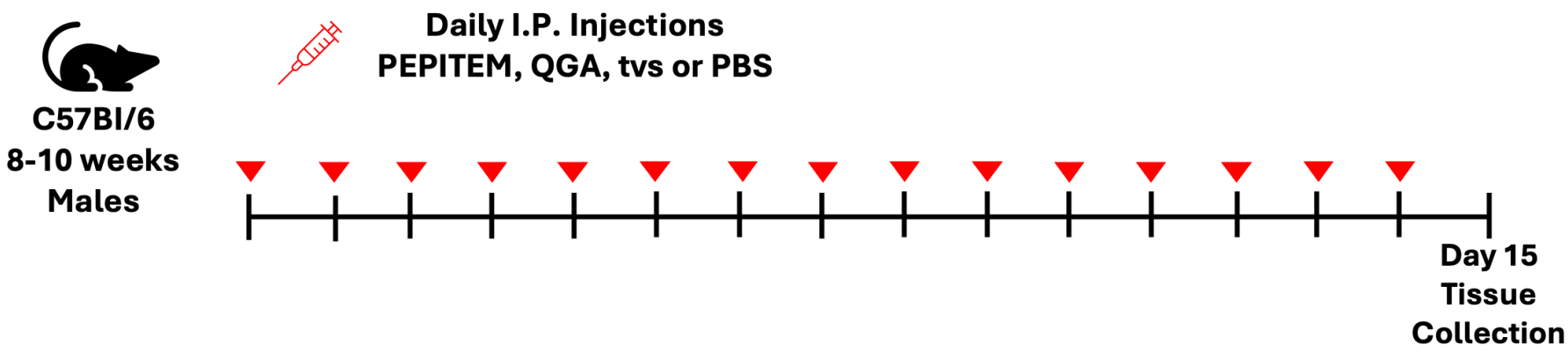


Figure 5.10 Model to study the effect of PEPITEM memetics on bone homeostasis. WT mice were given daily 300 µl i.p. injection containing vehicle control (PBS), or 645.8 µM PEPITEM, QGA or *tvs* for 14 days. On day 15 mice were culled by a Schedule 1 method (cervical dislocation), and tissue was collected for analysis.

To assess changes in bone formation μCT analysis of the tibiae was carried out. Trabecular changes were observed though isolation of the trabecular bone region below the proximal growth plate (Figure 5.11, A). Following 2-weeks of PEPITEM treatment, we saw a significant increase in the trabecular bone parameters, BV/TV (Figure 5.11, B) and trabecular number (Figure 5.11, E), and a decrease in trabecular separation (Figure 5.11, D). We observed no significant change in trabecular thickness (Figure 5.11, C), in contrast to our published data using PEGylated PEPITEM. Comparatively we saw no effect of either QGA or *tvs* on any of the trabecular bone parameters (Figure 5.11, B-E).

Previously, we have only observed PEPITEM to increase trabecular bone within the metaphysis, however analysis of trabecular bone further down into the diaphysis showed that PEPITEM, QGA and *tvs* caused trabecular elongation (Figure 5.12, A-B). To quantify this, we looked at BV/TV of the trabecular bone 200 slices below the metaphysis trabecular bone initially analysed (Figure 5.12, C). These data showed a significant increase in BV/TV in the PEPITEM treated mice compared to the PBS treated controls, suggesting PEPITEM is increasing trabecular elongation. Although a trend towards an increase was observed in the BV/TV of QGA and *tvs* treated mice was borderline significant ($P = 0.0588$ and $P = 0.0568$, respectively).

As seen previously we see no change in cortical parameters after 2-weeks PEPITEM treatment, additionally no changes were identified following tvs or QGA treatment (Figure 5.13, A-E).

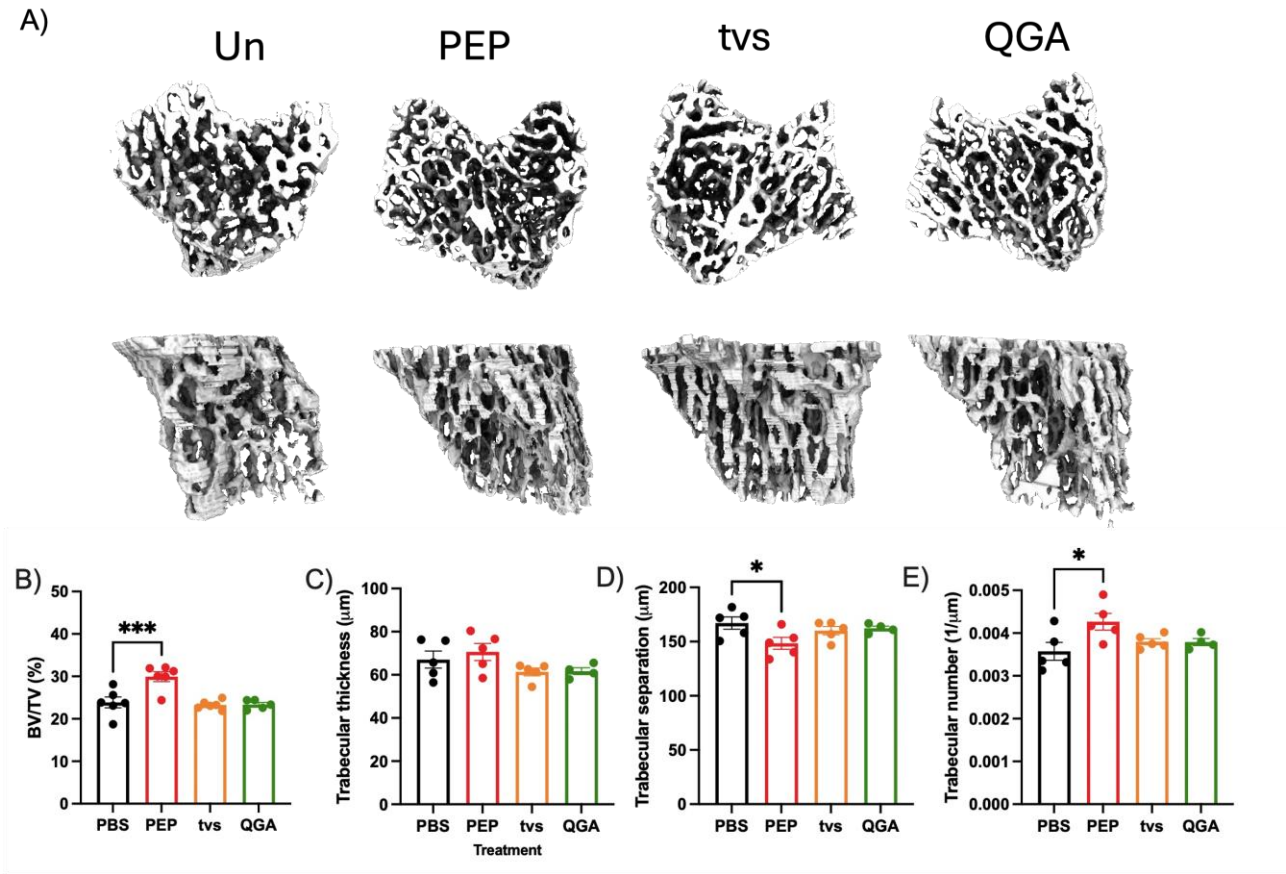


Figure 5.11 **PEPITEM but not peptide memetics alter trabecular bone parameters by µ-CT in homeostatic male mice.** Homeostatic male mice injected with daily i.p. injections of 300 µl of PBS vehicle (black, n = 5), or 300 µl containing 645.8 µM PEPITEM (red, n = 5), QGA (Green = 5) or *tvs* (orange = 5) for 14 days. Tibiae scanned by µ-CT and regions of interest were drawn around trabecular bone in the metaphysis to analyse trabecular parameters. (A) Representative images of transverse and coronal plane µ-CT 3D reconstructions from PBS, PEPITEM, *tvs* or QGA treated mice. (B-E) trabecular bone was quantified and analysed for (B) trabecular bone volume (BV/TV, %), (C**)** trabecular thickness (µm), (D) trabecular separation (µm) (E) trabecular number (1/µm). One way ANOVA showed significant effects of treatments for (A) $P < 0.01$, (C) $P < 0.05$ and (D) $P < 0.05$. Data are mean ± SEM for n=5 mice per treatment group. * = $P < 0.05$ and ** = $P < 0.01$ by Dunnett's multiple comparison.

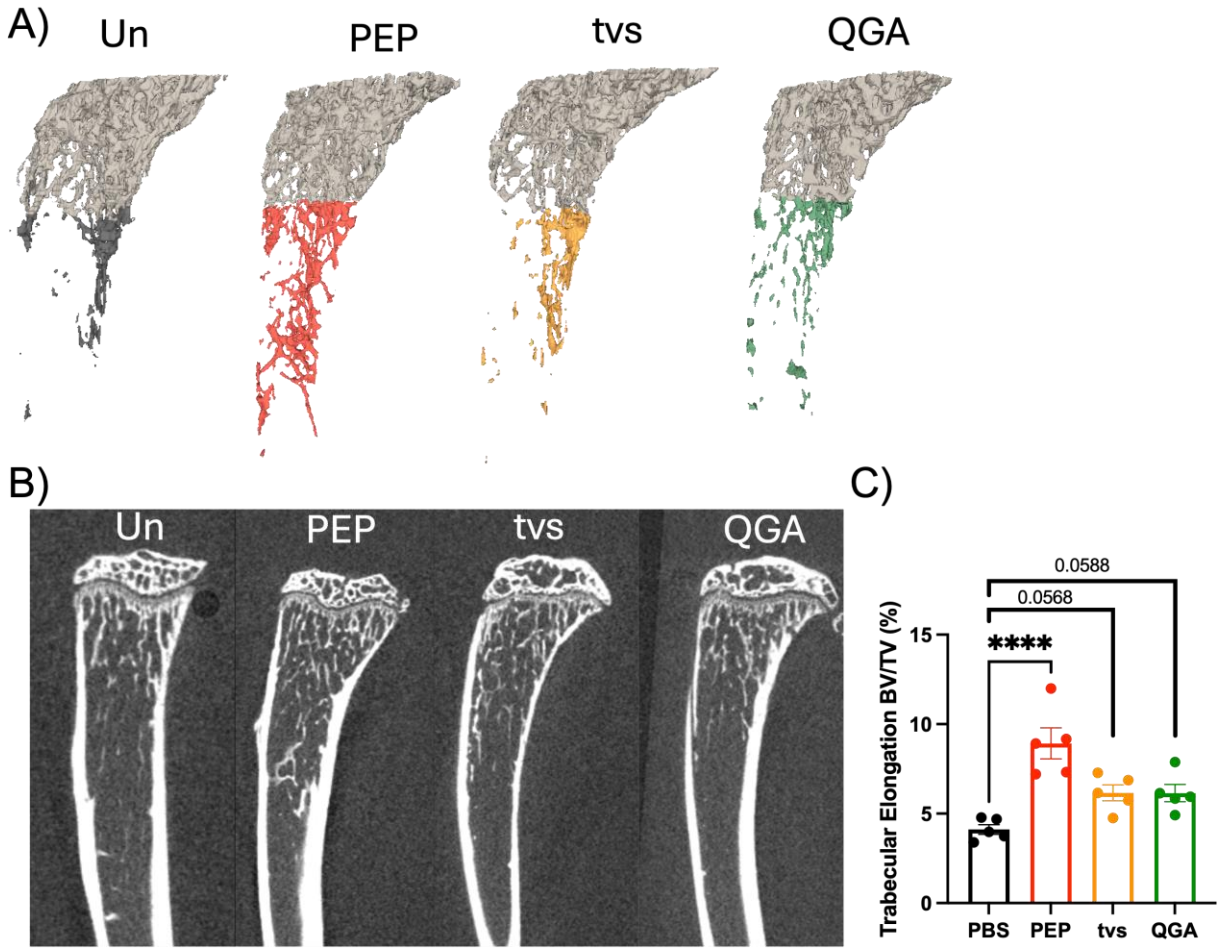


Figure 5.12 **PEPITEM and peptide memetics enhanced trabecular bone elongation by µ-CT in homeostatic male mice.** Homeostatic male mice injected with daily i.p. injections of 300 µl of PBS vehicle (black, n = 4), or 300 µl containing 645.8 µM of PEPITEM (red, n = 4), QGA (Green = 4) or *tvs* (orange = 4) for 14 days. Tibiae scanned by µ-CT and regions of interest were drawn around trabecular bone in the metaphysis to analyse trabecular elongation, where trabecular bone continues further than first 100 slices after growth plate. (A) Representative images of coronal plane µ-CT 3D reconstructions from PBS, PEPITEM, *tvs* or QGA treated mice. Elongated trabecular measurements highlighted. (B) 2D cross-section of µ-CT scanned tibia. (C) Trabecular bone volume (BV/TV, %) of elongated trabecular bone. ANOVA shows significant effect of treatment on (C) P<0.001 Data are mean ± SEM for n = 5 mice per treatment group. **** = P < 0.0001 by Dunnett's multiple comparison.

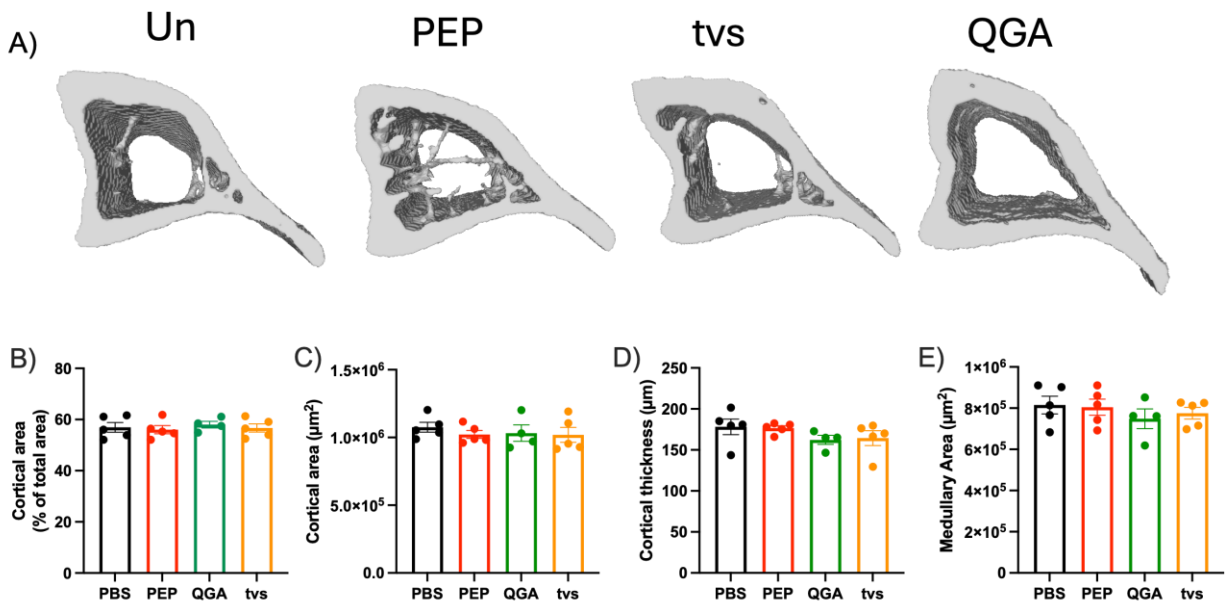


Figure 5.13 **PEPITEM and peptide memetics no not alter cortical bone parameters by µ-CT in homeostatic male mice.** Homeostatic male mice injected with daily i.p. injections of 300µl of PBS vehicle (black, n = 5), or 300µl containing 645.8 µM of PEPITEM (red, n = 5), QGA (Green = 5) or *tvs* (orange = 5) for 14 days. Tibiae scanned by µ-CT and regions of interest were drawn around cortical bone in the epiphysis to analyse cortical parameters. (A) Representative images of transverse plane µ-CT 3D reconstructions from PBS, PEPITEM, *tvs* or QGA treated mice. (B-E) Cortical bone was analysed for (B) cortical area (%), (C) total cortical area (µm^2) (D) Cross sectional thickness (µm), and (E) Medullary area (µm^2). Data are mean ± SEM for n = 5 mice per treatment group.

To further examine the effects of PEPITEM, QGA and *tvs* on homeostatic bone formation we performed histomorphology analysis looking at osteoblast number presented as a percentage bone osteoblast coverage (Ob.S/BS) and osteoid deposition presented as percentage of osteoid compared to trabecular bone surface area (OB/OS).

Osteoid was used to measure increases in matrix production in response to treatment, here we show that PEPITEM significantly increased osteoid production (Figure 5.14, A and B) similarly to that seen previously with PEG-PEPITEM[197]. We also saw an increase in QGA and *tvs*, however this trend is not statistically significant.

H&E staining was used to assess osteoblast number (Ob.S/BS) as a percentage of bone surface coverage. Here we saw no difference in osteoblast number following treatment compared to PBS control (Figure 5.15, A and B), agreeing with our published work and suggesting that PEPITEM or PEPITEM memetics do not affect osteoblast proliferation.

Following analysis of changes in bone formation, we also quantified changes in bone resorption through analysing change in the number of TRAP positive osteoclasts. Here we hypothesised based on data that PEPITEM and *tvs* will decrease osteoclast number as both were able to increase OPG secretion, whereas QGA did not. As observed previously we saw a significant reduction in the number of TRAP positive osteoclasts present following PEPITEM treatment (Figure 5.16). Although we do not see a significant decrease in osteoclast number following QGA and *tvs*, both show a trend towards a decrease (P= 0.0820 and P=0.3161, respectively) (Figure 5.16).

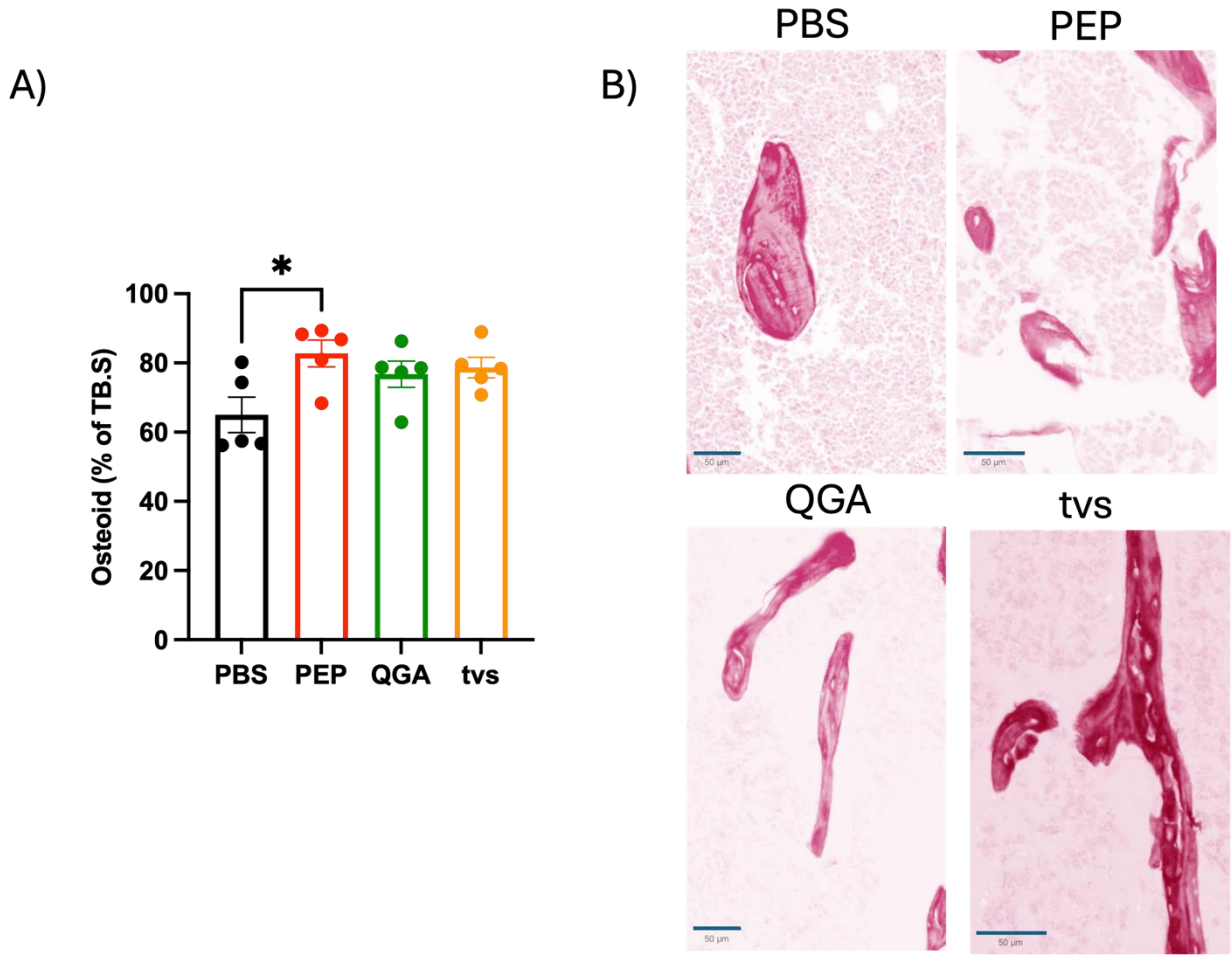


Figure 5.14 **PEPITEM memetics partially increased osteoblast production of osteoid**. Homeostatic male mice injected with daily i.p. injections of 300µl of PBS vehicle (black, n = 5), or 300 µl containing 645.8 µM of PEPITEM (red, n = 5), QGA (Green = 5) or *tvs* (orange = 5) for 14 days. Tibiae were decalcified, paraffin embedded, sectioned and stained for osteoid (Sirius red) (A) Levels of osteoid were measured as % of trabecular surface (TB.S). (B) Representative images of Sirius red staining from PBS or PEPITEM treated mice. ANOVA shows significant effect of treatment on osteoid production, $P < 0.05$. Scale bar, 50 µm Data are mean ± SEM for n = 5 mice per treatment group. * = $P < 0.05$ by Dunnett's multiple comparison.

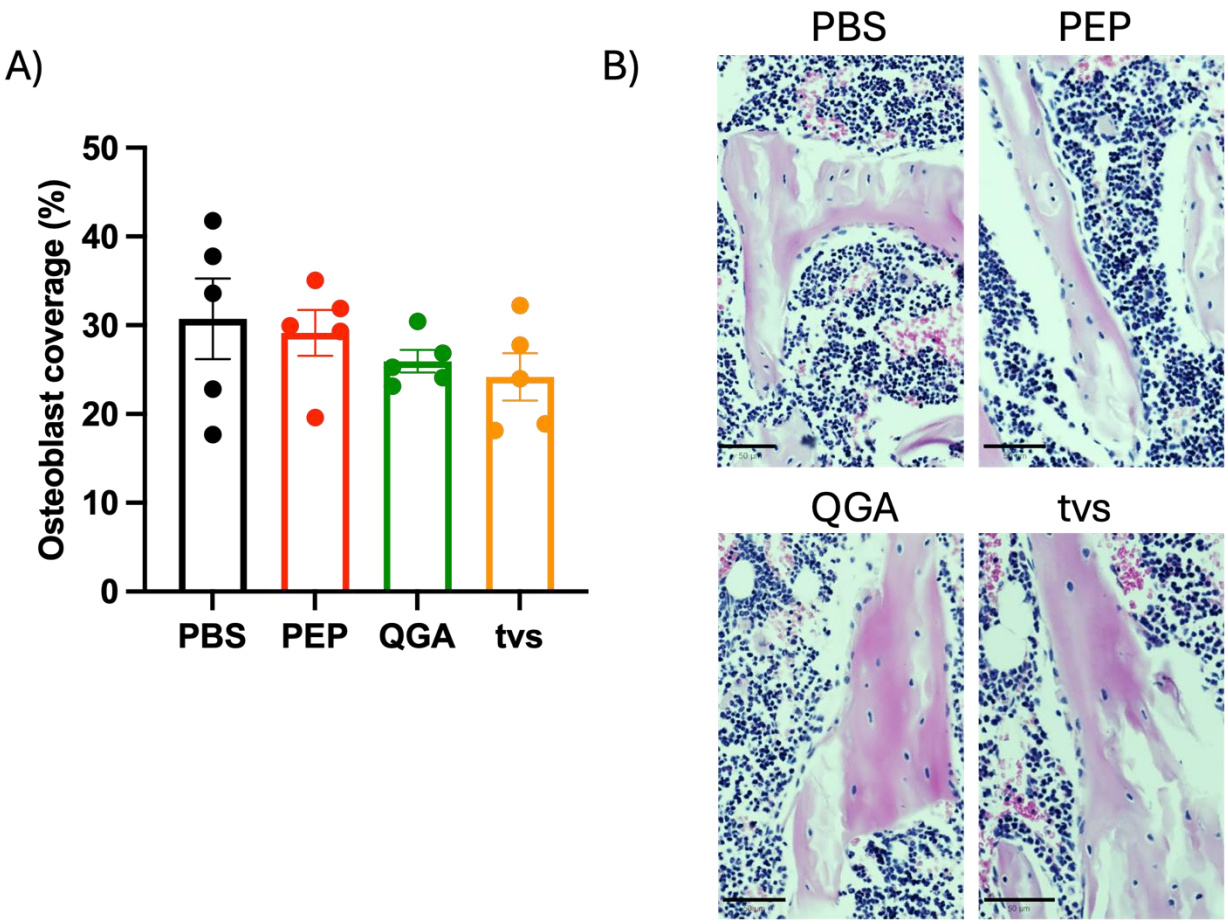


Figure 5.15 **PEPITEM memetics did not increase osteoblast number.** Homeostatic male mice injected with daily i.p. injections of 300µl of PBS vehicle (black, n = 5), or 300 µl containing 645.8 µM of PEPITEM (red, n = 5), QGA (Green = 5) or *tvs* (orange = 5) for 14 days. Tibiae were decalcified, paraffin embedded, sectioned and stained for H&E (A) Osteoblasts were quantified and measured as percentage of the total bone surface area, OB.S/BS. (B) Representative image of H&E stained tibia. Scale bar, 50 µm. ANOVA shows significant effect of treatment on (A) $P < 0.05$. Data are mean ± SEM for n = 5 mice per treatment group.

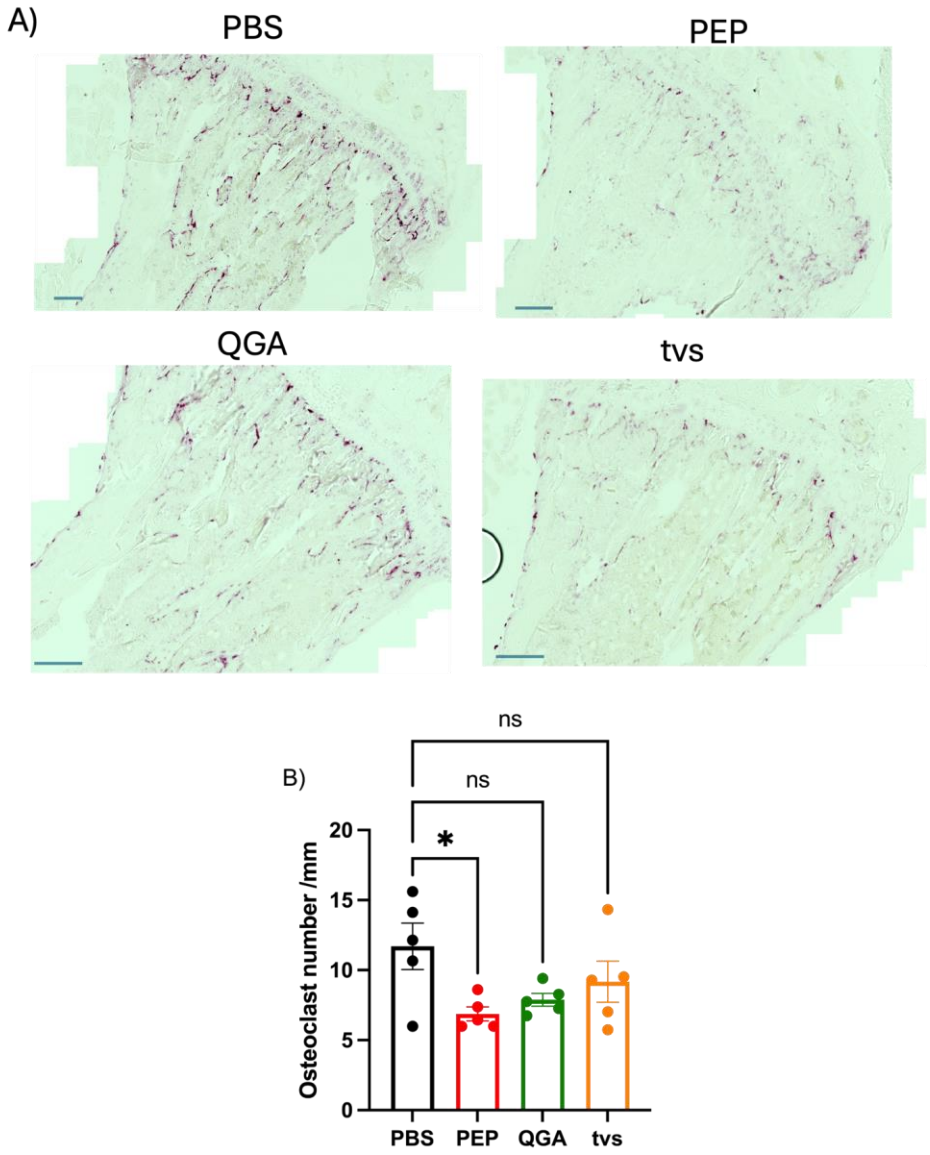


Figure 5.16 **PEPITEM memetic treatments partially reduce osteoclast number in male homeostatic mice.** Homeostatic male mice injected with daily i.p. injections of 300 µl of PBS vehicle (black, n = 5), or 300 µl containing 645.8 µM of PEPITEM (red, n = 5), QGA (Green = 5) or *tvs* (orange = 5) for 14 days. Tibiae were decalcified, paraffin embedded, sectioned and stained for TRAP. (A) Representative images of TRAP staining from PBS, PEPITEM, OQA or *tvs* treated mice. (B) the number of TRAP positive cells were measured as osteoclast number /mm^2 surface of trabecular bone. ANOVA shows significant effect of treatment (B) $P < 0.05$. Scale bar, 250 µm. Data are mean ± SEM for n = 5 mice. * = $P < 0.05$ by Dunnett's multiple comparison.

5.1.4 Peptide partially mimic PEPITEM function in models of osteoporosis

During a model of homeostatic bone remodelling, we saw trends in the effects of QGA and *tvs*. We hypothesized that based on the small changes observed these peptides may also have therapeutic potential in the presence of bone loss as seen with PEPITEM treatment. Our lab has previously used the ovariectomy (OVX) model of osteoporosis to explore the pro-anabolic properties of PEPITEM, therefore we used the same model to investigate QGA and *tvs*. We calculated the number of mice used in this experiment using the NC3Rs EDA software[635,636] using OVX BV/TV values of PEGylated PEPITEM treated mice[197] compared to control (PBS) for the power calculation.

Here we used the experimental design previously characterised. Female wild type mice were ovariectomised on day 0. 14-days post-surgery, mice were treated with PBS, PEPITEM, QGA or *tvs* (Figure 5.17). After 14-days of treatment (29-days post-OVX), tissues were collected. μCT analysis was performed to look at trabecular parameters following peptide treatments (Figure 5.18). When examining changes in trabecular parameters in response to PEPITEM we saw a significant increase in BV/TV (Figure 5.18, B) and trabecular number (Figure 5.18, E) in comparison to the PBS control group. Whereas no differences were observed for trabecular separation ($P>0.1$) or trabecular thickness ($P>0.1$). Previously, in this model PEGylated PEPITEM was shown to increase all four trabecular bone parameters[197], therefore PEGylation may increase PEPITEM function within bone.

There was a significant increase in BV/TV following *tvs* treatment ($P < 0.05$) compared to PBS, however no changes in any of the other trabecular parameters (Figure 5.18). Similarly, we only saw borderline significance of QGA treatment on BV/TV ($P = 0.0508$) but no changes

in other parameters (Figure 5.18), suggesting these memetics partially match the differences seen with PEPITEM treatment.

As we previously showed increased trabecular elongation into the diaphysis following PEPITEM and memetic treatment in resting mice, we looked at trabecular elongation following OVX. However following OVX the amount of trabecular bone detected in the diaphysis was negligible, therefore the data has not been included. Analysis of cortical bone parameters (Figure 5.19) showed no changes in cortical bone following PEPITEM, QGA or *tvs* treatment (Figure 5.19, A-E).

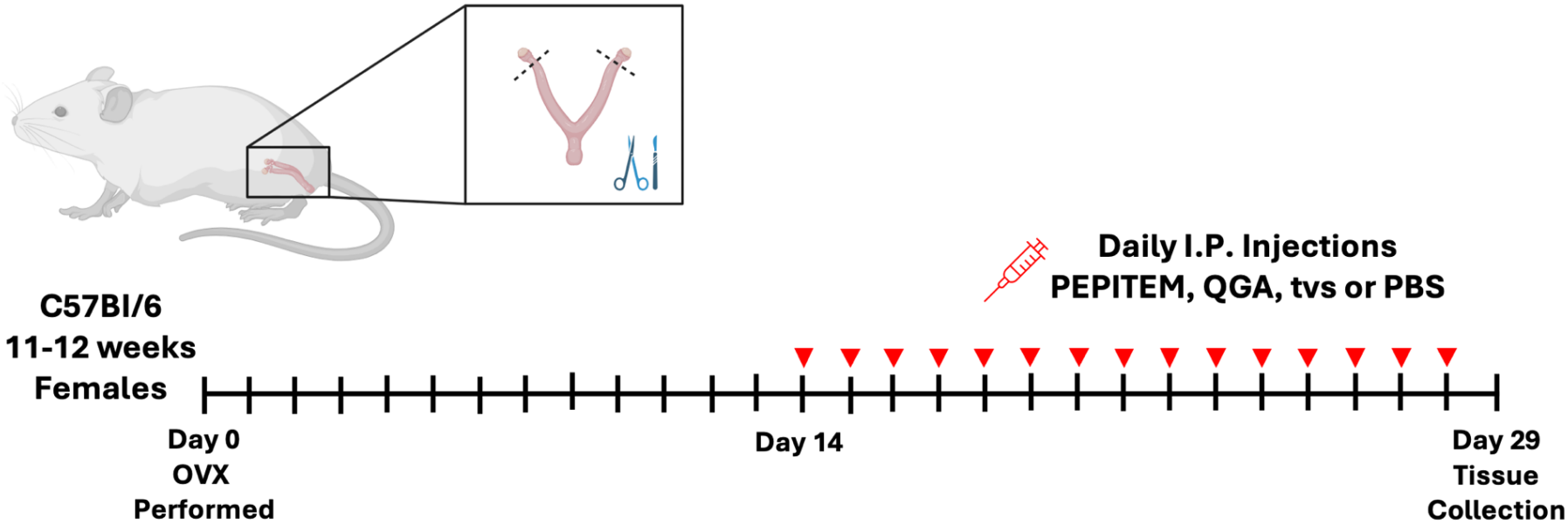


Figure 5.17 Model to study the effects of PEPITEM memetics on ovariectomized bone. Wild-type, female mice underwent an ovariectomy (OVX) on day 0 to initiate oestrogen dependent bone loss. 2-weeks post ovariectomy mice were given daily 300 µl i.p. injection containing vehicle control (PBS), or 645.8 µM PEPITEM, QGA or *tvs* for 14 days. On day 29 mice were culled, and tissue was collected for analysis.

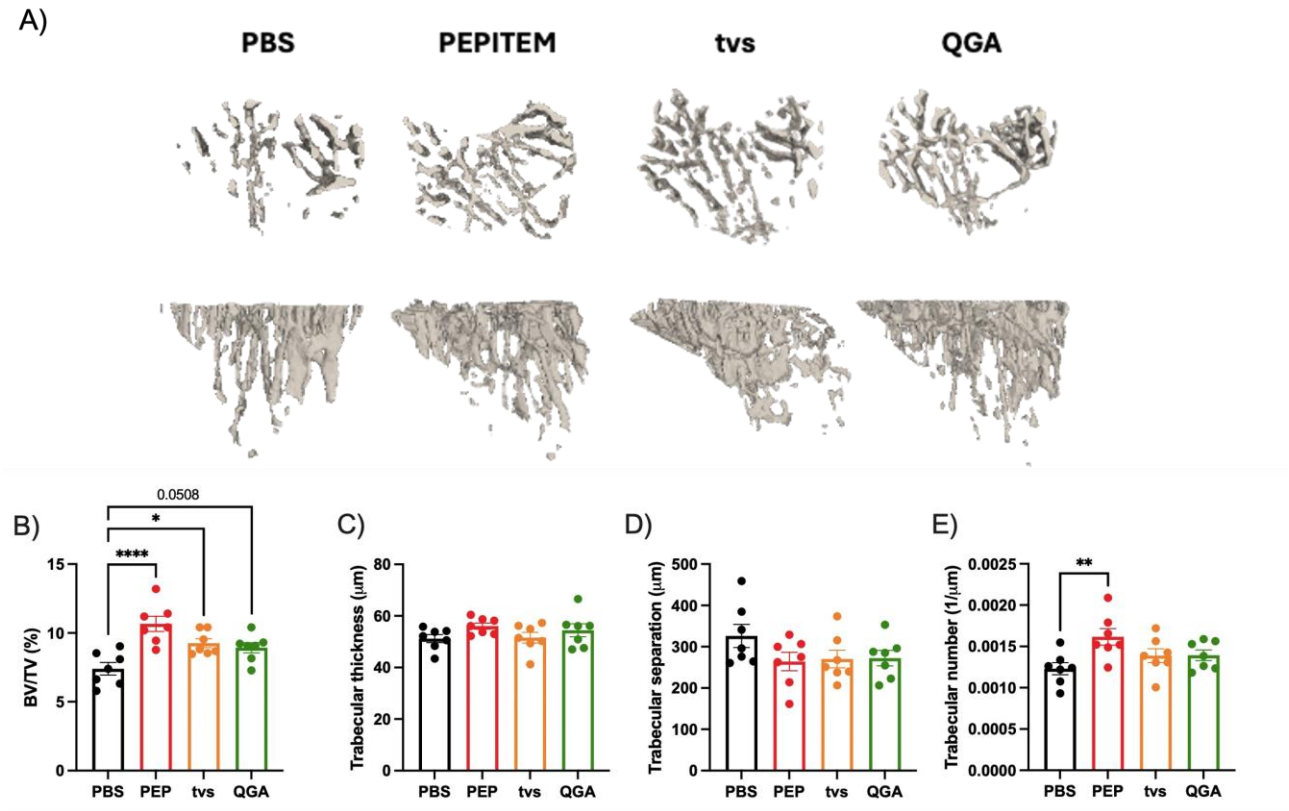


Figure 5.18 **PEPITEM and peptide memetics partly restore trabecular bone parameters by μ-CT in female mice following ovariectomy induced bone loss.** Female wild type mice underwent an ovariectomy (OVX) on day 0 to initiate oestrogen dependent bone loss. 2-weeks post ovariectomy mice were given daily 300 μl i.p. injection containing vehicle control (PBS) (black = 7), 645.8 μM PEPITEM (red = 7), QGA (green = 7) or *tvs* (orange = 7) for 14 days. Tibiae scanned by μ-CT and regions of interest were drawn around trabecular bone in the metaphysis to analyse trabecular parameters. (A) Representative images of transverse and coronal plane μ-CT 3D reconstructions from PBS, PEPITEM, *tvs* or QGA-treated mice. (B-E) trabecular bone was quantified and analysed for (B) trabecular bone volume (BV/TV, %), (C) trabecular thickness (μm), (D) trabecular separation (μm) (E) trabecular number (1/μm). One way ANOVA showed significant effects of treatments for (B) $P<0.01$, (D) $P<0.05$ and (E) $P<0.05$. Data are mean ± SEM for n = 7 mice per treatment group. * = $P < 0.05$ and **** = $P < 0.0001$ by Dunnett's multiple comparison.

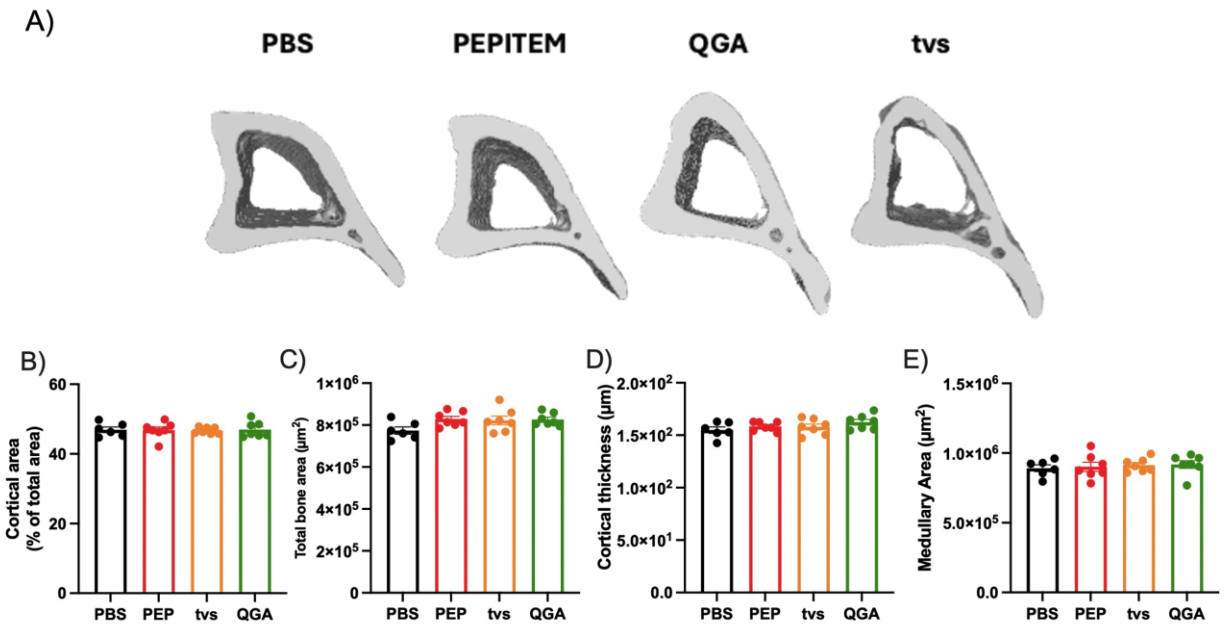


Figure 5.19 **Female wild type mice underwent an ovariectomy (OVX) on day 0 to initiate oestrogen dependent bone loss**. 2-weeks post ovariectomy mice were given daily 300 µl i.p. injection containing vehicle control (PBS) (black = 7), 645.8 µM of PEPITEM (red = 7), QGA (green = 7) or *tvs* (orange = 7) for 14 days. Tibiae scanned by µ-CT and regions of interest were drawn around cortical bone in the epiphysis to analyse cortical parameters. (A) Representative images of coronal plane µ-CT 3D reconstructions from PBS, PEPITEM, QGA or *tvs*-treated mice. (B-E) Cortical bone was analysed for (B) cortical area (%), (C) total bone area (μm^2) (D) Cross sectional thickness (µm), and (E) Medullary area (μm^2). Data are mean ± SEM for n = 7 mice per treatment group.

To examine the histomorphology changes caused by PEPITEM, QGA and *tvs* following ovariectomy we looked at osteoblast number presented as a percentage bone osteoblast coverage (Ob.S/BS) and osteoid deposition presented as percentage of osteoid compared to trabecular bone surface area (OB/OS).

Osteoid was used to measure increases in matrix production in response to treatment. Here we show that PEPITEM can significantly increase osteoid production (Figure 5.20, A and B), however we saw no change in osteoid production in either QGA or *tvs* (Figure 5.20, A).

H&E staining was used to assess osteoblast number (Ob.S/BS) as a percentage of bone surface coverage. Here we saw significant difference in osteoblast number following PEPITEM treatment compared to PBS control (Figure 5.21, A). As no effects of PEPITEM on proliferation were seen, this may suggest an anti-apoptotic role of PEPITEM within this model. Memetics did not impact osteoblast number *in vivo* (Figure 5.21, A).

Changes in bone resorption were investigated through analysis of the number TRAP positive osteoclasts. Here we also detected a significant reduction in osteoclast number following both PEPITEM and memetic treatments (Figure 5.22).

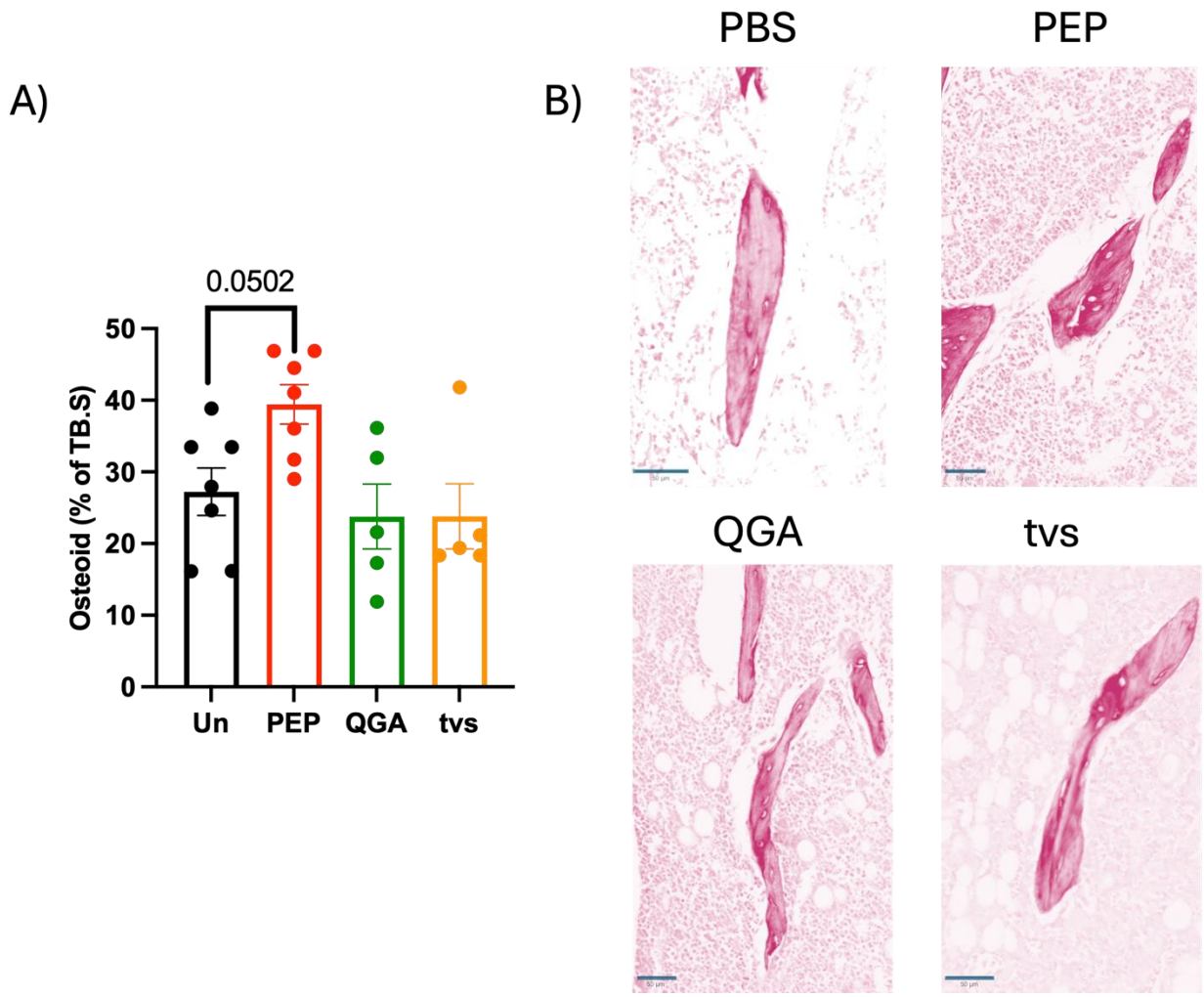


Figure 5.20 **Non-PEGylated PEPITEM increased osteoblast production in OVX female mice**. Female wild-type mice underwent an ovariectomy (OVX) on day 0 to initiate oestrogen dependent bone loss. 2-weeks post ovariectomy mice were given daily 300 µl i.p. injection containing vehicle control (PBS) (black = 7), 645.8 µM of PEPITEM (red = 7), QGA (green = 7) or *tvs* (orange = 7) for 14 days. Tibiae were decalcified, paraffin embedded, sectioned and stained for osteoid (Sirius red) (A) Levels of osteoid were measured as % of trabecular surface (TB.S). (B) Representative images of Sirius red staining from PBS or PEPITEM treated mice. Scale bar, 50 µm. ANOVA shows significant effect of treatment on (A) $P < 0.05$. Data are mean ± SEM for n = 7 mice per treatment group.

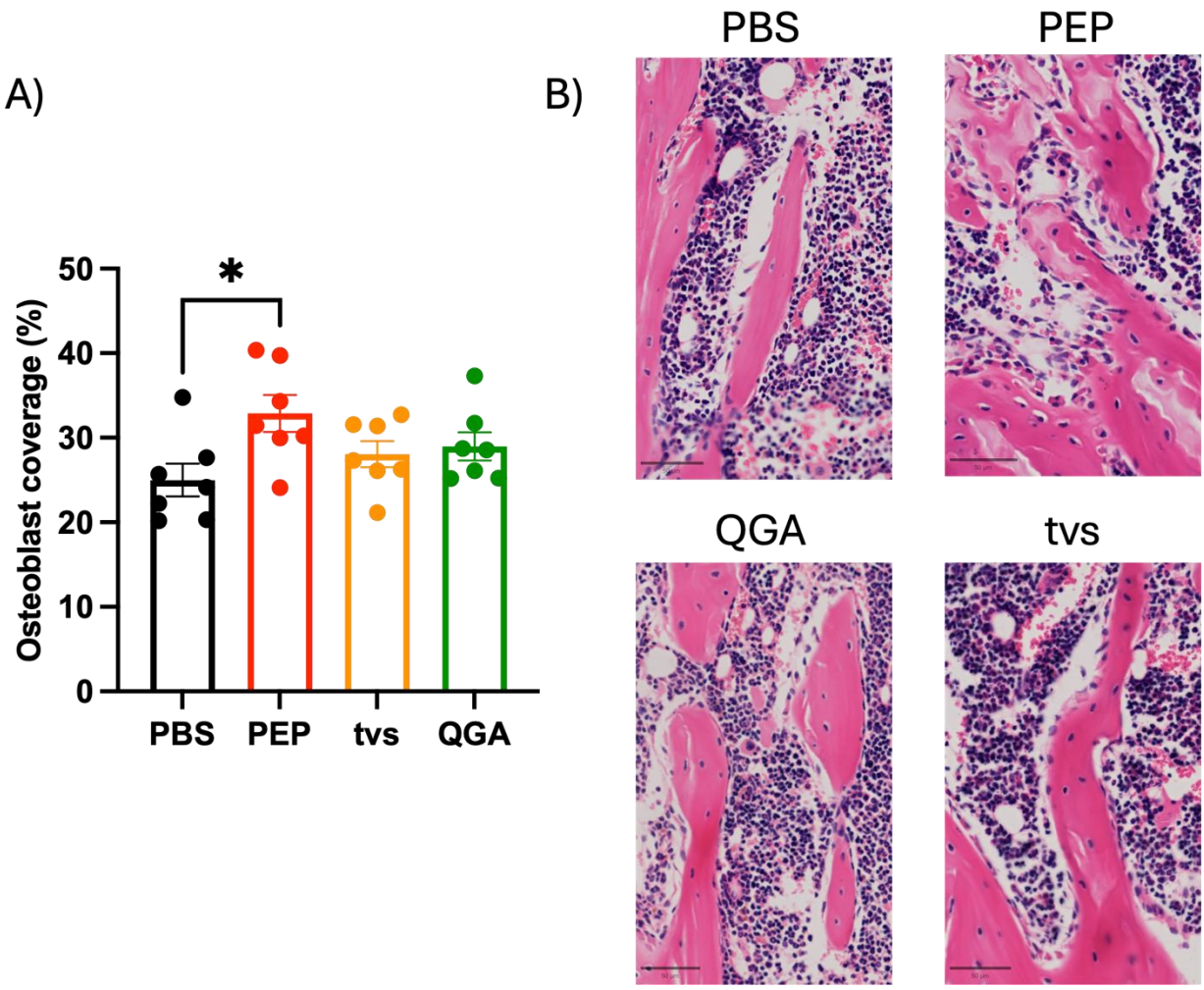


Figure 5.21 **PEPITEM increases osteoblast number in OVX model of osteoporosis.** Female wild type mice underwent an ovariectomy (OVX) on day 0 to initiate oestrogen dependent bone loss. 2-weeks post ovariectomy mice were given daily 300 µl i.p. injection containing vehicle control (PBS) (black = 7), 645.8 µM of PEPITEM (red = 7), QGA (green = 7) or *tvs* (orange = 7) for 14 days. Tibiae were decalcified, paraffin embedded, sectioned and stained for H&E (A) Osteoblasts were quantified and measures as percentage of the total bone surface area, OB.S/BS. (B) Representative image of H&E-stained tibia. Scale bar, 50 µm. ANOVA shows significant effect of treatment on (A) $P < 0.05$. Data are mean ± SEM for n=5 mice per treatment group. * = $P < 0.05$ by Dunnett's multiple comparison.

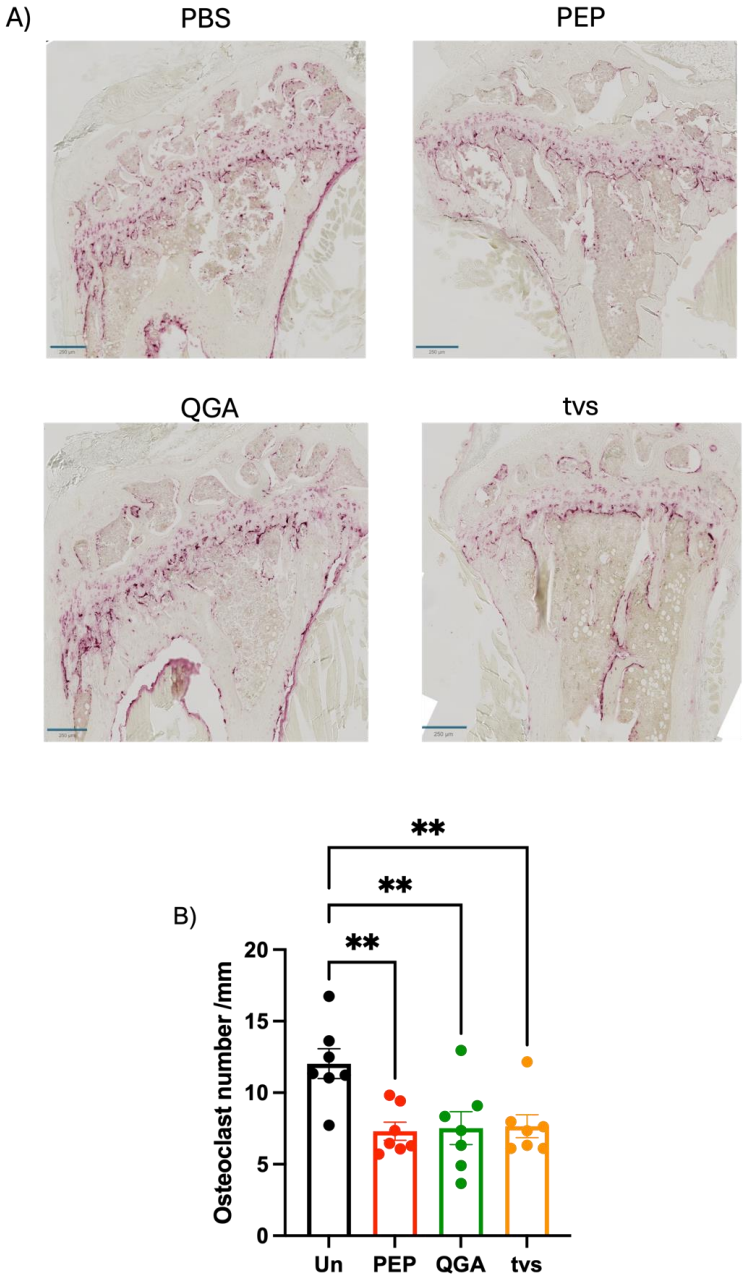


Figure 5.22 **PEPITEM memetic treatments partially reduce osteoclast number in female OVX mice.** Female wild type mice underwent an ovariectomy (OVX) on day 0 to initiate oestrogen dependent bone loss. 2-weeks post ovariectomy mice were given daily 300 µl i.p. injection containing vehicle control (PBS) (black = 7), 645.8 µM of PEPITEM (red = 7), QGA (green = 7) or *tvs* (orange = 7) for 14 days. Tibiae were decalcified, paraffin embedded, sectioned and stained for TRAP. (A) Representative images of TRAP staining from PBS, PEPITEM, OQA or *tvs* treated mice. (B) the number of TRAP positive cells were measured as osteoclast number /mm^2 surface of trabecular bone. Scale bar = 250 µm. Data are mean ± SEM for n=7 mice. ** = P < 0.01 by Dunnett's multiple comparison.

5.2 Discussion

Although PEPITEM shows promise as a therapeutic agent in the treatment of bone loss, its pharmacokinetic properties mean that daily injections are required. In this chapter we identify the actions of two novel PEPITEM memetics, QGA and *tvs*. The peptides are able to mimic or partially mimic PEPITEM responses, with a smaller amino acid sequence, therefore reducing the risk of enzymatic cleavage. Additionally, *tvs* which is based on the SVT trimer, is formed from D-isomer amino acids, which are less readily cleaved than natural L-isomer amino acids[634]. Therefore, the *tvs* peptide should be less readily cleared compared to the naturally occurring SVT peptide, prolonging its therapeutic action.

Both peptides were found to have similar effects on osteoblast activity, increasing ALP activity and collagen production *in vitro* and during homeostasis increasing trabecular bone formation and osteoid production *in vivo* without effecting overall osteoblast number. Using the OVX model both peptides were able to significantly increase BV/TV but failed to increase other trabecular parameters such as trabecular number. This was perhaps due to the experiment being underpowered, as power calculations were performed using previous BV/TV differences and not for the other parameters measured. Interestingly, within the OVX model we saw a significant increase in the number of osteoblasts in response to PEPITEM treatment. Previously osteoblast number within the OVX model was not examined[197], but we have reported no change in osteoblast proliferation *in vitro* and *in vivo* during homeostasis[197]. As oestrogen is an anti-apoptotic molecule for osteoblasts there is usually a significant decrease in osteoblast number in the OVX model[637], which can be seen when comparing the coverage of osteoblasts in the female homeostatic model to the OVX (58±2.2vs25±1.9,%). Therefore, PEPITEM may be acting to prevent osteoblast apoptosis in this model.

In vitro these peptides appeared to have a reduced effect on osteoclast formation with QGA failing to increase OPG secretion from osteoblasts. Comparatively *in vivo* both peptides were shown to partially decrease osteoclast number under homeostatic conditions and significantly decrease osteoclast number following ovariectomy. These data suggest that these peptide memetics may be acting to reduce osteoclast formation through an alternative mechanism.

5.2.1 PEPITEM contains bioactive regions

Here we show that altering the amino acid structure of PEPITEM can alter the efficacy of the peptide specifically its role in OPG secretion. Splitting the peptide in two, SVTEQGA and LSNEER, demonstrated that each end of the peptide has differing functions with SVTEQGA altering ALP activity, whilst LSNEER increased OPG secretion (at least *in vitro*). Alanine substitutions to amino acids on both the N- and C-terminal end of PEPITEM did not affect ALP responses but did impact OPG secretion, suggesting that specific amino acids within the PEPITEM sequence are required for changes in OPG secretion. Previous work has reported multiple cleavage sites within the PEPITEM sequence, which might be required to release the LSNEER portion of the peptide[193,331]. Two software packages (PROSPER and PROCLEAVE) predicted two cleavage sites within the PEPITEM sequence at residue 4 and 9, by glutamyl peptidase 1 (GGT1) and cathepsin G (CTSG) respectively[193,331]. Analysis of RNAseq data sets acquired in this thesis and previously in our lab, show that GGT1 but not CTSG is genetically expressed within isolated C.Obs, despite previous studies reporting that GGT1 is not expressed in osteoblasts, osteoclasts or chondrocytes[638]. The presence of GGT1

within our *in vitro* experiments may suggest that exogenously added PEPITEM may be cleaved at the 4th amino acid into two fragments SVT and QGAELSNEER[193,331], allowing for two independent actions of PEPITEM and indicating the reduced function of PEPITEM when this amino acid is altered.

Alternatively, the presence of two alternative actions of PEPITEM sub-sequences may indicate more than one mechanism of action of PEPITEM. In previous chapters we confirm that PEPITEM is acting at least partially though NCAM-1, with NCAM-1 antagonism reducing PEPITEM function ALP activity and OPG secretion. However as previously discussed there were multiple PEPITEM binding partners detected including the cell surface EH domain-containing protein 2 (EHD2), which was the other cell surface molecule detected [639], as well as other intercellular proteins such as Catenin delta-1 (CTNND1) and Nucleoredoxin (NXN). EHD2, has been implicated in multiple cellular processes[639], however very few studies have investigated the protein for its role in osteoblast function, with only one study to our knowledge implicating EHD2 in osteoblast function[640]. In this study EHD2 was identified on extracellular vesicles of mineralising human osteoblasts suggesting a role in cell-to-cell signalling[640], however no studies indicate EHD2 as a mediator of osteoblast maturation. Therefore, future work is required to look at the function of EHD2 in osteoblasts, investigating its effects on osteoblast maturation in order to understand if and how this protein may be involved in PEPITEM signalling.

In this thesis we did not follow up the PEPITEM binding partners which were found intracellularly because we have no data to suggest PEPITEM is able to cross the cell membrane. However, some of the intracellular binding partners showed higher binding than that seen with NCAM-1 the highest being CTNND1. AlphaFold predicts PEPITEM can bind to

the central portion of the armadillo domain within CTNND1 predominantly through amino acids towards the C-terminal of the peptide. The armadillo domain has previously been described to bind to and stabilise E-Cadherin and N-Cadherin[641]. N-Cadherin is important in osteogenesis and over expression of N-cadherin decreases osteoblast maturation through inhibition of WNT/PI3K/MAPK signalling[491,497,642,643]. PEPITEM binding may prevent the negative regulatory function of CTNND1, therefore increasing β-catenin signalling and WNT signalling. Based on these data we hypothesize that PEPITEM activation of β-catenin through binding to CTNND1. Therefore, as AlphaFold predictions of LSNEER region binding to CTNND1 β-catenin would not be upregulated following *tvs* or QGA treatment. However, before looking into these interactions our group must first identify whether PEPITEM and its related memetics can enter the cell. This can be done using fluorescently labelled peptides allowing for intracellular tracing.

5.2.2 PEGylation increases PEPITEM bioactivity

One of the overarching concerns with the use of peptide therapeutics is their short half-life, resulting in peptide therapies often requiring daily injection as seen in therapeutics like insulin[644] and PTH[645]. This has led to the development of new strategies to increase half-life of peptide therapeutics in order to reduce frequency of treatment, with the hope of enhancing patient compliance.

One broadly recognized technology used to extend therapeutic half-life is PEGylation[646], the addition of repeated ethylene oxide units (PEG), to the molecule or peptide of interest[647]. The addition of this highly hydrophilic and flexible chain was initially developed

to shield proteins from detection of the immune system, reducing the generation of neutralising antibodies[647]. However, it was since found to have the additional benefit of extending the circulating half-life of proteins[332]. Due to this, multiple therapies have since been modified to include various PEGylations to increase half-life, such as filgrastim (Neupogen)[648,649]. Used in the treatment of febrile neutropenia a common complication of chemotherapy[648,649], filgrastim is a granulocyte colony-stimulating factor that requires daily treatment during each chemotherapy cycle. However, has since been PEGylated to form Pegfilgrastim (Neulasta)[650]. Following PEGylation, the half-life of filgrastim was increased from 3.5hr to up to 80hr[651]. Pegfilgrastim now only requires one treatment per chemotherapy cycle compared to daily dosing required for its non-PEGylated predassessor[652]. This and other PEGylated therapies[646] show the therapeutic benefits of PEGylation.

Previously we have used a PEGylated form of PEPITEM[197,329,331,653], where a 352-PEG repeat was attached to the C-terminal of the PEPITEM sequence[331]. As PEGylation appeared to have no effects on PEPITEM function *in vitro*[331], the PEGylated peptide has been used in all *in vivo* experiments involving PEPITEM treatment since the first recorded PEPITEM publication. However, no one has compared the two peptides in the same model to observe the effects of the PEGylation on function, including on PEPITEMs role in bone remodelling. In this chapter we used non-PEGylated PEPITEM as we required comparison to our non-PEGylated memetics. This allowed for comparison between previous PEGylated PEPITEM results. In the homeostatic model the largest difference between PEGylated versus non-PEGylated effects was the lack of change in trabecular thickness seen following the non-PEGylated treatment, compared to after the PEGylated treatment where we saw an 8% increase in trabecular thickness compared to control[197]. Although there was no significant

change in trabecular thickness, the changes observed were comparable to those seen in response to PEGylated PEPITEM (PEGvsNon-PEG), BV/TV (29.8vs25.5%), trabecular number (20.2vs19.3%) and trabecular separation (8.3vs11.1%). In both treatments we saw no changes to cortical parameters. Additionally decrease in osteoclast numbers are also comparable (38.8vs41.2%).

Overall, these data suggest that PEGylated PEPITEM may have higher therapeutic capacity compared to non-PEGylated PEPITEM, with the additional effects to trabecular thickness. However, regarding cost effectiveness, PEGylation increases the cost peptide production therefore more detailed studies would be required determine the benefits of PEGylation from an economic standpoint.

5.2.3 PEPITEM and peptide memetics alter trabecular bone patterning

In this chapter we show an increase in trabecular extension into the bone diaphysis in response to PEPITEM treatment, whereas in typical murine long bone formation the trabecular bone is predominantly isolated to the metaphysis[654]. Few studies have reported this increased elongation of the trabecular therefore the exact cause of this elongation is unknown. There are potentially two explanations based on the current literature; (1) PEPITEM is acting on osteocytes to alter bone formation, (2) PEPITEM is acting on endothelial cells to alter vessel formation and angiotropism.

As described in previous chapters PEPITEM acts through altered β-catenin signalling, which has previously been shown to be a key regulator of early osteoblast differentiation[520,583,655,656]. However, others have also shown the importance of β-catenin in

mature osteoblasts/osteocytes[466,584,586,657]. Over-expression of β-catenin in osteocytes, led to increased trabecular bone formation and extension of trabecular bone within the femur into the diaphysis[466]. The level of trabecular bone was comparatively much higher in this model due to prolonged β-catenin activation, however β-catenin mediated osteocyte activity may result in the extension of trabecular bone into the diaphysis [466]. Previously our group has focused on the effect of PEPITEM in osteoblast and osteoclasts, primarily due to difficulty in the culture of osteocytes *in vitro*. In this thesis however we have used the SSBM, which holds the capability of culturing osteocyte like cells, characterised by the expression of podoplanin and dentin matrix acidic phosphoprotein 1 (DMP1)[378],these cells were detected after 8 and 12 weeks of culture within the SSBM constructs. PEPITEM and memetic treatment of constructs from 4 weeks increased osteoblast matrix production and mineralisation, as well as increasing OPG secretion. However, this effect was lost in the 12-week constructs. These data suggest that PEPITEM is unable to act on more mature osteoblast/osteocytes, or that PEPITEM function within osteocytes differs to the outcome measures used in this study. To understand this further we need to look at outcome measures related to osteocyte function, such as sclerostin secretion and the interconnectivity of the osteocyte network within the bone following PEPITEM treatment *in vivo*, should be investigated.

The second hypothesis is that the elongation of trabecular bone is caused by changes in bone vasculature. PEPITEM has previously been described to act on endothelial cells via CDH15, therefore PEPITEM may have additional functions within the bone through potential direct or indirect actions on blood vessels. The cardiovascular network serves multiple services to all organs in the body, providing vital nutrients and oxygen, as well as eliminating waste products such as CO_2[658,659]. The bone vasculature is vast and complicated with the

skeletal system receiving 10-15% of total cardiac output[660–663]. Researchers have identified specialised capillaries within the bone named, type-H and type-L vessels[93], each with specific endothelial cell properties that allow for distinct functions in bone formation. Type-H vessels have been shown to play a critical role in bone formation in both development, growth and repair[664–666]. Type-H vessels have been shown to be highways for osteoprogenitors, allowing for migration to the site of bone formation[667,668], through a process termed, angiotropism[667,668]. The type-H vessels have also been shown to regulate the architectural arrangement of the trabecular bone within the metaphasis[452]. There are multiple proteins involved in osteoblast-endothelial cell interactions, including the CD248-MMRN2-CLEC14A pathway[669]. Both Clec14a, a protein expressed on type-H vessel, and CD248, a protein expressed on osteoblasts, have been shown to negatively regulate osteoblast mineralisation[670–672]. In Clec14a knockout mice, there is a significant increase in trabecular bone formation coupled with increased trabecular elongationn[670,671], similar to that seen with PEPITEM treatment. Interestingly, the QGA trimer sequence is present in the MMRN2 protein, therefore interactions involving this sequence may be disrupted or mimicked in the presence of PEPITEM of the QGA trimer. The QGA sequence (87-89) does not fall in the know binding regions for CLEC14a (495-678) and CD248 (133-486)[669] but there may be other proteins able to interact via this region. Further investigation is required into how QGA may be involved in this interaction and whether PEPITEM is able to alter angiogenesis.

5.2.4 Do peptide memetics mimic PEPITEM function during homeostasis?

The delivery of exogenous PEPITEM to wild-type homeostatic mice provides insight into the potential actions of PEPITEM within bone remodelling in the absence of disease phenotypes such as osteoporosis. The data presented in this chapter and previous chapters demonstrates that under homeostatic conditions PEPITEM can increase bone formation and inhibit bone resorption through increase osteoblast activity and reducing osteoclast number[197]. Although we are currently unable to assess whether PEPITEM naturally is cleaved into its smaller memetics, here we assessed their homeostatic function to measure whether their action mimics that of PEPITEM.

Analysis of μCT parameters of both trabecular and cortical bone show no effect of either memetic, however when the tissues were examined at the cellular level we did observe effects of the tripeptides. Memetic treatments promoted bone formation, indicated by increased levels of osteoid, and inhibit bone resorption, indicated by reduced numbers of osteoclasts. The effects of the memetics on osteoid and osteoclast number are borderline significant likely due to underpowering of the study, as the power calculation was based on PEGylated-PEPITEM BV/TV effects. Using the differences seen here, a second power calculation was performed which shows that an additional n=4 per group would be required to reach statistical significance for osteoid production.

Contrary to our original hypothesis, we saw a reduction osteoclast number following QGA treatment despite observing no impact of QGA on OPG secretion *in vitro*, suggesting the involvement of an additional mediating factor. There are multiple osteoblast secreted proteins that decrease osteoclast function, such as WNT16[673]. Additionally, as we did not perform co-culture experiments as part of this piece of work, the effects of QGA on

osteoclasts may also be through altered direct osteoblast-osteoclast, such as FASL signalling[674]. These data suggest there may be additional signalling pathways involved in PEPTEM signalling allowing for QGA to alter osteoclast formation, without altering OPG production and further investigation is required to decipher these pathways. One hypothesis is that PEPITEM and memetics directly act on osteoclast precursors. Our group has previously shown that PEPITEM treatment alters the trafficking and polarisation of macrophages in models of ageing and arthritis, showing that PEPITEM is able to alter macrophage function[196,329,653]. Although PEPITEM does not directly act on macrophages to increase osteoclastogenesis[197], PEPITEM may be acting to alter macrophage trafficking and therefore altering the number of osteoclast precursors available. Additionally, PEPITEM peptide mimetics have been shown to decrease macrophage secretion of inflammatory cytokines, IL-6 and TNF-a (unpublished data), thus the peptides may be promoting an anti-inflammatory M2-like phenotype. M2-like macrophages have been shown to secrete osteogenic factors such as BMP-2[675] and TGF-β[676], therefore promoting osteoblast differentiation, whereas M1-like macrophages secret inducers of osteoclastogenesis such as IL-6 and IL-1β[677,678]. In addition to the secretion of varying pro- and anti-osteoclastogenic factors, macrophage polarisation has been linked to osteogenic potential, with macrophages which are primed with TNF-α have increased osteoclastogenic capacity compared to non-primed cells[679]. Therefore, it is possible that altered osteoclast numbers in response to the tripeptides in these experiments may be due to direct actions on macrophage biology, not solely due to osteoblast-osteoclast cross talk.

5.2.5 Peptide memetics compared to PEPITEM and current therapeutic for osteoporosis

Peptide memetics compared to PEPITEM and current therapeutic to look at the effect of PEPITEM memetics in pathological conditions we used the OVX model of osteoporosis. In this model we saw PEPITEM and peptide memetics were able to reduce bone loss following OVX, indicated by increased trabecular μCT parameters. In the early stages following oestrogen loss there is a significant increase in osteoclast formation and survival[680–683], due the inhibitory and pro-apoptotic action of oestrogen being lost[680]. Therefore, the increased number of osteoclasts is thought to be responsible for the initial OVX bone loss[680]. Based on this, it is likely the anti-osteoclastogenic function of QGA and *tvs* that mediates the increased BV/TV. It is at the later stages of the OVX model where reduced cortical bone can be observed. This decrease in cortical bone is caused by a reduction in osteoblast number due to increased apoptosis, mediated by the loss of the protective function of oestrogen[125,684]. Because of this, changes in cortical bone parameters are not always seen within this model[685–687], however longer study protocols (6-9 weeks post OVX) show decline in cortical bone parameters[688,689]. Therefore, to assess whether PEPITEM or tripeptides are able to prevent cortical bone loss a longer resting period between ovariectomy and treatment start is required. Alternatively other models of osteoporosis such as an aged mouse model[690], where reductions in cortical bone are more commonly described should be used.

In order to understand how PEPITEM and tripeptide treatment compares to current therapeutics we looked at similarly designed OVX studies using at current treatments. Firstly, comparing PEPITEM and peptide memetics to commonly used osteoporosis treatments, bisphosphonates and PTH. Before comparing studies, it is important to note differences in study design with many studies having increased differing treatment timeframes (1week-

12months) and additional differences upon start of treatment. Here we give PEPITEM post disease onset (2-weeks post OVX) whereas other studies will give prophylactic treatment or later in the disease progression.

Studies looking at bisphosphonates in the rodent models of osteoporosis show a significant effect on BV/TV in both prophylactic treatment[691] and treatment following disease onset[692]. As expected, these studies show a reduction in the number of osteoclast present after 8-12 weeks of treatment[691–693]. Comparatively PEPITEM was able to decrease osteoclasts following only 2-weeks treatment, whilst increasing osteoid suggesting there is a reduction in bone resorption coupled with an increase in formation. The peptide memetics unexpectedly only appear to decrease osteoclast number in both homeostatic and OVX model, but only increasing osteoid production under homeostatic conditions, suggesting that in the presence of bone loss and impaired osteoblast function, the memetic treatments lack the ability to affect both osteoblasts and osteoclasts. Unlike, PEPITEM or the memetics, studies have shown that bisphosphonate treatment was also able to increase cortical bone in OVX model after 8-weeks treatment[691], however here we saw no difference in cortical bone parameters following OVX in the presence or absence for therapeutic intervention. Suggesting in order to see how PEPITEM treatment compares to bisphosphonate therapies, we must use longer models of OVX and longer treatment regimes.

PTH treatment is often carried out over several weeks[687,689,694,695], however one study looking at a timeline of PTH treatment shows that effects on BV/TV were not statistically increased at 2 weeks, showing an increase of 12% respectively[688] comparatively to the 44% increase seen following PEPITEM or 20%, 25% increase following QGA or *tvs*. The effects of PTH were more prominent following 4-weeks of treatment, where treatment resulted in a

return to baseline[688]. In our study we see a return to 2-week baseline BV/TV values following treatments, however a prolonged study would be required to observe whether PEPITEM or peptide memetics were able to completely restore the bone lost following OVX. Interestingly, PTH was able to result in an increase in cortical bone (Ct.Ar and Ct.Th) following 2-weeks of treatment[688] despite no effect of OVX on the cortical bone. Differences between Roberts et al study protocol may account for differences in cortical bone changes. Both studies used C57BL/6 mice but at different ages underwent OVX surgery at 14-weeks compared to in our studies where mice were aged 11-12 weeks[688]. Additionally, Roberts and colleagues used *in vivo* imaging allowing for paired changes in bone volume whereas we used ex vivo analysis preventing us from observing changes in cortical parameters throughout treatment[688]. Other studies have also show an effect of PTH on cortical bone, but after longer treatment periods (8-weeks)[687]. We do not see an effect of either PEPITEM or the memetics on cortical bone parameters in this study, however we have previously seen cortical changes following longer treatment in chapter 3. PTH has also been shown positively regulate bone resorption increased osteocyte secretion of RANKL[696]. Prolonged PTH treatment can result in a net bone loss therefore required treatment breaks to prevent catabolic action[697]. Advantageously, alongside increasing osteoblast formation PEPITEM also causes a reduction in osteoclast formation, therefore is unlikely to cause a reduction in bone formation following prolonged use.

As we describe PEPITEM to have a dual response on both bone resorption and formation, we must compare it to one of the more novel osteoporosis treatments, anti-sclerostin antibodies, which also show a dual function. The first OVX study using an anti-sclerostin antibody was performed in rats, where treatments began 13 months after surgery

and were treated twice a week by subcutaneous injection. This study demonstrated that anti-sclerostin treatments can increase BV/TV by 57% compared to PBS controls, returning to SHAM-OVX levels[313]. Treatment was shown to increase osteoblast number by 223% compared to control, which coupled with a 227% increase in osteoid surface area[313]. Osteoclast number was also reduced by 77%, showing the dual function of anti-sclerostin treatment[313]. Due to the differences in study design within this study and other anti-sclerostin OVX studies[313,698–701] it is difficult to compare PEPITEM or tripeptide treatment. However, comparatively both anti-sclerostin and our peptides increase the same bone parameters influencing both osteoblasts and osteoclasts. It is to be noted that sclerostin expression is increased in the absence of sex steroid hormones[702–705], therefore it should be questioned whether anti-sclerostin is as effective in bone loss diseases with normal sex steroid activity. In wild type mice[312,706–708], anti-sclerostin is effective at increasing bone formation, however to a much lower degree than described in OVX models. One study showed a 25% increase in BV/TV in wild type mice after 5 weeks of anti-sclerostin treatment[706], which is comparable to 2-weeks of homeostatic PEPITEM (29.9%), *tvs* (23.36%) and QGA (23.27%). Suggesting that anti-sclerostin therapies are most effective in post-menopausal osteoporosis, but not for other causes of bone loss where sex hormones are present.

As mentioned, one of the main therapeutic benefits of PEPITEM and the memetics, is the dual effects treatment has increasing bone formation and reducing bone resorption, allowing for inhibition of the detrimental overactivation of osteoclasts whilst replacing previously lost bone. However, in relation to post-menopausal osteoporosis, PEPITEM and its memetics may have an additional benefit through its additional action on T-cell trafficking. Evidence suggests that T-cells play a large role in oestrogen-deficiency induced bone loss,

with studies showing that OVX does not cause trabecular or cortical bone loss in mice lacking functional T-cells[709–712]. The mechanism behind this is hypothesized to be due to increased TNF production from T-cells and increase thalamic T-cell production[593,711,713–717]. Thereby, PEPITEM and its memetics may also reduce OVX indicted bone loss through reduced T-cell trafficking into the bone tissue.

5.2.6 Conclusion

In conclusion, while PEPITEM shows promise as a treatment for bone loss, its need for daily injections limits its practicality. This chapter presents two novel PEPITEM memetics, QGA and *tvs*, which have previously not been explored within bone, are able to mimic PEPITEM's effects with smaller amino acid sequences, reducing enzymatic cleavage. Both peptides enhanced osteoblast activity, increasing ALP and collagen production *in vitro*, and promoted trabecular bone formation *in vivo* without altering overall osteoblast numbers. In the OVX model, they significantly increased BV/TV but did not affect other parameters, likely due to underpowering. Regarding osteoclasts, the peptides showed reduced effects on osteoclast formation *in vitro*, but *in vivo*, they decreased osteoclast numbers under homeostasis and significantly after ovariectomy. This suggests that QGA and *tvs* may reduce osteoclast formation through alternative mechanisms. Overall, these findings indicate that QGA and *tvs* are promising candidates for further research in treating bone loss.

6 General Discussion

6.1 Summary of Findings

The work presented in this thesis further expanded the current understanding of PEPITEMs endogenous function in bone and explored the potential therapeutic value of the peptide in musculoskeletal disorders. The key findings have been listed in context to the aims stated at the start of this project:

Aim I. Identify the mechanism of action of PEPITEM on osteoblasts

- Despite PEPITEM previously being shown to act through Cdh15 to increase Sphk2 activity and consequently S1P production[192], inhibition of Cdh15 was unable to prevent increases in ALP activity seen following PEPITEM treatment. Additionally, the treatment of osteoblasts with exogenous S1P did not elicit the same response as see with PEPITEM, demonstrating that PEPITEM is not acting through autocrine production of S1P. Furthermore, inhibition of S1P production was unable to prevent PEPITEM activity, suggesting that intracellular S1P signalling was also not required for PEPITEM function.
- NCAM-1 acts as a receptor for PEPITEM on osteoblasts, through binding to the NCAM-1 extracellular fibronectin-III type domain, demonstrated by in silico analysis. Inhibition of NCAM-1 using an antagonistic antibody was able to prevent PEPITEM activity, reducing alkaline phosphatase activity and metatarsal mineralisation.
- PEPITEM treatment elicits increase β-catenin signalling with osteoblasts, resulting in increased expression of osteoblast maturation marker Col1A1, suggesting that NCAM-1 mediates PEPITEM function through canonical WNT/β-catenin signalling.

Aim II. Explore potential mediators of PEPITEMs indirect actions on osteoclast function

- Osteoblasts secrete an anti-osteoclastic molecule in response to PEPITEM, as shown through media transfer of osteoblast secretome on to osteoclast precursors .
- S1P secreted from osteoblasts regulate osteoclastogenesis but does not mediate PEPITEM function.
- Osteoblast secretion of anti-osteoclastogenic molecule OPG is increased following PEPITEM, mediating osteoblast-osteoclast talk allowing PEPITEM to have indirect actions osteoclast formation.
- NCAM-1 inhibition prevents PEPITEM mediated OPG release, demonstrating that PEPITEM can be able to act though NCAM-1 to induce OPG secretion.

Aim III. Characterise the bioactive components of the PEPITEM sequence for investigation into therapeutic benefit.

- PEPITEM contains bioactive residues important for OPG secretion but not alkaline phosphatase activity, suggesting that PEPITEM function requires specific residues to be present for binding/activity.
- Use of the tripeptides, SVT and QGA, within the PEPITEM sequence can mimic PEPITEM function *in vitro*, through increased alkaline phosphatase activity and partial increases in OPG secretion.
- Homeostatic delivery of tripeptides memetics QGA and tvs can partially simulate PEPITEM responses *in vivo*, at a lower concentration compared to PEPITEM, increasing

osteoid production and reducing osteoclast number. However, tripeptides were unable to evoke changes in μ-CT parameters in the chosen timeframe and dosage.

- Therapeutic treatment using tripeptide memetics can moderately limit bone loss caused by OVX through reduction in osteoclast number but no apparent increase in osteoid production.

6.2 Mechanistic action of PEPITEM in Bone

Previously PEPITEM has been shown to reduce bone erosion in murine models of arthritis. The mechanism by which PEPITEM carries out this function is 2-fold, firstly PEPITEM can reduce immune infiltrate into the joint, shown through a reduction in T-cells, monocytes and neutrophils in the joint[570]. Secondly through direct actions on the bone, with PEPITEM being shown to increase bone formation and reduce bone resorption through direct actions of osteoblasts. We show that PEPITEM is acting though surface receptor NCAM-1, which has previously been linked to both intramembranous and endochondral bone formation[436,506]. Additionally, NCAM-1 has been shown to be important in MSC and osteoblast differentiation[5,6]. Previously, NCAM-14-3-3 interactions have been described for their role in axonal and dendritic differentiation in neurons[509,510], with the PEPITEM sequence within its parent protein being reported as one of six peptides being involved in the NCAM-14-3-3ζ interaction[509].

Downstream signalling of NCAM-1 has been reported to work through PI3k/Akt and WNT/β-catenin signalling[437]. The canonical WNT signalling has been shown to be important in the differentiation of osteoblasts, with osteoblasts showing increased activity in response to activators of this pathway such as LiCl[526,718]. 14-3-3ζ has also been shown to directly alter β-

catenin signalling, through direct binding to β-catenin and sequestering of β-catenin degradation enzyme GSK-3β[550–553]. Although the region of 14-3-3 involved in these interactions is unclear, these data show the importance of 14-3-3 proteins in β-catenin signalling. In this thesis we focused on exploring β-catenin signalling, however several of the genes identified in the RNAseq data set involve Akt signalling[445,447], which has also been shown to effect osteoblast maturation and have been found to be involved in NCAM-1 signalling[437]. Akt has previously been reported to phosphorylate β-catenin allowing for 14-3-3ζ interactions[550]. These data may indicate that there is an involvement of both Akt and β-catenin in PEPITEM function and signalling, however further investigation is required.

Activation of β-catenin signalling has also been shown to increase OPG secretion from osteoblasts, allowing for osteoblast-osteoclast communication and control of osteoclastogenesis[719,720]. Increase OPG secretions from osteoblasts treated with PEPITEM therefore explains reduced osteoclast numbers following PEPITEM treatment despite no direct effects on osteoclastogenesis. Previously studies have observed changes in RANKL signalling in response the 14-3-3 signalling[186], but to our knowledge changes in OPG secretion have not been reported. 14-3-3ζ was shown to suppress RANKL-induced signalling through direct actions on osteoclasts, where 14-3-3ζ prevented TRAF6-RANKL interactions[186]. We have previously reported that PEPITEM does not alter osteoclastogenesis therefore it is unlikely to act via the same pathways as the parent protein.

PEPITEMs dual effects on bone remodelling, lends itself as an effective therapeutic in the treatment of bone loss disorders such as osteoporosis, through increasing osteoblast activity and bone formation, whilst decreasing osteoclast activity, without completely halting necessary bone remodelling preventing formation of weakened bone as seen in long term

bisphosphonate treatment[721]. However, as we observe alterations in osteoclast number despite not observed changes in OPG secretion in vitro it opens up for the potential of other direct or indirect actions of PEPITEM on osteoclast formation which much be further explored.

6.3 Therapeutic potential of PEPITEM and Peptide memetics

In this thesis we delve deeper into the mechanism and function of the endogenous molecule, PEPITEM, to decipher its role in bone remodelling. Previously PEPITEM was shown to increase bone formation and reduce resorption, however the mechanism in which this occurred was unknown. Here we describe the PEPITEM-NCAM-1 axis, which can promote bone formation through promoting osteoblast maturation, whilst simultaneously reducing osteoclast activity through increase osteoblast secreted OPG.

The dual action of this peptide means PEPITEM can both increase bone formation and decrease bone resorption, unlike some current treatments like bisphosphonates and teriparatide.

Bisphosphonates are currently the first line of defence in the pharmacological treatment of osteoporosis[722]. The mechanism of action of these treatments is to primarily reduce bone resorption though the inhibition of osteoclast formation[242]. A reduction in osteoclast number prevents further bone loss, however due to the lack of resorption the balance of bone remodelling is lost resulting in increased risk of atypical fractures[723–725] caused by accumulation of microdamage[726]. We predict this to be less likely with PEPITEM as there is a less significant reduction in the number of osteoclasts allowing for both bone formation and resorption to continue. This hypothesis is supported by the pretence that PEPITEM is an

endogenous peptide, therefore is likely modulating bone remodelling during homeostasis without increased supplementation as we performed here.

Similarly to bisphosphonates teriparatide and other PTH related treatments have been shown to primarily effect only one side of the bone remodelling pathway, specifically increasing formation. PTH has been shown to increase bone formation through several different mechanisms, including an anti-apoptotic effect on osteoblasts[727] and increasing canonical WNT signalling through inhibition of SOST secretion in osteocytes[291,728–730]. Similarly, we show that PEPITEM may exert anti-apoptotic effects on osteoblasts shown through increase osteoblast numbers following OVX despite previously seeing no effects on proliferation *in vivo* or *in vitro*[197]. The mechanism by which PEPITEM may protect osteoblasts from apoptosis in the absence of oestrogen is so far unclear, however β-catenin signalling has been shown to reduce apoptosis of both osteoblast progenitors and differentiated osteoblasts[731]. Unlike PTH PEPITEM can also decrease osteoclast formation, allowing for the balance of bone remodelling to be tip towards formation, whereas PTH has been reported increase osteoclast number due to upregulation of RANKL[278–281,732,733]. Prolonged use of PTH has been shown to result in increased bone loss, as seen in hyperthyroidism[734], therefore PTH is recommended to be used intermittently to avoid catabolic effects[276], whereas as PEPITEM decreases osteoclast formation as well as increasing osteoblast activity it may allow for long term use without the need for treatment breaks or switching to anti-catabolic treatments.

The duality of PEPITEM therefore makes it more comparative to the use of Romosozumab, which can act on both osteoblasts to increase bone formation and inhibit osteoclast resorption, through inhibition of WNT inhibitor sclerostin[64]. The mechanism by which Romosozumab acts is similar to that of PEPITEM through increasing WNT/β-catenin

signalling to increase osteoblast activity and increased OPG secretion[314,698]. Current issues surrounding the use of Romosozumab lies in potential off target effects resulting in increased risk of cardiovascular events[324,326]. Although the prevalence of cardiovascular effects has been shown to only be higher in those with previously existing cardiovascular conditions[735], suggesting patient screening is required prior to treatment. Due to increased cardiovascular risk Romosozumab is currently only approved for the treatment of severe post-menopausal osteoporosis for 12-months, additionally after 12-month studies have shown that bone mineral density plateaus. Currently we have not identified and do not predict adverse effects with PEPITEM treatment due to its role as an endogenous peptide, however long term treatment is required to further understand any side effects. Like most monoclonal antibody therapies, Romosozumab is expensive to produce[736], comparatively peptide synthesis is relative cheap[737] allowing for mass production at a much lower cost, making treatment more economical and accessible.

As previously shown PEPITEM has a short half-life due to the nature of peptide therapeutics, therefore currently required daily treatment. PTH is used as a daily treatment suggesting that patients would be willing to opt for daily treatment[295]. However daily treatment leads to reduced patient adherence[295], therefore, we looked at the use of small memetics peptides from the PEPITEM sequence which are hypothesised to have a longer half-life due to reduced enzyme cleavage, therefore may require less frequent treatment. The peptides, QGA and tvs, partially mimic the response seen by PEPITEM, increasing ALP and/or OPG secretion *in vitro*, whilst increasing trabecular bone parameters and osteoid production *in vivo*. Additionally, both these peptides were able to decrease osteoclast number *in vivo*, despite QGA being unable to upregulate OPG secretion *in vitro*, which leads us to believe in a

secondary function of PEPITEM and related memetics at reducing osteoclast formation. We hypothesise that this may be due to direct actions on osteoclast precursors with PEPITEM and memetics being shown to alter macrophage polarisation and migration[196,329,570,653]. Alternatively, it may allude to additional alterations in osteoblast-osteoclast communication, however future experiments are required in order to understand this function further. In these experiments we did not assess the half-life of each memetic, it is assumed that these peptides will have a longer half-life based on their smaller amino acid sequence. Based on this hypothesis we can infer that the memetic treatments would have been able to have a longer period of action and therefore require fewer treatments. Meaning that although slightly less effective than the original peptide these emetics may have higher therapeutic potential. However radioactive tracer studies are required to assess whether these peptides to in fact have a longer half-life compared to PEPITEM alongside altered regime treatments such as once every week.

In addition to looking at peptide memetics of PEPITEM, the discovery of the PEPITEM pathway provides novel targets for bone loss. Previously NCAM-1 has been targeted as a treatment of neurological disorders[738], as well as some types of cancer[739]. Multiple peptides have been developed to target NCAM-1, including the peptides P2 and C3[738,740,741]. These peptides were synthesized as NCAM-1 memetics due to NCAM-1 acting as a ligand to itself[514,742]. Both have been shown to have agonistic properties on neurones to promote neurite outgrowth but have yet to be investigated for their actions in osteoblasts. However the actions of P2 peptide have been observed in BMSC, which show increased proliferation and migration, mitigated by PI3K/AKT or ERK signalling[740]. In this study they did not look at how P2 effected differentiation or effects on β-catenin signalling, therefore further experiments

comparing P2 and PEPITEM function are required. As these peptides were initially made to allow for therapeutic intervention in the brain, similarly to PEPITEM they are small with short half-life, therefore these peptides to require daily injections limiting their use in more chronic conditions such as osteoporosis.

While extending PEPITEM's half-life through smaller mimetics is promising, other methods can direct it specifically to bone tissue. One approach leverages the bone-binding properties of bisphosphonates, where PEPITEM can be linked to an inactive bisphosphonate creating a prodrug[743]. The prodrug is then able to bind to the bone surface, where PEPITEM is cleaved and released directly into the bone microenvironment. This targeted delivery reduces systemic clearance and prolongs PEPITEM availability at the treatment site.

Alternatively, recent advances in tissue engineering offer exciting new possibilities for PEPITEM delivery. Bone scaffolds are 3D matrices, which are formed of biomaterials such as collagens[744,745] and hydroxyapatite based bio-ceramics[746,747], designed to increase bone healing[748–750]. These scaffolds show promise in the delivery of drugs, including antibiotics, growth factors and anti-inflammatory drugs to the bone[748–750]. BMP-2 has previously been shown to improve fracture healing when incorporated into bone scaffolds[751]. Similarly to BMP-2, PEPITEMs structure and simple synthesis lends itself to delivery systems such as this. Additionally, as PEPITEM has both anti-inflammatory and pro-anabolic functions, the delivery via scaffold following fracture may enhance fracture healing and improve recovery time.

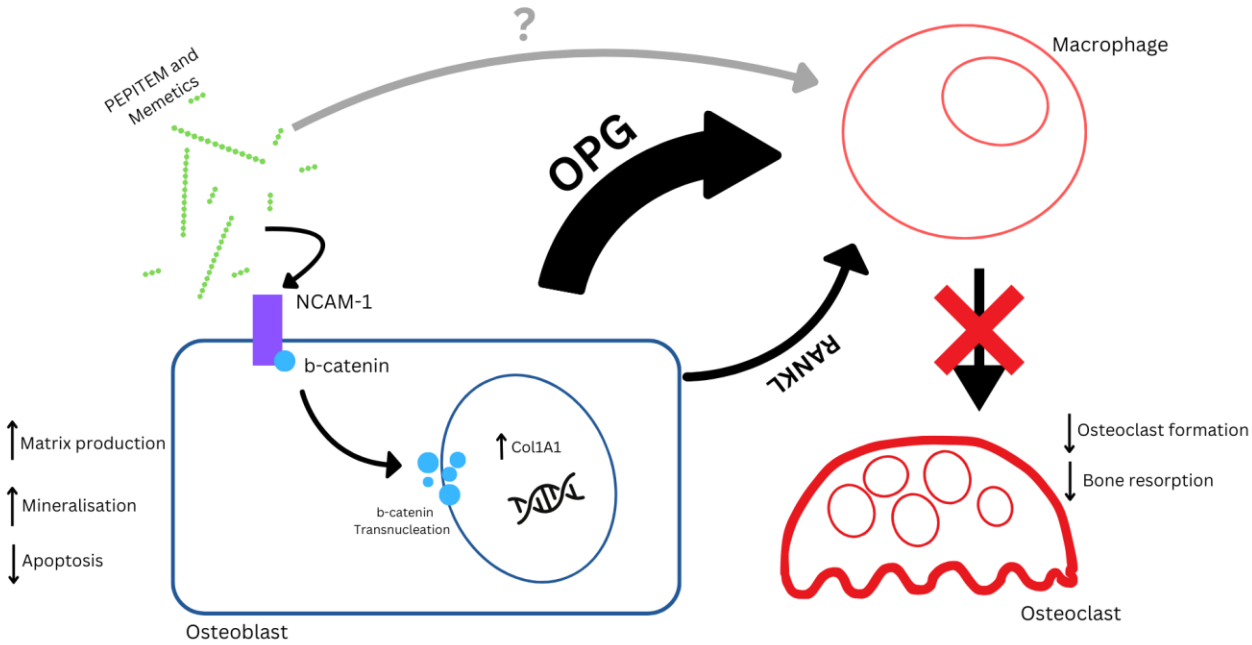


Figure 6.1 **Schematic of proposed PEPITEM signalling pathways in bone**. PEPITEM and peptide memetics were shown to increase trabecular bone volume *in vivo*, through increase osteoblast production of matrix (osteoid) and decrease the number of osteoclasts. *In vitro* PEPITEM was shown to bind to NCAM-1 activating downstream β-catenin signalling, resulting in increased osteoblast maturation (ALP activity and Col1A1 expression) and increase OPG secretion. Increased OPG secretion from osteoblasts inhibited osteoclast formation. PEPITEM memetic treatments increased osteoclast maturation (ALP) and partially increased OPG secretion *in vitro*. *In vivo* peptide memetics were able to decrease osteoclast number despite no increase in OPG secretion *in vitro*, hypothesised to be caused by PEPITEM and memetics on macrophage polarisation and differentiation capacity. Following ovariectomy PEPITEM prevented decreased osteoblast number caused by oestrogen deficiency suggesting PEPITEM leads to reduced apoptosis.

6.4 Study Limitations

The majority of this project was performed in murine samples or human cell lines (hFOb 1.19). This was primarily due to the lack of access to healthy human osteoblasts. We have previously reported the actions of PEPITEM in samples from both osteoporosis and osteoarthritis patients, showing that PEPITEM does have function within human osteoblasts, however the PEPITEM-NCAM-1 axis is yet to be confirmed in healthy human samples.

Additionally, although we were able to use 3D cell culture techniques which are replicate the *in vivo* bone environment, all cell cultures were performed in monocultures. *In vivo* bone cells exist in a complex 3D multicellular system allowing for cellular crosstalk, through the secretion of various pro-anabolic and pro-catabolic factors. These additional processes are also able to impact osteoblast development and differentiation and therefore may alter responses to PEPITEM.

Although we have functional data and in silico modelling suggesting that PEPITEM is able to bind to the NCAM-1 receptor, we were unable to confirm direct PEPITEM-NCAM-1 binding. In order to do this, we must use surface plasma resonance experiments, however due to the size of PEPITEM the signal to background noise predicted to be high therefore disrupting our ability to conclude PEPITEM-NCAM-1 binding.

Based on previous reports, we looked at β-catenin through NCAM-1, and although we do see increase β-catenin in response to PEPITEM we were unable to confirm colocalization between the two molecules, therefore we cannot exclude the potential that β-catenin signalling occurs as a result of a differing PEPITEM mechanism.

In vivo experiments are frequently used in the study of bone biology and in looking at treatment responses. However, there are significant differences in murine bone biology

comparatively to that in humans[752,753]. These differences in innate species biology, therefore, may alter PEPITEM responses in human patients. In the absence of innate biological differences between human and mouse, our *in vivo* data has some limitations. Although we explored the role of PEPITEM in homeostatic female and male mice, we only looked at the effects of PEPITEM within a female post-menopausal model of osteoporosis. Therefore, missing how PEPITEM may respond in osteoporosis with differing aetiology, such as ageing, orchiectomy and glucocorticoid induced osteoporosis. Future experiments are needed to explore whether the potential of PEPITEM as a therapeutic continues in other models of osteoporosis.

Additionally, all *in vivo* experiments were conducted in young mice (8-12 weeks). As bone changes with age[754], cellular activity and expression of proteins are altered[755]. We need to be aware that the differences seen in these mice may differ from changes within older mice when overall bone production and metabolic activity has reduced.

Here we look at PEPITEM as an endogenous peptide within the bone and observe it function during homeostasis. However, the source of PEPITEM within the bone is unclear. Osteoblasts express 14-3-3ς[756] and the cleavage enzymes[193] required for PEPITEM production[757–759] therefore may be capable of producing PEPITEM. However, in this thesis we did not look for the presence of PEPITEM in osteoblast cultures, therefore cannot conclude whether during homeostasis PEPITEM is present within bone.

We were unable to assess actions of memetics on primary human healthy or disease samples, meaning we cannot for conclude that the memetic treatments will have the same effect as PEPITEM in these samples. Therefore, future experiments are required to investigate whether the memetics have similar *in vitro* effect on primary human samples.

6.5 Future Experiments

Our observation in this thesis defines the likely mechanism of PEPITEM acting within bone in health and disease. However, there are several questions left unanswered and would require additional experiments to further our understanding of PEPITEM.

- Use of NCAM-1 knockout mice to observe whether PEPITEM response is affected by the removal of NCAM-1, in order to confirm it as the PEPITEM receptor.
- Confirm NCAM-1 signalling through β-catenin. Using NCAM-1 knockout cells to observe whether increase β-catenin activity is still present following PEPITEM treatment. Investigate co-localisation of NCAM-1 and β-catenin in osteoblasts to observe NCAM-1 ability to sequester and release β-catenin.
- Investigative studies of the NCAM-1-PEPITEM pathway and how it changes in human samples, looking at changes in age and disease groups such as osteoporosis and rheumatoid arthritis, in order to observe how this factors may affect PEPITEM function.
- Using PEPITEM in aged mouse models of osteoporosis (16-24 months[760]), as mice naturally develop an osteoporotic phenotype, it would be required to look at whether PEPITEM activity is effective in other forms of bone loss and whether PEPITEMs pro-anabolic function is maintained with age.
- Validate role of PEPITEM in oestrogen-deficiency induced bone loss using TUNEL staining for apoptotic sections from OVX treated and untreated mice.
- Further investigate PEPITEMs effects on macrophage polarisation and differentiation capacity to osteoclasts following PEPITEM treatment.
- PEPITEM showed high binding capacity to multiple intracellular proteins therefore investigation into the capability of PEPITEM entering the cell and the intracellular PEPITEM and tripeptide

function, using fluorescently labelled peptides to decipher other potential PEPITEM mechanisms.

- LSNEER showed bioactivity within osteoblasts *in vitro* however was not taken forward into *in vivo* testing, therefore future experiments should look at the actions of LSNEER *in vivo* on bone formation to help up further understand PEPITEM functioning.
- This thesis focused on the mechanism of action of PEPITEM on bone, however it is unclear whether PEPITEM is produced by bone cells or whether it is through b-cell crosstalk within the bone. Therefore, experiments are required to look at PEPITEM production from bone cells using mass spectrometry and investigations using b-cell cocultures to look at crosstalk. To provide further insight into homeostatic PEPITEM signalling in bone.
- Further investigation into the use of chemically altered peptide memetics, investigating differences in pharmacokinetics and pharmacodynamics compared to PEPITEM treatment, determining their therapeutic value.

6.6 Conclusion

This project provides novel insights to the mechanistic actions of the endogenous peptide, PEPITEM, and its role in bone homeostasis and disease. The discover of the PEPITEM-NCAM-1 pathway provides novel understandings into osteoblast function and potential new avenues for therapeutic intervention. The presence of bio-active regions within the PEPITEM sequence which maintain partial PEPITEM function *in vitro* and *in vivo*, provide new insight into the PEPITEM mechanism and potential new therapeutic targets for bone loss as these memetics may allow for less frequent treatment requirements compared to PEPITEM.

7 Bibliography:

1. Forwood, M. R. & Turner, C. H. Skeletal adaptations to mechanical usage: results from tibial loading studies in rats. *Bone* **17**, 197S-205S (1995).
2. Nomura, S. & Takano-Yamamoto, T. Molecular events caused by mechanical stress in bone. *Matrix Biol* **19**, 91–96 (2000).
3. Mason, D. J. *et al.* Mechanically regulated expression of a neural glutamate transporter in bone: A role for excitatory amino acids as osteotropic agents? *Bone* **20**, 199–205 (1997).
4. Rawlinson, S. C. F., Pitsillides, A. A. & Lanyon, L. E. Involvement of different ion channels in osteoblasts' and osteocytes' early responses to mechanical strain. *Bone* **19**, 609–614 (1996).
5. Gerstenfeld, L. C., Cullinane, D. M., Barnes, G. L., Graves, D. T. & Einhorn, T. A. Fracture healing as a post-natal developmental process: Molecular, spatial, and temporal aspects of its regulation. *Journal of Cellular Biochemistry* **88**, 873–884 (2003).
6. Marsell, R. & Einhorn, T. A. The biology of fracture healing. *Injury* **42**, 551–555 (2011).
7. Cowan, P. T. & Kahai, P. Anatomy, Bones. *StatPearls* (2021).
8. Cullinane, D. M. The role of osteocytes in bone regulation: Mineral homeostasis versus mechanoreception. *J Musculoskel Neuron Interact* **2**, 242–244 (2002).
9. Gilbert, S. Osteogenesis: The Development of Bones. in *Developmental Biology* (2000).
10. Breeland, G., Sinkler, M. A. & Menezes, R. G. Embryology, Bone Ossification. *StatPearls* (2021).
11. Hadjidakis, D. J. & Androulakis, I. I. Bone remodeling. *Annals of the New York Academy of Sciences* **1092**, 385–396 (2006).
12. Ott, S. M. Cortical or Trabecular Bone: What's the Difference? *American Journal of Nephrology* **47**, 373–375 (2018).

13. Oftadeh, R., Perez-Viloria, M., Villa-Camacho, J. C., Vaziri, A. & Nazarian, A. Biomechanics and Mechanobiology of Trabecular Bone: A Review. *Journal of Biomechanical Engineering* **137**, 0108021 (2015).

14. Clarke, B. Normal Bone Anatomy and Physiology. *Clinical Journal of the American Society of Nephrology : CJASN* **3**, S131 (2008).

15. Boskey, A. L., Spevak, L., Paschalis, E., Doty, S. B. & McKee, M. D. Osteopontin deficiency increases mineral content and mineral crystallinity in mouse bone. *Calcified tissue international* **71**, 145–154 (2002).

16. Aszódi, A., Bateman, J. F., Gustafsson, E., Boot-Handford, R. & Fässler, R. Mammalian skeletogenesis and extracellular matrix: what can we learn from knockout mice? *Cell structure and function* **25**, 73–84 (2000).

17. Downey, P. A. & Siegel, M. I. Bone Biology and the Clinical Implications for Osteoporosis. *Physical Therapy* **86**, 77–91 (2006).

18. Datta, H. K., Ng, W. F., Walker, J. A., Tuck, S. P. & Varanasi, S. S. The cell biology of bone metabolism. *Journal of clinical pathology* **61**, 577–587 (2008).

19. Florencio-Silva, R., Sasso, G. R. D. S., Sasso-Cerri, E., Simões, M. J. & Cerri, P. S. Biology of Bone Tissue: Structure, Function, and Factors That Influence Bone Cells. *BioMed Research International* **2015**, (2015).

20. Sims, N. A. & Gooi, J. H. Bone remodeling: Multiple cellular interactions required for coupling of bone formation and resorption. *Seminars in cell & developmental biology* **19**, 444–451 (2008).

21. Wang, X. *et al*. Role of mesenchymal stem cells in bone regeneration and fracture repair: a review. *International Orthopaedics* **37**, 2491 (2013).

22. Fujikawa, Y. *et al*. The effect of macrophage-colony stimulating factor and other humoral factors (interleukin-1, -3, -6, and -11, tumor necrosis factor-alpha, and granulocyte macrophage-colony

stimulating factor) on human osteoclast formation from circulating cells. *Bone* **28**, 261–267 (2001).

23. Boyce, B. F. & Xing, L. Functions of RANKL/RANK/OPG in bone modeling and remodeling. *Archives of biochemistry and biophysics* **473**, 139 (2008).
24. Crockett, J. C., Mellis, D. J., Scott, D. I. & Helfrich, M. H. New knowledge on critical osteoclast formation and activation pathways from study of rare genetic diseases of osteoclasts: focus on the RANK/RANKL axis. *Osteoporosis international : a journal established as result of cooperation between the European Foundation for Osteoporosis and the National Osteoporosis Foundation of the USA* **22**, 1–20 (2011).
25. Yoshida, H. *et al.* The murine mutation osteopetrosis is in the coding region of the macrophage colony stimulating factor gene. *Nature* **345**, 442–444 (1990).
26. Udagawa, N. *et al.* Osteoclast differentiation by RANKL and OPG signaling pathways. *Journal of bone and mineral metabolism* **39**, 19–26 (2021).
27. Sodek, J. & McKee, M. D. Molecular and cellular biology of alveolar bone. *Periodontology 2000* **24**, 99–126 (2000).
28. Hirotani, H., Tuohy, N. A., Woo, J.-T., Stern, P. H. & Clipstone, N. A. The Calcineurin/Nuclear Factor of Activated T Cells Signaling Pathway Regulates Osteoclastogenesis in RAW264.7 Cells *. *Journal of Biological Chemistry* **279**, 13984–13992 (2004).
29. Huang, H. *et al.* Osteoclast differentiation requires TAK1 and MKK6 for NFATc1 induction and NF-κB transactivation by RANKL. *Cell Death & Differentiation 2006 13:11* **13**, 1879–1891 (2006).
30. Blumer, M. J. F. *et al.* Role of tartrate-resistant acid phosphatase (TRAP) in long bone development. *Mechanisms of Development* **129**, 162 (2012).
31. Saftig, P. *et al.* Functions of cathepsin K in bone resorption. Lessons from cathepsin K deficient mice. *Advances in experimental medicine and biology* **477**, 293–303 (2000).

32. Mulari, M., Vääräniemi, J. & Väänänen, H. K. Intracellular membrane trafficking in bone resorbing osteoclasts. *Microscopy research and technique* **61**, 496–503 (2003).

33. Arana-Chavez, V. E. & Bradaschia-Correa, V. Clastic cells: mineralized tissue resorption in health and disease. *The international journal of biochemistry & cell biology* **41**, 446–450 (2009).

34. Takito, J., Inoue, S. & Nakamura, M. The Sealing Zone in Osteoclasts: A Self-Organized Structure on the Bone. *International journal of molecular sciences* **19**, (2018).

35. Qin, A. *et al.* V-ATPases in osteoclasts: structure, function and potential inhibitors of bone resorption. *The international journal of biochemistry & cell biology* **44**, 1422–1435 (2012).

36. Capulli, M., Paone, R. & Rucci, N. Osteoblast and osteocyte: games without frontiers. *Archives of biochemistry and biophysics* **561**, 3–12 (2014).

37. Baumann, K. Kindlin' the fate of mesenchymal stem cells. *Nature Reviews Molecular Cell Biology 2018 19:5* **19**, 279–279 (2018).

38. Grigoriadis, A. E., Heersche, J. N. M. & Aubin, J. E. Differentiation of muscle, fat, cartilage, and bone from progenitor cells present in a bone-derived clonal cell population: effect of dexamethasone. *The Journal of Cell Biology* **106**, 2139 (1988).

39. Okamoto, M., Murai, J., Yoshikawa, H. & Tsumaki, N. Bone morphogenetic proteins in bone stimulate osteoclasts and osteoblasts during bone development. *Journal of bone and mineral research : the official journal of the American Society for Bone and Mineral Research* **21**, 1022–1033 (2006).

40. Westendorf, J. J., Kahler, R. A. & Schroeder, T. M. Wnt signaling in osteoblasts and bone diseases. *Gene* **341**, 19–39 (2004).

41. Komori, T. Regulation of osteoblast differentiation by Runx2. *Advances in experimental medicine and biology* **658**, 43–49 (2010).

42. Cao, Y. *et al.* Osterix, a transcription factor for osteoblast differentiation, mediates antitumor activity in murine osteosarcoma. *Cancer research* **65**, 1124–1128 (2005).

43. M, F., E, H., B, B., R, B. & D, M. Molecular mechanisms of mesenchymal stem cell differentiation towards osteoblasts. *World journal of stem cells* **5**, 136 (2013).

44. Choi, H. K. *et al*. Vitamin C Activates Osteoblastogenesis and Inhibits Osteoclastogenesis via Wnt/β-Catenin/ATF4 Signaling Pathways. *Nutrients* **11**, (2019).

45. Rt, F., Bs, I. & Y, C. Effects of ascorbic acid on collagen matrix formation and osteoblast differentiation in murine MC3T3-E1 cells. *Journal of bone and mineral research : the official journal of the American Society for Bone and Mineral Research* **9**, (1994).

46. Rt, F. & Bs, I. Relationship between collagen synthesis and expression of the osteoblast phenotype in MC3T3-E1 cells. *Journal of bone and mineral research : the official journal of the American Society for Bone and Mineral Research* **7**, (1992).

47. Rt, F. & J, Y. Regulation of alkaline phosphatase by 1,25-dihydroxyvitamin D3 and ascorbic acid in bone-derived cells. *Journal of bone and mineral research : the official journal of the American Society for Bone and Mineral Research* **5**, (1990).

48. Ding, J. *et al*. TNF-alpha and IL-1beta inhibit RUNX2 and collagen expression but increase alkaline phosphatase activity and mineralization in human mesenchymal stem cells. *Life sciences* **84**, 499–504 (2009).

49. Foster, B. L. *et al*. Regulation of cementoblast gene expression by inorganic phosphate in vitro. *Calcif Tissue Int* **78**, 103–112 (2006).

50. Tada, H., Nemoto, E., Foster, B. L., Somerman, M. J. & Shimauchi, H. Phosphate increases bone morphogenetic protein-2 expression through cAMP-dependent protein kinase and ERK1/2 pathways in human dental pulp cells. *Bone* **48**, 1409–1416 (2011).

51. Maniatopoulos, C., Sodek, J. & Melcher, A. H. Bone formation in vitro by stromal cells obtained from bone marrow of young adult rats. *Cell Tissue Res* **254**, 317–330 (1988).

52. Freeman, F. E., Stevens, H. Y., Owens, P., Guldberg, R. E. & McNamara, L. M. Osteogenic Differentiation of Mesenchymal Stem Cells by Mimicking the Cellular Niche of the Endochondral Template. *Tissue Eng Part A* **22**, 1176–1190 (2016).

53. Stein, G. S. & Lian, J. B. Molecular mechanisms mediating proliferation/differentiation interrelationships during progressive development of the osteoblast phenotype. *Endocrine reviews* **14**, 424–442 (1993).

54. Nakashima, K. *et al.* The novel zinc finger-containing transcription factor osterix is required for osteoblast differentiation and bone formation. *Cell* **108**, 17–29 (2002).

55. Nakamura, H. Morphology, Function, and Differentiation of Bone Cells. *Journal of Hard Tissue Biology* **16**, 15–22 (2007).

56. Yoshiko, Y., Candeliere, G. A., Maeda, N. & Aubin, J. E. Osteoblast Autonomous Pi Regulation via Pit1 Plays a Role in Bone Mineralization. *Molecular and Cellular Biology* **27**, 4465 (2007).

57. Franz-Odendaal, T. A., Hall, B. K. & Witten, P. E. Buried alive: How osteoblasts become osteocytes. *Developmental Dynamics* **235**, 176–190 (2006).

58. Rochefort, G. Y., Pallu, S. & Benhamou, C. L. Osteocyte: the unrecognized side of bone tissue. *Osteoporosis international : a journal established as result of cooperation between the European Foundation for Osteoporosis and the National Osteoporosis Foundation of the USA* **21**, 1457–1469 (2010).

59. Bonewald, L. F. The Amazing Osteocyte. *Journal of Bone and Mineral Research* **26**, 229 (2011).

60. Manolagas, S. C. Birth and death of bone cells: basic regulatory mechanisms and implications for the pathogenesis and treatment of osteoporosis. *Endocrine reviews* **21**, 115–137 (2000).

61. Bonewald, L. F. & Johnson, M. L. Osteocytes, mechanosensing and Wnt signaling. *Bone* **42**, 606–615 (2008).

62. Tiede-Lewis, L. A. M. *et al.* Degeneration of the osteocyte network in the C57BL/6 mouse model of aging. *Aging* **9**, 2187–2205 (2017).

63. Han, Y., You, X., Xing, W., Zhang, Z. & Zou, W. Paracrine and endocrine actions of bone—the functions of secretory proteins from osteoblasts, osteocytes, and osteoclasts. *Bone Research* **6**, (2018).

64. Kim, J. *et al.* Sclerostin inhibits Wnt signaling through tandem interaction with two LRP6 ectodomains. *Nat Commun* **11**, 5357 (2020).

65. Xiong, J. & O'Brien, C. A. Osteocyte RANKL: New Insights into the Control of Bone Remodeling. *Journal of bone and mineral research : the official journal of the American Society for Bone and Mineral Research* **27**, 499 (2012).

66. Civitelli, R. Cell-Cell Communication in the Osteoblast/Osteocyte Lineage. *Archives of biochemistry and biophysics* **473**, 188 (2008).

67. Miller SC, de Saint-Georges L, Bowman BM, J. W. Bone lining cells: structure and function. *Scanning Microsc* **3**, 953–60 (1989).

68. Kahla, R. Ben & Barkaoui, A. Bone remodeling biology. *Bone Remodeling Process* 49–87 (2021) doi:10.1016/B978-0-323-88467-9.00002-3.

69. Andersen, T. L. *et al.* A Physical Mechanism for Coupling Bone Resorption and Formation in Adult Human Bone. *The American Journal of Pathology* **174**, 239 (2009).

70. von der Mark, K. & von der Mark, H. Immunological and biochemical studies of collagen type transition during in vitro chrondrogenesis of chick limb mesodermal cells. *J Cell Biol* **73**, 736–747 (1977).

71. Percival, C. J. & Richtsmeier, J. T. Angiogenesis and intramembranous osteogenesis. *Developmental Dynamics* **242**, 909–922 (2013).

72. Yoshida, T., Vivatbutsiri, P., Morriss-Kay, G., Saga, Y. & Iseki, S. Cell lineage in mammalian craniofacial mesenchyme. *Mech Dev* **125**, 797–808 (2008).

73. Ting, M.-C. *et al.* EphA4 as an effector of Twist1 in the guidance of osteogenic precursor cells during calvarial bone growth and in craniosynostosis. *Development* **136**, 855–864 (2009).

74. Rice, D. P. *et al*. Integration of FGF and TWIST in calvarial bone and suture development. *Development* **127**, 1845–1855 (2000).

75. Iseki, S. *et al*. Fgfr2 and osteopontin domains in the developing skull vault are mutually exclusive and can be altered by locally applied FGF2. *Development* **124**, 3375–3384 (1997).

76. Thompson, T. J., Owens, P. D. & Wilson, D. J. Intramembranous osteogenesis and angiogenesis in the chick embryo. *J Anat* **166**, 55–65 (1989).

77. Komori, T. *et al*. Targeted disruption of Cbfa1 results in a complete lack of bone formation owing to maturational arrest of osteoblasts. *Cell* **89**, 755–764 (1997).

78. Otto, F. *et al*. Cbfa1, a candidate gene for cleidocranial dysplasia syndrome, is essential for osteoblast differentiation and bone development. *Cell* **89**, 765–771 (1997).

79. Ortega, N., Behonick, D. J. & Werb, Z. Matrix remodeling during endochondral ossification. *Trends Cell Biol* **14**, 86–93 (2004).

80. Aghajanian, P. & Mohan, S. The art of building bone: emerging role of chondrocyte-to-osteoblast transdifferentiation in endochondral ossification. *Bone Res* **6**, 1–9 (2018).

81. Karsenty, G. & Wagner, E. F. Reaching a Genetic and Molecular Understanding of Skeletal Development. *Developmental Cell* **2**, 389–406 (2002).

82. Blair, H. C., Zaidi, M. & Schlesinger, P. H. Mechanisms balancing skeletal matrix synthesis and degradation. *Biochem J* **364**, 329–341 (2002).

83. Berendsen, A. D. & Olsen, B. R. Bone development. *Bone* **80**, 14–18 (2015).

84. Karl, A. *et al*. Thyroid Hormone-Induced Hypertrophy in Mesenchymal Stem Cell Chondrogenesis Is Mediated by Bone Morphogenetic Protein-4. *Tissue Eng Part A* **20**, 178–188 (2014).

85. Goldring, M. B., Tsuchimochi, K. & Ijiri, K. The control of chondrogenesis. *J Cell Biochem* **97**, 33–44 (2006).

86. Kronenberg, H. M. Developmental regulation of the growth plate. *Nature* **423**, 332–336 (2003).

87. Long, F. & Ornitz, D. M. Development of the endochondral skeleton. *Cold Spring Harb Perspect Biol* **5**, a008334 (2013).

88. Maes, C. & Kronenberg, H. M. Chapter 4 - Postnatal Bone Growth: Growth Plate Biology, Bone Formation, and Remodeling. in *Pediatric Bone (Second Edition)* (eds. Glorieux, F. H., Pettifor, J. M. & Jüppner, H.) 55–82 (Academic Press, San Diego, 2012). doi:10.1016/B978-0-12-382040-2.10004-8.

89. Zoetis, T., Tassinari, M., Bagi, C., Walthall, K. & Hurtt, M. Species Comparison of Postnatal Bone Growth and Development. *Birth defects research. Part B, Developmental and reproductive toxicology* **68**, 86–110 (2003).

90. Karimian, E. *et al.* Resveratrol Treatment Delays Growth Plate Fusion and Improves Bone Growth in Female Rabbits. *PLOS ONE* **8**, e67859 (2013).

91. Roach, H. I., Mehta, G., Oreffo, R. O. C., Clarke, N. M. P. & Cooper, C. Temporal Analysis of Rat Growth Plates: Cessation of Growth with Age Despite Presence of a Physis. *J Histochem Cytochem.* **51**, 373–383 (2003).

92. Roselló-Díez, A. & Joyner, A. L. Regulation of Long Bone Growth in Vertebrates; It Is Time to Catch Up. *Endocr Rev* **36**, 646–680 (2015).

93. Kusumbe, A., Ramasamy, S. & Adams, R. Coupling of angiogenesis and osteogenesis by a specific vessel subtype in bone. *Nature* **507**, (2014).

94. Ramasamy, S. K., Kusumbe, A. P., Wang, L. & Adams, R. H. Endothelial Notch activity promotes angiogenesis and osteogenesis in bone. *Nature* **507**, 376–380 (2014).

95. Carulli, C., Innocenti, M. & Brandi, M. L. Bone Vascularization in Normal and Disease Conditions. *Front Endocrinol (Lausanne)* **4**, 106 (2013).

96. Langen, U. H. *et al.* Cell-matrix signals specify bone endothelial cells during developmental osteogenesis. *Nat Cell Biol* **19**, 189–201 (2017).

97. Jilka, R. L. Biology of the basic multicellular unit and the pathophysiology of osteoporosis. *Medical and pediatric oncology* **41**, 182–185 (2003).

98. Raggatt, L. J. & Partridge, N. C. Cellular and molecular mechanisms of bone remodeling. *The Journal of biological chemistry* **285**, 25103–25108 (2010).

99. Kitaura, H. *et al*. Osteocyte-Related Cytokines Regulate Osteoclast Formation and Bone Resorption. *International Journal of Molecular Sciences* **21**, (2020).

100. Plotkin, L. I. Apoptotic osteocytes and the control of targeted bone resorption. *Current osteoporosis reports* **12**, 121 (2014).

101. Teti, A. Mechanisms of osteoclast-dependent bone formation. *Bonekey Rep* **2**, 449 (2013).

102. Xing, L. & Boyce, B. F. Regulation of apoptosis in osteoclasts and osteoblastic cells. *Biochemical and Biophysical Research Communications* **328**, 709–720 (2005).

103. Delaisse, J.-M. The reversal phase of the bone-remodeling cycle: cellular prerequisites for coupling resorption and formation. *BoneKEy reports* **3**, (2014).

104. Jensen, P. R., Andersen, T. L., Hauge, E. M., Bollerslev, J. & Delaissé, J. M. A joined role of canopy and reversal cells in bone remodeling--lessons from glucocorticoid-induced osteoporosis. *Bone* **73**, 16–23 (2015).

105. Murshed, M. Mechanism of Bone Mineralization. *Cold Spring Harbor Perspectives in Medicine* **8**, (2018).

106. Benedetti, M. G., Furlini, G., Zati, A. & Letizia Mauro, G. The Effectiveness of Physical Exercise on Bone Density in Osteoporotic Patients. *Biomed Res Int* **2018**, 4840531 (2018).

107. Man, J., Graham, T., Squires-Donelly, G. & Laslett, A. L. The effects of microgravity on bone structure and function. *NPJ Microgravity* **8**, 9 (2022).

108. Eimori, K. *et al*. Disrupted Bone Metabolism in Long-Term Bedridden Patients. *PLoS One* **11**, e0156991 (2016).

109. Qin, L., Liu, W., Cao, H. & Xiao, G. Molecular mechanosensors in osteocytes. *Bone Res* **8**, 1–24 (2020).

110. Frost, H. M. Bone 'mass' and the 'mechanostat': a proposal. *Anat Rec* **219**, 1–9 (1987).

111. Tatsumi, S. *et al*. Targeted Ablation of Osteocytes Induces Osteoporosis with Defective Mechanotransduction. *Cell Metabolism* **5**, 464–475 (2007).

112. Thompson, W. R., Rubin, C. T. & Rubin, J. Mechanical regulation of signaling pathways in bone. *Gene* **503**, 179–193 (2012).

113. Wang, Y., McNamara, L. M., Schaffler, M. B. & Weinbaum, S. A model for the role of integrins in flow induced mechanotransduction in osteocytes. *Proc Natl Acad Sci U S A* **104**, 15941–15946 (2007).

114. Li, X. *et al*. Connexin 43 is a potential regulator in fluid shear stress-induced signal transduction in osteocytes. *Journal of Orthopaedic Research* **31**, 1959–1965 (2013).

115. Sun, W. *et al*. The mechanosensitive Piezo1 channel is required for bone formation. *eLife* **8**, e47454.

116. Wang, L. *et al*. Mechanical sensing protein PIEZO1 regulates bone homeostasis via osteoblast-osteoclast crosstalk. *Nat Commun* **11**, 282 (2020).

117. Hendrickx, G. *et al*. Piezo1 Inactivation in Chondrocytes Impairs Trabecular Bone Formation. *Journal of Bone and Mineral Research* **36**, 369–384 (2021).

118. Liu, P. *et al*. Effects of Mechanical Stress Stimulation on Function and Expression Mechanism of Osteoblasts. *Front. Bioeng. Biotechnol.* **10**, (2022).

119. Sun, W. *et al*. Mechanical stimulation controls osteoclast function through the regulation of Ca2+-activated Cl− channel Anoctamin 1. *Commun Biol* **6**, 1–13 (2023).

120. Sun, W. *et al*. Anoctamin 1 controls bone resorption by coupling Cl- channel activation with RANKL-RANK signaling transduction. *Nat Commun* **13**, 2899 (2022).

121. Hu, Y. *et al*. The Critical Role of The Piezo1/β-catenin/ATF4 Axis on The Stemness of Gli1+ BMSCs During Simulated Microgravity-Induced Bone Loss. *Advanced Science* **10**, 2303375 (2023).

122. Xiao, Z. & Quarles, L. D. Physiological mechanisms and therapeutic potential of bone mechanosensing. *Rev Endocr Metab Disord* **16**, 115–129 (2015).

123. Calvi, L. M. *et al*. Activated parathyroid hormone/parathyroid hormone-related protein receptor in osteoblastic cells differentially affects cortical and trabecular bone. *The Journal of clinical investigation* **107**, 277–286 (2001).

124. Khosla, S., Oursler, M. J. & Monroe, D. G. Estrogen and the skeleton. *Trends in endocrinology and metabolism: TEM* **23**, 576–581 (2012).

125. Manolagas, S. C., Kousteni, S. & Jilka, R. L. Sex steroids and bone. *Recent Prog Horm Res* **57**, 385–409 (2002).

126. Negishi-Koga, T. & Takayanagi, H. Bone cell communication factors and Semaphorins. *BoneKEy reports* **1**, 183 (2012).

127. Frost, K., Naylor, A. J. & McGettrick, H. M. The Ying and Yang of Sphingosine-1-Phosphate Signalling within the Bone. *International Journal of Molecular Sciences* **24**, 6935 (2023).

128. LEWIS, J. W. CHARACTERISING THE THERAPEUTIC POTENTIAL OF PEPITEM IN AGE-RELATED BONE LOSS, SKELETAL REMODELLING AND REPAIR. (University of Birmingham, 2022).

129. el Bawab, S., Mao, C., Obeid, L. M. & Hannun, Y. A. Ceramidases in the regulation of ceramide levels and function. *Sub-cellular biochemistry* **36**, 187–205 (2002).

130. Ksia ̨zek, M., Chacińska, M., Chabowski, A. & Baranowski, M. Sources, metabolism, and regulation of circulating sphingosine-1-phosphate. *Journal of Lipid Research* **56**, 1271–1281 (2015).

131. Pralhada Rao, R. *et al*. Sphingolipid Metabolic Pathway: An Overview of Major Roles Played in Human Diseases. *Journal of Lipids* **2013**, 1–12 (2013).

132. Strub, G. M., Maceyka, M., Hait, N. C., Milstien, S. & Spiegel, S. Extracellular and Intracellular Actions of Sphingosine-1-Phosphate. *Advances in experimental medicine and biology* **688**, 141 (2010).

133. Maceyka, M., Harikumar, K. B., Milstien, S. & Spiegel, S. SPHINGOSINE-1-PHOSPHATE SIGNALING AND ITS ROLE IN DISEASE. *Trends in Cell Biology* **22**, 50 (2012).

134. Xiao, L. *et al.* SPHK1-S1PR1-RANKL Axis Regulates the Interactions Between Macrophages and BMSCs in Inflammatory Bone Loss. *Journal of Bone and Mineral Research* **33**, 1090–1104 (2018).

135. Ryu, J. *et al.* Sphingosine 1-phosphate as a regulator of osteoclast differentiation and osteoclast-osteoblast coupling. *EMBO Journal* **25**, 5840–5851 (2006).

136. Alvarez, S. E., Milstien, S. & Spiegel, S. Autocrine and paracrine roles of sphingosine-1-phosphate. *Trends in endocrinology and metabolism: TEM* **18**, 300–307 (2007).

137. Walker, J. M. *et al.* An Unanticipated Role for Sphingosine Kinase-2 in Bone and in the Anabolic Effect of Parathyroid Hormone. *Endocrinology* **162**, 1–13 (2021).

138. Bao, X. *et al.* Acid sphingomyelinase regulates osteoclastogenesis by modulating sphingosine kinases downstream of RANKL signaling. *Biochemical and Biophysical Research Communications* **405**, 533–537 (2011).

139. Brizuela, L. *et al.* Osteoblast-derived sphingosine 1-phosphate to induce proliferation and confer resistance to therapeutics to bone metastasis-derived prostate cancer cells. *Molecular oncology* **8**, 1181–1195 (2014).

140. Keller, J. *et al.* Calcitonin controls bone formation by inhibiting the release of sphingosine 1-phosphate from osteoclasts. *Nature Communications* **5**, 1–13 (2014).

141. Qi, T., Li, L. & Weidong, T. The Role of Sphingolipid Metabolism in Bone Remodeling. *Frontiers in cell and developmental biology* **9**, 752540 (2021).

142. Meshcheryakova, A., Mechtcheriakova, D. & Pietschmann, P. Sphingosine 1-phosphate signaling in bone remodeling: multifaceted roles and therapeutic potential. *Expert Opinion on Therapeutic Targets* **21**, 725 (2017).

143. Quint, P. *et al*. Sphingosine 1-phosphate (S1P) receptors 1 and 2 coordinately induce mesenchymal cell migration through s1p activation of complementary kinase pathways. *Journal of Biological Chemistry* **288**, 5398–5406 (2013).

144. Carpio, L. C., Stephan, E., Kamer, A. & Dziak, R. Sphingolipids stimulate cell growth via MAP kinase activation in osteoblastic cells. *Prostaglandins, Leukotrienes and Essential Fatty Acids (PLEFA)* **61**, 267–273 (1999).

145. Feehan, J., Kassem, M., Pignolo, R. J. & Duque, G. Bone From Blood: Characteristics and Clinical Implications of Circulating Osteogenic Progenitor (COP) Cells. *Journal of Bone and Mineral Research* **36**, 12–23 (2021).

146. Golan, K., Kollet, O. & Lapidot, T. Dynamic cross talk between S1P and CXCL12 regulates hematopoietic stem cells migration, development and bone remodeling. *Pharmaceuticals* **6**, 1145–1169 (2013).

147. Thuy, A. V., Reimann, C. M., Hemdan, N. Y. A. & Gräler, M. H. Sphingosine 1-phosphate in blood: Function, metabolism, and fate. *Cellular Physiology and Biochemistry* **34**, 158–171 (2014).

148. Spiegel, S. & Milstien, S. The outs and the ins of sphingosine-1-phosphate in immunity. *Nature Reviews. Immunology* **11**, 403 (2011).

149. Weske, S. *et al*. Targeting sphingosine-1-phosphate lyase as an anabolic therapy for bone loss. *Nature Medicine 2018 24:5* **24**, 667–678 (2018).

150. Ishii, T., Shimazu, Y., Nishiyama, I., Kikuta, J. & Ishii, M. The role of sphingosine 1-phosphate in migration of osteoclast precursors; An application of intravital two-photon microscopy. *Molecules and Cells* **31**, 399–403 (2011).

151. Ishii, M. *et al*. Sphingosine-1-phosphate mobilizes osteoclast precursors and regulates bone homeostasis. *Nature* **458**, 524–528 (2009).

152. Boyce, B. F. & Xing, L. Biology of RANK, RANKL, and osteoprotegerin. *Arthritis research & therapy* **9 Suppl 1**, (2007).

153. Tomimori, Y. *et al*. Evaluation of pharmaceuticals with a novel 50-hour animal model of bone loss. *Journal of bone and mineral research : the official journal of the American Society for Bone and Mineral Research* **24**, 1194–1205 (2009).

154. Hsu, L. C., Reddy, S. V., Yilmaz, Ö. & Yu, H. Sphingosine-1-phosphate receptor 2 controls podosome components induced by RANKL affecting osteoclastogenesis and bone resorption. *Cells* **8**, 1–19 (2019).

155. Price, S. T. Sphingosine 1-Phosphate Receptor 2 Regulates the Migration, Proliferation, and Differentiation of Mesenchymal Stem Cells. *International Journal of Stem cell Research & Therapy* **2**, 1–19 (2015).

156. Sassoli, C., Pierucci, F., Zecchi-Orlandini, S. & Meacci, E. Sphingosine 1-phosphate (S1P)/ S1P receptor signaling and mechanotransduction: Implications for intrinsic tissue repair/regeneration. *International Journal of Molecular Sciences* **20**, (2019).

157. Kong, Y., Wang, H., Lin, T. & Wang, S. Modulates Cell Migration in Human Bone Marrow-Derived Mesenchymal Stem Cells. **2014**, (2014).

158. Kong, Y., Wang, H., Lin, T. & Wang, S. Sphingosine-1-phosphate/s1p receptors signaling modulates cell migration in human bone marrow-derived mesenchymal stem cells. *Mediators of Inflammation* **2014**, (2014).

159. Rousselle, A. V. & Heymann, D. Osteoclastic acidification pathways during bone resorption. *Bone* **30**, 533–540 (2002).

160. Sun, Y. *et al*. Recent Advances in Osteoclast Biological Behavior. *Frontiers in Cell and Developmental Biology* **9**, 1–19 (2021).

161. Kikuta, J. *et al*. Sphingosine-1-phosphate-mediated osteoclast precursor monocyte migration is a critical point of control in antibone-resorptive action of active vitamin D. *Proceedings of the National Academy of Sciences of the United States of America* **110**, 7009–7013 (2013).

162. Ryu, J. *et al*. Sphingosine 1-phosphate as a regulator of osteoclast differentiation and osteoclast-osteoblast coupling. *The EMBO journal* **25**, 5840–5851 (2006).

163. Grey, A. *et al*. Osteoblastic cells express phospholipid receptors and phosphatases and proliferate in response to sphingosine-1-phosphate. *Calcified Tissue International* **74**, 542–550 (2004).

164. Hashimoto, Y. *et al*. Sphingosine-1-phosphate inhibits differentiation of C3H10T1/2 cells into adipocyte. *Molecular and cellular biochemistry* **401**, 39–47 (2015).

165. Hashimoto, Y. *et al*. Sphingosine-1-phosphate-enhanced Wnt5a promotes osteogenic differentiation in C3H10T1/2 cells. *Cell Biology International* **40**, 1129–1136 (2016).

166. Matsuzaki, E. *et al*. Sphingosine-1-phosphate promotes the nuclear translocation of β-catenin and thereby induces osteoprotegerin gene expression in osteoblast-like cell lines. *Bone* **55**, 315–324 (2013).

167. Higashi, K. *et al*. Sphingosine-1-phosphate/S1PR2-mediated signaling triggers Smad1/5/8 phosphorylation and thereby induces Runx2 expression in osteoblasts. *Bone* **93**, 1–11 (2016).

168. Choi, B. *et al*. Sphingosine-1-phosphate hinders the osteogenic differentiation of dental pulp stem cells in association with AKT signaling pathways. *International Journal of Oral Science* **14**, (2022).

169. Nishimura, R. *et al*. Smad5 and DPC4 Are Key Molecules in Mediating BMP-2-induced Osteoblastic Differentiation of the Pluripotent Mesenchymal Precursor Cell Line C2C12. *Journal of Biological Chemistry* **273**, 1872–1879 (1998).

170. Kim, J. M., Lin, C., Stavre, Z., Greenblatt, M. B. & Shim, J. H. Osteoblast-Osteoclast Communication and Bone Homeostasis. *Cells* **9**, 1–14 (2020).

171. Ahmed, N. *et al*. Characterization and expression of sphingosine 1-phosphate receptors in human and rat heart. *Frontiers in Pharmacology* **8**, 1–7 (2017).

172. Hsu, L.-C., Reddy, S. V., Yilmaz, Ö. & Yu, H. Sphingosine-1-Phosphate Receptor 2 Controls Podosome Components Induced by RANKL Affecting Osteoclastogenesis and Bone Resorption. *Cells* **8**, 17 (2019).

173. Spatz, J. M. *et al*. The Wnt Inhibitor Sclerostin Is Up-regulated by Mechanical Unloading in Osteocytes in Vitro. *The Journal of Biological Chemistry* **290**, 16744 (2015).

174. Zhang, J. N. *et al*. The role of the sphingosine-1-phosphate signaling pathway in osteocyte mechanotransduction. *Bone* **79**, 71–78 (2015).

175. Dobrosak, C. & Gooi, J. H. Increased sphingosine-1-phosphate production in response to osteocyte mechanotransduction. *Bone Reports* **7**, 114 (2017).

176. Xu, L. H., Shao, H., Ma, Y. H. V. & You, L. OCY454 Osteocytes as an in Vitro Cell Model for Bone Remodeling Under Mechanical Loading. *Journal of Orthopaedic Research* **37**, 1681–1689 (2019).

177. Obsilova, V. & Obsil, T. Structural insights into the functional roles of 14-3-3 proteins. *Front. Mol. Biosci.* **9**, (2022).

178. Ichimura, T. *et al*. Molecular cloning of cDNA coding for brain-specific 14-3-3 protein, a protein kinase-dependent activator of tyrosine and tryptophan hydroxylases. *Proc Natl Acad Sci U S A* **85**, 7084–7088 (1988).

179. Sluchanko, N. N. & Bustos, D. M. Intrinsic disorder associated with 14-3-3 proteins and their partners. *Prog Mol Biol Transl Sci* **166**, 19–61 (2019).

180. Adel, Y. & Sadeq, Y. 14-3-3η protein is associated with disease activity and osteoporosis in patients with rheumatoid arthritis. *Reumatologia* **60**, 384–391 (2022).

181. Liu, Y., Ross, J. F., Bodine, P. V. N. & Billiard, J. Homodimerization of Ror2 Tyrosine Kinase Receptor Induces 14-3-3β Phosphorylation and Promotes Osteoblast Differentiation and Bone Formation. *Molecular Endocrinology* **21**, 3050–3061 (2007).

182. Sanchez, C. *et al.* Comparison of secretome from osteoblasts derived from sclerotic versus non-sclerotic subchondral bone in OA: A pilot study. *PLoS ONE* **13**, (2018).

183. Schmidt, J. R. *et al.* Osteoblast-released Matrix Vesicles, Regulation of Activity and Composition by Sulfated and Non-sulfated Glycosaminoglycans. *Molecular & cellular proteomics : MCP* **15**, 558–572 (2016).

184. Bronisz, A. *et al.* Microphthalmia-associated transcription factor interactions with 14-3-3 modulate differentiation of committed myeloid precursors. *Molecular biology of the cell* **17**, 3897–3906 (2006).

185. Liu, Y., Xu, Y. & Shuai, Z. Mir-142-3P regulates MAPK protein family by inhibiting 14-3-3η to enhance bone marrow mesenchymal stem cells osteogenesis. *Sci Rep* **13**, 22862 (2023).

186. Ayyasamy, R. *et al.* 14-3-3ζ suppresses RANKL signaling by destabilizing TRAF6. *Journal of Biological Chemistry* **300**, (2024).

187. Naito, A. *et al.* Severe osteopetrosis, defective interleukin-1 signalling and lymph node organogenesis in TRAF6-deficient mice. *Genes Cells* **4**, 353–362 (1999).

188. Foucault, I., Liu, Y. C., Bernard, A. & Deckert, M. The Chaperone Protein 14-3-3 Interacts with 3BP2/SH3BP2 and Regulates Its Adapter Function. *Journal of Biological Chemistry* **278**, 7146–7153 (2003).

189. Levaot, N. *et al.* 3BP2-deficient mice are osteoporotic with impaired osteoblast and osteoclast functions. *The Journal of clinical investigation* **121**, 3244–3257 (2011).

190. Groza, T. *et al.* The International Mouse Phenotyping Consortium: comprehensive knockout phenotyping underpinning the study of human disease. *Nucleic Acids Research* **51**, D1038–D1045 (2023).

191. Kim, J. *et al.* 14-3-3ζ: A suppressor of inflammatory arthritis. *Proceedings of the National Academy of Sciences* **118**, e2025257118 (2021).

192. Chimen, M. *et al.* Homeostatic regulation of T cell trafficking by a B cell-derived peptide is impaired in autoimmune and chronic inflammatory disease. *Nature medicine* **21**, 467–475 (2015).

193. Nathan, P. INVESTIGATING THE PRODUCTION AND SECRETION OF PEPITEM, A REGULATOR OF LEUKOCYTE TRAFFICKING. (University of Birmingham, 2023).

194. Jin, J. *et al.* Proteomic, functional, and domain-based analysis of in vivo 14-3-3 binding proteins involved in cytoskeletal regulation and cellular organization. *Current biology : CB* **14**, 1436–1450 (2004).

195. Gardino, A. K., Smerdon, S. J. & Yaffe, M. B. Structural determinants of 14-3-3 binding specificities and regulation of subcellular localization of 14-3-3-ligand complexes: a comparison of the X-ray crystal structures of all human 14-3-3 isoforms. *Seminars in cancer biology* **16**, 173–182 (2006).

196. Kemble, S., Harford, L. E. & Mcgettrick, H. M. O013 New therapeutic avenues in rheumatoid arthritis: exploring the role of the adiponectin-pepitem axis. *Annals of the Rheumatic Diseases* **77**, A7–A7 (2018).

197. Lewis, J. W. *et al.* Therapeutic avenues in bone repair: Harnessing an anabolic osteopeptide, PEPITEM, to boost bone growth and prevent bone loss. *Cell Reports Medicine* **5**, 101574 (2024).

198. Zioupos, P., Kirchner, H. O. K. & Peterlik, H. Ageing bone fractures: The case of a ductile to brittle transition that shifts with age. *Bone* **131**, 115176 (2020).

199. Johannesdottir, F. *et al.* Age-Related Changes in Bone Density, Microarchitecture, and Strength in Postmenopausal Black and White Women: The SWAN Longitudinal HR-pQCT Study. *Journal of Bone and Mineral Research* **37**, 41–51 (2022).

200. Burr, D. B. Changes in bone matrix properties with aging. *Bone* **120**, 85–93 (2019).

201. Pignolo, R. J. *et al.* Defects in telomere maintenance molecules impair osteoblast differentiation and promote osteoporosis. *Aging Cell* **7**, 23–31 (2008).

202. Kim, H.-N. *et al.* DNA damage and senescence in osteoprogenitors expressing Osx1 may cause their decrease with age. *Aging Cell* **16**, 693–703 (2017).

203. Xu, P. *et al*. VDR activation attenuates osteoblastic ferroptosis and senescence by stimulating the Nrf2/GPX4 pathway in age-related osteoporosis. *Free Radical Biology and Medicine* **193**, 720–735 (2022).

204. Fang, C.-L., Liu, B. & Wan, M. "Bone-SASP" in Skeletal Aging. *Calcif Tissue Int* **113**, 68–82 (2023).

205. Sherk, V. D. & Rosen, C. J. Senescent and apoptotic osteocytes and aging: Exercise to the rescue? *Bone* **121**, 255–258 (2019).

206. Gorissen, B. *et al*. Hypoxia negatively affects senescence in osteoclasts and delays osteoclastogenesis. *J Cell Physiol* **234**, 414–426 (2018).

207. Chen, W. *et al*. Novel pycnodysostosis mouse model uncovers cathepsin K function as a potential regulator of osteoclast apoptosis and senescence. *Hum Mol Genet* **16**, 410–423 (2007).

208. Rose, S. & Maffulli, N. Hip fractures. An epidemiological review. *Bull Hosp Jt Dis* **58**, 197–201 (1999).

209. Cauley, J. A., Thompson, D. E., Ensrud, K. C., Scott, J. C. & Black, D. Risk of mortality following clinical fractures. *Osteoporos Int* **11**, 556–561 (2000).

210. Nieminen, S., Nurmi, M. & Satokari, K. Healing of femoral neck fractures; influence of fracture reduction and age. *Ann Chir Gynaecol* **70**, 26–31 (1981).

211. Clark, D., Nakamura, M., Miclau, T. & Marcucio, R. Effects of Aging on Fracture Healing. *Curr Osteoporos Rep* **15**, 601–608 (2017).

212. Hankenson, K. D., Zimmerman, G. & Marcucio, R. Biological perspectives of delayed fracture healing. *Injury* **45 Suppl 2**, S8–S15 (2014).

213. Kurdy, N. M., Weiss, J. B. & Bate, A. Endothelial stimulating angiogenic factor in early fracture healing. *Injury* **27**, 143–145 (1996).

214. Phillips, A. M. Overview of the fracture healing cascade. *Injury* **36 Suppl 3**, S5-7 (2005).

215. Einhorn, T. A. & Gerstenfeld, L. C. Fracture healing: mechanisms and interventions. *Nat Rev Rheumatol* **11**, 45–54 (2015).

216. Lopas, L. A. *et al.* Fractures in geriatric mice show decreased callus expansion and bone volume. *Clin Orthop Relat Res* **472**, 3523–3532 (2014).

217. Meyer, R. A. *et al.* Age and ovariectomy impair both the normalization of mechanical properties and the accretion of mineral by the fracture callus in rats. *J Orthop Res* **19**, 428–435 (2001).

218. Bergman, R. J. *et al.* Age-related changes in osteogenic stem cells in mice. *J Bone Miner Res* **11**, 568–577 (1996).

219. Baxter, M. A. *et al.* Study of telomere length reveals rapid aging of human marrow stromal cells following in vitro expansion. *Stem Cells* **22**, 675–682 (2004).

220. Nakahara, H., Goldberg, V. M. & Caplan, A. I. Culture-expanded human periosteal-derived cells exhibit osteochondral potential in vivo. *J Orthop Res* **9**, 465–476 (1991).

221. Lu, C. *et al.* Cellular basis for age-related changes in fracture repair. *J Orthop Res* **23**, 1300–1307 (2005).

222. Abou-Khalil, R. *et al.* Role of muscle stem cells during skeletal regeneration. *Stem Cells* **33**, 1501–1511 (2015).

223. Sethe, S., Scutt, A. & Stolzing, A. Aging of mesenchymal stem cells. *Ageing Res Rev* **5**, 91–116 (2006).

224. Gerstenfeld, L. C. *et al.* Impaired intramembranous bone formation during bone repair in the absence of tumor necrosis factor-alpha signaling. *Cells Tissues Organs* **169**, 285–294 (2001).

225. Schmidt-Bleek, K. *et al.* Inflammatory phase of bone healing initiates the regenerative healing cascade. *Cell Tissue Res* **347**, 567–573 (2012).

226. Thomas, M. V. & Puleo, D. A. Infection, inflammation, and bone regeneration: a paradoxical relationship. *J Dent Res* **90**, 1052–1061 (2011).

227. Varacallo, M. A. & Fox, E. J. Osteoporosis and its complications. *Med Clin North Am* **98**, 817–831, xii–xiii (2014).

228. Ilias, I., Milionis, C. & Zoumakis, E. An Overview of Glucocorticoid-Induced Osteoporosis. in *Endotext* (eds. Feingold, K. R. et al.) (MDText.com, Inc., South Dartmouth (MA), 2000).

229. Steinman, J. & Shibli-Rahhal, A. Anorexia Nervosa and Osteoporosis: Pathophysiology and Treatment. *J Bone Metab* **26**, 133–143 (2019).

230. Sherman, S. Defining the menopausal transition. *The American Journal of Medicine* **118**, 3–7 (2005).

231. WHO. Ageing and health. https://www.who.int/news-room/fact-sheets/detail/ageing-and-health#:~:text=At%20this%20time%20the%20share,2050%20to%20reach%20426%20million. (2022).

232. Rauner, M., Sipos, W. & Pietschmann, P. Age-dependent Wnt gene expression in bone and during the course of osteoblast differentiation. *Age (Dordr)* **30**, 273–282 (2008).

233. Stevens, J. R. *et al*. Wnt10b deficiency results in age-dependent loss of bone mass and progressive reduction of mesenchymal progenitor cells. *J Bone Miner Res* **25**, 2138–2147 (2010).

234. Stenderup, K., Justesen, J., Clausen, C. & Kassem, M. Aging is associated with decreased maximal life span and accelerated senescence of bone marrow stromal cells,. *Bone* **33**, 919–926 (2003).

235. Sözen, T., Özışık, L. & Başaran, N. Ç. An overview and management of osteoporosis. *Eur J Rheumatol* **4**, 46–56 (2017).

236. Melton, L. J., Achenbach, S. J., Atkinson, E. J., Therneau, T. M. & Amin, S. Long-term mortality following fractures at different skeletal sites: a population-based cohort study. *Osteoporos Int* **24**, 1689–1696 (2013).

237. Willers, C. *et al*. Osteoporosis in Europe: a compendium of country-specific reports. *Arch Osteoporos* **17**, 23 (2022).

238. Khosla, S. & Hofbauer, L. C. Osteoporosis treatment: recent developments and ongoing challenges. *Lancet Diabetes Endocrinol* **5**, 898–907 (2017).

239. Russell, R. G. G. Bisphosphonates: The first 40years. *Bone* **49**, 2–19 (2011).

240. Rogers, M. J. *et al.* Cellular and molecular mechanisms of action of bisphosphonates. *Cancer* **88**, 2961–2978 (2000).

241. Rogers, M. J., Mönkkönen, J. & Munoz, M. A. Molecular mechanisms of action of bisphosphonates and new insights into their effects outside the skeleton. *Bone* **139**, 115493 (2020).

242. Drake, M. T., Clarke, B. L. & Khosla, S. Bisphosphonates: Mechanism of Action and Role in Clinical Practice. *Mayo Clin Proc* **83**, 1032–1045 (2008).

243. Lin, J. H. Bisphosphonates: a review of their pharmacokinetic properties. *Bone* **18**, 75–85 (1996).

244. Black, D. M. *et al.* Randomised trial of effect of alendronate on risk of fracture in women with existing vertebral fractures. Fracture Intervention Trial Research Group. *Lancet* **348**, 1535–1541 (1996).

245. McClung, M. R. *et al.* Effect of risedronate on the risk of hip fracture in elderly women. Hip Intervention Program Study Group. *N Engl J Med* **344**, 333–340 (2001).

246. Harris, S. T. *et al.* Effects of risedronate treatment on vertebral and nonvertebral fractures in women with postmenopausal osteoporosis: a randomized controlled trial. Vertebral Efficacy With Risedronate Therapy (VERT) Study Group. *JAMA* **282**, 1344–1352 (1999).

247. Chesnut, C. H. *et al.* Effects of oral ibandronate administered daily or intermittently on fracture risk in postmenopausal osteoporosis. *J Bone Miner Res* **19**, 1241–1249 (2004).

248. Delmas, P. D. *et al.* Daily and intermittent oral ibandronate normalize bone turnover and provide significant reduction in vertebral fracture risk: results from the BONE study. *Osteoporos Int* **15**, 792–798 (2004).

249. Black, D. M. *et al.* Once-yearly zoledronic acid for treatment of postmenopausal osteoporosis. *N Engl J Med* **356**, 1809–1822 (2007).

250. Ahadzadeh Ardebili, A., Fu, T., Dunnewold, N., Aghajafari, F. & Billington, E. O. Bisphosphonates Preserve Bone Mineral Density and Suppress Bone Turnover Markers in Early Menopausal

Women: A Systematic Review and Meta-Analysis of Randomized Trials. *JBMR Plus* **7**, e10748 (2023).

251. Ott, S. M. Long-Term Safety of Bisphosphonates. *The Journal of Clinical Endocrinology & Metabolism* **90**, 1897–1899 (2005).
252. Simonet, W. S. *et al.* Osteoprotegerin: A Novel Secreted Protein Involved in the Regulation of Bone Density. *Cell* **89**, 309–319 (1997).
253. Kostenuik, P. J. *et al.* Denosumab, a fully human monoclonal antibody to RANKL, inhibits bone resorption and increases BMD in knock-in mice that express chimeric (murine/human) RANKL. *J Bone Miner Res* **24**, 182–195 (2009).
254. Törring, O. Effects of denosumab on bone density, mass and strength in women with postmenopausal osteoporosis. *Ther Adv Musculoskelet Dis* **7**, 88–102 (2015).
255. Watts, N. B. *et al.* Infections in postmenopausal women with osteoporosis treated with denosumab or placebo: coincidence or causal association? *Osteoporos Int* **23**, 327–337 (2012).
256. Anastasilakis, A. D. *et al.* Denosumab Discontinuation and the Rebound Phenomenon: A Narrative Review. *J Clin Med* **10**, 152 (2021).
257. Bone, H. G. *et al.* Effects of denosumab treatment and discontinuation on bone mineral density and bone turnover markers in postmenopausal women with low bone mass. *J Clin Endocrinol Metab* **96**, 972–980 (2011).
258. Miller, P. D. *et al.* Effect of denosumab on bone density and turnover in postmenopausal women with low bone mass after long-term continued, discontinued, and restarting of therapy: a randomized blinded phase 2 clinical trial. *Bone* **43**, 222–229 (2008).
259. McClung, M. R., Wagman, R. B., Miller, P. D., Wang, A. & Lewiecki, E. M. Observations following discontinuation of long-term denosumab therapy. *Osteoporos Int* **28**, 1723–1732 (2017).
260. Farias, V. *et al.* Three-year effect of bisphosphonates on bone mineral density after denosumab withdrawal: observations from a real-world study. *JBMR Plus* **8**, ziae044 (2024).

261. Stevenson, J. Prevention and treatment of osteoporosis in women. *Post Reprod Health* **29**, 11–14 (2023).

262. Manson, J. E. *et al*. The Women's Health Initiative Hormone Therapy Trials: Update and Overview of Health Outcomes During the Intervention and Post-Stopping Phases. *JAMA* **310**, 1353–1368 (2013).

263. Lufkin, E. G. *et al*. Treatment of postmenopausal osteoporosis with transdermal estrogen. *Ann Intern Med* **117**, 1–9 (1992).

264. Ryan, P. J., Harrison, R., Blake, G. M. & Fogelman, I. Compliance with hormone replacement therapy (HRT) after screening for post menopausal osteoporosis. *Br J Obstet Gynaecol* **99**, 325–328 (1992).

265. Lees, B. & Stevenson, J. C. The prevention of osteoporosis using sequential low-dose hormone replacement therapy with estradiol-17 beta and dydrogesterone. *Osteoporos Int* **12**, 251–258 (2001).

266. Lindsay, R., Gallagher, J. C., Kleerekoper, M. & Pickar, J. H. Effect of Lower Doses of Conjugated Equine Estrogens With and Without Medroxyprogesterone Acetate on Bone in Early Postmenopausal Women. *JAMA* **287**, 2668–2676 (2002).

267. Støer, N. C. *et al*. Menopausal hormone therapy and breast cancer risk: a population-based cohort study of 1.3 million women in Norway. *Br J Cancer* **131**, 126–137 (2024).

268. Osborne, C. K., Zhao, H. (Holly) & Fuqua, S. A. W. Selective Estrogen Receptor Modulators: Structure, Function, and Clinical Use. *JCO* **18**, 3172–3186 (2000).

269. Messalli, E. M. & Scaffa, C. Long-term safety and efficacy of raloxifene in the prevention and treatment of postmenopausal osteoporosis: an update. *International Journal of Women's Health* **1**, 11–20 (2010).

270. Delmas, P. D. *et al.* Efficacy of raloxifene on vertebral fracture risk reduction in postmenopausal women with osteoporosis: four-year results from a randomized clinical trial. *J Clin Endocrinol Metab* **87**, 3609–3617 (2002).

271. Ettinger, B. *et al.* Reduction of vertebral fracture risk in postmenopausal women with osteoporosis treated with raloxifene: results from a 3-year randomized clinical trial. Multiple Outcomes of Raloxifene Evaluation (MORE) Investigators. *JAMA* **282**, 637–645 (1999).

272. Lee, J. *et al.* Effect of Tamoxifen on the Risk of Osteoporosis and Osteoporotic Fracture in Younger Breast Cancer Survivors: A Nationwide Study. *Front Oncol* **10**, 366 (2020).

273. Bolognese, M. A. SERMs and SERMs with estrogen for postmenopausal osteoporosis. *Rev Endocr Metab Disord* **11**, 253–259 (2010).

274. Khan, M., Jose, A. & Sharma, S. Physiology, Parathyroid Hormone. in *StatPearls* (StatPearls Publishing, Treasure Island (FL), 2024).

275. Egbuna, O. I. & Brown, E. M. Hypercalcaemic and hypocalcaemic conditions due to calcium-sensing receptor mutations. *Best Pract Res Clin Rheumatol* **22**, 129–148 (2008).

276. Dobnig, H. & Turner, R. T. The effects of programmed administration of human parathyroid hormone fragment (1-34) on bone histomorphometry and serum chemistry in rats. *Endocrinology* **138**, 4607–4612 (1997).

277. O'Brien, C. A. *et al.* Control of bone mass and remodeling by PTH receptor signaling in osteocytes. *PLoS One* **3**, e2942 (2008).

278. Lee, S. K. & Lorenzo, J. A. Parathyroid hormone stimulates TRANCE and inhibits osteoprotegerin messenger ribonucleic acid expression in murine bone marrow cultures: correlation with osteoclast-like cell formation. *Endocrinology* **140**, 3552–3561 (1999).

279. Fu, Q., Jilka, R. L., Manolagas, S. C. & O'Brien, C. A. Parathyroid hormone stimulates receptor activator of NFkappa B ligand and inhibits osteoprotegerin expression via protein kinase A activation of cAMP-response element-binding protein. *J Biol Chem* **277**, 48868–48875 (2002).

280. Huang, J. C. *et al.* PTH differentially regulates expression of RANKL and OPG. *J Bone Miner Res* **19**, 235–244 (2004).

281. Ma, Y. L. *et al.* Catabolic effects of continuous human PTH (1--38) in vivo is associated with sustained stimulation of RANKL and inhibition of osteoprotegerin and gene-associated bone formation. *Endocrinology* **142**, 4047–4054 (2001).

282. Dempster, D. W., Cosman, F., Parisien, M., Shen, V. & Lindsay, R. Anabolic actions of parathyroid hormone on bone. *Endocr Rev* **14**, 690–709 (1993).

283. Jilka, R. L. Molecular and cellular mechanisms of the anabolic effect of intermittent PTH. *Bone* **40**, 1434–1446 (2007).

284. Kim, S. W. *et al.* Intermittent parathyroid hormone administration converts quiescent lining cells to active osteoblasts. *J Bone Miner Res* **27**, 2075–2084 (2012).

285. Wang, Y.-H., Liu, Y. & Rowe, D. W. Effects of transient PTH on early proliferation, apoptosis, and subsequent differentiation of osteoblast in primary osteoblast cultures. *Am J Physiol Endocrinol Metab* **292**, E594-603 (2007).

286. Locklin, R. M., Khosla, S., Turner, R. T. & Riggs, B. L. Mediators of the biphasic responses of bone to intermittent and continuously administered parathyroid hormone. *J Cell Biochem* **89**, 180–190 (2003).

287. Ogita, M., Rached, M. T., Dworakowski, E., Bilezikian, J. P. & Kousteni, S. Differentiation and proliferation of periosteal osteoblast progenitors are differentially regulated by estrogens and intermittent parathyroid hormone administration. *Endocrinology* **149**, 5713–5723 (2008).

288. Yu, B. *et al.* PTH Induces Differentiation of Mesenchymal Stem Cells by Enhancing BMP Signaling. *J Bone Miner Res* **27**, 2001–2014 (2012).

289. Ishizuya, T. *et al.* Parathyroid hormone exerts disparate effects on osteoblast differentiation depending on exposure time in rat osteoblastic cells. *J Clin Invest* **99**, 2961–2970 (1997).

290. Leaffer, D. *et al*. Modulation of osteogenic cell ultrastructure by RS-23581, an analog of human parathyroid hormone (PTH)-related peptide-(1-34), and bovine PTH-(1-34). *Endocrinology* **136**, 3624–3631 (1995).

291. Keller, H. & Kneissel, M. SOST is a target gene for PTH in bone. *Bone* **37**, 148–158 (2005).

292. Reeve, J. *et al*. Anabolic effect of human parathyroid hormone fragment on trabecular bone in involutional osteoporosis: a multicentre trial. *Br Med J* **280**, 1340–1344 (1980).

293. Divieti, P. *et al*. Receptors for the carboxyl-terminal region of pth(1-84) are highly expressed in osteocytic cells. *Endocrinology* **142**, 916–925 (2001).

294. Neer, R. M. *et al*. Effect of Parathyroid Hormone (1-34) on Fractures and Bone Mineral Density in Postmenopausal Women with Osteoporosis. *New England Journal of Medicine* **344**, 1434–1441 (2001).

295. Mulgund, M., Beattie, K. A., Wong, A. K. O., Papaioannou, A. & Adachi, J. D. Assessing adherence to teriparatide therapy, causes of nonadherence and effect of adherence on bone mineral density measurements in osteoporotic patients at high risk for fracture. *Therapeutic Advances in Musculoskeletal* **1**, 5–11 (2009).

296. Krege, J. H., Gilsenan, A. W., Komacko, J. L. & Kellier-Steele, N. Teriparatide and Osteosarcoma Risk: History, Science, Elimination of Boxed Warning, and Other Label Updates. *JBMR Plus* **6**, e10665 (2022).

297. Kocjan, T. *et al*. Switching to Denosumab or Bisphosphonates After Completion of Teriparatide Treatment in Women With Severe Postmenopausal Osteoporosis. *Endocrine Practice* **27**, 941–947 (2021).

298. G, H., T, D., Ba, C., H, B. & Tj, G. Binding Selectivity of Abaloparatide for PTH-Type-1-Receptor Conformations and Effects on Downstream Signaling. *Endocrinology* **157**, (2016).

299. Horwitz, M. J., Tedesco, M. B., Gundberg, C., Garcia-Ocana, A. & Stewart, A. F. Short-Term, High-Dose Parathyroid Hormone-Related Protein as a Skeletal Anabolic Agent for the Treatment of

Postmenopausal Osteoporosis. *The Journal of Clinical Endocrinology & Metabolism* **88**, 569–575 (2003).

300. Jolette, J. *et al.* Comparing the incidence of bone tumors in rats chronically exposed to the selective PTH type 1 receptor agonist abaloparatide or PTH(1–34). *Regulatory Toxicology and Pharmacology* **86**, 356–365 (2017).
301. Gold, D. T. *et al.* Treatment patterns in women with postmenopausal osteoporosis using abaloparatide: a real-world observational study. *Osteoporos Int* **35**, 1407–1415 (2024).
302. Bilezikian, J. P. *et al.* Abaloparatide in patients with mild or moderate renal impairment: results from the ACTIVE phase 3 trial. *Current Medical Research and Opinion* **35**, 2097–2102 (2019).
303. Bodenner, D., Redman, C. & Riggs, A. Teriparatide in the management of osteoporosis. *Clin Interv Aging* **2**, 499–507 (2007).
304. Lim, S. Y. & Bolster, M. B. Clinical Utility of Romosozumab in the Management of Osteoporosis: Focus on Patient Selection and Perspectives. *Int J Womens Health* **14**, 1733–1747 (2022).
305. Zhou, S. TGF-β regulates β-catenin signaling and osteoblast differentiation in human mesenchymal stem cells. *J Cell Biochem* **112**, 1651–1660 (2011).
306. Robling, A. G. *et al.* Mechanical stimulation of bone in vivo reduces osteocyte expression of Sost/sclerostin. *J Biol Chem* **283**, 5866–5875 (2008).
307. Pflanz, D. *et al.* Sost deficiency led to a greater cortical bone formation response to mechanical loading and altered gene expression. *Sci Rep* **7**, 9435 (2017).
308. Li, X. *et al.* Targeted deletion of the sclerostin gene in mice results in increased bone formation and bone strength. *J Bone Miner Res* **23**, 860–869 (2008).
309. Zhang, D. *et al.* The systemic effects of sclerostin overexpression using ΦC31 integrase in mice. *Biochem Biophys Res Commun* **472**, 471–476 (2016).

310. Brent, M. B., Brüel, A. & Thomsen, J. S. Anti-sclerostin antibodies and abaloparatide have additive effects when used as a countermeasure against disuse osteopenia in female rats. *Bone* **160**, 116417 (2022).

311. Toumi, H. *et al*. Effects of anti-sclerostin antibody and running on bone remodeling and strength. *Bone Reports* **2**, 52–58 (2015).

312. Cardinal, M. *et al*. Sclerostin-Antibody Treatment Decreases Fracture Rates in Axial Skeleton and Improves the Skeletal Phenotype in Growing oim/oim Mice. *Calcif Tissue Int* **106**, 494–508 (2020).

313. Li, X. *et al*. Sclerostin Antibody Treatment Increases Bone Formation, Bone Mass, and Bone Strength in a Rat Model of Postmenopausal Osteoporosis. *Journal of Bone and Mineral Research* **24**, 578–588 (2009).

314. Ominsky, M. S., Boyce, R. W., Li, X. & Ke, H. Z. Effects of sclerostin antibodies in animal models of osteoporosis. *Bone* **96**, 63–75 (2017).

315. Kim, S. W. *et al*. Sclerostin Antibody Administration Converts Bone Lining Cells Into Active Osteoblasts. *Journal of Bone and Mineral Research* **32**, 892–901 (2017).

316. Nioi, P. *et al*. Transcriptional Profiling of Laser Capture Microdissected Subpopulations of the Osteoblast Lineage Provides Insight Into the Early Response to Sclerostin Antibody in Rats. *Journal of Bone and Mineral Research* **30**, 1457–1467 (2015).

317. Boyce, R. *et al*. Decreased osteoprogenitor proliferation precedes attenuation of cancellous bone formation in ovariectomized rats treated with sclerostin antibody. *Bone Reports* **8**, (2018).

318. Taylor, S. *et al*. Time-dependent cellular and transcriptional changes in the osteoblast lineage associated with sclerostin antibody treatment in ovariectomized rats. *Bone* **84**, 148–159 (2016).

319. Ominsky, M. S., Niu, Q., Li, C., Li, X. & Ke, H. Z. Tissue-Level Mechanisms Responsible for the Increase in Bone Formation and Bone Volume by Sclerostin Antibody. *Journal of Bone and Mineral Research* **29**, 1424–1430 (2014).

320. Ominsky, M. S. *et al*. Two doses of sclerostin antibody in cynomolgus monkeys increases bone formation, bone mineral density, and bone strength*. *Journal of Bone and Mineral Research* **25**, 948–959 (2010).

321. Li, X. *et al*. Progressive Increases in Bone Mass and Bone Strength in an Ovariectomized Rat Model of Osteoporosis After 26 Weeks of Treatment With a Sclerostin Antibody. *Endocrinology* **155**, 4785–4797 (2014).

322. Morrell, A. E., Robinson, S. T., Ke, H. Z., Holdsworth, G. & Guo, X. E. Osteocyte mechanosensing following short-term and long-term treatment with sclerostin antibody. *Bone* **149**, 115967 (2021).

323. Romosozumab for treating severe osteoporosis | Guidance | NICE. https://www.nice.org.uk/guidance/ta791/chapter/1-Recommendations (2022).

324. Saag, K. G., Petersen, J. & Grauer, A. Romosozumab versus Alendronate and Fracture Risk in Women with Osteoporosis. *N Engl J Med* **378**, 195–196 (2018).

325. Lewiecki, E. M. *et al*. A Phase III Randomized Placebo-Controlled Trial to Evaluate Efficacy and Safety of Romosozumab in Men With Osteoporosis. *J Clin Endocrinol Metab* **103**, 3183–3193 (2018).

326. Cosman, F. *et al*. Romosozumab Treatment in Postmenopausal Women with Osteoporosis. *N Engl J Med* **375**, 1532–1543 (2016).

327. Zheng, J. *et al*. Lowering of Circulating Sclerostin May Increase Risk of Atherosclerosis and Its Risk Factors: Evidence From a Genome-Wide Association Meta-Analysis Followed by Mendelian Randomization. *Arthritis Rheumatol* **75**, 1781–1792 (2023).

328. Lems, W. F. & Raterman, H. G. Critical issues and current challenges in osteoporosis and fracture prevention. An overview of unmet needs. *Ther Adv Musculoskelet Dis* **9**, 299–316 (2017).

329. Hopkin, S. J. *et al*. Rejuvenation of leukocyte trafficking in aged mice through PEPITEM intervention. *npj Aging* **10**, 1–7 (2024).

330. Wang, L. *et al*. Therapeutic peptides: current applications and future directions. *Sig Transduct Target Ther* **7**, 1–27 (2022).

331. Apta, B. Investigating the Structure and Function of PEPITEM, a Novel Inhibitor of T cell Transmigration. (University of Birmingham, 2015).

332. Jevsevar, S., Kunstelj, M. & Porekar, V. G. PEGylation of therapeutic proteins. *Biotechnol J* **5**, 113–128 (2010).

333. Saviano, A. *et al*. PEPITEM, its tripeptide pharmacophores and their peptidomimetic analogues regulate the inflammatory response through parenteral and topical dosing in models of peritonitis and psoriasis. *Pharmacological Research* 107624 (2025) doi:10.1016/j.phrs.2025.107624.

334. Stein, M. *et al*. Why Animal Experiments Are Still Indispensable in Bone Research: A Statement by the European Calcified Tissue Society. *Journal of Bone and Mineral Research* **38**, 1045–1061 (2023).

335. Newman, E., Turner, A. S. & Wark, J. D. The potential of sheep for the study of osteopenia: current status and comparison with other animal models. *Bone* **16**, 277S-284S (1995).

336. Reichert, J. C. *et al*. The challenge of establishing preclinical models for segmental bone defect research. *Biomaterials* **30**, 2149–2163 (2009).

337. Hillier, M. L. & Bell, L. S. Differentiating Human Bone from Animal Bone: A Review of Histological Methods. *Journal of Forensic Sciences* **52**, 249–263 (2007).

338. Aerssens, J., Boonen, S., Lowet, G. & Dequeker, J. Interspecies Differences in Bone Composition, Density, and Quality: Potential Implications for in Vivo Bone Research*. *Endocrinology* **139**, 663–670 (1998).

339. den Boer, F. C. *et al*. New segmental long bone defect model in sheep: quantitative analysis of healing with dual energy x-ray absorptiometry. *J Orthop Res* **17**, 654–660 (1999).

340. Haffner-Luntzer, M. & Ignatius, A. Animal models for studying metaphyseal bone fracture healing. *eCM* **40**, 172–188 (2020).

341. Meakin, L. B., Price, J. S. & Lanyon, L. E. The Contribution of Experimental in vivo Models to Understanding the Mechanisms of Adaptation to Mechanical Loading in Bone. *Front Endocrinol (Lausanne)* **5**, 154 (2014).

342. Gomes, P. S. & Fernandes, M. H. Rodent models in bone-related research: the relevance of calvarial defects in the assessment of bone regeneration strategies - P S Gomes, M H Fernandes, 2011. https://journals.sagepub.com/doi/10.1258/la.2010.010085?url_ver=Z39.88-2003&rfr_id=ori:rid:crossref.org&rfr_dat=cr_pub%20%200pubmed#body-ref-bibr-LA-10-085C13 (2011).

343. Cancedda, R., Dozin, B., Giannoni, P. & Quarto, R. Tissue engineering and cell therapy of cartilage and bone. *Matrix Biol* **22**, 81–91 (2003).

344. Reddi, A. H. Morphogenesis and tissue engineering of bone and cartilage: inductive signals, stem cells, and biomimetic biomaterials. *Tissue Eng* **6**, 351–359 (2000).

345. Kong, Y. Y. *et al.* OPGL is a key regulator of osteoclastogenesis, lymphocyte development and lymph-node organogenesis. *Nature* **397**, 315–323 (1999).

346. Dougall, W. C. *et al.* RANK is essential for osteoclast and lymph node development. *Genes Dev* **13**, 2412–2424 (1999).

347. Li, J. *et al.* RANK is the intrinsic hematopoietic cell surface receptor that controls osteoclastogenesis and regulation of bone mass and calcium metabolism. *Proc Natl Acad Sci U S A* **97**, 1566–1571 (2000).

348. Lacey, D. L. *et al.* Osteoprotegerin ligand modulates murine osteoclast survival in vitro and in vivo. *Am J Pathol* **157**, 435–448 (2000).

349. Howe, K. *et al.* The zebrafish reference genome sequence and its relationship to the human genome. *Nature* **496**, 498–503 (2013).

350. Hur, M. *et al.* MicroCT-based phenomics in the zebrafish skeleton reveals virtues of deep phenotyping in a distributed organ system. *Elife* **6**, e26014 (2017).

351. Tonelli, F. *et al*. Zebrafish: A Resourceful Vertebrate Model to Investigate Skeletal Disorders. *Front. Endocrinol.* **11**, (2020).

352. Knopf, F. *et al*. Bone Regenerates via Dedifferentiation of Osteoblasts in the Zebrafish Fin. *Developmental Cell* **20**, 713–724 (2011).

353. Geurtzen, K. *et al*. Mature osteoblasts dedifferentiate in response to traumatic bone injury in the zebrafish fin and skull. *Development* **141**, 2225–2234 (2014).

354. Shah, A. N., Davey, C. F., Whitebirch, A. C., Miller, A. C. & Moens, C. B. Rapid reverse genetic screening using CRISPR in zebrafish. *Nat Methods* **12**, 535–540 (2015).

355. Watson, C. J. *et al*. Phenomics-Based Quantification of CRISPR-Induced Mosaicism in Zebrafish. *Cell Syst* **10**, 275-286.e5 (2020).

356. Kwon, R. Y., Watson, C. J. & Karasik, D. Using zebrafish to study skeletal genomics. *Bone* **126**, 37–50 (2019).

357. Lawrence, E. A. *et al*. The mechanical impact of col11a2 loss on joints; col11a2 mutant zebrafish show changes to joint development and function, which leads to early-onset osteoarthritis. *Philos Trans R Soc Lond B Biol Sci* **373**, 20170335 (2018).

358. Gistelinck, C. *et al*. Loss of Type I Collagen Telopeptide Lysyl Hydroxylation Causes Musculoskeletal Abnormalities in a Zebrafish Model of Bruck Syndrome. *J Bone Miner Res* **31**, 1930–1942 (2016).

359. Bellido, T. & Delgado Calle, J. Ex Vivo Organ Cultures as Models to Study Bone Biology. *JBMR Plus* **4**, e10345 (2020).

360. Cramer, E. E. A., Ito, K. & Hofmann, S. Ex vivo Bone Models and Their Potential in Preclinical Evaluation. *Curr Osteoporos Rep* **19**, 75–87 (2021).

361. Houston, D. A., Staines, K. A., MacRae, V. E. & Farquharson, C. Culture of Murine Embryonic Metatarsals: A Physiological Model of Endochondral Ossification. *J Vis Exp* 54978 (2016) doi:10.3791/54978.

362. Soucek, O. *et al.* Lithium rescues cultured rat metatarsals from dexamethasone-induced growth failure. *Pediatr Res* 1–12 (2024) doi:10.1038/s41390-024-03192-6.

363. Tong, Q., Raele, R., Bergen, D. & Hammond, C. Zebrafish Scale Regeneration In Toto and Ex Vivo Culture of Scales. *JoVE (Journal of Visualized Experiments)* e65396 (2024) doi:10.3791/65396.

364. Bakker, A. D. & Klein-Nulend, J. Osteoblast isolation from murine calvaria and long bones. *Methods Mol Biol* **816**, 19–29 (2012).

365. Soleimani, M. & Nadri, S. A protocol for isolation and culture of mesenchymal stem cells from mouse bone marrow. *Nat Protoc* **4**, 102–106 (2009).

366. Jonsson, K. B., Frost, A., Nilsson, O., Ljunghall, S. & Ljunggren, O. Three isolation techniques for primary culture of human osteoblast-like cells: a comparison. *Acta Orthop Scand* **70**, 365–373 (1999).

367. Ash, P., Loutit, J. F. & Townsend, K. M. Osteoclasts derived from haematopoietic stem cells. *Nature* **283**, 669–670 (1980).

368. Shah, K. M. *et al.* Osteocyte isolation and culture methods. *Bonekey Rep* **5**, 838 (2016).

369. Beresford, J. N., Graves, S. E. & Smoothy, C. A. Formation of mineralized nodules by bone derived cells in vitro: a model of bone formation? *Am J Med Genet* **45**, 163–178 (1993).

370. Lee, P. S. *et al.* Recapitulating bone development events in a customised bioreactor through interplay of oxygen tension, medium pH, and systematic differentiation approaches. *J Tissue Eng Regen Med* **13**, 1672–1684 (2019).

371. Borciani, G. *et al.* Co–culture systems of osteoblasts and osteoclasts: Simulating in vitro bone remodeling in regenerative approaches. *Acta Biomaterialia* **108**, 22–45 (2020).

372. Chen, S., Chen, X., Geng, Z. & Su, J. The horizon of bone organoid: A perspective on construction and application. *Bioact Mater* **18**, 15–25 (2022).

373. Scheinpflug, J. *et al.* Journey into Bone Models: A Review. *Genes (Basel)* **9**, 247 (2018).

374. Kong, Y. *et al.* Advance in the application of organoids in bone diseases. *Front. Cell Dev. Biol.* **12**, (2024).

375. Fois, M. G. *et al.* Mini-bones: miniaturized bone *in vitro* models. *Trends in Biotechnology* **42**, 910–928 (2024).

376. Kim, S. *et al.* Tissue extracellular matrix hydrogels as alternatives to Matrigel for culturing gastrointestinal organoids. *Nat Commun* **13**, 1692 (2022).

377. Finlay, M. *et al.* A detailed methodology for a three-dimensional, self-structuring bone model that supports the differentiation of osteoblasts towards osteocytes and the production of a complex collagen-rich mineralised matrix. Preprint at https://doi.org/10.12688/f1000research.130779.3 (2024).

378. Finlay, M. *et al.* Characterisation of osteoblast differentiation and activity within a self-structuring bone model. *The Journal of Bone and Mineral Research* (in review).

379. Roberts, B. C. *et al.* The longitudinal effects of ovariectomy on the morphometric, densitometric and mechanical properties in the murine tibia: A comparison between two mouse strains. *Bone* **127**, 260–270 (2019).

380. Naylor, A. J. *et al.* A Differential Role for CD248 (Endosialin) in PDGF-Mediated Skeletal Muscle Angiogenesis. *PLOS ONE* **9**, e107146 (2014).

381. Hardy, R. S. *et al.* 11 Beta-hydroxysteroid dehydrogenase type 1 regulates synovitis, joint destruction, and systemic bone loss in chronic polyarthritis. *J Autoimmun* **92**, 104–113 (2018).

382. Hemmatian, H. *et al.* Accuracy and reproducibility of mouse cortical bone microporosity as quantified by desktop microcomputed tomography. *PLOS ONE* **12**, e0182996 (2017).

383. Feldkamp, L., Davis, L. C. & Kress, J. Practical Cone-Beam Algorithm. *J. Opt. Soc. Am* **1**, 612–619 (1984).

384. Campbell, G. M. & Sophocleous, A. Quantitative analysis of bone and soft tissue by micro-computed tomography: applications to ex vivo and in vivo studies. *Bonekey Rep* **3**, 564 (2014).

385. Oliviero, S., Giorgi, M., Laud, P. J. & Dall'Ara, E. Effect of repeated in vivo microCT imaging on the properties of the mouse tibia. *PLOS ONE* **14**, e0225127 (2019).

386. Botsch, M. *et al*. Geometric Modeling Based on Polygonal Meshes. *ACM SIGGRAPH 2007 Papers - International Conference on Computer Graphics and Interactive Techniques* 1 (2007) doi:10.1145/1281500.1281640.

387. Cignoni, P. *et al*. *MeshLab: An Open-Source Mesh Processing Tool*. (The Eurographics Association, 2008).

388. Salih, M. M. Comparison between Conventional Decalcification and a Microwave-Assisted Method in Bone Tissue Affected with Mycetoma. *Biochemistry Research International* **2020**, 6561980 (2020).

389. Savi, F. M., Brierly, G. I., Baldwin, J., Theodoropoulos, C. & Woodruff, M. A. Comparison of Different Decalcification Methods Using Rat Mandibles as a Model. *J Histochem Cytochem* **65**, 705–722 (2017).

390. Ismaila, S., Ismail, M., Mahmud, R., Esmaile, M. & Abu Bakar, M. Z. Bone mass density estimation: Archimede's principle versus automatic X-ray histogram and edge detection technique in ovariectomized rats treated with germinated brown rice bioactives. *Clinical interventions in aging* **8**, 1421–31 (2013).

391. Bonucci, E. *et al*. Technical variability of bone histomorphometric measurements. *Bone Miner* **11**, 177–186 (1990).

392. Gaytan, F., Morales, C., Reymundo, C. & Tena-Sempere, M. A novel RGB-trichrome staining method for routine histological analysis of musculoskeletal tissues. *Sci Rep* **10**, 16659 (2020).

393. Rajfer, R. A. *et al*. Prevention of Osteoporosis in the Ovariectomized Rat by Oral Administration of a Nutraceutical Combination That Stimulates Nitric Oxide Production. *J Osteoporos* **2019**, 1592328 (2019).

394. Orriss, I. R., Hajjawi, M. O. R., Huesa, C., Macrae, V. E. & Arnett, T. R. Optimisation of the differing conditions required for bone formation in vitro by primary osteoblasts from mice and rats. *International Journal of Molecular Medicine* **34**, 1201–1208 (2014).

395. Kim, I. S. *et al.* Novel effect of biphasic electric current on in vitro osteogenesis and cytokine production in human mesenchymal stromal cells. *Tissue engineering. Part A* **15**, 2411–2422 (2009).

396. Kido, S. *et al.* Expression of RANK is dependent upon differentiation into the macrophage/osteoclast lineage: Induction by 1α,25-dihydroxyvitamin D 3 and TPA in a human myelomonocytic cell line, HL60. *Bone* **32**, 621–629 (2003).

397. Guo, J. *et al.* An allosteric-probe for detection of alkaline phosphatase activity and its application in immunoassay. *Frontiers in Chemistry* **6**, 618 (2018).

398. Orriss, I. R., Key, M. L., Hajjawi, M. O. R. & Arnett, T. R. Extracellular ATP Released by Osteoblasts Is A Key Local Inhibitor of Bone Mineralisation. *PLOS ONE* **8**, e69057 (2013).

399. Liu, M. *et al. Automated RNA Sample QC Using the Agilent 2200 TapeStation System*. (2014).

400. Ce, J., Ao, C. & Dk, W. Evaluation of isolation methods and RNA integrity for bacterial RNA quantitation. *Journal of microbiological methods* **75**, (2008).

401. Elbrecht, V. *et al. Testing the Potential of a Ribosomal 16S Marker for DNA Metabarcoding of Insects*. (2016). doi:10.7287/peerj.preprints.1855v1.

402. Kastanis, G. *et al.* In-Depth Comparative Analysis of Illumina ® MiSeq Run Metrics: Development of a Wet-lab Quality Assessment Tool. *Molecular Ecology Resources* **19**, (2018).

403. Babraham Bioinformatics - FastQC A Quality Control tool for High Throughput Sequence Data. https://www.bioinformatics.babraham.ac.uk/projects/fastqc/.

404. Bushnell, B. *BBMap: A Fast, Accurate, Splice-Aware Aligner*. https://www.osti.gov/biblio/1241166 (2014).

405. Dobin, A. *et al.* STAR: ultrafast universal RNA-seq aligner. *Bioinformatics* **29**, 15–21 (2013).

406. Liao, Y., Smyth, G. K. & Shi, W. featureCounts: an efficient general purpose program for assigning sequence reads to genomic features. *Bioinformatics* **30**, 923–930 (2014).

407. Liao, Y., Smyth, G. K. & Shi, W. The Subread aligner: fast, accurate and scalable read mapping by seed-and-vote. *Nucleic Acids Res* **41**, e108 (2013).

408. Ge, S. X., Son, E. W. & Yao, R. iDEP: an integrated web application for differential expression and pathway analysis of RNA-Seq data. *BMC Bioinformatics* **19**, 534 (2018).

409. Jumper, J. *et al.* Highly accurate protein structure prediction with AlphaFold. *Nature* **596**, 583–589 (2021).

410. Varadi, M. *et al.* AlphaFold Protein Structure Database: massively expanding the structural coverage of protein-sequence space with high-accuracy models. *Nucleic Acids Research* **50**, D439–D444 (2022).

411. Goddard, T. D. *et al.* UCSF ChimeraX: Meeting modern challenges in visualization and analysis. *Protein Sci* **27**, 14–25 (2018).

412. Pettersen, E. F. *et al.* UCSF ChimeraX: Structure visualization for researchers, educators, and developers. *Protein Sci* **30**, 70–82 (2021).

413. Protein complex prediction with AlphaFold-Multimer | bioRxiv. https://www.biorxiv.org/content/10.1101/2021.10.04.463034v2.full.

414. Guo, H.-B. *et al.* AlphaFold2 models indicate that protein sequence determines both structure and dynamics. *Sci Rep* **12**, 10696 (2022).

415. Mirdita, M. *et al.* ColabFold: making protein folding accessible to all. *Nat Methods* **19**, 679–682 (2022).

416. Mariani, V., Biasini, M., Barbato, A. & Schwede, T. lDDT: a local superposition-free score for comparing protein structures and models using distance difference tests. *Bioinformatics* **29**, 2722–2728 (2013).

417. Goel, P. N. *et al.* Suppression of Notch Signaling in Osteoclasts Improves Bone Regeneration and Healing. *Journal of orthopaedic research : official publication of the Orthopaedic Research Society* **37**, 2089–2103 (2019).

418. Lewis, J. W. CHARACTERISING THE THERAPEUTIC POTENTIAL OF PEPITEM IN AGE-RELATED BONE LOSS, SKELETAL REMODELLING AND REPAIR. (2022).

419. Price, S. T. *et al.* Sphingosine 1-Phosphate Receptor 2 Regulates the Migration, Proliferation, and Differentiation of Mesenchymal Stem Cells. *Int J Stem Cell Res Ther* **2**, 014 (2015).

420. Baker, B. S., Chen, Z., Larson, R. D., Bemben, M. G. & Bemben, D. A. Sex differences in bone density, geometry, and bone strength of competitive soccer players. *J Musculoskelet Neuronal Interact* **20**, 62–76 (2020).

421. Willinghamm, M. D. *et al.* Age-related changes in bone structure and strength in female and male BALB/c mice. *Calcif Tissue Int* **86**, 470–483 (2010).

422. Djuric, M. *et al.* Region-specific sex-dependent pattern of age-related changes of proximal femoral cancellous bone and its implications on differential bone fragility. *Calcif Tissue Int* **86**, 192–201 (2010).

423. Glatt, V., Canalis, E., Stadmeyer, L. & Bouxsein, M. L. Age-related changes in trabecular architecture differ in female and male C57BL/6J mice. *J Bone Miner Res* **22**, 1197–1207 (2007).

424. Callewaert, F., Sinnesael, M., Gielen, E., Boonen, S. & Vanderschueren, D. Skeletal sexual dimorphism: relative contribution of sex steroids, GH-IGF1, and mechanical loading. *J Endocrinol* **207**, 127–134 (2010).

425. Alswat, K. A. Gender Disparities in Osteoporosis. *J Clin Med Res* **9**, 382–387 (2017).

426. Parfitt, A. M. Misconceptions (2): turnover is always higher in cancellous than in cortical bone. *Bone* **30**, 807–809 (2002).

427. Finlay, M. Developing, characterising, and testing a humanised 3D in vitro bone model, capable of long-term osteocyte culture. (University of Birmingham, 2023).

428. Chimen, M. *et al.* Homeostatic regulation of T cell trafficking by a B cell-derived peptide is impaired in autoimmune and chronic inflammatory disease. *Nat Med* **21**, 467–475 (2015).

429. Frost, K. *et al.* The Species Effect: Differential Sphingosine-1-Phosphate Responses in the Bone in Human Versus Mouse. *International Journal of Molecular Sciences* **25**, 5118 (2024).

430. Mellacheruvu, D. *et al.* The CRAPome: a contaminant repository for affinity purification–mass spectrometry data. *Nat Methods* **10**, 730–736 (2013).

431. Cunningham, B. A. *et al.* Neural cell adhesion molecule: structure, immunoglobulin-like domains, cell surface modulation, and alternative RNA splicing. *Science* **236**, 799–806 (1987).

432. Skog, M. S. *et al.* Expression of neural cell adhesion molecule and polysialic acid in human bone marrow-derived mesenchymal stromal cells. *Stem Cell Research & Therapy* **7**, 113 (2016).

433. Shi, Y. *et al.* Neural cell adhesion molecule modulates mesenchymal stromal cell migration via activation of MAPK/ERK signaling. *Experimental Cell Research* **318**, 2257–2267 (2012).

434. Kim, W., Watanabe, H., Lomoio, S. & Tesco, G. Spatiotemporal processing of neural cell adhesion molecules 1 and 2 by BACE1 in vivo. *J Biol Chem* **296**, 100372 (2021).

435. Shah, C. Structural insights into membrane interaction and caveolar targeting of dynamin-like EHD2.

436. Lee, Y. S. & Chuong, C. M. Adhesion molecules in skeletogenesis: I. Transient expression of neural cell adhesion molecules (NCAM) in osteoblasts during endochondral and intramembranous ossification. *J Bone Miner Res* **7**, 1435–1446 (1992).

437. Cheng, B. F. *et al.* Neural Cell Adhesion Molecule Regulates Osteoblastic Differentiation Through Wnt/β-Catenin and PI3K-Akt Signaling Pathways in MC3T3-E1 Cells. *Frontiers in Endocrinology* **12**, 534 (2021).

438. Mao, X., Schwend, T. & Conrad, G. W. Expression and Localization of Neural Cell Adhesion Molecule and Polysialic Acid during Chick Corneal Development. *Investigative Ophthalmology & Visual Science* **53**, 1234–1243 (2012).

439. Yang, H. J. *et al.* A novel role for neural cell adhesion molecule in modulating insulin signaling and adipocyte differentiation of mouse mesenchymal stem cells. *Journal of Cell Science* **124**, 2552–2560 (2011).

440. Wang, X. *et al.* Mouse mesenchymal stem cells can support human hematopoiesis both in vitro and in vivo: the crucial role of neural cell adhesion molecule. *Haematologica* **95**, 884–891 (2010).

441. Wang, X. *et al.* Neural Cell Adhesion Molecule Contributes to Hemopoiesis-Supporting Capacity of Stromal Cell Lines. *Stem Cells* **23**, 1389–1399 (2005).

442. Roman-Roman, S. *et al.* Identification of genes regulated during osteoblastic differentiation by genome-wide expression analysis of mouse calvaria primary osteoblasts in vitro. *Bone* **32**, 474–482 (2003).

443. Wagner, W. *et al.* Adhesion of human hematopoietic progenitor cells to mesenchymal stromal cells involves CD44. *Cells Tissues Organs* **188**, 160–169 (2008).

444. Song, L. *et al.* Loss of wnt/β-catenin signaling causes cell fate shift of preosteoblasts from osteoblasts to adipocytes. *Journal of bone and mineral research : the official journal of the American Society for Bone and Mineral Research* **27**, 2344 (2012).

445. Zhang, Z., Guo, Y., Gao, X., Wang, X. & Jin, C. Role of histone methyltransferase KMT2D in BMSC osteogenesis via AKT signaling. *Regenerative Therapy* **26**, 775–782 (2024).

446. Otomo, H. *et al.* Flt-1 tyrosine kinase-deficient homozygous mice result in decreased trabecular bone volume with reduced osteogenic potential. *Bone* **40**, 1494–1501 (2007).

447. Xu, K. *et al.* SOD3 regulates FLT1 to affect bone metabolism by promoting osteogenesis and inhibiting adipogenesis through PI3K/AKT and MAPK pathways. *Free Radical Biology and Medicine* **212**, 65–79 (2024).

448. Khadilkar, S. S. Musculoskeletal Disorders and Menopause. *J Obstet Gynaecol India* **69**, 99–103 (2019).

449. Lu, D. *et al.* Temporal and Quantitative Transcriptomic Differences Define Sexual Dimorphism in Murine Postnatal Bone Aging. *JBMR Plus* **6**, e10579 (2021).

450. Collier, C. D. *et al.* Characterization of a reproducible model of fracture healing in mice using an open femoral osteotomy. *Bone Rep* **12**, 100250 (2020).

451. Kühnisch, J. *et al.* Multiscale, Converging Defects of Macro-Porosity, Microstructure and Matrix Mineralization Impact Long Bone Fragility in NF1. *PLOS ONE* **9**, e86115 (2014).

452. Ben Shoham, A. *et al.* Deposition of collagen type I onto skeletal endothelium reveals a new role for blood vessels in regulating bone morphology. *Development* **143**, 3933–3943 (2016).

453. Schini, M., Vilaca, T., Gossiel, F., Salam, S. & Eastell, R. Bone Turnover Markers: Basic Biology to Clinical Applications. *Endocrine Reviews* **44**, 417–473 (2023).

454. Welhaven, H. D. *et al.* The Cortical Bone Metabolome of C57BL/6J Mice Is Sexually Dimorphic. *JBMR Plus* **6**, e10654 (2022).

455. Choi, I. A., Umemoto, A., Mizuno, M. & Park-Min, K.-H. Bone metabolism – an underappreciated player. *npj Metab Health Dis* **2**, 1–10 (2024).

456. Zhao, H. *et al.* Integrative Bone Metabolomics—Lipidomics Strategy for Pathological Mechanism of Postmenopausal Osteoporosis Mouse Model. *Sci Rep* **8**, 16456 (2018).

457. Abe, K. & Aoki, Y. Sex differences in bone resorption in the mouse femur: A light and scanning electron-microscopic study. *Cell Tissue Res.* **255**, (1989).

458. Mun, S. H. *et al.* Sexual Dimorphism in Differentiating Osteoclast Precursors Demonstrates Enhanced Inflammatory Pathway Activation in Female Cells. *J Bone Miner Res* **36**, 1104–1116 (2021).

459. Paglia, D. N. *et al.* Runx1 Regulates Myeloid Precursor Differentiation Into Osteoclasts Without Affecting Differentiation Into Antigen Presenting or Phagocytic Cells in Both Males and Females. *Endocrinology* **157**, 3058–3069 (2016).

460. Valerio, M. S. *et al.* Sex-based differential regulation of bacterial-induced bone resorption. *J Periodontal Res* **52**, 377–387 (2017).

461. Desai, S., Lång, P., Näreoja, T., Windahl, S. H. & Andersson, G. RANKL-dependent osteoclast differentiation and gene expression in bone marrow-derived cells from adult mice is sexually dimorphic. *Bone Rep* **19**, 101697 (2023).

462. Sims, N. A. & Vrahnas, C. Regulation of cortical and trabecular bone mass by communication between osteoblasts, osteocytes and osteoclasts. *Archives of Biochemistry and Biophysics* **561**, 22–28 (2014).

463. Seeman, E. Age- and menopause-related bone loss compromise cortical and trabecular microstructure. *J Gerontol A Biol Sci Med Sci* **68**, 1218–1225 (2013).

464. Li, J. *et al.* Different bone remodeling levels of trabecular and cortical bone in response to changes in Wnt/β-catenin signaling in mice. *Journal of Orthopaedic Research* **35**, 812–819 (2017).

465. Jia, M. *et al.* Effects of constitutive β-catenin activation on vertebral bone growth and remodeling at different postnatal stages in mice. *PLoS One* **8**, e74093 (2013).

466. Tu, X. *et al.* Osteocytes mediate the anabolic actions of canonical Wnt/β-catenin signaling in bone. *Proceedings of the National Academy of Sciences* **112**, E478–E486 (2015).

467. Palacio-Mancheno, P. E., Larriera, A. I., Doty, S. B., Cardoso, L. & Fritton, S. P. 3D Assessment of Cortical Bone Porosity and Tissue Mineral Density Using High-Resolution Micro-CT: Effects of Resolution and Threshold Method. *J Bone Miner Res* **29**, 10.1002/jbmr.2012 (2014).

468. Cooper, D. M. L., Kawalilak, C. E., Harrison, K., Johnston, B. D. & Johnston, J. D. Cortical Bone Porosity: What Is It, Why Is It Important, and How Can We Detect It? *Curr Osteoporos Rep* **14**, 187–198 (2016).

469. Schneider, P., Meier, M., Wepf, R. & Müller, R. Serial FIB/SEM imaging for quantitative 3D assessment of the osteocyte lacuno-canalicular network. *Bone* **49**, 304–311 (2011).

470. Zuo, G. *et al.* Activation of HIFa Pathway in Mature Osteoblasts Disrupts the Integrity of the Osteocyte/Canalicular Network. *PLOS ONE* **10**, e0121266 (2015).

471. Hashimoto, Y. *et al.* Sphingosine-1-phosphate inhibits differentiation of C3H10T1/2 cells into adipocyte. *Mol Cell Biochem* **401**, 39–47 (2015).

472. Hashimoto, Y. *et al.* Sphingosine-1-phosphate-enhanced Wnt5a promotes osteogenic differentiation in C3H10T1/2 cells. *Cell Biology International* **40**, 1129–1136 (2016).

473. Carpio, L. C., Stephan, E., Kamer, A. & Dziak, R. Sphingolipids stimulate cell growth via MAP kinase activation in osteoblastic cells. *Prostaglandins, Leukotrienes and Essential Fatty Acids (PLEFA)* **61**, 267–273 (1999).

474. Matsuzaki, E. *et al.* Sphingosine-1-phosphate promotes the nuclear translocation of β-catenin and thereby induces osteoprotegerin gene expression in osteoblast-like cell lines. *Bone* **55**, 315–324 (2013).

475. Higashi, K. *et al.* Sphingosine-1-phosphate/S1PR2-mediated signaling triggers Smad1/5/8 phosphorylation and thereby induces Runx2 expression in osteoblasts. *Bone* **93**, 1–11 (2016).

476. Takeichi, M. Morphogenetic roles of classic cadherins. *Curr Opin Cell Biol* **7**, 619–627 (1995).

477. Overduin, M. *et al.* Solution structure of the epithelial cadherin domain responsible for selective cell adhesion. *Science* **267**, 386–389 (1995).

478. Cadwell, C. M., Su, W. & Kowalczyk, A. P. Cadherin tales: Regulation of cadherin function by endocytic membrane trafficking. *Traffic* **17**, 1262–1271 (2016).

479. Wallis, J., Moore, R., Smith, P. & Walsh, F. S. Cadherins: A review of structure and function. in *Biomembranes: A Multi-Volume Treatise* (ed. Lee, A. G.) vol. 3 127–157 (JAI, 1996).

480. Maître, J.-L. & Heisenberg, C.-P. Three Functions of Cadherins in Cell Adhesion. *Current Biology* **23**, R626–R633 (2013).

481. Donalies, M., Cramer, M., Ringwald, M. & Starzinski-Powitz, A. Expression of M-cadherin, a member of the cadherin multigene family, correlates with differentiation of skeletal muscle cells. *Proc Natl Acad Sci U S A* **88**, 8024–8028 (1991).

482. Paic, F. *et al*. Identification of Differentially Expressed Genes Between Osteoblasts and Osteocytes. *Bone* **45**, 682–692 (2009).

483. Cheng, S. L. *et al*. Human osteoblasts express a repertoire of cadherins, which are critical for BMP-2-induced osteogenic differentiation. *J Bone Miner Res* **13**, 633–644 (1998).

484. Gündüz, V., Kong, E., Bryan, C. D. & Hinds, P. W. Loss of the Retinoblastoma Tumor Suppressor Protein in Murine Calvaria Facilitates Immortalization of Osteoblast-Adipocyte Bipotent Progenitor Cells Characterized by Low Expression of N-Cadherin. *Mol Cell Biol* **32**, 2561–2569 (2012).

485. Turel, K. R. & Rao, S. G. Expression of the cell adhesion molecule E-cadherin by the human bone marrow stromal cells and its probable role in CD34(+) stem cell adhesion. *Cell Biol Int* **22**, 641–648 (1998).

486. Ferrari, S. L. *et al*. A role for N-cadherin in the development of the differentiated osteoblastic phenotype. *J Bone Miner Res* **15**, 198–208 (2000).

487. Kawaguchi, J., Kii, I., Sugiyama, Y., Takeshita, S. & Kudo, A. The Transition of Cadherin Expression in Osteoblast Differentiation from Mesenchymal Cells: Consistent Expression of Cadherin-11 in Osteoblast Lineage. *Journal of Bone and Mineral Research* **16**, 260–269 (2001).

488. Marie, P. J. *et al*. Cadherin-Mediated Cell-Cell Adhesion and Signaling in the Skeleton. *Calcif Tissue Int* **94**, 46–54 (2014).

489. Shin, C. S. *et al*. Relative abundance of different cadherins defines differentiation of mesenchymal precursors into osteogenic, myogenic, or adipogenic pathways. *J Cell Biochem* **78**, 566–577 (2000).

490. Lin, W. L., Chien, H. H. & Cho, M. I. N-cadherin expression during periodontal ligament cell differentiation in vitro. *J Periodontol* **70**, 1039–1045 (1999).

491. Cheng, S. L., Shin, C. S., Towler, D. A. & Civitelli, R. A dominant negative cadherin inhibits osteoblast differentiation. *J Bone Miner Res* **15**, 2362–2370 (2000).

492. Kii, I., Amizuka, N., Shimomura, J., Saga, Y. & Kudo, A. Cell-cell interaction mediated by cadherin-11 directly regulates the differentiation of mesenchymal cells into the cells of the osteo-lineage and the chondro-lineage. *J Bone Miner Res* **19**, 1840–1849 (2004).

493. Lai, C. F. *et al.* Accentuated ovariectomy-induced bone loss and altered osteogenesis in heterozygous N-cadherin null mice. *J Bone Miner Res* **21**, 1897–1906 (2006).

494. Greenbaum, A. M., Revollo, L. D., Woloszynek, J. R., Civitelli, R. & Link, D. C. N-cadherin in osteolineage cells is not required for maintenance of hematopoietic stem cells. *Blood* **120**, 295–302 (2012).

495. Radice, G. L. *et al.* Developmental defects in mouse embryos lacking N-cadherin. *Dev Biol* **181**, 64–78 (1997).

496. Di Benedetto, A. *et al.* N-cadherin and cadherin 11 modulate postnatal bone growth and osteoblast differentiation by distinct mechanisms. *J Cell Sci* **123**, 2640–2648 (2010).

497. Castro, C. H. M. *et al.* Targeted expression of a dominant-negative N-cadherin in vivo delays peak bone mass and increases adipogenesis. *J Cell Sci* **117**, 2853–2864 (2004).

498. Haÿ, E. *et al.* N-cadherin interacts with axin and LRP5 to negatively regulate Wnt/beta-catenin signaling, osteoblast function, and bone formation. *Mol Cell Biol* **29**, 953–964 (2009).

499. Lilien, J. & Balsamo, J. The regulation of cadherin-mediated adhesion by tyrosine phosphorylation/dephosphorylation of beta-catenin. *Curr Opin Cell Biol* **17**, 459–465 (2005).

500. Nelson, W. J. & Nusse, R. Convergence of Wnt, beta-catenin, and cadherin pathways. *Science* **303**, 1483–1487 (2004).

501. Ditlevsen, D. K., Povlsen, G. K., Berezin, V. & Bock, E. NCAM-induced intracellular signaling revisited. *J Neurosci Res* **86**, 727–743 (2008).

502. Hata, K., Maeno-Hikichi, Y., Yumoto, N., Burden, S. J. & Landmesser, L. T. Distinct Roles of Different Presynaptic and Postsynaptic NCAM Isoforms in Early Motoneuron–Myotube Interactions Required for Functional Synapse Formation. *J. Neurosci.* **38**, 498–510 (2018).

503. Polo-Parada, L., Bose, C. M., Plattner, F. & Landmesser, L. T. Distinct Roles of Different Neural Cell Adhesion Molecule (NCAM) Isoforms in Synaptic Maturation Revealed by Analysis of NCAM 180 kDa Isoform-Deficient Mice. *J. Neurosci.* **24**, 1852–1864 (2004).

504. Capkovic, K. L., Stevenson, S., Johnson, M. C., Thelen, J. J. & Cornelison, D. Neural cell adhesion molecule (NCAM) marks adult myogenic cells committed to differentiation. *Exp Cell Res* **314**, 1553–1565 (2008).

505. Bussolati, B. *et al.* Neural-cell adhesion molecule (NCAM) expression by immature and tumor-derived endothelial cells favors cell organization into capillary-like structures. *Exp Cell Res* **312**, 913–924 (2006).

506. Widelitz, R. B., Jiang, T.-X., Murray, B. A. & Chuong, C.-M. Adhesion molecules in skeletogenesis: II. Neural cell adhesion molecules mediate precartilaginous mesenchymal condensations and enhance chondrogenesis. *Journal of Cellular Physiology* **156**, 399–411 (1993).

507. Kato, J. *et al.* Contribution of neural cell adhesion molecule (NCAM) to hemopoietic system in monkeys. *Ann Hematol* **87**, 797–807 (2008).

508. Ilas, D. C. *et al.* The osteogenic commitment of CD271+CD56+ bone marrow stromal cells (BMSCs) in osteoarthritic femoral head bone. *Sci Rep* **10**, 11145 (2020).

509. Parcerisas, A. *et al.* NCAM2 Regulates Dendritic and Axonal Differentiation through the Cytoskeletal Proteins MAP2 and 14-3-3. *Cereb Cortex* **30**, 3781–3799 (2020).

510. Parcerisas, A. *et al*. New Partners Identified by Mass Spectrometry Assay Reveal Functions of NCAM2 in Neural Cytoskeleton Organization. *International Journal of Molecular Sciences* **22**, (2021).

511. Kulahin, N. & Walmod, P. S. The Neural Cell Adhesion Molecule NCAM2/OCAM/RNCAM, a Close Relative to NCAM. in *Structure and Function of the Neural Cell Adhesion Molecule NCAM* (ed. Berezin, V.) 403–420 (Springer, New York, NY, 2010). doi:10.1007/978-1-4419-1170-4_25.

512. Sanchez-Heras, E., Howell, F. V., Williams, G. & Doherty, P. The fibroblast growth factor receptor acid box is essential for interactions with N-cadherin and all of the major isoforms of neural cell adhesion molecule. *J Biol Chem* **281**, 35208–35216 (2006).

513. Francavilla, C. *et al*. The binding of NCAM to FGFR1 induces a specific cellular response mediated by receptor trafficking. *J Cell Biol* **187**, 1101–1116 (2009).

514. Kiselyov, V. V. *et al*. Structural Basis for a Direct Interaction between FGFR1 and NCAM and Evidence for a Regulatory Role of ATP. *Structure* **11**, 691–701 (2003).

515. Jacob, A. L., Smith, C., Partanen, J. & Ornitz, D. M. Fibroblast growth factor receptor 1 signaling in the osteo-chondrogenic cell lineage regulates sequential steps of osteoblast maturation. *Dev Biol* **296**, 315–328 (2006).

516. Tang, Y. *et al*. Fgfr1 deficiency in osteocytes leads to increased bone mass by enhancing Wnt/β-catenin signaling. *Bone* **174**, 116817 (2023).

517. Liu, R. *et al*. Neural cell adhesion molecule potentiates the growth of murine melanoma via β-catenin signaling by association with fibroblast growth factor receptor and glycogen synthase kinase-3β. *J Biol Chem* **286**, 26127–26137 (2011).

518. Duan, P. & Bonewald, L. The Role of the Wnt/β-catenin Signaling Pathway in Formation and Maintenance of Bone and Teeth. *Int J Biochem Cell Biol* **77**, 23–29 (2016).

519. Liu, J. *et al*. Wnt/β-catenin signalling: function, biological mechanisms, and therapeutic opportunities. *Sig Transduct Target Ther* **7**, 1–23 (2022).

520. Day, T. F., Guo, X., Garrett-Beal, L. & Yang, Y. Wnt/beta-catenin signaling in mesenchymal progenitors controls osteoblast and chondrocyte differentiation during vertebrate skeletogenesis. *Dev Cell* **8**, 739–750 (2005).

521. Glass, D. A. & Karsenty, G. Molecular bases of the regulation of bone remodeling by the canonical Wnt signaling pathway. *Curr Top Dev Biol* **73**, 43–84 (2006).

522. Silva, A. K., Yi, H., Hayes, S. H., Seigel, G. M. & Hackam, A. S. Lithium chloride regulates the proliferation of stem-like cells in retinoblastoma cell lines: a potential role for the canonical Wnt signaling pathway. *Mol Vis* **16**, 36–45 (2010).

523. Zhu, Z. *et al*. Lithium stimulates human bone marrow derived mesenchymal stem cell proliferation through GSK-3β-dependent β-catenin/Wnt pathway activation. *FEBS J* **281**, 5371–5389 (2014).

524. Li, L. *et al*. Acceleration of bone regeneration by activating Wnt/β-catenin signalling pathway via lithium released from lithium chloride/calcium phosphate cement in osteoporosis. *Sci Rep* **7**, 45204 (2017).

525. Posch, A. T. *et al*. Lithium chloride improves bone filling around implants placed in estrogen-deficient rats. *Archives of Oral Biology* **111**, 104644 (2020).

526. Clément-Lacroix, P. *et al*. Lrp5-independent activation of Wnt signaling by lithium chloride increases bone formation and bone mass in mice. *Proc Natl Acad Sci U S A* **102**, 17406–17411 (2005).

527. Loiselle, A. E., Lloyd, S. A. J., Paul, E. M., Lewis, G. S. & Donahue, H. J. Inhibition of GSK-3β Rescues the Impairments in Bone Formation and Mechanical Properties Associated with Fracture Healing in Osteoblast Selective Connexin 43 Deficient Mice. *PLOS ONE* **8**, e81399 (2013).

528. Bai, J., Xu, Y., Dieo, Y. & Sun, G. Combined low-dose LiCl and LY294002 for the treatment of osteoporosis in ovariectomized rats. *J Orthop Surg Res* **14**, 177 (2019).

529. Jin, Y. *et al*. Lithium chloride enhances bone regeneration and implant osseointegration in osteoporotic conditions. *J Bone Miner Metab* **35**, 497–503 (2017).

530. Huang, L. *et al*. Lithium chloride promotes osteogenesis and suppresses apoptosis during orthodontic tooth movement in osteoporotic model via regulating autophagy. *Bioactive Materials* **6**, 3074–3084 (2021).

531. Lewicki, M., Paez, H. & Mandalunis, P. Effect of lithium carbonate on subchondral bone in sexually mature Wistar rats. *Experimental and toxicologic pathology : official journal of the Gesellschaft fur Toxikologische Pathologie* **58**, (2006).

532. Dt, B. *et al*. Lithium inhibition of bone mineralization and osteoid formation. *The Journal of clinical investigation* **61**, (1978).

533. Harvey, B. M. *et al*. Effect of daily lithium chloride administration on bone mass and strength in growing broiler chickens,1. *Poultry Science* **94**, 296–301 (2015).

534. Henneman & Zimmerberg. Lack of effect of chronic lithium chloride on bone composition and metabolism. *Endocrinology* **94**, (1974).

535. Bellwinkel, S., Schäfer, A., Minne, H. & Ziegler, R. The effect of chronic lithium application on the mineral content of rat bone and soft tissues. *International pharmacopsychiatry* **10**, (1975).

536. Williams, L. J. *et al*. Lithium use and bone health in women with bipolar disorder: A cross-sectional study. *Acta Psychiatrica Scandinavica* **149**, 332–339 (2024).

537. Zamani, A., Omrani, G. R. & Nasab, M. M. Lithium's effect on bone mineral density. *Bone* **44**, 331–334 (2009).

538. Köhler-Forsberg, O., Rohde, C., Nierenberg, A. A. & Østergaard, S. D. Association of Lithium Treatment With the Risk of Osteoporosis in Patients With Bipolar Disorder. *JAMA Psychiatry* **79**, 454–463 (2022).

539. Bolton, J. M. *et al*. Fracture Risk From Psychotropic Medications: A Population-Based Analysis. *Journal of Clinical Psychopharmacology* **28**, 384 (2008).

540. Bolton, J. M. *et al*. Association of Mental Disorders and Related Medication Use With Risk for Major Osteoporotic Fractures. *JAMA Psychiatry* **74**, 641–648 (2017).

541. Vestergaard, P., Rejnmark, L. & Mosekilde, L. Reduced relative risk of fractures among users of lithium. *Calcif Tissue Int* **77**, 1–8 (2005).

542. Wilting, I. *et al.* Lithium use and the risk of fractures. *Bone* **40**, 1252–1258 (2007).

543. Liu, B., Wu, Q., Zhang, S. & Del Rosario, A. Lithium use and risk of fracture: a systematic review and meta-analysis of observational studies. *Osteoporos Int* **30**, 257–266 (2019).

544. Plenge, P. & Rafaelsen, O. J. Lithium effects on calcium, magnesium and phosphate in man: effects on balance, bone mineral content, faecal and urinary excretion. *Acta Psychiatr Scand* **66**, 361–373 (1982).

545. Cohen, O., Rais, T., Lepkifker, E. & Vered, I. Lithium carbonate therapy is not a risk factor for osteoporosis. *Horm Metab Res* **30**, 594–597 (1998).

546. Mak, T. W., Shek, C. C., Chow, C. C., Wing, Y. K. & Lee, S. Effects of lithium therapy on bone mineral metabolism: a two-year prospective longitudinal study. *J Clin Endocrinol Metab* **83**, 3857–3859 (1998).

547. Eren, Y., Yyldyz, M., Çivi, Y., Gündodar, D. & Özcankaya, R. P.1.175 The effects of lithium treatment on bone mineral density of bipolar patients. *European Neuropsychopharmacology* **13**, S249 (2003).

548. Su, J.-A. *et al.* Bipolar disorder and the risk of fracture: A nationwide population-based cohort study. *J Affect Disord* **218**, 246–252 (2017).

549. Wong, S. K., Chin, K.-Y. & Ima-Nirwana, S. The Skeletal-Protecting Action and Mechanisms of Action for Mood-Stabilizing Drug Lithium Chloride: Current Evidence and Future Potential Research Areas. *Front Pharmacol* **11**, 430 (2020).

550. Tian, Q. *et al.* Proteomic analysis identifies that 14-3-3ζ interacts with β-catenin and facilitates its activation by Akt. *Proceedings of the National Academy of Sciences* **101**, 15370–15375 (2004).

551. Fang, D. *et al.* PHOSPHORYLATION OF β-CATENIN BY AKT PROMOTES β -CATENIN TRANSCRIPTIONAL ACTIVITY. *J Biol Chem* **282**, 11221–11229 (2007).

552. Chang, T.-C. *et al.* 14-3-3σ Regulates β-Catenin-Mediated Mouse Embryonic Stem Cell Proliferation by Sequestering GSK-3β. *PLOS ONE* **7**, e40193 (2012).

553. Agarwal-Mawal, A. *et al.* 14-3-3 Connects Glycogen Synthase Kinase-3β to Tau within a Brain Microtubule-associated Tau Phosphorylation Complex *. *Journal of Biological Chemistry* **278**, 12722–12728 (2003).

554. Johnson, C. P. *et al.* Structural Studies of the Neural-Cell-Adhesion Molecule by X-ray and Neutron Reflectivity. *Biochemistry* **44**, 546–554 (2005).

555. Bottens, R. A. & Yamada, T. Cell-Penetrating Peptides (CPPs) as Therapeutic and Diagnostic Agents for Cancer. *Cancers (Basel)* **14**, 5546 (2022).

556. Heitz, F., Morris, M. C. & Divita, G. Twenty years of cell-penetrating peptides: from molecular mechanisms to therapeutics. *Br J Pharmacol* **157**, 195–206 (2009).

557. Xie, J. *et al.* Cell-Penetrating Peptides in Diagnosis and Treatment of Human Diseases: From Preclinical Research to Clinical Application. *Front Pharmacol* **11**, 697 (2020).

558. Schmidt, N., Mishra, A., Lai, G. H. & Wong, G. C. L. Arginine-rich cell-penetrating peptides. *FEBS Lett* **584**, 1806–1813 (2010).

559. Futaki, S., Hirose, H. & Nakase, I. Arginine-rich peptides: methods of translocation through biological membranes. *Curr Pharm Des* **19**, 2863–2868 (2013).

560. Borrelli, A., Tornesello, A. L., Tornesello, M. L. & Buonaguro, F. M. Cell Penetrating Peptides as Molecular Carriers for Anti-Cancer Agents. *Molecules* **23**, 295 (2018).

561. Xu, J. *et al.* Cell-penetrating peptide: a means of breaking through the physiological barriers of different tissues and organs. *Journal of Controlled Release* **309**, 106–124 (2019).

562. Cummings, S. R. *et al.* Denosumab for Prevention of Fractures in Postmenopausal Women with Osteoporosis. *New England Journal of Medicine* **361**, 756–765 (2009).

563. Feng, X. & McDonald, J. M. Disorders of Bone Remodeling. *Annu Rev Pathol* **6**, 121–145 (2011).

564. Matsuo, K. & Irie, N. Osteoclast-osteoblast communication. *Archives of biochemistry and biophysics* **473**, 201–209 (2008).

565. Matsuo, K. & Otaki, N. Bone cell interactions through Eph/ephrin. *Cell Adh Migr* **6**, 148–156 (2012).

566. Kim, J.-M., Lin, C., Stavre, Z., Greenblatt, M. B. & Shim, J.-H. Osteoblast-Osteoclast Communication and Bone Homeostasis. *Cells* **9**, 2073 (2020).

567. Bucay, N. *et al*. osteoprotegerin-deficient mice develop early onset osteoporosis and arterial calcification. *Genes Dev* **12**, 1260–1268 (1998).

568. Udagawa, N. *et al*. Osteoclast differentiation by RANKL and OPG signaling pathways. *Journal of bone and mineral metabolism* **39**, 19–26 (2021).

569. Lacey, D. L. *et al*. Osteoprotegerin ligand is a cytokine that regulates osteoclast differentiation and activation. *Cell* **93**, 165–176 (1998).

570. Wahid, M. *et al*. PEPITEM switches off the production of pro-inflammatory mediators to limit leukocyte trafficking into the inflamed joint. *World Congress Inflammation 2024 Absract* (2024).

571. Negishi-Koga, T. *et al*. Suppression of bone formation by osteoclastic expression of semaphorin 4D. *Nat Med* **17**, 1473–1480 (2011).

572. Chen, X. *et al*. Osteoblast–osteoclast interactions. *Connective Tissue Research* **59**, 99–107 (2018).

573. Hayashi, M. *et al*. Osteoprotection by semaphorin 3A. *Nature* **485**, 69–74 (2012).

574. Takahashi, T. & Strittmatter, S. M. PlexinA1 Autoinhibition by the Plexin Sema Domain. *Neuron* **29**, 429–439 (2001).

575. Toyofuku, T. *et al*. FARP2 triggers signals for Sema3A-mediated axonal repulsion. *Nat Neurosci* **8**, 1712–1719 (2005).

576. Zhao, C. *et al*. Bidirectional ephrinB2-EphB4 signaling controls bone homeostasis. *Cell Metabolism* **4**, 111–121 (2006).

577. Fu, W. *et al.* TNFR2/14-3-3ε signaling complex instructs macrophage plasticity in inflammation and autoimmunity. *J Clin Invest* **131**, e144016.

578. Dou, C. *et al.* Estrogen Deficiency–Mediated M2 Macrophage Osteoclastogenesis Contributes to M1/M2 Ratio Alteration in Ovariectomized Osteoporotic Mice. *Journal of Bone and Mineral Research* **33**, 899–908 (2018).

579. Wang, X. *et al.* Isobavachalcone prevents osteoporosis by suppressing activation of ERK and NF-κB pathways and M1 polarization of macrophages. *International Immunopharmacology* **94**, 107370 (2021).

580. Liu, L. *et al.* Inhibition of NF-κB and ERK signaling pathways in osteoclasts and M1 macrophage polarization: Mechanistic insights into the anti-osteoporotic effects of Pseudolaric acid B. *Life Sciences* **345**, 122592 (2024).

581. Wang, W., Liu, H., Liu, T., Yang, H. & He, F. Insights into the Role of Macrophage Polarization in the Pathogenesis of Osteoporosis. *Oxidative Medicine and Cellular Longevity* **2022**, 2485959 (2022).

582. Takase, N. *et al.* NCAM- and FGF-2-mediated FGFR1 signaling in the tumor microenvironment of esophageal cancer regulates the survival and migration of tumor-associated macrophages and cancer cells. *Cancer Letters* **380**, 47–58 (2016).

583. Hill, T. P., Später, D., Taketo, M. M., Birchmeier, W. & Hartmann, C. Canonical Wnt/β-Catenin Signaling Prevents Osteoblasts from Differentiating into Chondrocytes. *Developmental Cell* **8**, 727–738 (2005).

584. Glass, D. A. *et al.* Canonical Wnt Signaling in Differentiated Osteoblasts Controls Osteoclast Differentiation. *Developmental Cell* **8**, 751–764 (2005).

585. Holmen, S. L. *et al.* Essential role of beta-catenin in postnatal bone acquisition. *J Biol Chem* **280**, 21162–21168 (2005).

586. Kramer, I. *et al.* Osteocyte Wnt/beta-catenin signaling is required for normal bone homeostasis. *Mol Cell Biol* **30**, 3071–3085 (2010).

587. Baron, R. & Kneissel, M. WNT signaling in bone homeostasis and disease: from human mutations to treatments. *Nat Med* **19**, 179–192 (2013).

588. Maeda, K., Takahashi, N. & Kobayashi, Y. Roles of Wnt signals in bone resorption during physiological and pathological states. *J Mol Med (Berl)* **91**, 15–23 (2013).

589. Sapir-Koren, R. & Livshits, G. Osteocyte control of bone remodeling: is sclerostin a key molecular coordinator of the balanced bone resorption-formation cycles? *Osteoporos Int* **25**, 2685–2700 (2014).

590. Gitlin, M. Lithium side effects and toxicity: prevalence and management strategies. *Int J Bipolar Disord* **4**, 27 (2016).

591. Proell, V. *et al.* Orchiectomy upregulates free soluble RANKL in bone marrow of aged rats. *Bone* **45**, 677–681 (2009).

592. Li, X. *et al.* Increased RANK ligand in bone marrow of orchiectomized rats and prevention of their bone loss by the RANK ligand inhibitor osteoprotegerin. *Bone* **45**, 669–676 (2009).

593. Eghbali-Fatourechi, G. *et al.* Role of RANK ligand in mediating increased bone resorption in early postmenopausal women. *J Clin Invest* **111**, 1221–1230 (2003).

594. Fujiwara, Y. *et al.* RANKL (Receptor Activator of NFκB Ligand) Produced by Osteocytes Is Required for the Increase in B Cells and Bone Loss Caused by Estrogen Deficiency in Mice. *J Biol Chem* **291**, 24838–24850 (2016).

595. Ikeda, T., Utsuyama, M. & Hirokawa, K. Expression profiles of receptor activator of nuclear factor kappaB ligand, receptor activator of nuclear factor kappaB, and osteoprotegerin messenger RNA in aged and ovariectomized rat bones. *J Bone Miner Res* **16**, 1416–1425 (2001).

596. Franklin, M. *et al.* Dried plum prevents bone loss in a male osteoporosis model via IGF-I and the RANK pathway. *Bone* **39**, 1331–1342 (2006).

597. Fischer, V. *et al.* Role of Mast-Cell-Derived RANKL in Ovariectomy-Induced Bone Loss in Mice. *Int J Mol Sci* **24**, 9135 (2023).

598. Sunyer, T., Lewis, J., Collin-Osdoby, P. & Osdoby, P. Estrogen's bone-protective effects may involve differential IL-1 receptor regulation in human osteoclast-like cells. *J Clin Invest* **103**, 1409–1418 (1999).

599. Miyaura, C. *et al.* Endogenous bone-resorbing factors in estrogen deficiency: Cooperative effects of IL-1 and IL-6. *Journal of Bone and Mineral Research* **10**, 1365–1373 (1995).

600. Hofbauer, L. C. *et al.* Estrogen stimulates gene expression and protein production of osteoprotegerin in human osteoblastic cells. *Endocrinology* **140**, 4367–4370 (1999).

601. Streicher, C. *et al.* Estrogen Regulates Bone Turnover by Targeting RANKL Expression in Bone Lining Cells. *Scientific Reports* **7**, (2017).

602. Pierroz, D. D. *et al.* Are osteoclasts needed for the bone anabolic response to parathyroid hormone? A study of intermittent parathyroid hormone with denosumab or alendronate in knock-in mice expressing humanized RANKL. *J Biol Chem* **285**, 28164–28173 (2010).

603. McClung, M. R. *et al.* Denosumab in postmenopausal women with low bone mineral density. *N Engl J Med* **354**, 821–831 (2006).

604. Xiong, J. *et al.* Soluble RANKL contributes to osteoclast formation in adult mice but not ovariectomy-induced bone loss. *Nat Commun* **9**, 2909 (2018).

605. Zhang, T. *et al.* Aging Influences Fracture Healing on the Cellular Level and Alters Systemic RANKL and OPG Concentrations in a Murine Model. *Advanced Biology* **n/a**, 2300653 (2024).

606. Cao, J., Venton, L., Sakata, T. & Halloran, B. P. Expression of RANKL and OPG Correlates With Age-Related Bone Loss in Male C57BL/6 Mice. *Journal of Bone and Mineral Research* **18**, 270–277 (2003).

607. Piemontese, M., Xiong, J., Fujiwara, Y., Thostenson, J. D. & O'Brien, C. A. Cortical bone loss caused by glucocorticoid excess requires RANKL production by osteocytes and is associated with reduced OPG expression in mice. *American Journal of Physiology-Endocrinology and Metabolism* **311**, E587–E593 (2016).

608. T, N. *et al*. Insulinogenic sucrose+amino acid mixture ingestion immediately after resistance exercise has an anabolic effect on bone compared with non-insulinogenic fructose+amino acid mixture in growing rats. *Bone* **65**, (2014).

609. A, T., M, G., R, R., D, L. & Y, S. Endurance exercise and growth hormone improve bone formation in young and growth-retarded chronic kidney disease rats. *Nephrology, dialysis, transplantation : official publication of the European Dialysis and Transplant Association - European Renal Association* **31**, (2016).

610. Pichler, K. *et al*. RANKL is downregulated in bone cells by physical activity (treadmill and vibration stimulation training) in rat with glucocorticoid-induced osteoporosis. *Histol Histopathol* **28**, 1185–1196 (2013).

611. Scott, J. P. R. *et al*. The role of exercise intensity in the bone metabolic response to an acute bout of weight-bearing exercise. *J Appl Physiol (1985)* **110**, 423–432 (2011).

612. Kish, K., Mezil, Y., Ward, W. E., Klentrou, P. & Falk, B. Effects of plyometric exercise session on markers of bone turnover in boys and young men. *Eur J Appl Physiol* **115**, 2115–2124 (2015).

613. Bergström, I., Parini, P., Gustafsson, S. A., Andersson, G. & Brinck, J. Physical training increases osteoprotegerin in postmenopausal women. *J Bone Miner Metab* **30**, 202–207 (2012).

614. Mezil, Y. A. *et al*. Response of Bone Turnover Markers and Cytokines to High-Intensity Low-Impact Exercise. *Med Sci Sports Exerc* **47**, 1495–1502 (2015).

615. Esen, H. *et al*. Do walking programs affect C-reactive protein, osteoprotegerin and soluble receptor activator of nuclear factor-kappaβ ligand? *Turkish Journal of Biochemistry* **34**, 178–186 (2009).

616. Park, D. H. The Effects of Exercise Intensity Difference on Bone Metabolic Markers and Cytokines of the RANKL/RANK/OPG System in Korean Osteopenia Elderly Women. *Exercise Science* **26**, 87–95 (2017).

617. Kim, J., Kim, H.-J. & Kim, C.-S. Effects of 12-week combined exercise on RANKL/RANK/OPG signaling and bone-resorption cytokines in healthy college females. *J Exerc Nutrition Biochem* **23**, 13–20 (2019).

618. Marques, E. A. *et al*. Response of bone mineral density, inflammatory cytokines, and biochemical bone markers to a 32-week combined loading exercise programme in older men and women. *Arch Gerontol Geriatr* **57**, 226–233 (2013).

619. Marques, E. A. *et al*. Effects of resistance and aerobic exercise on physical function, bone mineral density, OPG and RANKL in older women. *Experimental Gerontology* **46**, 524–532 (2011).

620. Omiya, T. *et al*. Sustained anti-osteoporotic action of risedronate compared to anti-RANKL antibody following discontinuation in ovariectomized mice. *Bone Rep* **13**, 100289 (2020).

621. Elbers, L. P. B., Raterman, H. G. & Lems, W. F. Bone Mineral Density Loss and Fracture Risk After Discontinuation of Anti-osteoporotic Drug Treatment: A Narrative Review. *Drugs* **81**, 1645–1655 (2021).

622. Maré, A. D., D'Haese, P. C. & Verhulst, A. The Role of Sclerostin in Bone and Ectopic Calcification. *Int J Mol Sci* **21**, 3199 (2020).

623. Rosenfeld, L. Insulin: discovery and controversy. *Clin Chem* **48**, 2270–2288 (2002).

624. Quianzon, C. C. & Cheikh, I. History of insulin. *J Community Hosp Intern Med Perspect* **2**, 10.3402/jchimp.v2i2.18701 (2012).

625. Otvos, L. & Wade, J. D. Big peptide drugs in a small molecule world. *Front. Chem.* **11**, (2023).

626. Barman, P. *et al*. Strategic Approaches to Improvise Peptide Drugs as Next Generation Therapeutics. *Int J Pept Res Ther* **29**, 61 (2023).

627. Cabri, W. *et al*. Therapeutic Peptides Targeting PPI in Clinical Development: Overview, Mechanism of Action and Perspectives. *Front Mol Biosci* **8**, 697586 (2021).

628. Augustine, M. & Horwitz, M. J. Parathyroid Hormone and Parathyroid Hormone-related Protein Analogs as Therapies for Osteoporosis. *Curr Osteoporos Rep* **11**, 10.1007/s11914-013-0171–2 (2013).

629. Vyas, D. Identifying the core functional motif of the novel immune regulatory peptide, PEPITEM. (University of Birmingham, 2017).

630. Lefèvre, F., Rémy, M.-H. & Masson, J.-M. Alanine-stretch scanning mutagenesis: a simple and efficient method to probe protein structure and function. *Nucleic Acids Research* **25**, 447–448 (1997).

631. Hosono, Y. *et al.* Amide-to-ester substitution as a stable alternative to N-methylation for increasing membrane permeability in cyclic peptides. *Nat Commun* **14**, 1416 (2023).

632. Cummins, P. M. & O'Connor, B. Pyroglutamyl peptidase: an overview of the three known enzymatic forms. *Biochim Biophys Acta* **1429**, 1–17 (1998).

633. Awadé, A. C., Cleuziat, P., Gonzalès, T. & Robert-Baudouy, J. Pyrrolidone carboxyl peptidase (Pcp): an enzyme that removes pyroglutamic acid (pGlu) from pGlu-peptides and pGlu-proteins. *Proteins* **20**, 34–51 (1994).

634. Feng, Z. & Xu, B. Inspiration from the mirror: D-amino acid containing peptides in biomedical approaches. *Biomolecular concepts* **7**, 179 (2016).

635. du Sert, N. P. *et al.* The Experimental Design Assistant. *Nat Methods* **14**, 1024–1025 (2017).

636. Sert, N. P. du *et al.* The Experimental Design Assistant. *PLOS Biology* **15**, e2003779 (2017).

637. Bradford, P. G., Gerace, K. V., Roland, R. L. & Chrzan, B. G. Estrogen Regulation of Apoptosis in Osteoblasts. *Physiol Behav* **99**, 181–185 (2010).

638. Levasseur, R. *et al.* Reversible Skeletal Abnormalities in γ-Glutamyl Transpeptidase-Deficient Mice. *Endocrinology* **144**, 2761–2764 (2003).

639. Zhu, G., Zhang, H., Xia, M., Liu, Y. & Li, M. EH domain-containing protein 2 (EHD2): Overview, biological function, and therapeutic potential. *Cell Biochem Funct* **42**, e4016 (2024).

640. Morhayim, J. *et al*. Proteomic signatures of extracellular vesicles secreted by nonmineralizing and mineralizing human osteoblasts and stimulation of tumor cell growth. *The FASEB Journal* **29**, 274–285 (2015).

641. Hernández-Martínez, R., Ramkumar, N. & Anderson, K. V. p120-catenin regulates WNT signaling and EMT in the mouse embryo. *Proceedings of the National Academy of Sciences* **116**, 16872–16881 (2019).

642. Mbalaviele, G., Shin, C. S. & Civitelli, R. Cell-cell adhesion and signaling through cadherins: connecting bone cells in their microenvironment. *J Bone Miner Res* **21**, 1821–1827 (2006).

643. Guntur, A. R., Rosen, C. J. & Naski, M. C. N-cadherin adherens junctions mediate osteogenesis through PI3K signaling. *Bone* **50**, 54–62 (2012).

644. Using insulin | Information for the public | Type 1 diabetes in adults: diagnosis and management | Guidance | NICE. https://www.nice.org.uk/guidance/ng17/ifp/chapter/using-insulin (2015).

645. Teriparatide | Drugs | BNF content published by NICE. https://bnf.nice.org.uk/drugs/teriparatide/.

646. Gao, Y., Joshi, M., Zhao, Z. & Mitragotri, S. PEGylated therapeutics in the clinic. *Bioeng Transl Med* **9**, e10600 (2023).

647. Abuchowski, A., van Es, T., Palczuk, N. C. & Davis, F. F. Alteration of immunological properties of bovine serum albumin by covalent attachment of polyethylene glycol. *J Biol Chem* **252**, 3578–3581 (1977).

648. Rosa, R. G. & Goldani, L. Z. Cohort study of the impact of time to antibiotic administration on mortality in patients with febrile neutropenia. *Antimicrob Agents Chemother* **58**, 3799–3803 (2014).

649. Kuderer, N. M., Dale, D. C., Crawford, J., Cosler, L. E. & Lyman, G. H. Mortality, morbidity, and cost associated with febrile neutropenia in adult cancer patients. *Cancer* **106**, 2258–2266 (2006).

650. Yang, B.-B. & Kido, A. Pharmacokinetics and Pharmacodynamics of Pegfilgrastim. *Clin Pharmacokinet* **50**, 295–306 (2011).

651. Zamboni, W. C. Pharmacokinetics of pegfilgrastim. *Pharmacotherapy* **23**, 9S-14S (2003).

652. Ravangard, R., Bordbar, N., Keshavarz, K. & Dehghani, M. Pegfilgrastim Versus Filgrastim for Primary Prophylaxis of Febrile Neutropenia in Patients with non-Hodgkin's Lymphoma: A Cost-Effectiveness Study. *Asian Pac J Cancer Prev* **18**, 2703–2708 (2017).

653. Pezhman, L. *et al.* PEPITEM modulates leukocyte trafficking to reduce obesity-induced inflammation. *Clin Exp Immunol* **212**, 1–10 (2023).

654. Collins, C. J. *et al.* Bone Micro- and Nanomechanics. in *Encyclopedia of Biomedical Engineering* (ed. Narayan, R.) 22–44 (Elsevier, Oxford, 2019). doi:10.1016/B978-0-12-801238-3.99937-9.

655. Hu, H. *et al.* Sequential roles of Hedgehog and Wnt signaling in osteoblast development. *Development* **132**, 49–60 (2005).

656. Rodda, S. J. & McMahon, A. P. Distinct roles for Hedgehog and canonical Wnt signaling in specification, differentiation and maintenance of osteoblast progenitors. *Development* **133**, 3231–3244 (2006).

657. Jiao, Z. *et al.* SOST gene suppression stimulates osteocyte Wnt/β-catenin signaling to prevent bone resorption and attenuates particle-induced osteolysis. *J Mol Med* **101**, 607–620 (2023).

658. Burggren, W. W. *et al.* Comparative cardiovascular physiology: future trends, opportunities and challenges. *Acta Physiol (Oxf)* **210**, 257–276 (2014).

659. Watson, E. C. & Adams, R. H. Biology of Bone: The Vasculature of the Skeletal System. *Cold Spring Harb Perspect Med* **8**, a031559 (2018).

660. Filipowska, J., Tomaszewski, K. A., Niedźwiedzki, Ł., Walocha, J. A. & Niedźwiedzki, T. The role of vasculature in bone development, regeneration and proper systemic functioning. *Angiogenesis* **20**, 291–302 (2017).

661. Tomlinson, R. E. & Silva, M. J. Skeletal Blood Flow in Bone Repair and Maintenance. *Bone Res* **1**, 311–322 (2013).

662. Charkes, N. D., Makler, P. T. & Philips, C. Studies of skeletal tracer kinetics. I. Digital-computer solution of a five-compartment model of [18F] fluoride kinetics in humans. *J Nucl Med* **19**, 1301–1309 (1978).

663. Gross, P. M., Marcus, M. L. & Heistad, D. D. Measurement of blood flow to bone and marrow in experimental animals by means of the microsphere technique. *J Bone Joint Surg Am* **63**, 1028–1031 (1981).

664. Liu, X., Zhang, P., Gu, Y., Guo, Q. & Liu, Y. Type H vessels: functions in bone development and diseases. *Front Cell Dev Biol* **11**, 1236545 (2023).

665. Chen, K. *et al.* Osteoblast-derived EGFL6 couples angiogenesis to osteogenesis during bone repair. *Theranostics* **11**, 9738–9751 (2021).

666. Street, J. *et al.* Vascular endothelial growth factor stimulates bone repair by promoting angiogenesis and bone turnover. *Proc Natl Acad Sci U S A* **99**, 9656–9661 (2002).

667. Maes, C. *et al.* Osteoblast precursors, but not mature osteoblasts, move into developing and fractured bones along with invading blood vessels. *Dev Cell* **19**, 329–344 (2010).

668. Huang, C. *et al.* Spatiotemporal Analyses of Osteogenesis and Angiogenesis via Intravital Imaging in Cranial Bone Defect Repair. *J Bone Miner Res* **30**, 1217–1230 (2015).

669. Khan, K. A. *et al.* Multimerin-2 is a ligand for group 14 family C-type lectins CLEC14A, CD93 and CD248 spanning the endothelial pericyte interface. *Oncogene* **36**, 6097–6108 (2017).

670. Neag, G. *et al.* Type-H endothelial cell protein Clec14a orchestrates osteoblast activity during trabecular bone formation and patterning. (2024).

671. Neag, G. TARGETING THE NOVEL CD248-MMRN2-CLEC14A PATHWAY IN AGE-RELATED BONE LOSS. (University of Birmingham, 2022).

672. Naylor, A. J. *et al.* The Mesenchymal Stem Cell Marker CD248 (Endosialin) Is a Negative Regulator of Bone Formation in Mice. *Arthritis Rheum* **64**, 3334–3343 (2012).

673. Movérare-Skrtic, S. *et al*. Osteoblast-derived WNT16 represses osteoclastogenesis and prevents cortical bone fragility fractures. *Ulf H Lerner 1* **16**, 19–19 (2014).

674. Wang, L. *et al*. Osteoblast-induced osteoclast apoptosis by fas ligand/FAS pathway is required for maintenance of bone mass. *Cell Death Differ* **22**, 1654–1664 (2015).

675. Champagne, C. M., Takebe, J., Offenbacher, S. & Cooper, L. F. Macrophage cell lines produce osteoinductive signals that include bone morphogenetic protein-2. *Bone* **30**, 26–31 (2002).

676. Assoian, R. K. *et al*. Expression and secretion of type beta transforming growth factor by activated human macrophages. *Proc Natl Acad Sci U S A* **84**, 6020–6024 (1987).

677. Nakashima, T., Hayashi, M. & Takayanagi, H. New insights into osteoclastogenic signaling mechanisms. *Trends in Endocrinology & Metabolism* **23**, 582–590 (2012).

678. Takayanagi, H. Osteoimmunology: shared mechanisms and crosstalk between the immune and bone systems. *Nat Rev Immunol* **7**, 292–304 (2007).

679. Zhao, Z. *et al*. TNF Induction of NF-κB RelB Enhances RANKL-Induced Osteoclastogenesis by Promoting Inflammatory Macrophage Differentiation but also Limits It through Suppression of NFATc1 Expression. *PLoS One* **10**, e0135728 (2015).

680. Weitzmann, M. N. & Pacifici, R. Estrogen deficiency and bone loss: an inflammatory tale. *J Clin Invest* **116**, 1186–1194 (2006).

681. Nakamura, T. *et al*. Estrogen prevents bone loss via estrogen receptor alpha and induction of Fas ligand in osteoclasts. *Cell* **130**, 811–823 (2007).

682. Krum, S. A. *et al*. Estrogen protects bone by inducing Fas ligand in osteoblasts to regulate osteoclast survival. *EMBO J* **27**, 535–545 (2008).

683. Martin-Millan, M. *et al*. The Estrogen Receptor-α in Osteoclasts Mediates the Protective Effects of Estrogens on Cancellous But Not Cortical Bone. *Mol Endocrinol* **24**, 323–334 (2010).

684. Chen, J.-R. *et al*. Transient versus sustained phosphorylation and nuclear accumulation of ERKs underlie anti-versus pro-apoptotic effects of estrogens. *J Biol Chem* **280**, 4632–4638 (2005).

685. Li, Z., Kuhn, G., Schirmer, M., Müller, R. & Ruffoni, D. Impaired bone formation in ovariectomized mice reduces implant integration as indicated by longitudinal in vivo micro-computed tomography. *PLOS ONE* **12**, e0184835 (2017).

686. Watkins, M. P. *et al.* Bisphosphonates improve trabecular bone mass and normalize cortical thickness in ovariectomized, osteoblast connexin43 deficient mice. *Bone* **51**, 787–794 (2012).

687. Andersson, N., Lindberg, M. K., Ohlsson, C., Andersson, K. & Ryberg, B. Repeated in vivo determinations of bone mineral density during parathyroid hormone treatment in ovariectomized mice. (2001) doi:10.1677/joe.0.1700529.

688. Roberts, B. C. *et al.* PTH(1–34) treatment and/or mechanical loading have different osteogenic effects on the trabecular and cortical bone in the ovariectomized C57BL/6 mouse. *Sci Rep* **10**, 8889 (2020).

689. Alexander, J. M. *et al.* Human Parathyroid Hormone 1–34 Reverses Bone Loss in Ovariectomized Mice. *Journal of Bone and Mineral Research* **16**, 1665–1673 (2001).

690. Shim, J., Iwaya, C., Ambrose, C. G., Suzuki, A. & Iwata, J. Micro-computed tomography assessment of bone structure in aging mice. *Scientific Reports* **12**, (2022).

691. Camargos, G. V. *et al.* Mechanical competence of ovariectomy-induced compromised bone after single or combined treatment with high-frequency loading and bisphosphonates. *Sci Rep* **5**, 10795 (2015).

692. Mastaglia, S. R. *et al.* Vitamin D insufficiency reduces the protective effect of bisphosphonate on ovariectomy-induced bone loss in rats. *Bone* **39**, 837–844 (2006).

693. Seedor, J. G., Quartuccio, H. A. & Thompson, D. D. The bisphosphonate alendronate (MK-217) inhibits bone loss due to ovariectomy in rats. *J Bone Miner Res* **6**, 339–346 (1991).

694. Chen, J. *et al.* PTHG2 Reduces Bone Loss in Ovariectomized Mice by Directing Bone Marrow Mesenchymal Stem Cell Fate. *Stem Cells International* **2021**, 8546739 (2021).

695. Omiya, T. *et al*. The effect of switching from teriparatide to anti-RANKL antibody on cancellous and cortical bone in ovariectomized mice. *Bone* **107**, 18–26 (2018).

696. Xiong, J. & O'Brien, C. A. Osteocyte RANKL: New Insights into the Control of Bone Remodeling. *Journal of bone and mineral research : the official journal of the American Society for Bone and Mineral Research* **27**, 499–499 (2012).

697. Wein, M. N. & Kronenberg, H. M. Regulation of Bone Remodeling by Parathyroid Hormone. *Cold Spring Harb Perspect Med* **8**, a031237 (2018).

698. Stolina, M. *et al*. Temporal changes in systemic and local expression of bone turnover markers during six months of sclerostin antibody administration to ovariectomized rats. *Bone* **67**, (2014).

699. McDonald, M. M. *et al*. Inhibition of sclerostin by systemic treatment with sclerostin antibody enhances healing of proximal tibial defects in ovariectomized rats. *Journal of Orthopaedic Research* **30**, 1541–1548 (2012).

700. Li, S. *et al*. Sclerostin Antibody Mitigates Estrogen Deficiency-Inducted Marrow Lipid Accumulation Assessed by Proton MR Spectroscopy. *Front. Endocrinol.* **10**, (2019).

701. Florio, M. *et al*. A bispecific antibody targeting sclerostin and DKK-1 promotes bone mass accrual and fracture repair. *Nat Commun* **7**, 11505 (2016).

702. Kim, B.-J. *et al*. TNF-α mediates the stimulation of sclerostin expression in an estrogen-deficient condition. *Biochemical and Biophysical Research Communications* **424**, 170–175 (2012).

703. Fujita, K. *et al*. Effects of Estrogen on Bone mRNA Levels of Sclerostin and Other Genes Relevant to Bone Metabolism in Postmenopausal Women. *J Clin Endocrinol Metab* **99**, E81–E88 (2014).

704. Li, X. *et al*. Sclerostin Antibody Reverses Bone Loss by Increasing Bone Formation and Decreasing Bone Resorption in a Rat Model of Male Osteoporosis. *Endocrinology* **159**, 260–271 (2018).

705. Wang, A. *et al*. Effect of androgen deprivation therapy on serum levels of sclerostin, Dickkopf-1, and osteoprotegerin: a cross-sectional and longitudinal analysis. *Sci Rep* **11**, 14905 (2021).

706. Sinder, B. P. *et al.* Rapidly growing Brtl/+ mouse model of osteogenesis imperfecta improves bone mass and strength with sclerostin antibody treatment. *Bone* **71**, 115–123 (2015).

707. Perosky, J. E. *et al.* Single dose of bisphosphonate preserves gains in bone mass following cessation of sclerostin antibody in Brtl/+ osteogenesis imperfecta model. *Bone* **93**, 79–85 (2016).

708. Holdsworth, G. *et al.* Dampening of the bone formation response following repeat dosing with sclerostin antibody in mice is associated with up-regulation of Wnt antagonists. *Bone* **107**, 93–103 (2018).

709. Cenci, S. *et al.* Estrogen deficiency induces bone loss by enhancing T-cell production of TNF-alpha. *J Clin Invest* **106**, 1229–1237 (2000).

710. Gao, Y. *et al.* Estrogen prevents bone loss through transforming growth factor beta signaling in T cells. *Proc Natl Acad Sci U S A* **101**, 16618–16623 (2004).

711. Roggia, C. *et al.* Up-regulation of TNF-producing T cells in the bone marrow: a key mechanism by which estrogen deficiency induces bone loss in vivo. *Proc Natl Acad Sci U S A* **98**, 13960–13965 (2001).

712. Gao, Y. *et al.* IFN-gamma stimulates osteoclast formation and bone loss in vivo via antigen-driven T cell activation. *J Clin Invest* **117**, 122–132 (2007).

713. Grassi, F. *et al.* Oxidative stress causes bone loss in estrogen-deficient mice through enhanced bone marrow dendritic cell activation. *Proc Natl Acad Sci U S A* **104**, 15087–15092 (2007).

714. Tyagi, A. M. *et al.* Daidzein prevents the increase in CD4+CD28null T cells and B lymphopoesis in ovariectomized mice: a key mechanism for anti-osteoclastogenic effect. *PLoS One* **6**, e21216 (2011).

715. D'Amelio, P. *et al.* Estrogen deficiency increases osteoclastogenesis up-regulating T cells activity: a key mechanism in osteoporosis. *Bone* **43**, 92–100 (2008).

716. Ammann, P. *et al.* Transgenic mice expressing soluble tumor necrosis factor-receptor are protected against bone loss caused by estrogen deficiency. *J Clin Invest* **99**, 1699–1703 (1997).

717. Ryan, M. R. *et al*. An IL-7-dependent rebound in thymic T cell output contributes to the bone loss induced by estrogen deficiency. *Proc Natl Acad Sci U S A* **102**, 16735–16740 (2005).

718. Huang, T. *et al*. Effect of the Wnt signal-RANKL/OPG axis on the enhanced osteogenic integration of a lithium incorporated surface. *Biomater. Sci.* **7**, 1101–1116 (2019).

719. Mao, B. *et al*. LDL-receptor-related protein 6 is a receptor for Dickkopf proteins. *Nature* **411**, 321–325 (2001).

720. James, A. W. *et al*. NELL-1 in the treatment of osteoporotic bone loss. *Nat Commun* **6**, 7362 (2015).

721. Monzem, S. *et al*. Long-term bisphosphonate treatment coupled with ovariectomy in mice provokes deleterious effects on femoral neck fracture pattern and modifies tibial shape. *Bone Jt Open* **1**, 512–519 (2020).

722. Compston, J. Practical guidance for the use of bisphosphonates in osteoporosis. *Bone* **136**, 115330 (2020).

723. Bhadada, S. K. *et al*. Predictors of atypical femoral fractures during long term bisphosphonate therapy: A case series & review of literature. *Indian Journal of Medical Research* **140**, 46 (2014).

724. Giusti, A., Hamdy, N. A. T. & Papapoulos, S. E. Atypical fractures of the femur and bisphosphonate therapy: A systematic review of case/case series studies. *Bone* **47**, 169–180 (2010).

725. Patel, R. N., Ashraf, A. & Sundaram, M. Atypical Fractures Following Bisphosphonate Therapy. *Seminars in Musculoskeletal Radiology* **20**, 376–381 (2016).

726. Khan, A. A. & Kaiser, S. Atypical femoral fracture. *CMAJ* **189**, E542 (2017).

727. Jilka, R. L. *et al*. Increased bone formation by prevention of osteoblast apoptosis with parathyroid hormone. *J Clin Invest* **104**, 439–446 (1999).

728. Powell, W. F. *et al*. Targeted ablation of the PTH/PTHrP receptor in osteocytes impairs bone structure and homeostatic calcemic responses. *J Endocrinol* **209**, 21–32 (2011).

729. Rhee, Y. *et al*. PTH receptor signaling in osteocytes governs periosteal bone formation and intracortical remodeling. *J Bone Miner Res* **26**, 1035–1046 (2011).

730. Bellido, T. *et al.* Chronic elevation of parathyroid hormone in mice reduces expression of sclerostin by osteocytes: a novel mechanism for hormonal control of osteoblastogenesis. *Endocrinology* **146**, 4577–4583 (2005).

731. Almeida, M., Han, L., Bellido, T., Manolagas, S. C. & Kousteni, S. Wnt proteins prevent apoptosis of both uncommitted osteoblast progenitors and differentiated osteoblasts by beta-catenin-dependent and -independent signaling cascades involving Src/ERK and phosphatidylinositol 3-kinase/AKT. *J Biol Chem* **280**, 41342–41351 (2005).

732. Lee, S.-K. & Lorenzo, J. A. Regulation of receptor activator of nuclear factor-kappa B ligand and osteoprotegerin mRNA expression by parathyroid hormone is predominantly mediated by the protein kinase a pathway in murine bone marrow cultures. *Bone* **31**, 252–259 (2002).

733. Kondo, H., Guo, J. & Bringhurst, F. R. Cyclic adenosine monophosphate/protein kinase A mediates parathyroid hormone/parathyroid hormone-related protein receptor regulation of osteoclastogenesis and expression of RANKL and osteoprotegerin mRNAs by marrow stromal cells. *J Bone Miner Res* **17**, 1667–1679 (2002).

734. Dhanwal, D. K. Thyroid disorders and bone mineral metabolism. *Indian J Endocrinol Metab* **15**, S107–S112 (2011).

735. Vestergaard Kvist, A. *et al.* Cardiovascular Safety Profile of Romosozumab: A Pharmacovigilance Analysis of the US Food and Drug Administration Adverse Event Reporting System (FAERS). *J Clin Med* **10**, 1660 (2021).

736. San-Juan-Rodriguez, A., Parekh, N., Newman, T. V. & Hernandez, I. Pricing of Monoclonal Antibodies in the United States. *Global Journal on Quality and Safety in Healthcare* **1**, 4–5 (2020).

737. Sachdeva, S., Joo, H., Tsai, J., Jasti, B. & Li, X. A Rational Approach for Creating Peptides Mimicking Antibody Binding. *Sci Rep* **9**, 997 (2019).

738. Chu, C., Gao, Y., Lan, X., Thomas, A. & Li, S. NCAM Mimetic Peptides: Potential Therapeutic Target for Neurological Disorders. *Neurochem Res* **43**, 1714–1722 (2018).

739. Markovsky, E. *et al.* Targeting NCAM-expressing neuroblastoma with polymeric precision nanomedicine. *Journal of Controlled Release* **249**, 162–172 (2017).

740. Lan, X.-Y. *et al.* NCAM mimetic peptide P2 synergizes with bone marrow mesenchymal stem cells in promoting functional recovery after stroke. *J Cereb Blood Flow Metab* **44**, 1128–1144 (2024).

741. Berezin, V. & Bock, E. NCAM mimetic peptides: Pharmacological and therapeutic potential. *J Mol Neurosci* **22**, 33–39 (2004).

742. Kasper, C. *et al.* Structural basis of cell–cell adhesion by NCAM. *Nat Struct Mol Biol* **7**, 389–393 (2000).

743. Young, R. N. & Grynpas, M. D. Targeting therapeutics to bone by conjugation with bisphosphonates. *Current Opinion in Pharmacology* **40**, 87–94 (2018).

744. Calori, I. R., Braga, G., de Jesus, P. da C. C., Bi, H. & Tedesco, A. C. Polymer scaffolds as drug delivery systems. *European Polymer Journal* **129**, 109621 (2020).

745. Dang, J. M. & Leong, K. W. Natural polymers for gene delivery and tissue engineering. *Advanced Drug Delivery Reviews* **58**, 487–499 (2006).

746. Chocholata, P., Kulda, V. & Babuska, V. Fabrication of Scaffolds for Bone-Tissue Regeneration. *Materials* **12**, 568 (2019).

747. Ye, G. *et al.* Nanomaterial-Based Scaffolds for Bone Tissue Engineering and Regeneration. *Nanomedicine* **15**, 1995–2017 (2020).

748. Eusébio, D. *et al.* Chapter 28 - Drug delivery for bone tissue engineering. in *Advanced and Modern Approaches for Drug Delivery* (eds. Nayak, A. K., Hasnain, M. S., Laha, B. & Maiti, S.) 783–815 (Academic Press, 2023). doi:10.1016/B978-0-323-91668-4.00008-3.

749. V. K., A. D. *et al.* Dual drug delivery platforms for bone tissue engineering. *Front. Bioeng. Biotechnol.* **10**, (2022).

750. Oliveira, É. R. *et al.* Advances in Growth Factor Delivery for Bone Tissue Engineering. *International Journal of Molecular Sciences* **22**, 903 (2021).

751. Deininger, C. *et al.* Enhanced BMP-2-Mediated Bone Repair Using an Anisotropic Silk Fibroin Scaffold Coated with Bone-like Apatite. *Int J Mol Sci* **23**, 283 (2021).

752. Moreno-Jiménez, I. *et al.* Human and mouse bones physiologically integrate in a humanized mouse model while maintaining species-specific ultrastructure. *Sci Adv* **6**, eabb9265 (2020).

753. Bagi, C. M., Berryman, E. & Moalli, M. R. Comparative Bone Anatomy of Commonly Used Laboratory Animals: Implications for Drug Discovery. *Comp Med* **61**, 76–85 (2011).

754. Hoffseth, K. *et al.* Age-Dependent Changes in Bone Architecture, Patterning, and Biomechanics During Skeletal Regeneration. *Front. Cell Dev. Biol.* **9**, (2021).

755. Zhang, L. *et al.* Consequences of Aging on Bone. *Aging and disease* 0 (2023) doi:10.14336/AD.2023.1115.

756. N, F. *et al.* TBP, PPIA, YWHAZ and EF1A1 Are the Most Stably Expressed Genes during Osteogenic Differentiation. *International journal of molecular sciences* **23**, (2022).

757. Mosig, R. A. *et al.* Loss of MMP-2 disrupts skeletal and craniofacial development and results in decreased bone mineralization, joint erosion and defects in osteoblast and osteoclast growth. *Hum Mol Genet* **16**, 1113–1123 (2007).

758. Nichols, R. A., Niagro, F. D., Borke, J. L. & Cuenin, M. F. Mechanical Stretching of Mouse Calvarial Osteoblasts In Vitro Models Changes in MMP-2 and MMP-9 Expression at the Bone-Implant Interface. *J Oral Implantol* **42**, 138–144 (2016).

759. Tsai, C.-L. *et al.* c-Src-dependent transactivation of PDGFR contributes to TNF-α-induced MMP-9 expression and functional impairment in osteoblasts. *Bone* **60**, 186–197 (2014).

760. Jilka, R. L. The Relevance of Mouse Models for Investigating Age-Related Bone Loss in Humans. *J Gerontol A Biol Sci Med Sci* **68**, 1209–1217 (2013).

8 Appendix

```
#!/bin/bash
#SBATCH -J BBDuk_trim_loop      # A single job name for the array
#SBATCH -n 4                      # Number of cores
#SBATCH -N 1                      # All cores on one machine
#SBATCH --mem 8000                # in MB
#SBATCH -t 0-15:00                  # Maximum execution time (D-HH:MM)
#SBATCH -o job_%A_%a.log        # Standard output
#SBATCH -e job_%A_%a.log        # Standard error
#SBATCH --mail-type=FAIL,BEGIN,END
#SBATCH --account=mcgetthm-bone-pepitem
#SBATCH --qos castles

set -e

module purge; module load bluebear

module load FastQC/0.11.9-Java-11

fastqc `find . -name '*.fastq*' -print` --outdir=FASTQC
```

Figure 8.1 FastQC Script created in Sublime text and ran in Rstudio, adapted from scripts by Julia Manning

```
#!/bin/bash
#SBATCH -J BBDuk_trim_loop      # A single job name for the array
#SBATCH -n 4                      # Number of cores
#SBATCH -N 1                      # All cores on one machine
#SBATCH --mem 8000                # in MB
#SBATCH -t 0-15:00                  # Maximum execution time (D-HH:MM)
#SBATCH -o job_%A_%a.log        # Standard output
#SBATCH -e job_%A_%a.log        # Standard error
#SBATCH --mail-type=FAIL,BEGIN,END
#SBATCH --account=mcgetthm-bone-pepitem
#SBATCH --qos castles

set -e
module purge; module load bluebear # this line is required

module load MultiQC/1.9-foss-2019b-Python-3.7.4

multiqc ./FASTQC
```

Figure 8.2 MultiQC Script created in Sublime text and ran in Rstudio, adapted from scripts by Julia Manning



```
#!/bin/bash
#SBATCH -J BBDuk_trim_loop      # A single job name for the array
#SBATCH -n 4                      # Number of cores
#SBATCH -N 1                      # All cores on one machine
#SBATCH --mem 8000                # in MB
#SBATCH -t 0-15:00                  # Maximum execution time (D-HH:MM)
#SBATCH -o job_%A_%a.log        # Standard output
#SBATCH -e job_%A_%a.log        # Standard error
#SBATCH --mail-type=FAIL,BEGIN,END
#SBATCH --account=mcgetthm-bone-pepitem
#SBATCH --qos castles

set -e
module purge; module load bluebear # this line is required

module load BBMap/38.87-GCC-8.3.0
#module load R/4.0.0-foss-2020a

# Remove adapter contamination, polyA read throuhgh, and low quality read

for i in *.fastq.gz; do bbduk.sh in=$i out=trimmed_clean_$i \
ref=truseq_rna.fa.gz literal=AAAAAAAAAAAAAAAAAA \
k=13 \
ktrim=r \
useshortkmers=t \
mink=5 \
qtrim=r \
trimq=10 \
minlength=20; done

# in = chosen input file
# out = file name for out put
# ref = file of adapter sequences (and in our case, polyA tail)
# k = kmer size to use
# ktrim = r, means right-trimming
# mink allows use of shorter kmers at the end of reads
# qtrim = quality trim setting r trims right side only
# trimq = to Q10 using the Phred algorithrm,


# hdist - hamming distance, allows for mismatch
# flt = force trimming, set how mny you'd wnat it to trim
# maq = quality filtering, discards reads below threshold
# ktrim = N, masks all 35-mers - to do with entropy
```

Figure 8.3 Trimming Script created in Sublime text and ran in Rstudio, adapted from scripts by Julia Manning

```
#!/bin/bash
#SBATCH -J STAR_Align          # A single job name for the array
#SBATCH -n 4                        # Number of cores
#SBATCH -N 1                        # All cores on one machine
#SBATCH --mem 35000                  # in MB
#SBATCH -t 0-10:00                   # Maximum execution time (D-HH:MM)
#SBATCH -o job_%A_%a.log          # Standard output
#SBATCH -e job_%A_%a.log          # Standard error
#SBATCH --mail-type=FAIL,BEGIN,END
#SBATCH --account=mcgetthm-bone-pepitem
#SBATCH --qos castles

BB_WORKDIR=$(mktemp -d /scratch/${USER}_${SLURM_JOBID}.XXXXXX)
export TMPDIR=${BB_WORKDIR}

set -e

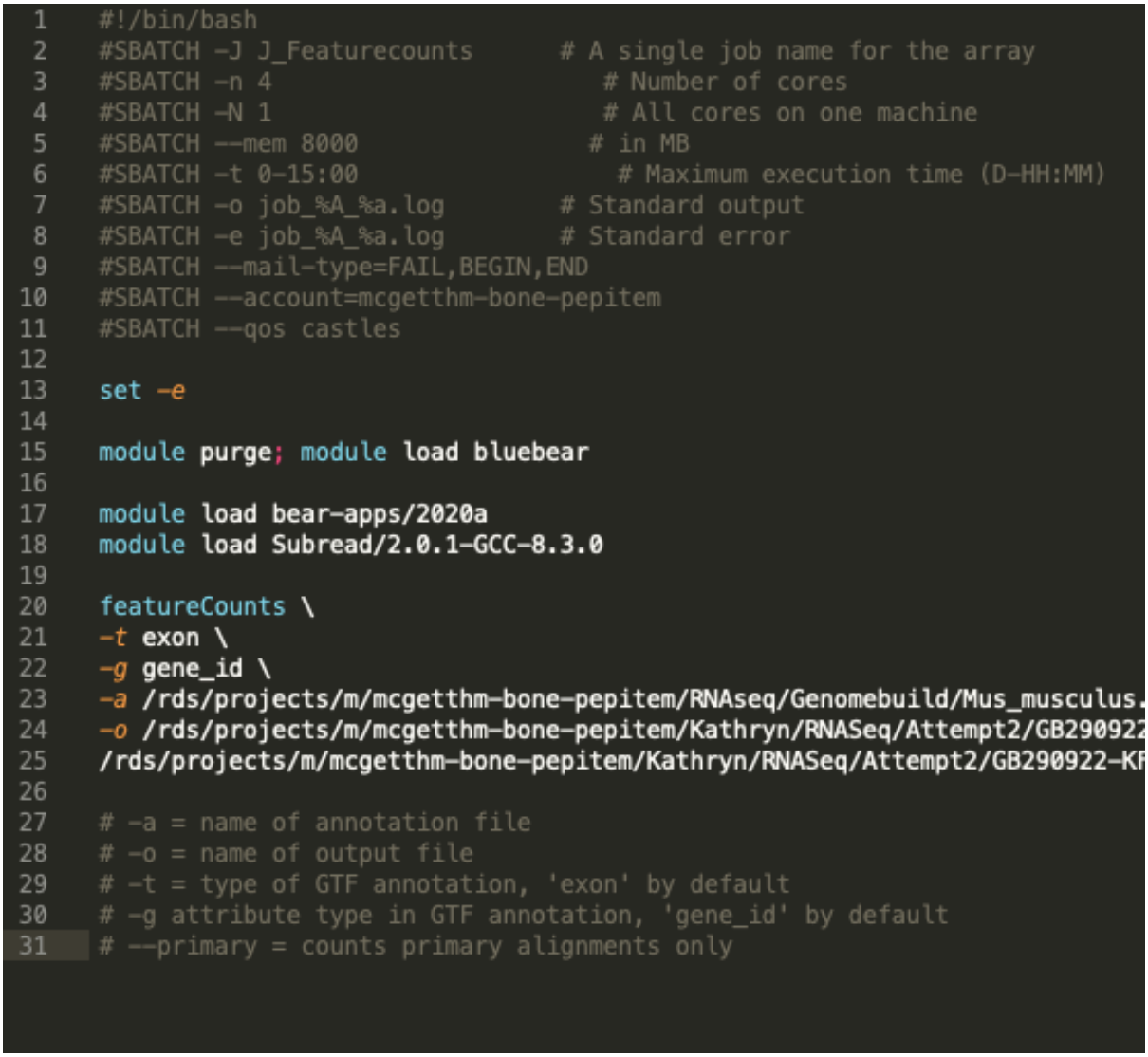
module purge; module load bluebear

module load STAR/2.7.2b-GCC-8.3.0

for i in *.fastq.gz; do STAR --runThreadN ${SLURM_NTASKS} \
--genomeDir /rds/projects/m/mcgetthm-bone-pepitem/RNAseq/Genomebuild \
--readFilesIn $i \
--readFilesCommand zcat \
--outFileNamePrefix aligned_$i \
--outSAMtype BAM SortedByCoordinate \
--outSAMunmapped Within \
--outSAMattributes Standard

test -d ${BB_WORKDIR} && /bin/cp -r ${BB_WORKDIR} ./
test -d ${BB_WORKDIR} && /bin/rm -rf ${BB_WORKDIR};
done
```

Figure 8.4 Align Script created in Sublime text and ran in Rstudio, adapted from scripts by Julia Manning



```
#!/bin/bash
#SBATCH -J J_Featurecounts      # A single job name for the array
#SBATCH -n 4                      # Number of cores
#SBATCH -N 1                      # All cores on one machine
#SBATCH --mem 8000                # in MB
#SBATCH -t 0-15:00                  # Maximum execution time (D-HH:MM)
#SBATCH -o job_%A_%a.log        # Standard output
#SBATCH -e job_%A_%a.log        # Standard error
#SBATCH --mail-type=FAIL,BEGIN,END
#SBATCH --account=mcgetthm-bone-pepitem
#SBATCH --qos castles

set -e

module purge; module load bluebear

module load bear-apps/2020a
module load Subread/2.0.1-GCC-8.3.0

featureCounts \
-t exon \
-g gene_id \
-a /rds/projects/m/mcgetthm-bone-pepitem/RNAseq/Genomebuild/Mus_musculus.
-o /rds/projects/m/mcgetthm-bone-pepitem/Kathryn/RNASeq/Attempt2/GB290922
/rds/projects/m/mcgetthm-bone-pepitem/Kathryn/RNASeq/Attempt2/GB290922-KF

# -a = name of annotation file
# -o = name of output file
# -t = type of GTF annotation, 'exon' by default
# -g attribute type in GTF annotation, 'gene_id' by default
# --primary = counts primary alignments only
```

Figure 8.5 Featurecounts Script created in Sublime text and ran in Rstudio, adapted from scripts by Julia Manning

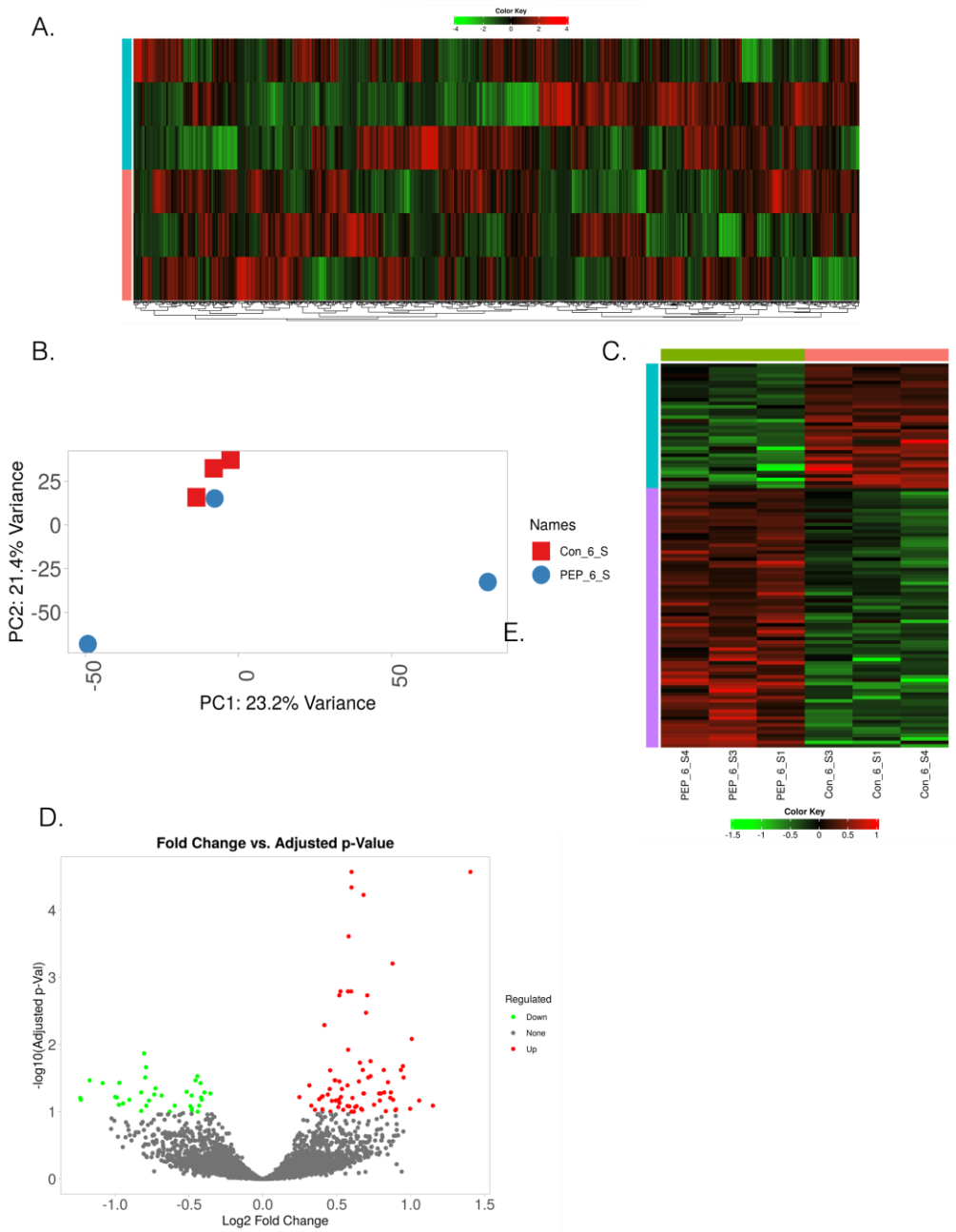


Figure 8.6 **Preprocessing of PEPITEM vs Control peptide RNAseq in iDEP.** C.Obs were plated for 24hr in osteogenic media before treatment with PEPITEM or control peptide for 6hr. RNA extracted and send for sequencing. Analysis preformed in iDEP. (A) Hierarchical clustering, (B) PCA analysis. (C) Heatmap of differentially expressed genes (DEGs), upregulated (red) and downregulated (green). (D) Volcano plot showing up and down regulated genes.

Table 8.1 All upregulated and downregulated genes following PEPITEM treatment compared to control peptide

Regulation	log2 Fold Change	Symbol	Chr
Up	1.40430776556747	Kmt2d	15q
	1.15024565487949	Flt1	5q
	1.05760092791329	Cpeb2	5q
	1.0073207049212	Rbm45	2q
	0.996559007758521	Lama2	10q
	0.952178517843655	Ptprm	17q
	0.947823623371367	Hivep2	10q
	0.934226403521769	Eng	2q
	0.901213704744887	Wdfy3	5q
	0.89702569683231	Fem1c	18q
	0.881391238649078	Dip2b	15q
	0.877883505427051	Zbtb20	16q
	0.866023036178446	Dram1	10q
	0.862128858338649	Patl1	19q
	0.846745380410452	Zfp568	7q
	0.83225947069035	Trrap	5q
	0.821490969991678	Arl13b	16q
	0.818505822258442	Rassf3	10q
	0.798118146421969	Zfp462	4q
	0.791758570825744	Brca2	5q
	0.78673474216748	Pcnx3	19q
	0.752321141728179	Arid1a	4q
	0.728727334748264	Nf1	11q
	0.728490160061874	Sacs	14q
	0.71317444560951	Nav2	7q
	0.706757934426878	Ubr4	4q
	0.698144342411609	Zfhx4	3q
	0.684570755941333	Usp24	4q
	0.681690402221993	Dst	1q
	0.680660086659274	Nav1	1q
	0.676263269282805	Diaph2	Xq
	0.671998492935553	Thsd7a	6q
	0.664900807472944	Ahnak	19q
	0.656539085200315	Sp1	15q
	0.649850897735021	Xrn1	9q
	0.633982450946088	Heatr5a	12q
	0.624441130291069	Phc3	3q
	0.615951905744821	Trio	15q
	0.606230239442185	Kmt2a	9q
	0.600361833824849	Ago3	4q
	0.600219331861358	Pcdh19	Xq
	0.599971791753937	Col12a1	9q
	0.59773839281501	Flnc	6q
	0.58553236973944	Hipk1	3q
	0.580697629173566	Golgb1	16q
	0.577300702390066	Dync1h1	12q
	0.57640041285326	Lrp1	10q
	0.572912603471088	Birc6	17q
	0.572343054102517	Tmem245	4q
	0.54450647950633	Prrc2a	17q
	0.535110268581313	Phip	9q
	0.528959887530308	Uggt1	1q

	0.525533520965761	Lpp	16q
	0.518896007730861	Fat1	8q
	0.518644419881584	Zfhx3	8q
	0.517627805029924	Mki67	7q
	0.513172915908124	Ylpm1	12q
	0.510496882653584	Dyrk2	10q
	0.493448659228275	Herc2	7q
	0.489793110321781	Macf1	4q
	0.486301541109151	Nfib	4q
	0.467458423558138	Sh3pxd2a	19q
	0.457252945009879	Pappa	4q
	0.455546160489084	Huwe1	Xq
	0.452468062965651	Purb	11q
	0.439834219941734	Golga4	9q
	0.416493712928052	Prrc2c	1q
	0.40514247754676	Col6a3	1q
	0.403062904310555	Ubr5	15q
	0.397811552206264	Igf2r	17q
	0.38156757024043	Myadm	7q
	0.352772156911008	Taok1	11q
	0.328218940767693	Nipbl	15q
	0.315132470594774	Tead1	7q
	0.247360900416806	Col1a1	11q
Down	-1.23481171180353	Rex1bd	8q
	-1.23010585840839	Pop5	5q
	-1.17099433291063	Mrpl11	19q
	-1.08294378277525	Ciao2b	8q
	-0.998050090509771	Cir1	2q
	-0.987369075921076	Cwc27	13q
	-0.973491012577354	Lamtor3	3q
	-0.970298295696761	Nab2	10q
	-0.944754965505827	Ccnt2	1q
	-0.902132781899503	Dhr7b	11q
	-0.822108448415377	Ubp1	9q
	-0.822100913458168	Rnf7	9q
	-0.802539677742481	Dhx40	11q
	-0.79510122822112	Gm8292	1q
	-0.789939896231761	Cenpw	10q
	-0.788201129897281	Nudt16l1	16q
	-0.769932193365714	Dhx30	9q
	-0.733875307178892	Lamtor5	3q
	-0.72561370033205	Med10	13q
	-0.684307667385217	Snhg18	15q
	-0.62883995396853	Tk1	11q
	-0.595363528291204	Ndufb11	Xq
	-0.514535959989639	Mrpl52	14q
	-0.489570358081693	Tnmd	Xq
	-0.481282814956995	Rps11	7q
	-0.480143879032629	Pcmt1	10q
	-0.479872476259173	Lrrc59	11q
	-0.455460664332768	Crk	11q

	-0.441999041257278	Rps23	13q
	-0.439943599153777	Nol7	13q
	-0.430077387508551	Gpx1	9q
	-0.421563308898329	Rps19	7q
	-0.418087519788854	Oxct1	15q
	-0.412833683151441	Atp6v0e	17q
	-0.394691300295738	Atpif1	4q
	-0.354813108044449	Rpl22	4q

International Journal of
Molecular Sciences

MDPI

Review

The Ying and Yang of Sphingosine-1-Phosphate Signalling within the Bone

Kathryn Frost, Amy J. Naylor * and Helen M. McGettrick

Rheumatology Research Group, Institute of Inflammation and Ageing, University of Birmingham, Birmingham B15 2TT, UK
* Correspondence: a.naylor@bham.ac.uk

Abstract: Bone remodelling is a highly active and dynamic process that involves the tight regulation of osteoblasts, osteoclasts, and their progenitors to allow for a balance of bone resorption and formation to be maintained. Ageing and inflammation are risk factors for the dysregulation of bone remodelling. Once the balance between bone formation and resorption is lost, bone mass becomes compromised, resulting in disorders such as osteoporosis and Paget's disease. Key molecules in the sphingosine-1-phosphate signalling pathway have been identified for their role in regulating bone remodelling, in addition to its more recognised role in inflammatory responses. This review discusses the accumulating evidence for the different, and, in certain circumstances, opposing, roles of S1P in bone homeostasis and disease, including osteoporosis, Paget's disease, and inflammatory bone loss. Specifically, we describe the current, often conflicting, evidence surrounding S1P function in osteoblasts, osteoclasts, and their precursors in health and disease, concluding that S1P may be an effective biomarker of bone disease and also an attractive therapeutic target for disease.

Keywords: osteoblast; osteoclast; S1P; bone mineral density; bone; osteoporosis

check for updates

Citation: Frost, K., Naylor, A.J., McGettrick, H.M. The Ying and Yang of Sphingosine-1-Phosphate Signalling within the Bone. *Int. J. Mol. Sci.* **2023**, *24*, 6935. https://doi.org/10.3390/ijms24086935

Academic Editor: Rodolfo Gómez

Received: 6 February 2023
Revised: 28 March 2023
Accepted: 4 April 2023
Published: 8 April 2023

Copyright: © 2023 by the authors. Licensee MDPI, Basel, Switzerland. This article is an open access article distributed under the terms and conditions of the Creative Commons Attribution (CC BY) license (https://creativecommons.org/licenses/by/4.0/).

1. Introduction

Despite its static appearance, bone is a highly dynamic tissue that is continually adapting to mechanical strain and damage. This bone remodelling process crucially involves two cell types (osteoblasts and osteoclasts) that communicate with each other within temporary bone modelling units (BMU) [1] and respond to changes in the local microenvironment to maintain homeostatic levels of bone formation and resorption. Disruption of this delicate balance can occur with age and in a variety of inflammatory disorders and cancer, leading to abnormal bone mineral density and increased risk of fracture [2]. Sphingosine-1-phosphate (S1P) is a member of the sphingolipid family that has previously been described to effect multiple cell functions such as survival [3], proliferation [4], and differentiation [5]. There is a growing body of evidence that indicates its importance in the bone pathology of several inflammatory diseases [6], and, more recently, its role in the maintenance of bone homeostasis throughout the life course has been identified. Here, we detail the current understanding of the different, and sometimes opposing, roles of S1P in bone remodelling and how these can appear divergent depending on the local milieu. We discuss the evidence that S1P impacts the onset and progression of bone diseases and identify areas where further research is required to ensure that the therapeutic potential of S1P can be effectively harnessed.

2. Bone Remodelling

Bone remodelling has two crucial functions in adults: the repair of damaged bone and the strengthening of existing bone tissue. In response to activating stimuli, such as mechanical strain, osteoclast precursors migrate to the bone surface where they undergo osteoclastogenesis [7]. Osteoclasts are large multinucleated cells that originate from the fusion of monocyte/macrophage haematopoietic lineage cells [8]. Mature osteoclasts directly mediate bone resorption through their release of chloride and hydrogen ions, which dissolve the alkaline hydroxyapatite mineral component of the bone [9]. The remaining collagen matrix is broken down via osteoclast-secreted lysosomal enzymes, matrix metalloproteinases (MMPs), and cathepsin K [10,11]. Following resorption, mesenchymal stem cell (MSC)-derived osteoblasts [12] replace the resorbed tissue by secreting osteoid, a type I collagen-rich organic extracellular matrix [12]. Over a period of several weeks, this matrix is mineralised with hydroxyapatite crystals to complete the bone remodelling process [13].

Bone remodelling is tightly regulated by the crosstalk between osteoblasts and osteoclasts and local environmental cues (damage, mechanical strain and hormones, e.g., parathyroid hormone—PTH), which all impact the balance of mineralisation and resorption to maintain homeostasis [14–16]. Many of the therapies for bone conditions stem from our understanding of the factors influencing osteoblast and osteoclast precursor migration, osteoblastogenesis, or osteoclastogenesis, which have enabled the enhancement of bone formation (e.g., PTH therapy) or the prevention of bone destruction (e.g., bisphosphonates). Despite these successes, there is an unmet clinical need for therapies that can prevent bone loss and repair damaged bone tissue. One newly identified potential therapeutic target is S1P.

3. Sphingosine-1-Phosphate

S1P is part of the sphingolipid metabolic pathway that also includes sphingosine and ceramide (Figure 1). Each metabolite has been shown to be involved in the survival, migration, and proliferation of osteoblast and osteoclast progenitor cells (reviewed by [17]). S1P is metabolised from ceramide via two reactions. First, ceramidase (CDase) converts ceramide into sphingosine in a reversible reaction with ceramide synthase (CerS) (reviewed by [18]). Sphingosine kinases (SPHK1 and SPHK2) then convert sphingosine to S1P. The phosphorylation of sphingosine can be reversed in the presence of sphingosine phosphate phosphatases (SPPase), or S1P lyase can irreversibly break down S1P into ethanolamine phosphate and hexadecenal [19]. Collectively, these reactions regulate extra- and intra-cellular sphingolipid concentrations, and thus the functional consequence of their signalling on the cell and surrounding cells (extensively reviewed by [20]).

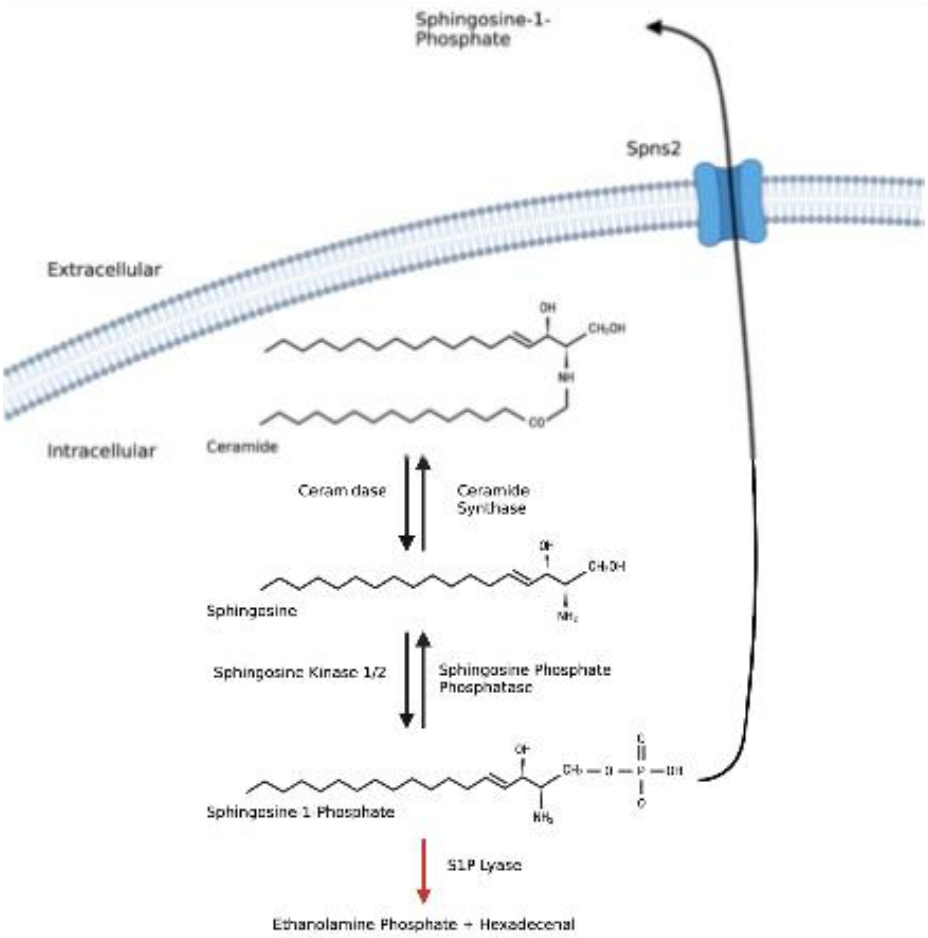


Figure 1. Sphingosine metabolic pathway. Ceramide, sphingosine, and sphingosine-1-phosphate can be metabolised into each other via various enzymes. Ceramide is converted into sphingosine through a reversible reaction by ceramidase (CDase) and ceramide synthase (CerS) [18]. Sphingosine frequently converted to sphingosine-1-phosphate via the two sphingosine kinases (SPHK1/2) [19]. S1P is metabolised back to sphingosine via sphingosine phosphate phosphatases (SPPase) or by an irreversible reaction by S1P lyase [19]. S1P is then exported out of the cell via spinster 2 (SPNS2). Created in Biorender.com.

4. S1P Signalling

S1P has both intracellular and extracellular functions in a variety of tissues (reviewed by [21]). One accepted principle within bone and other tissues is the sphingosine rheostat: here the intracellular levels of ceramide and S1P influence cell survival and proliferation, with ceramide being considered pro-apoptotic and S1P acting in an anti-apoptotic fashion [22]. No studies have looked at this rheostat directly in osteogenic cells; however, various studies have shown the similar actions of both ceramides and S1P. Additionally, there are few studies that directly investigate the role of intracellular S1P within bone cells [23,24]; therefore, reviews on the subject tend to infer functions based on other studies performed in other cell types.

4.1. Intracellular S1P Signalling

Current work investigating intracellular S1P within bone focuses on the action of the enzymes required for its production (SPHK1 or 2) rather than the bioactivity of S1P itself. Alterations in SPHK1 activity and/or expression result from altered autocrine signalling of the extracellular S1P receptors (S1PR1-5) due to the secretion of S1P, rather than altered intracellular S1P signalling [25]. Indeed, alterations in SPHK1 expression during osteoblast differentiation have been linked to the activation of S1PR1 signalling [23]. To the best of our knowledge, no studies have investigated the impact of intracellular osteoblastic SPHK1 and/or S1P signalling; however, it has been shown that the osteoclast-specific deletion of SPHK1 has no effect on bone mass in male or female mice [26]. Similarly, siRNA knockdown of SPHK1 in a murine macrophage cell line (RAW264) or in primary murine bone-marrow-derived macrophages had no effect on osteoclast maturation in response to RANKL [24]. Conversely, the upregulation of SPHK1, through the retroviral transfection of HA-tagged SPHK1, resulted in a moderate decrease in osteoclast maturation [24], suggesting that SPHK1 in osteoclasts acts as a negative regulator of osteoclastogenesis. The authors suggested that RANKL-mediated osteoclast activation results in an upregulation of SPHK1, which regulates the osteoclast function through the inhibition of c-FOS and NFATc1 via p38-dependent signalling [24]. Crucially, these differences were not observed in the presence of extracellular S1P, suggesting that they are mediated by either the intracellular action of SPHK1 or intracellular S1P [24]. These findings demonstrate the importance of intracellular S1P on osteogenesis and bone resorption and underscore the need for additional investigations into the intracellular receptors of S1P and their function in osteoclasts.

The inhibition of SPHK2 in the murine macrophage cell line RAW264 resulted in a reduction in c-FOS expression and subsequent osteoclastogenesis [27], identifying intracellular SPHK2 signalling as essential during the initial stages of osteoclastogenesis. In contrast, SPHK2$^{-/-}$ osteoclasts had normal resorptive activity in vitro, despite the observation that global SPHK2$^{-/-}$ mice have reduced trabecular bone mass [26]. This finding led to the in vivo phenotype being attributed to alterations in osteoblast formation, which was demonstrated by a reduction in collagen 1 gene expression and a significant impairment of the anabolic response to PTH within these mice [26]. Crucially, the impact of SPHK2 on PTH signalling was not determined, making it difficult to draw any firm conclusions about the exact role of intracellular S1P signalling in this process. These studies both postulate a role for SPHK2 in altering osteoclast or osteoblast function to drive changes within the bone architecture. One thing to consider with these studies is the fact that they focus solely on the intracellular kinase activity to infer the intracellular S1P function. However, increases in kinase activity leads to increased S1P production and therefore secretion, meaning differences could be due to autocrine signalling rather than intracellular activity. It is possible to overcome this issue by inhibiting SPSN2, thereby blocking S1P secretion; however, the interpretation of these results will be confounded by the assumptions of the sphingosine rheostat. Further research into the intracellular actions of S1P is urgently needed to enable the identification of potential intracellular targets that inhibit intracellular S1P function.

4.2. Extracellular S1P Signalling

In comparison to intracellular signalling, significantly more research has been conducted on the role of extracellular S1P signalling in the bone. Given the limited knowledge surrounding the S1P intracellular targets in bone, this review focusses predominantly on the functional consequence of the autocrine and paracrine actions of extracellular S1P. These include its actions directly on the cells within the bone and the mechanisms by which altered S1P cell–cell signalling results in impaired bone remodelling.

S1P is secreted by osteoblasts and osteoclasts, predominantly through the spinster 2 (SPNS2) transporter [28,29], allowing binding to one of the G-coupled protein S1PR. Osteoblasts, osteoclasts, and their precursors express four types of S1PR (S1PR1, -2, -3, and -4), which vary in expression levels across the maturation/differentiation status of the

cells [17] and are thought to play critical roles in bone cell migration, differentiation, and communication (Figure 2).

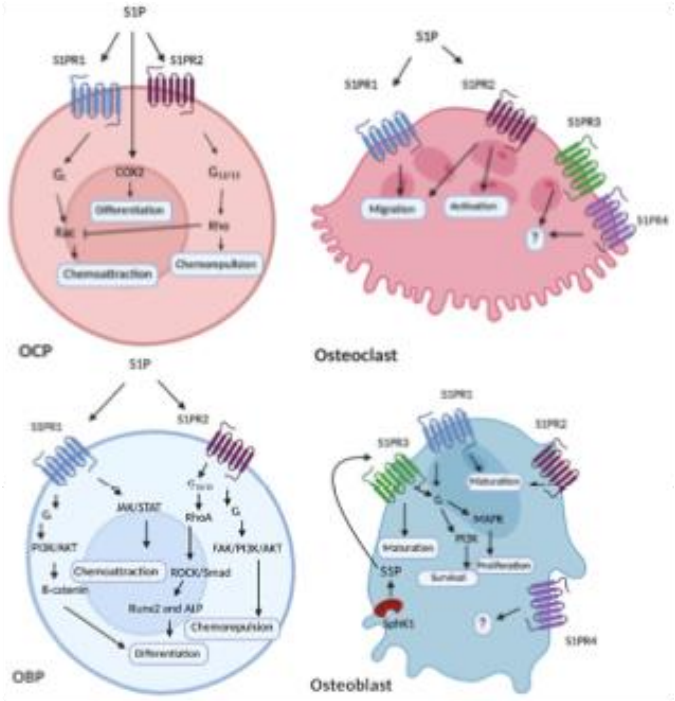


Figure 2. S1PR function in osteogenic cells. Schematic representation of the downstream signalling from S1PRs in osteoclast precursors (OCPs), osteoclasts (OCs), osteoblast precursors (OBPs), and osteoblasts (OBs). S1PRs are G-protein coupled receptors that activate various pathways and are present at different stages of OB and OC differentiation [17]. Within OCPs, S1PR1 and S1PR2 alter OC maturation via activation of Rho and Rac signalling pathways [24]. S1P can increase OCPs differentiation via Cox2, although the mechanism is not fully understood [24]. Although S1PR1-4 are expressed in OCs, the role of S1PR3 and S1PR4 are not currently understood [30]. S1PR1/2 can alter OC migration but the mechanisms underpinning this remain unclear. S1PR2 appears to be essential for OC activation. Within OBs, S1PR1 mediates OB differentiation via PI3K/AKT signalling and regulates migration via JAK/STAT signalling [31], resulting in chemoattraction in response to S1P [31], whereas S1PR2 increases OB differentiation via RhoA/ROCK/Smad signalling [30] and can also act through FAK/PI3K/AKT signalling to promote chemorepulsion. In OBs, S1PR1 increases OB proliferation [32] and survival via MAPK and PI3K signalling. S1PR1-3 are involved in mediating OB maturation through as of yet unknown signalling pathways. Activation of SphK1 in OBs promotes osteoblast maturation via autocrine S1P signalling through S1PR3 [23]. The function of S1PR4 in OBs is currently unknown. Created in Biorender.com.

5. S1P in Bone Precursors and Resident Cells

5.1. S1P as a Chemoattractant and Chemorepellent for Osteoclast Precursors

Osteoblast precursors (mesenchymal stem cells, MSCs) and osteoclast precursors (monocytes) are recruited into the bone tissue during periods of remodelling (reviewed by [30]) in response to CXCL12-CXCL4 and S1P-S1PR signalling (reviewed by [31]). S1P is detected in many different tissues; however, under homeostatic conditions, blood holds the highest concentration of S1P due to the secretion from red blood cells, thrombocytes, endothelial cells, and platelets (reviewed by [32]). Within blood, S1P is found bound to

albumin and lipoproteins, particularly HDL. Studies have demonstrated that S1P bound to albumin or HDL does not impact its ability to activate S1PRs, but rather creates a reservoir of S1P, keeping the S1P within circulation (reviewed by [32]). As total S1P is detected at higher concentrations in blood [33] and at lower concentrations within the bone [34], a concentration gradient is created along which osteoblast and osteoclast precursors migrate. The importance of this gradient in precursor migration was demonstrated when S1P breakdown was inhibited by either the inhibition or deletion of S1P lyase in vivo, causing the gradient to dissipate, resulting in increased bone mass and strength coupled with decreased osteoclast number [35]. The next sections will discuss the mechanisms and signalling pathways in which these actions are carried out.

5.2. Osteoclast Progenitors

Osteoclast precursor chemotaxis/migration has been shown to be dependent on the local S1P concentration: at low concentrations ($<10^{-7}$ M), osteoblast precursors (murine macrophages, RAW624.7) efficiently move through a Transwell filter towards S1P [36]. However, at higher concentrations (10^{-6} M), S1P repels the RAW624.7 cells, resulting in greater numbers remaining in the filter unable to move [36]. This observation raises a key question: how does S1P simultaneously attract and repel osteoclast precursors (monocytes)?

Osteoclast precursors express two of the S1P family of receptors, S1PR1 and S1PR2 [36]. siRNA knockdown of S1PR1 reduced osteoclast precursor migration at low S1P (10^{-9} M) concentrations, a phenomenon not observed following S1PR2 knockdown, indicating that S1P chemoattraction is mediated by S1PR1 [36]. Similar observations were made in wild-type mice treated intravenously with the S1PR1 agonist, SEW2871 (which causes receptor internalisation and mimics the inhibition of S1P activity), where increased numbers of osteoclast precursors were detected in the bloodstream [37], suggesting S1PR1 is responsible for keeping cells within circulation, where the S1P concentration is greater. Conversely, S1PR2 knockdown in osteoclast precursors (RAW264 cell line) enhanced migration towards S1P in vitro irrespective of S1P concentration, suggesting that S1PR2 negatively regulates osteoclast precursor migration [37]. Similarly, the administration of the S1PR2 antagonist, JTE013, increased monocytes in the circulation in vivo. Thus, S1PR2 is responsible for retaining osteoclast precursors within the tissue [36] or promoting migration from the circulation to the tissue. Collectively, the studies from this group have demonstrated opposing functions of S1PR1 and S1PR2 expressed by osteoclast precursors through the facilitation of chemotactic responses to S1P, thus regulating the migration of osteoclast precursors.

As previously described, RANKL is required for the differentiation of osteoclast precursors and is secreted from both osteoblasts and osteocytes (reviewed by [38]). Additionally, RANKL may also influence osteoclast precursor migration via its actions on S1PR1 [39,40]. For example, the intraperitoneal injection of RANKL induced a severe osteoporotic phenotype in mice that was reversed in the presence of the S1PR2 antagonist, JTE013 [39,40], indicating that RANKL directly impact S1P-related chemotaxis of osteoclast precursors. Therefore, RANKL appears to have a dual role in enhancing bone remodelling through (i) promoting the differentiation of osteoclast precursors and (ii) facilitating their migration into the bone.

5.3. Osteoblast Progenitors

S1P has also been investigated for its effect on osteoblast precursors (MSC). Primary murine MSCs express gene transcripts for all five of the S1PRs [41], whereas human bone-marrow-derived MSCs were only shown to express S1PR1-3 transcripts [42,43]. Of note, an additional amplification revealed an extremely low-level expression of S1PR4 and S1PR5 transcripts in human MSC [42], indicating that they are expressed at much lower levels compared to the murine MSC. It should be noted that the expression of S1PRs have also been shown to be influenced by culture density (3000–5000 cells/cm^2 vs. 15,000–20,000 cells/cm^2), where a marked increase in S1PR1 and S1PR3, but not S1PR2, gene expression was detected in the high-density cultures [42]. Therefore, alterations in

cell culture protocols and crosstalk between cells in culture may explain the conflicting findings within the literature. Unfortunately, the exact seeding density or plate sizes used are not always reported in sufficient detail within the current literature to establish this.

Similar to that described for the osteoblast progenitors, MSCs also display a concentration-dependent response to S1P [43] where human BM-MSC migrate towards low concentrations (1–10 nM) of S1P in a Transwell migration assay, whilst no migration was seen at higher concentrations (50–1000 nM) [43]. These data suggest that an S1P gradient is necessary for MSC migration. The opposing migratory properties of S1P on MSC movement have been, in part, attributed to the downstream signalling mediated by the different S1PRs; for instance, at low S1P concentrations, S1PR1 and S1PR3 downstream signalling occurred via Gi/ERK and supported migration, which was sensitive to S1PR1/3 or ERK1/2 pharmacological inhibitors in Transwell experiments [43]. By contrast, S1PR2 signalling via the $G_{12/13}$-RhoA-ROCK pathway inhibited migration, whilst the pharmacological inhibition of ROCK with Y27632 allowed for an increased migration at 1 nM [43]. The JTE-013-mediated inhibition of S1PR2 or genetic deletion ($S1PR2^{-/-}$) also inhibited migration in MSC scratch wound and Boyden chamber assays [41].

Despite the evidence above that the activation of S1PR2 results in the chemorepulsion of MSC in response to S1P, conflicting data indicate a role for S1PR2 in enhancing MSC migration via signalling crosstalk with S1PR1 [44]. Quint et al. showed that the pro-migratory response of the FAK/PI3K/AKT signalling is lost when JAK/STAT activity is inhibited, suggesting that the S1PR2-mediated activation of the FAK/PI3K/AKT signalling pathway induces the activation of S1PR1-mediated JAK/STAT signalling [44]. These data suggest that S1PR2 works in concert with, rather than against, S1PR1 to increase MSC migration.

The differences in S1P receptor roles in migration may be due to the origin of the progenitors (e.g., blood or tissue resident) and the experimental concentration of S1P used to activate the receptor. Unlike osteoclast progenitors, which often originate in the blood, the majority of MSC that differentiate into osteoblasts for bone remodelling are derived from the bone marrow or periosteum. These cells are not subjected to the high concentrations of S1P found within the blood. As such, the strength of any concentration gradient along which MSC are migrating is substantially reduced compared to that experienced by osteoclast progenitors. Moreover, the Quint study demonstrated that osteoclast-conditioned media acts as a chemoattractant to MSCs, increasing chemotaxis in an S1P-dependent manner (where migration was blocked in the presence of S1PR antagonists), thus suggesting that osteoclasts can recruit MSCs to the site of resorption [44]. Given that MSC responses to S1P vary dependent on S1P concentration, researchers should take care to use biologically relevant concentrations for their tissue of interest. One hypothesis is that smaller gradients in S1P concentrations are responsible for MSC chemotaxis to the bone surface opposed to those responsible for MSC recruitment from the blood.

6. Role of S1P in Mature Bone-Resident Cells

6.1. Osteoclasts

Osteoclasts are multinucleated cells involved in bone matrix demineralisation by releasing protons via vacuolar H^+-adenosine triphosphatase (H^+-ATPase), resulting in acidification of the resorption compartment and the release of calcium and phosphates (reviewed by [45]). The differentiation of monocytic osteoclast precursors into osteoclasts occurs within the bone remodelling compartment, where several molecules (M-CSF, RANKL, and OPG) drive osteoclastogenesis (reviewed by [46]). The most well-studied of these factors, RANKL, appears to at least partially elicit its osteogenic response via S1P signalling.

Following RANKL-induced osteoclastogenesis, there is an enhanced gene expression and the activity of SPHK1 and SPHK2, resulting in increasing in both intracellular and extracellular S1P [24]. Intracellular S1P was assessed by comparing extracellular S1P levels in culture media with concentrations within the cells (cell lysates) [24]. Mature osteoclasts express tartrate-resistant acid phosphatase (TRAP); therefore, the expression of this enzyme

is used as a marker of differentiation. SPHK1-induced intracellular S1P inhibited TRAP expression, as did the overexpression of SPHK1, whilst the siRNA knockdown of SPHK1 increased TRAP [24]. Ryu et al. demonstrated that RANKL increases the expression and also activation of p38 and ERK MAPKs in osteoclast precursors to promote osteoclastogenesis [24]. In cells treated with SPHK1 siRNA, there was an increase in p38 protein expression compared to those treated with control siRNA, whereas in SPHK1-overexpressing Mx-HA-SPHK1 cells, there was a significant decrease in p38 [24]. From these data, it is postulated that the SPHK1 upregulation and activation seen in response to RANKL results in increased intracellular S1P to induce a negative feedback loop, suppressing p38 signalling in osteoclast precursors and allowing the tight regulation of osteoclast differentiation [24] (Figure 3). Collectively, these studies suggest RANKL-mediated osteoclastogenesis is regulated though intracellular S1P; therefore, alterations in osteoclast S1P responses may result in osteoclastogenesis being unregulated, causing increased bone resorption. An enhanced understanding of how intracellular S1P inhibits p38 may enable the identification of new therapeutic targets to inhibit osteoclast formation and reducing bone formation.

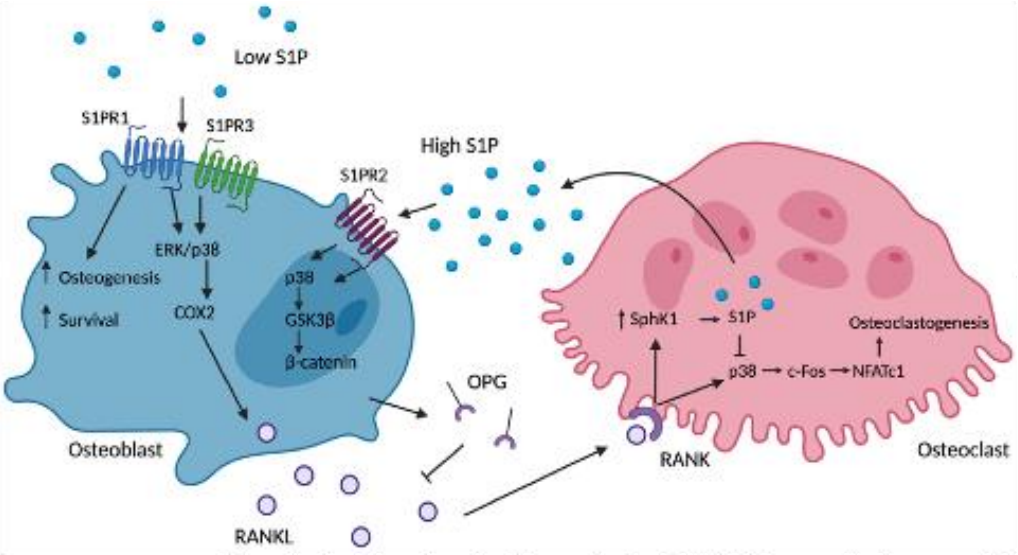


Figure 3. Osteoblast–Osteoclast Communication via S1P. S1P can act directly on osteoblasts via S1PR1/3 receptors to enhance osteoblast maturation and mineralisation [47]. S1PR1/3 also activates the ERK/p38 signalling pathway to enhance COX2 production [24,27]. COX2 then elicits the release of RANKL from osteoblasts to enhance osteoclastogenesis via p38-cfos-NFATc1 signalling [24]. RANK activation of osteoclasts by RANKL also upregulates SPHK1 expression and production, resulting in increased intracellular S1P, which inhibits p38. Inhibition of p38 causes a reduction in osteoclastogenesis, acting as a negative regulator of osteoclast maturation [24]. S1P released from osteoclasts increases extracellular S1P, which may act as a break on osteoclastogenesis through the S1PR2 receptor on osteoblasts, as S1PR2 acts to enhance the secretion of the RANKL decoy receptor osteoprotegerin (OPG) [40]. OPG acts to reduce further RANKL-mediated osteoclastogenesis through binding to RANKL. Created in Biorender.com.

The literature examining the effects of extracellular S1P on osteoclast precursors is both limited and conflicting: one study showed that exogenous S1P has no effect on osteoclastogenesis in bone marrow macrophages (BMM) in culture [24], whilst we have observed the increased differentiation of a murine macrophage-like cell line, RAW264.7, in response to S1P (unpublished observations). One possible explanation for this conflict could be the fact that the expression pattern of S1PR1 and S1PR2 alters during BMMs differentia-

of primary mouse calvarial osteoblasts (unpublished observations). By contrast, we were unable to detect the increases in osteoblast maturation and mineralisation previously reported using MC3T3s. These disparities may be due to differences in the osteogenic media used as both Higashi et al. and Choi et al. supplemented with steroids (dexamethasone or hydrocortisone), whilst neither Matsuzaki et al. nor we did [47,53].

Of all the S1P receptors expressed by MSCs and osteoblasts, the most well-studied in the context of osteoblastogenesis is S1PR2. Isolated murine BMSC from wildtype mice treated with JTE-013 or S1PR2$^{-/-}$ mice exhibited an enhance proliferation as assessed using an MTA assay [41]. Moreover, these cells had lower levels of the osteoblast differentiation marker osteopontin compared to wildtype untreated cells [41], suggesting S1P/S1PR2 signalling enhances osteoblastogenesis and that the inhibition of S1PR2 retains osteoblasts in a prolonged proliferative state.

Members of the SMAD signalling family are required for osteoblastogenesis [53], where SMAD4 forms heteromeric complexes with phosphorylated SMAD1/5/8, resulting in nuclear translocation and regulation of gene expression (e.g., RUNX2 [55]). At high S1P concentrations (2 µM), downstream signalling through ROCK and SMAD1/5/8 signalling led to enhanced RUNX2 gene expression and increased von Kossa staining (a measure of mineralisation) in the MC3T3 murine osteoblastic cell line [50]. These data suggest that S1PR2 is required for the differentiation and maturation of osteoblasts. By contrast, others have shown that S1PR2 inhibition increased adipocyte genetic markers FABP4 [41], suggesting that whilst S1PR2 promotes MSC differentiation, its function is not necessarily osteogenic-lineage specific.

Knockout mice have been used to investigate the function of S1PR1/3; however, S1PR1 global knockout in mice is embryonic lethal [50]. Osteoblast-specific S1PR1 deletion results in viable pups that have no detectable differences in bone formation at either 3 or 8 months [29]. Conversely, S1PR3 global knockout mice are viable and exhibit no developmental defects at 3 months; however, osteopenia is seen at 8 months [29]. This S1PR3$^{-/-}$-induced osteopenia is a result of a reduced bone formation rate demonstrated by reduced BV/TV (a measure of bone volume) and BFR/BS (a measure of bone formation over time), whilst parameters linked to resorption, e.g., serum osteocalcin(OcN)/bone morphogenic protein (BMP) and collagen degradation products (carboxy-terminal collagen crosslinks: CTX) remained unaffected [29]. Furthermore, when S1PR3$^{-/-}$ calvarial and bone-marrow-derived osteoblasts were cultured in the presence of S1P, there was a reduction in mineralisation compared to wildtype cells, suggesting reduced osteoblast maturation, although no other measurements of osteoblast maturation were assessed [29].

Although S1PR1 appears to have no role in post-natal bone remodelling, S1PR3 signalling is required for continued remodelling following skeletal maturation in mice, i.e., from mid-life onwards. Brizuela et al. demonstrated that SPHK1 mRNA expression increased with osteoblast maturation and that the inhibition of SPHK1 using an inhibitor (SK-II) or by the sequestration of S1P with a neutralising antibody reduced osteoblast maturation (as identified through reduced alkaline phosphatase activity and RUNX2 mRNA expression) [28]. A similar reduction in maturation was observed when the S1PR1/3 antagonist (VPC23019) was applied, but not when using specific S1PR1 (W146) or S1PR2 (JTE013) antagonists [28]. Taken together, these data suggest that S1P is essential for osteoblast maturation via S1PR3. As such, S1PR3 agonists may offer a therapeutic benefit in the treatment of catabolic bone disease in adults, but they are not expected to offer the same benefits to children.

7. Role in Osteogenic Communication

To regulate bone remodelling, osteoclasts and osteoblasts secrete a variety of factors that attract, activate, and inhibit each other (reviewed by [56]). This crosstalk is essential for normal bone remodelling, and if communication is disrupted, it results in altered bone formation and resorption. There is some evidence of the impact of S1P on this bidirectional crosstalk. Culturing naïve or activated macrophages with murine bone-marrow-

derived stem cells (BMSCs) was sufficient to induce the upregulation of SPHK1 and S1PR1 mRNA expression [23], suggesting that macrophages secrete molecules that induce SPHK1 and S1PR1 expression in the bone marrow niche. Additionally, co-culturing-activated macrophages with BMSCs resulted in increased RANKL production that was dependent on the activation of S1PR1, where the secretion of RANKL was lost following the siRNA knockdown of S1PR1 [23]. The authors postulate that osteoblast–osteoclast signalling activates S1PR1 and SPHK1, resulting in autocrine S1P/S1PR1 signalling that triggers increased RANKL production, which subsequently stimulates osteoclastogenesis within the co-culture [23] (Figure 3). This example highlights the complexity of S1P communication between osteogenic cells and emphasises the importance of such co-culture experiments.

The molecular mechanisms by which S1P acts as a communication molecule within bone is complex due to its varying roles in migration and differentiation and the sensitivity of its receptors to a fluctuating S1P concentration. The S1P-induced differentiation of MSCs into osteoblasts triggers the release of RANKL and subsequently the osteoclastic release of S1P [24]. This feed-forward mechanism allows the coupling of osteoblasts and osteoclasts, which is important for the regulation of bone remodelling. S1P has also been shown to stimulate RANKL expression in osteoblasts through the upregulation of COX2 via ERK and p38 MAPK pathways [24]. However, a model in which S1P purely stimulates the osteoblast release of RANKL, and its subsequent stimulation of osteoclastogenesis, does not explain the increased bone mass seen in response to S1P lyase inhibition or deletion [35]. The activation of osteoblast-expressed S1PR2 has been reported to cause the release of the soluble RANKL decoy molecules, OPG, via p38-GSK3β-β-catenin and noncanonical WNT5A-LRP5 signalling [23,35,54]. Given that S1PR2 has a lower affinity for S1P compared to S1PR1 [57], one hypothesis is that at low concentrations of S1P S1PR1/3, activation induces RANKL release. RANKL serves to activate osteoclasts and promote a further S1P release. As S1P concentrations increase, there is a shift in S1PR activation towards S1PR2, resulting in an alteration in the RANKL/OPG ratio in favour of OPG, which reduces bone resorption rates. An alternative explanation is that increased S1P results in S1PR1 internalisation, thereby reducing RANKL production and altering the RANKL/OPG ratio in favour of bone formation (Figure 3). Collectively, S1P bioavailability regulates the activation and the cessation of bone resorption.

Calcitonin has been shown to impact osteoclast–osteoblast communication via S1P. Calcitonin downregulates the gene expression of the S1P transporter, SPNS2, on primary murine osteoclasts [29] and is a negative regulator of bone formation. Calcitonin receptor knockout mice ($CALCR^{-/-}$) have increased trabecular bone volume and evidence of increased bone formation rate (serum alkaline phosphatase levels are increased) [29]. No effect on bone resorption markers (e.g., collagen breakdown products—CTX assay) were detected in these mice [29]. In response to calcitonin, Keller et al. observed that SPNS2 gene expression was downregulated in wild type osteoclasts [29]. This reduction in SPNS2 gene expression was coupled with a reduction in extracellular S1P, a difference that was not observed in the osteoclasts from $CALCR^{-/-}$ mice. These data indicate that calcitonin reduces S1P secretion from osteoclasts via the inhibition of SPNS2. The phenotype was lost in $CALCR^{-/-}$ mice when S1PR3 was knocked out in osteoblasts [29], suggesting that S1P secreted by osteoclasts in response to calcitonin acts to increase osteoblast maturation and mineralisation via S1PR3. Calcitonin acts to negatively regulate this circuit via the inhibition of osteoclastic secretion of S1P. Together, these data imply that calcitonin naturally regulates bone remodelling through altering S1P-mediated osteoclast–osteoblast communication.

As detailed above, the mechanisms by which S1P acts as a key regulator of bone remodelling (through communication between osteoblasts and osteoclasts) are starting to be uncovered. Challenges in the isolation and culture of osteocytes have limited research into how this S1P-mediated communication affects osteocytes. A recently developed osteocyte cell line (Ocy454 [58]) has been shown to increase the production of S1P in response to mechanical stimulation, which triggers the upregulation of SPHK1 and downregulation of SPPases (SGP11 and SGPP11) [59,60]. If confirmed in vivo, these data could indicate

that S1P functions in the activation of the bone remodelling cycle, attracting osteoclast and osteoblast precursors to the site of injury and promoting osteogenesis within the bone modelling unit. These findings suggest the existence of a positive feedback loop, whereby S1P is produced by osteocytes in response to mechanical stimulation which acts directly on osteocyte S1PRs to further increase S1P release [60]. Moreover, intracellular levels of S1P enhance calcium and prostaglandin E2 signalling in osteocytes (Ocy454 [61]), raising the possibility that S1P influences other osteocyte functions. Exactly how extracellular S1P and S1PR expression on osteocytes impacts communication with other bone resident cells following activation is unclear and further research is urgently required.

8. S1P in Catabolic Bone Diseases

8.1. Osteoporosis

Osteoporosis is a common bone disorder affecting 23.1% of women and 11.7% of men aged 18–95 globally [62]. The disorder is characterised by a decreased bone mineral density and bone strength, increased risk of fracture, reduced quality of life, and increased morbidity [62]. Osteoporosis develops due to a disturbance in the balance between osteoclast-mediated bone resorption and osteoblast-mediated bone formation, resulting in excessive resorption and net bone loss [62]. Although both sexes can be affected by osteoporosis, with the incidence rising with age, postmenopausal women are at the highest risk (reviewed by [63]).

Kim et al. (2016) and Bae et al. (2016) observed that osteoporosis patients display a higher ratio of S1P in their plasma compared to bone marrow, with an additional study by Ardawi et al. (2018) finding a positive correlation between osteoporosis-related fracture and S1P plasma levels [64–66]. Increased plasma levels of S1P steepen the concentration gradient between the tissues, resulting in the increased migration of osteoclast precursors to the bone parenchyma. Osteoporosis patients show an increased expression of bone resorption markers, despite no alterations in bone formation markers [64,67,68]. This increase in resorption can be attributed to the enhanced migration of osteoclast precursors into the tissue [64,67,68] (Figure 4). A large population-based cohort by Weske et al. (2018) demonstrated a strong positive correlation between plasma S1P and bone formation markers (procollagen type 1 N-terminal propeptide (PINP) [35]. In contrast to the aforementioned studies, increased calcium and a reduced bone resorption (C-terminal telopeptide of type 1 collagen—CTX) were also correlated with high plasma S1P levels [68]. The paucity of data in all these studies on the levels of S1P in the bone marrow and parenchyma (and therefore the ratio between bone and blood) makes their interpretation challenging. Ahn et al. reported decreased levels of S1P within the bone marrow of patients who experienced an osteoporotic hip fracture, suggesting that the S1P gradient is steepened by both changes in plasma and tissue S1P [69]. However, due to the high rate of turnover of S1P in bone, the accuracy of these measurements is uncertain.

The reliability of the S1P measurement is also a limiting factor. S1P can bind to carrier proteins, such as HDL, LDL, and albumin. Tests vary in their ability to detect the bound lipid, leading to the inaccurate detection of S1P bioavailability. Song et al. reported that bound S1P has distinct functions based on the related carrier protein [65], where for that which is albumin-bound but not HDL-bound, S1P was associated with an increased risk of osteoporotic fracture, indicating that HDL acts as a scavenger protein to reduce S1P function. However, the effects of albumin-bound S1P alone were lost following corrections for confounding factors [65], with only total S1P showing a significant difference in fracture risk. Clearly, further investigation is required to understand the involvement of S1P carrier proteins and the deleterious effects of S1P in osteoporosis.

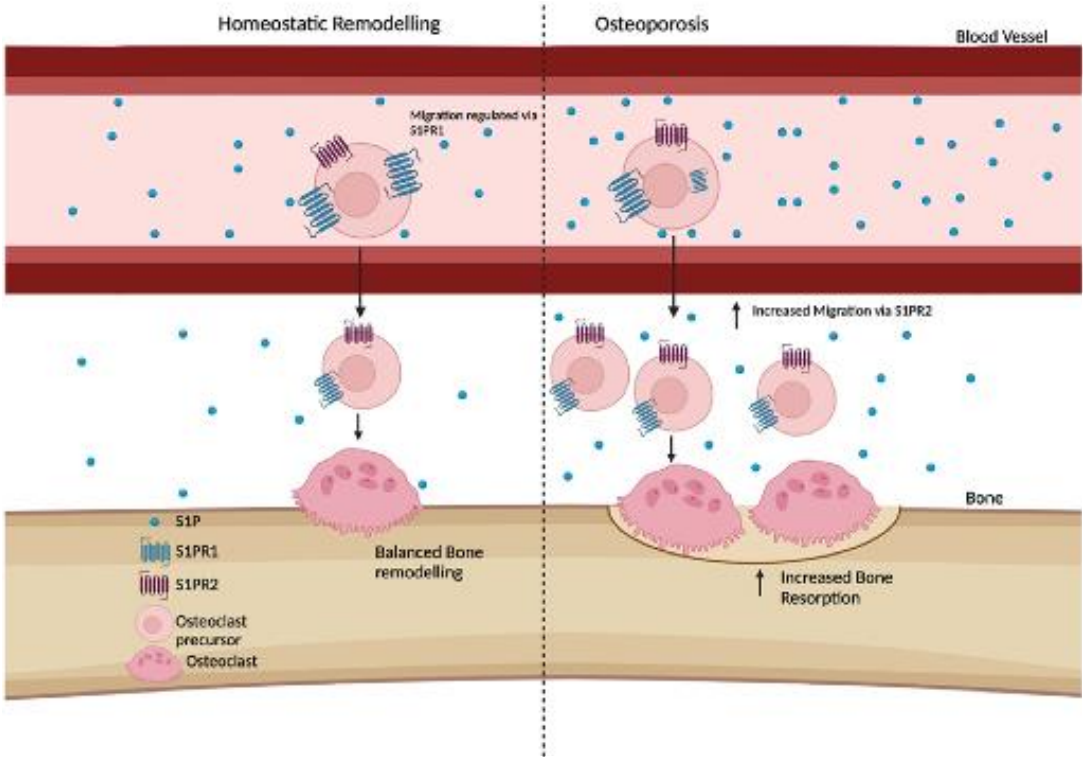


Figure 4. Osteoclast precursor migration is increased in osteoporosis due to increased plasma S1P. During typical homeostatic remodelling, it has been suggested that the S1P gradient allows for regulated migration of osteoclast precursors into the bone tissue via S1PR2 [35,36]. This is regulated via S1PR1, which opposes S1PR2, keeping some cells within circulation. Osteoporotic patients express increased plasma S1P [64–66]. This is thought to result in internalisation of the regulator receptor, S1PR1, causing increased migration of cells due to reduced opposition to S1PR2. Due to increased S1PR2 activity on osteoclast precursors, there are more migrating precursors that are thought to result in an increase in osteoclast numbers within the tissue, resulting in increased bone resorption. Created in Biorender.com.

As osteoporosis is most prevalent in postmenopausal women, substantial research has been performed investigating the association between S1P and oestrogen. Oestrogen plays an essential role in the development and maintenance of bone, having a variety of indirect and direct effects on formation and resorption [63]. The production of S1P has been linked to the activity of 17β-oestradiol (E2), and both S1P and oestrogen have been shown to enhance osteoblast proliferation [70]. E2 increased SphK1 mRNA expression and protein expression in human osteoblasts, whilst S1P caused an upregulation in ERβ but not Erα mRNA, as well as an increase in SPHK1 and S1PR1 [70]. It is likely that fluctuations in oestrogen may result in alterations within S1P signalling, but further research is required to identify whether the use of S1P signalling modulators could act as osteoporosis therapeutics.

The risk of osteoporosis is very strongly correlated with ageing, yet few studies have looked specifically at the effect of age on S1P as most participants were postmenopausal women [64,65,67,68,71,72]. The studies that have used patients undergoing hip replacement surgery [67,69] often have smaller sample sizes and predominantly include female participants who are over 50. Moreover, they also frequently fail to report sex differences. Although sex is recorded, it is often adjusted for rather than comparative data being pre-

sented; therefore, any sex differences in the role of S1P in bone are lost within the data. A recent review discussed the involvement of S1P in the dysregulation of nutrient sensing, cellular senescence, and proteostasis with age, and all these factors could impact bone remodelling [73]. Although there is substantial evidence of the role of S1P in age-related disease, such as osteoporosis, the role of age-related changes in S1P expression on bone function is required in order to establish whether it has any bearing on age-related decline in bone density.

Taken together, these data suggest that S1P could act as a potential biomarker for osteoporosis, allowing an earlier intervention prior to severe bone loss. Moreover, S1P poses an interesting therapeutic target for osteoporosis through the use of S1PR2 inhibitors, which would reduce bone resorption by partially inhibiting osteoclast precursor migration. Despite these exciting clinical benefits, considerable further research is required as highlighted here, especially dissecting the causal link between changes in S1P signalling within the bone with age and/or sex and increased risk of osteoporosis in postmenopausal women and the elderly.

8.2. Paget's Disease

Paget's disease of bone (PDB) is a chronic and progressive focal skeletal disorder [74] which can manifest as a monostotic (singular bone) or polyostotic (multiple bone) phenotype [75]. Typically, this disease affects adults over the age of 55, resulting in increased bone fragility and bone pain in the affected area [76]. PDB skeletal lesions are caused by increased bone resorption coupled with disorganised bone formation [77] and altered vascular infiltration. Histologically, PDB patients have increased numbers of osteoclasts, which are larger and display higher levels of activity compared to osteoclasts from healthy controls [78].

Although it is the altered morphology and activity of osteoclasts that drives pathogenesis in PDB, the increased secretion of molecules, such as S1P, from these osteoclasts also results in an altered osteoblast function [79]. It has been recently shown that osteoclasts from both PDB patients and the Measles virus nucleocapsid protein (MVNP) mouse model of PDB display an increased expression of S1PK1, resulting in increased S1P production [79]. Additionally, osteoblasts from PDB patients and MVNP mice express increased S1PR3, with no differences in the expression of S1PR1 and S1PR2, when compared to osteoblasts isolated from healthy controls [79]. An in vitro co-culture of osteoclasts and osteoblasts from MVNP mice showed an increased S1PR3 expression compared to control mice [79]. The activation of the S1PR3 receptor with the S1PR3 agonist VPC24191 enhanced the osteoblast differentiation and expression of RUNX2 and COL1A1 [79]. The S1PR3 antagonist VPC23019, which decreased levels of differentiation genes, such as Osterix, was observed [79]. These data suggest the involvement of S1P in Paget's disease, with a particular emphasis on the role of S1PR3, indicating a potential target for a future therapeutic to inhibit the dysregulation of osteoblasts. Further studies are required to identify which molecule(s) are mediating the upregulation of S1PR3 in osteoblasts. S1P is known to upregulate S1PR3 in other cell types, making it an obvious candidate for further investigation. Additional evidence revealing the link between S1P signalling within osteoblasts and osteoclasts and dysregulated function has the potential to identify novel therapeutic targets that might have clinical utility in PD in the future.

8.3. Inflammatory Diseases with Bone Damage

S1P has been known as a key driver of inflammation and is able to influence the migration of inflammatory cells and alter cytokine production (reviewed by [80]). Bone loss occurs both systemically and locally in several inflammatory diseases, such as rheumatoid arthritis (RA) and periodontitis (reviewed by [81]). In recent years, S1P has been investigated for its role in joint and bone inflammatory pathologies and mooted as a therapeutic target in several diseases.

8.3.1. Rheumatoid Arthritis

Rheumatoid arthritis (RA) is a common autoimmune disorder characterised by persistent inflammation of the synovium and the destruction of cartilage and bone. One study, looking at the presence of S1P within the synovium of RA patients, showed a significant increase in S1P [82]. Lai et al. assessed the involvement of S1P in the collagen-induced arthritis (CIA) model of RA. The inhibition of SPHK1 by pharmacological (N-N-Dimethylsphingosine—DMS) or siRNA knockdown highlighted its involvement in joint destruction and inflammation [82]. DMS-mediated inhibition significantly reduced joint erosion and inflammation, reducing the incidence and severity of arthritis [82]. Similar observations were made using siRNA knockdown, which collectively suggested that an increased production of S1P via SPHK1 is required for the progression of inflammatory arthritis in the CIA model [82].

A large variety of cell types are involved in the pathogenesis of RA, and much of the research in this area has focused on S1P involvement in non-osteogenic cell types (recently reviewed by [83]). To the best of our knowledge, no one has investigated the action of S1P specifically on osteoblasts during RA pathogenesis. Current research has worked on the assumption that increased S1P within the synovium will increase the migration of osteoclasts to the bone surface to cause increased bone resorption [84].

There are a few studies that have reported alterations in bone parameters or bone cells in animal models of inflammatory arthritis [85–87]. One study did observe reduced bone erosion when FTY720, a high-affinity agonist of S1PRs, was administered to the SKG mouse (described by [88]) that spontaneously develops arthritis [86]. However, no other bone parameters were reported; therefore, it cannot be determined whether the reduced erosion was due to reduced osteoclast function or reduced joint swelling and inflammation. Only two papers have looked in detail at osteoclasts within an inflammatory arthritis model [85,87]. Using the FAS-deficient MRL/lpr model of spontaneous inflammatory arthritis, the authors highlighted significant bone loss due to an increased number of osteoclasts [87]. The analysis of mandibular condyle tissue showed an upregulation of SPHK1 and S1PR1 gene expression and an increase in the number of SPHK1- and S1PR1-positive cells in these mice compared to uninflamed control animals [87]. The addition of the NF-κB inhibitor SN50 reduced the number of TRAP-positive cells and attenuated the subchondral trabecular bone loss seen in MRL/lpr mice [87]. Additionally, SN50 decreased the number of SPHK1- and S1PR1-positive cells, suggesting that FAS and S1P/S1PR1 signalling act in concert with NF-κB to exacerbate pathogenesis in this model [87]. When hTNFα transgenic mice were crossed with SPHK1$^{-/-}$ mice, a reduction in bone erosion was observed, with fewer mature osteoclasts in a location away from the bone margin being observed [88]. In the presence of excessive TNFα, SPHK1 or S1P production may be important for osteoclast maturation and activity, possibly due to changes in the S1P gradient that limit osteoclast precursor migration [85].

We also identified one clinical trial targeting the S1P pathway in RA (clinical trial: NCT00847886). The study involved LX3305, an inhibitor of S1P lyase that prevents the degradation of S1P. The inhibition of S1P lyase has been shown to increase bone mass [35] through the removal of the S1P gradient to reduce osteoclast precursors migration. The LX3305 phase 2 trial was completed in 2010; however, to date, the results of the trial have not been publicly reported.

8.3.2. Periodontitis

Periodontitis is an inflammatory disease of the oral cavity which results in the destruction of the alveolar bone and other structures that support the teeth. Left untreated, periodontitis can cause severe pain and tooth loss. Analysis of a large population-based cohort showed that the serum concentration of S1P was greatly upregulated in patients with moderate and severe periodontitis compared to healthy controls [89]. Additionally, the SPHK1 protein expression was upregulated in gingival tissue samples from participants

with periodontitis compared to healthy controls, suggesting that there are alterations in S1P metabolism in the context of periodontitis [89].

There are a number of identified risk factors for both periodontitis and RA: increasing age, female sex, smoking [90,91], and poor oral hygiene [92]. The effect of these environmental and biological risk factors on S1P production and function is likely to impact disease initiation and progression. Smoking alone has been implicated in the dysfunction of bone remodelling, resulting in reduced bone mass and bone mineral density, increasing the risk of osteoporosis [93]. The mechanisms surrounding this have been discussed at length in (review Al-Bashaireh et al., 2018 [93]). Overwhelming evidence suggests smoking can have direct effects on the bone by reducing osteogenesis and angiogenesis, as well as having indirect effects through alterations in antioxidant and cortisol production [93].

Research in other diseases (e.g., chronic obstructive pulmonary disease) has shown that smoking alters the S1P function by increasing levels of S1PRs and kinase activity [94,95]. Although the effect of smoking on S1P and other sphingolipids in the context of bone formation has not been formally studied, smoking has been shown to affect fracture healing [96,97]. Thymoquinone (TMQ) has previously been reported to increasing sphingolipid signalling in monocyte by increasing receptor mRNA expression [98]. Of relevance here, one study has investigated the effect of cigarette smoke on the efficacy of TMQ [97] in mice subjected to a model of bone healing. In this model, TMQ alone enhanced fracture healing, demonstrated by increased new bone formation, osteoblast number, and OPG:RANKL ratio [97]. Mice that received cigarette smoke (CS) alone or in addition to TMQ showed an increase in osteoblast number and OPG, with reduced RANKL expression [97]. Unfortunately, the mechanism of action of TMQ in relationship to the bone was not discussed in this study. Additional work is required to determine whether this is due to TMQ actions of S1PR expression, as previously shown [98].

Additionally, periodontitis is a risk factor for the development of RA [99], amongst other conditions, and, as such, aberrant S1P signalling within affected individuals could increase the frequency of comorbidity between these disorders and contribute to systemic bone damage. The above data suggest that S1P signalling is important within inflammation-mediated bone erosion. To understand the impact of S1P on bone formation and resorption in inflammatory disease, it is necessary to uncouple direct effects on the bone from the well-known effect of S1P on inflammation. Interventions that target S1P signalling will affect the bone and immune system, and separating the direct and indirect effects is extremely challenging. The current data suggest that there are alterations in S1P signalling in RA and periodontitis that drive inflammatory bone loss within these diseases. However, further research is required to unpack which are direct effects to enable the development of targeted therapeutics from the bone.

9. Conclusions

Increasing interest in the role of S1P in bone remodelling has revealed that it contributes to progenitor migration, homeostasis, and osteoblast/cyte–osteoclast communication. This review has shown that, although the field is in its infancy, there is a growing body of evidence indicating that S1P signalling is critical for bone homeostasis and that the disruption of these pathways can result in the dysregulation of bone remodelling. The notable actions of S1P in osteoblasts and osteoclasts are summarised in Table 1, along with their potential utility as therapeutic targets in the treatment of catabolic bone disease.

Gaps in the published data have led to the extrapolation of scientific dogma, such as the sphingosine rheostat, from other cell types, and this requires an urgent verification and examination of how the sphingosine rheostat within bone tissue alters S1P metabolism and how it may impact cell function and crosstalk. Going forward, the methodologies of any future study on this topic will need to be very carefully defined to allow an adequate interpretation of the data obtained. However, despite these limitations, the findings to date offer some hope that the S1P signalling pathway may be an attractive biomarker and/or therapeutic target for metabolic and inflammatory bone diseases in the future.

Table 1. Summary table outlining the effects of S1P on the different stages of bone remodelling and their potential as therapeutic targets in catabolic bone disorders.

Cell Type, Function	Effect of S1P Signalling	Therapeutic Application in Catabolic Bone Disorders	Ref
Osteoblast migration	S1PR1 and S1PR3 mediate chemoattraction to S1P—supports migration of precursors to the bone surface. S1PR2 has dual actions: low concentrations promote migration towards S1P. High concentrations cause chemo-repulsion.	Direct targeting of receptors is contraindicated due to expected off-target effects on osteoclasts. Targeting of downstream signalling could prove effective.	[43,44]
Osteoblast proliferation	Exogenous application of S1P increases proliferation. Inhibition of S1PR2 enhances proliferation but not differentiation.	Inhibition of S1PR2 enhances total osteoblast number but not their maturation. Unlikely to be effective therapeutically.	[41,52]
Osteoblast differentiation	S1P increases osteoblast differentiation. S1PR2 is required for osteoblast differentiation and maturation. Inhibition reduces differentiation. S1P signalling via S1PR3 is required for bone formation and maintenance.	S1PR3 is an interesting potential therapeutic target as (unlike, e.g., S1PR2) it has no alternative effects on osteoclasts. S1PR3 agonists likely to increase osteoblast differentiation and increase bone formation.	[29,41,47,50,51,53]
Osteoclast migration	S1PR1 is required for chemoattraction to S1P, maintaining osteoclast precursors within the circulation. S1PR2 is required for chemorepulsion towards S1P, promoting osteoclast precursors migration to tissue.	Inhibition of S1PR2 via antagonists (e.g., JTE013), may lower the number of osteoclasts present within bone tissue, reducing resorption.	[36,37,39,40]
Monocyte fusion	S1PR2 is required for monocyte fusion into osteoclasts, via regulation of podosome-adhesive proteins.	Inhibition of S1PR2 via antagonists (e.g., JTE013) prevents osteoclast formation, reducing resorption.	[40]
Osteoclast differentiation	SPHK1 is required for negative regulation of RANKL-mediated differentiation, through suppression of p38 signalling. The impact of exogenous S1P on osteoclast differentiation is unknown (incomplete data available).	Therapeutics that upregulate SPHK1 function or suppress p38 signalling may reduce mature osteoclasts.	[24,48]
RANKL production	Activation of S1PR1/3 on osteoblasts induces RANKL release, via activation of ERK/p38.	Reduction of RANKL-mediated osteoclast differentiation could be achieved through inhibition of osteoblast S1PR1/S1PR3 receptors or targeting the downstream signalling pathways.	[23]
OPG Production	Activation of S1PR2 on osteoblasts induces OPG release via GSK3β and β-catenin.	S1PR2 agonists or targeting of β-catenin-mediated secretion of OPG may reduce osteoclast numbers to prevent bone resorption.	[23,35,54]

Author Contributions: Conceptualisation, writing—original draft preparation and writing—review and editing—K.F., A.J.N. and H.M.M. Supervision, project administration and funding acquisition, A.J.N. and H.M.M. All authors have read and agreed to the published version of the manuscript.

Funding: KF was supported by supported by Ph.D. studentship funded by Chernajovksy Foundation. This work was also supported by an MRC (Medical Research Council) project, grant MR/T028025/1. AJN was supported by a Career Development Fellowship from Versus Arthritis #21743. This paper represents independent research part-funded by the MRC-Versus Arthritis Centre for Musculoskeletal Ageing Research MR/P021220/1. The views expressed are those of the authors and not necessarily those of the MRC or Versus Arthritis.

Institutional Review Board Statement: Not applicable.

Informed Consent Statement: Not applicable.

Data Availability Statement: No new data have been created.

Conflicts of Interest: All authors have no conflicts of interests to declare.

References

1. Jilka, R.L. Biology of the basic multicellular unit and the pathophysiology of osteoporosis. *Med. Pediatr. Oncol.* **2003**, *41*, 182–185. [CrossRef] [PubMed]
2. Feng, X.; McDonald, J.M. Disorders of bone remodeling. *Annu. Rev. Pathol. Mech. Dis.* **2011**, *6*, 121–145. [CrossRef] [PubMed]
3. Rutherford, C.; Childs, S.; Ohotski, J.; Mcglynn, L.; Riddick, M.; Macfarlane, S.; Tasker, D.; Pyne, S.; Pyne, N.J.; Edwards, J.; et al. Regulation of cell survival by sphingosine-1-phosphate receptor S1P1 via reciprocal ERK-dependent suppression of Bim and PI-3-kinase/protein kinase C-mediated upregulation of Mcl-1. *Cell Death Dis.* **2013**, *4*, e927. [CrossRef] [PubMed]
4. Wang, H.; Huang, H.; Ding, S.F. Sphingosine-1-phosphate promotes the proliferation and attenuates apoptosis of Endothelial progenitor cells via S1PR1/S1PR3/PI3K/Akt pathway. *Cell Biol. Int.* **2018**, *42*, 1492–1502. [CrossRef]
5. Zhao, Z.; Chen, Z.; Zhao, X.; Pan, F.; Cai, M.; Wang, T.; Zhang, H.; Lu, J.R.; Lei, M. Sphingosine-1-phosphate promotes the differentiation of human umbilical cord mesenchymal stem cells into cardiomyocytes under the designated culturing conditions. *J. Biomed. Sci.* **2011**, *18*, 37. [CrossRef] [PubMed]
6. Pérez-Jeldres, T.; Alvarez-Lobos, M.; Rivera-Nieves, J. Targeting Sphingosine-1-Phosphate Signaling in Immune-Mediated Diseases: Beyond Multiple Sclerosis. *Drugs* **2021**, *81*, 985–1002. [CrossRef]
7. Boyce, B.F. Advances in the regulation of osteoclasts and osteoclast functions. *J. Dent. Res.* **2013**, *92*, 860–867. [CrossRef]
8. Wang, X.; Wang, Y.; Gou, W.; Lu, Q.; Peng, J.; Lu, S. Role of mesenchymal stem cells in bone regeneration and fracture repair: A review. *Int. Orthop.* **2013**, *37*, 2491. [CrossRef]
9. Crockett, J.C.; Mellis, D.J.; Scott, D.I.; Helfrich, M.H. New knowledge on critical osteoclast formation and activation pathways from study of rare genetic diseases of osteoclasts: Focus on the RANK/RANKL axis. *Osteoporos. Int.* **2011**, *22*, 1–20. [CrossRef]
10. Blumer, M.J.F.; Hausott, B.; Schwarzer, C.; Hayman, A.R.; Stempel, J.; Fritsch, H. Role of tartrate-resistant acid phosphatase (TRAP) in long bone development. *Mech. Dev.* **2012**, *129*, 162. [CrossRef]
11. Saftig, P.; Hunziker, E.; Everts, V.; Jones, S.; Boyde, A.; Wehmeyer, O.; Suter, A.; von Figura, K. Functions of cathepsin K in bone resorption. Lessons from cathepsin K deficient mice. *Adv. Exp. Med. Biol.* **2000**, *477*, 293–303. [CrossRef]
12. Capulli, M.; Paone, R.; Rucci, N. Osteoblast and osteocyte: Games without frontiers. *Arch. Biochem. Biophys.* **2014**, *561*, 3–12. [CrossRef]
13. Yoshiko, Y.; Candeliere, G.A.; Maeda, N.; Aubin, J.E. Osteoblast Autonomous Pi Regulation via Pit1 Plays a Role in Bone Mineralization. *Mol. Cell. Biol.* **2007**, *27*, 4465. [CrossRef] [PubMed]
14. Siddiqui, J.A.; Partridge, N.C. Physiological bone remodeling: Systemic regulation and growth factor involvement. *Physiology* **2016**, *31*, 233–245. [CrossRef] [PubMed]
15. Negishi-Koga, T.; Takayanagi, H. Bone cell communication factors and Semaphorins. *Bonekey Rep.* **2012**, *1*, 183. [CrossRef] [PubMed]
16. Khosla, S.; Oursler, M.J.; Monroe, D.G. Estrogen and the skeleton. *Trends Endocrinol. Metab.* **2012**, *23*, 576–581. [CrossRef]
17. Qi, T.; Li, L.; Weidong, T. The Role of Sphingolipid Metabolism in Bone Remodeling. *Front. Cell Dev. Biol.* **2021**, *9*, 752540. [CrossRef]
18. el Bawab, S.; Mao, C.; Obeid, L.M.; Hannun, Y.A. Ceramidases in the regulation of ceramide levels and function. *Subcell. Biochem.* **2002**, *36*, 187–205. [CrossRef]
19. Ksia˙zek, M.; Chacińska, M.; Chabowski, A.; Baranowski, M. Sources, metabolism, and regulation of circulating sphingosine-1-phosphate. *J. Lipid Res.* **2015**, *56*, 1271–1281. [CrossRef]
20. Pralhada Rao, R.; Vaidyanathan, N.; Rengasamy, M.; Mammen Oommen, A.; Somaiya, N.; Jagannath, M.R. Sphingolipid Metabolic Pathway: An Overview of Major Roles Played in Human Diseases. *J. Lipids* **2013**, *2013*, 178910. [CrossRef]
21. Strub, G.M.; Maceyka, M.; Hait, N.C.; Milstien, S.; Spiegel, S. Extracellular and Intracellular Actions of Sphingosine-1-Phosphate. *Adv. Exp. Med. Biol.* **2010**, *688*, 141. [CrossRef]

22. Maceyka, M.; Harikumar, K.B.; Milstien, S.; Spiegel, S. Sphingosine-1-phosphate signaling and its role in disease. *Trends Cell Biol.* **2012**, *22*, 50. [CrossRef]
23. Xiao, L.; Zhou, Y.; Zhu, L.; Yang, S.; Huang, R.; Shi, W.; Peng, B.; Xiao, Y. SPHK1-S1PR1-RANKL Axis Regulates the Interactions Between Macrophages and BMSCs in Inflammatory Bone Loss. *J. Bone Miner. Res.* **2018**, *33*, 1090–1104. [CrossRef]
24. Ryu, J.; Kim, H.J.; Chang, E.J.; Huang, H.; Banno, Y.; Kim, H.H. Sphingosine 1-phosphate as a regulator of osteoclast differentiation and osteoclast-osteoblast coupling. *EMBO J.* **2006**, *25*, 5840–5851. [CrossRef]
25. Alvarez, S.E.; Milstien, S.; Spiegel, S. Autocrine and paracrine roles of sphingosine-1-phosphate. *Trends Endocrinol. Metab.* **2007**, *18*, 300–307. [CrossRef]
26. Walker, J.M.; Yao, G.Q.; Siu, E.; Zhu, M.; Sun, B.H.; Simpson, C.; Insogna, K.L. An Unanticipated Role for Sphingosine Kinase-2 in Bone and in the Anabolic Effect of Parathyroid Hormone. *Endocrinology* **2021**, *162*, bqab042. [CrossRef]
27. Bao, X.; Ogawa, T.; Se, S.; Akiyama, M.; Bahtiar, A.; Takeya, T.; Ishida-Kitagawa, N. Acid sphingomyelinase regulates osteoclastogenesis by modulating sphingosine kinases downstream of RANKL signaling. *Biochem. Biophys. Res. Commun.* **2011**, *405*, 533–537. [CrossRef] [PubMed]
28. Brizuela, L.; Martin, C.; Jeannot, P.; Ader, I.; Gstalder, C.; Andrieu, G.; Bocquet, M.; Laffosse, J.M.; Gomez-Brouchet, A.; Malavaud, B.; et al. Osteoblast-derived sphingosine 1-phosphate to induce proliferation and confer resistance to therapeutics to bone metastasis-derived prostate cancer cells. *Mol. Oncol.* **2014**, *8*, 1181–1195. [CrossRef]
29. Keller, J.; Catala-Lehnen, P.; Huebner, A.K.; Jeschke, A.; Heckt, T.; Lueth, A.; Krause, M.; Koehne, T.; Albers, J.; Schulze, J.; et al. Calcitonin controls bone formation by inhibiting the release of sphingosine 1-phosphate from osteoclasts. *Nat. Commun.* **2014**, *5*, 5215. [CrossRef] [PubMed]
30. Feehan, J.; Kassem, M.; Pignolo, R.J.; Duque, G. Bone From Blood: Characteristics and Clinical Implications of Circulating Osteogenic Progenitor (COP) Cells. *J. Bone Miner. Res.* **2021**, *36*, 12–23. [CrossRef] [PubMed]
31. Golan, K.; Kollet, O.; Lapidot, T. Dynamic cross talk between S1P and CXCL12 regulates hematopoietic stem cells migration, development and bone remodeling. *Pharmaceuticals* **2013**, *6*, 1145–1169. [CrossRef] [PubMed]
32. Thuy, A.V.; Reimann, C.M.; Hemdan, N.Y.A.; Gräler, M.H. Sphingosine 1-phosphate in blood: Function, metabolism, and fate. *Cell. Physiol. Biochem.* **2014**, *34*, 158–171. [CrossRef]
33. Spiegel, S.; Milstien, S. The outs and the ins of sphingosine-1-phosphate in immunity. *Nat. Rev. Immunol.* **2011**, *11*, 403. [CrossRef]
34. Meshcheryakova, A.; Mechtcheriakova, D.; Pietschmann, P. Sphingosine 1-phosphate signaling in bone remodeling: Multifaceted roles and therapeutic potential. *Expert Opin. Ther. Targets* **2017**, *21*, 725. [CrossRef] [PubMed]
35. Weske, S.; Vaidya, M.; Reese, A.; Von Wnuck Lipinski, K.; Keul, P.; Bayer, J.K.; Fischer, J.W.; Flögel, U.; Nelsen, J.; Epple, M.; et al. Targeting sphingosine-1-phosphate lyase as an anabolic therapy for bone loss. *Nat. Med.* **2018**, *24*, 667–678. [CrossRef]
36. Ishii, T.; Shimazu, Y.; Nishiyama, I.; Kikuta, J.; Ishii, M. The role of sphingosine 1-phosphate in migration of osteoclast precursors; An application of intravital two-photon microscopy. *Mol. Cells* **2011**, *31*, 399–403. [CrossRef]
37. Ishii, M.; Egen, J.G.; Klauschen, F.; Meier-Schellersheim, M.; Saeki, Y.; Vacher, J.; Proia, R.L.; Germain, R.N. Sphingosine-1-phosphate mobilizes osteoclast precursors and regulates bone homeostasis. *Nature* **2009**, *458*, 524–528. [CrossRef] [PubMed]
38. Boyce, B.F.; Xing, L. Biology of RANK, RANKL, and osteoprotegerin. *Arthritis Res. Ther.* **2007**, *9* (Suppl. S1), 1–7. [CrossRef]
39. Tomimori, Y.; Mori, K.; Koide, M.; Nakamichi, Y.; Ninomiya, T.; Udagawa, N.; Yasuda, H. Evaluation of pharmaceuticals with a novel 50-hour animal model of bone loss. *J. Bone Miner. Res.* **2009**, *24*, 1194–1205. [CrossRef]
40. Hsu, L.C.; Reddy, S.V.; Yilmaz, Ö.; Yu, H. Sphingosine-1-phosphate receptor 2 controls podosome components induced by RANKL affecting osteoclastogenesis and bone resorption. *Cells* **2019**, *8*, 17. [CrossRef]
41. Price, S.T. Sphingosine 1-Phosphate Receptor 2 Regulates the Migration, Proliferation, and Differentiation of Mesenchymal Stem Cells. *Int. J. Stem Cell Res. Ther.* **2015**, *2*, 14. [CrossRef] [PubMed]
42. Sassoli, C.; Pierucci, F.; Zecchi-Orlandini, S.; Meacci, E. Sphingosine 1-phosphate (S1P)/S1P receptor signaling and mechanotransduction: Implications for intrinsic tissue repair/regeneration. *Int. J. Mol. Sci.* **2019**, *20*, 5545. [CrossRef] [PubMed]
43. Kong, Y.; Wang, H.; Lin, T.; Wang, S. Sphingosine-1-phosphate/s1p receptors signaling modulates cell migration in human bone marrow-derived mesenchymal stem cells. *Mediat. Inflamm.* **2014**, *2014*, 565369. [CrossRef]
44. Quint, P.; Ruan, M.; Pederson, L.; Kassem, M.; Westendorf, J.J.; Khosla, S.; Oursler, M.J. Sphingosine 1-phosphate (S1P) receptors 1 and 2 coordinately induce mesenchymal cell migration through s1p activation of complementary kinase pathways. *J. Biol. Chem.* **2013**, *288*, 5398–5406. [CrossRef] [PubMed]
45. Rousselle, A.V.; Heymann, D. Osteoclastic acidification pathways during bone resorption. *Bone* **2002**, *30*, 533–540. [CrossRef]
46. Sun, Y.; Li, J.; Xie, X.; Gu, F.; Sui, Z.; Zhang, K.; Yu, T. Recent Advances in Osteoclast Biological Behavior. *Front. Cell Dev. Biol.* **2021**, *9*, 1–19. [CrossRef]
47. Choi, B.; Kim, J.E.; Park, S.O.; Kim, E.Y.; Oh, S.; Choi, H.; Yoon, D.; Min, H.J.; Kim, H.R.; Chang, E.J. Sphingosine-1-phosphate hinders the osteogenic differentiation of dental pulp stem cells in association with AKT signaling pathways. *Int. J. Oral Sci.* **2022**, *14*, 21. [CrossRef]
48. Kikuta, J.; Kawamura, S.; Okiji, F.; Shirazaki, M.; Sakai, S.; Saito, H.; Ishii, M. Sphingosine-1-phosphate-mediated osteoclast precursor monocyte migration is a critical point of control in antibone-resorptive action of active vitamin D. *Proc. Natl. Acad. Sci. USA* **2013**, *110*, 7009–7013. [CrossRef]
49. Grey, A.; Xu, X.; Hill, B.; Watson, M.; Callon, K.; Reid, I.R.; Cornish, J. Osteoblastic cells express phospholipid receptors and phosphatases and proliferate in response to sphingosine-1-phosphate. *Calcif. Tissue Int.* **2004**, *74*, 542–550. [CrossRef]

50. Hashimoto, Y.; Matsuzaki, E.; Higashi, K.; Takahashi-Yanaga, F.; Takano, A.; Hirata, M.; Nishimura, F. Sphingosine-1-phosphate inhibits differentiation of C3H10T1/2 cells into adipocyte. *Mol. Cell. Biochem.* **2015**, *401*, 39–47. [CrossRef]
51. Hashimoto, Y.; Kobayashi, M.; Matsuzaki, E.; Higashi, K.; Takahashi-Yanaga, F.; Takano, A.; Hirata, M.; Nishimura, F. Sphingosine-1-phosphate-enhanced Wnt5a promotes osteogenic differentiation in C3H10T1/2 cells. *Cell Biol. Int.* **2016**, *40*, 1129–1136. [CrossRef] [PubMed]
52. Carpio, L.C.; Stephan, E.; Kamer, A.; Dziak, R. Sphingolipids stimulate cell growth via MAP kinase activation in osteoblastic cells. *Prostaglandins Leukot. Essent. Fat. Acids* **1999**, *61*, 267–273. [CrossRef] [PubMed]
53. Matsuzaki, E.; Hiratsuka, S.; Hamachi, T.; Takahashi-Yanaga, F.; Hashimoto, Y.; Higashi, K.; Kobayashi, M.; Hirofuji, T.; Hirata, M.; Maeda, K. Sphingosine-1-phosphate promotes the nuclear translocation of β-catenin and thereby induces osteoprotegerin gene expression in osteoblast-like cell lines. *Bone* **2013**, *55*, 315–324. [CrossRef]
54. Higashi, K.; Matsuzaki, E.; Hashimoto, Y.; Takahashi-Yanaga, F.; Takano, A.; Anan, H.; Hirata, M.; Nishimura, F. Sphingosine-1-phosphate/S1PR2-mediated signaling triggers Smad1/5/8 phosphorylation and thereby induces Runx2 expression in osteoblasts. *Bone* **2016**, *93*, 1–11. [CrossRef]
55. Nishimura, R.; Kato, Y.; Chen, D.; Harris, S.E.; Mundy, G.R.; Yoneda, T. Smad5 and DPC4 Are Key Molecules in Mediating BMP-2-induced Osteoblastic Differentiation of the Pluripotent Mesenchymal Precursor Cell Line C2C12. *J. Biol. Chem.* **1998**, *273*, 1872–1879. [CrossRef]
56. Kim, J.M.; Lin, C.; Stavre, Z.; Greenblatt, M.B.; Shim, J.H. Osteoblast-Osteoclast Communication and Bone Homeostasis. *Cells* **2020**, *9*, 2073. [CrossRef] [PubMed]
57. Ahmed, N.; Linardi, D.; Decimo, I.; Mehboob, R.; Gebrie, M.A.; Innamorati, G.; Luciani, G.B.; Faggian, G.; Rungatscher, A. Characterization and expression of sphingosine 1-phosphate receptors in human and rat heart. *Front. Pharmacol.* **2017**, *8*, 1–7. [CrossRef]
58. Spatz, J.M.; Wein, M.N.; Gooi, J.H.; Qu, Y.; Garr, J.L.; Liu, S.; Barry, K.J.; Uda, Y.; Lai, F.; Dedic, C.; et al. The Wnt Inhibitor Sclerostin Is Up-regulated by Mechanical Unloading in Osteocytes in Vitro. *J. Biol. Chem.* **2015**, *290*, 16744. [CrossRef] [PubMed]
59. Zhang, J.N.; Zhao, Y.; Liu, C.; Han, E.S.; Yu, X.; Lidington, D.; Bolz, S.S.; You, L. The role of the sphingosine-1-phosphate signaling pathway in osteocyte mechanotransduction. *Bone* **2015**, *79*, 71–78. [CrossRef] [PubMed]
60. Dobrosak, C.; Gooi, J.H. Increased sphingosine-1-phosphate production in response to osteocyte mechanotransduction. *Bone Rep.* **2017**, *7*, 114. [CrossRef]
61. Xu, L.H.; Shao, H.; Ma, Y.H.V.; You, L. OCY454 Osteocytes as an in Vitro Cell Model for Bone Remodeling Under Mechanical Loading. *J. Orthop. Res.* **2019**, *37*, 1681–1689. [CrossRef] [PubMed]
62. Salari, N.; Ghasemi, H.; Mohammadi, L.; Behzadi, M.H.; Rabieenia, E.; Shohaimi, S.; Mohammadi, M. The global prevalence of osteoporosis in the world: A comprehensive systematic review and meta-analysis. *J. Orthop. Surg. Res.* **2021**, *16*, 1–20. [CrossRef]
63. Riggs, B.L. The mechanisms of estrogen regulation of bone resorption. *J. Clin. Investig.* **2000**, *106*, 1203. [CrossRef] [PubMed]
64. Ardawi, M.-S.M.; Rouzi, A.A.; Al-Senani, N.S.; Qari, M.H.; Elsamanoudy, A.Z.; Mousa, S.A. High Plasma Sphingosine 1-phosphate Levels Predict Osteoporotic Fractures in Postmenopausal Women: The Center of Excellence for Osteoporosis Research Study. *J. Bone Metab.* **2018**, *25*, 87. [CrossRef] [PubMed]
65. Song, H.E.; Lee, S.H.; Kim, S.J.; Kim, B.J.; Yoo, H.J.; Koh, J.M. Association of Circulating Levels of Total and Protein-Bound Sphingosine 1-Phosphate with Osteoporotic Fracture. *J. Investig. Med.* **2020**, *68*, 1295–1299. [CrossRef]
66. Lee, S.H.; Lee, J.Y.; Lim, K.H.; Lee, Y.S.; Kim, S.H.; Choi, S.; Cho, S.H.; Kim, J.S.; Koh, J.M. Associations of Circulating Levels of Sphingosine 1-Phosphate with the Trabecular Bone Score and Bone Mineral Density in Postmenopausal Women. *J. Clin. Densitom.* **2021**, *24*, 414–421. [CrossRef] [PubMed]
67. Kim, B.-J.; Shin, K.-O.; Kim, H.; Ahn, S.H.; Lee, S.H.; Seo, C.-H.; Byun, S.-E.; Chang, J.S.; Koh, J.-M.; Lee, Y.-M. The effect of sphingosine-1-phosphate on bone metabolism in humans depends on its plasma/bone marrow gradient. *J. Endocrinol. Investig.* **2016**, *39*, 297–303. [CrossRef]
68. Bae, S.J.; Lee, S.H.; Ahn, S.H.; Kim, H.M.; Kim, B.J.; Koh, J.M. The circulating sphingosine-1-phosphate level predicts incident fracture in postmenopausal women: A 3.5-year follow-up observation study. *Osteoporos. Int.* **2016**, *27*, 2533–2541. [CrossRef]
69. Ahn, S.H.; Koh, J.-M.; Gong, E.J.; Byun, S.; Lee, S.-Y.; Kim, B.-J.; Lee, S.H.; Chang, J.S.; Kim, G.S. Association of Bone Marrow Sphingosine 1-phosphate Levels with Osteoporotic Hip Fractures. *J. Bone Metab.* **2013**, *20*, 61–65. [CrossRef]
70. Tantikanlayaporn, D.; Tourkova, I.L.; Larrouture, Q.; Luo, J.; Piyachaturawat, P.; Witt, M.R.; Blair, H.C.; Robinson, L.J. Sphingosine-1-Phosphate Modulates the Effect of Estrogen in Human Osteoblasts. *JBMR Plus* **2018**, *2*, 217–226. [CrossRef]
71. Shahifar, N.; Samsudin, I.N.; Thambiah, S.C.; Yeap, S.S.; Sham, S.Y.Z.; Apannah, G.; Said, S.M.; Hew, F.L. Bone turnover markers and sphingosine-1-phosphate levels among the Chinese community in selangor, Malaysia and its correlation with bone density. *Malays. J. Med. Health Sci.* **2020**, *16*, 46–51.
72. Lee, S.H.; Lee, S.Y.; Lee, Y.S.; Kim, B.J.; Lim, K.H.; Cho, E.H.; Kim, S.W.; Koh, J.M.; Kim, G.S. Higher circulating sphingosine 1-phosphate levels are associated with lower bone mineral density and higher bone resorption marker in humans. *J. Clin. Endocrinol. Metab.* **2012**, *97*, 1421–1428. [CrossRef]
73. Li, S.; Kim, H.-E. Implications of Sphingolipids on Aging and Age-Related Diseases. *Front. Aging* **2021**, *2*, 797320. [CrossRef]
74. Paget, J. On a Form of Chronic Inflammation of Bones (Osteitis Deformans). *Med. Chir. Trans.* **1877**, *60*, 37–63. [CrossRef] [PubMed]
75. Ralston, S.H. Pathogenesis of Paget's disease of bone. *Bone* **2008**, *43*, 819–825. [CrossRef]

76. Shaker, J.L. Paget's Disease of Bone: A Review of Epidemiology, Pathophysiology and Management. *Ther. Adv. Musculoskelet. Dis.* **2009**, *1*, 107. [CrossRef] [PubMed]
77. Roodman, G.D.; Windle, J.J. Paget disease of bone. *J. Clin. Investig.* **2005**, *115*, 200–208. [CrossRef] [PubMed]
78. Harvey, L.; Gray, T.; Beneton, M.N.C.; Douglas, D.L.; Kanis, J.A.; Russell, R.G.G. Ultrastructural features of the osteoclasts from Paget's disease of bone in relation to a viral aetiology. *J. Clin. Pathol.* **1982**, *35*, 771. [CrossRef]
79. Nagata, Y.; Miyagawa, K.; Ohata, Y.; Petrusca, D.N.; Pagnotti, G.M.; Mohammad, K.S.; Guise, T.A.; Windle, J.J.; David Roodman, G.; Kurihara, N. Increased S1P expression in osteoclasts enhances bone formation in an animal model of Paget's disease. *J. Cell. Biochem.* **2021**, *122*, 335. [CrossRef]
80. Nagahashi, M.; Abe, M.; Sakimura, K.; Takabe, K.; Wakai, T. The role of sphingosine-1-phosphate in inflammation and cancer progression. *Cancer Sci.* **2018**, *109*, 3671. [CrossRef]
81. Redlich, K.; Smolen, J.S. Inflammatory bone loss: Pathogenesis and therapeutic intervention. *Nat. Rev. Drug Discov.* **2012**, *11*, 234–250. [CrossRef]
82. Lai, W.-Q.; Irwan, A.W.; Goh, H.H.; Howe, H.S.; Yu, D.T.; Valle-Oñate, R.; McInnes, I.B.; Melendez, A.J.; Leung, B.P. Anti-Inflammatory Effects of Sphingosine Kinase Modulation in Inflammatory Arthritis. *J. Immunol.* **2008**, *181*, 8010–8017. [CrossRef] [PubMed]
83. Burg, N.; Salmon, J.E.; Hla, T. Sphingosine 1-phosphate receptor-targeted therapeutics in rheumatic diseases. *Nat. Rev. Rheumatol.* **2022**, *18*, 335–351. [CrossRef] [PubMed]
84. Hutami, I.R.; Tanaka, E.; Izawa, T. Crosstalk between Fas and S1P1 signaling via NF-kB in osteoclasts controls bone destruction in the TMJ due to rheumatoid arthritis. *Jpn. Dent. Sci. Rev.* **2019**, *55*, 12. [CrossRef]
85. Baker, D.A.; Barth, J.; Chang, R.; Obeid, L.M.; Gilkeson, G.S. Genetic sphingosine kinase 1 deficiency significantly decreases synovial inflammation and joint erosions in murine TNFα-induced arthritis. *J. Immunol.* **2010**, *185*, 2570. [CrossRef]
86. Tsunemi, S.; Iwasaki, T.; Kitano, S.; Imado, T.; Miyazawa, K.; Sano, H. Effects of the novel immunosuppressant FTY720 in a murine rheumatoid arthritis model. *Clin. Immunol.* **2010**, *136*, 197–204. [CrossRef]
87. Hutami, I.R.; Izawa, T.; Mino-Oka, A.; Shinohara, T.; Mori, H.; Iwasa, A.; Tanaka, E. Fas/S1P1 crosstalk via NF-κB activation in osteoclasts controls subchondral bone remodeling in murine TMJ arthritis. *Biochem. Biophys. Res. Commun.* **2017**, *490*, 1274–1281. [CrossRef]
88. Sakaguchi, S.; Takahashi, T.; Hata, H.; Yoshitomi, H.; Tanaka, S.; Hirota, K.; Nomura, T.; Sakaguchi, N. SKG mice, a monogenic model of autoimmune arthritis due to altered signal transduction in T-cells. *Hered. Basis Rheum. Dis.* **2006**, 147–159. [CrossRef]
89. Moritz, E.; Jedlitschky, G.; Negnal, J.; Tzvetkov, M.V.; Daum, G.; Dörr, M.; Felix, S.B.; Völzke, H.; Nauck, M.; Schwedhelm, E.; et al. Increased Sphingosine-1-Phosphate Serum Concentrations in Subjects with Periodontitis: A Matter of Inflammation. *J. Inflamm. Res.* **2021**, *14*, 2883. [CrossRef]
90. Al Kawas, S.; Al-Marzooq, F.; Rahman, B.; Shearston, J.A.; Saad, H.; Benzina, D.; Weitzman, M. The impact of smoking different tobacco types on the subgingival microbiome and periodontal health: A pilot study. *Sci. Rep.* **2021**, *11*, 1113. [CrossRef] [PubMed]
91. Ishikawa, Y.; Terao, C. The Impact of Cigarette Smoking on Risk of Rheumatoid Arthritis: A Narrative Review. *Cells* **2020**, *9*, 475. [CrossRef]
92. Radwan-Oczko, M.; Duś-Ilnicka, I.; Richards, P.; Thomsen, A.M.; Rasmussen, C. Rheumatoid arthritis patients' oral health and disease activity. *Int. J. Rheum. Dis.* **2019**, *22*, 1538–1543. [CrossRef]
93. Al-Bashaireh, A.M.; Haddad, L.G.; Weaver, M.; Chengguo, X.; Lynch Kelly, D.; Yoon, S. The Effect of Tobacco Smoking on Bone Mass: An Overview of Pathophysiologic Mechanisms. *J. Osteoporos.* **2018**, *2018*, 1206235. [CrossRef] [PubMed]
94. De Cunto, G.; Brancaleone, V.; Riemma, M.A.; Cerqua, I.; Vellecco, V.; Spaziano, G.; Cavarra, E.; Bartalesi, B.; D'Agostino, B.; Lungarella, G.; et al. Functional contribution of sphingosine-1-phosphate to airway pathology in cigarette smoke-exposed mice. *Br. J. Pharmacol.* **2020**, *177*, 267–281. [CrossRef]
95. Goel, K.; Schweitzer, K.S.; Serban, K.A.; Bittman, R.; Petrache, I. Pharmacological sphingosine-1 phosphate receptor 1 targeting in cigarette smoke-induced emphysema in mice. *Am. J. Physiol.-Lung Cell. Mol. Physiol.* **2022**, *322*, L794–L803. [CrossRef] [PubMed]
96. Kolkesen Şahin, Ö.; Çina Aksoy, M.; Cihat AVUNDUK, M. Effects of resveratrol and cigarette smoking on bone healing: Histomorphometric evaluation. *Turk. J. Med. Sci.* **2016**, *46*, 1203–1208. [CrossRef] [PubMed]
97. Acikan, I.; Yaman, F.; Dundar, S.; Ozercan, I.H.; Atilgan, S.S. Protective effects of caffeic acid phenethyl ester (CAPE) and thymoquinone against cigarette smoke in experimental bone fracture healing. *J. Oral Biol. Craniofacial Res.* **2022**, *12*, 610–616. [CrossRef]
98. Barnawi, J.; Tran, H.B.; Roscioli, E.; Hodge, G.; Jersmann, H.; Haberberger, R.; Hodge, S. Pro-phagocytic Effects of Thymoquinone on Cigarette Smoke-exposed Macrophages Occur by Modulation of the Sphingosine-1-phosphate Signalling System. *COPD J. Chronic Obstr. Pulm. Dis.* **2016**, *13*, 653–661. [CrossRef] [PubMed]
99. Bingham, C.O., III; Moni, M. Periodontal disease and rheumatoid arthritis: The evidence accumulates for complex pathobiologic interactions. *Curr. Opin. Rheumatol.* **2013**, *25*, 345–353. [CrossRef]

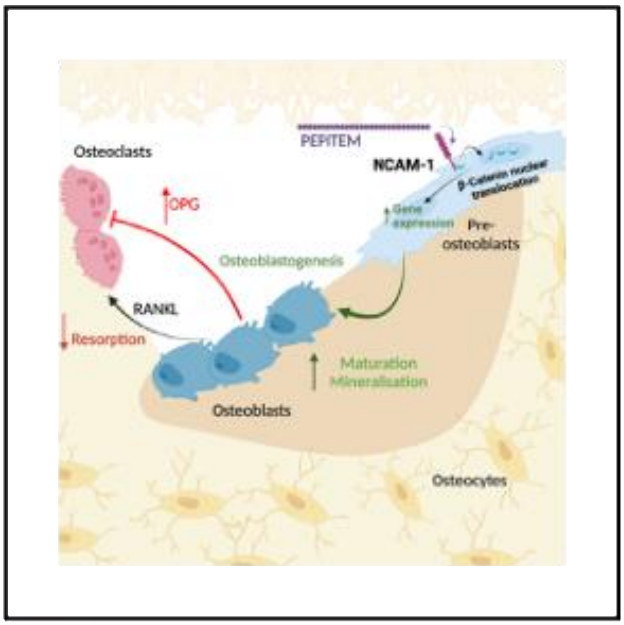
Disclaimer/Publisher's Note: The statements, opinions and data contained in all publications are solely those of the individual author(s) and contributor(s) and not of MDPI and/or the editor(s). MDPI and/or the editor(s) disclaim responsibility for any injury to people or property resulting from any ideas, methods, instructions or products referred to in the content.

Cell Reports
Medicine

Article

Therapeutic avenues in bone repair: Harnessing an anabolic osteopeptide, PEPITEM, to boost bone growth and prevent bone loss

Graphical abstract



Authors

Jonathan W. Lewis, Kathryn Frost, Georgiana Neag, ..., James R. Edwards, Amy J. Naylor, Helen M. McGettrick

Correspondence

h.m.mcgettrick@bham.ac.uk

In brief

Lewis and Frost et al. identify the anabolic activity of an endogenous osteopeptide (PEPITEM), revealing the cellular and molecular mechanisms by which PEPITEM regulates bone remodeling *in vitro* and in preclinical disease models, to promote new bone formation. They suggest that PEPITEM offers an alternative therapeutic option for bone loss diseases.

Highlights

- PEPITEM exerts anabolic osteogenic activity to regulate osteoblast-osteoclast coupling
- PEPITEM acts directly on osteoblasts to promote formation of new and stronger bone
- PEPITEM stimulates an inhibitory paracrine loop via OPG to limit bone resorption
- PEPITEM therapy halts disease-induced bone loss *in vivo*

Lewis et al., 2024, Cell Reports Medicine 5, 101574
May 21, 2024 © 2024 The Author(s). Published by Elsevier Inc.
https://doi.org/10.1016/j.xcrm.2024.101574

CellPress

Cell Reports Medicine

CellPress
OPEN ACCESS

Article

Therapeutic avenues in bone repair: Harnessing an anabolic osteopeptide, PEPITEM, to boost bone growth and prevent bone loss

Jonathan W. Lewis,[1,6] Kathryn Frost,[1,6] Georgiana Neag,[1] Mussarat Wahid,[1] Melissa Finlay,[1] Ellie H. Northall,[1] Oladimeji Abudu,[1] Samuel Kemble,[1] Edward T. Davis,[3] Emily Powell,[1] Charlotte Palmer,[4] Jinsen Lu,[4] G. Ed Rainger,[2] Asif J. Iqbal,[2] Myriam Chimen,[1] Ansar Mahmood,[5] Simon W. Jones,[1] James R. Edwards,[4] Amy J. Naylor,[1,7] and Helen M. McGettrick[1,7,8,*]

[1]Institute of Inflammation and Ageing, University of Birmingham, Birmingham B15 2WB, UK
[2]Institute of Cardiovascular Sciences, University of Birmingham, Birmingham B15 2TT, UK
[3]Royal Orthopaedic Hospital, Bristol Road, Birmingham B31 2AP, UK
[4]Botnar Research Centre, University of Oxford, Oxford OX3 7LD, UK
[5]Department of Trauma and Orthopaedics, University Hospitals NHS Foundation Trust, Edgbaston, Birmingham B15 2GW, UK
[6]These authors contributed equally
[7]These authors contributed equally
[8]Lead contact
*Correspondence: h.m.mcgettrick@bham.ac.uk
https://doi.org/10.1016/j.xcrm.2024.101574

SUMMARY

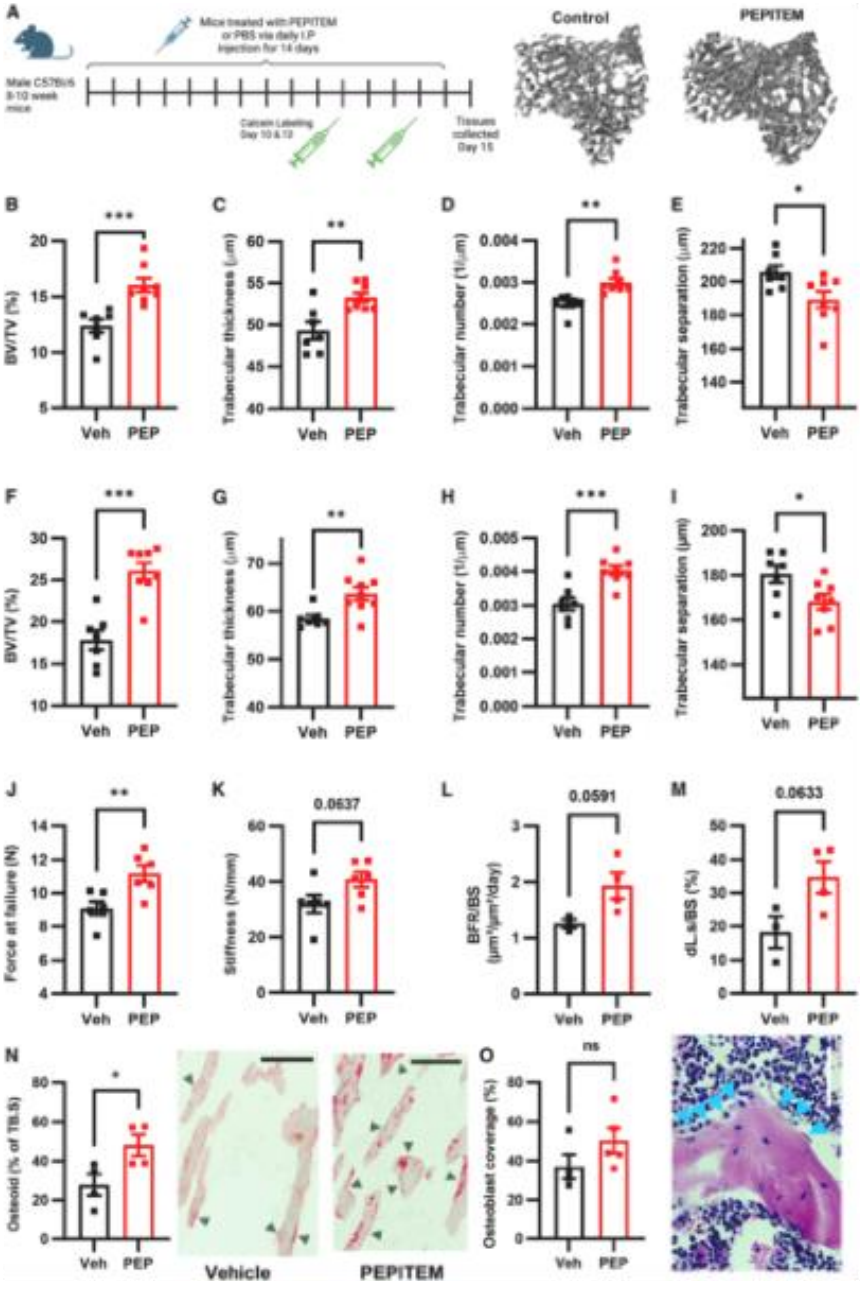
The existing suite of therapies for bone diseases largely act to prevent further bone loss but fail to stimulate healthy bone formation and repair. We describe an endogenous osteopeptide (PEPITEM) with anabolic osteogenic activity, regulating bone remodeling in health and disease. PEPITEM acts directly on osteoblasts through NCAM-1 signaling to promote their maturation and formation of new bone, leading to enhanced trabecular bone growth and strength. Simultaneously, PEPITEM stimulates an inhibitory paracrine loop: promoting osteoblast release of the decoy receptor osteoprotegerin, which sequesters RANKL, thereby limiting osteoclast activity and bone resorption. In disease models, PEPITEM therapy halts osteoporosis-induced bone loss and arthritis-induced bone damage in mice and stimulates new bone formation in osteoblasts derived from patient samples. Thus, PEPITEM offers an alternative therapeutic option in the management of diseases with excessive bone loss, promoting an endogenous anabolic pathway to induce bone remodeling and redress the imbalance in bone turnover.

INTRODUCTION

Bone is a highly active organ, undergoing continuous osteoblast-induced bone formation and osteoclast-mediated bone resorption throughout life. The process of bone remodeling is orchestrated by cross-talk among osteoblasts, osteoclasts, and osteocytes acting in concert to maintain structural integrity, repair damage, and respond to changes in activity and load.[1] Dysregulation of these pathways underpins numerous musculoskeletal (MSK) diseases where excessive bone resorption (e.g., osteoporosis, rheumatoid arthritis, periodontal disease, cancer-bone metastases) or abnormal bone formation (e.g., ankylosing spondylitis; heterotopic ossification) results in permanent loss of function, pain, increased risk of fracture, and frailty.[2] Osteoporosis is the most common bone disease globally, affecting over 54 million individuals in the United States and accounting for 3 million broken bones at a cost of ~$26 billion per annum.[3] There are no cures for bone damage. Existing therapies have predominantly focused on slowing the rate of bone damage (e.g., bisphosphonates; denosumab, saracatinib), with only a handful of drugs able to promote bone repair currently approved (e.g., parathyroid hormone—PTH or romosozumab).[4,5] Due to poor patient response, poor drug compliance, and drug-induced microfractures leading to atypical femur fractures, there is an urgent need to develop a new suite of therapies that lead to bone repair and regeneration in patients with MSK diseases to restore tissue homeostasis and functional integrity.

Approximately 10% of all bone in the human body is replaced annually, through a series of tightly coordinated sequential steps (reviewed by Kenkre and Bassett[6] and Delaisse et al.[7]). Hematopoietic myeloid cells (monocytes) recruited to the bone differentiate into mononuclear osteoclast precursors in response to M-CSF (macrophage colony stimulating factor) and later RANKL (receptor activator of nuclear factor-κB ligand) stimulation, before fusing together to form multinucleated mature osteoclasts. Within osteoclast resorption pits, locally released chloride and hydrogen ions dissolve the bone mineral, while proteases (matrix metalloproteinase

This is an open access article under the CC BY license (http://creativecommons.org/licenses/by/4.0/).



(legend on next page)

CellPress
OPEN ACCESS

[MMP], cathepsin K) digest the collagen matrix resulting in bone resorption. Replacement of this resorbed bone is performed by osteoblasts, derived from mesenchymal stem cells (MSCs), that become committed to the osteoblast lineage upon activation of the transcriptional regulator Runx2. As osteoblast precursors start to differentiate, they express increased amounts of collagen (*COL1A1*) and matrix proteins, which are deposited as an unmineralized osteoid. Maturing osteoblasts subsequently release alkaline phosphatase (ALP) into the collagen-rich matrix resulting in the deposition of hydroxyapatite crystals, mineralization of the matrix, and formation of new bone.

Physiological bone remodeling is tightly regulated by the intricate cross-talk between osteoblasts and osteoclasts at the bone surface and via signaling from osteocytes embedded within the bone tissue itself. Osteoblasts and osteocytes release both positive (RANKL, M-CSF) and negative (osteoprotegerin [OPG]) regulators of osteoclastogenesis to control the rate of bone resorption.[8] Conversely, osteoclasts and osteocytes produce anabolic stimuli that include sphingosine 1-phosphate,[9] Wnt/β-catenin proteins, and bone morphogenic proteins[10] that induce osteoblast precursor recruitment, differentiation, and survival. The highly conserved and ubiquitously expressed seven isoforms of the human 14-3-3 family act as adaptor proteins influencing the function of other proteins, and thus a multitude of signaling pathways, to regulate cellular responses (reviewed by Obsilova and Obsil[11]). The name 14-3-3 derives from the elution fraction (14^{th}) and subsequent position (3.3) on starch electrophoresis gel when the family was first identified in brain tissue.[12] Of particular relevance to bone homeostasis, two 14-3-3 family members have been reported to differentially regulate osteoblast function, with 14-3-3β[13] significantly reducing and 14-3-3ξ enhancing osteoblastogenesis.[14] We have previously identified a bioactive 14-amino acid peptide (PEPITEM) cleaved from 14-3-3ξ[15], which regulates the migration of monocytes (osteoclast precursors) into non-bone tissues during inflammation.[16,17] Here we investigated the ability of PEPITEM to directly influence bone remodeling under homeostatic conditions and subsequently the therapeutic efficacy of PEPITEM in models of excessive bone loss.

RESULTS

PEPITEM enhances bone formation and strength under homeostatic conditions

Initially we examined whether PEPITEM intrinsically regulated bone remodeling under basal conditions over a 2-week period (Figure 1A). PEPITEM therapy significantly increased bone volume (BV/TV), trabecular number, and thickness in both the tibia (Figures 1B–1D) and vertebrae (Figures 1F–1H) of adult mice, indicating that PEPITEM promotes bone formation. As expected, we observed a concomitant decrease in the gaps between individual trabeculae (trabecular separation [Figures 1E and I]), as the increased trabeculae created a denser, more interconnected trabecular network. Cortical bone turnover takes much longer than trabecular bone: ~4–6 weeks.[18] As expected, we observed no changes in the cortical bone following 2 weeks of PEPITEM treatment, but we did observe a significant increase in cortical bone parameters following 4 weeks of treatment (Figure S1). When comparing these findings with existing drugs targeting the bone, the effect size for PEPITEM on BV/TV at 2 weeks is comparable to that seen following treatment with the bisphosphonate zoledronic acid for 3 weeks[19] or PTH for up to 4 weeks.[20] Thus indicating PEPITEM is as efficient at inducing bone formation compared with current standard of care.

The enhanced trabecular parameters induced by PEPITEM translated to increased bone strength, with PEPITEM therapy significantly increasing the force at which bones fracture (Figure 1J) and tends to enhance bone stiffness (Figure 1K) compared with control-treated animals. Dynamic histomorphometry revealed increases in both the rate of bone formation (Figure 1L) and the overall mineralized bone surface (Figure 1M), demonstrating that PEPITEM induces bone mineralization leading to increased bone strength. Further supporting this, PEPITEM significantly increased the deposition of osteoid when compared with control animals (Figure 1O). Furthermore, PEPITEM treatment tended to increase osteoblast numbers when compared with vehicle, albeit not significantly (Figure 1P), suggesting increased bone mineralization was predominantly a result of increased osteoblast activity rather than absolute number. No detectable effect on the levels of the bone formation serum markers—soluble procollagen type 1 N-terminal propeptide

Figure 1. PEPITEM enhances bone formation and strength under homeostatic conditions

Healthy young mice injected with vehicle control (Veh, black) or PEPITEM-PEG (PEP, red) and then (B–E, L and M) tibiae, (F–I) vertebrae (L4–6), or (J and K) femurs were analyzed.

(A) Schematic representation of experiment and representative microCT images of tibiae trabecular bone.

(B and F) Percentage trabecular bone volume (BV/TV). $n = 7–8$ mice from three independent experiments.

(C and G) Trabecular thickness in μm. $n = 7–8$ mice from three independent experiments.

(D and H) Trabecular number per μm. $n = 7–8$ mice from three independent experiments.

(E and I) Trabecular separation in μm. $n = 7–8$ mice from three independent experiments.

(J and K) Femurs were subject to 3-point bend to assess (J) force at failure in N/mm and (K) stiffness in N for two femurs per mouse, $n = 3$ mice from one independent experiment.

(L and M) Dynamic histomorphometry of (L) bone formation rate normalized to bone surface perimeter (BFR/BS) as $\mu m^3/\mu m^2$/day and (M) length of double calcein labels normalized to total bone surface perimeter (dLs/BS) as a percentage. $n = 3–4$ for two independent experiments.

(N) Percentage of trabecular bone surface stained with picrosirius red representing osteoid compared with total trabecular bone surface area. $n = 4$ mice from two independent experiments (OB/BS).

(O) Number of osteoblasts in the tibiae from mice treated expressed as surface area of bone covered by osteoblasts as percentage of the total bone surface area (Ob.S/BS). $n = 4–5$ mice per group from two independent experiments. Representative image, where cyan arrows point to osteoblasts. Scale bar, 50 μm. Data are mean ± SEM. $^*p < 0.05$, $^{**}p < 0.01$, and $^{***}p < 0.001$ by unpaired t test.

(P1NP)—was observed in PEPITEM-treated compared with control-treated mice in this experiment (Figure S2). Collectively these data reveal the pro-osteogenic actions of PEPITEM in the absence of inflammation.

PEPITEM acts directly on osteoblasts to enhance bone mineralization and limit bone resorption

Osteoblasts and osteoclasts work in concert to balance bone formation and resorption—thus an increase in trabecular bone could result from an increase in osteoblast activity or a decrease in osteoclast activity. Using alkaline phosphatase activity as an early marker of osteoblast maturation and alizarin red to visualize the later occurrence of bone mineralization, we next investigated the direct effect of PEPITEM on osteoblast function *in vitro*. PEPITEM significantly increased alkaline phosphatase activity in the murine ST2 osteoblast cell line (Figure 2A), primary murine calvarial osteoblasts isolated from male and female mice (Figures 2B and 2C) and the human hFOb 1.19 osteoblast cell line (Figure 2D) in culture. Of note, PEPITEM had no effect on cell number when compared with untreated controls (Figure 2E), indicating the changes in ALP are not due to more cells being present. This heightened PEPITEM-induced ALP expression resulted in significantly enhanced osteoblast mineral production over time, as detected by increases in alizarin red concentration (Figures 2F–2H). No changes were seen in osteoblast maturation or mineralization when cells were treated with an alternative 14aa peptide sequence within 14-3-3ξ (parent protein of PEPITEM, Figures 2A–2D, 2F, and 2G), indicating that it is PEPITEM itself that exhibits osteogenic properties. Supporting these *in vitro* findings, PEPITEM significantly enhanced mineral formation within intact metatarsal bones cultured *ex vivo* (Figures 2I and 2J). These findings demonstrate that PEPITEM acts directly on osteoblasts in the bone microenvironment to increase mineral deposition and together with the increases in bone formation rate and osteoid deposition observed *in vivo* collectively support the anabolic role of PEPITEM in bone formation. Several questions remain unanswered: what is the receptor for PEPITEM on osteoblasts and can PEPITEM influence osteoclast function?

PEPITEM interaction with NCAM-1 leads to β-catenin translocation in osteoblasts

In the inflamed blood vascular bed, we have previously demonstrated that PEPITEM interacts with the adhesion molecule cadherin-15 (CDH15) on blood vascular endothelial cells to mediate its downstream immunomodulatory effects via sphingosine-1-phosphate (S1P).[15] While primary murine and human osteoblasts express CDH15 transcript and protein (Figure S3A–S3C), treating primary murine osteoblasts with a CDH15 agonistic antibody had no effect on bone mineralization (Figure S3D), suggesting that CDH15 is not responsible for mediating the actions of PEPITEM on osteoblasts. Moreover, increasing concentrations of S1P caused a dose-dependent reduction in alkaline phosphate activity, and thus osteoblast activity (Figure S3E), in contrast to the increase observed with PEPITEM. Collectively, these data strongly indicate that the osteogenic actions of PEPITEM are triggered by a previously undescribed mechanism, which is distinct from the immunopeptide actions described for leukocyte trafficking during an inflammatory challenge.

To identify a PEPITEM receptor on osteoblasts, we used a biotin-conjugated PEPITEM to "fish" for potential binding partners on the cell surface of calvarial osteoblasts. This peptide showed pro-osteogenic activity, inducing osteoblast maturation and mineralization to a similar amount seen by native PEPITEM (Figure S4), indicating that biotinylation did not inhibit PEPITEM's activity. PEPITEM-bound proteins eluted from osteoblast lysates were analyzed by mass spectrometry. Comparative analysis allowed exclusion of molecules identified in both control peptide and PEPITEM samples, and data were further filtered to include only those proteins associated with a membrane expression pattern using isoelectric point (Table S1). Of the top 10 hits, only two are known membrane proteins: NCAM-1 (CD56)[21] and EHD2 (EH domain containing protein 2).[22] Of these only NCAM-1 has previously been shown to be involved in osteoblastogenesis,[21] although expression was transient and lost as MSC differentiate into osteoblasts.[23,24] We detected both gene (Figure 3A) and protein expression of NCAM-1 in primary calvarial osteoblasts (Figures 3B and 3C), with western blot analysis revealing the presence of different NCAM-1 isoforms in osteoblasts—all of which increased in expression following PEPITEM treatment for 8 days (Figure 3C). To determine whether PEPITEM-enhanced osteoblast activity required NCAM-1, we treated osteoblasts with an NCAM-1 function blocking antibody or relevant immunoglobulin (Ig)G control in the presence of PEPITEM and assessed alkaline phosphatase activity. Inhibiting NCAM-1 blocked the effect of PEPITEM (Figure 3D), suggesting a role of NCAM-1 in mediating the effects of PEPITEM. Similarly, anti-NCAM-1 blocked PEPITEM-induced mineralization within intact metatarsal bones cultured *ex vivo* when compared with IgG1 treated controls (Figure 3E).

Previous evidence has shown that NCAM-1 regulation of osteoblast differentiation was mediated through Wnt/β-catenin and PI3K-AKT signaling pathways.[21] While PEPITEM had no effect on β-catenin gene expression (Figure 3F), we observed a significant increase in the amount of intracellular β-catenin protein in osteoblasts following a 60-min incubation with PEPITEM (Figures 3G and 3H). This change was ~1.9-fold higher than that observed with a known inducer of the β-catenin signaling pathway, lithium chloride.[25] In the presence of a Wnt ligand, β-catenin is known to translocate to the nucleus where it acts as a co-activator of the Wnt response elements in target genes.[26,27] Similarly, PEPITEM induced β-catenin nuclear translocation within 60 min to a comparable level as seen with lithium chloride (Figures 3G and 3I), strongly suggesting this pathway mediates PEPITEM-enhanced osteoblast activity. Further supporting this, we observed an increase in β-catenin activation within 15 min of PEPITEM treatment, reaching significance by 30 min (Figure 3J). Bulk RNA-sequencing analysis revealed 75 differentially regulated genes (DEGs) up-regulated and 36 down-regulated in osteoblasts after 6 h of treatment with PEPITEM compared with cells treated with control peptide (Tables S2, and S3). Of note, 17 of the 75 up-regulated DEGs were associated with osteoblast differentiation and skeletal development, including *col1a1*. Indeed, *col1a1* was significantly increased in response to PEPITEM following 6 h of treatment

CellPress
OPEN ACCESS

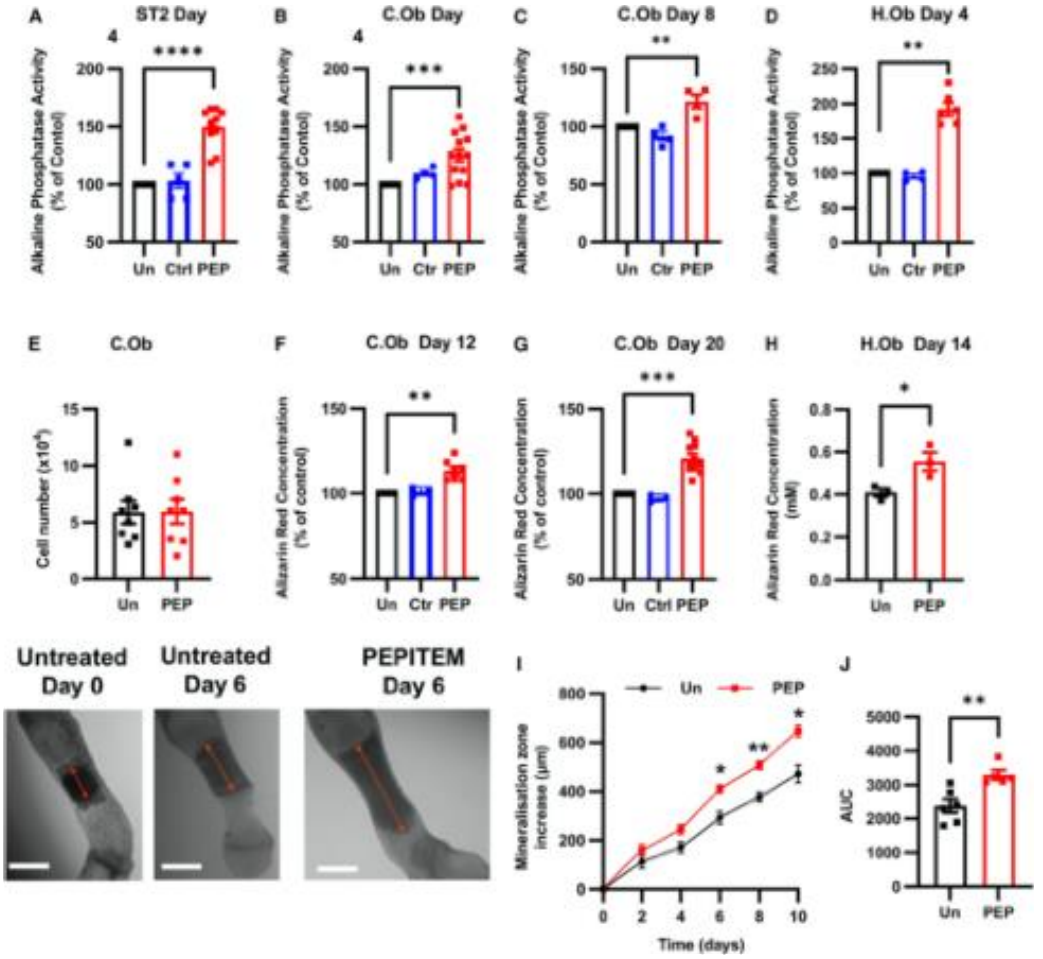


Figure 2. PEPITEM acts directly on osteoblasts to enhance bone mineralization and limit bone resorption

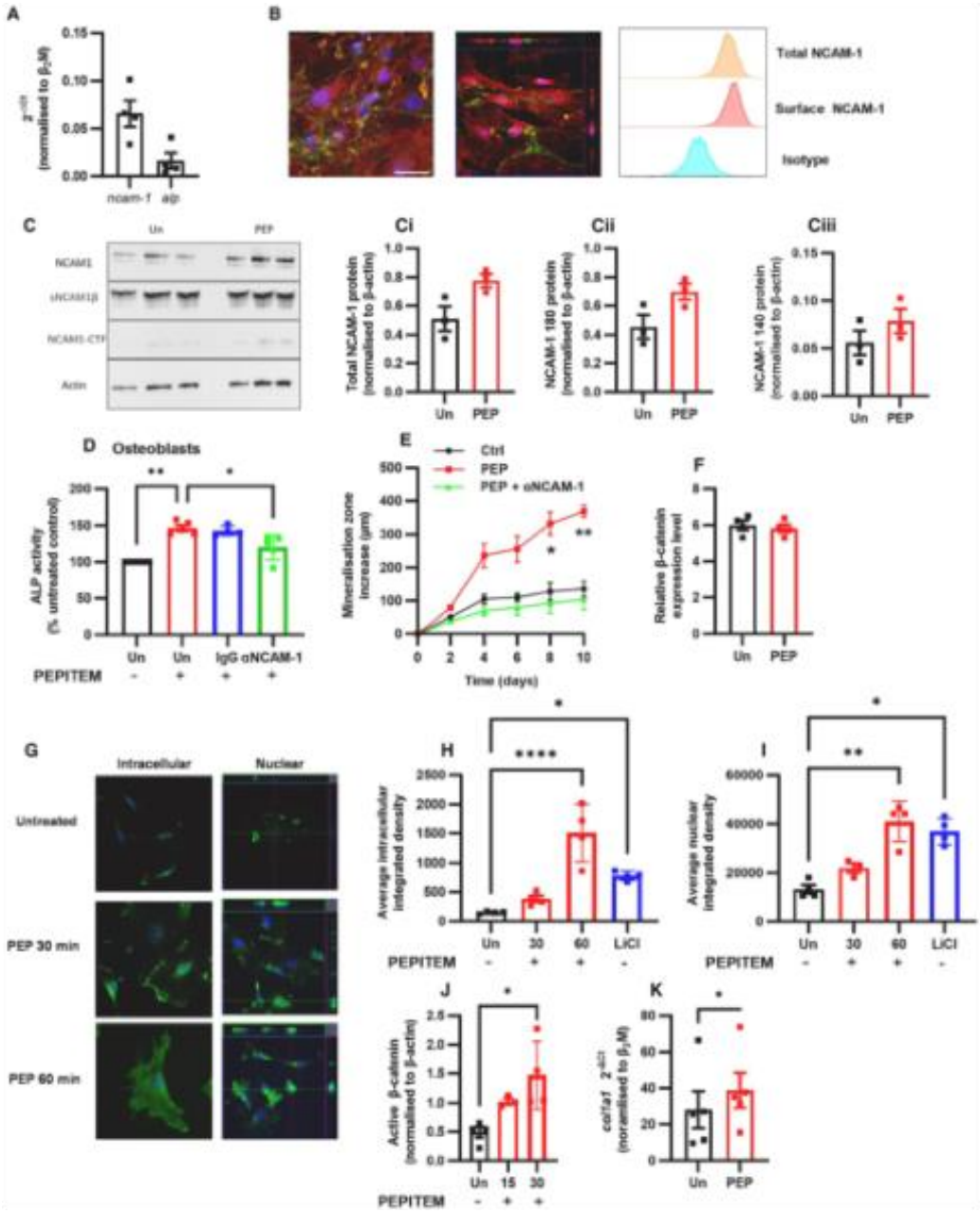
(A–D) Osteoblasts were cultured in osteogenic media (untreated, Un, black) supplemented with a control peptide (Ctr, blue) or PEPITEM (PEP, red). Alkaline phosphatase activity for (A) ST2 cells (n = 5–10), (B and C) primary calvarial (n = 4–13), or (D) hFOb 1.19 cells (n = 4–6) measured at day (A, B, and D) 4 or (C) 8 and normalized to percentage of untreated control. In (A–C), Kruskal-Wallis shows a significant effect of treatment, $p < 0.01$.

(E–H) (E) Proliferation of primary calvarial osteoblasts expressed as cell count × 10^4 cells, n = 8. Alizarin red concentration extracted from (F and G) calvarial osteoblasts or (H) hFOb 1.19 cells at day (F) 12 (n = 3–7) (G) 20 (n = 3–11), or (H) 14 (n = 3) expressed as percentage of untreated control or mM. In (F) and (G), Kruskal-Wallis, shows a significant effect of treatment, $p < 0.01$.

(I and J) Mineralization of metatarsal bones cultured without (untreated, un, black) or with PEPITEM (PEP, red) as representative images at different time points or plotted as (I) increase in mineral zone in µm or (J) area under the curve (AUC), n = 5–6. In (I), ANOVA shows a significant effect of treatment, $p < 0.001$. Data are mean ± SEM. *$p < 0.05$, **$p < 0.01$, ***$p < 0.001$, and ****$p < 0.0001$ by (A–C, F, and G) Dunn post-test, (D and H) Wilcoxon, (I) Bonferroni post-test between treatments for each time point, or (J) paired t test.

(Figure 3K), thus confirming induction of gene expression in response to β-catenin activation and nuclear translocation.

To further ascertain whether NCAM-1 is a receptor for PEPITEM, we used the AlphaFold2_Multimer neural network[28] coupled with ChimeraX[29] to generate five predicted 3-D models of PEPITEM binding/interacting with NCAM-1 (Figures 4A and 4B). NCAM-1 structurally has five IgG-like domains and two fibronectin-III-like domains.[30] Predicted model five indicates PEPITEM binding to the first fibronectin domain within the extracellular portion of NCAM-1 (Figures 4C–4E, and Table S4). We



(legend on next page)

also created 3-D models of PEPITEM interacting a peptide fragment of NCAM-1 containing the two fibronectin-III-like domains and IgG-like domain 5, observing much stronger predicted residue interactions compared with those obtained with the full NCAM-1 protein (Figures 4F and 4G). In this model, PEPITEM is interacting with the second fibronectin-III-like domain, with higher alignment scores (pLDDT score >70) than seen when PEPITEM is modeled with full-length NCAM-1 (Figures 4H–4J, and Table S4). Given EHD2 was also identified as a potential PEPITEM-binding partner expressed on the surface of osteoblasts, we created 3-D models predicting PEPITEM-End2 interactions (Figure S5). EHD2 consists of an N-terminal extended GTPase domain, a helical domain, and a C-terminal Eps15-homology domain.[31] While *in silico* analysis suggests PEPITEM binds to the GTPase domain of EHD2, the predicted scores (pLDDT score 70 > 50) were lower than those seen in the NCAM-1-PEPITEM models (Figure S5). The combination of the predictive 3-D models and functional studies strongly suggest that PEPITEM mediates its effects via the NCAM-1-β-catenin signaling pathway, while also revealing a second potential binding partner in EHD2.

PEPITEM acts indirectly on osteoclasts to reduce bone resorption

The interplay between osteoblast and osteoclast activity is carefully controlled, where increases in osteoblast activity are often matched with enhanced osteoclastogenesis (leading to increased bone resorption) to ensure balance is maintained. For this reason, it was necessary to assess the impact of PEPITEM on osteoclast function. Analysis of bone sections from mice treated with PEPITEM revealed a significant reduction in osteoclast numbers when compared with the treatment controls (Figure 5A), as measured by the presence of tartrate-resistant acid phosphatase (TRAP)-positive multinucleated cells. Similarly, PEPITEM significantly reduced mineral resorption when whole murine bone marrow was cultured with osteoclast-stimulating factors (M-CSF and RANKL) on specialist hydroxyapatite-coated plates (Figure 5B). As the action of PEPITEM appeared to also influence osteoclast number and function, we subsequently assessed whether this was mediated by direct action on the osteoclasts or the consequence of paracrine signaling from a neighboring cell type (e.g., osteoblast) that would be present in the *in vivo* samples and in the whole bone marrow extract assay.

Osteoclasts are derived from peripheral blood $CD14^+$ monocytes following stimulation with RANKL and M-CSF. If PEPITEM binds directly to pre-osteoclasts to influence osteoclastogenesis, we predicted a reduction in osteoclast formation and mineral resorption in its presence. However, we observed no difference in the number of TRAP-positive osteoclasts when either the murine macrophage cell line RAW264.7 (Figure 5C) or primary human monocytes (Figure 5D) were differentiated into osteoclasts in the presence of PEPITEM. Induction of osteoclastogenesis was confirmed by significant up-regulation of the osteoclast genes *ACP5*, *ATP6V1B1*, and *CTSK* in primary human monocytes treated with RANKL (Figure S6). By contrast, a known inhibitor of osteoclasts (the bisphosphonate, zoledronic acid) significantly reduced the number of murine and human-derived osteoclasts (Figures 5C and 5D). Furthermore, PEPITEM had no effect on osteoclast resorption capacity, with the same degree of dentine resorption seen when compared with untreated cells (Figure 5E). These data clearly show that PEPITEM has no direct effects on osteoclast differentiation or activity and indicates that paracrine signaling cascades induced by PEPITEM within the bone microenvironment are likely to be responsible for the reduction in osteoclast number observed *in vivo* and in the whole murine bone marrow culture experiments.

PEPITEM induces osteoblasts to release a soluble mediator, which inhibits osteoclast function

Osteoblasts can regulate osteoclastogenesis through paracrine signaling often through the RANKL-OPG axis. Osteoblasts secrete both RANKL and OPG, which have opposing functions—RANKL binds to its receptor (RANK) on monocytes to induce their differentiation to osteoclasts; while OPG acts as a decoy receptor for RANKL, inhibiting its binding to RANK and thus limiting osteoclast differentiation.[32] Given this ability of osteoblasts to control osteoclastogenesis, we examined the possibility that the negative regulation of osteoclast function was due to production of a soluble agent released by osteoblasts in response to PEPITEM. To test this hypothesis, we collected the secretome/supernatant from PEPITEM-treated osteoblasts and transferred this onto osteoclast precursors (Figure 6A). Osteoclastogenesis in murine (Figure 6B) and human (Figure 6C) precursors was significantly inhibited in the presence of conditioned media from PEPITEM-treated osteoblasts, suggesting the presence of an inhibitory agent. When osteoblasts were treated with PEPITEM in the presence of

Figure 3. PEPITEM signaling through NCAM-1 on osteoblasts leads to b-catenin translocation

(A, F, and K) Gene expression of (A) *ncam-1*, *alpl*, (F) *β-catenin*, and (K) *col1a1* in osteoblasts expressed as $2^{-\Delta CT}$ of β_2M or relative expression level from bulk-RNA-sequencing, $n = 3–6$.

(B) Representative confocal images of NCAM-1 (green), RUNX2 (red) expression, and DAPI (blue) from two independent experiments and histograms of total and surface NCAM-1 expression as assessed by flow cytometry.

(C) Representative gel for 3 independent experiments analyzing (Ci) total, (Cii) 180, or (Ciii) 140 NCAM-1 isoforms following treatment without (Un) or with PEPITEM (PEP) normalized to β-actin, $n = 3$.

(D and E) Osteoblasts or metatarsals were left untreated (Un, black) or treated with PEPITEM (PEP, red), IgG control antibody (blue), or anti-NCAM-1 antibody (green). (D) Alkaline phosphatase activity normalized to percentage of untreated osteoblasts, $n = 4$. (E) Metatarsal mineralization increased in μm over time, $n = 3$.

(G–J) Osteoblasts were untreated (Un, black) or treated with PEPITEM (PEP, red) or lithium chloride (LiCl, blue). (G) Representative images of β-catenin intracellular and nuclear expression pattern (green). Average β-catenin (H) intracellular or (I) nuclear localisation at 30 and 60 min expressed as integrated density, $n = 4–5$. (J) Active β-catenin protein expression at 15 and 30 min as band intensity (AUC) relative to β-actin loading control, $n = 3–4$. (D) Kruskal-Wallis or (E, G, and H) ANOVA shows a significant effect of treatment, $p < 0.001$. Data are mean ± SEM. $^*p < 0.05$, $^{**}p < 0.01$, and $^{****}p < 0.0001$ by (D) Dunn or (E, G, and H) Bonferroni post-test, or (J) paired t test. Scale bar, (B) 50 μm; (G) 100 μm.

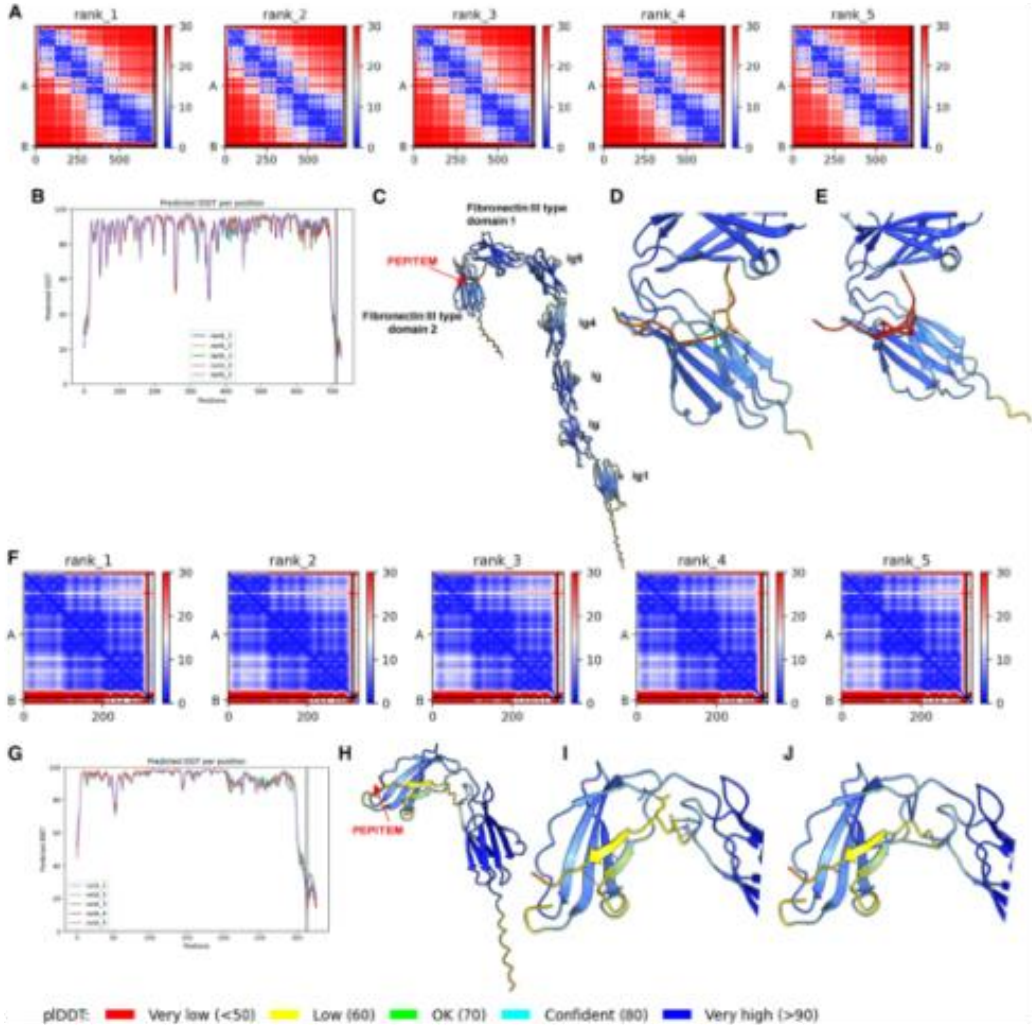


Figure 4. 3-D predictive modeling of PEPITEM interaction with NCAM-1

(A–E) Full-length NCAM-1 extracellular domain or (F–J) fibronectin-III like domain were run with PEPITEM in (A and B, F and G) AlphaFold-Multimer followed by analyzed of rank 1 model (C–E and H–J) using ChimeraX. Predicted aligned error heatmap for five models of (A) NCAM-1 or (F) fibronectin-III like domain and PEPITEM, where blue and red indicate low or high error, respectively.

(B and G) pLDDT score for each residue in the predicted models for (B) NCAM-1 or (G) fibronectin-III like domain.

(C and H) ChimeraX modeling of rank 1 model for PEPITEM interactions with (C) NCAM-1 or (H) fibronectin-III colored by pLDDT.

(D and E, I and J) Magnified view of binding location of PEPITEM on NCAM-1 revealing (D) four and (I) nine predicted hydrogen bonds—high likelihood (blue), low (orange)—and (E) 17 and (J) 13 pseudobonds based on a distance of 3 Å, confidence indicated by pLDDT color as above.

Brefeldin A (a chemical inhibitor of the golgi), they were no longer able to generate the osteoclast inhibitory agent(s) (Figure 6D). Importantly, as PEPITEM does not influence osteoclasts directly (Figures 5C–5E), these data strongly indicate that osteoblasts are releasing a soluble mediator in response to PEPITEM that inhibits osteoclast function.

Given this, we next assessed OPG and RANKL levels in the conditioned media released from osteoblasts following PEPITEM

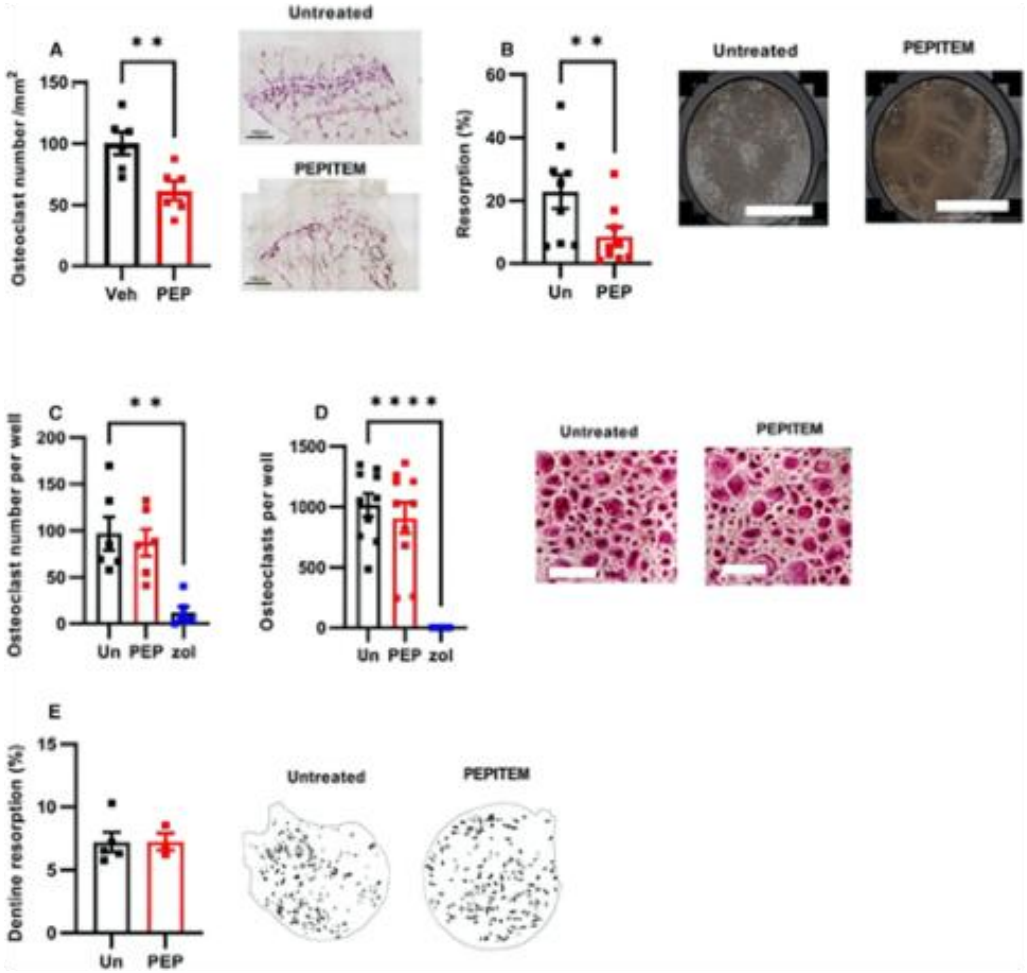


Figure 5. PEPITEM acts indirectly on osteoclasts to reduce bone resorption

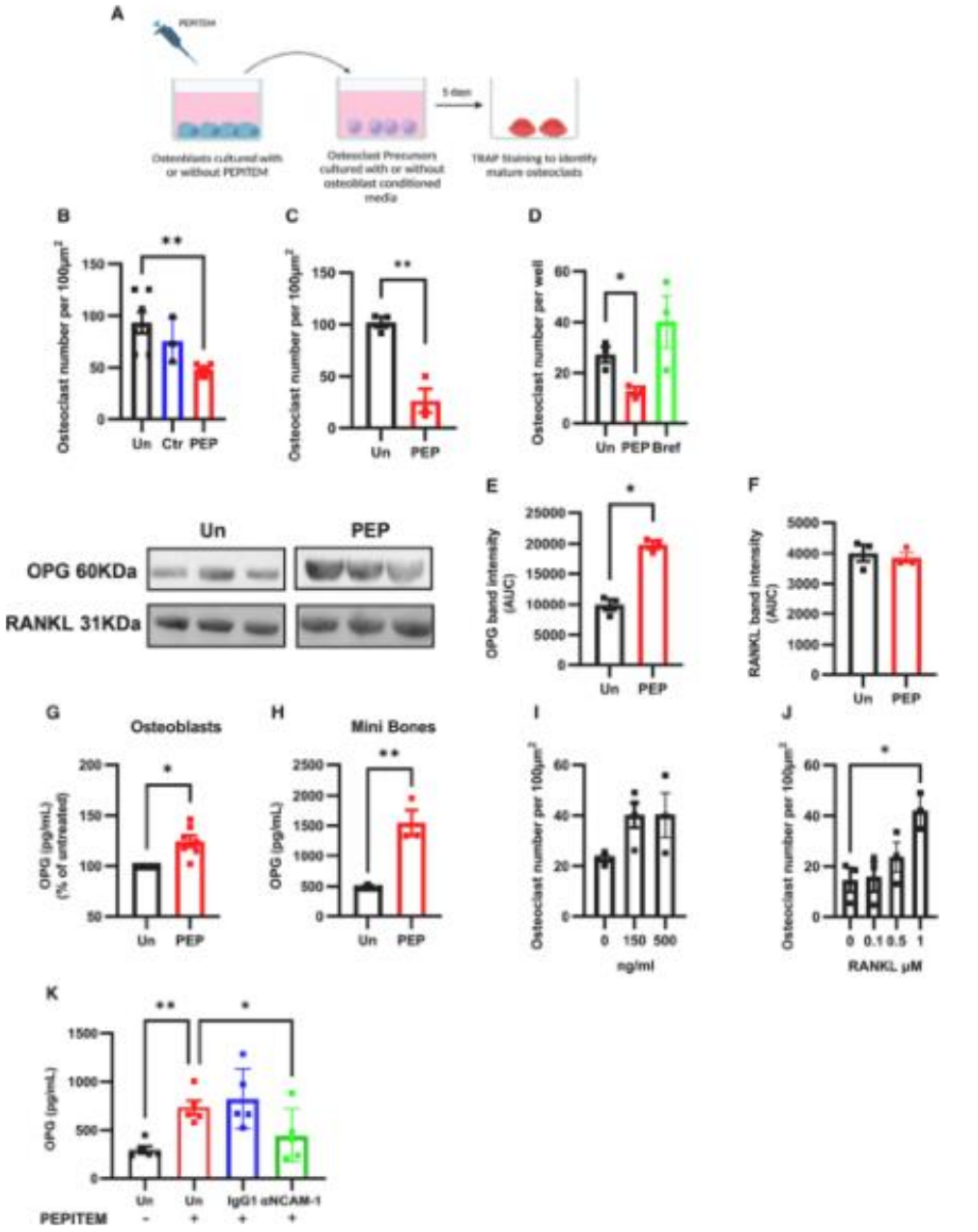
(A) Number of TRAP-positive multinucleated cells in the tibiae from mice treated with control (Veh, black, $n = 8$) or PEPITEM-PEG (PEP, red, $n = 6$) expressed as number of osteoclasts per mm^2. $^{**}p < 0.05$ by unpaired t test.

(B) Osteoclast resorption on hydroxyapatite plates as percentage of total area for whole murine bone marrow cells left untreated (Un, black, $n = 9$) or with PEPITEM (PEP, red, $n = 9$). $^{**}p < 0.05$ by paired t test.

(C and D) Number of TRAP-positive osteoclasts cells per well differentiated from (C) RAW264.7 ($n = 6$) or human peripheral blood monocytes ($n = 10$) either left untreated (Un, black) or treated with PEPITEM (PEP, red) or with zoledronic acid (zol, blue). ANOVA showed a significant effect of treatment on osteoclast number, $p < 0.01$. $^{**}p < 0.01$ and $^{****}p < 0.0001$ by Dunnett post-test.

(E) Human peripheral blood monocytes derived osteoclast resorption of dentine slices calculated from image masks (see inserts) as percentage of total area following treatment without (untreated, Un, black, $n = 6$) or with PEPITEM (PEP, red, $n = 3$). Data are mean ± SEM. Scale bar, (A and D) 500 μm; (B) 1,000 μm.

treatment. Significantly more OPG protein was detected in supernatants from PEPITEM-treated osteoblasts or 3-D human minibones organoids compared with untreated controls as assessed by western blot (Figure 6E) and ELISA (Figures 6G and 6H). By contrast, the amount of osteoblast-derived RANKL protein remained unchanged following PEPITEM treatment (Figure 6F). To ascertain whether OPG was truly the osteoblast agent responsible for inhibiting osteoclastogenesis, we used an OPG neutralizing antibody to deplete OPG from the PEPITEM-treated osteoblast conditioned media prior to adding it to the osteoclast



(legend on next page)

CellPress
OPEN ACCESS

precursors. Depleting OPG from the osteoblast conditioned media reversed the effects of PEPITEM on osteoclastogenesis, such that numbers of osteoclasts significantly increased (Figure 6I). To further confirm these observations, we undertook a competition assay, adding increasing concentrations of RANKL to the OPG-rich PEPITEM-treated osteoblast conditioned media. As expected, RANKL was able to outcompete PEPITEM-induced OPG, such that at 500 ng/mL RANKL the indirect inhibitory effects of PEPITEM on osteoclastogenesis were lost (Figure 6J). Finally, we assessed whether blocking NCAM-1 signaling impacted PEPITEM-induced OPG in osteoblasts. Significantly lower OPG concentrations were detected in conditioned media from anti-NCAM-1+PEPITEM-treated osteoblasts compared with those treated with PEPITEM in the presence of IgG1 control (Figure 6K). Collectively these data indicate that in response to PEPITEM signaling through NCAM-1, osteoblasts release OPG, which in turn negatively regulate osteoclast numbers, leading to an overall reduction in bone resorption and increase in bone density.

PEPITEM reverses bone loss in age-related musculoskeletal diseases

Osteoporosis is the most commonly occurring MSK condition, resulting in a net loss of cancellous bone and increased risk of fracture. To date, most osteoporosis medications target the activity of the osteoclast (e.g., bisphosphates, denosumab) to prevent further bone loss, but are unable to induce bone repair. Recent advances have enabled the development of anabolic agents, such as teriparatide (a parathyroid hormone mimic) and romosozumab, that can induce new bone formation but have limitations clinically—teriparatide is only effective for 24 months[33] and romosozumab has been associated with cardiovascular events.[34] Therefore, new drugs targeting the endogenous repair processes elicited by osteoblasts are urgently required. Given the pro-osteoblastogenic actions of PEPITEM revealed above, we sought to investigate the therapeutic efficacy of PEPITEM in a model of excessive bone loss.[35]

Osteoporosis onset is linked with menopause and the symptoms can be replicated *in vivo* upon the removal of the ovaries, where bone loss is evident as early as 2 weeks post-surgery (Fig S7). PEPITEM therapy limited the amount of trabecular bone loss triggered by ovariectomy (Figure 7A) with comparable levels of bone volume density (BV/TV), trabecular number, and thickness in the tibia of PEPITEM-treated mice at 4 weeks and those at the start of the 2-week therapy regimen (Figures 7B–7D). In contrast, there was a significant reduction in all these parameters in mice treated with vehicle control. As expected, we observed the reverse changes in trabecular separation (Figure 7E), indicating that PEPITEM therapy maintained a higher level of interconnectivity within the trabecular network during the onset of osteoporosis. Similar findings were seen in an inflammatory model of bone erosion, where PEPITEM treatment significantly reduced bone damage in arthritic mice when compared with vehicle-treated animals (Figure 7F). Using osteoblasts from aged patients (Table S5), we asked whether these cells were responsive to PEPITEM therapy. Crucially, PEPITEM significantly increased osteoblast maturation (Figures 7G and 7H) and mineralization (Figure 7I). These data highlight that PEPITEM could be used as an alternative and early clinical intervention to reverse the impact of age-related MSK diseases.

DISCUSSION

Dysregulation of bone remodeling underpins numerous MSK disorders resulting in substantive health care and socioeconomic costs through the permanent loss of function, pain, increased risk of fracture, and frailty in patients. Here we have described that the endogenous peptide, PEPITEM, regulates anabolic and catabolic activity in the bone. Specifically, PEPITEM acts directly on osteoblasts to induce new bone formation to increase bone strength. Simultaneously, PEPITEM triggers the release of the anti-osteoclastogenic regulator, OPG, from osteoblasts to limit bone resorption. Mechanistically, PEPITEM operates through a known bone regulating pathway—inducing rapid translocation of β-catenin to the nucleus to alter gene expression within osteoblasts (Figure 6). Crucially, PEPITEM therapy halted any further bone loss following ovariectomy and was effective at inducing bone formation by osteoblasts isolated from aged donors with osteoarthritis. Of note, we observed no sexual dimorphism in the response of cells, mice, or patients to PEPITEM. The dual bioactivity of PEPITEM is rare within the current portfolio of drugs available for MSK diseases, shared only by romosozumab, thus offering an alternative approach that promotes bone formation and repair while simultaneously redressing the imbalance in bone turnover.

PEPITEM can be endogenously cleaved from its parent protein 14-3-3ξ.[15] Of the seven members of the 14-3-3 family, only two have been previously postulated to play a role in bone development and remodeling. Using short hairpin RNA to inhibit 14-3-3β significantly reduced bone growth and osteoblast number *ex vivo* and reduced MSC osteoblastogenesis *in vitro*, indicating it has an anti-anabolic role within the bone.[13] By contrast, small interfering RNA (siRNA) knockdown of 14-3-3ξ (and thus

Figure 6. PEPITEM induces osteoblasts to release a soluble mediator, which inhibits osteoclast function

Figure360▷ For a Figure360 author presentation of Figure 6, see https://doi.org/10.1016/j.xcrm.2024.101574.

(A–K) Schematic representation of protocol. (B and E–G) Murine macrophage-like RAW264.7 cell line or (C and D) human peripheral blood monocytes were cultured with conditioned media from (B–G and K) primary murine calvarial osteoblasts, or (H) mini-bones cultured alone (untreated, Un, black), with a control peptide (Ctr, blue), PEPITEM either alone (PEP, red) or (D) in combination with Brefeldin A (Bref, green), (I) anti-OPG antibody, (J) RANKL, or (K) anti-NCAM-1 antibody.

(B–D, I, and J) Number of TRAP-positive osteoclasts expressed per 100 mm^2. Data are mean ± SEM from $n = 3$–4, or (B) $n = 7$ independent experiments. $^*p < 0.05$ and $^{**}p < 0.01$ by (B, D, and I) Dunnett's post-test.

(E, G, H, and K) OPG and (F) RANKL protein in supernatants expressed as (E and F) band intensity (AUC), (G) percentage of untreated calvarial osteoblasts, (H) pg/mL for human mini-bone organoids or (K) calvarial osteoblasts. Data are mean ± SEM from $n = 3$–4, (K) $n = 5$, or (G) $n = 7$ independent experiments. $^*p < 0.05$ and $^{**}p < 0.01$ by paired *t* test, (G) Wilcoxon, (H) unpaired *t* test, or (K) Dunnett's post-test.

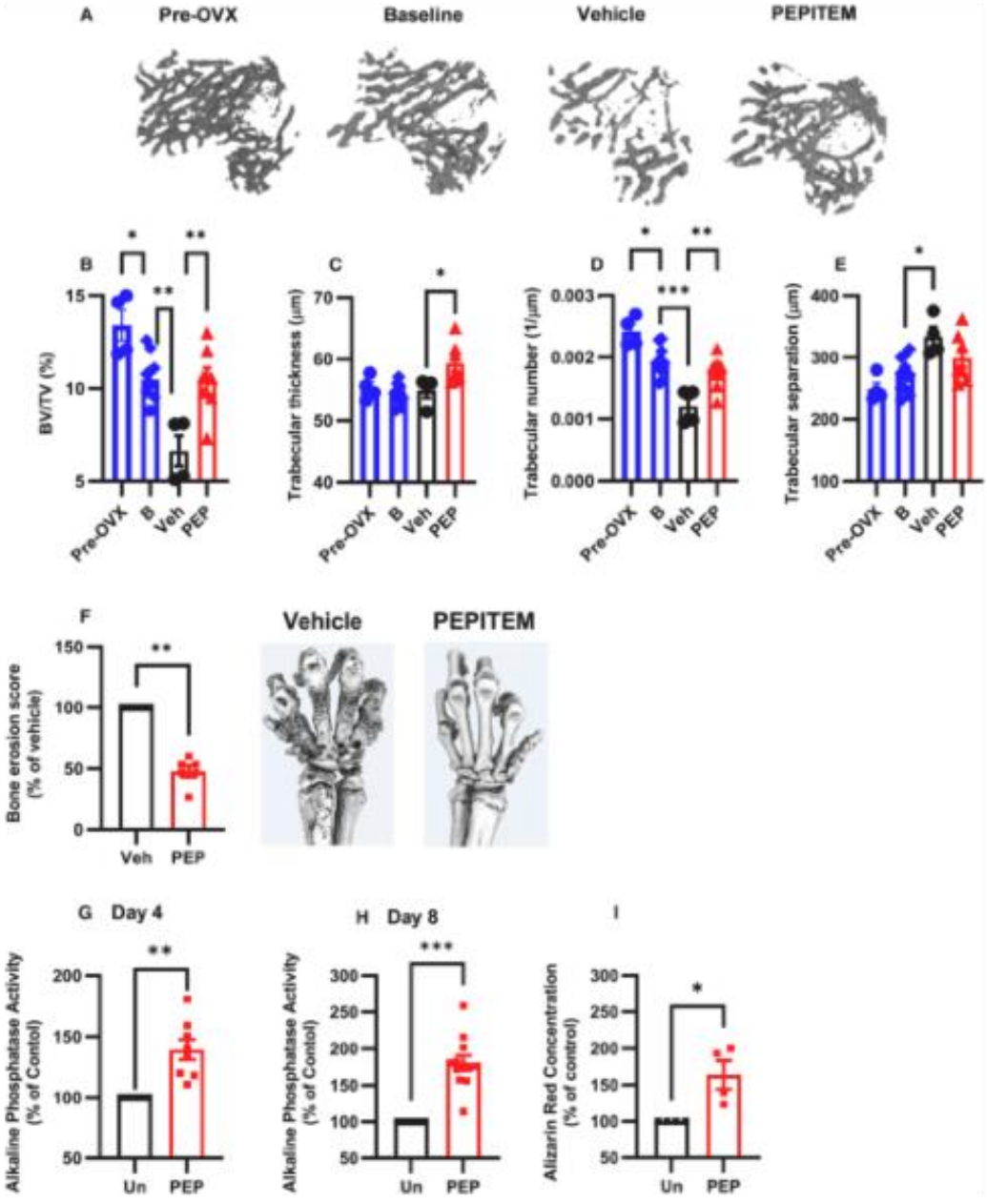


Figure 7. PEPITEM reverses bone loss related to musculoskeletal diseases

(A–E) Osteoporosis was induced for 2 weeks prior to mice being injected with vehicle control (Veh, black, $n = 4$) or PEPITEM-PEG (PEP, red, $n = 8$) for a further 2 weeks. Baseline samples were analyzed 2 weeks post-surgery before treatment started (B, blue, $n = 10$).

(legend continued on next page)

PEPITEM) significantly reduced osteoblastogenesis *in vitro*—with osteoblast precursors showing diminished expression of maturation markers (*runx2*, *alp*, *col1a1*, *bmp*) resulting in reduced maturation/alkaline phosphatase activity and mineral production.[14] However, and in contrast to our findings with PEPITEM, overexpression of 14-3-3ξ had no impact on BV/TV or trabecular number in resting Balb/c mice over the 6-week time frame of the experiment.[14] Possible explanations for these differences include the use of different strains of mice; the time point chosen for the analysis (2 vs. 6 weeks); the type and bioactivity of treatment (bioactive peptide vs. microRNA antagomir induced up-regulation of 14-3-3ξ and required subsequent proteolytic cleavage). Overexpression of 14-3-3ξ was able to partially reverse ovariectomy-induced loss of cancellous bone density and trabecular number over 6 weeks of treatment in Balb/c mice.[14] Importantly, these changes were comparable to those we observed with only 2 weeks of PEPITEM therapy, suggesting the pre-processed peptide represents a better therapeutic option. This is further supported by the ubiquitous expression pattern and multitude of cellular responses elicited by 14-3-3ξ and its up-regulation in various cancers (reviewed by Obsilova and Obsil[11]), which collectively make it a poor candidate for drug development. Conversely, PEPITEM circulates within serum of healthy individuals and its levels have been shown to decline with age,[15] making it a strong therapeutic candidate and putative causative factor in age-related bone loss.

NCAM-1 is transiently expressed within the bone: its expression is maximal in osteoblast precursors,[24] diminishing with maturation or long-term culture[23] so that it is lost entirely in mature osteocytes.[24] Indeed, osteoblast differentiation was significantly inhibited *in vitro* when NCAM-1 was silenced using either plasmid-based transfection of MC3T3-E1 cells or use of MSC from NCAM-1 knockout mice.[21] When NCAM-1 was silenced, osteoblasts exhibited reduced total β-catenin and PI-3K protein[21] and activation of Wnt/β-catenin in the absence of NCAM-1 restored osteoblastogenesis.[21] β-catenin is essential for the differentiation[26] and survival[27] of osteoblasts and its signaling role in the bone remodeling process is relatively well understood. Sclerostin binds to the Wnt receptor LRP5/6, inhibiting Wnt from binding to its receptor and therefore preventing signaling via the canonical Wnt signaling pathway. An absence of signaling via this pathway causes β-catenin to be targeted for ubiquitination and subsequent proteasomal degradation. Romosozumab (anti-sclerostin antibody) exerts its bone-anabolic effect by preventing sclerostin binding to the LRP5/6, allowing Wnt to bind, which inhibits ubiquitination of β-catenin and enables its translocation to the nucleus where it induces transcription of *RUNX2* and *OPG* to cause osteoblast maturation. Here, we show that PEPITEM rapidly induced β-catenin activation and nuclear translocation to enhance the expression of genes involved in osteoblast differentiation, including *col1a1*, as well as driving increased secretion of OPG—a known Wnt target.[36] Our *in silico* analysis predicts binding of PEPITEM to the FIII domain of NCAM-1, a region in which FGFR1 has been shown to bind and signal.[37–39] FGFR1 is important in regulating osteoblastogenesis: deficiency in osteoblast precursors results in maintenance of stem-like properties and blockade of differentiation and mineral deposition.[40] However, within mature osteoblasts[40] and osteocytes lack of FGFR1 drives bone formation by increasing the amount of active β-catenin, leading to increased OPG release.[41] Of note, we observe similar findings in response to PEPITEM, with increased active β-catenin within 15 min. Thus, it is possible that PEPITEM is binding to NCAM-1 directly or indirectly inhibits FGFR1 activation, driving increased β-catenin activity, osteoblast maturation, and mineralization, and OPG secretion resulting in enhanced bone formation and reduced osteoclastogenesis. However, further studies, such as site-directed mutagenesis or inhibition of the NCAM-1 FIII domain (FGFR1 binding site) are now required to conclusively prove this.

Of note, NCAM-1 is not the only PEPITEM-binding partner within the bone. Cadherin-15 was originally identified as the PEPITEM receptor and is expressed by osteoblasts and osteocytes[42]; however, our *in vitro* data indicate no role for cadherin-15 in mediating the activities of PEPITEM within the bone. Our co-immunoprecipitation studies revealed an additional nine potential binding partners with reported roles in bone homeostasis, of which eight were intracellular proteins with enzyme activity, roles in signaling pathways, or vesicle/ER trafficking of proteins. Of these intracellular proteins, nucleoredoxin, sec31A, and catenin delta-1 (p120) had high predicted interaction scores (pLTTD >90) with PEPITEM when analyzed using AlphaFold coupled with ChimeraX (data not shown), suggesting the possibility the PEPITEM influences intracellular responses in osteoblasts. Focusing on surface-expressed binding partners, EHD2 was also identified as a potential PEPITEM interactor. Little is known about the role of EHD2 in the bone, although its expression has been reported in osteoblastic-cell lines where it is thought to contribute to tumor suppression in the context of osteosarcoma.[43] In other mesenchymal stem cell-derived cells (e.g., adipocytes), EHD2 is known to stabilize calveolin-1 to regulate lipid uptake[44] through the protein kinase A-cAMP signaling pathway.[45] There is no evidence to date to indicate that EHD2 responses are linked to the β-catenin

(A) Representative 3-D microCT renders of trabecular bone.
(B) Percentage trabecular bone volume (BV/TV).
(C) Trabecular thickness in μm.
(D) Trabecular number per μm.
(E) Trabecular separation in μm. In B–E, ANOVA showed significant effect of time and treatment on all bone parameters, $p < 0.05$.
(F) Arthritis was induced, and mice were injected with vehicle control (Veh, black, $n = 5$) or PEPITEM-PEG (PEP, red, $n = 5$) for 2 weeks, prior to analysis by microCT. Bone erosion score expressed as a percentage of vehicle control.
(G–I) Alkaline phosphatase activity at day (G) 4 ($n = 8$) or (H) 8 ($n = 12$) or (I) alizarin red concentration at day 18 ($n = 4$) normalized to percentage of untreated control for osteoblasts from aged patients left untreated (Un, black) or treated with PEPITEM (PEP, red). Data are mean ± SEM. $^{*}p < 0.05$, $^{**}p < 0.01$, and $^{***}p < 0.001$ by (B–E) Dunnett's post-test compared with PBS control treatment at 4 weeks, (F–H) Wilcoxon, or (I) Mann-Whitney U.

translocation we observe upon PEPITEM treatment but further studies, including surface plasmon resonance, are necessary to reveal whether PEPITEM can interact with these other potential binding partners, and the functional consequence of such interactions, if they occur.

The balance between bone formation and bone resorption is largely controlled by the amount of RANKL and OPG produced by cells in the bone. Indeed, pharmaceutical companies have taken advantage of manipulating the RANKL-OPG ratio by developing biologics that either block RANKL (denosumab—anti-RANKL antibody) or reduce its endogenous production (romosozumab). By contrast, PEPITEM acts to enhance the production of the endogenous anti-osteoclastogenic factor, OPG, by osteoblasts without impacting RANKL levels—thereby swinging the balance in favor of bone formation without impacting the ability of osteoclasts to resorb regions of damaged or weak bone tissue via normal bone remodeling.

Bisphosphates are the current standard of care for osteoporosis, yet poorly managed long-term use is associated with increased incidence of microfractures and atypical femur fractures due to the absence of bone remodeling. Of the other remaining treatment options, only romosozumab has dual bioactivity—impacting both osteoblast and osteoclast function, as described for PEPITEM. Comparing mode of actions, PEPITEM is endogenously produced and acts directly on osteoblasts to stimulate osteoblastogenesis, while the humanized monoclonal antibody romosozumab works by removing the osteoblast inhibitor sclerostin to facilitate bone formation. Furthermore, PEPITEM stimulates osteoblast release of the endogenous inhibitor OPG, while romosozumab limits RANKL release to reduce bone resorption. The early data on the clinical efficacy of romosozumab appears exciting; however, this only appears effective over a relatively short term (maximum duration of treatment is 12 months) with reports of increased cardiovascular events in patients.[34] As an endogenous osteogenic peptide with the capacity to regulate osteoblast-osteoclast coupling in health and disease, PEPITEM offers the real possibility for maintenance or restoration of bone homeostasis over the long-term to prevent osteoporosis and fragility fractures. For this to be realized, prolonged treatment protocols are now required in a variety of bone disease models to ascertain the quality of the bone formed in response to PEPITEM therapy.

Conclusions

PEPITEM exerts osteogenic properties—whereby its osteogenic activity regulates osteoblast-osteoclast coupling leading to enhanced bone formation and moderating bone resorption in health, with age, and in disease (osteoporosis and rheumatoid arthritis) to redress the imbalance in bone turnover. Further studies are now urgently required to ascertain the therapeutic potential of PEPITEM or a PEPITEM-based agent in the clinical management of patients with excessive bone loss.

Limitations of the study

This study revealed 10 potential PEPITEM-binding partners on osteoblasts (listed in Table S1). Of these, we further investigated the role of one (NCAM-1) *in vitro* and *ex vivo*, but not *in vivo* in the murine models. Our *in silico* modeling provides a predicted analysis for protein-protein interactions, but it is important to consider surface plasma resonance and X-ray crystallography are the gold standard techniques to determine receptor-ligand interactions and these were not performed in the current study. The proposed molecular mechanism does not directly link NCAM-1 signaling to β-catenin activation and translocation—site-directed mutagenesis-type studies are needed for this. Finally, the use of PEPITEM therapy *in vivo* requires further pharmacokinetic and pharmacodynamic studies in a broader range of applications (e.g., fracture models, immobilization studies) in mice and other species, prior to translation into clinical use.

STAR★METHODS

Detailed methods are provided in the online version of this paper and include the following:

- KEY RESOURCES TABLE
- RESOURCE AVAILABILITY
  - Lead contact
  - Materials availability
  - Data and code availability
- EXPERIMENTAL MODEL AND STUDY PARTICIPANT DETAILS
  - Animals studies
  - Human participants
  - Cell lines and primary cell cultures
- INDUCTION OF MYOCYTE DIFFERENTIATION
- METHOD DETAILS
  - microCT analysis
  - Mechanical testing of murine femurs
  - Tissue analysis
  - Osteoblast maturation and mineralisation assays
  - Metatarsal methods
  - Human self-structuring bone organoids
  - Western blot
  - Co-immunoprecipitation and mass spectrometry
  - NCAM expression by flow cytometry
  - NCAM-1-PEPITEM interactions
  - NCAM1 and RUNX2 staining
  - β-catenin signaling
  - Osteoclast resorption assays
  - Secretome assays
  - ELISA
  - Gene expression
- QUANTIFICATION AND STATISTICAL ANALYSIS

SUPPLEMENTAL INFORMATION

Supplemental information can be found online at https://doi.org/10.1016/j.xcrm.2024.101574.

ACKNOWLEDGMENTS

Analysis was conducted using the Imaging Suite and Advanced Mass Spectrometry Facility funded by the University of Birmingham, and the microCT facility within the "Science City Research Alliance" was funded by Advantage West Midlands and the European Regional Development Fund. The authors acknowledge all study participants, research staff at the Royal Orthopaedic Hospital NHS Foundation Trust (Birmingham) and Russell's Hall Hospital, Dudley for obtaining consents and screening, and the orthopedic surgeons David Dunlop and Matthew Revell. Dynamic histomorphometry analysis was performed by members of the Skeletal Analysis Laboratories (University of Sheffield). This paper represents independent research partly funded by the MRC-Versus Arthritis Centre for Musculoskeletal Ageing Research (MR/P021220/1) and the Research into Inflammatory Arthritis Centre Versus Arthritis (RACE)

(grant number 22072). The views expressed are those of the author(s) and not necessarily those of the MRC or Versus Arthritis. Finally, we acknowledge the help and support provided by Elspeth Insch, as the patient research partner for this study. J.W.L., K.F., and G.N. were supported by PhD studentships funded by the Medical Research Council -Versus Arthritis Centre for Musculoskeletal Ageing Research PhD studentship (MR/R502364/1) and British Society for Research on Ageing - Chernajovsky Foundation PhD Scholarship. M.C. was supported by a Royal Society Dorothy Hodgkin Fellowship (DH16044). M.F. was supported by the National Centre for the Replacement, Refinement and Reduction of Animals in Research (NC3Rs NC/S001646/1). S.W.J. received funding from Versus Arthritis (21530; 21812) to provide tissue resources to support this work. A.J.N. was supported by a Versus Arthritis Career Development Fellowship (21743). This work was also supported by a Medical Research Council project grant MR/T028025/1 and the UK SPINE Knowledge Exchange Network.

AUTHOR CONTRIBUTIONS

J.W.L., K.F., G.N., M.W., M.F., O.A., S.K., E.P., C.P., J.L., and M.C. contributed to investigation and formal analysis. G.E.R., A.J.I., E.T.D., A.M., and S.W.J. contributed to resources. J.R.E., A.J.N., and H.M.M. contributed to conceptualization, formal analysis, funding acquisition, project administration, resources, supervision, and writing - original draft. All authors contributed to the writing – review and editing.

DECLARATION OF INTERESTS

H.M.M., G.E.R., A.J.I., and M.C. hold patents on the use of PEPITEM in bone diseases and other inflammatory conditions (US9597368B2; US9839671B; EP2802342; JP6055845; CN104168910B; US-2021-0100870-A1; GB2301317.0; PCT/GB2023/052013). H.M.M. and A.J.I. have received funding from Roche.

Received: December 5, 2023
Revised: February 29, 2024
Accepted: April 23, 2024
Published: May 21, 2024

REFERENCES

1. Bolamperti, S., Villa, I., and Rubinacci, A. (2022). Bone remodeling: an operational process ensuring survival and bone mechanical competence. Bone Res. *10*, 48. https://doi.org/10.1038/s41413-022-00219-8.
2. Feng, X., and McDonald, J.M. (2011). Disorders of bone remodeling. Annu. Rev. Pathol. *6*, 121–145. https://doi.org/10.1146/annurev-pathol-011110-130203.
3. Rashki Kemmak, A., Rezapour, A., Jahangiri, R., Nikjoo, S., Farabi, H., and Soleimanpour, S. (2020). Economic burden of osteoporosis in the world: A systematic review. Med. J. Islam. Repub. Iran *34*, 154. https://doi.org/10.34171/mjiri.34.154.
4. Kim, B., Cho, Y.J., and Lim, W. (2021). Osteoporosis therapies and their mechanisms of action (Review). Exp. Ther. Med. *22*, 1379. https://doi.org/10.3892/etm.2021.10815.
5. Xu, H., Wang, W., Liu, X., Huang, W., Zhu, C., Xu, Y., Yang, H., Bai, J., and Geng, D. (2023). Targeting strategies for bone diseases: signaling pathways and clinical studies. Signal Transduct. Target. Ther. *8*, 202. https://doi.org/10.1038/s41392-023-01467-8.
6. Kenkre, J.S., and Bassett, J. (2018). The bone remodelling cycle. Ann. Clin. Biochem. *55*, 308–327. https://doi.org/10.1177/0004563218759371.
7. Delaisse, J.M., Andersen, T.L., Kristensen, H.B., Jensen, P.R., Andreasen, C.M., and Søe, K. (2020). Re-thinking the bone remodelling cycle mechanism and the origin of bone loss. Bone *141*, 115628. https://doi.org/10.1016/j.bone.2020.115628.
8. Kramer, I., Halleux, C., Keller, H., Pegurri, M., Gooi, J.H., Weber, P.B., Feng, J.Q., Bonewald, L.F., and Kneissel, M. (2010). Osteocyte Wnt/β-Catenin Signaling Is Required for Normal Bone Homeostasis. Mol. Cell Biol. *30*, 3071–3085. https://doi.org/10.1128/MCB.01428-09.
9. Frost, K., Naylor, A.J., and McGettrick, H.M. (2023). The Ying and Yang of Sphingosine-1-Phosphate Signalling within the Bone. Int. J. Mol. Sci. *24*, 6935. https://doi.org/10.3390/ijms24086935.
10. Pederson, L., Ruan, M., Westendorf, J.J., Khosla, S., and Oursler, M.J. (2008). Regulation of bone formation by osteoclasts involves Wnt/BMP signaling and the chemokine sphingosine-1-phosphate. Proc. Natl. Acad. Sci. USA *105*, 20764–20769. https://doi.org/10.1073/pnas.0805133106.
11. Obsilova, V., and Obsil, T. (2022). Structural insights into the functional roles of 14-3-3 proteins. Front. Mol. Biosci. *9*, 1016071. https://doi.org/10.3389/fmolb.2022.1016071.
12. Moore, B.W. (1967). Specific acidic proteins of the nervous system. Physiological and Biochemical Aspects of Neverous Integration, pp. 343–349.
13. Liu, Y., Ross, J.F., Bodine, P.V.N., and Billiard, J. (2007). Homodimerization of Ror2 tyrosine kinase receptor induces 14-3-3(beta) phosphorylation and promotes osteoblast differentiation and bone formation. Mol. Endocrinol. *21*, 3050–3061. https://doi.org/10.1210/me.2007-0323.
14. Yin, P., Shi, Q., Xiao, F., Zhao, B., Yu, W., Wu, K., and Peng, K. (2020). Inhibition of miR-22 promotes differentiation of osteoblasts and improves bone formation via the YWHAZ pathway in experimental mice. Arch. Med. Sci. *16*, 1419–1431. https://doi.org/10.5114/aoms.2019.89979.
15. Chimen, M., McGettrick, H.M., Apta, B., Kuravi, S.J., Yates, C.M., Kennedy, A., Odedra, A., Alassiri, M., Harrison, M., Martin, A., et al. (2015). Homeostatic regulation of T cell trafficking by a B cell-derived peptide is impaired in autoimmune and chronic inflammatory disease. Nat. Med. *21*, 467–475. https://doi.org/10.1038/nm.3842.
16. Matsubara, H., Shimizu, Y., Arai, M., Yamagata, A., Ito, S., Imakiire, T., Tsunoda, M., Kumagai, H., and Oshima, N. (2020). PEPITEM/Cadherin 15 Axis Inhibits T Lymphocyte Infiltration and Glomerulonephritis in a Mouse Model of Systemic Lupus Erythematosus. J. Immunol. *204*, 2043–2052. https://doi.org/10.4049/jimmunol.1900213.
17. Pezhman, L., Hopkin, S.J., Begum, J., Heising, S., Nasteska, D., Wahid, M., Ed Rainger, G., Hodson, D.J., Iqbal, A.J., Chimen, M., and McGettrick, H.M. (2023). PEPITEM modulates leukocyte trafficking to reduce obesity-induced inflammation. Clin. Exp. Immunol. *212*, 1–10. https://doi.org/10.1093/cei/uxad022.
18. Parfitt, A.M. (2002). Misconceptions (2): turnover is always higher in cancellous than in cortical bone. Bone *30*, 807–809. https://doi.org/10.1016/S8756-3282(02)00735-4.
19. Zhu, E.D., Louis, L., Brooks, D.J., Bouxsein, M.L., and Demay, M.B. (2014). Effect of bisphosphonates on the rapidly growing male murine skeleton. Endocrinology *155*, 1188–1196. https://doi.org/10.1210/en.2013-1983.
20. Zweifler, L.E., Koh, A.J., Daignault-Newton, S., and McCauley, L.K. (2021). Anabolic actions of PTH in murine models: two decades of insights. J. Bone Miner. Res. *36*, 1979–1998. https://doi.org/10.1002/jbmr.4389.
21. Cheng, B.F., Feng, X., Gao, Y.X., Jian, S.Q., Liu, S.R., Wang, M., Xie, Y.F., Wang, L., Feng, Z.W., and Yang, H.J. (2021). Neural Cell Adhesion Molecule Regulates Osteoblastic Differentiation Through Wnt/β-Catenin and PI3K-Akt Signaling Pathways in MC3T3-E1 Cells. Front. Endocrinol. *12*, 667953. https://doi.org/10.3389/fendo.2021.667953.
22. Guilherme, A., Soriano, N.A., Bose, S., Holik, J., Bose, A., Pomerleau, D.P., Furcinitti, P., Leszyk, J., Corvera, S., and Czech, M.P. (2004). EHD2 and the novel EH domain binding protein EHBP1 couple endocytosis to the actin cytoskeleton. J. Biol. Chem. *279*, 10593–10605. https://doi.org/10.1074/jbc.M307702200.
23. Roman-Roman, S., Garcia, T., Jackson, A., Thelhaber, J., Rawadi, G., Connolly, T., Spinella-Jaegle, S., Kawai, S., Courtois, B., Bushnell, S., et al. (2003). Identification of genes regulated during osteoblastic differentiation by genome-wide expression analysis of mouse calvaria primary

osteoblasts in vitro. Bone *32*, 474–482. https://doi.org/10.1016/s8756-3282(03)00062-8.

24. Lee, Y.-S., and Chuong, C.-M. (1992). Adhesion molecules in skeletogenesis: I. transient expression of neural cell adhesion molecules (NCAM) in osteoblasts during endochondral and intramembranous ossification. J. Bone Miner. Res. *7*, 1435–1446. https://doi.org/10.1002/jbmr.5650071211.
25. Case, N., Ma, M., Sen, B., Xie, Z., Gross, T.S., and Rubin, J. (2006). Beta-catenin levels influence rapid mechanical responses in osteoblasts. J. Biol. Chem. *283*, 29196–29205. https://doi.org/10.1074/jbc.M801907200.
26. Glass, D.A., and Karsenty, G. (2006). Molecular bases of the regulation of bone remodeling by the canonical Wnt signaling pathway. Curr. Top. Dev. Biol. *73*, 43–84. https://doi.org/10.1016/s0070-2153(05)73002-7.
27. Day, T.F., Guo, X., Garrett-Beal, L., and Yang, Y. (2005). Wnt/beta-catenin signaling in mesenchymal progenitors controls osteoblast and chondrocyte differentiation during vertebrate skeletogenesis. Dev. Cell *8*, 739–750. https://doi.org/10.1016/j.devcel.2005.03.016.
28. Evans, R., O'Neill, M., Pritzel, A., Antropova, N., Senior, A., Green, T., Žídek, A., Bates, R., Blackwell, S., Yim, J., et al. (2022). Protein complex prediction with AlphaFold-Multimer. Preprint at bioRxiv. https://doi.org/10.1101/2021.10.04.463034.
29. Pettersen, E.F., Goddard, T.D., Huang, C.C., Meng, E.C., Couch, G.S., Croll, T.I., Morris, J.H., and Ferrin, T.E. (2021). UCSF ChimeraX: Structure visualization for researchers, educators, and developers. Protein Sci. *30*, 70–82. https://doi.org/10.1002/pro.3943.
30. Johnson, C.P., Fragneto, G., Konovalov, O., Dubosclard, V., Legrand, J.F., and Leckband, D.E. (2005). Structural studies of the neural-cell-adhesion molecule by X-ray and neutron reflectivity. Biochemistry *44*, 546–554. https://doi.org/10.1021/bi048263j.
31. Shah, C., Hegde, B.G., Morén, B., Behrmann, E., Mielke, T., Moenke, G., Spahn, C.M.T., Lundmark, R., Daumke, O., and Langen, R. (2014). Structural insights into membrane interaction and caveolar targeting of dynamin-like EHD2. Structure *22*, 409–420. https://doi.org/10.1016/j.str.2013.12.015.
32. Boyce, B.F., and Xing, L. (2008). Functions of RANKL/RANK/OPG in bone modeling and remodeling. Arch. Biochem. Biophys. *473*, 139–146. https://doi.org/10.1016/j.abb.2008.03.018.
33. Lindsay, R., Krege, J.H., Marin, F., Jin, L., and Stepan, J.J. (2016). Teriparatide for osteoporosis: importance of the full course. Osteoporos. Int. *27*, 2395–2410. https://doi.org/10.1007/s00198-016-3534-6.
34. Saag, K.G., Petersen, J., Brandi, M.L., Karaplis, A.C., Lorentzon, M., Thomas, T., Maddox, J., Fan, M., Meisner, P.D., and Grauer, A. (2017). Romosozumab or Alendronate for Fracture Prevention in Women with Osteoporosis. N. Engl. J. Med. *377*, 1417–1427. https://doi.org/10.1056/NEJMoa1708322.
35. Lei, Z., Xiaoying, Z., and Xingguo, L. (2009). Ovariectomy-associated changes in bone mineral density and bone marrow haematopoiesis in rats. Int. J. Exp. Pathol. *90*, 512–519. https://doi.org/10.1111/j.1365-2613.2009.00661.x.
36. Glass, D.A., Bialek, P., Ahn, J.D., Starbuck, M., Patel, M.S., Clevers, H., Taketo, M.M., Long, F., McMahon, A.P., Lang, R.A., and Karsenty, G. (2005). Canonical Wnt Signaling in Differentiated Osteoblasts Controls Osteoclast Differentiation. Dev. Cell *8*, 751–764. https://doi.org/10.1016/j.devcel.2005.02.017.
37. Sanchez-Heras, E., Howell, F.V., Williams, G., and Doherty, P. (2006). The fibroblast growth factor receptor acid box is essential for interactions with N-cadherin and all of the major isoforms of neural cell adhesion molecule. J. Biol. Chem. *281*, 35208–35216. https://doi.org/10.1074/jbc.M608655200.
38. Francavilla, C., Cattaneo, P., Berezin, V., Bock, E., Ami, D., de Marco, A., Christofori, G., and Cavallaro, U. (2009). The binding of NCAM to FGFR1 induces a specific cellular response mediated by receptor trafficking. J. Cell Biol. *187*, 1101–1116. https://doi.org/10.1083/jcb.200903030.
39. Kiselyov, V.V., Skladchikova, G., Hinsby, A.M., Jensen, P.H., Kulahin, N., Soroka, V., Pedersen, N., Tsetlin, V., Poulsen, F.M., Berezin, V., and Bock, E. (2003). Structural basis for a direct interaction between FGFR1 and NCAM and evidence for a regulatory role of ATP. Structure *11*, 691–701. https://doi.org/10.1016/s0969-2126(03)00096-0.
40. Jacob, A.L., Smith, C., Partanen, J., and Ornitz, D.M. (2006). Fibroblast growth factor receptor 1 signaling in the osteo-chondrogenic cell lineage regulates sequential steps of osteoblast maturation. Dev. Biol. *296*, 315–328. https://doi.org/10.1016/j.ydbio.2006.05.031.
41. Tang, Y., Yang, P., Jin, M., Huang, S., Chen, H., Chen, L., Yang, J., and Su, N. (2023). Fgfr1 deficiency in osteocytes leads to increased bone mass by enhancing Wnt/β-catenin signaling. Bone *174*, 116817. https://doi.org/10.1016/j.bone.2023.116817.
42. Paic, F., Igwe, J.C., Nori, R., Kronenberg, M.S., Franceschetti, T., Harrington, P., Kuo, L., Shin, D.G., Rowe, D.W., Harris, S.E., and Kalajzic, I. (2009). Identification of differentially expressed genes between osteoblasts and osteocytes. Bone *45*, 682–692. https://doi.org/10.1016/j.bone.2009.06.010.
43. Fan, H., Liu, T., Tian, H., and Zhang, S. (2020). TUSC8 inhibits the development of osteosarcoma by sponging miR-197-3p and targeting EHD2. Int. J. Mol. Med. *46*, 1311–1320. https://doi.org/10.3892/ijmm.2020.4684.
44. Morén, B., Hansson, B., Negoita, F., Fryklund, C., Lundmark, R., Göransson, O., and Stenkula, K.G. (2019). EHD2 regulates adipocyte function and is enriched at cell surface–associated lipid droplets in primary human adipocytes. Mol. Biol. Cell *30*, 1147–1159. https://doi.org/10.1091/mbc.E18-10-0680.
45. Fryklund, C., Morén, B., Shah, S., Grossi, M., Degerman, E., Matthaeus, C., and Stenkula, K.G. (2021). EH Domain-Containing 2 Deficiency Restricts Adipose Tissue Expansion and Impairs Lipolysis in Primary Inguinal Adipocytes. Front. Physiol. *12*, 740666. https://doi.org/10.3389/fphys.2021.740666.
46. Gaytan, F., Morales, C., Reymundo, C., and Tena-Sempere, M. (2020). A novel RGB-trichrome staining method for routine histological analysis of musculoskeletal tissues. Sci. Rep. *10*, 16659. https://doi.org/10.1038/s41598-020-74031-x.
47. Finlay, M., Hill, L.A., Neag, G., Patel, B., Chipara, M., Lamont, H.C., Frost, K., Patrick, K., Lewis, J.W., Nicholson, T., et al. (2023). A detailed methodology for the long-term in vitro culture and analysis of three-dimensional, self-structuring bone models generated from cell lines or primary osteoblastic cell populations [version 1; peer review: awaiting peer review]. F1000Res. *12*, 357. https://doi.org/10.12688/f1000research.130779.1.
48. Guo, H.-B., Perminov, A., Bekele, S., Kedziora, G., Farajollahi, S., Varaljay, V., Hinkle, K., Molinero, V., Meister, K., Hung, C., et al. (2022). AlphaFold2 models indicate that protein sequence determines both structure and dynamics. Sci. Rep. *12*, 10696. https://doi.org/10.1038/s41598-022-14382-9.
49. Varadi, M., Anyango, S., Deshpande, M., Nair, S., Natassia, C., Yordanova, G., Yuan, D., Stroe, O., Wood, G., Laydon, A., et al. (2022). AlphaFold Protein Structure Database: massively expanding the structural coverage of protein-sequence space with high-accuracy models. Nucleic Acids Res. *50*, D439–d444. https://doi.org/10.1093/nar/gkab1061.
50. Goddard, T.D., Huang, C.C., Meng, E.C., Pettersen, E.F., Couch, G.S., Morris, J.H., and Ferrin, T.E. (2018). UCSF ChimeraX: Meeting modern challenges in visualization and analysis. Protein Sci. *27*, 14–25. https://doi.org/10.1002/pro.3235.
51. Elbrecht, V., Taberlet, P., Dejean, T., Valentini, A., Usseglio-Polatera, P., Beisel, J.N., Coissac, E., Boyer, F., and Leese, F. (2016). Testing the potential of a ribosomal 16S marker for DNA metabarcoding of insects. PeerJ *4*, e1966. https://doi.org/10.7717/peerj.1966.
52. Kastanis, G.J., Santana-Quintero, L.V., Sanchez-Leon, M., Lomonaco, S., Brown, E.W., and Allard, M.W. (2019). In-depth comparative analysis of Illumina(®) MiSeq run metrics: Development of a wet-lab quality assessment tool. Mol. Ecol. Resour. *19*, 377–387. https://doi.org/10.1111/1755-0998.12973.

CellPress
OPEN ACCESS

53. Wingett, S.W., and Andrews, S. (2018). FastQ Screen: A tool for multi-genome mapping and quality control. F1000Res. *7*, 1338. https://doi.org/10.12688/f1000research.15931.2.

54. Bushnell, B. BBMAP: A fast, accurate, splice-aware aligner. No. LBNL-7065E. Ernest Orlando Lawrence Berkeley National Laboratory, Berkeley, CA (2014).

55. Howe, K.L., Achuthan, P., Allen, J., Allen, J., Alvarez-Jarreta, J., Amode, M.R., Armean, I.M., Azov, A.G., Bennett, R., Bhai, J., *et al.* (2021). Ensembl 2021. Nucleic Acids Res. *49*, D884–d891. https://doi.org/10.1093/nar/gkaa942.

56. Dobin, A., Davis, C.A., Schlesinger, F., Drenkow, J., Zaleski, C., Jha, S., Batut, P., Chaisson, M., and Gingeras, T.R. (2013). STAR: ultrafast universal RNA-seq aligner. Bioinformatics *29*, 15–21. https://doi.org/10.1093/bioinformatics/bts635.

57. Liao, Y., Smyth, G.K., and Shi, W. (2014). featureCounts: an efficient general purpose program for assigning sequence reads to genomic features. Bioinformatics *30*, 923–930. https://doi.org/10.1093/bioinformatics/btt656.

58. Liao, Y., Smyth, G.K., and Shi, W. (2013). The Subread aligner: fast, accurate and scalable read mapping by seed-and-vote. Nucleic Acids Res. *41*, e108. https://doi.org/10.1093/nar/gkt214.

59. Ge, S.X., Son, E.W., and Yao, R. (2018). iDEP: an integrated web application for differential expression and pathway analysis of RNA-Seq data. BMC Bioinf. *19*, 534. https://doi.org/10.1186/s12859-018-2486-6.

STAR★METHODS

KEY RESOURCES TABLE

REAGENT or RESOURCE	SOURCE	IDENTIFIER
Antibodies		
Anti-Cadherin-15 Antibody, clone: 12G4	Sigma-Aldrich	Cat: 05-852; RRID: AB_390133
Anti-NCAM-1 Antibody, clone: MEM-188	Thermo Fisher Scientific	Cat: MA1-19129; RRID: AB_1073124
Rabbit IgG1 Isotype Control Antibody	Invitrogen	Cat: 02-6102; RRID: AB_2532938
Anti-RANKL Antibody, clone: 3F2E1	Proteintech	Cat: 66610-1-Ig; RRID: AB_2881970
Anti-OPG polyclonal Antibody	Bio-Techne	Cat: AF459-SP; RRID: AB_3553
Anti-β-actin polyclonal Antibody	Sigma-Aldrich	Cat: A2066; RRID: AB_476693
Goat Anti-Mouse IgG HRP-conjugated Antibody	Bio-Rad	Cat: 1706516; RRID: AB_2921252
Goat Anti-Rabbit IgG HRP-conjugated Antibody	Merck Millipore	Cat: 401393; RRID: AB_437797
Anti-β-catenin polyclonal Antibody	Merck Millipore	Cat: 06-734; RRID: AB_310231
Donkey Anti-Goat IgG 647-conjugated Antibody	Thermo Fisher Scientific	Cat: A21447; RRID: AB_2535864
Goat anti-Rat IgG 546-conjugated Antibody	Thermo Fisher Scientific	Cat: A11081; RRID: AB_2534125
Goat anti-Rabbit IgG 488-conjugated Antibody	Thermo Fisher Scientific	Cat: A11034; RRID: AB_2576217
Anti-CD56 (NCAM) Antibody, clone: 5.1H11	Thermo Fisher Scientific	Cat: AB5032; RRID: AB_2291692
Anti-RUNX2 Antibody, clone: 232902	Bio-Techne	Cat: MAB2006-SP; RRID AB_2184526
Rabbit Non-phospho (Active) β-Catenin (Ser33/37/Thr41) (D13A1) Antibody	Cell Signaling	Cat: 8814T; RRID AB_11127203
Biological samples		
Murine Tibias and Spines	C57BL/6J male mice	N/A
Murine Tibias and Spines	Ovariectomy female C57BL/6J mice	N/A
Embryonic metatarsals	C57BL/6J embryonic (E14.5) mice	N/A
Hind Limbs	Collagen induced arthritis male DBA-1 mice	N/A
Human bone chips	Royal Orthopedic Hospital, Birmingham	N/A
Small dentine disks	Gift from Prof James Edwards, University of Oxford	N/A
Chemicals, peptides, and recombinant proteins		
PEPITEM-PEG (SVTEQGAELSNEER- PEG(352)-Amide)	Cambridge Bioscience	N/A
PEPITEM (SVTEQGAELSNEER)	Cambridge Bioscience	N/A
Control peptide (EQAERYDDMAACMK)	Cambridge Bioscience	N/A
biotinylated PEPITEM (Biotin-SVTEQGAELSNEER)	Cambridge Bioscience	N/A
biotinylated control peptide (Biotin-EQAERYDDMAACMK)	Cambridge Bioscience	N/A
Complete Freund's Adjuvant	Sigma-Aldrich	Cat: F5881
Bovine collagen II	Gift from Prof Richard Williams, University of Oxford, UK	N/A
Sphingosine-1-phosphate	Sigma-Aldrich	Cat: S9666
Recombinant Mouse RANKL	Abcam	Cat: Ab129136
Recombinant Human M-CSF	R&D systems	Cat: 216-MC-005/CF
Recombinant Human RANKL	R&D systems	Cat: 390-TN-010/CF
Zoledronic acid hydrate	Cambridge Biosciences	Cat: CAY14984
Recombinant Mouse FGFR1	Sino Biological	Cat: 50186-M02H
Critical commercial assays		
Alizarin Red S Staining Quantification Kit	Caltag+Medsystems	Cat: 8678
BCA assay	Thermo Fisher Scientific	Cat: 23225

(Continued on next page)

Continued

REAGENT or RESOURCE	SOURCE	IDENTIFIER
EasySep™ Human Monocyte Isolation Kit	STEMCELL Technologies	Cat: 19359
Osteo Assay Surface Multiple Well Plate	Corning	Cat: CLS3987
Mouse Osteoprotegerin Quantikine ELISA Kit	R&D systems	Cat: MOP00
Human Osteoprotegerin DuoSet ELISA Kit	R&D systems	Cat: DY805
Mouse RANKL Quantikine ELISA Kit	R&D systems	Cat: MTR00
Rat/Mouse Total procollagen type-1 N terminal propeptide (P1NP) EIA	RatLaps	Cat: AC-33F1
RNeasy Kit	Qiagen	Cat: 74104
High-Capacity cDNA Reverse Transcription Kit	Applied Biosystems	Cat: 10400745
Deposited data		
Bulk RNAseq	SRA	http://www.ncbi.nlm.nih.gov/bioproject/1099588
Experimental models: Cell lines		
Murine calvarial osteoblasts (C.Ob)	C57BL/6J	N/A
ST2	Gift from Prof James Edwards, University of Oxford	N/A
Primary Human Osteoblasts	Royal Orthopedic Hospital, Birmingham	N/A
hFOb 1.19	ATCC	CRL-3602
Primary human bone-derived mesenchymal stem cells	Lonza	C-14090
Murine bone marrow osteoclast precursors	C57BL/6 WT	N/A
RAW264.7	ATCC	TIB-71
Human Monocytes	healthy volunteers	N/A
C2C12	ATCC	CRL-1772
Experimental models: Organisms/strains		
C57BL/6J male mice	Charles River	N/A
Ovariectomy female C57BL/6J mice	Charles River or Envigo	N/A
Collagen induced arthritis male DBA-1 mice	Charles River or Envigo	N/A
Oligonucleotides		
Ncam1 (Mm01149710_m1)	Thermo Fisher Scientific	Cat: 4331182
Alpl (Mm00475834_m1)	Thermo Fisher Scientific	Cat: 4331182
Cdh15 (Mm00483191_m1)	Thermo Fisher Scientific	Cat: 4331182
CDH15 (Hs00170504_m1)	Thermo Fisher Scientific	Cat: 4331182
ACP5 (Hs00356261_m1)	Thermo Fisher Scientific	Cat: 4331182
ACP6 (Hs00212563_m1)	Thermo Fisher Scientific	Cat: 4331182
CTSK (Hs00166156_m1)	Thermo Fisher Scientific	Cat: 4331182
MRS1 (Hs00234007_m1)	Thermo Fisher Scientific	Cat: 4331182
Col1a1 (Mm00801666_g1)	Thermo Fisher Scientific	Cat: 4331182
Software and algorithms		
NRecon 1.6.1.5	Bruker	N/A
DataViewer	Bruker	https://www.bruker.com/en/products-and-solutions/preclinical-imaging/micro-ct/3d-suite-software.html
CTAn v1.12	Bruker	https://www.bruker.com/en/products-and-solutions/preclinical-imaging/micro-ct/3d-suite-software.html
Osteomeasure	Osteometrics	https://www.osteometrics.com/

(Continued on next page)

Continued

REAGENT or RESOURCE	SOURCE	IDENTIFIER
ImageJ	National Institute for Health	https://imagej.nih.gov/ij/
ImageJ FIJI	ImageJ	https://imagej.net/software/fiji/downloads
AlphaFold2_multimer	Google colab	https://colab.research.google.com/github/sokrypton/ColabFold/blob/main/AlphaFold2.ipynb#scrollTo=mbaIO9pWjaN0
Gen5	BioTek	N/A
Uniprot database using Protein Discovery 2.2	Thermo Fisher Scientific	N/A
Sequest HT algorithm	Thermo Fisher Scientific	N/A
ChimeraX	UCSF	https://www.cgl.ucsf.edu/chimerax/
Zen Blue software	ZEISS	N/A
FlowJo	BD Life Sciences	N/A
Other		
Skyscan 1172 micro-CT scanner	Bruker	N/A
ElectroForce® BioDynamic® 5500	Bose	N/A
ZEISS Axioscan Z1	ZEISS	N/A
Synergy HT plate reader	BioTek	N/A
Cytation 5 microscope	Biotek	N/A
170V current PowerPac Basic Power supply	Bio-Rad	Cat: 1645050
Trans-Blot turbo transfer system	BioRad	Cat: 1704150
ChemiDOC MP Imaging System	BioRad	N/A
100V current PowerPac Basic Power supply	Bio-Rad	Cat: 1645050
UltiMate® 3000 HPLC series	Dionex	N/A
QExactive HF Orbitrap mass spectrometer	Thermo Fisher Scientific	N/A
Triversa Nanomate nanospray source	Advion Biosciences	N/A
LSM 780 confocal microscope	ZEISS	N/A
LightCycler 480	Roche	Cat: 04729749001

RESOURCE AVAILABILITY

Lead contact

Further information and requests for resources and reagents should be directed to and will be fulfilled by the lead contact, Helen McGettrick (h.m.mcgettrick@bham.ac.uk).

Materials availability

This study did not generate unique reagents. Key resources are outlined in the resources table.

Data and code availability

- Bulk RNA-seq data have been deposited at SRA (http://www.ncbi.nlm.nih.gov/bioproject/1099588) and are publicly available as of the date of publication. Accession numbers are listed in the key resources table.
- This paper does not report original code.
- Any additional information required to reanalyze the data reported in this paper is available from the lead contact upon request.

EXPERIMENTAL MODEL AND STUDY PARTICIPANT DETAILS

Animals studies

Mice were purchased from Charles River or Envigo, and were maintained in a specific pathogen free facility, with free access to food and water. Environmental conditions were: 21 ± 2°C, 55 ± 10% relative humidity and a 12 h light-dark cycle.

Eight-week-old, male, C57Bl/6J resting wild type (WT) mice were given daily intra-peritoneal (IP) injections of equivalent volume of vehicle control (PBS), or pegylated PEPITEM (300 μg, sequence SVTEQGAELSNEER- PEG(352)-Amide; both from Cambridge

CellPress
OPEN ACCESS

Research Biochemicals Limited; Cambridge, UK) for 14 or 28 days. On day 8 and day 12, mice were given 20 mg/kg calcein (Sigma-Aldrich) by IP injection.

Alternatively, 12-week-old, female C57Bl/6J underwent ovariectomy. Fourteen days later, mice were culled to acquire baseline measurements or given daily IP injections of either vehicle control (PBS) or PEPITEM-PEG (300 μg) for 14 days. Ovariectomy is only possible on female mice, and the effects of PEPITEM on male mice during osteoporosis-related bone loss were not explored.

Alternatively, 8-week-old, male DBA-1 were administered s.c. injection of bovine collagen II (CII, 100 μg, gift from Prof Richard Williams, University of Oxford, UK) 1:1 with complete Freund's adjuvant, followed by boost at day 21 with CII in incomplete Freund's adjuvant. Between days 21–35 mice were given daily IP injections of either vehicle control (PBS) or PEPITEM-PEG (300 μg).

Following treatment, mice were culled and bones from the hind limbs and spine were dissected, cleaned of muscle and fat before fixation in 10% neutral-buffered formalin (4% v/v formaldehyde in phosphate buffered saline - PFA) for 24 h and stored in 70% ethanol at 2-8°C until analysis.

In all experiments, littermates were randomly assigned to experimental groups within the same cages.

Animal studies were regulated by the Animals (Scientific Procedures) Act 1986 of the United Kingdom and performed under Personal Project Licence (PE5985209) at the Biomedical Services Unit, University of Birmingham, which holds a section 2C Establishment Licence. Approval was granted by the University of Birmingham's Animal Welfare and Ethical Review Body and all ethical guidelines were adhered to whilst carrying out this study.

Human participants

Primary human osteoblasts were isolated from aged (between 55 and 80 years old) predominantly female patients undergoing joint replacement surgery at the Royal Orthopedic Hospital, Birmingham (Table S5). The skewing of participants sex to females is equivalent to osteoporosis incidence. Power calculations based on preliminary data indicated 10 participants per group per analysis were required. Sample size used is recorded within the legend for Figure 7. In all experiments utilising human samples, the same patient samples were included in all conditions. The study was conducted in compliance with the Declaration of Helsinki. All human samples were obtained with written, informed consent and approval from the Human Biomaterial Resource Center (Birmingham, UK), South East Scotland Research Ethics Committee (16/SS/0172) or University of Birmingham Local Ethical Review Committee.

Cell lines and primary cell cultures

Osteoblasts

Primary murine calvarial osteoblasts (C.Ob) were isolated from male and female postnatal day 3–5 C57BL/6J WT mice as previously described[39] and cultured in basal murine osteoblast media [α-MEM, supplemented with 2 mM L-glutamine, 100 μg/mL streptomycin, 100U/ml penicillin (all from Sigma-Aldrich) and 10% fetal bovine serum (Biosera)], prior to use at passage (P)1. Gene expression for specific osteoblast progenitor and maturation markers, along with capacity to differentiate into osteoblasts and form mineral were used to authenticate the cell lineage.

Murine osteoblast precursor stromal P1 cell line (ST2) were cultured in basal osteoblast murine media and used before P9.

Primary human osteoblasts were isolated from aged patients undergoing joint replacement surgery at the Royal Orthopedic Hospital, Birmingham (Table S5) using the outgrowth method from bone chips as previously described[40] and cultured in basal human osteoblast media [DMEM, 2 mM L-glutamine, 100 μg/mL streptomycin, 100 U/ml penicillin, 1% non-essential amino acid solution, 2 mM β-glycerol phosphate, 50 μg/mL L-ascorbic acid (all from Sigma-Aldrich) and 10% fetal bovine serum (Biosera)], prior to use at P1-4. Gene expression for specific osteoblast progenitor and maturation markers, along with capacity to differentiate into osteoblasts and form mineral were used to authenticate the cell lineage.

Human osteoblast cell line (hFOb 1.19) were cultured in DMEM/F-12, no phenol red (Fisher scientific, cat; 21041025) supplemented with 10% FBS and 0.3 mg/mL G418 (Sigma-Aldrich, cat; 4727878001) at 35.5°C for 3 days, before moving cells to 37°C and culturing in osteogenic media (basal culture media plus 10-8M menadione and 100 μg/ml ascorbic acid (all from Sigma-Aldrich).

Primary human bone marrow-derived mesenchymal stem cells (MSC) from healthy donors were purchased from Lonza Ltd (Basel, Switzerland) at P2 and expanded/cultured in MSCGM Bulletkit (Lonza), prior to use at P5. Cells were plated (3×10^4) in 6 well plates or 1.5×10^4 in 12 well plates and allowed to adhere for 24 h before changing to osteogenic media (Lonza, cat: PT-3002) with media changes every 3 days.

Osteoclasts

Murine bone marrow osteoclast precursors were isolated from the hindlimb tibias and femurs of 8-week-old male and female C57BL/6J WT mice by centrifugation at 10,000 g for 15 s in murine basal osteoclast media.[46] The pellet was dispersed using a 25G needle before addition of murine basal osteoclast media and filtration through a 70 μm pore filter. Gene expression for specific osteoclast progenitor and maturation markers, along with capacity to differentiate into osteoclasts and resorb mineral were used to authenticate the cell lineage.

Murine macrophage-like cell line RAW264.7 (TIB-71; ATCC) were cultured in basal osteoclast media.

Primary human peripheral mononuclear cells (PBMC) were isolated from the blood of male and female healthy volunteers as previously described.[47] Monocytes were negatively selected from PBMC resuspended in MACs buffer using EasySepTM Human Monocyte Isolation Kit, as per manufacturer's instructions (Stem Cell, Cambridge, UK).

INDUCTION OF MYOCYTE DIFFERENTIATION

Immortalised murine myoblast cell line C2C12 (CRL-1772, ATCC) were cultured in DMEM supplemented with 2 mM L-glutamine, 100 μg/mL streptomycin and 100 U/ml penicillin (all from Sigma-Aldrich) for 24 h, prior to differentiation in DMEM supplemented with 2% horse serum (Sigma-Aldrich) for 8 days.

METHOD DETAILS

microCT analysis

Limbs and spines were placed vertically into the Skyscan 1172 micro-CT scanner (Bruker; Kontich, Belgium) and imaged every 0.45° as previously described.[37] Images were reconstructed using NRecon 1.6.1.5 (Bruker) by two independent researchers and subsequently analyzed blinded and independently. Briefly, scanning misalignment was calculated and automatic compensation was applied, followed by a beam hardening correction of 20% and a ring artifact correction of 4. Cross-sectional images were reconstructed using the Feldkamp algorithm. Spinal cross-sectional images were subsequently rotated to 3D coronal view in DataViewer (Bruker).

Trabecular and cortical bone parameters were calculated from cross-sectional images and 3D images generated using the CTAn v1.12 software (Computed Tomography Analyser; Bruker). Comparing CTAn images to original CT images allowed a manual global threshold that differentiated "real" bone from background noise to be applied. Regions of interest (ROIs) beginning at the distal-most point of the proximal growth plate were drawn around trabecular bone. 100 slices were included (total region of 1370μm) for tibiae and 14 (total region of 192 μm) for the spine. The "despeckle" CTAn plugin was used to remove white pixels from 3D space, then analyzed as 2D images or converted to a 3D mesh using a marching cube algorithm in CTAn, before meshes were visualised in MeshLab 1.3.2 (ISTI-CNR, Italy). Quantitative data was generated by the "3D analysis" plugin (CTAn) and percentage trabecular bone volume/tissue volume (BV/TV %); average (mean) trabecular number per μm as 1/μm; average (mean) trabecular thickness in μm and average (mean) trabecular separation in μm are shown. For the arthritis model, images were scored for degree of erosion (0 = normal, 1 = roughness; 2 = pitting or 3 = full thickness holes) and the extent of damage (0 = none, 1 = a few small areas; 2 = multiple small to medium sized areas or 3 = multiple medium to large sized areas). Data were presented as bone erosion as a percentage of the vehicle treated animals.

Mechanical testing of murine femurs

Femurs were cleaned of all muscle and tested to the point of failure in the 3-point bending test using the ElectroForce BioDynamic 5500 (Bose, ElectroForce Systems Group, Minnesota, USA) as previously described.[37] A 22 N load cell was placed under the bone and set to descend at 1 mm/min. Force and displacement data were generated as displacement (mm) against force (N) measured every second. Data were expressed as bone stiffness (N/mm; gradient of the rising portion) and force at failure (N; maximum load supported by the bone).

Tissue analysis

Dynamic histomorphometry of calcein-labelled bone embedded in plastic was performed at the University of Sheffield by the Skelet.AL team (Sheffield, UK). Sagittal sections of the tibia (8 μm) were cut at 3 depths, 30 μm apart, and the endocortical bone surface was imaged using Osteomeasure software (Osteometrics, Georgia, USA). Six fields of view were taken along both the medial and lateral surfaces starting 0.33 mm from the growth plate, totalling a distance of 3.6 mm[38]. Bone formation rate normalised to bone surface perimeter (BFR/BS) was expressed as μm3/μm2/day and the length of double calcein labels normalised to total bone surface perimeter (dL.s/BS) was expressed as a percentage.

Osteoclast or osteoblast number in tibial bone formalin-fixed paraffin-embedded (FFPE) sections were analyzed by immunohistochemistry for tartrate-resistant acid phosphatase (TRAP) activity or haematoxylin and eosin (H&E) staining, respectively. Sections were deparaffinised using Xylene (VWR), followed by rehydration in decreasing concentrations of ethanol (100%, 90%, 80%, 70%) and finished with two washes with de-ionised water.

For H&E staining, deparaffinised slides underwent serial staining for haematoxylin (Pioneer Research Chemicals) and eosin (Pioneer Research Chemicals). Slides cleared in xylene for two 5 min incubation. Slides mounted in xylene-based mounting medium (Merck) and imaged using the ZEISS Axioscan Z1. Images analyzed using ImageJ by two independent researchers, where total bone surface starting 100 μm under the growth plate was measured and a ROI created. From this ROI area of bone which had osteoblasts present were measured, where an osteoblast was characterised as multiple cuboidal cells lining the bone. Osteoblast number presented as percentage bone osteoblast coverage (Ob.S/BS).

For analysis of osteoid deposition,[48] rehydrated slides were stained with 0.04% Fast Green for 30 min before being rinsed in running water for 1 min. Sections were then stained with 0.1% sirius red dissolved in picric acid for a total of 1h. Finally, sections were rinsed in water, dehydrated in ethanol and cleared in xylene before being mounted with xylene-based mounting medium (Merck). Slides were imaged using the ZEISS Axioscan Z1 and analyzed using ImageJ by two independent researchers. Briefly, an ROI was created around trabecular bone below the growth plate and total trabecular bone surface area was measured. Surface area of red staining on the surface of the bone was then measured and presented as percentage of osteoid compared to trabecular bone surface area (OB/OS).

CellPress
OPEN ACCESS

For TRAP staining deparaffinised slides were submerged for 30 min at 37°C in the TRAP staining solution [0.11 mM sodium acetate anhydrous (VWR), 0.074mM L-(+)-Tartaric acid (Fisher Scientific), 2% (v/v) glacial acetic acid supplemented with 1.6M Fast Red Violet LB salt and 2% (v/v) 58 mM Naphthol AS-MX (all from Sigma-Aldrich) diluted in 2- ethoxyethanol (Alfa Aesar, Lancashire, UK)]. Slides were mounted using immuno-mount (Fisher Scientific) and imaged using the ZEISS Axioscan Z1. Images were color separated in ImageJ using CIELAB color space (L*A*B*), where L* (lightness) and B* (blue/yellow) were set as 0 to remove colors that are not red. Manual thresholding on A* (green/magenta) to limit visible spectrum to pink osteoclasts. Osteoclasts were counted manually using the ImageJ cell counter plugin, normalised to the area of the ROI, and presented as osteoclasts/mm^2.

Osteoblast maturation and mineralisation assays

Osteoblasts were seeded at 10^4 cells/well into 48 well plates and cultured in either basal media or osteoblastogenic media [murine/human basal media supplemented with 10 mM β-glycerol phosphate and 50 μg/mL L-ascorbic acid (Sigma-Aldrich)] for up to 21 days. In some cases, media was supplemented with either: 10 ng/mL PEPITEM (sequence: SVTEQGAELSNEER), 10 ng/mL control peptide (sequence: EQAERYDDMAACMK, both from Cambridge Bioscience), 10 μg/mL cadherin-15 agonist antibody (cat: 05–852; Sigma-Aldrich), 3 μg/mL anti-NCAM-1 antibody (clone MEM-188; Thermo Fisher), IgG1 isotype control antibodies (3 μg/mL, Invitrogen cat; 02–6102) or increasing concentrations of sphingosine-1-phosphate (S1P, Sigma-Aldrich). Supernatants were collected at various timepoints for analysis in secretome assays, by ELISA or western blot (see sections below). For western blot analysis, cells were serum starved for 24h prior to centrifugation of supernatants at 10000 rcf for 20 min. Supernatants were stored at −80°C until use.

Osteoblast maturation was assessed in technical triplicate by quantifying alkaline phosphatase activity. Briefly, cells were lysed in RIPA buffer (Sigma-Aldrich) for 30 min on ice, harvested using a cell scraper and centrifuged at 13,000g for 10 min. A 1:4 ratio of cell lysate to alkaline phosphatase yellow (pNPP) liquid substrate for ELISA (Sigma-Aldrich) were incubated for 45 min in the dark at 37°C with agitation (SciQuip, Shropshire, UK) before being quantified using a Synergy HT plate reader with absorbance set at 405 nm. Data are expressed as percentage of control (%).

Osteoblast mineralisation was assessed using the Alizarin Red S Staining Quantification Kit in technical duplicate and following manufacturer's instructions (Caltag+Medsystems, Buckingham, UK). Entire wells were imaged using the Cytation 5 microscope and Gen5 software (both Biotek). The alizarin red stain was quantified by dye extraction as per manufacturer's instructions and absorbance read using a Synergy HT plate reader with absorbance set at 405 nm. The concentration of alizarin red (mM) was quantified using a standard curve generated from known concentration standards and expressed as a percentage of the untreated control.

Metatarsal methods

Hind limbs from embryonic day (E)14.5–15.5 mice were removed, and metatarsals dissected under a dissection microscope in α-MEM (Sigma-Aldrich) diluted 1:13 with sterile PBS, plus 2 mg/mL BSA. The metatarsals were cultured in α-MEM, supplemented with 2 mM L-glutamine, 100 μg/mL streptomycin, 100 U/ml penicillin, 0.2% BSA, 5 μg/mL L-ascorbic acid and 1 mM β-glycerol phosphate (all from Sigma-Aldrich) for 5 days prior to the start of the experiment. Subsequently, metatarsals were treated ± PEPITEM alone, with IgG1 or anti-NCAM-1 antibody. Metatarsals were imaged every other day and data expressed as increase in mineralisation zone in μm.

Human self-structuring bone organoids

Three-dimensional self-structuring bone models (SSBM) containing hFOb 1.19 were created as previously described.[47] SSBM were cultured in osteogenic media (DMEM/F-12, no phenol red with 10% FBS, 0.3 mg/mL G418, 10^{-8}M Menadione and 100 μg/mL Ascorbic acid (as detailed above) at 37°C and 5% CO_2 for 4 weeks prior to addition of treatment - with or without 10 ng/mL PEPITEM or control peptide for 8 days. Three days prior to analysis, constructs were moved into fresh plates with fresh media ± treatments to ensure that only encapsulated cells (and not populations growing outside of the construct on the tissue culture plastic) were included in the analysis. Conditioned media from the last 72 h of culture was collected and analyzed by OPG ELISA (see below).

Western blot

Cells were incubated in RIPA buffer (Sigma-Aldrich) for 30mins on ice, prior to storage at −80°C. Total protein was assessed using BCA assay (ThermoScientific) according to manufacturer's guidelines. Samples were diluted 1:5 with SDS Laemmli buffer (Bio-Rad, cat-1610737), heated at 95°C for 10min prior to loading into 10% gels (Nu-Page, cat -NP0326BOX). Proteins were separated using a 170V current PowerPac Basic Power supply (cat-1645050) for 50 min, then the gel was transferred on to a PVDF membrane using the Trans Biot Turbo mini 0.2 μm (cat-1704156) and Trans-Blo turbo transfer system (all from BioRad).

Membranes were blocked with 5% milk (Marvel – Premier Foods, Ireland) diluted in PBS containing 1% TWEEN 20 (Sigma-Aldrich) for 1h under agitation, then incubated with the following primary antibodies diluted in 5% milk overnight at 4°C: anti-RANKL (1:3000, clone:3F2E1, Proteintech); anti-OPG polyclonal (1:3000, cat: AF459-SP Bio-techne); anti-NCAM- (1:1000 clone MEM-18, ThermoFisher Scientific); or anti-β-actin polyclonal (1:1000, cat:A2066, Sigma-Aldrich) or anti-none-phosphorylated β-catenin (1:10000, cat:8814T, Cell Signaling). Membranes were then washed with PBS-T and incubated with the relevant HRP-conjugated antibodies for 1h: mouse, 1:3000, cat:1706516, BioRad) or rabbit (1:5000, cat:401393, Millipore). Membranes were washed as

described and treated with Clarity Western Peroxide Reagent and Clarity Western Luminol/Enhancer Reagent 1:1 (cat: 1705061) prior to imaging using ChemiDOC MP Imaging System (both from BioRad). Band intensity was measured using ImageJ FIJI software.

Co-immunoprecipitation and mass spectrometry

C.Ob were cultured in osteoblastogenic media for 24h then moved to FBS free osteoblastogenic media containing 0.1mg BSA ±3 μg/mL biotinylated PEPITEM (seq: Biotin-SVTEQGAELSNEER; Cambridge Bioscience) or biotinylated control peptide (seq: Biotin-EQAERYDDMAACMK) for 4 h at 4°C. Cells were washed in ice-cold PBS followed by incubation on ice in ice-cold Triton phosphate lysis buffer [50 mM Tris-HCL, pH 7.5; 150 mM NaCl; 1% Triton X-100; Protease and phosphatase inhibitor (Roche)] for 30 min. Lysates were centrifuged for 20 min at 600 g at 4°C, supernatant collected and stored at −80°C prior to use.

Pierce High-Capacity Streptavidin Chromatography Cartridges (ThermoFisher Scientific, cat: 87739) were equilibrated with Triton phosphate lysis buffer at a flow rate of 0.5–2 mL/min. Supernatants were then passed through the column at a flow rate of 0.5-1 mL/min and fractions were collected. Columns were washed ×5 with Triton phosphate lysis buffer prior to elution of bound proteins using 50% ACN with 1% trifluoroacetic acid (TFA; ThermoFisher). Fractions containing the eluted proteins were then dried in a vacuum centrifuge overnight. Samples resuspended in 8 M urea in 2% SDS and 20μL of the resuspended sample was added to 5 μL of SDS Laemmli buffer (Bio-Rad, cat: 1610737) prior to incubation at 95°C for 10min

Proteins in the samples were separated using a 4–12% Bis-Tris gels (Nu-Page, cat: NP0326BOX) using a 100V current PowerPac Basic Power supply (cat: 1645050; BioRad) for 90 min. Separation gels were stained with Bio-Safe Coomassie stain (cat: 1610786, BioRad) for 1 h room temperature with shaking, prior to washing ×4 in PBS. Regions with bands of high Coomassie blue staining were cut into 5 sections and stored in PBS. Samples were then sent for peptide identification, performed by the Mass Spectrometry Facility (School of Biosciences, University of Birmingham, UK).

Briefly, trypsin digested samples (≤10μg of protein) were incubated in 100 mM ammonium bicarbonate (pH 8) and 10 mM dithiothreitol for 30 min at 56°C. Cooled samples were incubated at room temperature in 50mM iodoacetamide for 30 min, prior to addition of trypsin gold (6 ng/μL; Promega, Southampton, Hampshire, UK) and incubation 37°C overnight. Peptide concentration and separation was performed using UltiMate 3000 HPLC series (Dionex, Sunnyvale, CA USA). Samples were added to precolumn (Thermo Scientific Acclaim PepMap 100 C18 HPLC Columns) and separated in Nano Series Standard Columns using a gradient of 3.2%–44% solvent B (0.1% formic acid in acetonitrile) for 30 min. Columns were washed with 90% mobile phase B, re-equilibrated with 3.2% mobile phase B and eluted directly (~350 nL/min) via a Triversa Nanomate nanospray source (Advion Biosciences, NY) into a QExactive HF Orbitrap mass spectrometer (ThermoFisher Scientific).

Data were analyzed using Uniprot database using Protein Discovery 2.2 software, Sequest HT algorithm (Thermo Fisher). Precursor mass tolerance was 10 ppm and the MS/MS mass tolerance was 0.02 Da. Data were filtered with a false discovery rate of 0.01, and proteins with at least two high confidence peptides were accepted as a real hit. Quality control screening was performed on protein/peptide hits to remove expected contaminants and also hits that appeared in both control peptide and PEPITEM samples. The remaining potential PEPITEM binding partners were initially ranked using Sequest score, and subsequently filtered based on an isoelectric point score of 4–7 corresponding to proteins associated with the plasma membrane. Extensive literature analysis was performed on the top 10 binding partners looking for specific roles in bone biology.

NCAM expression by flow cytometry

Calvarial osteoblasts were grown in osteogenic media before being fixed prior to removal from well plates and subsequently resuspended in MACs buffer (PBS supplemented with, 0.5% EDTA, and 0.6% BSA (all from Sigma)). Cells were stained with anti-CD56 (NCAM) PE (1:50, clone 5.1H11, ThermoFisher Scientific). Samples were filtered and acquired using Fortessa-X20. Data were analyzed offline using FlowJo (V-10.2.6).

NCAM-1-PEPITEM interactions

Protein Uniprot sequences from the above mass spectrometry were ran alongside PEPITEM (SVTEQGAELSNEER) to predict PEPITEM-potential binding partner interactions in AlphaFold2_multimer using Google colab[46,49] to predict both peptide-protein interactions and binding strength. The predicted local distance difference test (pLDDT) was used to select the models with the highest predicted confidence, which were further analyzed using ChimeraX[29,50] to create a 3-D rendering of the interaction.

NCAM1 and RUNX2 staining

Calvarial osteoblasts seeded onto coverslips in 6 well plates (1 x 10^4 cells/well) were cultured in osteogenic media for 24h. Cells were fixed in 10% buffered formaldehyde for 15 min at room temperature, followed by three washes in PBS. Samples were permeabilised in 0.1% Triton X-100 (Sigma) for 10 min, followed by 1h 1% BSA (Sigma) blocking at room temperature. Samples were stained with an anti-NCAM1 (AB5032, 2 μg/mL in PBS) and anti-RUNX2 antibody (MAB2006, 10 μg/mL in PBS, Bio-Techne) for 3 h at room temperature, washed three times in PBS before incubation with secondary antibody (1:2000; ThermoFisher Scientific, cat: A11081 and 1:4000; ThermoFisher Scientific, cat: A11034) for 40 min at room temperature in the dark, washed as above and mounted with DAPI mounting media (Invitrogen) and dried overnight prior to storage at −20°C. Images were taken on a ZEISS LSM 780 confocal microscope and analyzed using Zen Blue software (ZEISS).

CellPress
OPEN ACCESS

β-catenin signaling

Calvarial osteoblasts seeded onto coverslips in 6 well plates (1 x 10^4 cells/well) were cultured in osteogenic media for 24 h before treating with PEPITEM (10 ng/mL, for up to 1 h) or lithium chloride (20 mM for 3 h). Cells were fixed in 10% buffered formaldehyde for 15 min at room temperature, followed by three washes in PBS. Samples were stained with a polyclonal β-catenin primary antibody (4 μg/mL in PBS, Merck, cat: 06–734) for 2h at room temperature. Coverslips were washed three times in PBS before incubation with secondary antibody (1:4000; ThermoFisher Scientific, cat: A21447) for 40 min at room temperature in the dark. Coverslips were washed as described before being gently removed from the wells and excess liquid removed. Coverslips were mounted using DAPI mounting media (Invitrogen), dried overnight prior to storage at −20°C. Images were taken on a ZEISS LSM 780 confocal microscope and analyzed using Zen Blue software (ZEISS). Using ImageJ FIJI software (v2.3.1/1.53f), masks were created for individual cells and their nuclei. Relative intensity was measured in both the whole cell and DAPI positive regions, DAPI measurements were then subtracted from the whole cell recordings. Data presented as average integrated density per nucleus or per 100 μm cell area.

Osteoclast resorption assays

Murine bone marrow osteoclast precursor cells (10^6 cells/well) or RAW264.7 cells (8x10^3cells/well) were seeded onto Osteoassay plates (Corning Inc.) or standard 48-well plates and cultured in either basal media or murine osteoclastogenic media [murine basal media supplemented with 50 or 10 ng/mL RANKL (Abcam, cat: Ab129136)] for up to 7 days. Alternatively, primary human monocytes were seeded into 12-well (10^6 cells/well) or 96-well plates (2 x 10^5 cells/well) containing small dentine disks in human osteoclastogenic media (human osteoclast basal media supplemented with 25 ng/mL *m*-CSF and 25 ng/mL RANKL (both R&D systems). In some cases, media was supplemented with either: 10 ng/mL PEPITEM, 10 ng/mL control peptide, or 1 μM zoledronic acid hydrate (Cambridge Biosciences).

Osteoclast differentiation was assessed by measuring TRAP using a method similar to that described above. Briefly, cultured cells were fixed in 10% PFA for 15 min and then incubated with the TRAP staining solution for 30 min at 37°C. Wells were washed three times in distilled water before imaging using the Cytation5 microscope (Agilent) with BioTek Gen5 software. Number of osteoclasts per well were analyzed using ImageJ and expressed as osteoclasts per 100 m^2.

Osteoclasts seeded into OsteoAssay plates were removed by a 5 min incubation in 10% H_2O_2. Plates were washed in PBS, allowed to air dry and imaged using the Cytation5 microscope with Gen5. Hydroxyapatite resorption was then analyzed in ImageJ FIJI by color thresholding areas of resorption and calculating the percentage of resorption per area/well.

Dentine disks were treated with 1M NH_4OH for 24h, washed and air dried. Dentine resorption pits were stained with 0.5% Toluidine Blue in 0.5% Boric acid for 2min, before being washed, air dried and mounted onto slides using DPX mountant (Sigma-Aldrich). z stack images of the dentine were acquired using the Axioscan Z1 slide scanner (ZEISS). A manual mask of the stained resorption pits was created using ImageJ FIJI software allowing for resorption area to be measured. Data were expressed as percentage of total dentine disk resorbed.

Secretome assays

RAW264.7 (6–8 x 10^3 cells/well) were cultured with 50 ng/mL RANKL in basal murine osteoblast media or conditioned media from treated osteoblasts for 5 days, prior to staining for TRAP (as above). Prior to addition to RAW264.7 cells, conditioned media from PEPITEM-treated osteoblasts was supplemented with 50 ng/mL RANKL along with either: 0.15 or 0.5 μg/mL OPG polyclonal neutralising antibody (cat: AF459, Biotechne, UK) or an IgG control antibody (0.5 μg/mL, Invitrogen, cat: 02–6102). In competition assays, conditioned media was supplemented with 50, 100 or 500 ng/mL RANKL (Abcam).

ELISA

Osteoprotegerin (OPG) or RANKL concentrations (pg/mL) in osteoblast supernatants were measured in technical duplicates using R&D Quantikine ELISA kits as per manufacturer's instructions (R&D Systems) using a Synergy HT plate reader with absorbance set at 405nm. Data were expressed as a percentage of the untreated control. Serum was analyzed for RatLaps total procollagen type-1 N terminal propeptide (P1NP) by a competitive ELISA as per the manufacturer's instructions and read using a Synergy HT plate reader at 405nm. A 4- parameter logistical curve fit was applied to the data to calculate P1NP serum concentrations (ng/mL).

Gene expression

RNA was extracted using the RNeasy Kit as per manufacturer's instructions (Qiagen). 500ng RNA was converted to cDNA using a high-capacity cDNA reverse transcription kit following the manufacturer's instructions (Applied Biosystems). Gene-specific Applied Biosystems Assay-on-Demand TaqMan primers were diluted 1:10 in master mix (Applied Biosystems), before plating into 384 LightCycler plates along with 2.75 μL of diluted cDNA (1:5) in dH2O. Samples were run in technical triplicates and analyzed on the LightCycler 480. Data were normalised to β_2-microglobin and expressed as $2^{-\Delta Ct}$.

Alternatively, library preparation was performed on samples with RIN of >7 using the Lexogen QuantSeq 3′ mRNA-Seq Library Prep Kit FWD for Illumina (Illumina, California). Samples that passed library prep were pooled in equal volumes and quality checked by the Genomics service using the Agilent TapeStation DNA 1000 tape (Aligent) and DNA HS Qubit (Fisher Scientific). Sequencing was then performed using the NextSeq 500 (Illumina), where the run had a Yield (Gbp) of 43.58 and an average %Q30 of 91.17, indicating a successful run and analysis could be performed in house.[51,52] Data generated were provided in fastq format, where quality of

each sample could be checked using FASTQC and MULTIQC packages in Rstudio (RStudio Public-benefit corporation).[53] Four reads were generated for each sample, which were combined and subsequently trimmed. Trimming was performed using BBMap to remove the polyA tail, low quality RNA (Using the Phred quality score algorithm) and contaminating adaptor regions.[54]

In order to align the genome, a genome index was created using a pre-assembled genome from ensembl.[55] The "Mus_musculus.GRCm39.104.gtf" genome and corresponding primary assembly file were used to create the genome used for our analysis. Trimmed sequences were then aligned to the genome using the STAR align package and the Encode standard settings.[56] MultiQC was performed on FastQC files generated from the aligned samples and each parameter was checked to ensure quality of pre-processing. Feature counts were produced using the Subread package to generate a table of gene counts.[57,58] The produced feature counts were then loaded and analyzed using iDep.[59] IDep correctly identified the samples as *Mus musculus* and rlog transformation was selected. Genes were then ranked by standard deviation using hierarchical clustering. Samples were then plotted on a PCA plot using first and second principal components. The Dseq2 package was then used to identify upregulated and downregulated genes. Genes were analyzed using GO term analysis.

QUANTIFICATION AND STATISTICAL ANALYSIS

Data are expressed as mean ± SEM unless otherwise stated. To ensure the data met the assumptions for each statistical test, normality was assessed using Kolmogorov-Smirnov test. Univariant analysis was performed using unpaired t-test, paired t-test or Wilcoxon signed-rank test. Multi-variant analysis was performed using ANOVA or Kruskal-Wallis followed by Dunnett's, Bonferroni or Dunn post-hoc test. For the purposes of visualisation (*) $p < 0.05$ was deemed to be statistically significant. The statistical parameters, including the value of n and what n entails, are reported in the relevant methods sections and within each figure legend.